RILEM Bookseries

Kamal Henri Khayat
Dimitri Feys *Editors*

Design, Production and Placement of Self-Consolidating Concrete

Proceedings of SCC2010, Montreal, Canada, September 26–29, 2010

Springer

Design, Production and Placement of Self-Consolidating Concrete

RILEM BOOKSERIES

Volume 1

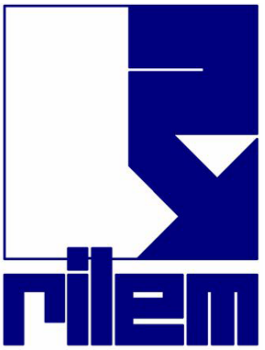

For other titles published in this series, go to
www.springer.com/series/8781

Kamal Henri Khayat • Dimitri Feys
Editors

Design, Production and Placement of Self-Consolidating Concrete

Proceedings of SCC2010, Montreal, Canada,
September 26–29, 2010

Springer

Editors
Kamal Henri Khayat
Université de Sherbrooke
Québec, Canada

Dimitri Feys
Université de Sherbrooke
Québec, Canada

ISBN 978-90-481-9663-0 e-ISBN 978-90-481-9664-7
DOI 10.1007/978-90-481-9664-7
Springer Dordrecht Heidelberg London New York

Library of Congress Control Number: 2010932809

Cover design: eStudio Calamar S.L.

Printed on acid-free paper

Springer is part of Springer Science+Business Media (www.springer.com)

Table of Contents

Theme 3: Rheology and Workability of SCC

Theme 4: Production and Placement of SCC

Theme 5: Flow Modeling of SCC

Preface

Dear Colleagues,

We are pleased to organize the Sixth International RILEM Symposium on SCC and the Fourth North-American Conference on the Design and Use of SCC, held on Sept 26-29, 2010 in Montreal, Quebec, Canada. The RILEM series of symposia started in 1999 in Stockholm, followed by Tokyo in 2001, Reykjavik in 2003, Chicago in 2005, and Ghent in 2007 with a steadily increasing number of papers, participants, and interest from across the globe. Due to the growing success of SCC, regional conferences have been organized, such as the North-American Conference on the Design and Use of SCC held in Chicago in 2002, 2005, and 2008; the International Symposium on Design, Performance and Use of SCC held in Changsa, China in 2005 and in Beijing, China in 2009; as well as the 2nd International Conference on Advances in Concrete Technology in the Middle East: SCC held in Abu Dhabi in 2009. It can be concluded that these regional Conferences and Symposia were highly successful and reached a far more international audience than anticipated.

Nearly 100 papers were submitted for these proceedings from which the International Scientific Committee selected 37 contributions covering a wide range of timely and original subjects from around the world. We would like to acknowledge the input of the International Scientific Committee for providing critical input to guarantee high quality of these peer-reviewed proceedings. We invite you to explore a wealth of information in the electronic proceedings. Topics covered in this conference include SCC Mix Design, Chemical Admixtures, Rheology and Workabilty, Production and Placement, Flow Modeling, Formwork Pressure, Hardened Properties, Bond Strength, Fiber-Reinforced SCC, Economics, Worker's Health, Environmental Benefits, and Case Studies. These papers reflect significant advances made in research, design, and implementation of SCC worldwide during the last years. Nearly 130 papers will be presented during the three parallel sessions in addition to other papers discussed during the poster session at the conference.

We would like to greatly acknowledge all the Authors for sharing their expertise and knowledge as well as our Sponsors for their generous support that is critical for the success of the conference.

Special thanks go to the Honorary Advisory Committee and the International Technical Committee for their advice and help in promoting the conference.

We would like to thank the Organizers of this conference: l'Université de Sherbrooke, RILEM, la fédération internationale du béton (*fib*), the Center for Advanced Cement Based Materials (ACBM), and le Centre de Recherche sur les Infrastructures en Béton (CRIB) as well as the Local Organizing Committee for their diligent work and commitment to bring this conference to great success!

The Editors,

Kamal Henri Khayat
Dimitri Feys
Université de Sherbrooke, Canada

September, 2010

Conference Committees

Conference Chair

K.H. Khayat, *Université de Sherbrooke, Canada*

Honorary Advisory Committee

A. Skarendahl, *Sweden, chair of SCC 1999, Stockholm*
H. Okamura, *Japan, chair of SCC 2001, Tokyo*
O. Wallevik, *Iceland, chair of SCC 2003, Reykjavik*
S. Shah, USA, *chair of SCC 2005 and SCC 2008, Chicago*
G. De Schutter, *chair of SCC 2007, Ghent*

International Technical Committee

O. Wallevik, *IBRI, Iceland* (chair)
A. Bentur, *Technion, Israel*
M. Geiker, *Technical University of Denmark, Denmark*
T.A. Hammer, *SINTEF, Norway*
J. Kim, *Fosroc, South Korea*
R. Munn, *University of New South Wales, Australia*
S. Nagataki, *Aichi Institute of Technology, Japan*
M. Ouchi, *Kochi University, Japan*
J. Walraven, *Delft University, The Netherlands*
P. Yan, *Tsinghua University, China*

International Scientific Committee

G. De Schutter, *Ghent University, Belgium* (co-chair)
N. Roussel, *LCPC, France* (co-chair)
H. Abdelgader, *Al-fateh University, Lybia*
G. Agranati, *Politécnica de Madrid, Spain*
S. Amziane, *Université Blaise-Pascal, France*
E. Attiogbe, *BASF Construction Chemicals, USA*
C. Bédard, *The Euclid Chemical Company, Canada*

H. Beitzel, *FH Trier, Germany*
P. Billberg, *CBI, Sweden*
B. Blair, *Lafarge North America, USA*
W. Brameshuber, *University Aachen, Germany*
F. Cussigh, *Vinci Construction, France*
J. Daczko, *BASF Construction Chemicals, USA*
Y. Deshpande, *Michigan Technological University, USA*
P. Domone, *University College London, UK*
L. Ferrara, *Politecnico di Milano, Italy*
C. Ferraris, *National Institute of Standards and Technology, USA*
R. Ferron, *University of Texas at Austin, USA*
R. Flatt, *Sika, Switzerland*
J.V. Gruber, *Bechtel Power Corporation, USA*
S. Grünewald, *Hurks Beton / TU Delft, the Netherlands*
A. Kanellopoulos, *University of Cyprus, Cyprus*
M. Khrapko, *CBE Consultancy, New Zealand*
E. Koehler, *W.R. Grace & Co., USA*
M. Lachemi, *Ryerson University, Canada*
D. Lange, *University of Illinois, USA*
C. Lanos, *Université de Rennes 1, France*
A. Leemann, *EMPA, Switzerland*
D. Ludirdja, *Vulcan Materials Company, USA*
P. Lura, *EMPA, Switzerland*
C. Mazzotti, *University of Bologna, Italy*
C.V. Nielsen, *Danish Technological Institute, Denmark*
C. Ozyildirim, *Virginia Transportation Research Council, USA*
M. Pagé, *Handy Chemicals, Canada*
A. Perrot, *Université de Bretagne Sud, France*
B. Persson, *Lund Institute of Technology, Sweden*
A.K. Schindler, *Auburn University, USA*
W. Schmidt, *BAM Berlin, Germany*
C. Shi, *Hunan University, China*
K. Sideris, *Democritus University of Thrace, Greece*
K.R. Sompura, *Sika Corporation, USA*
M. Sonebi, *Queen's University, Belfast, UK*
A. Tagnit-Hamou, *Université de Sherbrooke, Canada*
C. Talbot, *Omya Inc,, USA*
L.N. Thrane, *Danish Technological Institute, Denmark*
F. Toussaint, *Pôle technologique Lafarge, France*
M. Vachon, *ESSROC, USA*
K. van Breugel, *TUDelft, The Netherlands*
S. Vanikar, *Federal Highway Administration, USA*
G. Ye, *TUDelft, The Netherlands*
W. Zhu, *University of the West of Scotland, Paisley, UK*

Local Organizing Committee

K.H. Khayat, *Université de Sherbrooke, Canada* (chair)
O. Bonneau, *Université de Sherbrooke, Canada*
G. Breton, *Université de Sherbrooke, Canada*
C. Couture, *Université de Sherbrooke, Canada*
Y. Denommé, *Handy Chemicals, Canada*
D. Feys, *Université de Sherbrooke, Canada*
R. Gagné, *Université de Sherbrooke, Canada*
G. Lemieux, *The Euclid Chemical Company, Canada*
B. Tighiouart, *Université de Sherbrooke, Canada*
A. Yahia, *Université de Sherbrooke, Canada*

Theme 1: Mix Design for SCC

Design and Flow of Powder-type SCC with Crushed Aggregates

Andreas Huss[1] and Hans W. Reinhardt[2]

[1] Materialprüfungsanstalt Universität Stuttgart, Germany
[2] Department of Construction Materials, University of Stuttgart, Germany

Abstract. The paper describes a new approach to determine the volume of the cement paste required to produce SCC irrespective of the granulometric characteristics of the aggregate. A test vessel has been designed which enables the determination of the void ratio of the aggregate and the necessary paste volume. The method has been applied to various aggregate (crushed quartz porphyry, crushed muschelkalk, gravel, fluvial sand). SCC mixtures have been designed according to the new approach, and it turned out that it has a good predictive potential as the mixture composition is concerned.

Introduction

A certain amount of cement paste is required to produce powder type SCC. This amount largely depends on the granulometric characteristics of the aggregates used. The amount of cement paste required to produce SCC is usually determined empirically on the basis of fresh concrete tests, or is assumed on the basis of the experience gained so far (see e.g. [1-3[3]). Since this situation is not satisfying, a method to determine the required cement paste volume which is not purely empirical has been developed, which is termed aggregate-packing test (APT).

Void Ratio and Amount of Cement Paste Required

As central point of the research, a method and a test vessel were developed to determine experimentally the amount of cement paste ($V_{CP,req}$) required for powder type SCC. In this process, the aggregate to be used in the SCC is examined directly, including any influence that may result from the granulometric characteristics of the aggregate. The method examines the aggregate fractions larger than 0.125 mm in size in the composition in which it is to be used in the

K.H. Khayat and D. Feys (eds.), *Design, Production and Placement of Self-Consolidating Concrete*, RILEM Bookseries 1,
DOI 10.1007/978-90-481-9664-7_1, © RILEM 2010

concrete. For this purpose, a wetted, homogenized sample of the aggregate is fed into the test vessel (Figure 1) up to its top edge, without compaction.

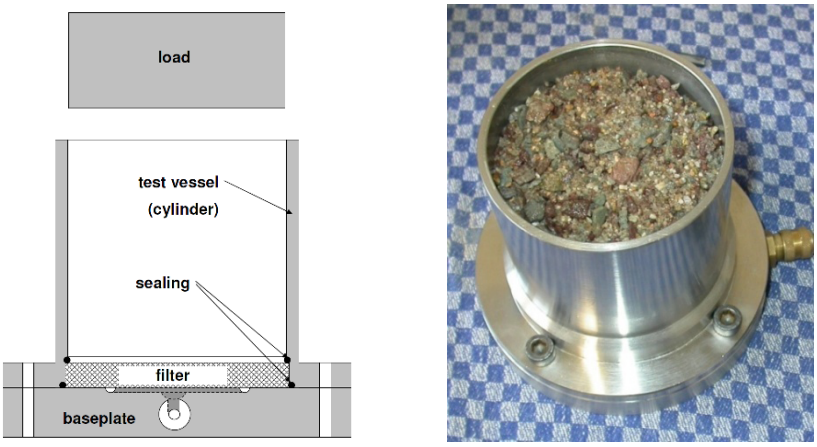

Figure 1. Test vessel, left: cross-section, right: picture.

The vessel is then flooded with water from its bottom up to the top edge. The sample collapses during flooding and settles in a loose arrangement as a result of the reduction in, or elimination of, the friction between the particles and due to the mass of the aggregate. Following a saturation period, the water is siphoned off again through the bottom vessel section under controlled conditions. In the investigations presented in this article, the settlement condition of the aggregate mixture after water discharge is referred to as "non-compacted". In this condition, the amount of water physically bound in the aggregate is determined ($V_{W,nc}$) by weighing. In the next step, the aggregate is compacted under a defined load of 1.972 kg ($\triangleq$ 3.1 kPa) by vibration, and the total volume (solids and voids) of the compacted aggregate ($V_{A,c}$) is determined geometrically, as well as the void volume in compacted state ($V_{V,c}$) via the concentration of solids. The concentration of solids is calculated using the particle volume V_A ($= m_A / \rho_A$) and the volume of the compacted aggregate $V_{A,c}$. The amount of cement paste required to produce SCC ($V_{CP,req}$) in cubic meters per cubic meter of SCC is calculated using Eqn. (1).

$$V_{CP,req}/V_{SCC} = (V_{V,c} + V_{CP,sp})/V_{SCC} = (1 - V_A/V_{A,c}) + V_{W,nc}/V_{A,c} \quad (1)$$

Figure 2 shows the two situations. Figure 2a illustrates the non-compacted state with cement paste around the grains and in the voids. Figure 2b illustrates the state of the compacted aggregate with the cement paste in the remaining voids ($V_{V,c}$) and the surplus cement paste ($V_{CP,sp}$) which is necessary in order to cause self-compactibility.

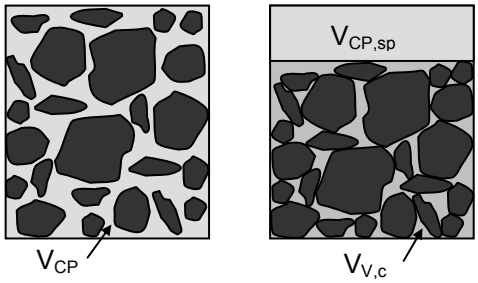

Figure 2. Aggregate in non-compacted (a) and compacted state (b) with cement paste.

Aggregate Tests

Aggregates conforming to DIN EN 12620 were used for the tests. The coarse fractions in excess of 2 mm consisted of gravel (K), crushed quartz porphyry (Q) and crushed muschelkalk (shell limestone) (WI); the fine 0-2 mm fractions comprised fluvial sand (-F) and crushed quartz porphyry sand (-Q). The tests to determine the void ratio and the amount of cement paste required were carried out for aggregates with a particle size distribution in accordance with grading curves A16, AB16, ABB16 and B16 as specified in DIN 1045-2.

The composition of the aggregate mixtures referred to as ABB16 was in the range between grading curves AB16 and B16. This composition is largely equivalent to the "ideal grading curve" with a Fuller exponent of n = 0.5. It was selected to achieve a high packing density on the basis of own tests and analyses and information available in the literature. Figure 3 shows a comparison of the voids of dry aggregate mixtures according to DIN 1097-3 with the voids measured in wet mixtures in the aggregate-packing test.

It should be noted that the wall effect of the test vessel was not considered. If the wall effect is estimated according to [4], the values measured in the APT range from approximately 1% to 4%, i.e. from approx. 4 to 15 dm^3 per m^3 of SCC, above the actual values. However, since this constitutes a systematic error, no correction was made for the purpose of the comparison shown in Figure 4 and for the other considerations contained in this paper.

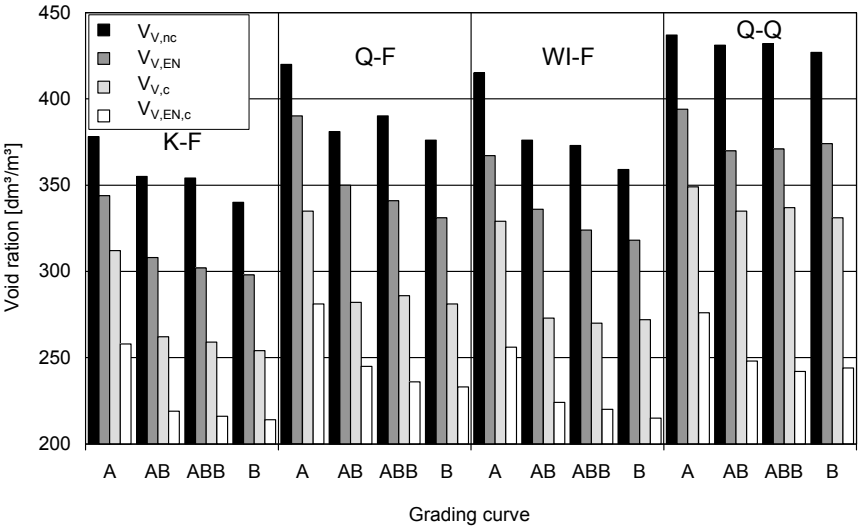

Figure 3. Void ratios of aggregate mixtures K-F; Q-F; WI-F and Q-Q in the case of grading curve variation. Non-compacted ($V_{V,nc}$) and compacted ($V_{V,c}$), as well as to the dry aggregate mixture on the basis of DIN EN 1097-3, non-compacted ($V_{V,EN}$) and compacted ($V_{V,EN,c}$).

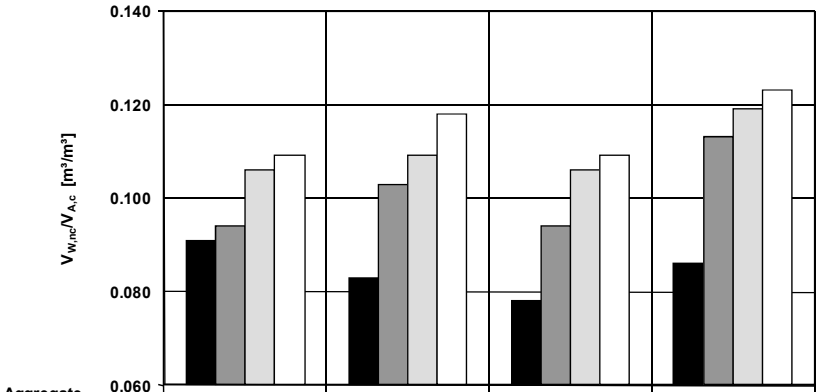

Aggregate	K-F	Q-F	WI-F	Q-Q
A16 (0/4: 36%)	0.091	0.083	0.078	0.086
AB16 (0/4: 45%)	0.094	0.103	0.094	0.113
ABB16 (0/4: 51%)	0.106	0.109	0.106	0.119
B16 (0/4: 56%)	0.109	0.118	0.109	0.123

Figure 4. Physically bound water ($V_{W,nc}$)/volume of aggregate mixture ($V_{A,c}$), tested with the aggregate-packing test (APT) method whilst varying the grading curve.

In the tests carried out, a larger void ratio was found in the aggregate-packing test than in the dry aggregate mixture test on the basis of DIN EN 1097-3. This outcome is attributed to the varying boundary conditions of the testing methods and to the fact that the fines fraction below 0.125 mm is missing in the APT method. In addition, it is assumed that the aggregates tested in dry condition segregate when being fed into the test vessel, and during compaction. This became particularly apparent for the tested aggregate that included crushed sand (-Q), where the void volume decreased much more significantly during compaction in dry condition as a result of the trickling-down fine particles, compared to aggregate tested in wet condition. For this reason, this paper uses the void volume $V_{V,c}$ determined in the APT in compacted condition as a parameter in Eqn. (1) to calculate the void volume for a zero cement paste layer thickness.

The amount of cement paste required for the production of SCC ($V_{CP,req}$) was determined on the basis of the results of the aggregate-packing test, using Eqn. (1). The volumes shown in Figure 4 have been determined using the amount of physically bound water during the APT. As expected, these volumes increase along with a higher fines ratio, i.e. in line with the increase in the aggregate surface. Although this ability to bind water mainly depends on the fines ratio, the most unfavorably shaped crushed quartz porphyry (Q) are clearly visible (Figure 4) because of the higher amount of water bound in the AB, ABB and B mixtures, in which the same fluvial sand (-F) was used. The particle surface of crushed sand (-Q), which is significantly higher than that of fluvial sand, is considered the main cause of the higher water-binding capacity of the Q-Q aggregate mixture tested.

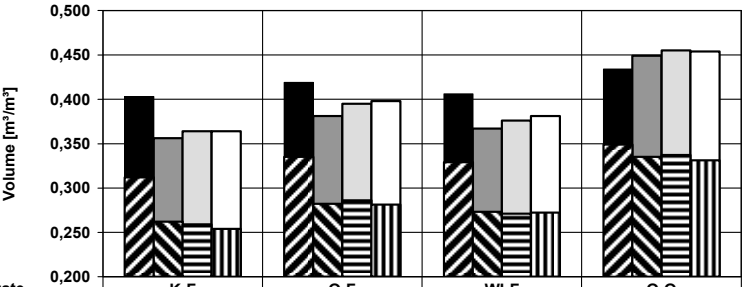

	Aggregate	K-F	Q-F	WI-F	Q-Q
$V_{CP,req}$	A16 (0/4: 36 %)	0,403	0,419	0,406	0,434
	AB16 (0/4: 45 %)	0,356	0,381	0,367	0,449
	ABB16 (0/4: 51 %)	0,364	0,395	0,376	0,455
	B16 (0/4: 56 %)	0,364	0,398	0,381	0,454
$V_{V,c}$	A16	0,312	0,335	0,329	0,349
	AB16	0,262	0,282	0,273	0,335
	ABB16	0,259	0,286	0,271	0,337
	B16	0,254	0,281	0,272	0,331

Figure 5. Amount of cement paste required ($V_{CP,req}$) = void ratio in compacted condition ($V_{V,c}$) + ($V_{W,nc}$)/($V_{A,c}$) according to Figure 4, tested with the aggregate-packing test (APT) whilst varying the grading curve.

Figure 5 shows the amount of cement paste determined for grading curves A16, AB16, ABB16 and B16 in the aggregate-packing test. In line with expectations, the amount of cement paste required that was determined for crushed aggregate was higher than that of aggregates containing gravel. Likewise, the cement paste amount was higher for crushed sand compared to fluvial sand. The amount of cement paste required ($V_{CP,req}$) that had been determined for the ABB16 size fractions was used as input parameters to calculate the mixture of the SCCs tested.

Powder-type SCC Mix Design

To produce the SCCs under study, the above-described aggregates consisting of gravel and fluvial sand (K-F), crushed quartz porphyry and fluvial sand (Q-F), crushed muschelkalk and fluvial sand (WI-F) and crushed quartz porphyry and crushed sand (Q-Q) were used with a ratio of particles smaller than 4 mm in size that amounted to approx. 50% by mass (ABB16 grading curve). The mixture was determined using the known material volume calculation by defining the cement paste volume and the volume-related cement/additive and water/powder (V_W/V_P). The paste volume was considered to include all constituents smaller than 0.125 mm (cement, concrete additions, and fines in aggregate mixtures), the added water quantity, the concrete admixture and the air contained in the fresh concrete.

The composition of the SCCs examined was compared to the cement paste volume $V_{CP,req}$ that had been determined in the aggregate-packing test, and with paste volumes above and below this value. As an addition, limestone filler or fly ash was added at a 1:1 ratio in relation to the volume of the cement used (CEM II/A-LL 32.5 R). These high addition ratios resulted from the C30/37 strength class to be complied with. The 28 days compressive strength of the concretes produced ranged from 40 to 50 MPa. To achieve higher target strengths, it appears feasible to increase the ratio of cement whilst reducing the addition content by a corresponding margin without significantly altering the other constituents of the mixture.

Since dry aggregate mixtures were used to produce the concrete mixtures, the absorption capacity of the aggregates was also considered. For this purpose, the aggregate mixtures were sprayed with water during a continuous motion until the surfaces of the coarse particles appeared just slightly damp, without any visible shiny spots. The fine aggregates were sprayed with water until the first signs of adhesion of particles to each other or to the vessel wall became apparent. According to experience, the results of this quick test for densely packed aggregate are usually in the water absorption range specified in the DIN EN 1097-3. The addition of water derived from water absorption ranged from 6 to 9 kg/m^3. To determine the ratio of water volume (V_W) to powder volume (V_P), initial tests were performed with pure cement paste in accordance with the SCC Guideline [5]. It

turned out, however, that this approach was not helpful when it came to designing a large number of different mixtures.

One of the difficulties encountered was the issue of how to reflect the powder content in the aggregate. In addition, an incremental development of the mix design through the determination of the amount of water required (cement and addition), cement paste and mortar tests and fresh concrete testing would have been very complex. For this reason, the mix designs were based on approximate values for the V_W/V_P that were taken from the literature (e. g. [1-3]) and from own preliminary tests with a Portland limestone cement (CEM II/A-LL 32.5 R) and fly ash (FA) or limestone filler (LF). These values were then used to calculate the mixture compositions. For the mix designs investigated, the ratios selected amounted to V_W/V_P = 0.88 and V_W/V_P = 0.90 for limestone filler and fly ash, respectively.

The extent to which the selected water-powder ratios were suitable to produce a suspension was tested for specific mixtures by measuring the "shear resistance" during the production of fresh concrete. In this procedure, the amount of water required for the conversion of the mixture (consisting of cement, addition and mineral aggregate) to a suspension was determined in an experimental setup. This volume was termed the minimum amount of water (w_{min}) and was derived from the "shear resistance" curve of the aggregate, which was indirectly captured via the input power of the compulsory mixer [6].

Own experience has shown that any water volume in excess of the minimum amount is tolerable as long as there are no signs of segregation (bleeding) of the fresh concrete, for instance in the form of "water shifting" occurring during the slump test. It is not possible, however, to go below the minimum amount of water since this would no longer provide the conditions under which a suspension, and thus SCC, can be produced. Only when the minimum amount of water w_{min} has been exceeded will it be possible to produce a SCC from the suspension by adding a plasticizer.

The measurement of "shear resistance" depending on water addition provides a quick and convenient method to determine the amount of water required for SCC.

The following fresh concrete parameters of the SCCs were measured [7]:

- Slump flow with and without J-ring (sf_J; sf)
- Blocking tendency in accordance with pr EN 12350-12 across the difference in height within/outside the J-ring (blocking step st_J)
- V-funnel flow time (t_V) in accordance with pr EN 12350-9
- Air void ratio in the 8 dm^3 vessel in accordance with DIN EN 12350-7.

A slump flow target value of 690 mm was defined. The V-funnel flow target value was defined as a range of 14 ± 3 s according to [1]. At a constant V_W/V_P, the

degree of flow was set by the amount of added plasticizer alone. The scope of the tests did not include an optimization of the paste composition.

The SCCs' blocking tendency was determined visually and by the blocking step st_J during the slump test. From the literature, values of $st_J \leq 20$ mm were taken as a criterion for non-blocking SCC. In the SCCs investigated, blocking was found when the actual cement paste volume was lower than the required paste volume $V_{CP,req}$ established in the aggregate-packing test.

For the SCCs produced with crushed quartz porphyry sand (-Q), it was found that their V-funnel flow time t_V equaled approx. 7 s, and was thus significantly lower than the 14 ± 3 s target range. Despite this short V-funnel flow time, no signs of sedimentation were identified at sawn-open concrete cylinders for the mixtures in which the paste volume exceeded the calculated paste volume by 15 or 20 dm^3/m^3.

Due to the high amount of plasticizer used, some of the air void ratios determined during the tests were as low as 0.6% by volume in the SCCs with reduced paste content. The SCCs with a paste volume that corresponded to the paste volume $V_{CP,req}$ calculated in the APT showed a very good degree of self-compaction with air void ratios between 1.0% and 1.5% by volume.

When the paste content was very low it was impossible to reliably reach the target range (sf approx. 690 mm, $st_J \leq 20$ mm and $t_V = 14 \pm 3$ s) in the tests carried out by adjusting the amount of plasticizer alone. Nor was it possible, under these conditions, to produce a SCC on the basis of a visual assessment. Starting from a paste volume equivalent to the volume $V_{CP,req}$ determined in the APT, it was possible to produce SCCs with added FA and LF that met practical requirements.

Summary and Outlook

In summary, the following conclusions can be drawn from the above considerations and tests with regard to the mix design of powder-type SCC with ABB 0/16 aggregates:

- The aggregate-packing test (APT) is a practice-oriented method to determine the required paste volume ($V_{CP,req}$) for powder type SCC. By testing the mineral aggregate to be used for concrete production directly, this method delivers an integral description of the granulometric characteristics of aggregates. When the required paste volume has been determined, the mix design can be reduced to the known material volume calculation.
- The fact that the paste volume required for SCC production can be determined in the aggregate-packing test (APT) makes it possible to focus on the optimization of the cement paste. In this regard, the measurement of the power of the laboratory mixer made in the course of the tests has proven

to be a quick and accurate method to determine the required minimum amount of water. Starting from the paste volume and minimum amount of water required, SCCs can be optimized in a targeted fashion, especially with respect to the selection and dosing of the plasticizer.

- Tests that are currently being carried out with other sands should verify the findings arrived at to date. In parallel, the practical feasibility of the proposed design concept in the production of SCC at the ready-mixed concrete plant is to be investigated.

References

[1] Lemmer, C. (2003), A production approach for SCC as derived from experimental studies, PhD Thesis, Technische Universität Darmstadt (in German).

[2] Marquardt, I. (2002), A mixing concept for SCC based on the volume parameters and the water demand of the constituent elements, PhD Thesis, University Rostock, Bull. 7 of Faculty of Civil Engineering, (in German).

[3] Kordts, S. (2005), Production and control of workability properties of SCC, PhD Thesis, Technische Universität Berlin (in German).

[4] Sedran, T. and de Larrard, F. (1999), Optimization of self compacting concrete thanks of packing model. PRO 7: 1st International RILEM Symposium on Self-Compacting Concrete, Å. Skarendahl and Ö. Petersson (Eds.), pp. 321-332.

[5] German Association of Structural Concrete (2003), Guideline for self-compacting concrete (in German).

[6] Huss, A. and Reinhardt, H.W. (2009), Powder-type SCC with crushed mineral aggregates. *Concrete Plant + Precast Technology*, vol. 75, n. 8, pp. 4-12 and n. 9, pp. 22-34.

[7] Pade, C. (2005), Test methods for SCC, Danish Technological Institute, Denmark.

"Structural Design with Flowable Concrete" - A *fib*-Recommendation for Tailor-Made Concrete

Steffen Grünewald[1], Liberato Ferrara[2] and Frank Dehn[3]

[1] Delft University of Technology/Hurks Beton, The Netherlands
[2] Politecnico di Milano, Italy
[3] University of Leipzig/MFPA Leipzig, Germany

Abstract. Flowable concrete (either compacted with some vibration or self-compacting) is becoming a widely applied building material. Due to its flowable nature, reinforcing bars can become an obstacle, mixture components may float or segregate and the casting technique determines the orientation of fibers, if any. An increasing range of components is available to optimize concrete concerning rheological and hardened state properties and for the application under consideration. Flowable concrete offers an extended range of engineering properties and the potential for product innovation.
fib Task Group (TG) 8.8 "Structural Design with Flowable Concrete" started in 2009 to facilitate the use of innovative flowable materials for the design of concrete structures. Taking into account research findings and practical experience, the main objectives of fib TG 8.8 are to write a state-of-the-art report and recommendations on the structural design with flowable concrete. fib TG 8.8 considers three aspects of flowable concrete: material properties, production effects and structural boundary conditions.
This paper discusses the scope of fib TG 8.8 concerning the characteristics and the potential of flowable concrete and presents related design standards. fib TG 8.8 aims at promoting the application of flowable concrete, improving and adapting the concrete design and the production technology and its implementation in guidelines and codes.

Introduction

Aim of fib Task Group 8.8

Design recommendations for flowable concrete will most likely be instrumental to promote and facilitate the application of highly flowable and self-compacting

K.H. Khayat and D. Feys (eds.), *Design, Production and Placement of Self-Consolidating Concrete*, RILEM Bookseries 1,
DOI 10.1007/978-90-481-9664-7_2, © RILEM 2010

concretes, either plain or fiber-reinforced, including high and ultra-high performance fiber-reinforced concrete (UHPFRC). In contrast to traditionally vibrated concrete, highly flowable concrete requires little or no vibration energy to be placed. This implies that not only the mixture composition but also the production process have to be "tailored" to the devised application, finally aiming at an optimized structural performance. Successful construction with flowable concrete hence implies a "holistic" approach (Fig. 1), which encompasses optimizing the material composition to the achievement of the targeted fresh and hardened state properties together with the adjusted manufacturing process and the conception of the type and the shape of a structure.

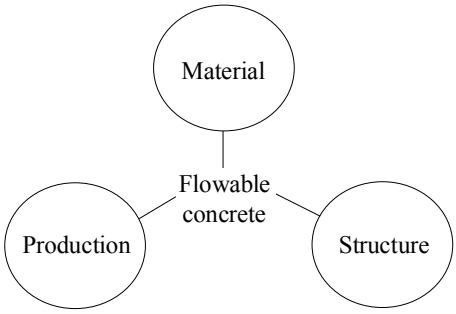

Figure 1. Structural performance as a result of three components: material behavior, production effects and structural boundaries.

Benefits and bottlenecks of flowable concrete

The application of flowable concrete has benefits related to productivity (i.e. lower production costs, and a higher casting rate), working circumstances (reduced noise and dust emissions), casting circumstances (i.e. casting of densely-reinforced sections and remote casting) and environment-friendly production (e.g. filler and aggregates can be waste/recycled materials). With flowable concrete, the effect of vibration (when not properly carried out, affects the quality of concrete) is eliminated or reduced [1]. Major benefits of applying SCC are a more homogenous concrete, a better visual appearance, a lower variation of strength and a more durable concrete [2, 3]. Vibrating traditional concrete can also affect the local air content and consequently the strength and the durability of concrete, especially the freeze-thaw resistance [2].

Strength and durability are the two main features of concrete structures which have to be considered for the design. Since flowable concrete may significantly differ from vibrated concrete in the mixture composition (for example the paste content is usually higher), characteristics during setting, hardening as well as properties in

the hardened state may be affected [4], which has to be adequately taken into account by designers and engineers. These issues will be addressed by fib TG 8.8.

The aesthetical appearance of concrete often is an important criterion to decide what mixture will be applied for a structure. The type and the content of the powders and the composition of the paste mainly determine the color and the variation of color. Producing flowable concrete with fillers or pigments allows altering the color compared to a mixture that contains only cement as a powder. Flowable concrete usually contains a higher powder content and, if well-executed, fair-faced structures can be produced. The elimination of vibration or casting with a minimum of compaction energy largely reduces color inhomogeneities of the concrete surface. In this context, fib TG 8.8 intends to strongly cooperate with the new fib Task Group on "Aesthetics of Concrete Surfaces" (fib TG 8.9).

Cussigh [5] and Desmyter [6] discussed the potential and the drawbacks of SCC; most aspects also describe the situation of flowable concrete in general. The need for high quality materials, for a higher accuracy of production equipment and for special formwork, higher material costs, stringent quality control requirements and a lack of standards possibly explain why the market-share of ready-mix SCC is low (Cussigh reported only 3% in France [5]) and why the precast industry may be more prone to implement SCC. With SCC, it is required to specify in advance where the supplier's responsibility ends during production (i.e. concerning the surface appearance or blowholes). Higher material costs, an increased complexity and higher risks hinder a more widespread application of SCC in spite of many proven benefits. The difference in material costs of SCC compared to vibrated concrete decreases at increasing compressive strength. Applying ready-mix SCC involves more actors (i.e. owner, supplier, contractor) compared to the production of prefabricated elements with SCC. The fragmentation of the building industry and the prime focus on cost competition are main barriers for innovation [6]. Four issues have hence to be addressed to increase the market-share of the SCC-technology: to provide robust and reliable concrete mixtures, to involve industry in R&D-activities, to transfer knowledge and to develop accepted standards. Flowable concrete and SCC are important to further industrialize prefabricated and cast-in-place concrete construction, to improve the quality of concrete structures and to carry out projects more economically profitable.

Flowable concrete with fibers

Flowable fiber-reinforced concrete (FFRC) combines the benefits of flowable concrete in the fresh state and an enhanced performance of fiber-reinforced concrete (FRC) in the hardened state. By adding fibers to flowable concrete bar reinforcement can be replaced, crack widths reduced, the durability improved and the load bearing capacity of a structure increased. The size of the fibers relative to the rebar spacing affects the passing ability. By optimizing the mixture composition and balancing filling ability and segregation resistance, concrete can

be self-compacting or highly flowable at a relative high fiber content. The fibers are not only carried but also transported in flowable concrete. The production circumstances can affect the orientation of fibers and the structural performance [7]. The potential of tailor-made concrete was demonstrated with recent developments like Engineered Cementitious Composites (ECC) and UHPFRC. Both concrete types can be self-compacting at high fiber contents (2-2.5 Vol.-%). Figure 2 compares different concrete types concerning the compressive strength and the fiber content. A relatively large area is not yet covered by standards and practical experience is lacking.

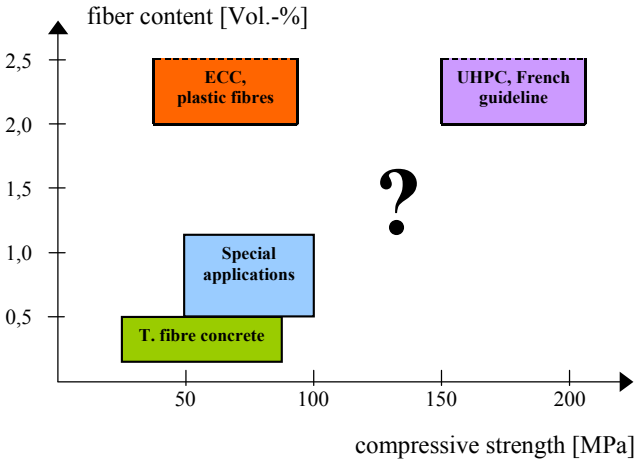

Figure 2. Common range of different concrete types concerning compressive strength and fiber content.

The application of optimized fiber-reinforced concrete might be an economic alternative for either typical SCC- or FRC-applications. Examples of applications with self-compacting fiber-reinforced concrete are slabs on grade, overlays, prefabricated prestressed beams, roof elements, sheet piles, tunnel segments, thin walls and façade panels. Without conventional reinforcement (rebars) any structural shape can be produced. The minimum thickness of elements without rebars is no longer determined by the concrete cover. Additional benefits are savings in mass, and the reduction of storage and transport volumes. The overall economic efficiency (time- and cost-effectiveness) of the construction process can be improved with flowable concrete. Due to the special characteristics of flowable FRC new fields of application can be explored.

Design recommendations for flowable concretes

Numerous publications and conferences reflect the research efforts in the field of high-performance concrete during the past two decades. “High” performance has been achieved concerning i.e. durability, increased fracture toughness, improved deflection and strain hardening behavior, better flowability (even self-leveling behavior) and very high compressive and bond strengths. The research activities established trust in new materials. Concrete can be optimized to obtain a specific, tailor-made structural performance and as a consequence, new products or structures can be developed. Several commissions act worldwide to establish design recommendations for high-performance concrete. fib TG 8.8 will provide an overview of material characteristics including the influence of production and how this can be translated in structural design guidelines. Examples of recent standards and ongoing commissions for flowable concrete are:

Self-compacting concrete

- European Standards (additional rules: FprEN 206-9 [8]; test methods: FprEN 12350 parts 8-12 [9])
- RILEM TC MPS: Mechanical Properties of Self-Compacting Concrete

Fiber-reinforced concrete

- fib Task Group 8.3: Fiber-reinforced concrete
- Fiber-SCC: Concept for a Norwegian guideline [10]
- ECC-recommendation, Japan [11]
- RILEM TC 208-HFC: High Performance Fiber-Reinforced Cementitious Comp.

UHPC-recommendations

- AFGC UHPFRC-recommendation, France [12]
- UHPFRC-recommendation, Japan [13]
- fib Task Group 8.6: Ultra-High Performance Fiber-Reinforced Concrete

fib TG 8.3 is preparing a design recommendation for FRC and fib TG 8.6 aims at completing in 2010 a design recommendation for UHPFRC. Important aspects of both recommendations will be included in the new Model Code, like the effect of the dispersion and the orientation of the fibers and a description of how material tests should be carried out. The material characteristics, the shape of an element and the applied production technique also determine the performance of a structure. The orientation of the fibers, which is affected by the flowability and the casting process, can be taken into account by testing specimens cut from a full-scale sample in different directions and positions.

Characterization of Flowable Concretes

Characteristics in the fresh state

Flowable concrete, in comparison to conventional vibrated concrete, is characterized by a thicker paste layer around the aggregates that minimizes the friction of the grains and allows obtaining a low yield value that promotes the flow. For low strength classes, the relative water dosage (water to powder volume) of vibrated concrete usually is higher compared to flowable concrete at an equivalent strength. However, at a lower paste content and with a higher number of contact points connecting the aggregates, the flowability of vibrated concrete is lower. Vibrated high-strength concrete already can have high flowability due to high cement content and increased paste content. Midorikawa et al. [14] varied the grading and the content of sand in mortar (ratio s/m). The water to powder volume ratio (V_w/V_p) and the superplasticizer content (superplasticizer/powder by mass; SP/P) were adjusted until a flow diameter of 245+/-10 mm and a flow time of 10+/-1 s were obtained. The cone and the mortar funnel are described by Okamura et al. [15]. Figures 3 and 4 show the increase of the dosages of water and superplasticizer at increasing sand content (sands: Ar, Br and Cr), respectively.

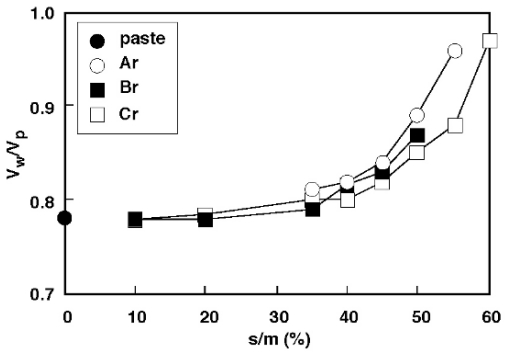

Figure 3. Relationship between the fine aggregate volume and the water to powder volume ratio (V_w/V_p) [14].

A higher flowability of concrete can be obtained by adjusting the rheology of the paste and the content of paste in concrete [16]. Once a certain paste content is exceeded (at a fixed composition of the paste), the flowability does not increase anymore since the flow behavior is already determined by the paste. Table I lists mixture compositions of a traditionally vibrated concrete (TC: C55/67) [17], 2 SCC's (at a low and a high powder content) [18, 19], an ECC (with polyvinyl-alcohol fibers: P) [20] and a UHPFRC-mixture (with steel fibers: S) [21]. Mixture TC was designed for a slump higher than 15 cm.

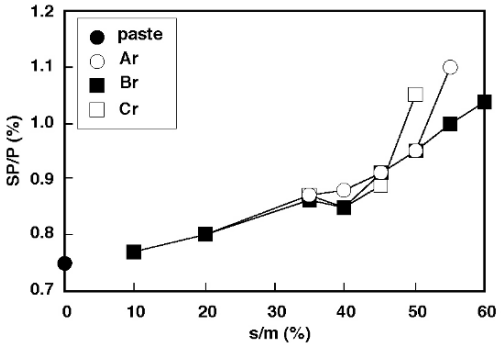

Figure 4. Relationship between the fine aggregate volume and the superplasticizer content (SP/P) [14].

Table I. Mixture composition of five flowable concretes.

Mixture component	**TC** [17] [kg/m^3]	**SCC 1** [18] [kg/m^3]	**SCC 2** [19] [kg/m^3]	**ECC** [20] [kg/m^3]	**UHPC** [21] [kg/m^3]
CEM III/B 42.5 N	300	-	-	-	-
CEM I 52.5 R/CEM I 52.5 N	100	-	360	-	-
Silica fume	-	-	-	-	169
Cement	-	232	-	583	1114
Fly ash	-	-	-	700	-
Limestone filler	-	84	240	-	-
Water	159	186	165	298	209
Viscosity-Modifying Agent	-	1.3	-	-	-
Plasticizer/superplasticizer	6.4	1.3	3.6	15	40
Sand 0/0.25	-	-	-	467	-
Sand 0/2	-	117	-	-	-
Sand 0/4	830	-	-	-	-
Sand 0/5 or 0/6	-	-	853	-	1072
Sand 0/8	-	1160	-	-	-
Gravel 2/8	-	-	263	-	-
Gravel 4/16	975	-	-	-	-
Gravel 8/16	-	543	434	-	-
Fibers	-	-	-	26 (P)	234 (S)
Powders	400	316	600	1283	1283
Aggregates	1805	1820	1550	467	1072
w/b (excl. water in plasticizer)	0.40	0.59	0.28	0.23	0.16

During compaction, flow into place, or after casting, solid particles/components may segregate or float. Examples of inhomogeneities are the sinking of steel fibers towards the bottom of the mould, the alignment of fibers in the direction of compaction, the segregation/floating of powder and color particles. Five aspects contribute to the stability of flowable concrete: a high yield value, a high plastic

viscosity, thixotropy, the supporting lattice effect and a reduced ability of liquid/slurry migration in the shearing zone [22]. The homogeneity of flowable concrete also depends on the duration and the energy of compaction and the passing ability. Vibrated concrete usually has a better air stability, which is besides filling the mould an important reason to compact the concrete. A major risk involved in the application of flowable concrete is whether the concrete remains within the range of specified rheological characteristics; the characteristics in the fresh state have to be as constant as possible throughout the production. Since the characteristics of the mixture components, the aggregate moisture content and other boundary conditions fluctuate or change to some degree, flowable concrete has to be optimized and designed with sufficient robustness (the ability to compensate deviations) [23]. A surprising variety of types of SCC has been applied worldwide due to different traditions in countries to produce concrete and the availability and the price of the mixture components.

Characteristics in the hardened state

Differences in the mixture composition explain different characteristics in the hardened state compared to vibrated concrete. Domone [24] summarized details of the production of 68 SCC-structures and considers SCC a "family of mixtures", that varies in wide range of properties, component materials and mixture proportions. An air-entraining agent was applied in 30 case-studies and a viscosity-modifying agent in 34 cases. In case the robustness (slump flow change with more or less water) of SCC was investigated, mixtures with a viscosity-modifying agent were more robust. The powder content was in the range of 425-625 kg/m^3; mixtures with a viscosity-modifying agent contained in average 30 kg/m^3 less powder. Compared to vibrated concrete, the paste and the powder contents of SCC usually are higher, the volume of coarse aggregate is reduced, the water to powder ratio is lower and the superplasticizer dosage is higher. Domone [25] compared the mechanical characteristics of SCC and vibrated concrete at a comparable compressive strength. Table II shows his findings and adds (sometimes in contradiction) conclusions of other studies [1, 17, 26].

The addition of fibers affects the workability of concrete; the maximum size, the distribution, the content and the shape of the aggregates have to be considered to optimize the workability [27] and the maximum fiber content [28]. The possibility of orienting the fibers along the flow direction of fresh concrete has been also clearly demonstrated. In order to fully benefit the structural performance, the casting process must be designed to consider the flow direction, along which fibers may be aligned, to match as close as possible with the direction of the principal tensile stress in the specimen/structure or to counteract the orientation of fibers.

Concerning engineering properties, SCC and vibrated concrete are often applied without taking differences into account. fib TG 8.8 aims at describing and clarifying reasons for differences, which enable designers to tailor-made flowable

concrete, paying due consideration to the influence of processing (i.e. casting, flow, finishing) on the material and structural performance as well as addressing the needs for suitably adapted production and quality control methods.

Table II. Characteristics of SCC in the hardened state compared to vibrated concrete (+: higher; -: lower).

Reference	Domone [25]	Book SCC [1]	Den Uijl [17]	DAfStb [26]
Mechanical characteristics				
Tensile strength	+/-	+	+	+
Elastic modulus	-	-	+/-	-
Variation in situ-strength	+/-	-	no conclusion	-
Variation of surface strength	no conclusion	-	no conclusion	no conclusion
Time-dependent deformation				
Drying shrinkage	no conclusion	+/-	+	+
Creep	no conclusion	+/-	-	+
Bond				
Shear strength	+/-	+/-	no conclusion	no conclusion
Bond with reinforcement	+/-	+/-	+/-	+/-
Shear on surfaces	no conclusion	no conclusion	+/-	no conclusion
Bond strands	+/-	+/-	+/-	no conclusion
Anchorage length strands	+/-	+/-	-	no conclusion
Structural performance				
Beam: load capacity	+/-	no conclusion	no conclusion	no conclusion
Beam: deflection/strain	+	no conclusion	no conclusion	no conclusion

Conclusions

This paper describes the scope of fib TG 8.8 “Structural Design with Flowable Concrete”. Flowable concrete is a tailor-made, high-performance material. The transfer of knowledge and the completion of design recommendations are essential steps to exploit its full potential. The application of flowable concrete requires taking into account material properties, production effects and structural boundaries on the flow and during hardening. Design recommendations for flowable concrete can level the ground and pave the way for innovations.

References

[1] De Schutter, G., Bartos, P.J.M., Domone, P. and Gibbs, J. (2008), Self-Compacting Concrete, Whittles Publishing, Scotland.

[2] Wallevik, O.H. and Nielsson, I. (1999), Self-Compacting Concrete – A rheological approach, Proc. of the Int. Workshop on SCC, Kochi, Ozawa, K. and Ouchi, M. (Eds), JSCE, pp. 136-159.

[3] Ferrara, L. (2009), Statistical properties of steam-cured plant-produced SCC for prestressed precast applications, Proc. 2nd Int. Symp. on Design, Performance and Use of SCC, Beijing, C. Shi et al. (Eds.), pp. 483-494.
[4] RILEM TC205-DSC (2007), State-of-the-Art report: Durability of Self-Compacting Concrete, De Schutter, G. and Audenaert, K. (Eds.).
[5] Cussigh, F. (2007), SCC in practice: opportunities and bottlenecks, Proc. 5th Int. RILEM Symp. on SCC, Ghent, De Schutter, G. and Boel, V. (Eds.), pp. 21-28.
[6] Desmyter, J.R. (2007), Barriers to the application of cast-in-place SCC, Proc. 5th Int. RILEM Symp. on SCC, Ghent, De Schutter G. and Boel, V. (Eds.), pp. 373-378.
[7] Ferrara, L., di Prisco, M. and Khurana, R.S. (2008), Tailoring optimum performance for structural use of self consolidating SFRC, Proc. Befib 2008, 7th Int. RILEM Symp. on FRC, Chennai, R. Gettu (Ed.), pp. 739-750.
[8] CEN, European committee for standardization (2009), Fpr 206-9: Concrete – Part 9: Additional rules for self-compacting concrete (SCC).
[9] CEN, European committee for standardization (2009), FprEN 12350, Testing fresh concrete: Slump flow test (part 8), V-funnel test (part 9), L box test (part 10), Sieve segregation test (part 11), J-ring test (part 12).
[10] Thorenfeldt E.V. et al. (2006), Steel Fibre Reinforcement in Concrete, Guidelines for Design, Execution and Control, Sintef, Trondheim, Norway (in Norwegian).
[11] Japanese Society of Civil Engineers (2008), Recommendations for Design and Construction of High Performance Fiber Reinforced Cement Composites with multiple fine cracks, www.jsce.or.jp/committee/concrete/e/hpfrcc_JSCE.pdf.
[12] AFGC (2002), Ultra-High Performance Fibre-Reinforced Concretes, Interim Recommendations.
[13] Japan Society for Civil Engineers (2006), Recommendation for Design and Construction of Ultra High Strength Fiber Reinforced Concrete Structures (Draft).
[14] Midorikawa, T., Pelova, G.I. and Walraven, J.C. (2001), Application of "The Water Layer Model" to self-compacting mortar with different size distribution of fine aggregate, Proc. 2nd Int. Symp. on SCC, Tokyo, Ozawa, K. and Ouchi, M. (Eds.), COMS Engineering Corporation, pp. 237-247.
[15] Okamura, H., Maekawa, K. and Ozawa, K. (1993), High Performance Concrete, Gihodo Publishing (in Japanese).
[16] Bui, V.K., Akkaya, J. and Shah, S.P. (2002), Rheological model for self-consolidating concrete, *ACI Materials Journal*, vol. 99, no. 6, pp. 549-559.
[17] Den Uijl, J. (2002), Background Report: CUR-Recommendation – Self-compacting concrete, CUR Gouda (in Dutch).
[18] Müller, F.V. and Wallevik, O.H. (2008), Benefits of filler material on rheology in Eco-SCC, Proceedings of the 3rd North American Conference on the Design and Use of SCC, to be published.

[19] Desnerck, P., Taerwe, L. and De Schutter, G. (2007), Experimental determination of bond strength of reinforcing bars in SCC, Proc. of the 5th Int. RILEM Symp. on SCC, Ghent, De Schutter, G. and Boel, V. (Eds.), pp. 659-664.

[20] Wang, S. and Li, V.C. (2006), High-early-strength engineered cementitious composites, *ACI Materials Journal*, vol. 103, n. 2, pp. 97-105.

[21] Hajar, Z., Lecointre, D., Simon, A. and Petitjean, J. (2004), Design and construction of the world first Ultra-High Performance Concrete road bridges, 1st Int. Symposium on UHPC, Kassel, Schmidt, M. et al. (Eds.), pp. 39-48.

[22] Wallevik, O.H. (2003), Rheology – A scientific approach to develop self-compacting concrete, Proc. 3rd Int. Symp. on SCC, Reykjavik, Wallevik, O.H. and Níelson, I., (Eds.), pp. 23-34.

[23] Rigueira, J.W., García-Taengua, E. and Serna-Ros, P. (2009), Self-consolidating concrete robustness in continuous production regarding fresh and hardened state properties, *ACI Materials Journal*, vol. 106, n. 3, pp. 301-307.

[24] Domone, P.L. (2006), Self-compacting concrete, An analysis of 11 years of case-studies, *Cement & Concrete Composites*, vol. 28, pp. 197-208.

[25] Domone, P.L. (2007), A review of the hardened mechanical properties of self-compacting concrete, *Cement & Concrete Composites*, vol. 29, pp. 1-12.

[26] DAfStb - Deutscher Ausschuss für Stahlbeton (2001), State-of-the-art Report Self-Compacting Concrete, Reinhardt, H.W. et al. (Eds.), Heft 516, Beuth Verlag (in German).

[27] Ferrara, L., Park, Y.D. and Shah, S.P. (2007), A method for mix-design of fiber reinforced self compacting concrete, *Cement and Concrete Research*, vol. 37, pp. 957-971.

[28] Grünewald, S. (2004), Performance-based design of self-compacting fibre reinforced concrete, PhD Thesis, Concrete Structures Group, TU Delft, Delft University Press.

Effect of Material Constituents and Mix Design on Performance of SCC for Precast, Prestressed Girders

Guillaume Lemieux[1], Soo-Duck Hwang[2] and Kamal H. Khayat[2]

[1] The Euclid Chemical Company, Canada
[2] Université de Sherbrooke, Canada

Abstract. An extensive investigation was undertaken to evaluate the influence of binder type, water-to-cementitious materials ratio (*w/cm*), type of coarse aggregate, and maximum size of aggregate (MSA) on workability and strength development of self-consolidating concrete (SCC) designated for precast, prestressed bridge girders. In total, 30 SCC mixtures were investigated. In total, 24 mixtures were non air-entrained and were prepared using crushed aggregate or gravel with three MSA of 10, 14, and 20 mm. The *w/cm* was set to a relatively low value of 0.33 and a higher value of 0.38. Three different binder compositions were investigated. The effect of slump flow consistency on performance was also investigated. Test results indicate that SCC made with the higher *w/cm* exhibited superior fluidity retention, passing ability, and filling capacity. Mixtures proportioned with the lower *w/cm* developed greater stability. Mixtures made with the crushed aggregate of 10 mm MSA exhibited greater passing ability, higher filling capacity, and better retention of air content than similar SCC prepared with 14 and 20 mm MSA. Mixtures proportioned with the gravel had superior passing ability, filling capacity and similar stability compared to those made with crushed aggregate of the same MSA.

Introduction

The use of self-consolidating concrete (SCC) for the manufacturing of precast, prestressed elements provides the benefits of increased rate of production, improved safety, reduced labour need and lower noise levels at manufacturing plants. Guidelines for selection of mixture parameters and mixture optimization of SCC are critical for the implementation of such technology. Compared to conventional vibrated concrete, there are a number of factors that should be taken into consideration to a greater degree when designing SCC. This includes the type and shape of coarse aggregate, type of cement and supplementary cementitious

K.H. Khayat and D. Feys (eds.), *Design, Production and Placement of Self-Consolidating Concrete*, RILEM Bookseries 1,
DOI 10.1007/978-90-481-9664-7_3, © RILEM 2010

materials, and *w/cm*. The selection of material constituents and mixture proportioning for precast, prestressed applications should be diligently selected to achieve required workability, surface finish characteristics, early-age strength, design strength, as well as durability.

The design of precast, prestressed concrete members is typically 35 to 41 MPa. This is easily achieved with low *w/cm* SCC that usually develops 28-day compressive strengths greater than 55 MPa. Concrete for precast, prestressed girder elements typically need to achieve a minimum release compressive strength of 28 MPa within 18 hours as per AASHTO LRFD Bridge Design Specifications 1998 [1]. This study was undertaken to evaluate the influence of binder type, *w/cm*, coarse aggregate type and nominal aggregate size on key workability characteristics and compressive strength development of SCC designated for the construction of precast, prestressed bridge girders.

Experimental Program

Testing program

A parametric study was undertaken to evaluate the influence of key mixture parameters and material properties on workability and compressive strength development of SCC designated for precast, prestressed girders. As presented in Table I, 24 non air-entrained SCC mixtures (No. 1 to 24) were prepared to evaluate workability, stability, and strength development characteristics. The mixtures were prepared using either crushed aggregate or gravel with maximum size aggregate (MSA) of 10, 14, or 20 mm, *w/cm* of 0.33 and 0.38, and three different binder compositions: Type MS cement (similar to ASTM Type I/II) as well as Type HE cement (similar to ASTM Type III) with either 30% slag or 20% Class F fly ash replacement. Three SCC mixtures (No. 25 to 27), similar to mixtures No. 1 to 3, having relatively low slump flow of 600 to 640 mm and three other mixtures (No. 28 to 30) similar to mixtures No. 4 to 6 with high slump flow values of 710 to 760 mm were prepared. These mixtures (No. 25 to 30) were used to evaluate the effect of fluidity level on workability and strength development. Testing program details are given in Table II.

Several 100 x 200 mm cylinders were sampled within 10 minutes after cement and water contact to determine compressive strength and modulus of elasticity. The cylinders were cast in one lift without any mechanical consolidation. The cylinders were cured under three different curing conditions, as summarized in Table III. In some cases, the curing regime was modified to achieve the targeted release compressive strength of 35 MPa at 18 hours.

Table I. Experimental program.

Mixture #	Aggregate type and MSA				Type and content of binder			*w/cm*	
	Crushed 20 mm	Crushed 10 mm	Crushed 14 mm	Gravel 14 mm	Type MS 480 kg/m^3	Type HE + 30% Slag 460 kg/m^3	Type HE + 20% fly ash 460 kg/m^3	0.33	0.38
1	x				x			x	
2	x					x		x	
3	x						x	x	
4	x				x				x
5	x					x			x
6	x						x		x
7		x			x			x	
8		x				x		x	
9		x					x	x	
10		x			x				x
11		x				x			x
12		x					x		x
13			x		x			x	
14			x			x		x	
15			x				x	x	
16			x		x				x
17			x			x			x
18			x				x		x
19				x	x			x	
20				x		x		x	
21				x			x	x	
22				x	x				x
23				x		x			x
24				x			x		x
25 26 27	• Low filling ability, slump flow of 600-640 mm • *w/cm* of 0.33, Type HE+30% slag, crushed aggregate with MSA of 20 mm								
28 29 30	• High filling ability, slump flow of 710-760 mm • *w/cm* of 0.38, Type HE+30% slag, crushed aggregate with MSA of 20 mm								

Table II. Testing program.

Property	Test method		Test age
Filling ability	Slump flow and T-50	ASTM C 1611	10 and 40 min
Passing ability	J-Ring	ASTM C 1621	
	L-box	[2]	
Filling capacity	Caisson filling capacity	[3]	
Stability	Surface settlement	[4]	24 hours
	Column segregation	ASTM C 1610	10 min
	Visual stability index	ASTM C 1611	10 and 40 min
	Stability of air	ASTM C 231	Over 40 min
Mechanical properties	Compressive strength	ASTM C 684	18 hours air and steam curing 28 and 56 days moist curing
	Modulus of elasticity	ASTM C 469	18 hours steam curing

Table III. Concrete curing condition in this investigation.

Curing methods	Stages	Details
Steam curing	I	Ambient temperature for 2 hours after water-cement contact
	II	Temperature raised for 2 hours
	III	Concrete temperature maintained for 10 hours
	IV	Temperature decreases over 2 hours to ambient temperature
	V	Air curing until age of testing at 18 hours
Moist curing	I	18 hours in molds with wet burlap at 23 ± 2°C
	II	Moist-cured at 23 ± 2°C until testing age
Air curing	I	18 hours in molds with wet burlap at 23 ± 2°C
	II	Air-dried at 23 ± 2°C until testing age

Material properties

The grain-size distributions of three types of crushed aggregates with MSA of 10 mm, 14 mm, 20 mm, and gravel with MSA of 14 mm conforming to AASHTO T 27 and river-bed sand conforming to AASHTO T 27 are summarized in Table IV. The particle-size distributions are within the AASHTO recommended maximum and minimum limits.

Table IV. Grain-size distribution and properties of coarse aggregate and sand.

Sieve opening	Sand	Crushed aggregate			Gravel
	0 to 5 mm	20 mm MSA	14 mm MSA	10 mm MSA	14 mm MSA
25 mm	100	100	100	100	100
20 mm	100	99	100	100	100
14 mm	100	68	95	100	99
10 mm	100	40	69	100	94
5 mm	98	7	18	13	32
2.5 mm	85	1	4	2	1
1.25 mm	72	1	3	2	-
630 µm	55	-	-	-	-
315 µm	32	-	-	-	-
160 µm	9	-	-	-	-
Pan	2	0	0	0	0
Specific gravity	2.66	2.72	2.71	2.73	2.66
Absorption, %	1.12	0.31	0.44	0.38	1.26

Chemical and physical properties of cements and supplementary cementitious materials used throughout the project are shown in Table V. The specific gravity values of Type MS, Type HE, fly ash, and blast-furnace slag are 3.14, 3.15, 2.53, and 2.95, respectively, and the Blaine fineness values are 390, 530, 410, and 400 m^2/kg, respectively. The aggregate and supplementary cementitious materials employed in this investigation are widely used in North America. The high-range water-reducing admixture (HRWRA) is a polycarboxylate ether-based admixture

with a moderate slump retention capacity. Its density and solid content are 1.05 and 27%, respectively.

Table V. Physical properties and chemical composition of cement, fly ash, and blast-furnace slag.

Cement and supplementary cementitious materials	Type MS cement	Type HE cement	Class F fly ash	Blast-furnace slag
Physical properties				
Specific gravity	3.14	3.15	2.53	2.95
Blaine specific surface area, m^2/kg	390	530	410	400
Passing No. 325 (45 µm), %	91	99	90	92
Chemical composition, %				
SiO_2	21.4	20.0	52.4	36.0
Al_2O_3	4.6	5.4	27.2	10.4
Fe_2O_3	2.9	2.3	8.3	1.5
CaO	63.3	63.5	4.5	42.9
MgO	2.0	1.4	0.96	6.7
SO_3	3.4	4.4	0.05	0.48
K_2O	0.94	1.1	2.33	0.37
Na_2O	0.07	0.15	0.20	0.17
Na_2O eq*	0.69	0.88	1.74	0.41
LOI	0.98	0.80	2.73	0.41
Bogue composition, %				
C_3S	50.0	54.9	-	-
C_2S	23.7	15.8	-	-
C_3A	7.4	10.5	-	-
C_4AF	8.8	6.9	-	-

*Na_2O equivalent = Na_2O + 0.64 K_2O

Tests Results and Discussion

Evaluation scheme

The evaluation of the relative effect of mixture constituents and mix design parameters was carried out by comparing the relative performance of each parameter on the overall performance of the concrete in terms of workability and mechanical properties. These properties are assigned weighting factors to reflect their relative significance on SCC performance (Table VI).

The relative performance of the various workability and mechanical property responses are ranked at three levels, as follows:

- III high performance (3 points)
- II medium performance (2 points)
- I low performance (1 point)

These rankings are based on the relative performance specifications presented in Table VII. The total scores of fresh and hardened properties for each tested mixture parameter are determined to obtain a global evaluation of each parameter. Material constituent and mix design parameter with the highest total scores is ranked as "1", which represents the best performance of the material in terms of fresh and hardened properties. On the other hand, a ranking of "4" is given to the material constituent and mix design parameter that yielded the lowest global performance. The values for global performance scores relative to maximum score in each material constituent and mixture parameter category are taken as 100%, 93% to 99%, 85% to 92%, and less than 85% for rankings of 1, 2, 3, and 4, respectively.

Table VI. Weighing factors for evaluated workability and mechanical properties.

Property (i)	SCC behavior	Weighing factor (WF)	Score obtained
1	HRWRA demand	× 1	(I, II, or III) × 1
2	Slump flow retention over 30 min	× 1	(I, II, or III) × 1
3	Passing ability	× 1	(I, II, or III) × 1
4	Filling capacity	× 2	(I, II, or III) × 2
5	Static stability	× 2	(I, II, or III) × 2
Total fresh properties			$\sum_{i=1}^{5}(I, II, or\ III)_i \times (WF)_i$
6	18-hour compressive strength steam-cured	× 3	(I, II, or III) × 3
7	18-hour compressive strength air-cured	× 1	(I, II, or III) × 1
8	56-day compressive strength moist-cured	× 2	(I, II, or III) × 2
9	18-hour elastic modulus steam-cured	× 2	(I, II, or III) × 2
Total hardened properties			$\sum_{i=6}^{9}(I, II, or\ III)_i \times (WF)_i$
Global performance			$\sum_{i=1}^{9}(I, II, or\ III)_i \times (WF)_i$

Effect of binder type on SCC performance

The binder content and composition are shown to have a direct influence on HRWRA demand, fluidity retention, temperature rise, early-age strength, and mechanical properties at 28 and 56 days. Among the three binder types that were used in the parametric study, mixtures made with Type HE cement and 20% Class F fly ash exhibited better workability compared to similar mixtures prepared with Type MS cement or Type HE cement and 30% slag replacement. SCC made with Type HE cement and 20% fly ash had a total score of 18 compared to 16 and 15 for SCC with Type MS and Type HE cement and 30% slag, respectively. As illustrated in Table VIII, the SCC mixtures with 20% Class F fly ash developed

high levels of fluidity retention, passing ability, filling capacity, and static stability. SCC proportioned with Type HE cement and 30% slag exhibited relatively low passing ability and spread between slump flow and J-Ring flow greater than 100 mm.

Table VII. Relative performance of SCC for precast, prestressed applications.

		Relative performance level		
		Low	Medium	High
Filling ability	Slump flow	600 - 640 mm	640 - 700 mm	700 - 735 mm
Fluidity retention	Slump flow at 10 min – slump flow at 40 min	≥ 65 mm	25 - 65 mm	≤ 25 mm
Passing ability	L-box blocking ratio (h_2/h_1)	0.5 - 0.6	0.6 - 0.7	≥ 0.7
	Slump flow – J-Ring flow	75 - 100 mm.	50 - 100 mm	≤ 50 mm
Filling capacity	Caisson filling capacity	70% - 75%	75% - 90%	≥ 90%
Air stability	Air volume at 10 min – air volume at 40 min	≥ 1.5%	0.5% - 1.5%	≤ 0.5%
Static stability	Max. surface settlement	≥ 0.5%	0.3% - 0.5%	≤ 0.3%
	Column segregation index	≥ 5%	2% - 5%	≤ 2%
Comp. strength	18-hour compressive strength (air-cured)	≤ 14 MPa	14 - 21 MPa	≥ 21 MPa
	18-hour compressive strength (steam-cured)	≤ 31 MPa	31 - 38 MPa	≥ 38 MPa
	56-day compressive strength (moist-cured)	≤ 55 MPa	55 - 69 MPa	≥ 69 MPa
Modulus of elasticity	18-hour modulus of elasticity (steam-cured)	≤ 28 GPa	28 - 35 GPa	≥ 35 GPa

Table VIII. Effect of binder type on SCC performance.

SCC Behavior	Binder type		
	Type MS	Type HE I 30% Slag	Type HE I 20% FA
HRWRA demand (× 1)	III	II	II
Slump flow retention (× 1)	I	II	III
Passing ability (× 1)	II	I	III
Filling capacity (× 2)	III	II	II
Static stability (× 2)	II	III	III
Total fresh properties	**16**	**15**	**18**
18-hour compressive strength steam-cured (× 3)	II	II	II
18-hour compressive strength air-cured (× 1)	III	II	II
56-day compressive strength (× 2)	II	II	III
18-hour modulus of elasticity (× 2)	II	II	II
Total hardened properties	**17**	**16**	**18**
Global performance	**33**	**31**	**36**
Ranking	**2**	**3**	**1**

Regardless of the binder type, the evaluated mixtures developed similar compressive strengths after 18 hours of steam curing and 56 days of moist curing. Concrete with Type HE cement and 20% fly ash had the highest score for mechanical properties, which is mainly due to its highest 56-day compressive strength. It is important to note that the performance comparison and recommendations presented here are based on the materials tested in this study. Variations in constituent material characteristics can yield different results.

Effect of maximum aggregate size and type on SCC performance

The size and type of coarse aggregate were shown to have a marked effect on the passing ability, filling capacity, and static stability of SCC, as presented in Table IX. The MSA should be selected given the minimum clearance between the reinforcement and clear cover over the reinforcement, as well as the geometry of the cast element. The reduction in MSA can enhance segregation resistance.

Table IX. Effect of aggregate size and type on SCC performance.

SCC Behavior	Aggregate size and type			
	Crushed 20 mm	Crushed 10 mm	Crushed 14 mm	Gravel 14 mm
HRWRA demand (× 1)	III	I	II	II
Slump flow retention (× 1)	NS	NS	NS	NS
Passing ability (× 1)	I	III	II	III
Filling capacity (× 2)	I	III	II	III
Static stability (× 2)	II	III	III	III
Total fresh properties	**10**	**16**	**14**	**17**
18-hour compressive strength steam-cured (× 3)	II	II	III	II
18-hour compressive strength air-cured (× 1)	III	II	II	II
56-day compressive strength (× 2)	II	III	III	I
18-hour modulus of elasticity (× 2)	III	II	II	II
Total hardened properties	**19**	**18**	**21**	**14**
Global Performance	**29**	**34**	**35**	**31**
Ranking	**4**	**1**	**2**	**3**

From a workability point of view, SCC made with crushed aggregate of 10 mm MSA exhibited greater passing ability, spread between slump flow and J-Ring flow diameters lower than 50 mm, and caisson filling capacity higher than 90%. Mixtures made with crushed aggregate of 10 mm MSA had a total score of 16, compared to 14 and 10 for those with crushed aggregate of 14 and 20 mm MSA, respectively. In particular, mixtures containing 20 mm MSA exhibited relatively low filling capacity (caisson filling capacity less than 70%) and relatively low resistance to segregation (column segregation index higher than 5%). SCC made with 10 mm MSA exhibited similar static stability as concrete made with the larger MSA. As in the case of workability, mixtures made with crushed aggregate of 10 mm MSA developed higher or similar compressive strength than those with 14 and

20 mm MSA after 18 hours of steam curing and 56 days of moist curing. In terms of global performance, SCC made with crushed aggregate of 10 or 14 mm MSA exhibited the highest performance, as indicated in Table IX.

SCC made with gravel (14 mm MSA) developed a greater filling capacity than concrete with crushed aggregate of 14 mm MSA. The former had a high level of passing ability (h_2/h_1 greater than 0.7 and spread between slump flow and J-Ring flow less than 50 mm) as well as high filling capacity (caisson filling capacity greater than 90%). Both SCC types exhibited similar segregation resistance (medium level: column segregation index of 2% to 5%). Mixtures made with gravel developed lower compressive strength and modulus of elasticity than similar concrete prepared with crushed aggregate of the same MSA. In terms of global performance, SCC with crushed aggregate offered better performance than those made with gravel (overall score of 35 versus 31).

Effect of w/cm and fluidity level on SCC performance

As presented in Table X, SCC mixtures proportioned with 0.38 *w/cm* had better workability characteristics than those with 0.33 *w/cm*. The former exhibited superior fluidity retention, passing ability, and filling capacity than SCC prepared with 0.33 *w/cm*. On the other hand, SCC proportioned with 0.33 *w/cm* developed greater static stability and higher 18-hour steam-cured compressive strengths as well as 56-day strength. Air-cured SCC made with 0.33 *w/cm* exhibited lower 18-hour compressive strength than air-cured concrete of 0.38 *w/cm* due to the higher HRWRA required to achieve the target slump flow of the former concrete. No significant difference was found in the modulus of elasticity determined at 18 hours between SCC made with 0.33 or 0.38 *w/cm*.

Table X. Effect of *w/cm* and fluidity level on SCC performance.

SCC Behavior	*w/cm*		Fluidity level		
	0.33	0.38	Low	Medium	High
HRWRA demand (× 1)	II	III	NA	NA	NA
Slump flow retention (× 1)	II	III	III	III	I
Passing ability (× 1)	II	III	I	II	III
Filling capacity (× 2)	II	III	I	II	III
Static stability (× 2)	III	II	III	II	I
Total fresh properties	**16**	**19**	**12**	**13**	**12**
18-hour compressive strength steam-cured (× 3)	III	II	III	III	II
18-hour compressive strength air-cured (× 1)	II	III	III	III	II
56-day compressive strength (× 2)	III	II	III	III	II
18-hour modulus of elasticity (× 2)	III	III	III	III	II
Total hardened properties	**23**	**19**	**24**	**24**	**16**
Global performance	**39**	**38**	**36**	**37**	**28**
Ranking	**I**	**I**	**II**	**I**	**IV**

SCC with 0.38 *w/cm* can be successfully used to secure a minimum release compressive strength of 35 MPa and 56-day design strength of 55 MPa. Such concrete can be used for casting highly reinforced and restricted structural elements given its excellent passing ability and filling capacity. Higher release and design strengths may necessitate the use of SCC with lower *w/cm*.

Workability responses and mechanical properties of SCC designed for relatively high, medium, and low slump flow values of 700 to 735 mm, 640 to 700 mm, and 600 to 640 mm, respectively, are compared in Table X. Mixtures with low and medium slump flow values exhibited similar levels of passing ability (medium), filling capacity (medium), and resistance to surface settlement (high). Mixtures with high fluidity (slump flow) exhibited high passing ability and filling capacity, but relatively medium to low static stability. SCC of high slump flow had slightly lower overall workability score of 12 than that with medium fluidity (13). Concrete with high fluidity developed lower compressive strength at 18 hours of steam curing and 56 days of moist curing in addition to lower 18-hour modulus of elasticity than SCC with low slump flow. In general, SCC mixtures of medium fluidity developed the best overall performance for casting highly reinforced precast, prestressed girders.

Conclusions

Based on the results presented in this paper, the following conclusions can be made:

- The use of crushed coarse aggregate with MSA of 14 mm, *w/cm* of 0.38, and Type HE cement with 20% Class F fly ash provide good overall performance in terms of overall workability;
- The HRWRA demand can be reduced by the use of MSA 20 mm crushed aggregate, *w/cm* of 0.38, and Type MS cement;
- The use of crushed aggregate with MSA of 14 mm, *w/cm* of 0.33, and Type HE cement with 20% Class F Fly ash can lead to greater mechanical properties; and
- If the precast/prestressed concrete girder does not present high level of congestions of reinforcement, SCC with relatively low to medium slump flow values of 620 ± 20 mm and 670 ± 30 mm, respectively, can be sufficient to assure adequate filling of the formwork.

Acknowledgements

This work was sponsored by the American Association of State Highway and Transportation Officials and was conducted in the National Cooperative Highway Research Program, which is administered by the Transportation Research Board of

the National Research Council. This project was performed under NCHRP Project 18-12 [5]. The help and support of Dr. Hoi-Keun Lee and Dr. Wu Jian Long is especially acknowledged.

References

[1] AASHTO (1998), AASHTO LRFD bridge design specification, 2nd edition. American Association of State Highway and Transportation Officials, Washington D.C.

[2] Petersson. O. et al. (1996), A model for self-compacting concrete. Proceeding of International RILEM Conference on Production Methods and Workability of Concrete, Paisley, pp. 489-490.

[3] Yurugi, M. et al. (1993), Mix proportion of highly workable concrete, Proceeding of Concrete 2000, Dundee, Scotland, pp. 579-589.

[4] Khayat, K.H. (1999), Workability, testing, and performance of self-consolidating concrete, *ACI Materials Journal*, vol. 96, n. 3, pp. 346-353.

[5] Khayat, K.H. and Mitchell, D. (2008), National Cooperative Highway Research Program (NCHRP) 18-12 Project, Self-consolidating concrete for precast, prestressed concrete bridge elements. Final report.

Robustness by Mix Design – A New Approach for Mixture Proportioning of SCC

Peter Ramge[1] and Ludger Lohaus[2]

[1] Berlin, Germany
[2] Institute of Building Material Science, Leibniz University Hanover, Germany

Abstract. Robustness is the ability of a concrete mixture to satisfy its defined requirement profile despite any unfavorable influences, they may be predictable or unpredictable. The objective of this study is to investigate ways to increase the robustness of SCC by means of specific mixture proportioning, especially in the fine grain and powder range. The Superplasticizer Based Approach and the characteristic boundary consistency curves are tools whereby the general robustness of grain compositions can be estimated. Furthermore the Superplasticizer based Water Demand is proven to be a useful tool to characterize grain compositions concerning their packing density, which in turn is an important information to ensure the necessary surplus of fines in the overall mixture proportioning. By several examples it is demonstrated how little changes in the powder composition can cause major changes in concrete properties and how such influences can be determined effectively.

Introduction

Robustness in SCC primarily stands for the stability against segregation and bleeding, but also implies the ability to maintain the workability properties despite any unfavorable conditions or changes. This can be changes in the characteristic properties of the raw materials as well as changes in the ambient conditions, like temperature or mixing process. As those influences cannot be eliminated a priori, the aim must be to minimize their impact on the change of the concrete properties. Therefore one possible approach is the use of a distinct mixture proportioning. Thereby the proportioning of a robust mixture may well differ from one of a mixture that was optimized regarding a specific aspect. The fresh concrete properties of SCC are strongly influenced by the actual packing state of the solids. The packing state of the powder components is however influenced by the dispersing effect of the superplasticizers (SP). Therefore the effects of SP have to

K.H. Khayat and D. Feys (eds.), *Design, Production and Placement of Self-Consolidating Concrete*, RILEM Bookseries 1,
DOI 10.1007/978-90-481-9664-7_4, © RILEM 2010

be included directly in the determination of the parameters needed for the development of robust self-compacting concretes and mortars. According to the mix design of Okamura [1] the development of a SCC starts with the paste, followed by the adjustment of the mortar. Only once the mortar provides sufficient performance the next step is taken. Perhaps not all properties observed on paste and mortar have significant influence on the concrete, but nevertheless proper performance of paste and mortar is a precondition for proper SCC performance. Therefore, the robustness of paste and mortar is dealt with in this paper.

The Superplastisizer Based Approach

Water demand / characteristic consistency

In general the water demand of any granular mixture is dependent on the specific surface and the packing density. For coarse aggregates the packing density is the dominant parameter. However in [2] it is confirmed that also for fine powders within the particle size range of cement still the measurable value of the water demand is mainly influenced by the packing density and not by the specific surface.

Amongst the various methods to determine the water demand the most common ones are the β_p-value according to Okamura [1], the water demand at standard consistency according to EN 196-3 [3], and the water demand according to Puntke [2]. These methods were developed for the binary system of granular mixture and water. They do not include the effects of SP. As high performance concretes (SCC in particular) are always produced by using SP it seems to be necessary to include these effects in the determination of the characteristic properties.

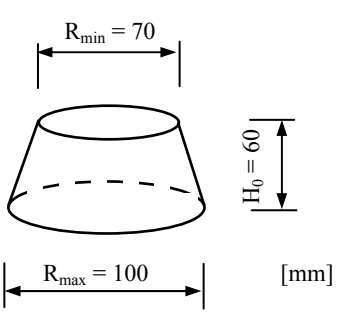

Figure 1. The Haegermann cone as used for the β_p value according to Okamura and the experiments of the Superplasticizer Based Approach.

The Superplasticizer Based Approach [4, 5] describes the attainable consistency of a paste including SP in dependence of the volumetric ratio of the fluid ingredients to the solids. The conception of the model is illustrated in Figure 2. Similar to Okamura, the experimental measurements to determine the consistency are carried out with the Haegermann cone according to [6]. The dimensions of this cone are depicted in Figure 1. For each granular mixture a certain consolidation point (C-point) exists when just enough water is present to fill all the voids but no additional water to enable flowing of the paste or mortar. For mixtures without SP this point corresponds with the β_p -value according to Okamura, which is expressed as the volumetric water / powder (V_w/V_p-value) or more general as the fluid / solid (V_f/V_s-value), including also the coarser particles like sand if present. For mixtures without SP the slump flow increases almost linearly for increasing V_f/V_s-values above the C-point.

Already low contents of PCE-based SP cause a significant increase in the slump flow in comparison to a mixture without SP, whereas the C-point is dropped significantly. Increasing the SP dosage, the consistency can be increased to a specific maximum value (boundary consistency) for each V_f/V_s. At that point the so called saturation limit is reached [7]. Now the paste shows almost no yield stress, so that an additional SP dosage cannot lower the yield stress any further, therefore no wider slump flow can be observed. The maximum consistency decreases at low V_f/V_s until the C-point is reached. Following the characteristic boundary consistency curve, with increasing V_f/V_s, the so called segregation point (S-point) is reached. In the illustration this point appears as a bending point. In some cases it is a sharp bend, in other cases it might be a wider transition zone. In [8] it was proven in several experiments by evaluating the density distribution of hardened paste specimens that this bend corresponds with the onset of significant sedimentation. Sedimentation often occurs already at V_f/V_s where visual effects of segregation such as bleeding cannot yet be seen on the fresh mortar specimens. Above the S-point the paste is no longer stable, the solids tend to separate, and therefore a practical application is not reasonable in this range. The behavior changes with lower V_f/V_s below the S-point. In this area it is possible to design concretes with high SP contents, even beyond the saturation limit. These pastes are extremely flowable associated with stability against segregation. At further decrease of the V_f/V_s, the maximum attainable slump flow value decreases. Due to the dispersion and the related reduction of the agglomerates, a very high packing density can be obtained, significantly higher than without superplasticizer. The minimum attainable C-point is called “Superplasticizer-based Water Demand” (SPWD). This characteristic value is significantly lower than the β_p-value according to Okamura. It is likewise lower than the water demand according to Puntke or EN 196-3. Close to this point the maximum attainable consistency is limited by the V_f/V_s. For a given powder mixture the characteristic boundary consistency cannot be exceeded by means of higher SP dosage, only by changing the V_f/V_s.

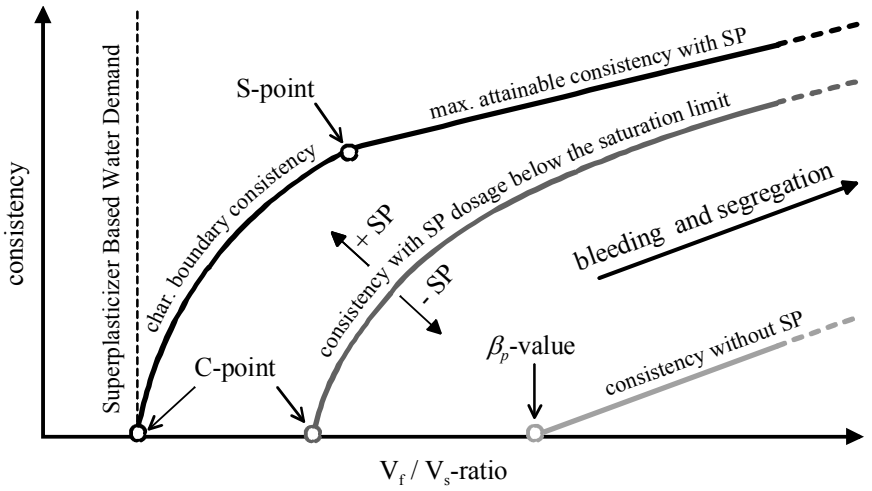

Figure 2. Model of the Superplasticizer Based Approach.

The model is valid for all powders or powder mixtures that would be adequate for the determination of the β_p-value according to Okamura. These are mainly cements and other mineral binders as well as fine inert powders, also in combination with fine grained sand. But as for the β_p-value the experiments do not give satisfying results, if the material is too coarse (e.g. sand only), because the fluid's viscosity is too low to hold up and carry the particles in the suspension.

Figure 3 shows an example for a characteristic curve. In this case, the bend in the curve occurs at a V_f/V_s of about 0.34 to 0.36. From the evaluation of the density distribution of hardened mortar specimens the inset of significant sedimentation could be detected slightly above these values, however during the slump flow experiments no bleeding or other segregation phenomena could be observed visually. In Figure 3 it can be clearly seen that only a very small change in the V_f/V_s (in this case from 0.21 to 0.20) can change the mortar's consistency from a homogeneous paste to a crumbly mixture without cohesion. This "loss of cohesion point" is introduced as L-point. In the given example the L-point and the C-point (where flowing starts) lay close together, but they are not identical. In other cases (depending on the mixture proportioning) they may be identical or lay further apart providing a wider V_f/V_s-range in which a homogeneous cohesive, yet not flowing paste is obtained.

For the determination of the sedimentation the fresh paste or mortar is cast into a test tube. After hardening the balance point is determined. As these specimens provide high l/d, deviations in the density distribution caused by significant sedimentation can be determined reliably despite the existing uncertainties. For

quantitative analyze however this method would need to be specified more precisely but for the qualitative analyze to determine the inset point of sedimentation it is well sufficient.

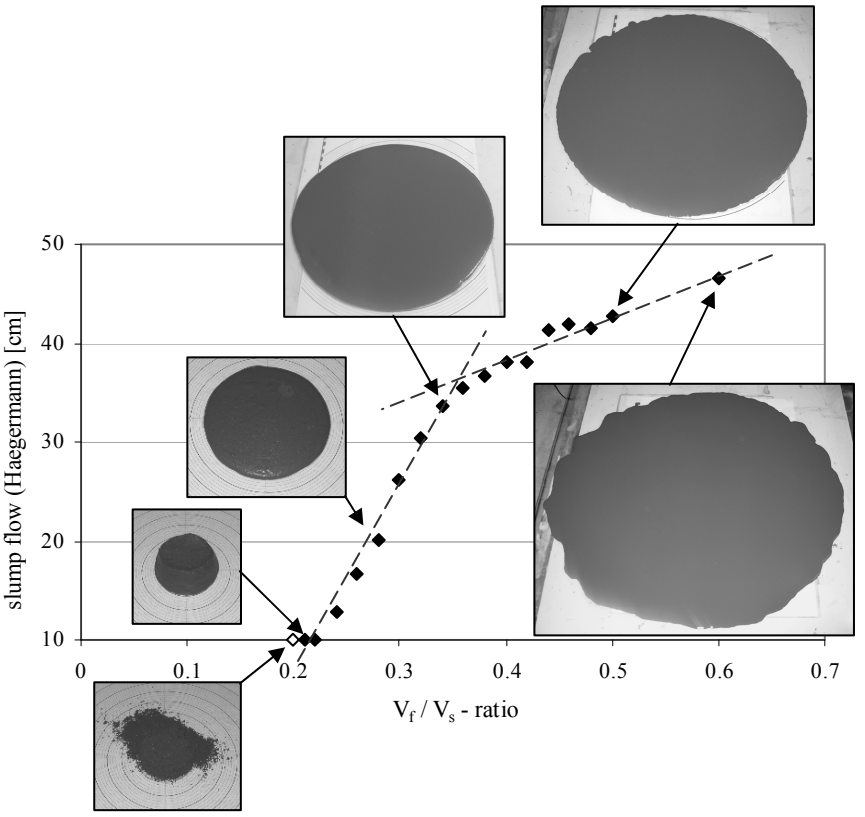

Figure 3. Example of a characteristic boundary curve.

Surplus of fines / precondition for proper flowability

One premise to reduce bleeding and segregation risk in SCC is to avoid unnecessary amounts of free water. However a certain minimum of free water is necessary for the needed flowability and the self-consolidating behavior. Therefore the solid content, especially in the paste, has to be rather high. Choosing a granular lattice with the maximum possible packing density would however not be appropriate for SCC. Theoretically this mixture can flow as soon as more fluid phase is present as needed to fill the voids. But this movement is only possible at a very low speed and can stop easily. In Figure 4a such a mixture is illustrated. (This

is only an illustration of a very simplified 2D-model which does not represent the real 3D-situation but it is well sufficient to visualize the general effect that will also occur in a real 3D granular mixture.) For proper flowing it is necessary that all particles (especially the bigger ones) can freely move relatively to each other. If one of the bigger particles in a packing optimized mixture wants to change its position (Figure 4b) this is only possible by leaving a gap behind it, that has to be filled again with surrounding material (finer particles plus fluid phase).

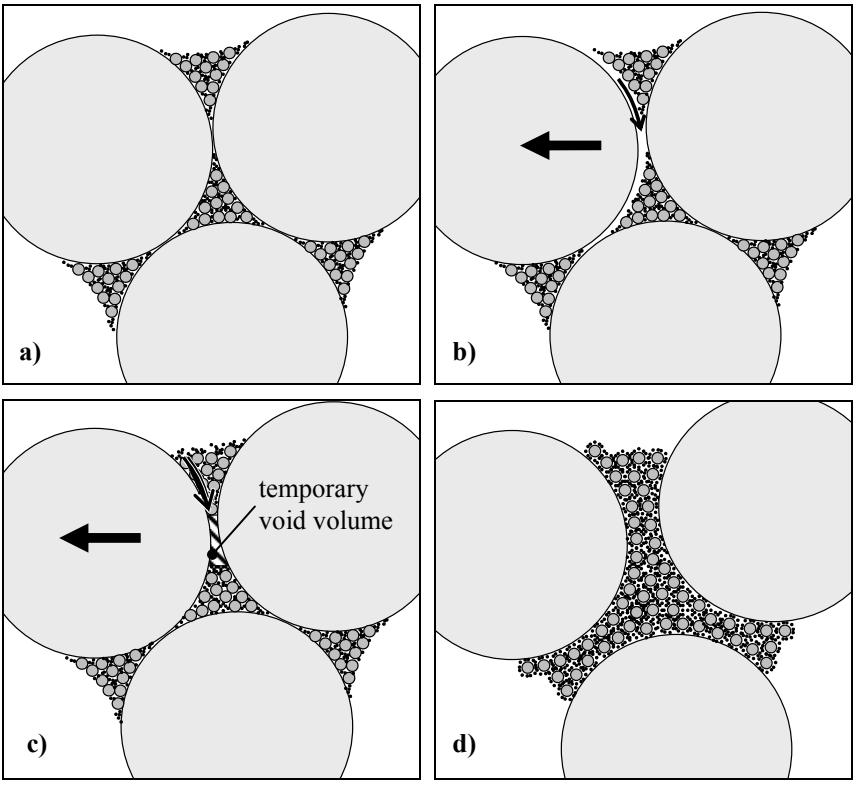

Figure 4. Necessity of a surplus of fines to secure flowability.

In mixes containing lots of fines and ultra fines this can lead to a local blocking situation (Figure 4c). Due to the generally high solid content and the high packing density the effective diameters of the granular pore system are very small so that the fluid phase can move only very slowly. Until the gap between two bigger grains is large enough to be filled with medium sized grains, the temporary void can only be filled with fluid, which drastically limits the velocity of the bigger grains. In general this effect is one of the reasons for shear thickening behavior. In extreme cases it can lead to a total stagnation of the paste or mortar through only a

minor change in the water content or the granular proportions in the mixture. For a robust mixture it is therefore necessary to have a surplus of fines as illustrated in Figure 4d. As long as for each grain size level a dominance of the finer grain is guaranteed by a sufficient surplus of fines also gap graded grain distributions are possible. Continuous grain distributions are however to be preferred for the sake of robustness.

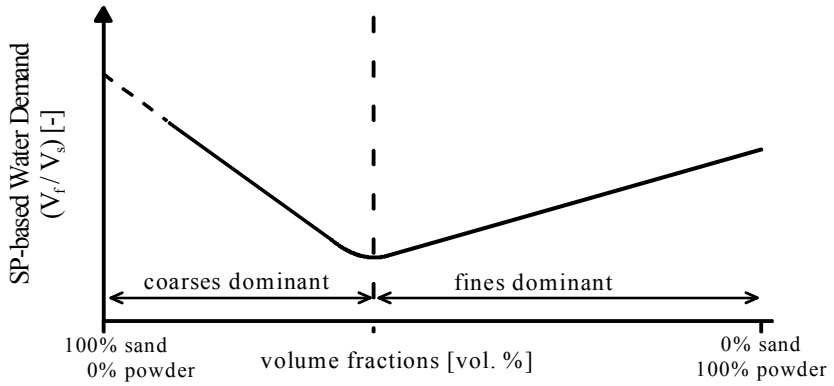

Figure 5. General relations between dominance conditions and packing density.

As illustrated in Figure 5, regarding a binary mixture the mixing ratio at which the fine and the coarse particles are co-dominant marks the mixing ratio with the highest achievable packing density [9]. Increasing the contents of either coarse or fine particles decreases the packing density of the mixture and causes either the coarse or the fine particles to be the dominant phase. To ensure a sufficient surplus of fines the mixing ratio which leads to the maximum packing density needs to be known. Based on this "optimum" mixing ratio the content of the fines can now be increased systematically.

Already Schwanda confirmed in the mid-1950s that the dominance of the fine aggregates is necessary for robust and cost-effective concrete (in his case ordinary concrete) [10]. Due to the inter-particular forces being eliminated widely by the SP, the same general rules can be applied also for the fines and ultra fines in the paste. That means that the so called optimal mixing ratio, which is the start point for the enhancement of the fines, can be precalculated using any appropriate theoretical model, for example de Larrard [9] or Schwanda [10]. However, the authors suggest a combination of calculations and laboratory tests to reduce the overall work amount. It is not necessary to precalculate the actual packing density or the water demand of the mixture, only the mixing ratio at this point is important. Once a granular mixture is composed it is far more exact and target-oriented to determine the fluid demand for the aimed consistency in a laboratory test than calculating it on basis of a theoretical model.

Recent Experiments / Results

In recent examinations [8, 11] it was confirmed that mineral stabilizers such as silica fume (SF) play an important role for the robustness. Adding a reasonable amount of SF in a self-compacting mortar enhances the stable range in the boundary consistency curve. In the beginning the slope of the curve becomes almost linear just like it is known from the β_p-value. The SF is not fully dispersed, although the SP dosage may be above the saturation limit. Due to their size the SF flocculations act as stabilizers but do not negatively influence the general flowability of the paste, as cement flocculations would do.

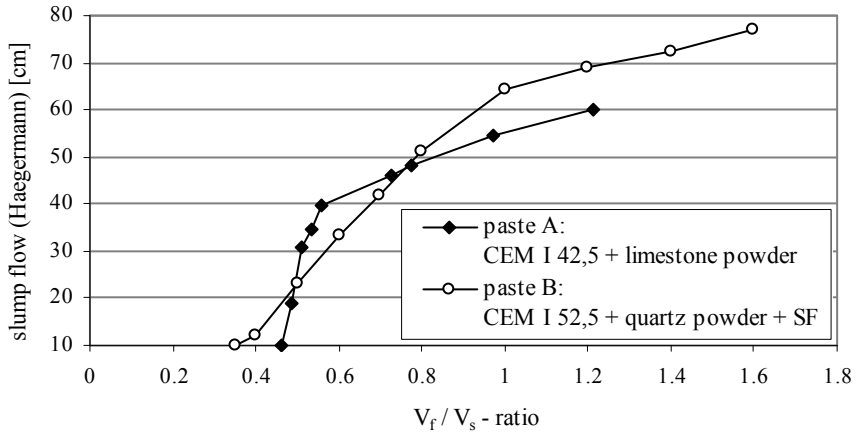

Figure 6. Example for characteristic consistency curves of pastes with different powder composition.

For the practical use granular mixtures that show a long shallow (preferably linear) slope in the characteristic consistency curve are most suitable for tough application conditions, as the consistency can be adjusted in a rather wide range. Changes in the water demand caused by environmental influences or changes in the properties of one component can be buffered by the adjustment of the consistency through the fluid dosage without changing the general properties of the mixture. Figure 6 shows an example of characteristic boundary consistency curves of two paste mixtures. At a V_f/V_s-value of 0.49 both curves show roughly the same consistency expressed by a slump flow of around 22 cm (measured with the Haegermann cone). Paste A is rather sensitive to changes in the V_f/V_s. At $V_f/V_s = 0.46$ this paste does not flow any more whereas at a V_f/V_s of 0.55 a slump flow of nearly 40 cm is reached and the paste starts to be unstable. For paste B the same variation in the V_f/V_s only means an increase in the slump flow from 18 to 29 cm. Paste B does not show significant sedimentation effects until a V_f/V_s of 1.0. If sand was added to that mixture at $V_f/V_s = 1.0$ this would surely segregate, but the paste itself is stable.

On basis of paste B further investigations were carried out with mortar. Therefore, a fine quartz sand (0.1-0.5 mm) was added to the paste. The maximum packing density was found at a mixing ratio of about 60% sand volume to 40% powder volume. The original powder composition of the paste as seen in Figure 6 showed a SF volume content of roughly 22%. The characteristic boundary consistency of the mortar was investigated for several sand / powder, whereby also the SF content in the powder was varied. In Figure 7 two examples are given for mortars with 54% and 46% sand content respectively. Considering the packing maximum at 60% sand content, in both mortars the fines are dominant.

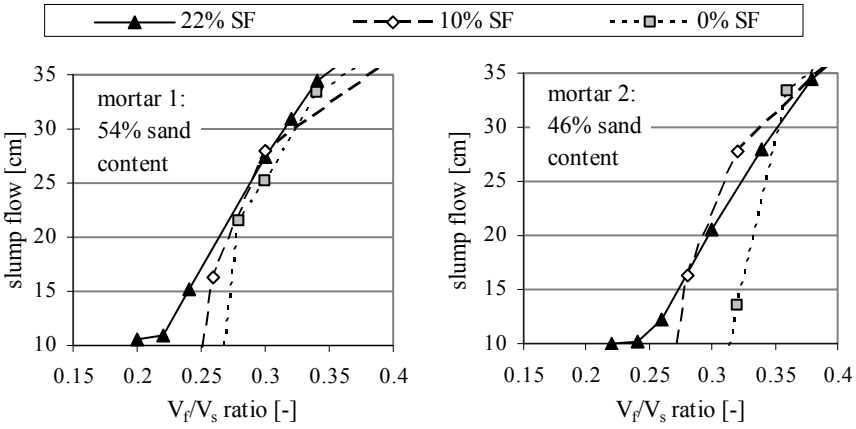

Figure 7. Characteristic consistency curves for a mortar with 54% and 46% sand content respectively, with the SF content in the powder fraction being varied.

In comparison to the paste as shown in Figure 6, the mortars seem to segregate already shortly above slump flow values of 30 cm, indicated by the bending of the curve. But this is not an unexpected behavior for a self-compacting mortar. Much more of interest is the behavior below slump flow values of 30 cm. Here a decrease of the SF content increases the slope, which indicates a higher sensitivity to fluctuations in the water content. With the mortars containing 10% or 0% SF in the powder fraction, it was not even possible to demonstrate the C-point in an actual experiment. Decreasing the V_f/V_s in 0.02 steps in the test series led from a flowing paste directly to an inhomogeneous crumbly mixture without cohesion in only one step. For the sake of extrapolation, such experiments, in which no homogenous paste was producible, are defined as slump flow values of 0 cm to enable them to be distinguished from experiments with homogeneous cohesive, yet not flowing paste.

In a further step the SF content was exchanged by a fine fly ash ($d_{max} < 10$ µm). The results are presented in Figure 8. Basis of these variations was mortar 2 with 22% SF in the powder composition. Concerning the filling ability, shown in the

maximum attainable packing density, or the minimum V_f/V_s-value, the changes are of minor significance. However the changes in the robustness are immense. As soon as more than 25% of the SF is exchanged by the fly ash, the slope of the boundary consistency curves increases drastically. For the range of 15 to 25 cm the gradient, expressed as Δ slump flow / Δ V_f/V_s, is interpolated and visualized in the right chart of Figure 8. In comparison, the mortars without SF as shown in Figure 7 show gradients of 405 and 495 respectively for the same observation range. By comparing the gradients the robustness of the mortar can be classified.

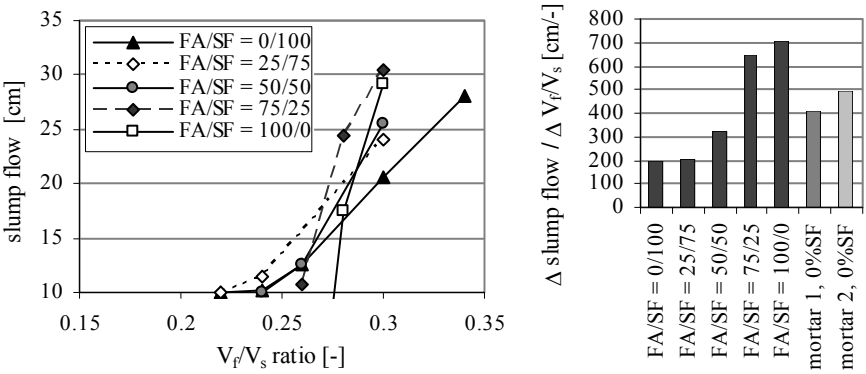

Figure 8. SF being exchanged by fly ash in mortar 2.

For the verification of the positive effect further investigations on silica fume pastes were carried out. However it was technically not possible to determine the characteristic boundary consistency of a 100% silica fume paste. Therefore mixtures of SF and quartz sand (QS) were investigated. Considering the grain size of the sand (0.1-0.5 mm) in comparison to the SF, according to [9] a significant granular interaction is not to be expected.

Experiments were carried out with normal tap water as well as with water including high SP dosages. In this test series the behavior near the C-point was of special interest therefore measurements to determine the S-point were not carried out. Figure 9 shows the measured C-points plotted against the SF/QS. With water the V_f/V_s-values, where the C-point is reached, are rather high and decrease with decreasing SF content until a minimum attainable V_f/V_s-value is found at a SF/QS of about 20/80. Unlike the SF-free mortars in Figure 7, it was possible for each mixture to produce a homogeneous not flowing paste with V_f/V_s-values significantly lower than the C-point. Finally a certain V_f/V_s-value was reached, below which only a crumbly mixture could be obtained. This V_f/V_s-value marks the “loss of cohesion point” (L-point).

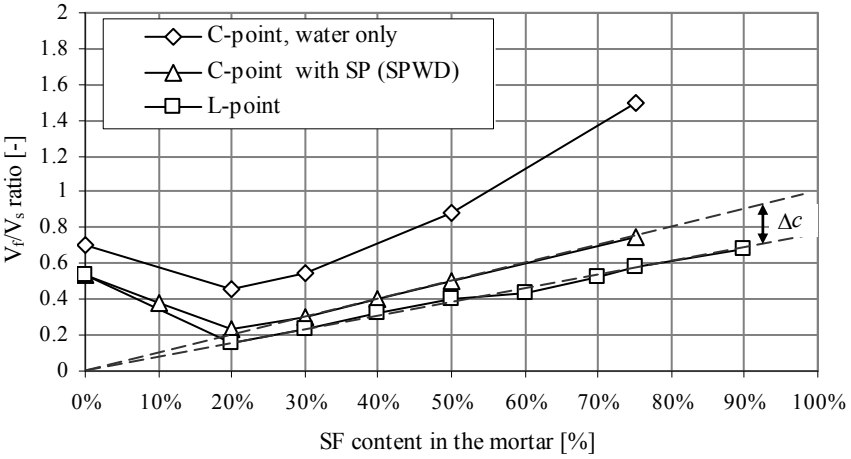

Figure 9. C-points and L-points for SF / QS mixtures.

For high SP dosages, the C- point is identical with the SPWD. For the range of fines being dominant, SPWD and SF content correlate almost linearly, perfectly fitting Schwanda's packing theories [10]. However the SPWD values are still higher than the L-point values, which means, that in this case the densest possible packing is not attained at the SPWD point but at the L-point. In mixtures with low SF content or no SF the SPWD point and the L-point are often identical or very close together. The difference between the C-point and the L-point marked as Δc in Figure 9, is an indication of a high yield stress. On basis of such mixtures robust mortars can be produced that maintain a proper yield stress despite a high SP dosage even above the saturation limit.

Conclusions and Outlook

With the Superplasticizer Based Water Demand a useful value to characterize cementitious powder mixtures is presented. Not only a boundary value for the maximum attainable packing density can be found but also a curve describing the boundary consistency of a paste or mortar composition. This is valuable information for the mixture proportioning. As basis for a robust SCC paste compositions should be used that exhibit a shallow, preferably linear, slope in the beginning of the boundary consistency curve.

For enhancing the robustness of SCC, a mix design is suggested, that secures a surplus of fines for each grain size level. This surplus will assure that for each grain size level the coarse particles will not become dominant despite any unfavorable influences (changes in the dosage, changes in the characteristic properties of the raw materials). Through this mixture proportioning voids, caused

by the granular setup of the coarser particles, can be avoided successfully. Therefore it is possible to adjust the consistency of SCC by adjusting its fluid content which guarantees proper flowability and filling ability of the mixture, which in turn is the condition for reproducible hardened concrete properties.

Silica fume was shown as a useful stabilizer as it does not fully disperse with the commonly used PCE-based superplasticizers. The superplasticizers however do have a significant impact on Silica fume as well, even in the absence of cement.
Besides necessary concrete scale tests, further research should be done to study the influence of boundary conditions like changes in the temperature or the mixing process on the robustness. In addition it should be investigated how these negative effects can be avoided respectively minimized by means of mixture proportioning.

References

[1] Okamura, H. and Ozawa, K. (1995), Mix Design for Self-Compacting Concrete, *Concrete Library of JSCE*, n. 25 pp. 107-120.

[2] Puntke, W. (2002), Water Demand of Fine Granular Compositions, *Beton,* vol. 51, n. 5, pp. 242-248 (in German).

[3] European Committee for Standardization: EN 196 – Methods of testing cement, (2005).

[4] Lohaus, L., Ramge, P., Höveling, H. and Anders, S. (2007), Superplasticizer-Based Approach for Optimized Pastecomposition and Robustness of SCC, In: Procedings of the 5th Int. RILEM Symposium on Self-Compacting Concrete - SCC 2007, De Schutter, G., Boel, V. (Eds) RILEM Publications S.A.R.L. Bagneux, pp 89-94.

[5] Lohaus, L. and Ramge, P. (2008), Robustness of UHPC – A new Approach for mixture Proportioning, In: Procedings of the 2nd Int. Symposium on Ultra HighPerformance Concrete, Fehling E., Schmidt M. Stürwald S. (Eds), Kassel University Press, Kassel, pp. 113-120.

[6] European Committee for Standardization: EN 459-2 – Building lime – Part 2: Test methods, (2002).

[7] Spanka, G., Grube, H. and Thielen, G. (1995), Mode of Action of Liquefying Concrete Admixtures, *Beton*, vol. 44, n. 11, pp. 802-808 and n. 12, pp. 876-881 (in German).

[8] Weicken, H. and Kotsinas, P (2007), Investigations on Mixture Optimisation and Robustness of Pastes and Mortars by Means of the Superplasticizer Based Approach, project thesis, Institute of Building Materials, Leibniz University Hanover, Hanover (in German).

[9] de Larrard, F. (1999), Concrete Mixture proportioning: a scientific approach. Modern Concrete Technology Series 9, E&FN Spon, London.

[10] Schwanda, F. (1956), The Optimal Grain Composition for Coarse Aggregates in Concrete*, Der Bauingenieur,* vol. 31, pp. 41-46 (in German).

[11] Lagos, C. (2007), Investigations on the Robustness of UHPC-Mixtures, Institute of Building Materials, Leibniz University Hanover, Hanover (in German).

Theme 2: Chemical Admixtures

Smart Polycarboxylate Design for SCC in Precast Applications

Lukas Frunz, Didier Lootens, Robert J. Flatt, Franz Wombacher and Ulf Velten

Sika Technology AG, Zürich, Switzerland

Abstract. Concretes for self-compacting concrete (SCC) applications have to combine a high fluidity and fluidity retention with high segregation resistance. This optimal rheological behaviour is obtained by combining a suitable aggregate grading curve with correct rheological properties of the suspending matrix (i.e. the cement paste). It is shown in this paper how these rheological properties can be influenced by polycarboxylate-based superplasticizers. Furthermore it is shown that relatively easy tests can be used to access the rheological properties of both the fresh cement paste and the concrete quantitatively. It is demonstrated that a new superplasticizer leads to an improved robustness in the formulation of SCC.

Introduction

Self-compacting concrete (SCC) is more and more used in many different applications ranging from ready-mix concrete to precast concrete. To fulfill all the different requirements in such different applications, excellent control of the key characteristics defining the quality of the SCC is necessary. Admixtures are used to control these key characteristics which are: slump flow, flow retention, speed of flow, segregation resistance (static and dynamic) and strength development.

Superplasticizers are extensively used in modern SCC to improve workability (i.e. slump flow and flow retention) [1]. Addition of these admixtures influences the results of slump and slump flow measurements which can be related to yield stress [2-4]. Yield stress is one of the two rheological parameters that describe Bingham fluids and that allow a good description of cementitious materials [3]. The other parameter is the viscosity which affects the flow speed of the SCC. While it was generally accepted that superplasticizers would not much influence the plastic viscosity, some recent papers have re-examined this issue [5, 6]. Both parameters, yield stress and viscosity, may have an influence on static and/or dynamic

K.H. Khayat and D. Feys (eds.), *Design, Production and Placement of Self-Consolidating Concrete*, RILEM Bookseries 1,
DOI 10.1007/978-90-481-9664-7_5, © RILEM 2010

segregation. It is one goal of this article to investigate the effect of superplasticizers on these parameters and on the segregation behaviour of the SCC.

Furthermore it is reported that, depending on their nature and dosage, polycarboxylate superplasticizers can induce a retardation that slows strength development. Especially in precast applications, a fast strength development is crucial. Therefore it is a second goal of this article to investigate how a new polycarboxylate superplasticizer, which is especially designed for SCC in precast applications yielding faster strength development (Table II), influences yield stress, viscosity and segregation behaviour of the SCC, compared to more common polycarboxylate polymers.

Materials and Methods

Superplasticizers

The three model polymers used in this study are polycarboxylate based comb-polymers made by polymer analogous esterification reaction. They are named A, B and C. Polymers A and B are common polycarboxylates; polymer C is a new polymer especially designed for SCC applications and more specifically for SCC in precast applications. This new polymer is very insensitive towards sulphates [7] and shows excellent strength development (Table II). All samples are used as 30 wt% solutions and are defoamed with commercially available defoamers.

Cement paste

Preparation. A dry premix of 2680 g of a cement mixture of three CEM I (CEM I 42.5 from three different suppliers), 610 g fly ash and 700 g limestone powder is prepared. The paste is prepared by mixing this premix with water containing the superplasticizer during 2 minutes at 2000 rpm; after 1 minute waiting time the paste is remixed for 10 seconds and then the measurements are performed. The dosage of the superplasticizer is adapted for the initial spread to be 180 mm at water to cement ratio (*w/c*) 0.415. The other *w/c* values were 0.427, 0.44 and 0.452. These values correspond to a relative water increase of 3% for each step. The superplasticizer dosage is kept constant for all *w/c*.

Yield stress measurement. The paste is filled in a cylinder of 51 mm in height and 50 mm in diameter. The cylinder is lifted and the diameter of the produced cake taken as the spread value. All the measured spreads are less than 220 mm, in that range of spread, the surface tension effect can be neglected .The spread can then be linked to the yield stress according to simple equation (1) [4]:

$$\tau_0 = \frac{225\,\rho\,g\,V^2}{128\,\pi^2\,R^5} \tag{1}$$

Marsh cone test. A Marsh cone with a cone height of 278 mm, an upper diameter of 152 mm, a lower diameter of 10 mm and a cylindrical section length of 58 mm is used. A sample of 1.7 ±0.05 liter of the paste is transferred into the funnel. The balance below it is connected to a computer and the mass variation of the falling paste is recorded with the commercially available software [8]. The mass variation over time m is saved and the evolution of the flow rate Q is computed. Assuming a Newtonian limit, the wall shear rate $\dot{\gamma}_R$ in the cylindrical section is calculated from the flow rate according to Eqn. (2):

$$\dot{\gamma}_R = \frac{4Q}{\pi R^3} \tag{2}$$

The wall shear stress σ_R in the lower diameter is calculated according to Eqn. (3) by considering the pressure difference ΔP between the entrance and the exit:

$$\sigma_R = \frac{\Delta P}{2L} R \tag{3}$$

These equations are valid for Newtonian fluids; however, in the shear rate range of the measurements presented in this paper, the viscosity is almost independent of the shear rate, which allows the use of these equations. The pressure difference is simply calculated by considering the hydrostatic pressure developed by the cement in the cone according to Eqn. (4):

$$\Delta P = \rho g h \tag{4}$$

Where ρ is the density of the paste, g the gravitational acceleration and h the height of the cement paste in the cone. The height of the cement paste in the cone is derived from the measurement of the mass of cement.

Concrete

Preparation. A concrete with 375 kg/m^3 cement, 85 kg/m^3 fly ash and 170 liter/m^3 water was used. The exact composition of the used concrete is given in Table I. The cement used was a mixture of three CEM I 42.5 in proportions of 1/1/1. The fines (cement, fly ash and limestone powder) of the concrete were in the same ratio as used for the cement paste tests.

The above mentioned composition was mixed dry in a forced pan mixer for 30 seconds. Then the water containing the superplasticizer was added and mixing was continued for 90 seconds. The dosage of the superplasticizer was adjusted in order to reach a slump flow of the concrete of 68 ±2 cm at *w/c* of 0.45. The other *w/c* were 0.463, 0.477 and 0.49. This corresponds to a relative water increase of 3% for

each step (i.e. 5 liter/m^3), as for the paste experiments. For all *w/c* the dosage of the superplasticizer was also kept constant.

Table I. Composition of the used concrete.

	Limestone powder	0-1 mm	1-4 mm	4-8 mm	8-16 mm	Fly ash	Cement
Mass [kg]	2.8	9.1	13.5	9.5	15.1	2.43	10.67

Slump flow and V-funnel measurements. Slump flow and V-funnel measurements are done according to drafts for the European norms prEN 12350-8: SCC slump-flow test and prEN 12350-9: SCC V-funnel test. The V-funnel test is used to measure the viscosity of the concrete. The concrete is poured in with the base flap closed, then the flap is opened and the outflow time is measured. In this study, as for the Marsh cone, the V-funnel is equipped with a balance, so that the evolution of the concrete weight flowing out of the V-funnel can be recorded. The flow rate Q is computed and the shear rate in the bottom parallelepiped (length L, thickness D) is obtained by assuming a Newtonian regime and using Eqn. (5):

$$\dot{\gamma}_R = \frac{6Q}{D^3} \tag{5}$$

The shear stress in this part is calculated according to Eqn. (3) by considering the pressure difference ΔP between the entrance and the exit. In this case, the radius R is replaced by half the thickness D. Again, the simple equations used for the V-funnel are valid for a Newtonian fluid, which is relevant in the shear rate range of the measurement.

Setting time. Temperature curves over time were measured with a data logger. A concrete specimen of 2.6 liters was taken just after the mixing of the concrete and put in an insulated box. The recorded temperature curve was evaluated by taking the point when temperature starts to increase as "initial setting" and the time at which the maximum temperature is reached as "T_{max}".

Segregation test. A quantitative measurement of the static segregation of the prepared concretes was done according to a draft version for the European norm for testing fresh concrete prEN 12350-11 part 11: self-compacting concrete. This test is based on a sieve analysis of a fresh concrete specimen after 15 minutes resting time. The amount of concrete passing the sieve as percentage of the total concrete amount poured on the sieve is taken as the degree of segregation.

Results and Discussions

Effect of the water to cement ratio on the yield stress

The effect of the water to cement ratio (*w/c*) on the yield stress of the cement paste and of the concrete has been investigated by flow spread and slump flow measurements. On pastes, the dosage of the polymers was chosen to have a spread of about 180 mm with a *w/c* of 0.415. The dosage was kept constant for other *w/c*. The evolution of the spread as a function of the *w/c* for the three polymers is presented in Figure 1 on the left side. The corresponding yield stress evolution calculated by Eqn. (1) is presented on the right side of Figure 1.

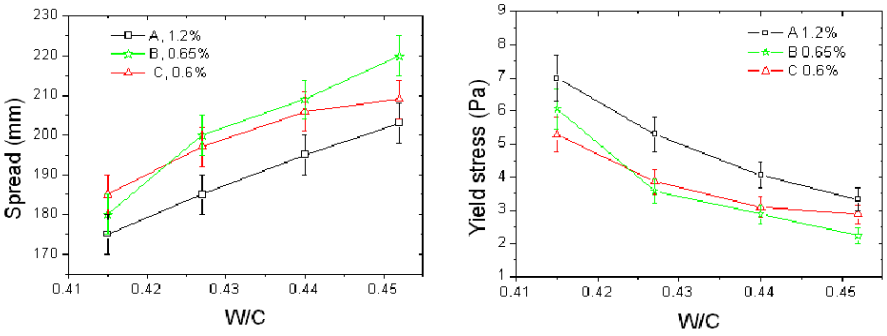

Figure 1. Left: spread of the cement paste as a function of the water to cement ratio for the three polymers. Right: calculated yield stress as a function of the water to cement ratio for the three polymers.

The yield stress measured for the three polymers with *w/c* from 0.415 to 0.455 ranges from 2 to 7 Pa. The decrease of the yield stress of the paste upon water addition is smaller for polymer C than for the other two polymers.

Analogous experiments have been made in concrete: the evolution of the slump flow of the three polymers with *w/c* is represented on the left side of Figure 2. The slump flows (and the corresponding yield stresses) of the concretes containing polymer B and C are a little less influenced by addition of water than the one containing polymer A.

A direct comparison of the yield stresses measured on the cement pastes and on the concrete is shown on the right side of Figure 2. A higher *w/c* had to be used in concrete due to water adsorption of the aggregates. A linear correlation of the cement paste yield stress and the concrete yield stress is found. Since we are working with a fixed granular skeleton and the yield stress changes induced by additional water are of the same type in cement paste and concrete, it is expected

that the *w/c* difference between concrete and paste only shifts the results but does not influence the fundamental linear correlation.

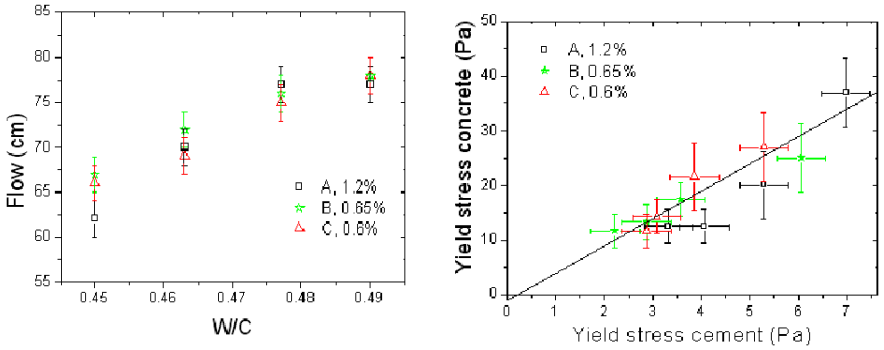

Figure 2. Left: evolution of the slump flow as a function of the *w/c* for the three polymers A, B and C. Right: comparison of the yield stress of the concrete with the yield stress of the corresponding cement paste.

Effect of the water to cement ratio on the viscosity

The effect of the polymer type and of the water to cement ratio on the viscosity is studied for both cement paste and concrete. The measurements of the viscosity are made with the Marsh cone for the fresh cement paste and with the V-funnel for the concrete. In this study, the Marsh cone and the V-funnel are used as capillary rheometer to measure the evolution of the viscosity as a function of the shear rate. The left side of Figure 3 shows the evolution of the viscosity as a function of the shear rate extrapolated from the Marsh cone measurement using Eqn. (2) and (3).

The viscosity is constant over almost the entire range of shear rates for the four tested *w/c*. This validates indirectly our calculation assumptions. It allows a simple determination of the viscosity. The viscosity is represented as a function of *w/c* for the different polymers on the right side of Figure 3. The obtained viscosities were verified by measuring fluids with known viscosities in the same way. The Marsh cone data were also evaluated with a slightly more complicated procedure known from literature [9]. The obtained values for viscosities were very similar. The viscosity decreases with increasing *w/c* from about 1.3-1.8 Pa·s to 0.6-0.9 Pa·s for all three tested polymers. A slightly bigger change in viscosity upon water addition is found for polymer C.

The same measurements are performed in concrete with the V-funnel. The evolution of the viscosity as a function of the shear rate is extrapolated from Eqn. (4) and (3). The left side of Figure 4 represents the evolution for polymer A. For all tested polymers and the entire *w/c* range, the viscosity measured is almost independent on the shear rate. The viscosity can therefore be extrapolated from

these measurements. The dependence of the viscosity on *w/c* for the three polymers is represented on the right side of Figure 4. The influence of additional water on the viscosity of the fresh concrete is similar for polymers A and B and a little more pronounced for polymer C.

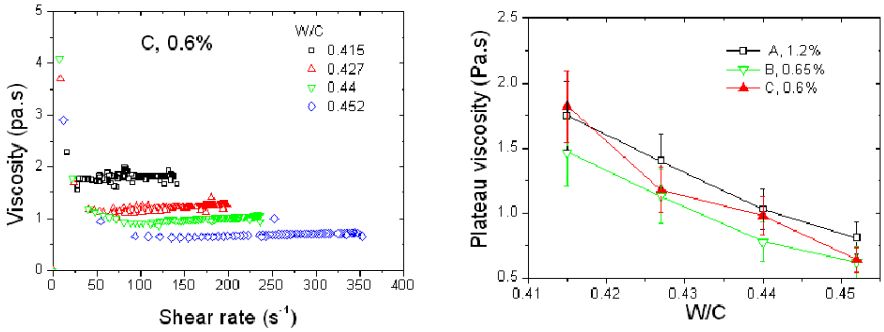

Figure 3. Left: viscosity of the cement paste containing polymer C as a function of the shear rate at different *w/c*. Right: viscosities as a function of the water to cement ratio for the 3 tested polymers.

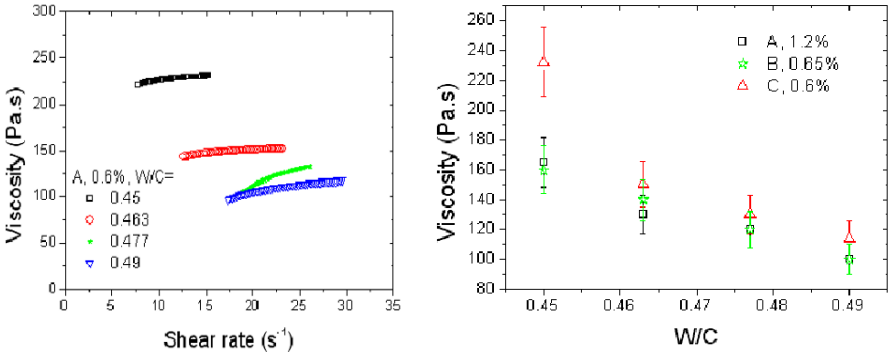

Figure 4. Left: concrete viscosities as a function of the shear rate for polymer A at different *w/c*. Right: dependence of the viscosity on *w/c* for the three polymers.

Effect of the yield stress on the segregation

In SCC it is important to ensure the absence of segregation to guarantee the homogeneity of the mechanical properties of the final structure. Segregation can be either dynamic when occurring during the placement of the concrete or static when occurring after its placement and before setting. The segregation test we used is a measure for the static segregation.

The segregation of the aggregates happens due to the sedimentation of the aggregates under their own weight. It is linked to the rheological properties of the dispersing medium, in our case the cementitious matrix. The ratio between the gravitational force acting on an aggregate and the restoring force due to the yield properties of the cement paste matrix gives an approximation of the size of the particle that will stay in place under static conditions. A critical yield stress can be calculated above which a particle has a limited sedimentation. For a sphere of a diameter D and of a density ρ_α, the ratio K of plastic effects of the matrix to gravity effects is represented by Eqn. (6):

$$K = \frac{\tau_y}{gD(\rho_a - \rho_m)} \tag{6}$$

τ_y is the yield stress of the matrix, g the gravitational constant and ρ_m the density of the matrix. According to Jossic *et al.* [10], Atapattu *et al.* [11] or Beris *et al.* [12] a critical ratio K_s can be defined as a stability criterion above which sedimentation is negligible. K_s lies between 0.045 and 0.10. Expressed in these terms, the results of Roussel [13] would give a value of K_s of 0.056. The relatively broad limits of K_s are due to the effect of the particle roughness and shape, but also due to the matrix nature. Taken these limits, the range of the minimum yield stress needed to avoid sedimentation of an aggregate of 16 mm (density of 2600 kg/m^3) in a matrix with a density of 2000 kg/m^3 is between 4 to 10 Pa.

The relation between the yield stress of the cement paste and of the concrete for our mix design is represented on the right side of Figure 2. A yield stress of the cement paste ranging from 4 to 10 Pa corresponds to a yield stress of the concrete from 15 to 40 Pa. This means that a segregation of the concrete would definitely be expected to occur when the yield of the concrete is smaller than 15 Pa.

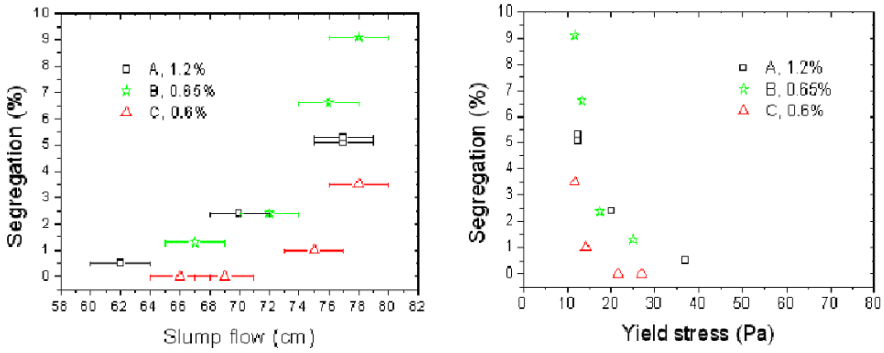

Figure 5. Measured segregation of the concrete as a function of slump flow (left) and yield stress (right).

To examine this expectation, the degree of segregation as a function of the measured slump flow and the corresponding yield stress is shown in Figure 5. As expected, segregation increases when the yield stress of the fresh concrete decreases. No measurable segregation occurs when the yield of the concrete is higher than 40 Pa. This limit is shifted to 25 Pa for the concrete prepared with polymer C. Significant segregation occurs when the yield stress is smaller than 15 Pa. These results are in good agreement with the theoretical prediction.

Robustness of a SCC formulation

A correct control of the rheological properties of the matrix allows the production of a workable and segregation-free SCC. However, important characteristics of a SCC are not only its absolute rheological properties but also their robustness. This means that they must not be much affected by any small variation in the composition or amount of any of the concrete components. In addition, the setting time and strength development are very important.

Robustness. Many of the industrial concrete mixers are equipped with an ampere-meter which allows the adjustment of the mix. This is essentially a measure of the force needed for the mixing of the SCC and can be expected to be directly linked to the viscosity of the concrete owing to the high shear regime during concrete production [14]. Because this measurement is used to check concrete workability, we conclude that production plants are essentially adapting the water content on the basis of a viscosity measurement. The variation in the water content therefore counteracts any component variation that impacts viscosity, as for example, the grading or humidity of the aggregates, the sulphate content of the cement, etc.

Due to the complexity of the mixer design and the accuracy of this measurement, an accuracy of ± 20% on the concrete viscosity can be assumed. This represents the range of variations that may be measured randomly without any single component having changed. We therefore proceed to evaluate the impact of such random variations on concrete properties. The right side of Figure 4 shows that a change of 20% in viscosity corresponds to a change in *w/c* of about 0.02 in our mix design. This variation of the *w/c* also has an impact on the yield stress of the SCC as shown on the left side of Figure 2.

For example, a concrete with 680 mm slump flow and showing no apparent segregation would go to showing slump flow of 750 mm for which the segregation is important and of about 10%. In terms of yield stress this means going from 28 to 17 Pa. In this case, the small variation of added water can therefore be relatively critical for the stability of the SCC. The smaller the impact of additional water the more robust is the SCC.

Because of the above mentioned quality control in the field (adjustment of viscosity by addition of water), the issue of robustness can be looked at by

checking the dependence of the yield stress on the viscosity. If this dependence is small, then a change of ± 20% in viscosity would have only a small impact on yield stress and no negative impact on the segregation stability. In contrast, if the dependence is big, the same change in viscosity would have a big impact on the segregation stability.

The dependence of the cement paste spread and of the concrete slump flow on the viscosity is presented in Figure 6. It can be seen that for the new polymer C the dependence is in both cement paste and concrete the smallest of the three polymers, meaning that it is the most robust of the three.

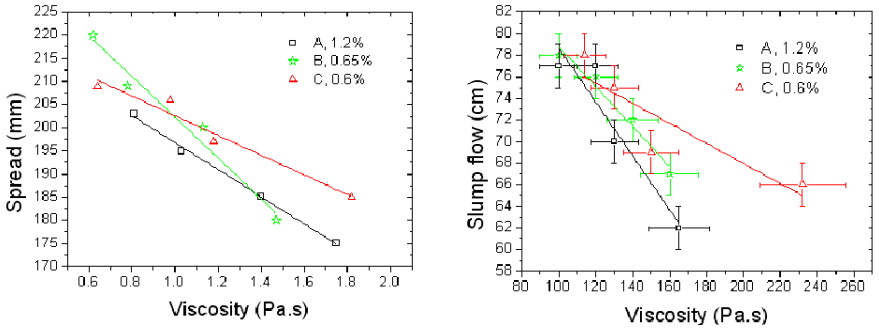

Figure 6. Left: cement paste spread as a function of the viscosity for the three polymers. Right: same representation for the fresh concrete.

Control of the setting time. Depending on their structure and dosage, polycarboxylate-based superplasticizers can have a retarding effect on the hydration of the cement. The new polymer C was developed to reduce this retarding effect. Initial setting and T_{max} are listed in Table II. Polymer C has the fastest hydration behaviour of the three polymers.

Table II. Setting time of the concrete.

	Polymer A	Polymer B	Polymer C
Initial setting [h]	9.8	5	3.7
T_{max} [h]	23	18	15.5

Conclusions

Complete quantitative characterizations of the rheological properties of both cement paste and concrete have been made based on well established classical tests. Simple physical analysis allows the determination of yield stresses from spread tests and of viscosities from V-funnel measurements for concrete and from

Marsh cone tests for cement paste. The evolution of viscosity and yield stress with *w/c* was influenced by the polymer. The results also demonstrate that the rheological properties of the cement paste are well correlated with those of the fresh concrete. This correlation allows the analysis of the segregation occurring in the early ages of the SCC based on cement paste yield stress and viscosity. The degree of segregation occurring is dependent on yield stress and only little influenced by the polymers used.

From a practical point of view, it is important to recognize that many concrete plants adjust the water content based on an indirect measurement of concrete viscosity. Random variations within the accuracy of such instruments lead to changes in water content that can be detrimental to segregation resistance. We demonstrate that a robust SCC can be obtained when the yield stress of the concrete is less dependent on the viscosity of the concrete. This can be influenced by the polymer. It has turned out that the new polymer C shows a more robust behaviour in this sense than the common polycarboxylate polymers it was compared to.

References

[1] Flatt, R.J. (2001), In: *Polymers in Particulate Systems: Properties and Applications*, Hackley, V.A., Somasundran, P. and Lewis, J.A. (Eds.), Surfactant Science Series, Marcel Dekker Inc, pp. 247-294.

[2] Banfill, P.F.G. (Ed.) (1991), In: *The rheology of fresh cement and concrete*, Spon, 373p..

[3] Roussel, N. (2006), *Mater. Struct.*, vol. 39, n. 4, pp. 501-509.

[4] Roussel, N. et al. (2005), *Cem. Conc. Res.*, vol. 35, pp. 817-822.

[5] Winnefeld, F. et al. (2007), *Cem. Conc. Compos.*, vol. 29, pp. 251-262.

[6] Yamada, K. et al. (2000), *Cem. Conc. Res.*, vol. 30, pp. 197-207.

[7] Zimmermann, J. et al. (2009), In: *Superplasticizers and other chemical admixtures in concrete*, Proc. 9th ACI Int. Conf. (Seville), Holland, T.C., Gupta, P.R., Malhotra, V.M. (Eds.), ACI, pp. 165-175.

[8] http://us.mt.com/global/en/home/supportive_content/product_documentation/product_brochures/balancelink.rxHgAwXLuMvM.MediaFileComponent.html/BalanceLink_en.pdf

[9] Roussel, N. et al. (2005), *Cem. Conc. Res.*, vol. 35, pp. 823-830.

[10] Jossic, L. and Magnin, A. (2001), *Les cahiers de Rhéologie*, n. 1, pp. 55-64 (in French).

[11] Atapattu, D.D. et al. (1995), *J. Non-Newton. Fluid Mechan.*, vol. 59, n. 2-3, pp. 245-265.

[12] Beris, A.N. et al. (1985), *J. Fluid. Mechan.*, vol. 158, pp. 219-244.

[13] Roussel, N. (2006), *Mater. Stuct.*, vol. 39, n. 1, pp. 75-83.

[14] Chopin, D. (2003), Mixing of High-Performance and Self-Compacting Concretes – Optimisation of the mixing time, Ph.D. Thesis, Laboratoire Central des Ponts et Chaussées, France (in French).

Effects of Superplasticizer and Viscosity-Modifying Agent on Fresh Concrete Performance of SCC at Varied Ambient Temperatures

Wolfram Schmidt[1], Jos Brouwers[2], Hans-Carsten Kühne[1] and Birgit Meng[1]

[1] BAM Federal Institute for Materials Research and Testing, Germany
[2] Eindhoven Technical University, The Netherlands

Abstract. Varying ambient temperatures in plants or on construction sites during casting of SCC can cause serious problems affecting the fresh concrete performances, such as rheological properties and setting time, with consequences for the hardened properties in the structure. By sensible choices of the components, the robustness of SCC mixtures against temperature variations can be improved. However, this aspect has not been the focus of intensive research yet. In this study the effects of varied ambient temperatures on the early performance of differently composed SCC mixtures are investigated, with emphasis on changes in rheology, early deformations, heat evolution and setting. Focus is placed on the study of the influence of the polycarboxylate ether molecule type as well as different viscosity-modifying agents on the temperature robustness. Effects on the relevance for practical concrete applications are evaluated, which will provide a reliable framework of possible actions on the appropriate use of admixtures for SCC.

Introduction

It is often stated that self-compacting concrete (SCC) can only function well, when the mixture composition is perfectly adjusted and the ambient conditions are within narrow limits. Thus, SCC is typically limited to precast applications, although the technology offers many opportunities for the construction site as well. The flow properties of SCC are controlled by the composition of paste and aggregates as well as their respective ratio in the concrete. Regarding the rheology of the paste matrix, the adsorption of superplasticizer molecules on the surfaces of clinker phases and early hydrate phases plays an important role [1, 2]. In case of SCC, polycarboxylate ether superplasticizers (PCE) are mostly used. Positively charged clinker and reaction phases, like C_3A and ettringite, interact with the negatively charged backbones of the PCE molecules [3]. In this process, superplasticizer

K.H. Khayat and D. Feys (eds.), *Design, Production and Placement of Self-Consolidating Concrete*, RILEM Bookseries 1,
DOI 10.1007/978-90-481-9664-7_6, © RILEM 2010

molecules compete with the sulphate ions and interact with the calcium ions in the pore solution [4, 5]. The processes are time dependent, since newly built reaction phases, e.g. ettringite, provide additional adsorption surfaces. The higher the anionic backbone charge density, the quicker the molecules adsorb on surfaces. The lower the charge density, the slower but the more polymers can adsorb. In case of high dosages, some molecules will not adsorb directly but time dependent [3, 6]. Typically highly charged PCEs are used for quick performance over a short period of time, whereas lowly charged PCEs are used if flow retention is required. Sensible choice of PCE at particular ambient conditions can optimize the flow performance or the robustness against varying total water contents resulting from either poor production control or varying moisture contents of the components. An optimized PCE for particular conditions, however, does not inevitably have to be the best choice at differing ambient conditions. At varied temperatures, the hydration can be accelerated or slowed down, which affects the interaction between PCE, cement and hydrates significantly.

In the case of ready-mix concrete, surrounding conditions may change unexpectedly, and it is not possible to have an individual optimum superplasticizer modification for all expectable situations. Robustness is often only linked to the performance stability against variations in quality and quantity of the concrete's constituents such as water, cement, admixtures, aggregates, or human and technological shortcomings during casting [7-11]. The stability against ambient climatic conditions at otherwise identical specifications is only rarely observed. The interaction between PCE and mineral components is highly affected by the ambient temperature. Hence, the relevant question for casting on site is not only, which PCE can optimize the performance, but also which SCC mixture parameters can buffer negative effects caused by temperature dependent varying binder-PCE-interactions. In this, the impact of additions and viscosity-modifying agents (VMA) has to be considered. Additions may also provide positive surface charges, causing interactions with PCE. VMA has strong impact on the rheology of cementitious materials, overlapping or interfering with the effects of PCE [12]. In order to better understand temperature effects, systematic investigations were performed at varied temperatures with a powder type SCC and a VMA stabilized SCC. Focus was put on rheological concrete properties as well as on setting, heat evolution and autogenous deformations.

Experimental Setup and Investigations

Two characteristic concrete mixture compositions were generated, which are demonstrated in Table I:

- The powder type mixture (POW) used in the investigations is a modification of an SCC, originally developed without any VMA according to the approach of Okamura [13]. In order to better point out effects of VMA, in the modified concrete (POW) the limestone filler content of the original

Okamura type was reduced by 50 kg/m³. The missing filler was compensated by VMA. By this modification, yielding a water-powder ratio of 0.31 and a total powder content of still 560 kg/m³, the basic characteristics of a powder type SCC remain largely untouched, while the role of VMA for the functioning of the SCC is increased.

- The mixture called COM is a combined approach between powder and admixture stabilization. The powder content is higher than in ordinary concrete but significantly smaller than in the POW mixture. Due to the missing powder, high contents of VMA are required to achieve segregation stability and self-compacting flow properties.

These basic mixture compositions were then adjusted by combination of three types of PCE and two types of VMA, in such a way that a slump flow diameter between 650 and 700 mm was obtained 30 minutes after mixing. This specification was made in order to provide sufficient workability retention with regard to the casting on the construction site, where temperature changes are most likely to occur. The PCEs in use are commercial products with comparable side chain and backbone length, differing characteristically in their graft chain density, which determines the backbone's ionic strength and thus the adsorption velocity. For a better display of the results, this paper focuses only on the PCEs with highest and lowest charge density (PCE1 and PCE2), since SCC with the medium charge density polymer always performed within the range of these. Viscosity-modifying agent VMA1 was based on modified potato starch, whereas VMA2 was based on Diutan Gum. When introduced into water only, both VMAs increase plastic viscosity but only VMA2 generates a significant yield stress. When added to water-solid suspensions, both VMAs significantly increase plastic viscosity and yield stress [12, 14]. Thus, particle immobilization (VMA1) and fluid-phase stabilization (VMA2) can be distinguished. Table II provides an overview of the characteristics and dosages of admixtures to achieve the defined flow performance.

Rheological concrete investigations were performed by using a CONTEC Rheometer-4SCC. The rheometer is an impeller based transportable system, which measures the electric current at varied rotational speed [9]. When applying a Bingham curve on the results, qualitative information about yield stress (G-Yield) and viscosity (H-Viscosity) of flowable concrete can be obtained. Changes of the rheological properties can be displayed qualitatively, but the results cannot be converted to fundamental rheological units as possible with a co-axial cylinder rheometer. The rheological test protocol is given in Table III. The first step includes 5 seconds of pre-shearing in order to assure measuring at steady state. In order to avoid deviations due to the change of the rotational speed, only the last 4 seconds of each step were used for the calculation of the Bingham curve. The rheometric investigations were conducted in a large climate chamber at 5, 20 and 30°C. In advance, it was ensured that the raw materials including water were adjusted to the particular test climate. 30 l of concrete were mixed for the tests in a

compulsory mixer according to the mixing procedure given in Table IV. Mixing steps were conducted at 70 revolutions per second. The investigations were performed 0, 30, 60, and 90 minutes subsequently. Before testing the rheological properties at 30 minutes, the concrete was reintroduced in the mixer and stirred intensively. By this, the transportation to the job-site in a truck mixer should be simulated. For later testing times, the concrete was only softly stirred in the rheometer in order to avoid effects of possibly separated aggregates.

Table I. Mixture composition for basic SCC types.

	POW	COM
Normal Portland Cement*	310 kg/m³	350 kg/m³
Limestone Filler	250 kg/m³	130 kg/m³
Water	175 kg/m³	175 kg/m³
Sand (0.1-4 mm) **	808 kg/m³	848 kg/m³
Aggregate (4-16 mm)	791 kg/m³	831 kg/m³
* CEM I 42.5; total alkali content: 0.89 wt.-% Clinker comp. [wt.-%]: C_3S=55.8; C_2S=19.6; C_3A=8.2; C_4AF=6.8 ** Washed and dried sand, fraction below 125 µm < 1.5% by volume, fraction below 250 µm < 20.0% by volume		

Table II. Admixture adjustments for defined performance at 20°C.

VMA	PCE	Ionic backbone strength	POW		COM	
			PCE solids	VMA	PCE solids	VMA
			wt.-% of cem.	wt.-% of water	wt.-% of cem.	wt.-% of water
VMA1 (Starch ether)	PCE1	low	0.62	0.035	0.68	0.24
	PCE2	high	0.38	0.035	0.44	0.24
VMA2 (Diutan Gum)	PCE1	low	0.57	0.002	0.66	0.02
	PCE2	high	0.36	0.002	0.42	0.02

Table III. Testing protocol for rheometric concrete investigations.

Step	1	2	3	4	5	6	7	8	9
Speed [s^{-1}]	0.45	0.40	0.35	0.30	0.25	0.20	0.15	0.10	0.05
Duration [s]	10	5	5	5	5	5	5	5	5

Table IV. Mixing protocol for concrete investigations.

Step	Duration [s]	Action
1	60	Dry mixing
2	60	Addition of 2/3 of total water
3	30	Wet mixing + addition of VMA
4	60	Addition of remaining water mixed with PCE
5	30	Scraping walls of mixing pan
6	120	Mixing
7	120	Resting phase
8	120	Mixing

The early age properties were determined by measuring setting, autogenous deformations as well as heat evolution of the mixtures at 5, 20 and 30°C. Since the particular effects of VMA on the early properties go beyond the scope of this paper, the presented results focus on the influence of PCE. For these demonstrated tests, binder paste was used. Since the sand used in the basic concrete mix design (Table I) did neither provide high contents of fines nor large surfaces compared to the powders, consideration of the powder fraction from sand and water absorption of sand and aggregates would only modify the paste composition to small extent. Hence, the pastes for these tests were generated from cement, limestone filler, water and superplasticizers to the same volumetric ratio as in the concrete mixture given in Tables I and II.

Since the particular adjustment of admixtures was conducted on SCC, the thus generated pastes, if sand and aggregates were added, can be considered to function properly at 20°C. The aim of the demonstrated research was to learn more about the influence of the PCE molecule type on the paste components and to illuminate effects taking place on paste level. Therefore the pastes were not furthermore changed characteristically or optimized. Particularly the PCE-powder ratio should remain untouched in order to point out effects of the PCE modification and to avoid that observed effects are rather resulting from differing PCE solid contents. Furthermore, the water-powder ratios were not changed to better distinguish characteristics of powder type and combination type binders. However, without the stabilizing effect of the sand and aggregates, the COM pastes tended to segregation, which had to be avoided since this would critically affects the measurement of the deformations and the setting. In order to safely avoid segregation of the COM specimens at all observed temperatures, the VMA contents were increased by factor 2 compared to the concrete mixes. By this, the general characteristics of the pastes, such as the ratio of powder to water and solid PCE, respectively, remained untouched. Since the VMA content was kept constant for all paste tests, this allowed observing the effect of different PCE types. It has to be stated that the effects observed with these pastes do not have to be representative for the respective concretes, since numerous influencing factors

have been excluded. To which extent the demonstrated results provide validity on full concrete scale will be subject of future research.

For the investigations of the setting, an automatic Vicat device was used. Measurements took place under water at particular temperature. Early deformations were measured with a shrinkage cone, where the mortar is given into a cone tapered downwards. On the flat top surface, a laser reflector is placed, measuring continuously the change in height. The top angle of 60 ° allows for similar deformations in height and width. Only the cone walls can be tempered, therefore the investigations were conducted in a climate chamber at particular temperature. In order to avoid exchange with the surrounding air, the cones were fully covered by foil. Since the minutes between mixing and first measurement remain undefined, a quantitative determination of the deformations is not possible. The method, however, provides information on rate of deformation. It cannot distinguish between deformations caused by settlement or shrinkage. When a sensible starting time for the observations can be defined (e.g. after final set) the deformations can be quantified. The heat flow investigations were performed in an isothermal heat flow calorimeter type TAM Air. The cells were calibrated to the particular investigation climate. The above described tests were conducted in parallel from one single mixture in order to avoid effects resulting from different test conditions. A repeatable mix regime that has proven to homogenize the powder well was applied constantly. Each test was conducted at least twice for each mixture and admixture adjustment.

Results and Discussion

Yield stress was influenced much more by the surrounding conditions and the admixture adjustment than viscosity. Therefore, the demonstrated results focus on G-yield, which can be linked to the slump flow behaviour of the mixes. Figure 1 shows the evolution of the G-Yield of the POW mixtures with time depending on temperature, PCE and VMA. At 5°C neither PCE type nor VMA type affect the performance and the performance retention of the POW mixes. At higher temperatures PCE1 retains the yield stress constantly, whereas PCE2 causes a time dependent increase of the yield stress. The latter effect is boosted by higher temperature. Due to the performance loss at 30°C no further measurement could be conducted later than 30 minutes, when PCE2 was used. Generally the influence of VMA is negligible. Only at 20°C in combination with PCE2, VMA1 provides better yield stress retention than VMA2. Figure 2 shows the respective results for the COM mixtures. Due to the higher content of VMA, their performance depends on both PCE and VMA type. At 5°C concrete with PCE2 provides a significantly lower yield stress than with PCE1. This effect occurs in comparable magnitude for both VMA types. In addition, concrete with VMA1 provides significantly lower yield stress than with VMA2. Both stabilizing agents provide characteristic retention behaviour, which is independent of the PCE type. VMA1 causes constant

stiffening, whereas VMA2 causes an initial stiffening effect which reduces again with increasing time. Effects of VMA and PCE superpose so that the only mixture that can be considered self-compacting is the mixture with PCE2 and VMA1.

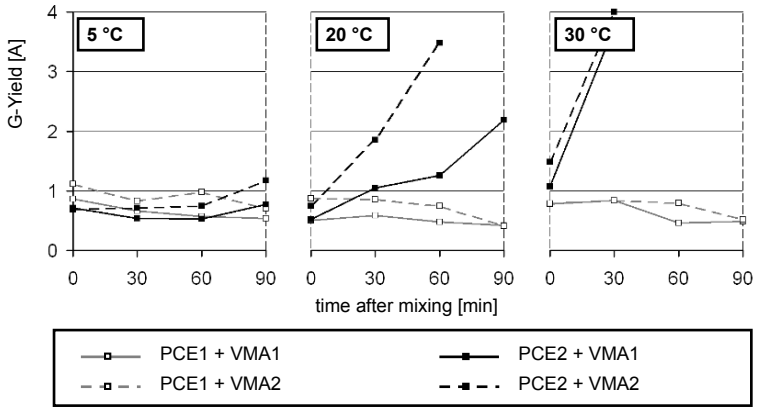

Figure 1. POW mixtures at varied temperatures, PCEs and VMAs.

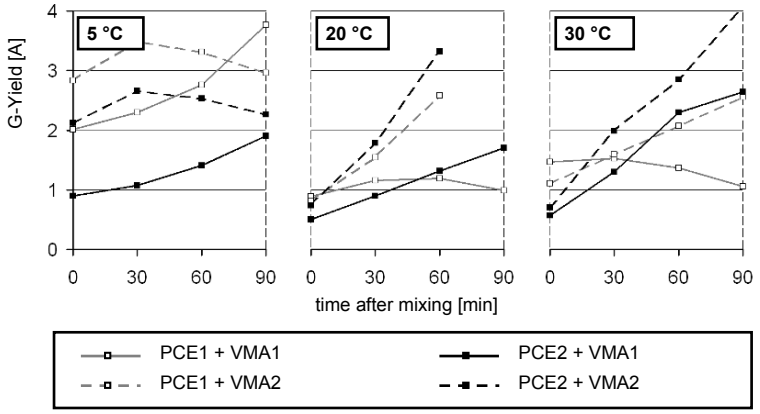

Figure 2. COM mixtures at varied temperatures, PCEs and VMAs.

At 20°C the influence of the VMA on yield stress is much stronger than the effect of the PCE. Independent of the PCE type, both mixes with VMA1 retain the performance better than those with VMA2. At 30°C, effects of both, VMA and PCE, can be noticed. Initially PCE2 provides much lower yield stress than PCE1 but then the yield stress increases quickly. PCE1 generally provides better yield

stress retention. Mixtures with VMA1 provide lower yield stress. The only mixture that performs well over the whole time includes PCE1 and VMA1.

The results presented in Figures 1 and 2 can be explained by PCE adsorption that depends on hydration progress and backbone charge density as well as on the stabilizing mechanism caused by the mix design and the VMA. Since the flow behaviour of the POW mixture is strongly dependent on particle distribution and optimized water content, the influence of low temperatures on the yield stress is small. The hydration is slowed down and thus the adsorption of polymers on hydration phases is low. Therefore the influence of the PCE type is negligible. At higher temperatures, the hydration takes place much quicker, causing stronger effect of the PCE type. The highly charged polymers of PCE2 are quickly consumed so that any further hydration causes stiffening, whereas the lower charged PCE1 still provides polymers for adsorption in the solution. Hence, PCE1 generally provides better robustness against temperature effects. The influence of the VMA is generally low on the POW mixtures, since it is only added in small amount. The flow performance of the COM mixtures depends rather on the VMA than on the optimum adjustment of particles and water demand. Since the COM mixtures provide water in overabundance, the temperature effect on the performance of VMA2, which rather stabilizes the fluid phase, is much stronger than on VMA1, which immobilizes the particles. At low temperatures, precipitation of aluminates and solubility of sulphates is slowed down as well as their reaction. Therefore, less adsorption sites are available for the PCE molecules than at higher temperature, when ettringite can be shaped quickly. Hence the PCE with high backbone charge density performs significantly better than the one with low charge density. Since the performance loss related to the initial performance of both PCEs is comparable, it can be assumed that even after a long period of time no distinct adsorption of PCE1 takes place. This can be explained by anions from the pore solution occupying the adsorption spaces for the polymers. Effects of VMA superpose the PCE performance, and VMA2 causes a distinct performance loss. Hence, only the combination of PCE2 and VMA1 performs stable at low temperature. At 20 and 30°C the hydration proceeds faster and the PCEs' dependency on the hydration process gains prominence. This causes low initial yield stress combined with poor performance retention for SCC with highly charged PCE. With increasing temperature, the hydration is accelerated causing increasingly poorer performance retention at the use of PCE2. Since the flowability of these mixtures is supplementary determined by the high available volume of water, however, the significance is much smaller than it is for the POW mixtures.

In summary, the POW mixtures provide stable performance at a wide temperature range, when a low charge density polymer is used, whereas a highly charged polymer might cause poor performance retention at high temperatures. COM mixtures require a highly charged polymer at cold temperatures to provide workability at all, while at higher temperature the influence of the PCE is less significant. Hence, POW mixtures are very robust at low temperatures and prone to

failure at high temperature against effects of the PCE type. Vice versa, COM mixtures are sensitive against PCE effects at low temperatures and more robust at high temperatures. However, since the used PCE also determines the overall amount of adsorbable polymers in the bulk system, and the adsorbed surfaces influence the hydration progress, the effect of the PCE continues still after casting, since it can have a strong influence on the setting behaviour.

Figure 3 demonstrates the influence of the PCE on the setting behaviour for the COM mixtures at 5 and at 30°C. In order to provide comparable flow properties of the concrete, the low charge backbone PCE has to be added in significantly higher solid content (see Table II). Therefore, compared to PCE2, the setting is significantly retarded, since at full consumption of PCE more molecules occupy the surfaces of hydration products, thus slowing down the setting. This observation fits in with the results of the heat flow calorimetry. Retarding effects that were caused by the choice of PCE and the respective amount of solid molecules could qualitatively be observed at the heat flow curves as well. In order to underline this, the first derivative of the heat flow was calculated, which can be entitled as the heat flow rate (Figure 4). For all temperatures the maximum heat flow rate peak occurs at the time of the final set, which underlines the strong correlation between heat evolution and setting. This is valid for all observed temperatures.

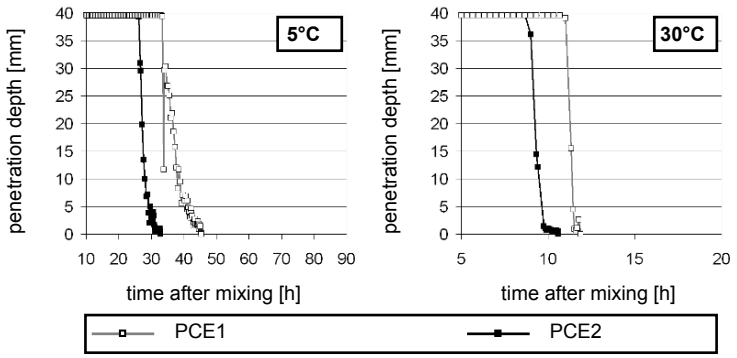

Figure 3. Needle penetration depth at 5 and 30°C of COM paste.

The time dependency of the autogenous deformations, the deformation rate, which when approaching zero indicates the transition towards a slow deformation process, was strongly related to temperatures. At 5°C the approximation towards zero occurred for the demonstrated examples of the COM pastes around 44 hours at 5°C and around 21 hours at 30°C, independent of PCE type or solid content. If deformation progresses are independent of the PCE solid content but the final set is strongly depending on the PCE solid content, this suggests taking a closer look at those deformations after the final set. Deformations occurring earlier take place still in plastic state, which makes the occurrence of lasting cracks unlikely. After

the final set, deformations take place in elastic state while the strength is still low, making the mortar prone to cracks in particular at this time.

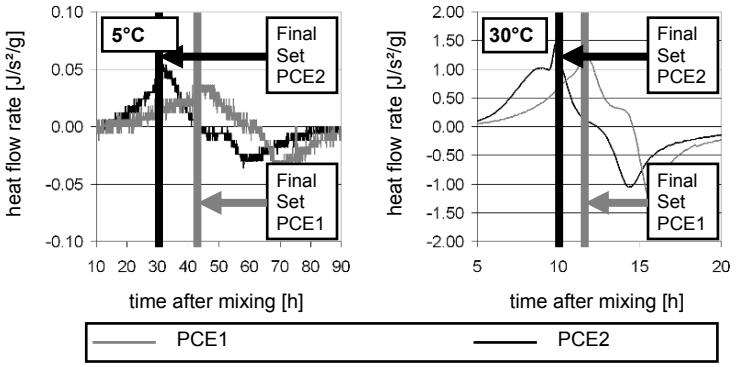

Figure 4. Heat flow rate depending on PCE type compared to time of final set.

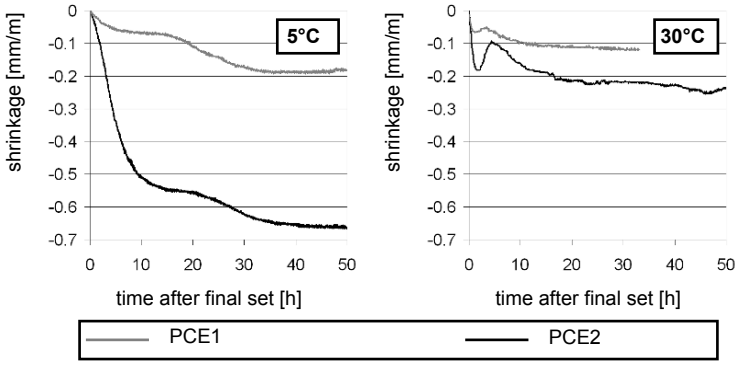

Figure 5. Deformations after final set depending on PCE type.

Figure 5 shows the deformations of the mortars with PCE1 and PCE2 that only occur after the final set at low and high temperatures. Since at all temperatures the shrinkage rate approaches zero with PCE1 and PCE2 approximately at the same time, but PCE2 always sets much earlier than PCE1, the highly charged PCE2 produces larger deformations than the lowly charged PCE1 at this stage. The higher amount of polymers that is required to provide the demanded concrete flow performance with PCE1 reduces the susceptibility to early cracks due to set retardation. Furthermore, the shrinkage deformations after the final set are generally higher at 5°C than at 30°C. This effect can be attributed to a slower development of stiffness at low temperatures, causing low resistance against deformations over a longer period of time. Temperature effects on deformations

after setting are more prominent with PCE2. The deformations at 5°C are roughly two times as high with PCE1 and roughly three times as high with PCE2 as at 30°C. The earlier setting due to the lower amount of polymers occurs most significantly at low temperatures (Figure 3). The long period of time between the setting of PCE1 and PCE2 at 5°C causes that the influence of temperature on deformations after setting is significantly higher on pastes when the highly charged PCE is used.

Summary and Outlook

Rheological investigations as well as investigations of early properties of two types of SCC at varied temperatures and at varied admixture compositions have shown that although the performance of all modifications was comparable at 20°C, significant performance differences occur at varied temperatures.

- Since temperature effects on the performance of SCC are mainly initiated by the temperature dependent hydration velocity, robustness improvement can be achieved by sensible choice of a fitting PCE polymer.
- At low temperatures, the powder type SCC is less affected by the choice of PCE, whereas at high temperatures PCE with high ionic strength of the backbone can cause rapid stiffening.
- The VMA type SCC requires a highly charged PCE at low temperatures, whereas at high temperatures the effect of PCE is less prominent.
- Besides temperature effects that can be related to PCE, temperature effects on the VMA have to be considered for the VMA type SCC. In the demonstrated research, starch ether was less prone to temperature effects than Diutan Gum.
- Since the charge density of the polymers' backbone also determines the amount of solids that have to be added to achieve certain flowability, the required PCE for a defined flow performance strongly affects the early concrete properties.
- Higher PCE solid contents slow down the setting and the heat flow. While it is likely that at 20 and 30°C these effects are not of practical importance, at low temperatures, the delay can be crucial.
- Since early deformations in the observed pastes are rather temperature and mixture dependent but, unlike the setting, less affected by the polymer type, retarded setting helps minimizing the risk of early cracks.

The research has shown that a reasonable mixture composition as well as the admixture setup can improve the robustness against effects of the ambient temperature on performance and performance retention. Furthermore, influences on the early properties caused by the superplasticizer type have been shown. These results, however, were demonstrated on the basis of binder pastes, which do not have to be representative for the respective concrete mixes, particularly at low temperatures, which in combination with the high PCE contents caused severe set

retardation. In order to show the relevance for the concrete scale, they have to be validated by concrete tests in future investigations.

References

[1] Schober, I. and Flatt, R.J. (2006), Studying Admixtures with the 5C Rheometer, 8th CANMET/ACI International Conference on Superplasticizers and other chemical Admixtures in Concrete, Malhotra, V.M. (Ed.), American Concrete Institute, pp. 93-104.

[2] Schober, I. and Flatt, R.J. (2006), Optimizing Polycaboxylate Polymers, 8th CANMET/ACI International Conference on Superplasticizers and other chemical Admixtures in Concrete, Malhotra, V.M. (Ed.), Am. Conc. Institute, pp. 169-184.

[3] Plank, J. and Hirsch, C. (2007), *Cem. Conc. Res.*, vol 37, n. 4, pp. 537-542.

[4] Plank, J., Bassioni, G., Dai, Z., Keller, H., Sachsenhauser, B. and Zouaoui, N. (2006), Recent advances in interactions between cement and polycarboxylate superplasticizers, 16th International Conference on Building Materials - ibausil, Stark, J. (Ed.), FIB, vol. I, pp. 579-598 (in German).

[5] Yamada, K., Ogawa, S. and Hanehara, S. (2001), *Cem. Conc. Res.* vol. 31, n. 3, pp. 375-383.

[6] Petit, J.-Y., Khayat, K.H. and Wirquin, E. (2006), *Cem. Conc. Res.*, vol. 36, n. 5, pp. 832-841.

[7] bibm, CEMBUREAU, EFCA, EFNARC, ERMCO (2005), The European Guidelines for Self-Compacting Concrete, http://www.efnarc.org.

[8] Terpstra, J. (2005), Stabilizing self-levelling concrete with polysaccharide additive, 1st International Symposium on Design, Performance and Use of Self-Consolidating Concrete, Yu, Z.,Shi, C., Khayat, K.H., Xie, Y. (Eds.), RILEM Publications SARL, pp. 207-213.

[9] Wallevik, O.H., Kubens, S. and Mueller, F. (2007), Influence of cement-admixture interaction on the stability of production properties of SCC, 5th International RILEM Symposium on Self-Compacting Concrete, De Schutter, G., Boel, V. (Eds.), RILEM Publications SARL, pp. 211-216.

[10] Nunes, S., Figueiras, H., Milheiro Oliveira, P., Coutinho, J.S. and Figueiras, J. (2006), *Cem. Conc. Res.*, vol 36, n. 12, pp. 2115-2122.

[11] Hamada, D., Hamai, T., Shimoda, M., Shonaka, M. and Takahashi, H. (2006), Development of New Superplasticizer Providing Ultimate Workability, 8th CANMET/ACI Int.Conf. on Superplasticizers and other chemical Admixtures in Concrete, Malhotra, V.M. (Ed.), American Concrete Institute, pp. 31-50.

[12] Schmidt, W., Kuehne, H.-C. and Meng, B. (2009), Temperature related Effects on Self-Consolidating Concrete due to Interactions between Superplasticizers, supplemental Admixtures and Additions, 9th ACI International Conference on Superplasticizers and Other Chemical

Admixtures in Concrete - Suppl. Papers, Malhotra, V.M. (Ed.), American Concrete Institute, pp. 135 - 147.

[13] Okamura, H. and Ozawa, K. (1995), *Conc. Lib. of JSCE*, pp. 107-120.

[14] Schmidt, W., Kuehne, H.-C. and Meng, B. (2010), Influence of ambient temperature conditions on the effect of stabilising polymers in cementitious building materials, 13th International Congress on Polymers in Concrete, Aguiar, J.B., Jalali, A., Camoes, A., Ferreira, R.M. (Eds.), Univ. of Minho, pp. 240-248.

Selecting Admixtures to Achieve Application-Required Rheology

Eric Koehler, Ara Jeknavorian and Stephen Klaus

W.R. Grace & Co., Cambridge, MA, USA

Abstract. SCC can encompass a wide range of concrete rheology. Previous research has shown the importance of specific rheological characteristics for application requirements such as reduced formwork pressure, increased static and dynamic segregation resistance, and increased pumpability. The required rheological characteristics for different applications are discussed in terms of yield stress, plastic viscosity, and thixotropy. Micromortar rheology measurements were conducted with four different high-range water reducers (HRWR) and two different water/cement ratios to demonstrate potential differences in rheology due to HRWR selection. The results indicated that HRWR selection can significantly impact micromortar rheology.

Introduction

Concrete must be able to flow under its own mass, pass through reinforcement, and resist segregation in order to be considered self-consolidated concrete (SCC). However, SCC can be further optimized for individual application requirements, such as for reduced formwork pressure, increased static and dynamic segregation resistance, and improved pumpability. Therefore, the rheology of SCC can vary widely based on application requirements or even regional preferences [1]. Mixture proportions can be altered in numerous ways to achieve the desired SCC rheology [2]. In particular, admixture selection can impact rheology [3-5]. In this paper, the effects of four different commercially available high-range water reducers (HRWRs) on the rheology of micromortar are examined.

Rheology of SCC

SCC rheology is typically measured in terms of static yield stress, dynamic yield stress, plastic viscosity, and thixotropy [6]. Static yield stress is defined as the

K.H. Khayat and D. Feys (eds.), *Design, Production and Placement of Self-Consolidating Concrete*, RILEM Bookseries 1,
DOI 10.1007/978-90-481-9664-7_7, © RILEM 2010

minimum stress to initiate flow from rest. Dynamic yield stress is the minimum stress to maintain flow. Plastic viscosity expresses the increase in shear stress with increasing shear rate once the yield stress has been exceeded. The difference between static and dynamic yield stress is due to thixotropy, which is defined as the reversible, time-dependent decrease in viscosity at a given shear rate. When a thixotropic material is at rest, a three-dimensional network structure develops over time due to factors such as colloidal forces. The application of shear causes a breakdown of this network structure and a reorientation or deformation of particles or flocs, resulting in a reduction in viscosity at a constant shear rate or shear stress. After shear is applied for sufficient time, the material reaches an equilibrium condition where the viscosity is at a minimum for the given shear rate or shear stress. When the application of shear is stopped, the three-dimensional network structure reforms and the original viscosity is eventually restored [7].

SCC can exhibit high formwork pressure due to its high flowability [8-12]. The maximum possible formwork pressure is hydrostatic pressure, which is the product of the concrete density and the height of concrete above the given point. Not all SCC mixtures exhibit hydrostatic pressure. The extent of horizontal pressure depends on the rheological properties of the concrete and changes in these rheological properties over time [9-12]. When concrete is at rest in forms, the gradual build-up of a thixotropic structure results in an increase in the static yield stress. Concrete is typically placed in forms gradually in lifts, which allows sufficient time for the build-up of a thixotropic structure and a reduction in formwork pressure in the lower lifts before the upper lifts are placed. Therefore, both thixotropy and static yield stress have been related to formwork pressure [10-12]. To reduce the extent of horizontal formwork pressure, SCC mixtures should exhibit low dynamic yield stress in order to flow under their own mass and a fast increase in static yield stress due to thixotropy for reduced formwork pressure [10].

Segregation resistance can be described in terms of dynamic segregation resistance when concrete is flowing or static segregation resistance when concrete is a rest. Dynamic segregation resistance has been shown to increase with increased yield stress and plastic viscosity, reduced maximum aggregate size, improved aggregate grading, and reduced difference in density between paste and aggregate [13].

Static segregation resistance is achieved when the downward gravitational force acting on an individual aggregate particle is offset by an upward buoyant force and the rheology of the paste [14-16]. Additionally, the lattice effect – that is, the effect of neighboring aggregate particles – can reduce segregation potential. The descent of an individual particle in a Bingham fluid has been related to a minimum yield stress [6, 16]. If the yield stress is too low to prevent a particle from settling, the rate of settlement is a function of viscosity. When concrete is placed and comes to rest at its final location, the static yield stress increases due to thixotropy, which results in increased segregation resistance over time. Immediately after the

concrete comes to rest, the dynamic yield stress is equal to the static yield stress. Therefore, thixotropy is important to ensuring segregation resistance. Since low dynamic yield stress is important for ensuring self-flow in SCC, it is typically advantageous to increase thixotropy while maintaining low dynamic yield stress in order to prevent static segregation. Further, the robustness of SCC with respect to segregation resistance has been shown to be dependent on mixture proportions, including HRWR selection, based on the workability box concept [4].

Concrete pumpability has been shown to be a function of plastic viscosity and yield stress [16, 17]. Decreasing plastic viscosity reduces the pump pressure to achieve a given flow rate or increases the flow rate at a given pump pressure. However, if plastic viscosity is too low such that the concrete is no longer stable, blockage of the pump can occur. In addition, mixtures with high viscosity are often described qualitatively as being sticky or cohesive.

Experimental Methods

Rheology measurements were conducted on micromortar mixtures, which consisted of ordinary Portland cement, water, fine silica sand with maximum size of 0.4 mm, and HRWR. The micromortars were prepared at water/cement (w/c) of 0.40 and 0.50 (Table I). For each w/c, three different commercially available polycarboxylate-based HRWRs (denoted PC-4, PC-5, and PC-8) and one commercially available naphthalene-based HRWR (denoted NSFC) were tested at four different dosages each. The HRWR dosages varied among HRWR and were selected to achieve a range of yield stresses typical of the micromortar in SCC. All HRWR dosages were expressed as percent HRWR solids on cement (% s/c).

Table I. Micromortar Mixture Proportions (% volume).

w/c	Cement	Sand	Water
0.40	24.3	45.0	30.6
0.50	22.6	41.8	35.6

A bench-top laboratory rheometer with vane geometry was used. The vane had four blades and was 25 mm in diameter and 37.5 mm in height. The outer cup had a diameter of 27.5 mm. The vane was positioned with a 12.4 mm vertical gap from the bottom of the cup. A water bath maintained the temperature of the micromortar at 23°C.

Each rheology test consisted of a pre-shear, rest period, and shear rate sweep. The pre-shear was used increase the consistency of shear history after loading material into the rheometer. The purpose of the rest period was to allow a build-up of the

thixotropic structure following the standard pre-shear. The shear rate sweep was used to determine rheological parameters.

Immediately after the completion of mixing, micromortar was loaded into the rheometer and pre-sheared at a shear rate of 50 s^{-1} for 30 s. The micromortar was then left undisturbed for a 300 s rest period. The shear rate sweep involved increasing and then decreasing the shear rate from 5 to 30 to 5 s^{-1}. The up and down sweeps each consisted of 7 equally spaced shear rates. Each shear rate was maintained for 3 s for the up sweep and 7 s for the down sweep, with torque and rotation speed measurements recorded for the last 2 s of each shear rate increment. However, the maximum shear rate of 30 s^{-1} was maintained for 62 s to ensure full breakdown of the thixotropy structure.

Dynamic yield stress and plastic viscosity were calculated based on the Bingham model from the down sweep portion of the shear stress versus shear rate curve. Thixotropy was calculated as the area between the up and down sweep shear stress versus shear rate curves between shear rates of 6 and 24 s^{-1} [7]. A typical rheometer test result is shown in Figure 1. No visible segregation was observed during the testing.

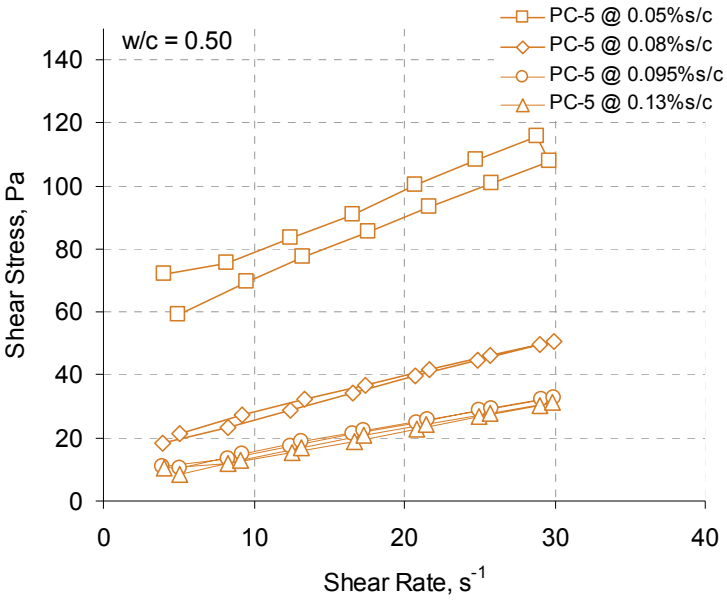

Figure 1. Typical rheometer measurements.

Experimental Results and Discussion

The use of micromortar rather than concrete allowed a more direct comparison of the effects of HRWR on rheology. For example, Erdem et al. [18] provided a summary of past published research using micromortar to predict concrete properties. Other research has shown the effect of HRWR on concrete rheology directly [4].

Figures 2 and 3 show that increasing the HRWR dosage resulted in reduced yield stress and plastic viscosity for all w/c and HRWRs combinations. The reductions in yield stress and plastic viscosity with increased HRWR dosage were due to the release of water between previously flocculated cement particles, which itself resulted from increased inter-particle repulsive forces within the cement floc. As expected, micromortar mixtures with increased w/c exhibited lower yield stress and plastic viscosity.

Figure 4 shows that with only a few exceptions (PC-8 at w/c of 0.50 and PC-4 at the highest dosage for both w/c), increasing the HRWR dosage reduced thixotropy. Because thixotropy is caused by the reversible formation of a flocculated structure driven by Brownian motion, the greater dispersion of cement particles through HRWR addition or the greater separation between particles due to higher w/c resulted in reduced thixotropy.

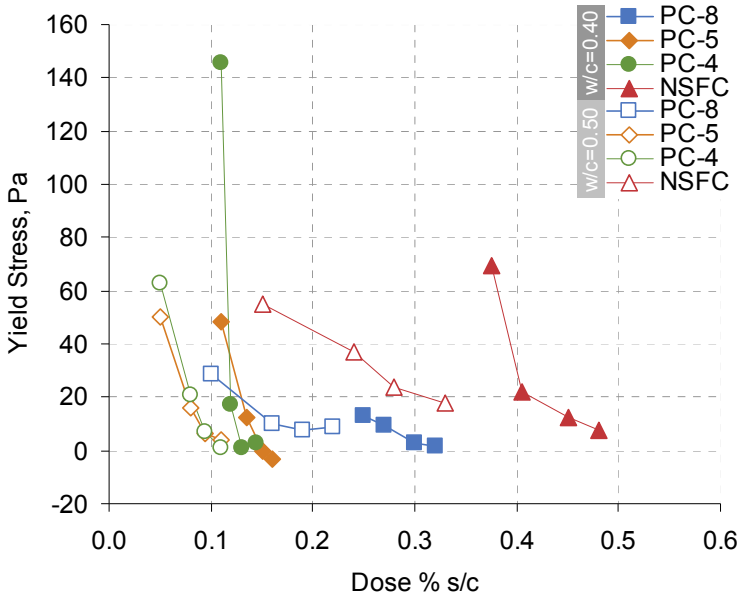

Figure 2. Effect of HRWR dose on dynamic yield stress.

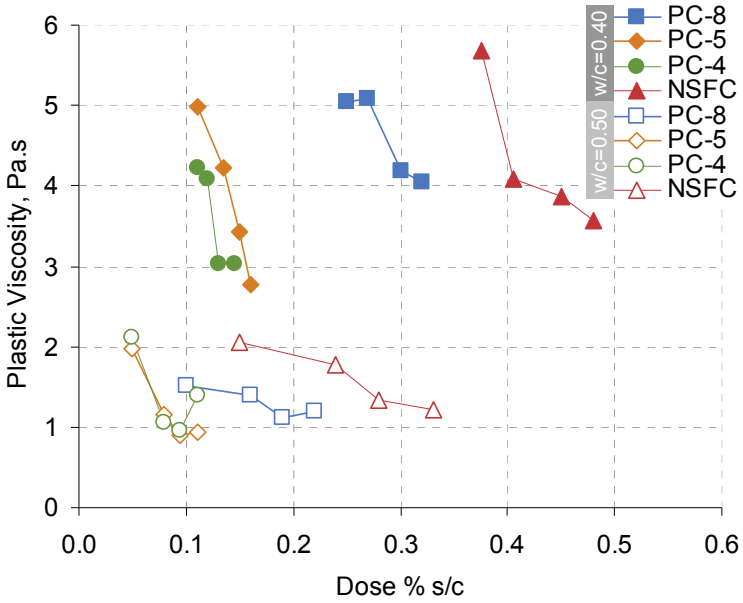

Figure 3. Effect of HRWR dose on plastic viscosity.

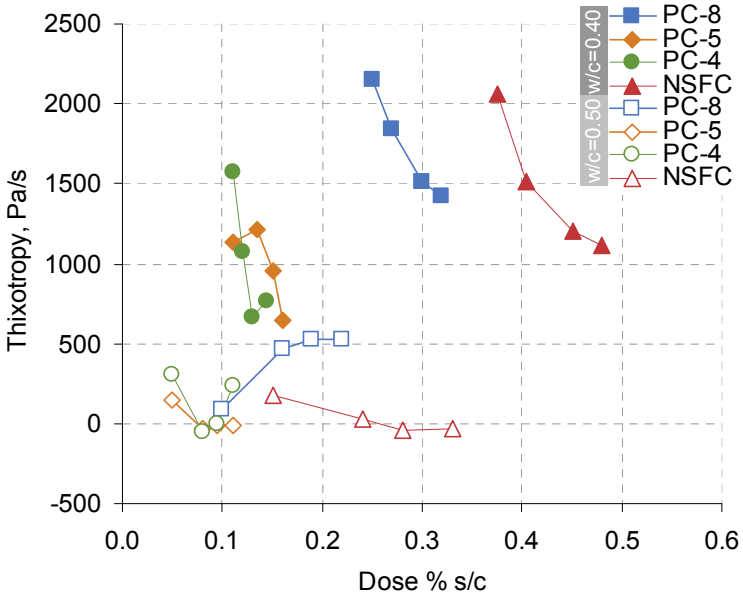

Figure 4. Effect of HRWR dose on thixotropy.

It was possible to reduce the yield stress to near zero for all HRWRs. For a given yield stress, however, plastic viscosity and thixotropy varied widely depending on the w/c and HRWR, as shown in Figures 5 and 6. The yield stress of micro-mortar must be near zero to enable concrete to flow under its own mass and be considered SCC; however, plastic viscosity can vary widely and the concrete still be considered SCC. Differences in plastic viscosity or thixotropy at a given yield stress can be used to optimize rheology for specific applications.

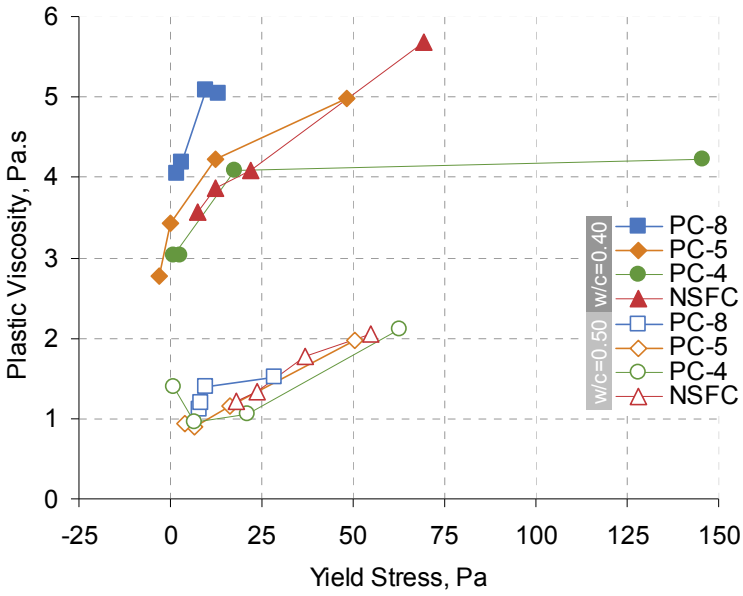

Figure 5. Comparison of dynamic yield stress and plastic viscosity.

As expected, higher w/c at a given yield stress resulted in lower plastic viscosity and thixotropy. For a given yield stress and w/c, the polycarboxylate-based HRWRs could be ranked in order of increasing plastic viscosity as PC-4 < PC-5 < PC-8. The plastic viscosity of NSFC was generally between that of PC-4 and PC-5. The higher viscosity associated with PC-5 and PC-8 may be beneficial in reducing static and dynamic segregation. The lower plastic viscosity associated with PC-4 may be suitable where reduced stickiness or greater pumpability is desired. For a given yield stress and w/c, the polycarboxylate-based HRWRs could be ranked in order of increasing thixotropy as PC-4 < PC-5 < PC-8. The thixotropy of NSFC was generally similar to that of PC-5. The higher thixotropy associated with PC-5 and PC-8 may be beneficial for reduced formwork pressure and higher static and dynamic segregation resistance. Although not measured in this testing, the NSFC HRWR would be expected to exhibit shorter workability retention and a longer delay in setting time relative to the three PC-based HRWRs.

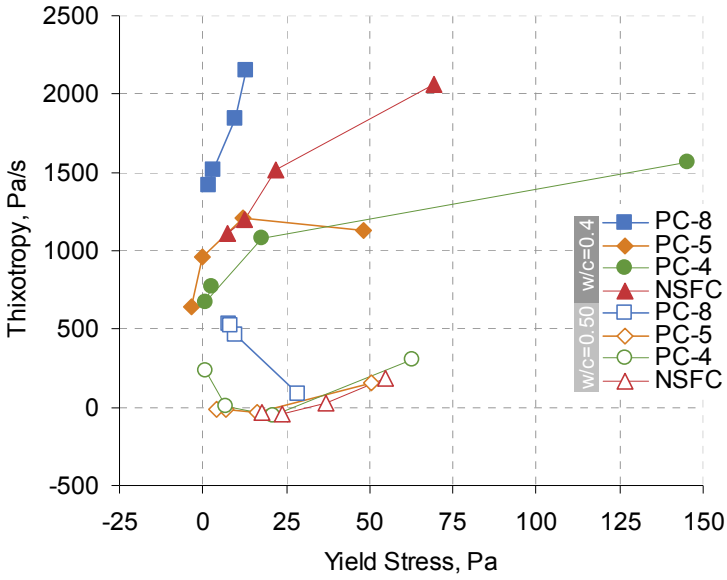

Figure 6. Comparison of dynamic yield stress and thixotropy.

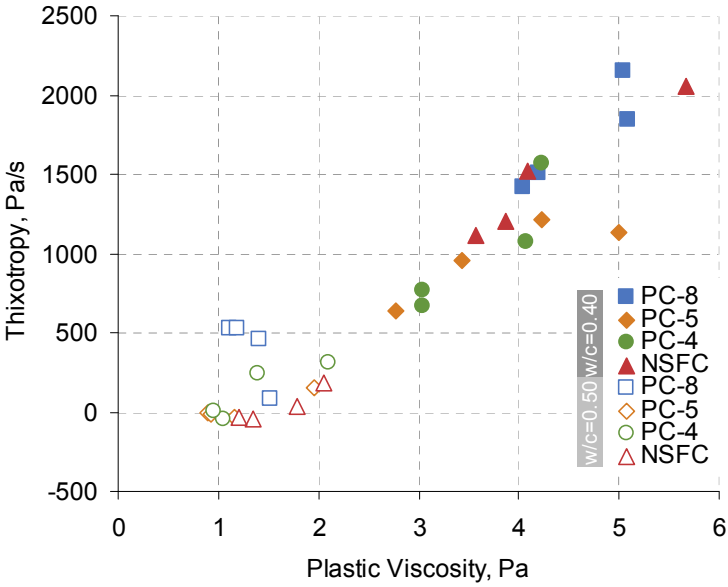

Figure 7. Relationship between plastic viscosity and thixotropy.

Figure 7 shows that thixotropy and plastic viscosity were correlated when w/c and HRWR were changed. The increased spacing between cement particles – whether due to lower solid particle content or increased inter-particle repulsive forces between cement particles – resulted in both lower plastic viscosity and thixotropy. Further test data are needed to determine whether this correlation is valid across other changes in mixture proportions. It should be noted that PC-8 provided increased thixotropy at lower plastic viscosities, which may allow increased pumpability without sacrificing segregation resistance or formwork pressure characteristics.

Conclusions

Rheological measurements showed that different HRWRs resulted in significantly different micromortar rheology. All HRWRs were capable of reducing the yield stress to near zero, which is necessary to ensure that concrete flows under its own mass. However, there were large differences in plastic viscosity and thixotropy for the different HRWRs. Therefore, HRWR selection can be important in optimizing application-specific SCC requirements, such as reduced formwork pressure, increased static and dynamic segregation resistance, and improved pumpability. Plotting plastic viscosity and thixotropy against yield stress is one way of comparing the rheology of different micromortar or concrete mixtures. Further, results from micromortar rheology measurements should be confirmed in concrete mixtures.

References

[1] Wallevik, O. (2005), Why Is SCC Different from Country to Country?, Proceedings of SCC 2005, ACBM, Chicago, IL.

[2] Koehler, E.P. and Fowler, D.W. (2007), ICAR Mixture Proportioning Procedure for SCC. International Center for Aggregates Research (Report 108-1F), Austin, TX.

[3] Mikanovic, N. and Jolicoeur, C. (2008), Influence of Superplasticizers on the Rheology and Stability of Limestone and Cement Pastes, *Cement and Concrete Research*, vol. 38, pp. 907-919.

[4] Jeknavorian, A.J., Koehler, E.P., Geary, D. and Malone, J. (2008), Concrete Rheology with High-Range Water Reducers With Extended Slump Flow Retention, Proceedings of SCC 2008, Chicago, IL.

[5] Khayat, K.H. and Assaad, J. (2006), Effect of w/cm and High-Range Water-Reducing Admixture on Formwork Pressure and Thixotropy of Self-Consolidating Concrete, *ACI Materials Journal*, vol. 103, pp. 186-193.

[6] Koehler, E.P. and Fowler, D.W. (2008), Static and Dynamic Yield Stress Measurements of SCC, Proceedings of SCC 2008, Chicago, IL.

[7] Barnes, H.A. (1997), Thixotropy – A Review, *Journal of Non-Newtonian Fluid Mechanics,* vol. 70, pp. 1-33.

[8] Tejeda-Dominguez, F. and Lange, D.A. (2005), Formwork Pressure of SCC for Tall Wall Field Applications. *Journal of Transportation Research Record,* vol. 1914, pp. 1-7.

[9] Khayat, K. and Assaad, J. (2005), Use of Rheological Properties of SCC to Predict Formwork Pressure, Proceedings of SCC 2005, Chicago, IL.

[10] Koehler, E.P., Keller, L. and Gardner, N.J. (2007), Field Measurements of SCC Rheology and Formwork Pressures, Proceedings of the SCC 2007 Conference, Ghent, Belgium.

[11] Roussel, N. (2006), A Thixotropy Model for Fresh Fluid Concretes: Theory, Validation and Applications. *Cement and Concrete Research*, vol. 36, pp. 1797-1806.

[12] Billberg, P. (2007), Form Pressure Generated by Self-Compacting Concrete — Influence of Thixotropy and Structural Behavior at Rest, Doctoral Thesis, Royal Institute of Technology, Stockholm.

[13] Shen, L., Struble, L. and Lange, D. (2009), Modeling Dynamic Segregation Resistance of Self-Consolidating Concrete, *ACI Materials Journal*, vol. 106, pp. 375-380.

[14] Shen, L., Struble, L. and Lange, D. (2009), Modeling Static Segregation Resistance of Self-Consolidating Concrete, *ACI Materials Journal,* vol. 106, pp. 367-374.

[15] Saak, A.W., Jennings, H.M. and Shah, S.P. (2001), New Methodology for Designing Self-Compacting Concrete, *ACI Materials Journal*, vol. 98, pp. 429-439.

[16] Koehler, E.P., Brooks, W., Mogan, E. and Neuwald, A. (2009), Application of Rheology Measurements to Enable and Ensure Concrete Performance, Proceedings of the NRMCA Concrete Technology Forum, Cincinnati, OH.

[17] Feys, D., De Schutter, G. and Verhoeven, R. (2009), Rheology and Pumping of Self-Compacting Concrete, Proceedings of Tenth ACI International Conference on Recent Advances in Concrete Technology and Sustainability Issues, Seville, Spain.

[18] Erdem, T.K., Khayat, K.H. and Yahia, A. (2009), Correlating Rheology of Self-Consolidating Concrete to Corresponding Concrete Equivalent Mortar. *ACI Materials Journal*, vol. 106, pp. 154-160.

Theme 3: Rheology and Workability of SCC

Effect of Cement on Superplasticizer Adsorption, Yield Stress, Thixotropy and Segregation Resistance

Dirk Lowke, Thomas Kränkel, Christoph Gehlen and Peter Schießl

Technische Universität München, Centre for Building Materials (cbm), Munich, Germany

Abstract. The successful application of self-compacting concrete depends more and more on the exact knowledge of the rheological properties during mixing, handling and placement. Rheological investigations with mortar compositions of similar flowability reveal that different Portland cements of similar fineness affect static yield stress and thixotropy differently. Higher amounts of superplasticizer added to adjust flowability reduce the static yield stress and thixotropy of the mortar and the segregation resistance of the equivalent concrete. This behaviour can be explained by superplasticizer adsorption and surface coverage by the adsorbed polymer on the cement particles. Surface coverage affects inter-particle forces as well as nucleation probability at the surface. An increase in superplasticizer dosage leads to a higher surface coverage by polymers. At higher surface coverage the effective layer thickness increases and causes a reduction in the maximum attraction between the particles. Furthermore, the number of available nucleation sites decreases and the bridging distance between the particles increases. Less force is needed to disperse the particles, static yield stress and thixotropy become lower. The results illustrate the importance of understanding the inter-particle interactions in concrete if rheological properties, workability and segregation resistance are to be controlled.

Thixotropy and Yield Stress

The yield stress τ_0 is defined as the minimum shear stress necessary to cause a liquid to flow. At stresses τ above this value, the additional shear stress (τ - τ_0) applied to the liquid determines the flow rate. The yield stress originates in the microstructure of the fluid which is able to store mechanical work as deformation energy. In cementitious suspensions, such structures form between the powder particles and early hydration products. From a rheological point of view, these structures may be regarded as rigid solid bodies which determine the behaviour of

K.H. Khayat and D. Feys (eds.), *Design, Production and Placement of Self-Consolidating Concrete*, RILEM Bookseries 1,
DOI 10.1007/978-90-481-9664-7_8, © RILEM 2010

the fluid at low shear rates. Thus the application of a low stress to such a non-Newtonian fluid does not immediately result in viscous flow, but viscoelastic behaviour, Figure 1 left. The stress gradually increases with deformation. Destruction of the structure and viscous flow at constant shear stress occur after prolonged application of shear.

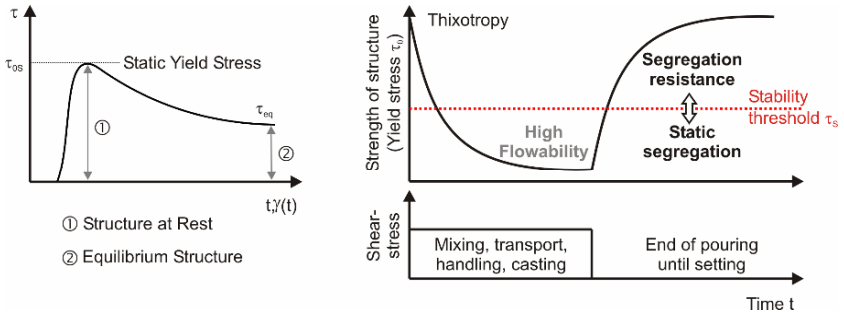

Figure 1. Evolution of shear stress τ at a very low constant shear rate and static yield stress τ_{0S} (left) and microstructural strength during production of concrete members (right).

The yield stress of cementitious suspensions varies with time, a behaviour known as thixotropy. In general, thixotropy is the ability of a previously undisturbed fluid to (a) reduce shear resistance during the application of constant shear stress or deformation and (b) to regain the original state in a finite time interval after shear has been removed, Figure 1 right. This time dependent change in shear resistance may be explained by reversible changes in the strength of the microstructure caused by shear. Shear results in the destruction of part of the undisturbed microstructure which reforms after the termination of shear [1, 2]. Recent research [3, 4] indicates that the build-up of a percolation network with time is mainly caused by nucleation of hydration products between the powder particles. Owing to the thixotropy of cementitious suspensions, it is necessary to distinguish between static and dynamic yield stress [2, 5, 6]. The static yield stress τ_{0S} characterizes the stress which must be overcome to set the undisturbed microstructure in motion. The dynamic shear stress τ_{0D} characterizes the minimum shear stress needed to maintain the flow of a fluid already in motion or the shear stress necessary to set a fluid in motion after a short rest period.

The static yield stress is larger than the dynamic yield stress because the complete undisturbed structure must be overcome at the beginning, Figure 1 left. Part of the undisturbed structure is already destroyed in the case of the dynamic yield stress. The magnitude of the static yield stress depends on the time elapsed since the shear was removed. The structure reforms progressively until a maximum shear stress is reached [2]. Immediately after the structure has been destroyed, the static yield

stress is equivalent to the dynamic yield stress. It is possible to draw conclusions on thixotropy by evaluating the static yield stress as a function of time.

Low yield stress is necessary to achieve self-compacting concrete. This enables entrapped air to escape and gives a good self-leveling ability. These requirements impose an upper limit on the yield stress. Opposed to this, the yield stress must be sufficiently high to prevent segregation of the coarse aggregate particles which therefore imposes a lower limit on yield stress [7]. This is determined by the shear stress at the surface of the largest aggregate particles. Thixotropy is particularly important if the critical yield stresses required for flowability and segregation resistance are very close. During concreting, pronounced thixotropic behaviour can lead to a very low yield stress which provides the required workability and air removal properties, Figure 1 right. A rapid increase in yield stress is then possible during the subsequent rest period in the formwork enabling a high segregation resistance. Thixotropy permits the production of highly flowable concrete with a high segregation resistance.

Materials and Methods

Three Portland cements and ground limestone as a mineral addition were used in the investigations. The density of the materials was determined by helium pycnometry, the mineralogical composition by X-ray diffraction and the mean particle diameter of the powder materials by laser granulometry, Table I. Quartz sand with a 0/2 mm grading and a density of 2.6 g/cm³ were used with 4/16 mm river gravel having a density of 2.8 g/cm³. The mixes were prepared with a commercial polycarboxylate ether based superplasticizer (SP) with 35% solids in aqueous solution and a mean molecular mass of 44.500 g/mol.

Table I. Characteristics of powder materials.

	Alite [wt.%]	Belite [wt.%]	C_3A [wt.%]	C_4AF [wt.%]	$CaSO_4$ [wt.%]	ρ [g/cm ³]	d_{50} [µm]
CEM.A	62.3	10.5	8.0	6.7	4.3	3.1	13.3
CEM.B	68.8	5.2	8.7	6.1	3.8	3.1	15.2
CEM.C	69.6	5.2	5.3	10.8	4.4	3.1	18.9
Ground limestone	-	-	-	-	-	2.8	5.3

In the first series of investigations, three mortars were prepared using the different cements (150 L/m³) with 150 L/m³ ground limestone, 300 L/m³ water and 400 L/m³ sand. The volumetric water-to-powder ratio V_w/V_p was 1.0 and the *w/b* was 0.35. The slump flow with the mini cone (8 min after water addition) was adjusted to 255 ± 5 mm by varying the superplasticizer dosage, Table II. The

investigations aimed to quantify the effect of the three cements on yield stress and thixotropy at similar workability. The robustness of the mortar with respect to water overdosage was investigated by increasing the water content of the three mortars by 15 L/m^3 without changing superplasticizer dosage. An increase in water content of this order of magnitude, caused by, for example, inaccurate determination of the moisture content of the sand, is relevant to field practice. The amount of additional water chosen reflects the range of overdosage occurring in construction practice.

In order to determine the segregation resistance of the corresponding concretes, mixes were prepared by adding coarse aggregate to the three mortars. The concretes contained 67.8 vol.% mortar and 32.2 vol.% 4/16 mm gravel. The superplasticizer dosage was adjusted to yield a slump flow of 710 ± 15 mm. The effect of water overdosage on segregation resistance also was investigated with the concretes. The water content of the concretes was raised by 10 L/m³ equivalent to 15 L/m³ with respect to the volume of mortar in the mix. Again, the amount of superplasticizer was kept constant.

Table II. SP dosage, SP adsorption and flowability of mortar and concrete.

Mortar	Designed water content Comparable flowability 255 ± 5 mm			Increased water content +15 L/m³ SP content unmodified		
Cement	CEM.A	CEM.B	CEM.C	CEM.A	CEM.B	CEM.C
SP [wt.%$_{CEM}$]	0.52	0.38	0.31	0.50	0.38	0.31
SP adsorbed [mg/g]	0.57	0.49	0.40	-	-	-
Mini slump [mm]	252	258	255	289	289	295
Concrete	**Designed water content Comparable flowability 710 ± 15 mm**			**Increased water content +10 L/m³ SP content unmodified**		
Cement	CEM.A	CEM.B	CEM.C	CEM.A	CEM.B	CEM.C
SP [wt.%$_{CEM}$]	0.62	0.56	0.44	0.62	0.56	0.44
Slump flow [mm]	708	705	721	771	764	761

In addition, three pastes with the same composition of cement, limestone and water as the mortars and concretes were prepared to determine superplasticizer adsorption. Pore solution was expressed from the pastes 15 min after water addition [8]. The total organic carbon (TOC) content of the pore solution and the superplasticizer solution were determined by high-temperature oxidation of the organic ingredients. The amount of adsorbed superplasticizer was calculated as the difference between the TOC of the added superplasticizer solution and the pore solution of the mortar.

The rheological measurements of static yield stress and thixotropy were performed 10 min after water addition using a rheometer with a rotating ball with a radius r of 10 mm, see Figure 2 left. The ball geometry was used to simulate aggregate sedimentation in self-compacting concrete, i.e. the geometrical boundary conditions during sedimentation are incorporated in the rheological measurement. Before commencing the measurements, the mortar was subjected to high shear stress for 30 s in order to break up agglomerates (structural breaking) enabling the subsequent observation of structure formation. The measurement of static yield stress starts 30 s after structure breaking. The force of resistance F_{res} needed to move the ball through the mortar suspension was measured after waiting periods of 35, 60, 120 and 150 s during which the mixture was at rest. Each measurement was performed at the very low rotational speed of $5 \cdot 10^{-4}$ m/s ($\dot{\gamma} \approx 0.05$ s^{-1}). Owing to the low shear rates used in the investigations, the resistance force F_{res} measured is mainly due to the intrinsic yield stress of the mortar. Neglecting the shear force due to the rotational motion, an upper bound of static yield stress τ_{0S} was calculated from the results of the rheological investigations using $\tau_{0S} = Y_G F/(2 \pi r^2)$, $Y_G = 0.14334$, according to [9]. In addition, the dynamic yield stress was calculated from the slump flow measurements using $\tau_{0D} = 225 \rho g V^2/(128 \pi^2 R^5)$, according to [10]. The first derivative of the yield stress as a function of time is a measure of the thixotropy A_{thix}.

The segregation stability was assessed for the mortars with the ball penetration test in which the free penetration depth of a sphere of defined diameter and density was measured [11, 12]. The density of 2.75 g/cm^3 and diameter of 15 mm of the sphere correspond to the coarse aggregate particles, so the test simulates the segregation behaviour of the coarse aggregate.

The segregation behaviour of the self-compacting concretes was determined using the cylinder segregation test in which the concrete is poured into three vertically stacked cylinders with a total height of 450 mm [11, 13]. After a given segregation time, the individual cylinders are separated and the content of coarse aggregate determined for each cylinder. The degree of segregation Δm is the maximum deviation of the coarse aggregate from the average content for the whole concrete specimen.

Results and Discussion

The dynamic yield stress and development of static yield stress τ_0 during variations of the rest period after destruction of the microstructure (mixing time 30 s) are shown in Figure 2 right. The dynamic yield stresses ($t_P = 0$) for the different mortars with the designed water content (open symbols) are similar at 9.7 ± 0.6 Pa. Afterwards, the static yield stress increases with the duration of the rest period (thixotropy) and dependent on the cement used. The mortars increased their static yield stress by a factor of 5 to 12 within a few minutes. 150 s after structure

breaking, the yield stress of the mortars with the designed water ranges from 55 Pa (CEM.A) to 121 Pa (CEM.C). As already mentioned, robustness with respect to water overdosage was determined by adding 15 L/m^3 water to each mix, Figure 2 right. As expected, a considerable loss of yield stress and thixotropy occurred, but the order of the different cements was preserved.

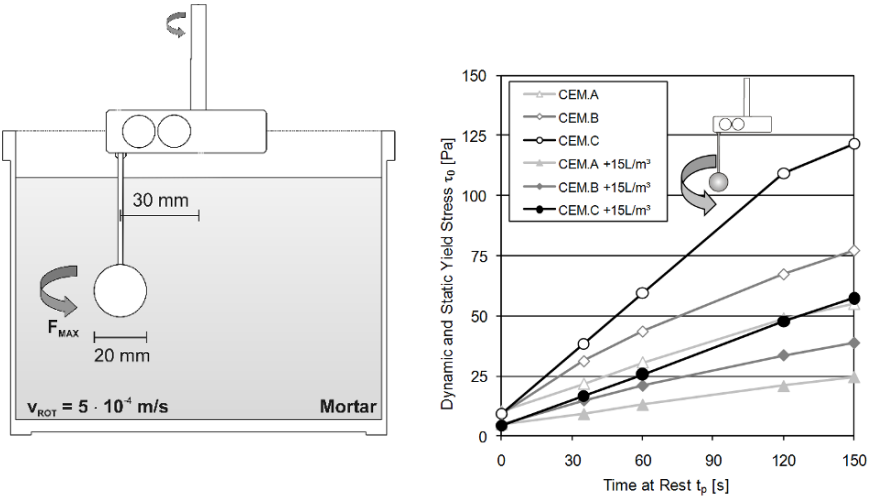

Figure 2. Rheometer for the measurement of static yield stress and thixotropy (Schleibinger) (left) as well as dynamic ($t_p = 0$) and static yield stress of mortar with three Portland cements in dependence of time at rest after structural breaking. Open symbols: designed water content, full symbols: with water overdosage (left).

Interestingly, the relative residual yield stress (ratio of yield stress with additional water, to the one with designed water content $\tau_{0,15L} / \tau_{0,0L}$) is similar for all mixes, 46%, and does not vary significantly with time. This indicates that water addition does not affect the dispersion and bond strength of coagulated particles, but just the actual volume fraction Φ and thus the number of direct particle contacts. According to [14, 15, 16] the dependence of yield stress on volume fraction in weakly flocculated suspensions can be described by

$$\tau_0 = m \frac{\Phi(\Phi - \Phi_{perc})^2}{\Phi_{max}(\Phi_{max} - \Phi)} \tag{1}$$

where Φ_{max} is the geometrical maximum packing of the solids, Φ_{perc} is a percolation threshold, and m is a factor that accounts for inter-particle forces, particle size and particle size distribution. Since, in this case, $\tau_{0,15L} / \tau_{0,0L}$ is almost time independent, Eqn. (1) can be modified to predict both dynamic yield stress and the development of static yield stress $\tau_0(t)$. An additional factor $b(t) = (1+\lambda)$ is

introduced, following [2], which describes the change in bond strength with time, Eqn. (2).

$$\tau_0(t) = b(t) \cdot m \cdot \frac{\Phi(\Phi - \Phi_{perc})^2}{\Phi_{max}(\Phi_{max} - \Phi)} \tag{2}$$

The factor *b(t)* is independent of solid volume fraction, at least in the range decisive for robustness. By normalizing the static yield stress data using the value for the dynamic yield stress, the relative static yield stress $\tau_{0,S}(t)/\tau_{0D}$ of the mortars with designed water content is equal to the mortars with water overdosage, Figure 3 left. Since evolution of relative static yield stress $\tau_{0,S}(t)/\tau_{0D}$ for each cement is independent of volume fraction, it is concluded that the increase in strength of the microstructure is due to an increase in strength of direct particle contacts. The strength of particle bonding is governed by inter-particle forces and nucleation of hydration products between the particles.

The development of bond strength between the particles and thus thixotropy is strongly affected by cement and superplasticizer. A larger increase in yield stress, i.e. a more pronounced thixotropic behaviour, was observed for the mortars made with cement C and a low superplasticizer dosage than for the mortars with cement A and a higher superplasticizer dosage. This effect was investigated in more detail by determining the amount of superplasticizer adsorbed on the particle surfaces, Table II. The relationship between superplasticizer adsorption and thixotropy is shown in Figure 3 right. Smaller amounts of adsorbed superplasticizer appear to increase thixotropy of mortar of the same composition and flowability, but made with different cements of a comparable granulometry. This behaviour can be explained by surface coverage θ by the adsorbed polymer. Surface coverage affects inter-particle forces as well as nucleation probability at the surface. The effect on inter-particle forces is based on changes in average layer thickness of the adsorbed polymer at varying coverage. Sub-monolayer coverage relates to a thinner effective layer thickness. At low superplasticizer dosage, one can assume a linear relationship between dosage and surface coverage and thus effective layer thickness [17]. Assuming a comparable surface area, the investigated cements possess different surface coverage und layer thickness. Since the maximum inter-particle force is proportional to the inverse square of layer thickness ($F_{max} \propto \delta^{-2}$) [17], the inter-particle forces between particles increase with decreasing superplasticizer adsorption. If the maximum inter-particle force is compared with the thixotropy, we can observe a linear relationship, Figure 3 right. A decrease in superplasticizer dosage leads to a thinner polymer layer and therefore an increase in the maximum attraction between the particles. More force is needed to disperse the particles, static yield stress and thixotropy are higher. However, results of Roussel [3] and Oesterheld [4] indicate that the build-up of a percolation network over time is mainly caused by nucleation of hydration products between the powder particles. This would mean the increase of thixotropy at low

superplasticizer adsorption can be explained by an increase of available nucleation sites and a decrease of the bridging distance.

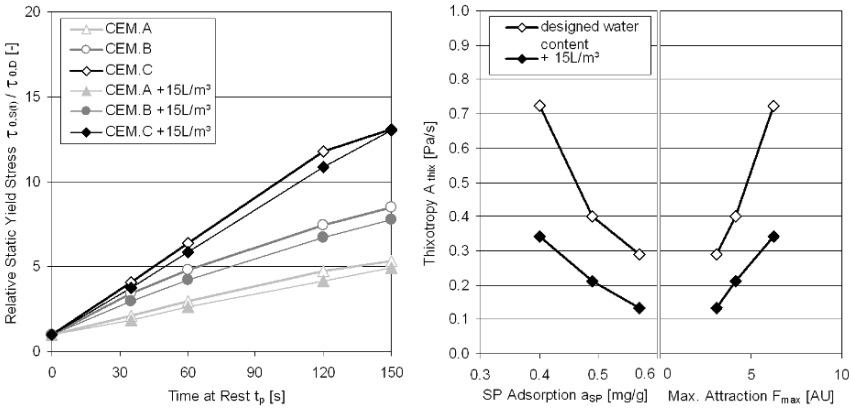

Figure 3. Relative static yield stress evolution $\tau_{0,S}(t)/\tau_{0D}$ (left) and thixotropy A_{thix} in dependence of superplasticizer adsorption a_{SP} and maximum attractive force F_{max} (right).

To demonstrate the significance of the rheological parameters on segregation resistance and robustness it will be shown how the bulk properties of concrete are determined by the rheological properties of the mortar. In the ball penetration test, no penetration was discernible for the as-designed mortars. Thus Figure 4 left just shows the results of the ball penetration test for the three cements in mortar with 15 L/m^3 additional water. It is apparent that the depth of penetration depends on the cement used and is echoed by the segregation behaviour of the corresponding concrete, Figure 4 right. None of the concretes made with the designed water content showed significant signs of segregation. In contrast, the additional 10 L/m^3 water in concrete made with cement A resulted in a 27% departure of the amount of coarse aggregate in the bottom cylinder from the average value, i.e. this concrete was no longer stable. However, more water in the concretes with cement B and C did not lead to instability.

The results of the ball penetration test and cylinder segregation test correlate very well. It is therefore possible to draw conclusions on the real sedimentation behaviour of concrete based on the properties of the mortar. Both the sedimentation behaviour of the concrete and the penetration of the ball in the mortar depend on the rheological properties of the mortar. The mortar must be able to support the mass of the coarse aggregate through the friction at the surface of the aggregate particles, whereby the yield stress, which depends on the size of the coarse aggregate, must not be surpassed [7]. Since the decrease in dynamic yield stress of mortar at water overdosage was independent of cement used, the

thixotropy becomes the main parameter with respect to segregation resistance of the concretes. Thus, the lower static yield stress and thixotropy (CEM.A < CEM.B < CEM.C), the lower is the segregation resistance at increased water content. With addition water, the concrete with cement C exhibited a distinctly higher stability than the concrete with cement A, Figure 4. This is because the resistance of the mortar with cement C was higher due to a much faster development of structure (thixotropy), Figure 3 left.

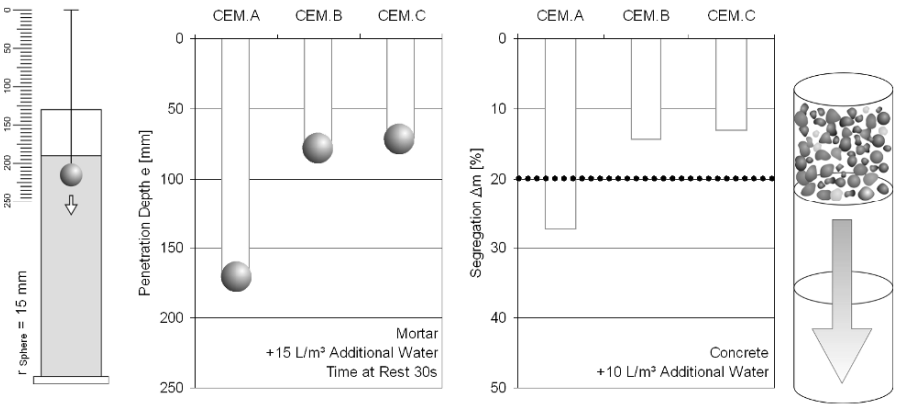

Figure 4. Ball penetration test with mortar, penetration depth in dependence of cement used (left) and cylinder segregation test with concrete, departure of coarse aggregate content Δm from average mixture value.

Conclusions

The relationship between concrete workability, the rheological properties of the corresponding mortar and the particle interactions responsible for the behaviour of fresh concrete are considered using self-compacting concrete as an example. Concretes of the same composition were mixed with different Portland cements of similar fineness where the superplasticizer dosage was varied to adjust flowability to a similar value. A reduction in static yield stress and thixotropy of the corresponding mortar was observed with superplasticizer dosage. This was clearly related to a reduction in the segregation resistance of the equivalent concretes.

Yield stress and thixotropy are determined by the interaction of particles in the suspension of cementitious materials. A correlation was found between thixotropy, superplasticizer adsorption and maximum attractive force between particles. An increase in superplasticizer dosage leads to a higher surface coverage by polymers. At higher surface coverage the effective layer thickness increases and causes a reduction in the maximum attraction between the particles. Furthermore, the

number of available nucleation sites decreases and the bridging distance between the particles increases.

The present results illustrate the importance of considering inter-particle interactions in order to understand fresh concrete properties like workability, segregation and formwork pressure - properties that are often difficult to control in field conditions. This is particularly necessary for better reliability in the production of high performance concrete such as SCC. By the choice of suitable combinations of cement and additions, knowledge of inter-particle interactions can help to control yield stress, thixotropy, robustness and thus the required behaviour of the final mix.

Acknowledgments

The authors would like to thank Prof. Olafur Wallevik, Dr. Robert Flatt and Dr. Robin Beddoe for the fruitful discussions about robustness and inter-particle forces. The work was financially supported by the German Research Foundation (DFG).

References

[1] Roussel, N. (2005), *Cem Con Res.*, vol. 35, n. 9, pp. 1656-1664.
[2] Roussel, N. (2006), *Cem Con Res.*, vol. 36, n. 10, pp. 1797–1806.
[3] Roussel, N. (2010), Lecture at DTU-RILEM Doctoral Course "Flow of fresh Cement-Based Materials", Lyngby, April 12-16, 2010.
[4] Oesterheld, S., Wallevik, J.E. and Wallevik, O.H. (2009), In: *Rheology of Cement Suspensions such as Fresh Concrete*, Rilem Pro 68, Rilem Publications, Bagneux, pp. 163-170.
[5] Billberg, P. (2005), In: *SCC 2005*, Proc. of the 4th Int. Rilem Symposium on SCC. Hanley Wood Publication, Addison, pp. 583-589.
[6] Orvalez, G. and Roussel, N. (2007), In: *SCC 2007*, Proc. of the 5th Int. Rilem Symposium on SCC, Rilem Publications, Bagneux, pp. 285-290.
[7] Roussel, N. (2006), *Materials and Structures*, vol. 39, n. 1, pp. 81-91.
[8] Lowke, D. and Schießl, P. (2009), In: *Rheology of Cement Suspensions such as Fresh Concrete*, Rilem Pro 68, Rilem Publications, Bagneux, pp. 45-54.
[9] Beris, A.N., Tsamopoulos, J.A., Armstrong, R.C. and Brown, R.A. (1985), *J. Fluid Mech.*, vol. 158, pp. 219-244.
[10] Roussel, N., Stefani, C. and Leroy R. (2005), *Cem. Con. Res.*, vol. 35, n. 5, pp. 817-822.
[11] Lowke, D., Kränkel, T. and Schießl, P. (2009), In: *Design, Performance and Use of SCC*, Rilem Pro 65, Rilem Publications, Bagneux, pp. 183-193.

[12] Lowke, D. (2004), In: *5th International PhD-Symposium in Civil Engineering*, A.A. Balkema Publishers, Leiden, pp.717-724.
[13] Lowke, D., Wiegrink, K.-H. and Schießl, P. (2003), In: *SCC 2003*, Proc. of the 3rd Int. Symposium on SCC, Rilem Pub. Pro 33, pp. 365-366.
[14] Flatt, J.R. and Bowen, P. (2006), *J. Am. Ceram. Soc.*, vol. 89, n. 4, pp. 1244-1256
[15] Flatt, J.R. and Bowen, P. (2007), *J. Am. Ceram. Soc.*, vol. 90, n. 4, pp. 1038-1044.
[16] Roussel. N., Lemaître, A., Flatt, J.R. and Coussot, P. (2010), *Cem. Con. Res.*, vol. 40, pp. 77-84.
[17] Kjeldsen, A.M., Flatt, J. R. and Bergström, L. (2006), *Cem. Con. Res.*, vol. 36, pp. 1231-1239.

Effect of Metakaolin on the Rheology of Self-Consolidating Concrete

A.A.A. Hassan, M. Lachemi and K.M.A. Hossain

Department of Civil Engineering, Ryerson University, Toronto, Canada

Abstract. This study deals with the rheological properties of self-consolidating concrete (SCC) incorporating various percentages of metakaolin (MK) and silica fume (SF) as a partial replacement of cement. Plastic viscosity and yield stress were evaluated at different slump flow values using a concrete viscometer. The effect of high range water reducing admixture (HRWRA) dosage and the total time for flow, the time to reach 500 mm diameter (T50), and the final diameter of the slump flow test were also investigated and studied in this research program. The results showed that the plastic viscosity and the yield stress increase with the increase of the percentage of MK. The results also demonstrated a correlation between the final slump flow diameter and the yield stress similar to that presented in the literature.

Introduction

Self-consolidating concrete (SCC) is a high performance high flowable concrete that can be placed and compacted under its self-weight with no vibration effort and achieves good consolidation without segregation even in a very congested structural member [1-3]. The production of SCC commonly involves using supplementary cementing materials (SCM) such as fly ash, slag and/or silica fume (SF) [4-6]. Silica fume is considered as one of the most effective and widely used SCM that greatly increases the strength and significantly reduces the concrete permeability. However, utilizing SF in SCC is of a limited use because of the difficulty in obtaining the desired SCC workability.

Metakaolin (MK) is a relatively new mineral admixture; it has been successfully used in concrete as (SCM) since 1990. MK has a comparable pozzolanic reactivity as that of SF which significantly modifies the concrete micro-structure and enhances the overall mechanical and durability performance of concrete [7-9]. Nowadays, the recent discovery of MK (known as whitemud) resources in

K.H. Khayat and D. Feys (eds.), *Design, Production and Placement of Self-Consolidating Concrete*, RILEM Bookseries 1,
DOI 10.1007/978-90-481-9664-7_9, © RILEM 2010

southern Saskatchewan (one of the largest deposits of kaolin in North America) allows MK to be used economically in concrete.

The particle size of MK is much finer than cement but not as fine as SF. Hence, MK may require less amount of high-range water-reducing admixture (HRWRA) than SF to obtain the same slump flow [10, 11]. MK has a number of other benefits as well; it has a creamier texture, generates less bleed water, and has better finishability than concrete with SF [10, 12]. Therefore, developing SCC containing MK is beneficial and requires more investigation since it is expected to have comparable mechanical and durability performance to SF concrete – at a lower price and with better workability.

A number of researchers have studied the workability of normal concrete containing MK. Some of them have concluded a loss of workability while others found either no effect or enhanced workability when using MK in concrete [13-16]. However, it is generally acknowledged that MK tends to adversely affect the workability of normal concrete but shows better workability than concrete with SF.

Caldarone et al. [10] found that concrete with MK requires 25 to 35% less HRWRA than concrete with silica fume to achieve a comparable slump of 120 to 180 mm at water to binder ratio of 0.36 to 0.38. The reduction in HRWRA demand resulted in MK concrete having less sticky consistency and better finish than SF concrete. Ding and Li [11] concluded that MK offered a much better workability than did SF for the same mixture proportions. Concrete mixtures with 5 to 10% MK had a slightly higher slump than the control mixture. Even when the replacement level of MK was increased to 15%, the slump was only decreased by approximately 10%. For SF concrete, the slump value showed only a small decrease at the replacement level of 5% and then decreased almost linearly with an increase of SF content to 15%.

The fresh properties of concrete containing MK were also tested by Balaguru [17]. MK concrete containing type I and II cements were investigated in his study. Balaguru concluded that for type I cement, the addition of MK resulted in either no influence or slight increase in slump. In the case of type II cement, MK reduced the slump slightly and the magnitude of the decrease was more pronounced in high strength concrete.

The viscosity and yield value of fresh concrete mixture are considered the main factors that influence the concrete workability. SCC mixture should have a low yield value to ensure high deformation and good flowability [18]. However, the yield value should not be very low otherwise segregation could occur under static conditions [19]. In addition, SCC require moderate to high viscosity in order to keep the mixture homogeneous and prevent segregation. Although segregation is not a factor in mixtures with very high viscosity, designing a very high viscosity

SCC warrants a reduction in the concrete flowability and workability. Meanwhile very low viscosity mixtures assure solid particles segregation. Therefore, a specific range of yield stresses and plastic viscosities should be maintained in order to produce successful SCC mixtures [20].

Cyr and Mouret [21] studied the rheological behavior of cement paste containing MK and SF in order to evaluate their potential for incorporation into SCC. Their results concluded that MK enhanced the viscosity of cement paste which is beneficial for SCC as it slows down the particles sedimentation and enhances the dispersion of solids in the plastic state. Their result also concluded that SF decreases the viscosity and increases the superplasticizers demand which makes this admixture incompatible with the properties expected for SCC.

Limited information about the rheological properties of SCC containing MK is available in the literature. The main objective of this research is to investigate the rheological properties of SCC containing various amount of MK (0, 3, 8, 15, and 25%) as a partial replacement of cement. The rheological properties of SCC containing 8% SF were also investigated for comparison. The tested mixtures were evaluated based on some fresh properties such as slump flow, time to reach 500 mm diameter (T50), and total slump flow time as well as the yield stress values and plastic viscosity using Contec concrete viscometer.

Experimental Program

Materials

The MK used in this investigation was delivered from southern Saskatchewan. The Sum of SiO_2, Al_2O_3, Fe_2O_3 in SF and MK were 90.3% and 93.6% respectively. Type GU Canadian cement similar to ASTM Type I was also used as cementitious materials. Natural sand and 10 mm maximum size stone were used as fine and coarse aggregates, respectively. The coarse and fine aggregates each had a specific gravity of 2.70 and water absorptions of 0.5 and 0.64%, respectively. High range water reducing admixture (HRWRA) similar to Type F of ASTM C 494 was used to adjust the flowability of SCC mixtures. The specific gravity, volatile mass, and pH of the HRWRA were 1.2, 62% and 9.5 respectively.

Mixture proportions and mixture details

The mixture proportions of SCC containing different percentages of MK and SF are presented in Table I. A total of 18 SCC mixtures were tested in this program.

Table I. Mixture proportions and the 28-day compressive strengths of the 650 mm slump flow diameter concrete mixtures.

Mixture ID	% of SCM (by mass)	w/b	Water, kg/m^3	Cement, kg/m^3	SCM, kg/m^3	Aggregates (kg/m^3)		28-day comp. strength, MPa
						Fine	Coarse	
Control	0%	0.4	180	450	0	930	900	40.2
8SF	8% (SF)	0.4	180	414	36	923	893	45.9
3MK	3% (MK)	0.4	180	436	13.5	929	899	39.4
8MK	8% (MK)	0.4	180	414	36	926	896	45.6
15MK	15% (MK)	0.4	180	382	67	923	893	45.9
25MK	25% (MK)	0.4	180	337	112	919	889	48.9

The 18 mixtures consisted of 6 main mixtures categorized by the amount of SCM as a partial replacement of cement. Each one of the 6 mixtures was divided into 3 mixtures that had different amounts of HRWRA to obtain variable slump flow values. The 6 main mixtures included four mixtures containing 3, 8, 15, and 25% of MK (3MK, 8MK, 15MK, and 25MK), one mixture containing 8% of SF (8SF), and one control mixture containing no SCM. The decision of choosing 8SF was based on a preliminary investigation which showed that 8% of SF was the best percentage in terms of 28-day compressive strength. The plastic viscosity, yield stress, amount of HRWRA, slump flow diameter, T50, and the total flow time of the slump flow were measured and recorded for each one of the 18 mixtures (Table II). The T50 and the total time of the slump flow test were recorded accurately using a video tape recorder. No air entraining admixtures were used in any mixture. The 28-day compressive strength and the fresh properties of all the tested mixtures are presented in Tables I and II.

Results and Discussions

Compressive strength

One additional mixture with a slump flow of around 650 ± 10 mm was performed for each of the 6 main tested concrete mixtures to obtain the 28-day compressive strength. Three 100 × 200 mm concrete cylinders were tested for each mixture and

Table II. Rheological properties of the tested mixtures.

	HRWR L/m^3	Viscosity, Pas	Slump Flow			Yield Stress Pa	At 3460 mL/m^3 HRWR	At 650 mm slump flow diameter			
			Ø mm	T50 mm	Total time, 's'		Yield stress, Pa	Visc., Pa.s	Total time, 's'	T50, 's'	HRWR mL/m^3
8SF	3.5	18.0	500	5.5	5.5	60.3	60.3	15.1	22.5	2.5	4600
	4.2	16.4	590	3	13.7	26.4					
	4.6	15.1	650	2.5	22.6	17.3					
Con-trol	1.9	17.7	475		3.4	63.8	21.3	15	22.5	2.4	3700
	2.7	15.6	570	3.5	10.8	36.6					
	3.6	15	645	2.5	21.9	17.2					
3MK	2.3	28.2	470		5.6	76.3	21.1	19	23.1	2.2	4100
	3.5	22.5	600	3	16.5	21.1					
	3.8	20.5	630	2.5	20.5	18.7					
8MK	3.5	26.5	560	3	8.8	35.1	35.1	21.5	23.8	2.7	4300
	4.0	25.2	610	3.2	15.8	22.1					
	4.4	20.6	660	2.6	25.5	15.8					
15MK	3.8	31.1	570	3.9	11.4	39.8	52.5	28	30.5	3.8	4430
	4.2	29.8	620	3.8	24.7	22.3					
	4.6	25.9	680	3.7	36.1	16.1					
25MK	3.1	36.3	325		2		69.0	36.5	36	4.4	4700
	3.5	39.9	500	7.1	7.1	69.0					
	5.0	37.1	685	3.8	43.9	17.4					

the average value was recorded (Table I). The results showed that the addition of MK increased the 28-day compressive strength of SCC. As the amount of MK increased, the 28-day compressive strength slightly increased. Replacement of cement by up to 25% of MK increased the compressive strength by about 22% compared to the control mixture. This result is in agreement with the findings of other researchers in which the increase of compressive strength with the increase of the percentage of MK was observed [16, 22]. Also, the addition of 8% SF was similar to that of 8% MK in terms of strength enhancement. Both 8SF and 8MK SCC mixtures obtained 14% extra compressive strength than that of the control mixture.

HRWRA

Table II presents the demand of HRWRA at 650 mm slump flow diameter (estimated from the relationship curves of the HRWRA demand versus slump flow diameter for each mixture) for each mixture type. As seen from the table, the demand of HRWRA increased by about 27% when the percentage of MK in SCC mixtures increased from 0 to 25%. However, the addition of MK appears to require less HRWRA than the addition of SF. The addition of 8% SF required 7% extra HRWRA than the addition of 8% MK. This result is in agreement with other studies which show that MK offers much better workability than SF for a given mixture proportions [10, 11].

Viscosity

After the viscosity was measured at different slump flow diameters for all tested mixtures, the viscosity at 650 mm slump diameter was estimated (using the relationship curves of the viscosity versus slump diameter for each mixture) for each mixture type. Table II presents the results of the viscosity at 650 mm slump flow versus each mixture type. The table shows that as the percentage of MK increased in SCC mixtures, the viscosity increased. The maximum viscosity (36.5 Pa.s) occurred at 25% replacement of cement by MK and this value was around 2.4 times the viscosity of the control mixture. The table also shows that the addition of 8% SF did not affect the viscosity of SCC mixture (8SF had a similar viscosity to that of the control mixture) while the addition of 8% MK showed 43% higher viscosity than that of the control mixture.

In addition, Table II shows a direct relation between the viscosity and the total flow time as well as the T50 of the slump flow. As the viscosity of a 650 mm slump SCC mixtures increased, the total slump flow time and the T50 increased. This result agrees with other intervention studies [23] which showed an increase of plastic viscosity with the increase of T50. The results of this investigation also revealed that the amount of HRWRA in SCC mixtures did not appear to affect the viscosity of the concrete mixtures and this fact was proved from the result of 8SF mixture which required 24% extra HRWRA than the control mixture (to obtain the same slump flow diameter) and had similar viscosity to it.

Yield stress

Table II presents the results of the yield stress at different slump flow diameters for all tested concrete mixtures. Since the amount of HRWRA affects the yield stress of the mixture, the yield stress was estimated at a constant HRWRA amount [3460 mL/m^3, amount that gives a reasonable slump flow diameter (630 mm) in the control mixture] in order to evaluate the effect of MK and SF on the yield stress. The results of the yield stress at 3460 mL/m^3 HRWRA are presented in Table II. The table shows that as the percentage of MK increased in SCC mixtures, the yield

stress increased. Replacement of cement by 25% of MK increased the yield stress of the control mixture by 3.2 times. Meanwhile, the addition of SF showed higher influence on the yield stress than the addition of MK. Replacement of cement by 8% SF showed 72% higher yield stress than the replacement of 8% MK (at 3460 mL/m^3 HRWRA).

Figure 1 presents a relationship between the experimental results of the yield stress and the final slump flow diameter for the 18 concrete mixtures. The figure also compares the experimental results of the yield stress with the results calculated by Roussel and Coussot [24] equation. It appears from the figure that there is a direct relation between the final slump flow diameter and the yield stress of the concrete mixtures regardless of the mixture proportions. In addition, the results of the experimental investigation showed the same trend of variation as that of Roussel and Coussot equation.

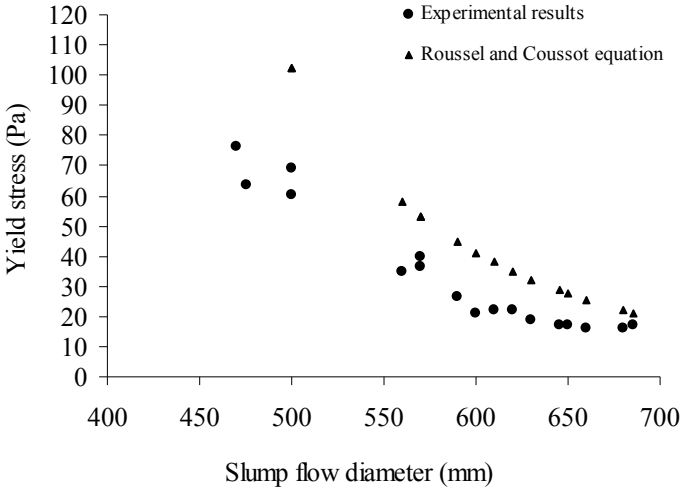

Figure 1. Slump flow diameter and yield stress for all tested concrete mixtures.

Conclusions

The following conclusions are drawn from the study:

- As the percentage of MK in SCC mixture increases, the 28-day compressive strength increases. Replacement of cement by up to 25% of MK increased the 28-day compressive strength of the control mixture (0%MK) by 22%. Also, both MK and SF were similar in terms of strength enhancement at the same level of cement replacement.

- The addition of MK increases the demand of HRWRA in SCC mixtures. Replacement of cement by 25% MK in SCC mixture having 650 mm slump flow diameter increased the demand of HRWRA by 27%. Also, the addition of SF appears to require extra HRWRA than the addition of MK in a given SCC mixture proportion.
- The plastic viscosity increased as the percentage of MK was increased in SCC mixtures. Replacement of cement by 25% MK increased the viscosity of the control mixture by 2.4 times. Also, replacement of cement by 8% SF did not have any effect on the viscosity while replacement of cement by 8% MK increased the viscosity of SCC mixture by 43%.
- The result of this investigation revealed a direct relation between the viscosity of SCC mixtures and both the total time and the T50 of the slump flow test at a given slump flow diameter. As the viscosity of a 650 mm slump SCC mixture increased, the total time and the T50 increased.
- The yield stress increased as the percentage of MK was increased in SCC mixtures, the maximum yield stress occurred at 25% replacement of cement by MK which was 3.2 times that of the control mixture (at a constant HRWRA amount of 3460 mL/m^3). Also, addition of SF showed higher influence on the yield stress than the addition of MK for given mixture proportions.
- The results of all the tested concrete mixtures showed a direct relation between the final slump flow diameter and the yields stress regardless of the mixture proportions. In addition, the results of the experimental investigation showed the same trend of variation as that of Roussel and Coussot equation.

References

[1] Khayat, K.H., Paultre, P. and Tremblay, S. (2001), Structural performance and in-place properties of self-consolidating concrete used for casting highly reinforced columns, *ACI Mater J*, vol. 98, n. 5, pp. 371-378.

[2] Hassan, A.A.A., Hossain, K.M.A. and Lachemi, M. (2009), Bond strength of deformed bars in reinforced self-consolidating concrete beams, *Constr and Building Mater* (In press).

[3] Hassan, A.A.A., Hossain, K.M.A. and Lachemi, M. (2008), Behavior of full-scale self-consolidating concrete beams in shear, *Cem Concr Comp*, vol. 30, n. 7, pp. 588-596.

[4] Bouzoubaâ, N. and Lachemi, M. (2001), Self-compacting concrete incorporating high volumes of class Fly ash: Preliminary results, *Cem Concr Res*, vol. 31, n. 3, pp. 413-420.

[5] Lachemi, M., Hossain, K.M.A., Lambros, V. and Bouzoubaâ, N. (2003), Development of cost effective self-compacting concrete incorporating fly

ash, slag cement or viscosity modifying admixtures, *ACI Mater J* , vol. 100, n. 5, pp. 419-425.

[6] Lachemi, M., Hossain, K.M.A., Lambros, V., Nkinamubanzi, P.C. and Bouzoubaâ, N. (2004), Self compacting concrete incorporating new viscosity modifying admixtures, *Cem Concr Res,* vol. 24, n. 6, pp.917-926.

[7] Siddique, R. and Klaus, J. (2009), Influence of metakaolin on the properties of mortar and concrete: A review, *Applied Clay Science*, vol. 43, pp. 392-400.

[8] Barnes, P., Bensted, J. and Jones, T.R. (2003), Structure and Performance of Cements, 2nd edition. Chapter 15, Metakaolin as pozzolanic addition to concrete, England, pp. 372-398.

[9] Hubertova, M. and Hela, R. (2007), The effect of metakaolin and silica fume on the properties of lightweight self consolidating concrete, *ACI Publication SP-243-3*, American Concrete Institute, Detroit, pp. 35-48.

[10] Caldarone, M.A., Gruber, K.A. and Burg, R.G. (1994), High-reactivity metakaolin: A new generation mineral admixture, *Concrete International*, vol. 16, n. 11, pp. 37-40.

[11] Ding, J. and Li, Z. (2002), Effects of metakaolin and silica fume on properties of concrete, *ACI Mater J*, vol. 99, n. 4, pp. 393–398.

[12] Balogh, A. (1995), High-reactivity metakaolin, *Aberdeen's Concr Constr.,* vol. 40, n. 7, 604p.

[13] Justice, J.M., Kennsion, L.H., Mohr, B.J., Beckwith, S.L., McCormick, L.E., Wiggins, B., Zhang, Z.Z. and Kurtis, K.E. (2005), Comparison of two metakaolins and a silica fume used as supplementary cementitious materials, *ACI SP-228*, Detroit, pp. 213-236.

[14] Razak, H.A. and Wong, H.S. (2001), Effect of incorporating metakaolin on fresh and hardened properties of concrete, *ACI SP-200-19*, Detroit, pp. 309-324.

[15] Brooks. M.A. and Johari (2001), Effect of metakaolin on creep and shrinkage of concrete, *Cem Concr Comp*, vol. 23, n. 6, pp. 495-502.

[16] Bonakdar, M., Bakhshi and Ghalibafian, M. (2005), Properties of high-performance concrete containing high reactivity metakaolin, *ACI SP-228*, Detroit, pp. 287-296.

[17] Balaguru, P. (2001), Properties of normal- and high strength concrete containing metakaolin, *ACI SP-199*, Detroit, pp. 737-756.

[18] Khayat, K.H. (2000), Optimization and performance of air-entrained, self compacting concrete, *ACI Mater J*, vol. 97, n. 5, pp. 526-535.

[19] Saak, A.W., Jennings, H.M. and Shah, S.P. (2001), New methodology for design self-compacting concrete, *ACI Mater J*, vol. 98, n. 6, pp. 429-439.

[20] Fujiwara, H., Nagataki, S., Otsuki, N. and Endo, E. (1996), Study on reducing unit powder content of high-fluidity concrete by controlling powder particle size distribution, *Conc Lib of Japan Soc of Civ Eng*, vol. 28, pp. 117-128.

[21] Mouret, M. and Cyr, M. (2003), Rheological characterization of superplasticized cement pastes containing mineral admixtures:

Consequences on self-compacting concrete, *ACI SP-217-16*, Detroit, pp. 241-255.

[22] Curcio, F., Deangelis, B.A. and Pagliolico, S. (1998), Metakaolin as a pozzolanic microfiller for high performance mortars, *Cem Concr Res*, vol. 28, pp. 803-804.

[23] Ferraris, C.F., Brower, L.E., Beaupre, D., Chapdelaine, F., Domone, P., Koehler, E.P., Shen, L., Sonebi, M., Struble, L., Tepke, D., Wallevik, O. and Wallevik, J.E. (2004), Comparison of Concrete Rheometers: International Tests at MB (Cleveland, OH, USA) in May 2003, NISTIR 7154, 47 pp.

[24] Roussel, N. and Coussot, P. (2005), Fifty-cent rheometer for yield stress measurements: From slump to spreading flow, *Journal of Rheology*, vol. 49, n. 3, pp. 705-718.

Segregation of Coarse Aggregates in Self-Compacting Concrete

Peter Ramge[1], Tilo Proske[2] and Hans-Carsten Kühne[1]

[1] BAM Federal Institute for Materials Research and Testing, Berlin, Germany
[2] Institut für Massivbau, Technische Universität Darmstadt, Germany

Abstract. A major requirement on self-compacting concrete (SCC) is the resistance to any kind of separation. In the presented studies the segregation behavior of aggregates was analyzed systematically. The rheology of self-compacting mortars was dealt with at first. Following, the segregation of particles of different size, shape and density in various mortars was examined. The aim was to find an analytical relation to estimate the risk of sedimentation, using the characteristics of the particles and those of the mortars. The classification of the aggregates according to their potential segregation is rather simple. But the description of the segregation resistance of the mortar is much more difficult. It is not possible to evaluate a mortar solely based on the rheological properties. The mixture composition must always be considered as well. Tests on concrete samples were conducted additionally to determine the influence of the overall system of SCC on the sedimentation of the aggregates.

Introduction

Several approaches describing the sedimentation of aggregates in SCC are commonly known. In recent years a lot of research was carried out in this field, theoretical as well as experimental works [1-10]. In some cases only single particles in a homogeneous fluid are regarded whereas in other cases the complex polydisperse system of concrete is considered. Applying Stoke's law to a single particle it becomes obvious that the viscosity of the surrounding medium controls the sinking speed whereas a stagnation of the movement is only caused by a distinct yield stress τ_0. Several authors [1-6] describe a critical particle diameter d_{lim} as defined in Eqn. (1).

$$d_{\text{lim}} = C \cdot \frac{\tau_0}{\Delta\rho \cdot g} \tag{1}$$

K.H. Khayat and D. Feys (eds.), *Design, Production and Placement of Self-Consolidating Concrete*, RILEM Bookseries 1,
DOI 10.1007/978-90-481-9664-7_10, © RILEM 2010

For $d > d_{\text{lim}}$ sedimentation occurs. C is a model-depending constant, with values between 1.5 [3] and 20.97 [1]. In [6] Roussel, however, proves 1.5 to be wrong. He concludes that the minimum possible theoretical value lies at 4.71. The key question of the above approach is the correct assumption of the effective yield stress τ_0 and the shape and location of the activated shear area.

However concrete is a polydisperse mixture, in which the coarse aggregates do not move without interaction with other aggregates. In [6] Roussel explains that in a Bingham fluid the solid fraction content in an area where sedimentation took place is always lower than in a Newtonian fluid. The sedimented particles do not reach the highest possible packing state that would be expected for a random particle packing. Due to the yield stress of the fluid, the movement of two particles towards each other comes to a stop at a certain gap distance. That means that, depending on the combination of yield stress and solid fraction content, stable mixtures can exist with none of the particles sedimenting, even if the yield stress is proven to be too low to keep a single particle. Even if there is no connected granular lattice, the activated shear area is enlarged and thus the sedimentation resistance enhanced. De Larrard [11] describes the sedimentation risk in dependence of the grain size distribution. His comparing parameter depends on the packing density status of each single grain size fraction and allows the relative classification of grain compositions in order to their potential sedimentation risk. Figure 1 illustrates the difference between a pure rheological approach and a combined (rheological and granular) approach of the sedimentation phenomenon.

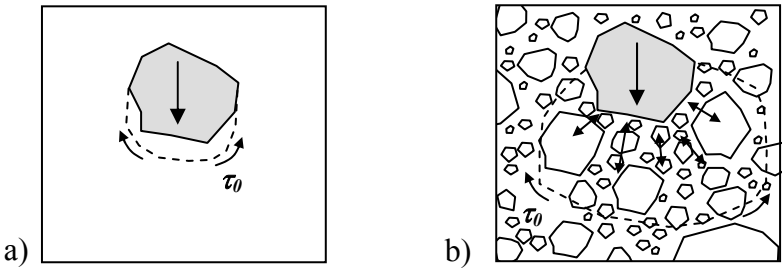

Figure 1. Pure rheological (a) versus combined (b) approach of sedimentation.

Experimental Program

The experimental program was divided into three parts. The first part was focused on self-compacting mortars. The aim was to design and produce several mortars with a certain range of slump flow diameters (*sm*) (measured with the Haegermann cone) and V-funnel times (t_v) (measured with the mortar funnel). On each of these mortars rheological investigations were carried out to characterize the variety of

mortars and to find a correlation between the classical values *sm* and t_v and the rheological properties such as yield stress τ_0 and plastic viscosity η_{pl}. In the second part some mortars of part one were selected to study the sedimentation behavior of single coarse particles of different kind. In the third part concrete specimens were produced based on the mortars to verify how the results of part one and two can be transferred to concrete scale, where a particle interaction of the coarse aggregates has to be considered.

The targeted *sm* values of the mortars in the first part were 22 cm, 24.5 cm and 27 cm. For each *sm* value three different V-funnel times were aimed, 7 sec, 10 sec and 15 sec, respectively. This matrix of combinations was applied for mortars with 40% as well as 50% sand content. Only one of these 18 different mortars corresponded to a mortar as suggested in Okamura's mix design [12] with $sm = 24.5$ cm, $t_v = 10$ sec and 40% sand content. The detailed mixture proportioning of the mortars can be found in [13]. Directly after mixing *sm* and t_v were measured, then a series of several rheological measurements was carried out continuously over a period of up to 90 min with additional measurements of *sm* and t_v in between. Rheometer measurements with a stirrer were carried out to produce flow curves in order to determine the Bingham parameters τ_0 and η_{pl}. This experimental setup, (Figure 2, left) does not allow analytical calculation of the flow profile. Therefore the gained parameters are not the real Bingham parameters, but a yield moment T_0 and a moment gradient called η_{rel}. However these parameters are assumed to be proportional to τ_0 and η_{pl}.

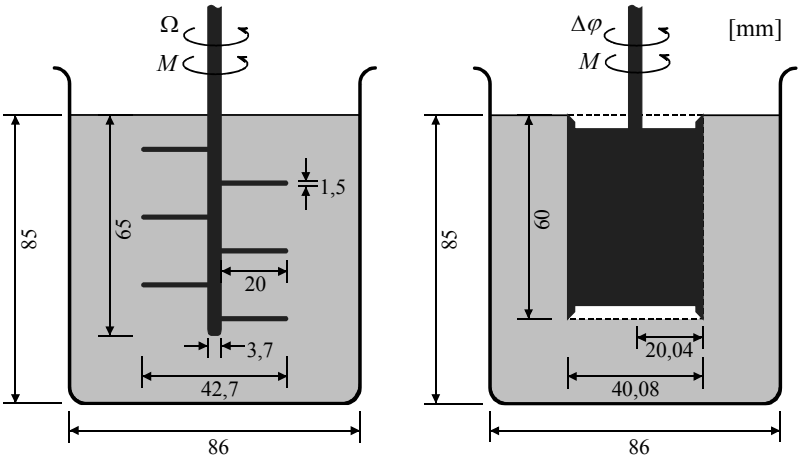

Figure 2. Experimental setup for the determination of the relative flow curves (left) and the direct measurement of the yield stress at rest (right).

A second setup was used for the direct measurement of the yield stress at rest (Figure 2, right). A cylindrical probe, coated with waterproof sandpaper to avoid surface slip, was used. Due to its construction, after immersing the cylinder in the mortar an air pocket forms underneath its bottom, assuring that shear stress is transmitted only through the lateral area. If a small rotation displacement $\Delta\varphi$ is applied, a certain torque will be measured, which decreases after the end of the movement. But due to the mortars yield stress τ_0 the detectable torque will converge to a certain value above zero. As soon as τ_0 is reached in the lateral area, no further movement takes place, and thus no further decrease of the measured torque. The static yield stress can now be calculated based on the remaining torque value and the lateral area of the cylinder. This yield stress at rest is introduced as τ_{00} to emphasize that is was measured at zero movement and to distinguish it from the Bingham parameter τ_0 that normally is derived from the regression of the flow curve from measurement points with different shear velocities.

In the second part several individual particles were embedded in 15 x 15 x 15 cm³ cube specimens of selected mortars. The particles should cover a vast range of size, shape and density. Besides rounded and crushed ordinary aggregates also heavy aggregates and lightweight aggregates were used. Additionally glass spheres and steel spheres were investigated. Table I gives an overview of the used particles.

Table I. Overview of the used particles.

material	shape	density [Mg/m³]	used diameter [mm]	abbreviation
river gravel	naturally rounded	2.59	8, 11, 16, 32	rg
limestone	crushed	2.69	8, 11, 16, 25, 45	ls
granite	crushed	2.72	8, 11, 16	gr
barite	crushed	4.12	8, 11, 16	bar
expanded clay	spherical	≈ 0.74	8, 16	ec
glass spheres	spheres	2.47	11, 16, 25	gla
steel spheres	spheres	7.85	10, 15, 18	st

Directly after filling the cube moulds with the self-compacting mortar, the particles were placed on the surface and if needed be gently pushed in until just covered by the surrounding mortar. The moulds were left at rest until hardened. To examine the location of the individual particles, the hardened specimens were split. The sedimentation level was defined as the proportion of sinking depth to maximal possible sinking depth. A sedimentation level of 100% means that the particle reached the bottom of the 150 mm cube mould. Figures 3 and 4 show examples of some split specimens. The lightweight aggregates in Figure 4 did not sink but rose

from the bottom; this was realized by closing the mold and turning it around after inserting the particles.

In the third part SCCs were produced on basis of the mortars used in part two. By varying the mortar volume and the ratio of 2-8 mm and 8-16 mm gravel in the mixture proportioning, concretes with different sedimentation potentials were produced. At first the mortar was mixed. Then the gravel was added and the concrete was adjusted to a slump flow value of 750-800 mm (Abrams cone) by further addition of superplasticizer (SP). To evaluate the sedimentation behavior, horizontal prismatic specimens 15 x 15 x 70 cm³ were cast and sawn open in longitudinal and transversal direction after hardening. In Figure 8-10 some samples are presented.

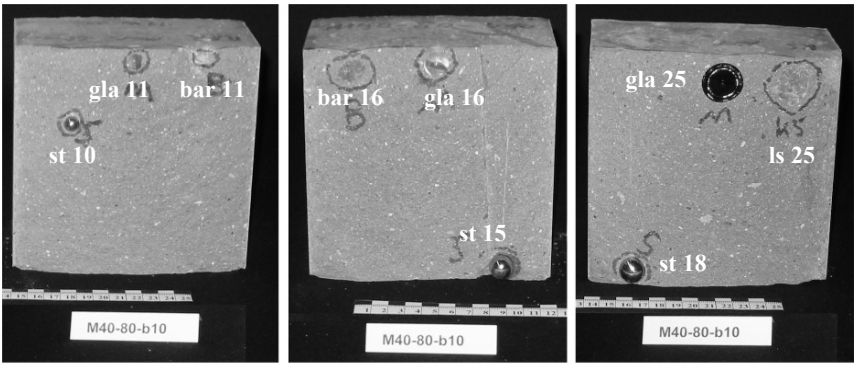

Figure 3. Sedimentation of particles in the same mortar (sm = 24 cm, t_v = 10 sec).

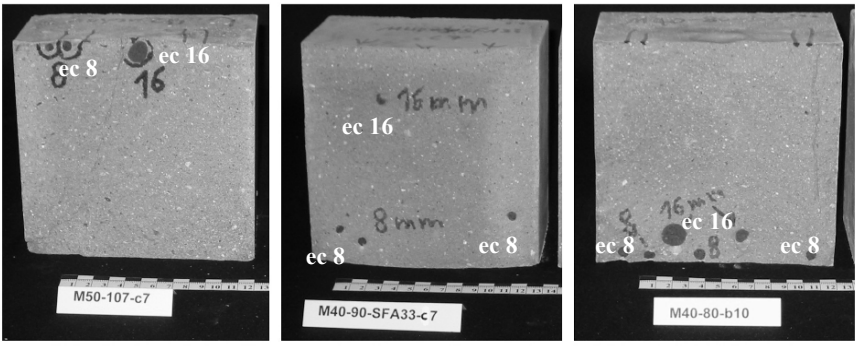

Figure 4. Rising of lightweight aggregates in different mortars.

Results and Evaluation

It was found that the classical properties *sm* and t_v as well as the relative Bingham parameters T_0 and η_{rel} showed a distinct linear behavior over the time, at least for the relevant timeframe of the experiments. This allows the interpolation of the values for a time 10 min after mixing for the following analysis. Even though the mortar was never really at rest during the regarded time the effect may still be caused by thixotropic behavior as described in [14-18]. The common claim that the water-powder ratio controls the V-funnel time whereas the SP dosage controls the slump flow value could be confirmed in the own experiments.

In literature several correlations between empirical tests and rheological properties exist. In [19, 20] the correlation of the viscosity to the Marsh cone flow is investigated. The own results show that t_v and η_{rel} correlate in a similar way. In [21-25] the correlation of the yield stress to slump and spread is dealt with. For the own results the general correlation of T_0 with *sm* was described with a logarithmic function in the same manner as done in [24]. It was found that if only mortars of a similar mixture proportioning are analyzed, the individual correlation fits very well as seen in Figure 5 (left). So unlike in the theoretical case of an ideal Bingham fluid it can be seen, that not solely the yield stress, represented in T_0, controls *sm* but also the viscosity and the granular properties seem to have an influence. However, it must be taken in account that these properties may also have influenced the measurement of T_0. As described above the experimental setup with the stirrer does not allow determining the "real" yield stress. Considering τ_{00} and *sm* a similar correlation can be seen. In Figure 5 (right) *sm* values of various different mixtures are plotted versus τ_{00}.

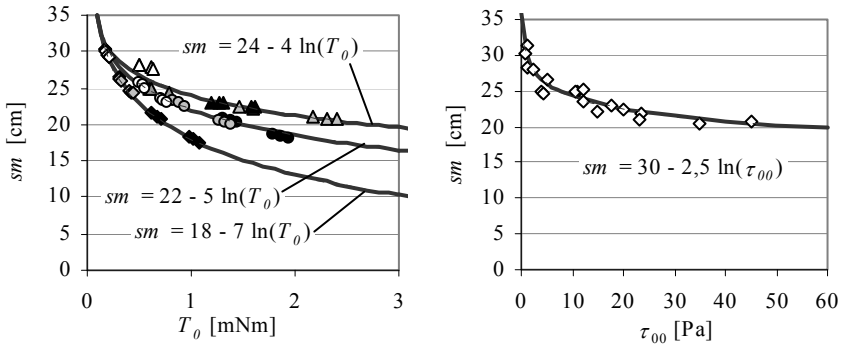

Figure 5. Correlation of T_0 (left) and τ_{00} (right) with sm.

Even though the relation between τ_{00} and *sm* can be described with one single equation for all different mixtures, due to the scattering of the values, it is not possible to conclude from a measured *sm* value to τ_{00}. Regarding T_0 and τ_{00} both

values do not correlate well. In this case the regression coefficient only reaches $R^2 = 0.72$. This is a strong indication that the yield stress at rest is in general independent of the T_0 or τ_0 value which is derived from a flow curve. In other words: having derived τ_0 from a flow curve the behavior of a coarse aggregate in the concrete at rest cannot be described. The yield stress derived from a flow curve is not the input parameter needed for the rheological models described in Eqn. (1); they rather need τ_{00}, the yield stress at rest.

Some of the single particles did not sink at all, some reached the bottom of the mould, whereas others stopped in-between. At rest, sedimentation is hindered as long as the shear stress that the grain implements on the surrounding mortar is lower than τ_{00}. The driving force is the gravitation resulting from the density difference. With random shaped particles the activated shear area cannot be calculated analytically. However, it is believed that this shear area is proportional to the projection area A_p that the particle features in direction of its movement. With the introduction of α_F as a constant of proportionality, the stress that a particle applies to the mortar can be described with Eqn. (2).

$$\tau = \frac{V_i \cdot \Delta\rho \cdot g}{\alpha_F \cdot A_{p,i}} \tag{2}$$

The density of the aggregates can be determined easily by common methods. For the particle volume V_i and the projection area $A_{p,i}$ mean values, gained by means of photo optical particle analysis, can be used. Knowing a sample's mass m and its number of particles n counted in a photo optical measurement, the mean volume of the particles can be calculated with Eqn. (3).

$$\overline{V_i} = \frac{m}{n \cdot \rho} \tag{3}$$

To evaluate the results a value to distinguish the potential sedimentation risk of each particle, the relative sedimentation exposure S_E is introduced in Eqn. (4).

$$S_E = \frac{\overline{V_i} \cdot \Delta\rho \cdot g}{\overline{A}_{p,i}} \tag{4}$$

To enhance the accuracy of the determined values the samples should be clustered in different narrow bordered grain fractions for the photo optical analysis. S_E is not an absolute value, but a relative parameter, to compare different aggregates regarding their potential segregation risk.

Figure 6 shows how the grain shape influences the segregation risk. In this case the flat elliptic shaped grain exhibits a far lower sedimentation exposure than the spherical grain. Considering single particles the sedimentation exposure will raise drastically if the grain would be turned by 90°. Considering a bulk of grains in a

real concrete, the orientation of the grains will be statistically distributed and therefore the determination of the projection area A_p by means of a photo optical particle analysis seems reasonable. The measured values represent the statistical distribution of all possible projection areas. Figure 7 shows the results of the particle sedimentation versus the relative sedimentation exposure S_E for those test specimens where significant sedimentation occurred. It can be seen that depending on the mortar's properties, the sinking depth correlates with the sedimentation exposure S_E. In Table II the properties of the mortars are given. In general the sinking depth s can be calculated by integrating the sinking speed over the time as described in Eqn. (5).

$$s = \begin{cases} A & for \quad S_E \le C(t) \\ A + \int_t B(t) \cdot \left(S_E - C(t)\right) \quad dt & for \quad S_E > C(t) \end{cases} \tag{5}$$

The parameter A describes a term for an independent start displacement that may be caused by external disturbances. $B(t)$ describes a time depending term for the viscosity, controlling the sinking speed and $C(t)$ describes a time depending term considering the yield stress, controlling start and end of the movement. If $S_E \le C(t)$ no sedimentation occurs at rest. However with the available data it was not possible to calculate B and C.

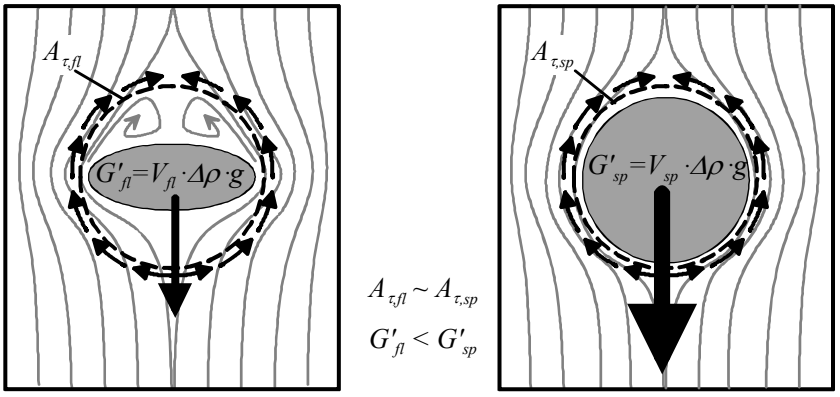

Figure 6. Flat shaped grain (left) and a spherical grain (right) in comparison.

Table II. Properties of the mortars shown in Figure 7.

mortar no.	sand content	sm [cm]	t_v [sec]	ρ [Mg/m³]	mortar no.	sand content	sm [cm]	t_v [sec]	ρ [Mg/m³]
M-a	40%	22.0	26.0	2.29	M-f	40%	28.5	11.4	2.30
M-b	40%	27.8	13.0	2.29	M-g	50%	30.0	8.0	2.26
M-c	50%	28.0	10.0	2.27	M-h	50%	29.5	6.9	2.25
M-d	40%	29.0	15.0	2.28	M-i	40%	29.0	5.4	2.22
M-e	40%	25.3	13.0	2.30	M-j	40%	30.0	5.0	2.22

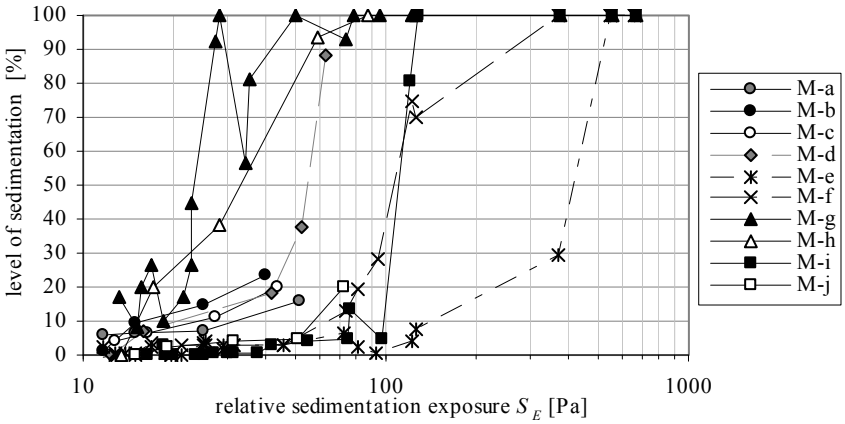

Figure 7. Level of sedimentation versus relative sedimentation exposure S_E.

Comparing the mortars it is obvious that the evaluation of the sedimentation resistance of a mortar solely on basis of τ_0 and η_{pl} or *sm* and t_v respectively is not sufficient. Furthermore the mixture proportioning, for example the sand content, has an impact. Having two mortars with different sand contents and similar rheological properties measured with *sm* and t_v, the one with the higher sand content has the lower sedimentation resistance. Comparing mortars M-g to M-j in Table II and Figure 7 this becomes obvious. To exhibit the same rheological properties for the mortar with the higher sand content the viscosity and yield stress of the paste need to be lower. This results in less stability of the sand in the mortar. Even if the sand itself may well be carried in the mortar without any sedimentation, a bigger particle will sink, if the paste is not able to activate the surrounding sand grains to enlarge the activated shear area. However this does not mean that a mortar without sand would be best. The above mentioned observations count for sand contents in the range commonly used in SCC mortars, bordered by economical and technical aspects.

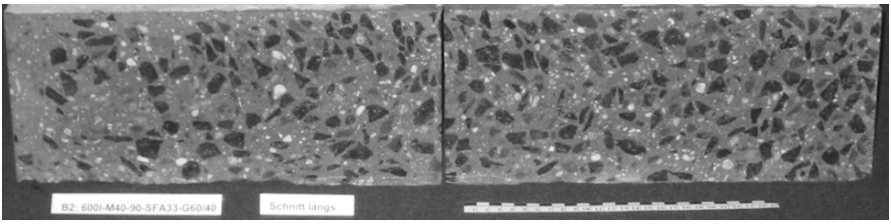

Figure 8. Concrete sample without sedimentation.

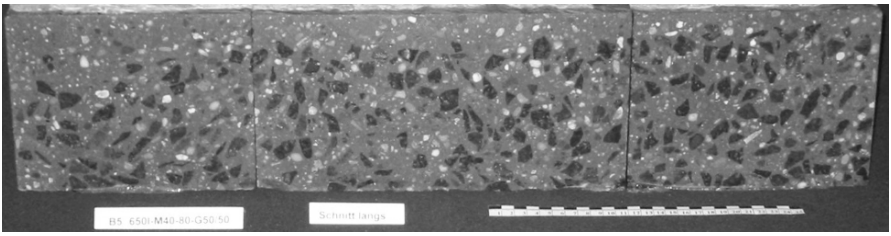

Figure 9. Concrete sample with significant sedimentation.

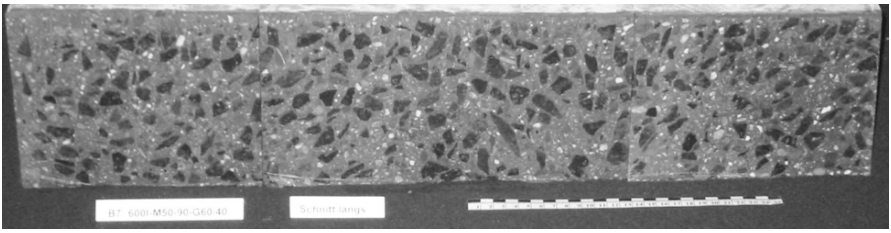

Figure 10. Concrete sample with evenly distributed coarse aggregates despite heavy segregation behavior.

Regarding the concrete specimens, a strong influence of the mortar content on the segregation behavior could be observed. High mortar contents allow achieving the aimed concrete properties (*sm* and t_v) by using a mortar with high yield stress. Thus the coarse aggregates are rather stable in the mix. Decreasing the mortar content, the mortar's rheological properties have to be changed to achieve the same concrete properties, thus increasing the sedimentation risk. However by increasing the amount of coarse aggregates the supporting effect of the granular lattice and thus the segregation resistance is improved. Figure 8 shows a concrete with good sedimentation stability whereas Figure 9 shows significant sedimentation. On the first view the coarse aggregates in Figure 10 are well distributed. However, this concrete showed heavy segregation features. Due to the high aggregate content this segregation is only visible in the first top centimeter. Taking a closer look a 1-2 mm pure paste layer without sand was detected on the top.

Conclusions

It could be shown that the overall mixture proportioning has a significant influence on sedimentation (segregation). As stated also in [6], it is never sufficient to classify the sedimentation risk of coarse aggregates solely based on rheological measurements on SCC. Concerning the sedimentation potential of the aggregates the relative sedimentation exposure (S_E) was introduced to rank comparable aggregate compositions. Besides the grain density, the necessary input values can be gained by photo optical measurements. The sedimentation resistance is mainly controlled by the yield stress of the mortar. The viscosity is only of minor importance. At rest the yield stress of the mortar must be able to prevent all aggregates from moving. A high viscosity cannot stop the segregation of particles; it can only control the speed of the movement. However, the viscosity should not be too low, to limit the distance the aggregates may move at times when the yield stress is disrupted by unexpected external influences. Having the choice between a high viscous mixture with low yield stress and a low viscous mixture with high yield stress in terms of segregation risk the latter should always be favored.

References

[1] Beris, A.N. et al. (1985), Creeping motion of a sphere through a Bingham plastic, *Journal of Fluid Mechanics*, vol. 158, pp. 219-244.

[2] Petrou, M.F. et al. (2000), A unique experimental method for monitoring aggregate settlement in concrete, *Cement and Concrete Research*, vol. 30, n. 5, pp. 809-816.

[3] Saak, A.W., Jenning, H. and Shah, S. (2001), New methodology for designing self-compacting concrete, *ACI Materials Journal*, vol. 98, n. 6.

[4] Jossic, L. and Magnin, A. (2001), Drag and stability of objects in a yield stress fluid, *Les Cahiers de Rhéologie*, vol. 18, n. 1 (in French).

[5] Bethmont, S. (2003), Defining the stability criterion of a sphere suspended in a cement paste: A way to study the segregation risk in self-compacting concrete (SCC), In: Proceedings of the 3rd International Symposium on Self-Compacting Concrete, Reykjavik.

[6] Roussel, N. (2006), A theoretical frame to study stability of fresh concrete *Materials and Structures*, vol. 39, n. 1, pp. 81-91.

[7] D'Aloia Schwartzentruber, L., Bethmont, S., Ladouceur, L. and Rossi, P. (2007), A step towards the design of stable self compacting concrete, In: Proceedings of the 5th Int. RILEM Symposium on Self-Compacting Concrete - SCC 2007, De Schutter, G., Boel, V. (Eds) RILEM Publications S.A.R.L. Bagneux, pp. 143-148.

[8] Bethmont, S., Tailhan, J.-L., D'Aloia Schwartzentruber, L. and Rossi, P. (2007), Role of the granular lattice solid fraction in the stability of self compacting concrete (SCC), In: Proceedings of the 5th Int. RILEM

Symposium on Self-Compacting Concrete - SCC 2007, De Schutter, G., Boel, V. (Eds) RILEM Publications S.A.R.L. Bagneux, pp. 149-154.

[9] Shen, L., Struble, L. and Lange, D. (2009), Modeling static segregation of self-consolidating concrete, *ACI Materials Journal*, vol. 106, n. 6, pp. 367-374.

[10] Shen, L., Struble, L. and Lange, D. (2009), Modeling dynamic segregation of self-consolidating concrete, *ACI Materials Journal*, vol. 106, n. 6, pp. 375-380.

[11] de Larrard, F. (1999), Concrete Mixture Proportioning, A Scientific Approach, E & FN Spon, an imprint of Routledge, London.

[12] Okamura, H. and Ozawa, K. (1995), Mix design for self-compacting concrete, *Concrete Library of JSCE,* no. 25.

[13] Ramge, P. (2005), Investigations on the segregation behaviour of coarse aggregates in self-compactng concrete, Diploma Thesis, Technische Universität Darmstadt (in German).

[14] Roussel, N. (2006), A thixotropy model for fresh fluid concretes: Theory, validation and applications, *Cement and Concrete Research*, vol. 36, n. 10, pp. 1789-1796.

[15] Roussel, N. (2007), A thixotropy model for fresh fluid concretes: Theory and applications, In: Proceedings of the 5th Int. RILEM Symposium on Self-Compacting Concrete - SCC 2007, De Schutter, G., Boel, V. (Eds) RILEM Publications S.A.R.L. Bagneux, pp. 267-272.

[16] Ovarlez, G. and Roussel, N. (2007), Structuration rate of fresh SCC: Influence of the state of shear during rest, In: Proceedings of the 5th Int. RILEM Symposium on Self-Compacting Concrete - SCC 2007, De Schutter, G., Boel, V. (Eds) RILEM Publications S.A.R.L. Bagneux, pp. 285-290.

[17] Billberg, P. (2007), Formwork pressure when using SCC – A doctoral project, In: Proceedings of the 5th Int. RILEM Symposium on Self-Compacting Concrete - SCC 2007, De Schutter, G., Boel, V. (Eds) RILEM Publications S.A.R.L. Bagneux, pp. 491-496.

[18] Roussel, N. (2005), Steady and transient flow behaviour of fresh cement pastes, *Cement and Concrete Research*, vol. 35, n. 9, pp. 1656-1664.

[19] Roussel, N. and Leroy, R. (2005), The Marsh cone: a test or a rheological apparatus?, *Cement and Concrete Research*, vol. 35, n. 5, pp. 823-830.

[20] Leroy, R. and Roussel, N. (2005), The Marsh Cone as a viscometer: Theoretical analysis and practical limits, *Materials and Structures*, vol. 38, n. 1, pp. 25-30.

[21] Roussel, N. and Coussot, P. (2005), "Fifty-cent rheometer" for yield stress measurements: From slump to spreading flow, *Journal of Rheology*, vol. 49 n. 3, pp. 705-718.

[22] Roussel, N., Stefani, C. and Leroy, R. (2005), From mini-cone test to Abrams cone test: measurement of cement-based materials yield stress using slump tests, *Cement and Concrete Research*, vol. 35, n. 5, pp. 817-822.

[23] Jarny, S., et al. (2005), Rheological behavior of cement pastes from MRI velocimetry, *Cement and Concrete Research*, vol. 35, n. 10, pp. 1873-1881.
[24] Flatt, R.J., Larosa, D. and Roussel, N. (2006), Linking yield stress measurements: Spread test versus Viskomat, *Cement and Concrete Research*, vol. 36, n. 1, pp. 99-109.
[25] Roussel, N. (2006), Correlation between yield stress and slump: Comparison between numerical simulations and concrete rheometers results, *Materials and Structures*, vol. 39, n. 4, pp. 501-509.

Estimating Measurement Artifacts in Concrete Rheometers from MRI Measurement on Model Materials

H. Hafid[1,2], G. Ovarlez[2], F. Toussaint[3], P.H. Jezequel[3] and N. Roussel[1]

[1] Université Paris Est, Laboratoire Central des Ponts et Chaussées, Paris, France
[2] Université Paris Est, Laboratoire Navier, Champs sur Marne, France
[3] Lafarge Centre de Recherche, Saint Quentin Fallavier, France

Abstract. Measurement artifacts in concrete or mortar rheometers often prevent the user from having access to absolute correct values of the rheological parameters of the tested material. As there does not exist any rheometer giving access to the "correct" or "real" values of these parameters, it is even not possible to estimate the order of magnitude of the error induced by these artifacts. It is however possible to have access to the local and real rheological behavior law by measuring local velocities and local concentrations of particles through Magnetic Resonance Imaging (MRI) techniques. In this paper, we compare macroscopic measurements and local MRI measurements of the behavior of suspensions of natural sand particles and bi-disperse spherical particles in model yield stress fluids (emulsions). In doing so, we seek to illustrate the potential consequences of artifacts on the measurements of the flow curve of cementitious materials. We reach the conclusions that particle migration is at the origin of the discrepancy between concrete rheometers.

Introduction

Because of the inherent difficulty of measuring viscosity and because of the fundamental role of yield stress during casting processes, most studies dealing with fresh cementitious materials properties mainly focus on static and/or dynamic yield stress [1]. This parameter can be assessed through rheometers but also through empirical test such as slump or slump flow [2, 3], L-box [4], mini slump [5] or channel flow [6]. Even if marsh cone [7] or V-funnel test results are sometimes correlated to viscosity, only rheometers give access to the value of the plastic viscosity. However, it has been shown recently that artifacts are systematically involved during measurements of viscosity on dense systems containing both fluid

K.H. Khayat and D. Feys (eds.), *Design, Production and Placement of Self-Consolidating Concrete*, RILEM Bookseries 1,
DOI 10.1007/978-90-481-9664-7_11, © RILEM 2010

and particles [8, 9]. For example, shear induced migration [8, 10] or shear induced settling [9] of particles may occur within the gap. Moreover, flow frequently localize in the gap (*i.e.* plug flow) [8, 11, 12]. These artifacts seem generally able to induce an apparent non-Newtonian behavior that is not representative of the actual behavior of the material. These artifacts, which strongly depend on the rheometer and the shear flow geometry used, could be at the origin of the strong discrepancy between the absolute values of the rheological parameters measured using various concrete rheometers [13, 14]. It was indeed shown in [13, 14] that this discrepancy can reach up to a factor 4 between two rheometers measuring the properties of the same material. It is however possible to overcome these artifacts and have access to the local and real rheological behavior law. In order to do so, it is possible to identify the rheological behavior of the studied suspension by measuring local velocities [8, 11, 12] and local concentrations of particles [8] through Magnetic Resonance Imaging (MRI) of the material. In this paper, we compare macroscopic measurements and local MRI measurements of the behavior of suspensions of natural sand particles and bi-disperse spherical particles in model yield stress fluids (emulsions). In doing so, we seek to illustrate the potential consequences of artifacts on the measurements of the flow curve of cementitious materials. It has to be noted that we focus here on migration and settling of non colloidal particles neglecting therefore the consequences of bleeding and migration of cement grains. In the first part, we present the studied materials and experimental protocols. In a second part, we discuss the migration and sedimentation of particles and plug flow measured with MRI. Finally, we compare the flow parameters obtained from macroscopic measurements with the real local values obtained from MRI. We conclude that, once plug flow is taken into account, it is the particle migration that most strongly affects the measurements of the rheological parameters.

Materials and Procedures

We study in this paper the rheological behavior of suspensions of particles in a model yield stress fluid. Suspensions of coarse particles in cement pastes have been recently shown to behave like any suspensions of particles in any other yield stress fluid [15] from a purely rheological point of view. Their behavior finds its origin in the hydro-dynamical interactions between the inclusions. That is why we chose to suspend our particles in water in oil emulsions, which have been shown to be simple yield stress fluids [16]: this avoids all the complexity linked to setting and thixotropy, while providing a good measurement of the variations of the rheological properties of cement pastes as a function of the coarse particle volume fraction [15]. Oil is the continuous phase (23% by mass) in which water droplets (77% by mass) are mixed. The emulsions yield stress was varied between 10 and 20 Pa. The coarse particles are either sand or polystyrene particles. The polystyrene particles are a mixture of particles of diameter 0.08 mm (30% by

mass) and 0.5 mm (70% by mass). The coarse particles volume fractions studied in this paper is 35% for the sands and 55% for polystyrene particles. The maximum packing fraction of the dry mixture was measured by vibration and was of the order of 0.7. Three sands were studied. The first one was a naturally rounded sand (S_1). The two other sands S_2 and S_3 were crushed sands. They differed by their roughness (*i.e.* characteristic dimension of the grain surface defects), the sand S_3 displaying a rougher surface than the sand S_2. Three sand grains sizes were studied (160-200 μm, 315-400 μm and 800-1000 μm). The orders of magnitudes of the maximum packing fractions ϕ_m of the dry sand assemblies were measured by vibration and were of the order of 0.65. The experiments were performed within a wide gap Couette type rheometer coupled with MRI [8, 11, 12, 16]. MRI was used to measure the velocity and concentration profiles of the material inside the gap of the geometry, while a Bohlin® C-VOR 200 rheometer was used to measure the torque for the same protocol and flow history. The inner cylinder radius R_i was 4.15 cm while the radius of the outer cylinder R_e was 6 cm. The two cylinders were covered with sandpaper with a roughness of 180 μm to prevent any slippage. The experimental protocol was divided in two parts. An increasing rotation velocity ramp from 4 to 100 rpm (each step lasting for 20 s) was followed by a decreasing rotation velocity ramp from 100 to 5 rpm corresponding to a shear rate from 0.5 to 10.5 s^{-1}. In the case of the polystyrene beads, a 100 rpm rotation velocity was maintained for one hour between these two ramps in order to reach a steady concentration profile in the gap. In the case of the sands tested here, this phase did not exist as it would induce sedimentation.

Experimental Results

Artifact N°1: migration

No matter the tested material, the rotation of the inner cylinder causes a migration of the particles towards the outer cylinder (see Figs. 1(a) and 1(b)). It is often considered in cementitious materials literature that this migration is a slow phenomenon and that it is therefore possible to measure the behavior of the system before any migration of the particles perturb the measured data. This common belief comes from the literature of migration in Newtonian suspensions (see [8] for a review), where it was indeed observed that it is usually a slow diffusive phenomenon. However, it has been recently shown that, at very high particle volume fraction, depending on the flow history, migration may be in some cases very rapid (it can take a strain smaller than 100 to induce migration) and thus unavoidable [8]. Consistently with these last observations, in our experiments, we have observed that migration occurs almost instantaneously when we shear the material: at the end of the first velocity ramp, the material is already heterogeneous, showing that migration occurs in less than 100 strain unities. It is

possible to roughly estimate in the simple case of a Bingham fluid the local consequences of these variations on the local rheological properties in the cases illustrated above by using the relations from [14] and applied to cementitious material in [17], which allow for the computation of the yield stress $\tau_c(\phi)$ and plastic viscosity $\mu_p(\phi)$ as a function of the local concentration of particles.

$$\frac{\tau_c(\phi)}{\tau_c(0)} = \sqrt{\frac{1-\phi}{(1-\phi/\phi_m)^{2.5\phi_m}}} \tag{1}$$

$$\frac{\mu_p(\phi)}{\mu_p(0)} = (1-\phi/\phi_m)^{-2.5\phi_m} \tag{2}$$

According to the above relations, in the case of the polystyrene particles, the local variation of the yield stress and plastic viscosity should respectively be of the order of 20% and 50%. In the case of the sand studied here, these variations are of the order of 5% and 10%. Note that it is at high volume fraction, which is the interesting domain for mix design, that the consequences of these variations on the local rheological behavior are the strongest. This is due to the high sensitivity of the rheological parameters when the particle volume fraction is close to the maximum packing fraction. It can finally be noted that the results obtained here are for coaxial cylinder geometry and may be different in the case of a Vane tool.

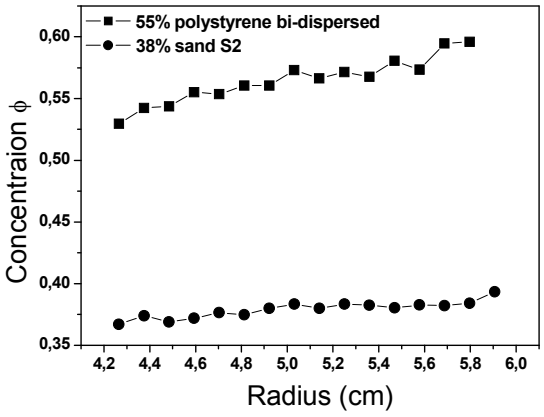

Figure 1. Radial concentration profiles in the cell for a suspension containing 55% of polystyrene bi-dispersed particles in an emulsion, suspension containing 38% of sand S_2, after the ascending rotation speed ramp.

Artifact N°2: sedimentation

Another measurement artifact is the shear induced sedimentation of particles during the rheological measurements. Concentration profiles along the vertical direction of our Couette cell were recorded after every rotation step of the inner cylinder. These profiles are shown in Figs. 2(a) and 2(b).

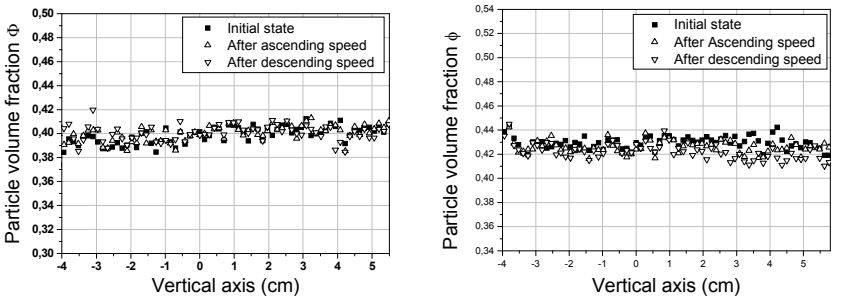

(a) (b)

Figure 2. Concentration profiles along the axis Z of the cell of a suspension containing 39% of sand S_1 160-200 µm in an emulsion (a) and a suspension containing 43% of sand S_2 800-1000µm (b).

The particle concentration variation induced by shear induced sedimentation for most of the materials tested in this study is less important than the one induced by radial migration. It is, for example, negligible in Fig. 2(a) and of the order of 5% in the upper part of the material in Fig. 2(b). It can be noted that although both mixtures were stable at rest, the sedimentation in Fig. 2(b) occurs during flow. According to Eqs. (1) and (2), it can be estimated that the variations induced by sedimentation on the local values of the yield stress and plastic viscosity in the upper part of the material during the test shown in Fig. 2(b) should be respectively of the order of 5% and 15%.

Artifact N°3: plug flow

We plot in Fig. 3 the relative tangential flowing velocity (*i.e.* the ratio between the tangential velocity and the tangential velocity at the inner cylinder surface) as a function of the radius within the gap for a suspension of sand S_2 in an emulsion. It is first possible to observe that the slip velocity at the surface of the inner cylinder is negligible. We naturally observe a decrease in velocity along the gap and two distinct zones: one sheared zone and one unsheared zone. The boundary between these two zones is located at a critical radius r_c. r_c increases with the rotation speed of the inner cylinder and when the concentration increases. Our results show

that shape and size of particles have an influence on r_c. This measurement artifact described as "plug flow" prevents the operator from the direct computation of the shear rate within the gap. It is nevertheless possible to compute the material constitutive law for a homogeneous material by using the Nguyen and Boger approach (see below).

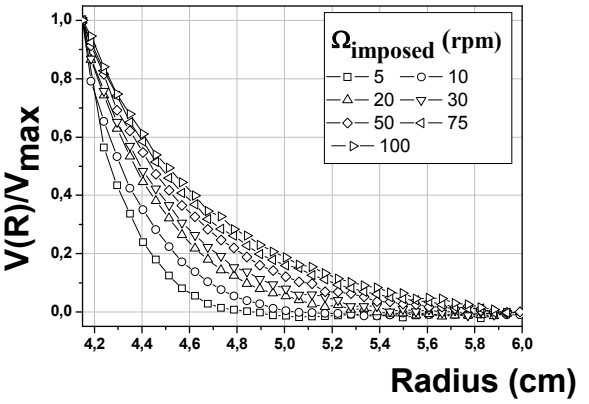

Figure 3. Relative tangential velocity (i.e. ratio between the tangential velocity and the tangential velocity at the inner cylinder surface) as a function of the radius within the gap for a suspension of sand S_2 in an emulsion.

Local vs. Macroscopic Measurement

In this section, we compare the flow curves obtained from conventional rheometry and from a reconstruction technique of the "real" flow curve of the material obtained by MRI (*i.e.* via measurements of the local flow velocity and therefore local shear rates within the gap, and of the "true" local concentration of the material). This technique is better described in [8, 11].

Local measurement

The shear stress distribution $\tau(r)$ within the gap is known everywhere in the material. It is obtained from macroscopic measurement. It reads

$$\tau(r) = C/2\pi Hr^2 \tag{3}$$

where C is the torque applied on the inner cylinder. The local shear rate is deduced from the velocity profiles measured with MRI and is computed using:

$$\dot{\gamma}(r) = V(r)/r - dV(r)/dr \tag{4}$$

Macroscopic measurement

The classical way to calculate shear stress and shear rate from macroscopic torque and rotation velocity consists in a) calculate shear stress at the surface of the inner cylinder ($r = r_i$) using Eqn. (3) ; b) calculate shear rate as $\dot{\gamma} = 2\pi\Omega / \delta$ where δ is the rheometer gap. The obtained flow curve is shown in Fig. 4 for a suspension containing 38% of sand S_2 in an emulsion. These macroscopic measurements can be corrected using the method proposed by Nguyen and Boger [12, 18] in order to take into account the plug flow zone. The shear rate is calculated from the macroscopic measurements using the following equation:

$$\dot{\gamma}(\tau(r_i)) = 2C\frac{d\Omega}{dC} = 2\Omega\frac{d\ln\Omega}{d\ln C} \tag{5}$$

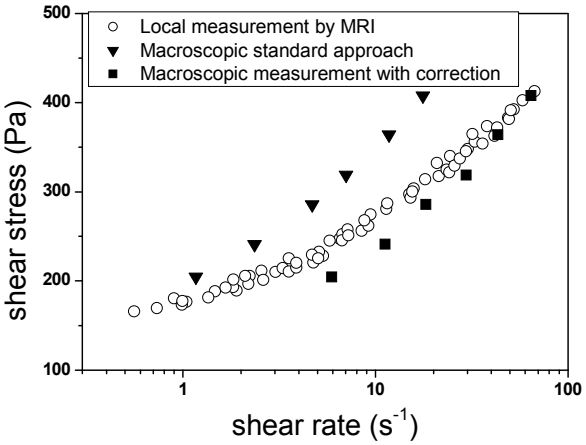

Figure 4. Macroscopic and local flow curves for a suspension containing 38% sand S_2 in an emulsion.

The shear stress is calculated as above. The corrected flow curve is shown in Fig. 4. The obtained flow curve is then fitted with a Herschel-Bulkley model $\tau(\dot{\gamma}) = \tau_c + \eta_{HB}\dot{\gamma}^n$ where τ_c is the yield stress, η_{HB} is the consistency and n is the flow index (equal to 0.5 for an emulsion). In Fig. 4, the corrected macroscopic measurement gives τ_c = 121.1 Pa and η_{HB} = 36.4 Pa.s$^{-0.5}$ whereas the local flow curve obtained from MRI gives τ_c=172.9 Pa, η_{HB}= 31.2 Pa.s$^{-0.5}$.

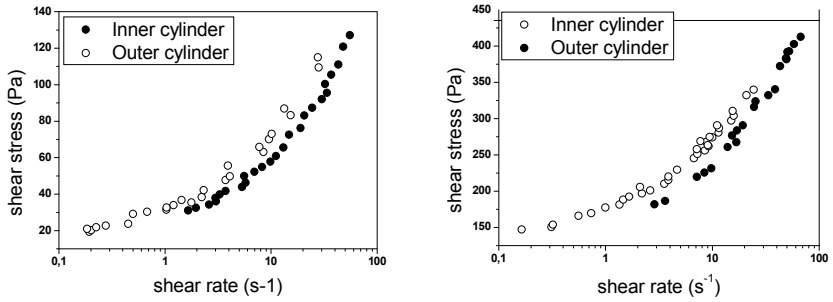

(a) (b)

Figure 5. Flow curves computed from local MRI measurements for a suspension containing 52% of polystyrene particles (a) and a suspension containing 38% of sand S_2.

The error between local and macroscopic measurement is of the order of 30% for yield stress and 20% for consistency for the material studied in Fig. 4. The origin of this discrepancy stands in the fact that the Nguyen and Boger approach is valid only for a homogeneous distribution of particles within the material, which is not the case here. The value of the difference between local and macroscopic measurements can then be understood by observing the change in the local behavior of the material between the zone located close to the inner cylinder (where the particle volume fraction is lower) and the zone located close to the outer cylinder (where the particle volume fraction is higher). In each zone, we measure the local velocity profiles, compute the local shear rates and use the reconstruction technique described above to compute the local behavior law of the tested material (see Fig. 5). We observe flow curves, which differs between the inner and outer cylinder. For the suspension containing 38% of sand S_2 shown in Fig. 5(b), the particle volume fraction variation between the inner and outer zones (between 37 and 39%) leads to a variation between the local flow curves of the order of 20%.

Effect of Volume Fraction on Artifacts

In the above sections, illustrations of artifacts were given for various particle volume fractions. In this section, we focus on the effect of this specific parameter on the rheological measurement of yield stress and Herschel-Bulkley consistency. Even if it was shown in the previous sections that it is at the lowest particle volume fractions that the migration is the strongest, it is for the highest particle volume fractions that the consequences of this migration on the measurement of the yield stress and plastic viscosity of the material are the strongest. In the case of the highest particle volume fractions tested in this paper, the induced error is of the

order of 20% (see Figs. 6(a) and 6(b)). This error seems however to increase strongly as the volume fraction tends towards the maximum packing fraction. As already explained above, this is due to the high sensitivity of the rheological parameters in these regimes. It is possible to roughly extrapolate from the results in Figs. 6(a) and 6(b) that, at higher particle volume fractions (*i.e.* particle volume fractions typical of concrete), the induced error could reach value of the order of several tens of percentage in the case of yield stress and a factor of order 10 in the case of consistency. This means that particle migration, which strongly depends on the rheometer geometry, could explain the discrepancy between concrete rheometers described in [13, 14]. One could object that most concrete rheometers protocol demonstrates that no segregation occurs in the sample by measuring the torque at a given rotation speed before and after the test procedure. However, we have seen in our experiments that most of the migration occurs after a few rotations of the inner cylinder. This means that the measurement of the initial torque before any test is already effected by this initial migration and that this verification is not sufficient to ensure that no particle migration occurs in the sample.

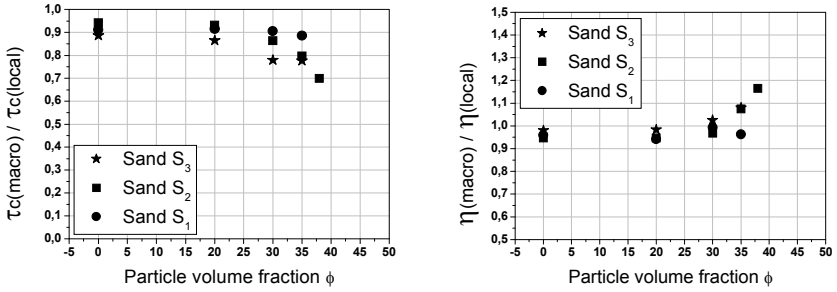

(a) (b)

Figure 6. Ratio between measured macroscopic yield stress and local yield stress as a function (a) and ratio between measured macroscopic consistency and local consistency (b) as a function of the particle volume fraction (sand size 160-200 microns).

Conclusions

In this paper, we have compared macroscopic measurements and local MRI measurements of the behavior of suspensions of natural sand particles and bi-disperse spherical particles in emulsions. In doing so, the potential consequences of artifacts on the measurements of the flow curve of cementitious materials are illustrated. In the first part, we presented the studied materials and experimental protocols. In a second part, we discussed the migration and sedimentation of

particles and plug flow measured with MRI. Finally, we compared the flow parameters obtained from macroscopic measurements with the real local values obtained from MRI and we concluded that, once plug flow is taken into account, it is the particle migration that most strongly effects the measurement of the rheological parameters.

References

[1] Roussel, N. (2007), Rheology of fresh concrete: from measurements to predictions of casting processes, *Materials and Structures*, vol. 40, n. 10, pp. 1001-1012.

[2] Roussel, N. (2006), Correlation between yield stress and slump: Comparison between numerical simulations and concrete rheometers results, *Materials and Structures*, vol. 39, n. 4, pp. 501-509.

[3] Roussel, N. and Coussot, P. (2005), "Fifty-cent rheometer" for yield stress measurements: from slump to spreading flow, *Journal of Rheology*, vol. 49, n. 3, pp. 705-718.

[4] Nguyen, T.L.H., Roussel, N. and Coussot, P. (2006), Correlation between L-box test and rheological parameters of an homogeneous yield stress fluid, *Cem. Concr. Res.,* vol. 36, n. 10, pp. 1789-1796.

[5] Roussel, N., Stefani, C. and Le Roy, R. (2005), From mini cone test to Abrams cone test : measurement of cement based materials yield stress using slump tests, *Cem. Concr. Res.,* vol. 35, n. 5, pp. 817-822.

[6] Roussel, N. (2007), The LCPC BOX: a cheap and simple technique for yield stress measurements of SCC, *Materials and Structures*, vol. 40, n. 9, pp. 889-896.

[7] Roussel, N. and Le Roy, R. (2005), The Marsh cone: A test or a rheological apparatus?, *Cem. Concr. Res.*, vol. 35, n. 5, pp. 823-830.

[8] Ovarlez, G., Bertrand, F. and Rodts, S. (2006), Local determination of the constitutive law of a dense suspension of non-colloidal particles through magnetic resonance imaging, *Journal of Rheology*, vol. 50, pp. 259-292.

[9] Ovarlez, G., Barral, Q. and Coussot, P. (2010), Three-dimensional jamming and flows of soft glassy materials, *Nature Materials,* vol. 9, n. 2, pp. 115-119.

[10] Leighton, D. and Acrivos, A. (1987), The shear-induced migration of particles in concentrated suspensions, *J. Fluid Mech,* vol. 181, pp. 415-439.

[11] Jarny, S., Roussel, N., Rodts, S., Bertrand, F., Le Roy, R. and Coussot, P. (2005), Rheological behavior of cement pastes from MRI Velocimetry, *Cem. Concr. Res.*, vol. 35, n. 10, pp. 1873-1881.

[12] Jarny, S., Roussel, N., Le Roy, R. and Coussot, P. (2008), Modelling thixotropic behavior of fresh cement pastes from MRI measurements, *Cem. Concr. Res.*, vol. 38, pp. 616-623.

[13] Ferraris, C.F. and Brower, L.E., editors (2001), Comparison of concrete rheometers: International tests at LCPC (Nantes, France) in October, 2000,

National Institute of Standards and Technology Interagency Report (NISTIR) 6819.

[14] Ferraris, C.F. and Brower, L.E., editors (2004), Comparison of concrete rheometers: International tests at MB (Cleveland OH, USA) in May, 2003, National Institute of Standards and Technology Interagency Report (NISTIR) 7154.

[15] Mahaut, F., Mokeddem, S., Chateau, X., Roussel, N. and Ovarlez, G. (2008), Effect of coarse particle volume fraction on the yield stress and thixotropy of cementitious materials, *Cem. Concr. Res.*, vol. 38, pp. 1276-1285.

[16] Ovarlez, G., Rodts, S., Coussot, P., Goyon, J. and Colin, A. (2008), Wide gap Couette flows of dense emulsions: Local concentration measurements, and comparison between macroscopic and local constitutive law measurements through magnetic resonance imaging, *Physical Review,* E 78, 036307.

[17] Chateau, X., Ovarlez, G. and Trung, K.L. (2008), Homogenization approach to the behavior of suspensions of non-colloidal particles in yield stress fluids, *Journal of Rheology,* vol. 52, pp. 489-506.

[18] Nguyen, Q.D. and Boger, D.V. (1987), Characterization of yield stress fluids with concentric cylinder viscometers, *Journal of Rheology*, vol. 26, pp. 508-515.

Evaluation of Fresh Properties of Self-Consolidating Concrete under Long Transportation Time and Extreme Temperature

Nader Ghafoori and Hamidou Diawara

Department of Civil and Environmental Engineering, University of Nevada, Las Vegas, USA

Abstract. The investigation presented herein was intended to study the influence of long transportation time and extreme temperature on the fresh performance of self-consolidating concrete. The study is useful in simulating concrete mixing and hauling by means of concrete truck mixer during extreme temperature. Temperatures of 43 and -0.5^{o}C, to simulate hot and cold weathers, were used to evaluate the unconfined workability (slump flow), flow rate (T_{50}), and dynamic stability (VSI) of the matrices transported for 60 and 80 minutes. Mixing and transporting under the temperature of 21^{o}C and transportation duration of 10 minutes was adopted as the control condition. Polycarboxylate-based high range water-reducing admixture (HRWRA) and viscosity-modifying admixture (VMA) were used to produce self-consolidating concretes with slump flow of 635 ± 25 mm, VSI of 0, and T_{50} of 2 to 5 seconds. The test results revealed that the self-consolidating concrete mixed and transported under extreme temperature experienced slump flow loss in elevated temperature and slump flow gain in cold environment, when compared to the equivalent concrete produced under the reference condition. While the flow rate/plastic viscosity of the selected matrix increased in the cold temperature, the concrete remained highly stable irrespective of the selected temperature.

Introduction

Self-consolidating concrete (SCC) is a highly flowable and non-segregating matrix that can spread into place, fill the formwork, and encapsulate the reinforcement without mechanical consolidation [1]. It provides better consolidation around reinforcement, reduces noise due to the elimination of vibration, improves surface

K.H. Khayat and D. Feys (eds.), *Design, Production and Placement of Self-Consolidating Concrete*, RILEM Bookseries 1,
DOI 10.1007/978-90-481-9664-7_12, © RILEM 2010

appearance, enhances working conditions and safety, and reduces in-place cost when compared to vibrated concrete.

Lengthy hauling time and extreme temperature (due to excessive hot or cold weather) can adversely affect the fresh properties of concrete by accelerating or retarding the rate of moisture loss and the rate of cement hydration [2]. For self-consolidating concrete, it is manifested in the form of slump flow loss. Slump flow loss can be defined as the loss of consistency in fresh concrete with elapsed time. It is a normal phenomenon which is related to the intrinsic nature of concrete. The influence of long transporting time under extreme temperature on the fresh performance of self-consolidating concrete is presented in the subsequent sections.

Research Objective

The study presented herein was intended to evaluate the effect of long transportation time and extreme hot and cold temperature on the fresh properties of a self-consolidating concrete mixture. Laboratory room temperatures of 43 and -0.5^{o}C to simulate hot and cold weathers, respectively, were used to evaluate the freshly-mixed self-consolidating concretes transported for 60 and 80 minutes. Under the above selected temperatures, the unconfined workability, flow rate, and dynamic segregation resistance were assessed at the end of the hauling time, and compared to the equivalent fresh properties obtained at the control condition, i.e.: fresh matrix hauled for 10 minutes at normal room temperature of 21^{o} C.

Experimental Program

Raw materials

The cementitious materials used in all mixtures consisted of ASTM C150 [3] Type V Portland cement and ASTM C 618 [4] class F fly ash. Their physico-chemical characteristics are shown in Table I. The fine aggregate used had bulk and saturated surface dry specific gravity, absorption, and fineness modulus of 2.75 and 2.78, 0.8%, and 3.0, respectively. The coarse aggregate had a nominal maximum size equal to 12.50 mm and complied with ASTM C 33 [5] size number 7. Its bulk and saturated surface dry specific gravity, absorption, and dry-rodded unit weight were 2.77 and 2.79, 0.6%, 1634 kg/m^3, respectively. Other concrete constituents were tap water, polycarboxylate-based high-range water reducing admixture (HRWRA) complying with the ASTM C 494 [6] Type F requirements and viscosity-modifying admixture (VMA).

Table I. Chemical and physical properties of Portland cement and fly ash.

Chemical Composition	Portland Cement, (%)	Fly Ash, (%)
SiO_2	20.64	58.9
AL_2O_3	3.4	20.5
Fe_2O_3	3.4	5.6
CaO	63.5	7.5
MgO	4.7	
SO_3	2.4	0.4
Na_2O equivalent	0.46	-
K_2O	-	-
C_2S	9	-
C_3S	66	-
C_3A	4	-
Loss on Ignition	1.2	0.3
Insoluble residue	0.14	-
Fineness Blaine, cm^2/g	3810	-

Mixture proportion

The mixture constituents and proportion used for the investigation are shown in Table II. The matrix was prepared with a constant water-to-cementitious materials ratio of 0.4, a uniform cement content of 391 kg/m^3, and a constant amount of fly ash representing 20% of the cement mass. In proportioning the aggregates content, particular attention was given to the coarse-to-fine aggregate ratio due to its critical role in generating sufficient amount of mortar for the selected self-consolidating concrete. The ASTM C 29 [7] was used to determine the compacted bulk unit weight and the calculated void content using different ratios of the combined coarse and fine aggregates. The optimum volumetric coarse-to-fine aggregate ratio, utilized in the proportioning of the concrete constituents, was found at 0.52/0.48. The optimum (minimum) dosages of the high range water-reducing admixture (HRWRA) and viscosity-modifying admixture (VMA) used at the control condition (hauling time of 10 minutes and temperature of 21°C) are presented in Table II. These dosages were obtained by evaluating the consistency and stability of concrete using different trial batches until a satisfactory slump flow of 635± 25 mm; T_{50} of 2 to 5 sec, and a visual stability index of 0 were attained.

Mixing, sampling and testing

Laboratory trial mixtures were used to produce the intended self-consolidating concrete. An electric counter-current pan mixer with a capacity of 0.028 m^3 was used to blend concrete components. In simulating the influence of hauling time on the fresh SCCs, a concrete mixer with variable velocity was needed. An

environmental chamber to simulate hot or cold temperature conditions was built around the mixing apparatus. The walls, roof and floor of the room were made with plywood and insulated with polystyrene foam to maintain a uniform temperature throughout the experiments. The hot temperatures were generated by a heater while a cooling unit was used to produce the cold temperatures. A temperature regulator, which was connected to the heating and cooling units and assisted by multiple probes, maintained the target temperature within ± 2°C margins. A separate control unit also monitored and recorded the relative humidity of the environmental chamber. Prior to the actual mixing, the concrete's dry ingredients (i.e., aggregate, cement and fly ash) were stored in the environmental chamber for 24 hours or until they reached the target temperature.

Table II. Mixture components and proportion.

Portland cement (kg/m^3)	Fly ash (kg/m^3)	*w/cm*	Fine aggregate (kg/m^3)	Coarse aggregate (kg/m^3)	Admixtures (ml/100 kg)	
					HRWRA[1]	VMA[2]
391	78	0.40	849	922	209	26

[1]High range water reducing admixture, [2]Viscosity-modifying admixture

Prior to the actual mixing, the concrete dry ingredients were stored in the environmental chamber for 24 hours or until they reached the target temperature. The mixing water was kept at a constant temperature of 21 ± 2°C to avoid any interference with the rate of cement hydration. At the completion of each batching, the temperature of concrete was measured and remained within 2 ± 1°C of the ambient temperature.

The mixing sequence consisted of blending the coarse aggregate with 1/3 of the mixing water for 2 minutes, followed by the fine aggregate with 1/3 of the mixing water for another 2 minutes, and the cementitious materials with the remaining 1/3 of the mixing water for 3 minutes. Finally, the required amount of HRWRA and VMA (as reported earlier) were added and blending of the matrix continued for an additional 3 minutes, followed by a 2-minute rest and resumption of mixing for 2 additional minutes. From that point on the mixing speed (14.5 rpm) was changed to an agitating speed (7.25 rpm) until the end of the desired hauling time was achieved. The hauling time was defined as the elapsed time between the first contact of water and cementitious materials to the beginning of concrete discharge. At the completion of each mixing and hauling, the fresh self-consolidating concretes were evaluated for the unconfined workability (measured by the slump flow), the flow rate or viscosity by inference (evaluated by the T_{50} time), the dynamic segregation resistance (assessed by the visual stability index (VSI)), and J-ring passing ability (determined by the J-ring test); in accordance with the ASTM C 1611 [8] and C 1621 [9].

Discussion of Results

For the purpose of this study, the combination of hauling times of 60 and 80 minutes and temperatures of 43 and -0.5°C were considered. The term "TxHy" is used throughout the discussion to indicate the mixing condition and environment. "Tx" stands for the temperature "x", and "Hy" represents the hauling time "y." The test results for the slump flow, T_{50} time, and visual stability index (VSI) at the selected combined hauling time and temperature are presented in Table III.

Slump flow loss

TxHy versus T21H10. In this section, the slump flow of the selected self-consolidating concrete exposed to the combination of hauling time and temperature are compared to the matrix hauled for 10 minutes under the reference temperature of 21 ± 2°C (T21H10 condition). Table III documents the slump flow losses. In comparing to T21H10 condition, the selected self-consolidating concretes hauled for 60 and 80 minutes experienced 55% and 65% decreases in slump flow at the temperature of 43°C, respectively. The combined transportation duration and cold temperature (i.e., -0.5°C), also caused decreases in slump flow when compared to T21H10, but to a lesser extent. On average, the losses were about 23% and 29% after 60 and 80 minutes of hauling time, respectively.

TxHy versus T21Hy. This section is intended to compare the slump flows obtained for the matrices transported for the same duration under different temperatures to those obtained under the control temperature (21 ± 2°C) of the equivalent hauling time. As it can be seen in Table III, the self-consolidating concretes batched and hauled in different temperatures for 10, 60, and 80 minutes experienced slump flow losses in hot conditions and gains in cold environments when compared to the equivalent concretes produced at the control temperature. When the selected self-consolidating concrete was hauled for 10, 60, and 80 minutes under 43°C, it experienced reductions in slump flow of about 26%, 37%, and 45%, respectively, when compared to the slump flow of the equivalent matrix under T21Hy condition. Contrary to the results of hot temperatures, the unconfined workability of the selected self-consolidating concretes improved during mixing and hauling under a cold environment when compared to that of the control matrix in T21Hy. As it can be seen in Table III, the increase was 3%, 8%, and 10% when the matrices were hauled for 10, 60, and 80 minutes.

Table III. Fresh properties of 625 mm self-consolidating concrete at various hauling times and temperatures.

Temp.[a] (°C)	Hauling time (minute)	Measured slump flow (mm)	T_{50} (sec.)	VSI	Slump flow change vs. T21H10 (mm)	Slump flow change vs. T21Hy (mm)
43	10[b]	480	-[c]	0	-171	-171
	60	292	-	0	-359	-171
	80	229	-	0	-422	-190
21	10[b]	651	2.79	0	0	0
	60	464	-	0	-187	0
	80	419	-	0	-232	0
-0.5	10[b]	673	2.50	0	22	22
	60	502	-	0	-149	38
	80	462	-	0	-189	43

[a]Control temperature
[b]Control hauling time
[c]The T_{50} time could not be measured since the slump flow was less than the recommended 508 mm

Change in flow rate. The T_{50} times was used to evaluate the flow rate or viscosity by inference of the fresh self-consolidating concrete. The T_{50} at TxHy condition was compared to those obtained at the control condition of T21H10, i.e. 2.79 seconds. In general, the flow rate of the selected self-consolidating concretes was increased when the mixture was exposed to the combination of hauling time and temperature. Irrespective of the selected transportation time, in elevated temperatures of 43°C the T_{50} times of the selected self-consolidating concrete were not available for measurement since their spreads were less than the recommended 508 mm. On the other hand, when self-consolidating concretes were hauled in cold environment the flow rate of the matrix increased at the hauling times of 10 minutes or less.

Change in dynamic stability. In general, the dynamic stability of the selected 635 mm self-consolidating concrete was not affected by the hot or cold temperatures and always remained highly stable.

Mechanism of slump flow loss or gain

The fundamental mechanism of slump flow loss or gain induced by the combination of hauling time and hot or cold temperatures is illustrated by the flow chart of Figure 1. It can be explained through the increase or decrease in

adsorption amount of admixture per specific surface area of concrete mortar (Ads/SSAm), the contribution of aggregate's moisture content, and the partial evaporation of mixing water [10].

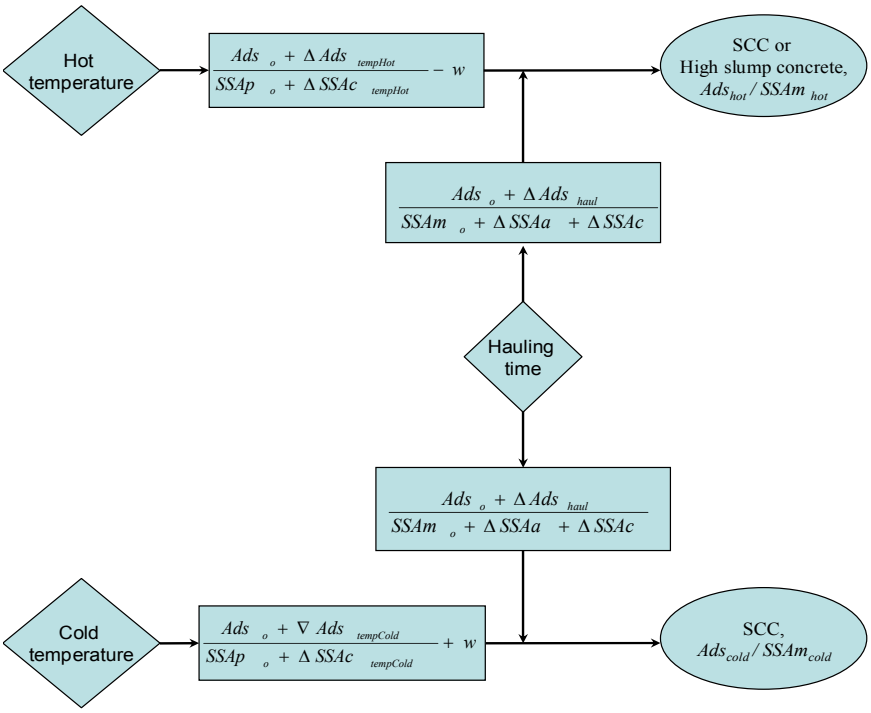

LEGEND
Ads_o = *Adsorption amount of admixture at the control condition of T21H10*
$SSAm_o$ = *Specific surface area of concrete mortar at T21H10*
$SSAp_o$ = *Total specific surface area of concrete paste at T21H10*
$\Delta SSAa$ = *Increase in SSAm due to the grinding of aggregates and cement during hauling*
$\Delta SSAc$ = *Increase in SSAm or SSAp due to the growth of cement hydrated products*
$\Delta Ads_{tempHot}$ = *Increase in adsorption due to hot temperature*
$\nabla Ads_{tempCold}$ = *Decrease in adsorption due to cold temperature*
$\Delta SSAc_{tempHot}$ = *Increase in SSAm due to hot cement hydration*
$\Delta SSAc_{tempCold}$ = *Increase in SSAm due to cold cement hydration*
w = *mixing water contribution*

Figure 1. Mechanism of slump flow loss induced by the combined hauling time and temperature.

When the temperature of the mixing room increased from -0.5 to 21 to 43°C, the contribution of aggregates' moisture content to the total mixing water became

more pronounced [10]. It required about 2 to 3 kg/m^3 of additional mixing water to maintain the same slump flow. Although not measured, it is also suspected that a portion of the mixing water was evaporated and/or absorbed once it become in contact with the hot aggregates and cementitious materials, thus reducing the amount of water necessary to assist the admixture in dispersing cement particles. Otherwise accounted in the design of the matrix at extreme temperatures, the corresponding aggregates' moisture contribution can affect significantly the mixing water requirement, and thus the yield stress and plastic viscosity of concrete in general and self-consolidating concrete in particular.

The contribution of the hauling time to the increase in SSAm was attributed to the grinding of aggregate and cement particles, and the growth of cement hydrated products, whereas the role of the temperature was explained through the growth of cement hydrated products.

The direct measurement of adsorption Ads was beyond the scope of this investigation. However, the ultraviolet-visible (UV/Vis) spectroscopy was used to determine the cement-water-superplasticizer solution concentration of free admixture, from which correlations with the amount of adsorption were made. Diawara [10] found that while the concentration of HRWRA molecule remained fairly uniform at temperatures ranging from 14 to 36^{o}C, it decreased as the temperature moved toward the extreme cold and hot temperatures. Table IV documents the UV/Vis test results.

Table IV. HRWRA concentration at various hauling times and temperatures.

Mixing condition	Total concentration of admixture (g/L)
T-0.5H10	24.92
T-0.5H60	48.97
T-0.5H80	49.02
T21H10	44.49
T21H60	82.45
T21H80	82.99
T43H10	30.87
T43H60	68.83
T43H80	69.37

The contribution of Ads to the fresh performance of the trial matrix was derived from the superposition of Ads_{haul} from hauling time and Ads_{temp} from the temperature. Diawara [10] also reported that the concentration of free admixture in cement-water solution increased as hauling time increased up to 80 minutes. Beyond that time, gradual decreases were recorded as longer hauling times of 100, 140, and 180 minutes were used. The increase or decrease in admixture

concentration led to an increase or decrease in admixture adsorption on cement particle. Despite the increase in free admixture concentration, the total released carboxylic group (COO^-) from the PC-HRWRA could not produce enough electrostatic and steric hindrance repulsive forces in dispersing cement particles to avoid the loss in slump flow. Based on the prior evidence on the role of hauling time on specific surface area of concrete mortar, it can be concluded that the increase in SSAm was sufficient to overtake the increase in Ads. As a result, decreases in fresh properties of the fresh self-consolidating concretes were observed, indicating that the contribution of the specific surface area in slump flow loss was greater than that of the admixture adsorption.

Considering the abovementioned discussions, the slump flow loss or gain of self-consolidating concrete exposed to the combination of hauling times and extreme temperatures can be expressed in the following mathematical form:

Slump flow loss or gain =

$$f\left\{\frac{Ads}{SSAm}, w\right\} = \frac{Ads_{haul} + Ads_{temp}}{SSAm_{haul} + SSAm_{temp}} + (w_o + w_t)_{temp} \quad (1)$$

where: $\frac{Ads}{SSAm}$ = Adsorption amount of admixture per specific surface area of concrete mortar

Ads_{haul} = Adsorption amount of admixture induced by hauling time

Ads_{temp} = Adsorption amount of admixture induced by temperature

$SSAm_{haul}$ = Specific surface area of concrete mortar generated by hauling time

w = Contribution of the mixing water

w_o = Contribution of the mixing water at the control temperature

w_t = Contribution of the mixing water at the target temperature (could be ±)

Prediction of SCC slump flow at TxHy

The measured slump flow at the TxHy condition can be related to the target slump flow, the hauling time and the temperature by determining the most suitable statistical predictive equation using a 95% confidence level. The relationships are as follows:

In hot temperature:

$$SF_{measured} = -3.4021h_t - 7.0002t_h + 0.2354SF \quad (2)$$

Or $SF_{measured} = ah_t + bt_h + cSF$

In cold temperature:

$$SF_{measured} = -2.5162h_t - 0.2070t_c + 1.0314SF \quad (3)$$

Or $SF_{measured} = ah_t + bt_c + cSF$

where: $SF_{measured}$ = Slump flow measured at TxHy condition (mm)

h_t = Hauling time (minute), with 10 minutes ≤ h_t ≤ 80 minutes

t_h = Hot temperature (°C) with 21°C ≤ t_h ≤ 43°C (tolerance ± 2°C)

t_c = Cold temperature (°C) with -0.5°C ≤ t_c ≤ 14°C (tolerance ± 2°C)

SF = Target slump flow (mm), with 635 mm ≤ SF ≤ 711 mm (tolerance ± 25 mm).

The predictive equations were tested for accuracy using R^2 (regression value) and S (standard deviation). Correlations between the data predicted from the regression equations and the actual results were evaluated using F and T tests. The regression equations (2) and (3) produced R^2 and S values of 96.7% and 20.82 mm; and 95% and 18.32 mm, respectively, indicating a good relationship between the dependent variable (slump flow loss) and the independent variables (initial slump flows, hauling times and hot or cold temperatures). F and T tests were performed to confirm the significance of coefficients a, b, c, and d in the regression models. The following results were found.

For Eqn. (2):
Prob(t) = 0.0000, 0.0000 and 0.0000, for a, b and c, respectively; Prob(F) = 0.0000.

For Eqn. (3):
Prob(t) = 0.000, 0.7458 and 0.000 for a, b and c, respectively; Prob(F) = 0.000.

In general, the F and T tests results indicated that all independent variables, i.e. hauling time, temperature, and initial slump flow had a similar influence on the predicted slump flow losses. The higher value of Prob(t) for the coefficient b of Eqn. (3) indicates that the magnitude of the cold temperature has little influence in the prediction of the slump flow loss.

Conclusions

The following conclusions can be drawn from the test results:

- In general, the self-consolidating concrete batched and transported for a long time in hot or cold temperatures experienced slump flow losses in hot conditions, and gains in cold temperatures when compared to the equivalent concretes produced at the control temperature of T21H10 (i.e., 10-minute

hauling time under normal room temperature of 21°C). Under all selected temperatures, the slump flow decreased with the increase in hauling time.

- The flow rate/plastic viscosity (measured by the T_{50} time) of the selected self-consolidating concretes were also affected by the combination of hauling time and temperature. Irrespective of the selected temperatures, the selected matrix experienced progressive and excessive losses in slump flow with increases in hauling time and their T_{50} times could not be evaluated.
- The changes in fresh properties of plastic self-consolidating concretes can be explained through the increase or decrease in adsorption amount of admixture per specific surface area of concrete mortar (Ads/SSAm), the contribution of aggregate's moisture content, and partial evaporation of mixing water. However, despite the augmentation in Ads, the increase in SSAm was sufficient to decrease the Ads/SSAm, resulting in further reduction (in hot temperature) or conservation (in cold temperature) of the unconfined workability for the trial self-consolidating concretes.
- The statistical equations to predict the actual slump flow of the self-consolidating concrete prepared and transported for different hauling times, and hot and cold temperatures; showed significant relationships between the dependent and independent variables.

Acknowledgements

The authors would like to acknowledge the financial support of the Nevada Department of Transportation, Grant number P 077-06-803. Thanks are also given to a number of admixture manufacturers and concrete suppliers who contributed materials and equipments used in this investigation. Their names are withheld to avoid any concern of commercialization or private interest.

References

[1] American Concrete Institute (2007), Self-Consolidating Concrete, Reported by the Committee 237, pp. 30.

[2] Kosmatka, S.H., Kerkhoff, B. and Panarese, W.C. (2002), Design and Control of concrete Mixtures, 14th Edition, Portland Cement Association, Skokie, Illinois, 358 pp.

[3] American Society for Testing and Materials (2004), Standard Specification for Portland Cement, (ASTM C 150), *Annual Book of ASTM Standards*, vol. 4.01, pp. 150-157.

[4] American Society for Testing and Materials (2004), Standard Test Method for Coal Fly Ash and Raw or Calcined Natural Pozzolan for Use as a Mineral Admixture in Concrete, (ASTM C 618), *Annual Book of ASTM Standards*, vol. 4.02, pp. 319-312.

[5] American Society for Testing and Materials (2004), Standard Specification for Concrete Aggregates, (ASTM C 33), *Annual Book of ASTM Standards*, vol. 4.02, pp. 10-16.
[6] American Society for Testing and Materials (2004), Standard Specification for Chemical Admixture for Concrete, (ASTM C 494), *Annual Book of ASTM Standards*, vol. 4.02, pp. 271-279.
[7] American Society for Testing and Materials (2004), Standard Test Method for Bulk Density ("Unit Weight") and Voids in Aggregate, (ASTM C 29), *Annual Book of ASTM Standards*, vol. 4.02, pp. 1-4.
[8] American Society for Testing and Materials (2005), Standard Test Method for Slump Flow of Self-Consolidating Concrete, (ASTM C 1611), *Annual Book of ASTM Standards*, vol. 4.02, pp. 36-41.
[9] American Society for Testing and Materials (2005), Standard Test Method for Passing Ability of Self-Consolidating Concrete by J-Ring, (ASTM C 1621), *Annual Book of ASTM Standards*, vol. 4.02, pp. 42-45.
[10] Diawara, H. (2008), Parametric Study of Self-Consolidating Concrete, Ph.D. Dissertation, University of Nevada, Las Vegas (UNLV), USA, 370 pp.

Theme 4: Production and Placement of SCC

Similarities and Differences of Pumping Conventional and Self-Compacting Concrete

Dimitri Feys[1], Geert De Schutter[2], Ronny Verhoeven[3] and Kamal H. Khayat[1]

[1] Department of Civil Engineering, Université de Sherbrooke, Québec, Canada
[2] Magnel Laboratory for Concrete Research, Department of Structural Engineering, Faculty of Engineering, Ghent University, Belgium
[3] Hydraulics Laboratory, Department of Civil Engineering, Faculty of Engineering, Ghent University, Belgium

Abstract. In practice, self-compacting concrete (SCC) is considered as a simple extension of conventional vibrated concrete (CVC) when pumping is concerned. The same equipment, materials, pumping procedures and guidelines used for CVC are applied when pumping SCC. On the other hand, it has been clearly shown that the rheological properties and the mix design of SCC are different than CVC. Can the same pumping principles employed for CVC be applied for SCC? This paper compares the some published results of pumping of CVC with those for SCC. A first striking difference between pumping of CVC and SCC is the flow behaviour in the pipes. The flow of CVC is a plug, surrounded by a lubricating layer, while during the flow of SCC, part of the concrete volume itself is sheared inside the pipe. As a result, the importance of viscosity increases in case of SCC. Due to the low yield stress of SCC, the behaviour in bends is different, but quite complex to study. Due to the lower content of aggregate and better stability of SCC, as it is less prone to internal water migration, blocking is estimated to occur at lower frequency in case of SCC.

Introduction

Pumping of concrete is a worldwide applied casting method enabling fast and efficient concrete placement. For conventional vibrated concrete (CVC), the results of scientific investigations and practical guidelines can be easily found in literature [1-4], while for self-compacting concrete (SCC), the number of investigations published is quite restricted [5-7]. On the contrary, SCC is largely applied in the concrete industry and is often placed by means of pumping. In practice, it is assumed that pumping of SCC is similar to pumping of CVC, and that the same

K.H. Khayat and D. Feys (eds.), *Design, Production and Placement of Self-Consolidating Concrete*, RILEM Bookseries 1,
DOI 10.1007/978-90-481-9664-7_13, © RILEM 2010

rules would apply. On the other hand, SCC is a different concrete with a different composition and rheological behaviour [7, 8]. Therefore, it is important to know if the rules for CVC would apply for SCC.

This paper compares the literature results for pumping of CVC with the results obtained during a research project on pumping of SCC. It will point out the main differences in mix design and rheological properties between the two concrete types and the consequences of these differences on the main parameters influencing the pumping pressure.

Experiments on SCC

Test setup

Pumping experiments on SCC were conducted with a truck-mounted piston pump, having two cylinders alternately pushing concrete inside the pipeline and pulling concrete from the reservoir of the pump. A powerful valve in the pump switches the connection between the pipes and the cylinders when the pushing cylinder is empty and the pulling cylinder is full. The output discharge rate of the pump could be varied over 10 different steps from the lowest step: 4-5 l/s (defined as step 1) to the highest step: 40 l/s (step 10). During the experiments, the maximum discharge rate was restricted to 19-20 l/s (step 5) for safety reasons.

Behind the pump, two different types of loop circuits were installed using steel pipes with an inner diameter of 106 mm: a short circuit with a length of approximately 25 m (Figure 1), and long circuits with lengths varying between 80 and 105 m. In both types of circuits, the pressure loss was measured in a straight horizontal section by means of two pressure sensors, located approximately 10 m from each other. As a back-up for the each pressure sensor, three strain gauges were attached to the outer wall of the pipe. As pipe deformation can be related to the occurring pressure [1], strain gauges were also attached to the pipe walls in other locations than the pressure sensors to monitor pressure evolution in the long circuits, including sections containing a bend.

As the theoretical volume of a pumping cylinder is 83.1 liter, the discharge rate was determined indirectly by measuring the time between two changes of the pumping valve, which corresponds to the contents of one pumping cylinder. This measuring method was verified by pumping the concrete present inside a full cylinder into a reservoir suspended with a load cell to a rolling bridge. By measuring the variations of the mass of the concrete discharged into the reservoir with time, the discharge rate was calculated. Both measurement methods were shown to deliver similar discharge rates.

Figure 1. Short pumping circuit (25 m).

Testing procedure

As the volume of concrete required for the pumping tests was 1.5 and 3.25 m^3 for the short and long circuits, respectively, the concrete was prepared in a ready-mix plant and delivered to the laboratory in a time span of approximately 45 min. After filling the pipe with concrete over 10 min for the short circuit, the first test could be started around 60 min following water-cement contact. For the long circuits, the quantity of priming mortar appeared to be insufficient to avoid blocking during the filling of the pipes and consequently, the first test was started at later concrete ages: between 1 and 2 hours. The tests on fresh concrete indicate that even at this age, the concrete still has self-compacting properties.

The testing procedure consisted of pumping the concrete at the five lowest available discharge rates, in a descending order (steps 5 to 1) and maintaining each discharge rate for five full strokes (Figure 2). In this way, pressure loss, measured as the pressure difference between the two pressure sensors divided by the separation distance, vs. discharge rate curve could be obtained in relatively short period (4 min). This procedure was repeated at 30-min intervals until the workability of the concrete decreased below the SCC level. Simultaneously to the pumping experiment, rheological properties of the SCC were determined using a Tattersall Mk-II rheometer [7, 9] in addition to standard characterization of SCC workability (slump flow, V-funnel and sieve stability in addition to unit weight and air content).

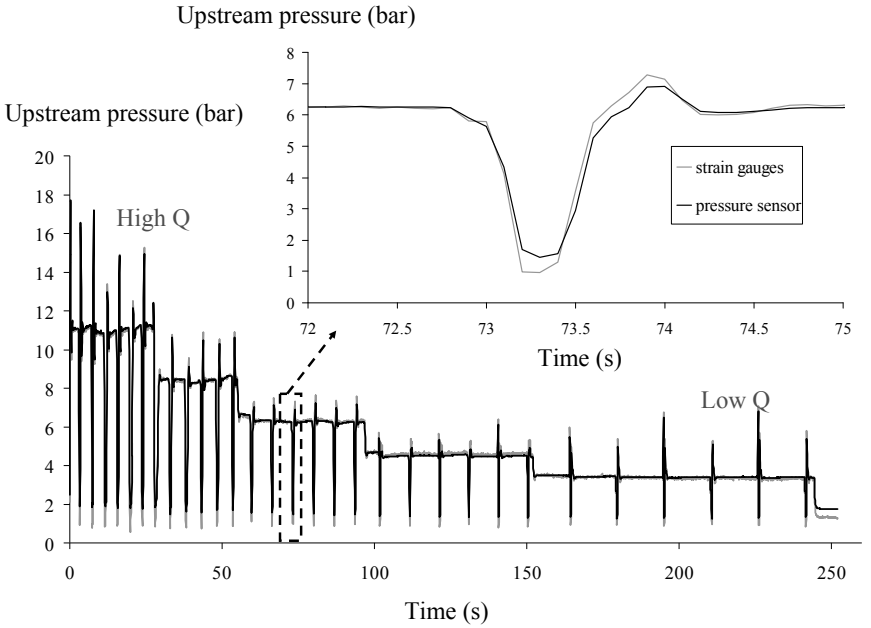

Figure 2. Upstream pressure variation with time, clearly indicating the five different discharge rate steps.

Concrete composition

In total, 19 different concrete mixtures were produced for the pumping tests. The mixture proportioning of these concretes are given in Table I. Most of the mixtures were prepared using ordinary high strength Portland cement (CEM I with 52.5 MPa cement strength at 28 days), limestone filler, natural sand, rounded river-bed gravel with maximal size of 16 mm and polycarboxyl-ether superplasticizer with a long workability retention. As can be seen in Table I, the mixture proportioning is based on the powder-type method for SCC mix design [8]. Four of the concrete mixtures were commercial products supplied by the ready-mix concrete producer. Mixtures SCC 14-17 were pumped in the long circuits, the others were used in the short circuit.

Table I. Concrete compositions.

Composition [kg/m^3]	SCC 0	SCC 1	SCC 2	SCC 3	SCC 4	SCC 5	SCC 6	SCC 7	SCC 8	CVC 1
Gravel 8/16	Commercial mixture	434	434	434	459	434	434	434	434	Commercial mixture
Gravel 2/8		263	263	263	278	263	263	263	263	
Sand 0/5		853	853	853	901	853	853	853	853	
CEM I 52.5 N		360	360	360	300	360	360	360	360	
Limestone Filler		239	239	239	200	239	239	239	239	
Water		165	165	165	165	165	165	165	165	
SP [l/m^3]		11	11	15.22	12.16	20.95	13.33	12.69	14.44	
Initial SF [mm]	740	640	720	690	710	710	720	650	680	190*

Composition [kg/m^3]	SCC 9	SCC 10	SCC 11	SCC 12	SCC 13	SCC 14	SCC 15	SCC 16	SCC 17
Gravel 8/16	410	434	410	434	434	434	Commercial mixture	434	Commercial mixture
Gravel 2/8	248	263	248	263	263	263		263	
Sand 0/5	805	853	805	853	853	853		853	
CEM I 52.5 N	400	360	400	360	360	360		360	
Limestone Filler	300	239	300	239	239	239		239	
Water	165	165	165	165	165	160		165	
SP [l/m^3]	18.15	11				21.9			
Initial SF [mm]	850	800	700	675	700	640	650	700	700

*slump

Comparison between CVC and SCC

Mix design and rheological properties

As stated in the previous sections, the mix design of SCC differs from CVC in order to enhance the flowability, reduce blocking due to accumulation of aggregates and avoid segregation. The amount of coarse aggregates in SCC is reduced and the viscosity of the concrete is increased by means of viscosity-modifying agents (VMA), or by increasing the amount of fine particles in the concrete, or by combining both. In this experimental project, the powder-type method was applied, by adding limestone filler to the concrete.

The rheological behaviour of fresh concrete is mostly described by means of the Bingham model (defining a yield stress and a plastic viscosity) [9-11], when transient behaviour, like thixotropy is not considered [11]. As generally known, SCC has a low yield stress, resulting in a high slump value [12]. The order of magnitude for the yield stress is between 10 and 100 Pa for SCC, while it can achieve several thousands of Pascals for CVC. For “pumpable” conventional vibrated concrete, the yield stress roughly varies between 100 and 1000 Pa [1]. The viscosity of SCC is increased by means of VMA or an additional amount of small

particles to prevent segregation of the coarse aggregates. As a result, the viscosity of SCC is generally higher than the viscosity of CVC.

Behaviour law in pipes

The movement of concrete in pipes can be determined by two physical processes: flow or friction [1, 13]. In case friction is negligible, the deformation of concrete in pipes occurs according to the hydrodynamic laws, and as concrete has a high viscosity, the occurrence of turbulence in straight sections is quite rare. As a result, the flow is laminar, and rheological principals for dense suspensions can be applied.

The pressure gradient during pumping does not only push the concrete through the pipeline, but also tends to move the water among the granular skeleton [13]. In this case, the water content is no longer homogeneous along the conveying pipeline and in zones suffering a reduction in water, the stress is no longer transferred through the liquid, but by friction among aggregates. Browne and Bamforth examined both behaviour laws for the movement of concrete in pipes and concluded that the frictional behaviour causes a significantly higher pressure to pump the concrete, compared to the hydrodynamic behaviour [13]. Also in practice, “pumpable” CVC contains relatively large amount of fine particles to reduce friction, and stable concrete is less prone to friction than unstable mixtures.

As discussed in the previous section, special care is taken to avoid segregation in case of SCC, by adding VMA or more fine particles [8]. In theory, SCC should flow in the pipes according to hydrodynamic laws, which is confirmed by the conducted experiments. No blocking was observed during regime conditions (after insertion), even when a segregating concrete was fed into the pump (SCC 9 and 10). During the start-up of pumping, on the other hand, the experiments on the long circuits indicate a large amount of blockings due to a lack of fine particles at the concrete front, causing friction between coarse aggregate particles. The amount of fine particles at the concrete front decreases, as they stick to the pipe wall to lubricate the concrete and as they need to fill the space in the rubber seals installed in the connections between the pipes. Blocking during start-up was reported by Kaplan as the most frequent blocking occurrence [1] and can be prevented by inserting a priming mortar in the pipes before the pumping of concrete starts.

Flow in straight sections – velocity profile

In order to estimate the velocity profile of different types of concrete flowing through pipes, the theoretical framework for laminar flow in cylindrical pipes will be introduced, which is known as the Poiseuille formula in case of Newtonian liquids. The shear stress at the wall of the pipe is related to the pressure loss by equilibrium of forces (Eqn. (1)):

$$\tau_w = \Delta p \cdot R / 2 \tag{1}$$

where: τ_w = wall shear stress (Pa)
Δp = pressure loss per unit of length (Pa/m)
R = radius of the pipe (m)

The shear stress varies linearly with the pipe radius, from zero in the center, to the maximum value at the wall (τ_w). Incorporating the rheological behaviour law into the shear stress profile delivers the shear rate distribution, which can be integrated to obtain the velocity profile. The presence of a yield stress causes a zone with zero shear rate in the center, resulting in a constant velocity, also known as the plug. The larger the yield stress, the larger the plug radius and in the limit, no flow should occur if the wall shear stress is equal to or smaller than the yield stress of the concrete. As the yield stress of CVC is quite high, this would result in elevated pressure to start the flow of CVC. In order to facilitate its movement in pipes, concrete creates a water-cement layer of lower rheological properties near the wall [1-2]. As a result, the concrete can move much faster through the pipes and flow is observed even if the wall shear stress is lower than the yield stress of the bulk concrete.

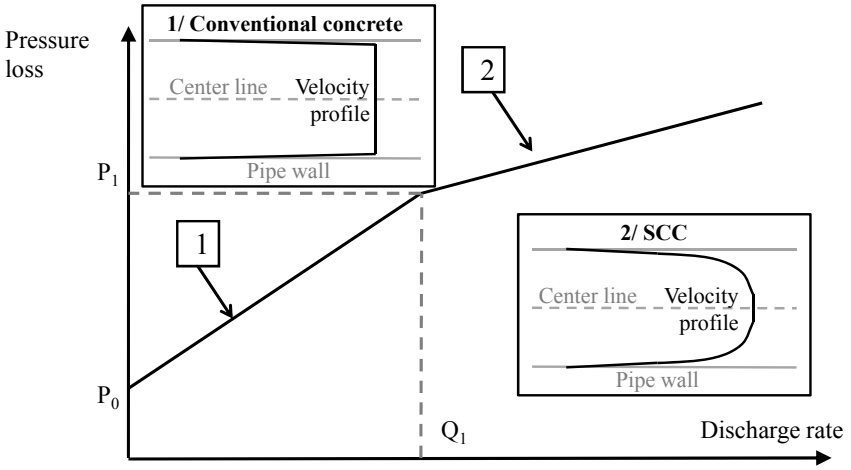

Figure 3. Distinction between pure plug flow with a lubrication layer (zone 1) and plug flow with a lubrication layer and partly sheared concrete (zone 2), based on pressure loss – discharge rate curve. (Q1, P1) represents the theoretical point where the wall shear stress equals the concrete yield stress. Figure after Kaplan [1].

Kaplan made a distinction between two different types of velocity profiles of the pressure loss – discharge rate curve, as can be seen in Figure 3 [1]. In zone 1, on the left side, the pumping parameters are only governed by the properties of the lubrication layer, as the wall shear stress is lower than the concrete yield stress. In zone 2, the flow parameters are governed by both the properties of the lubrication layer and the properties of the concrete. The velocity profile in zone 1 consists of a plug (constant velocity) and a large velocity gradient near the wall due to the lubrication layer [1, 2], while in zone 2, the velocity profile consists of a plug, a large velocity gradient near the wall and a smaller velocity gradient in between, because the concrete itself is also sheared [1, 7]. Conventional concrete has a rather high yield stress and in most cases is situated in zone 1, while SCC has a rather low yield stress, and is mostly situated in zone 2.

SCC also creates a lubrication layer near the wall during pumping, as the theoretical framework delivers significantly larger pressure losses at a certain discharge rate, compared to the experiments [7]. On the other hand, as the yield stress is low, a large part of the concrete is sheared, and a good relationship between the viscosity of the concrete and pressure loss can be established. This relationship is dependent on the discharge rate (Figure 4).

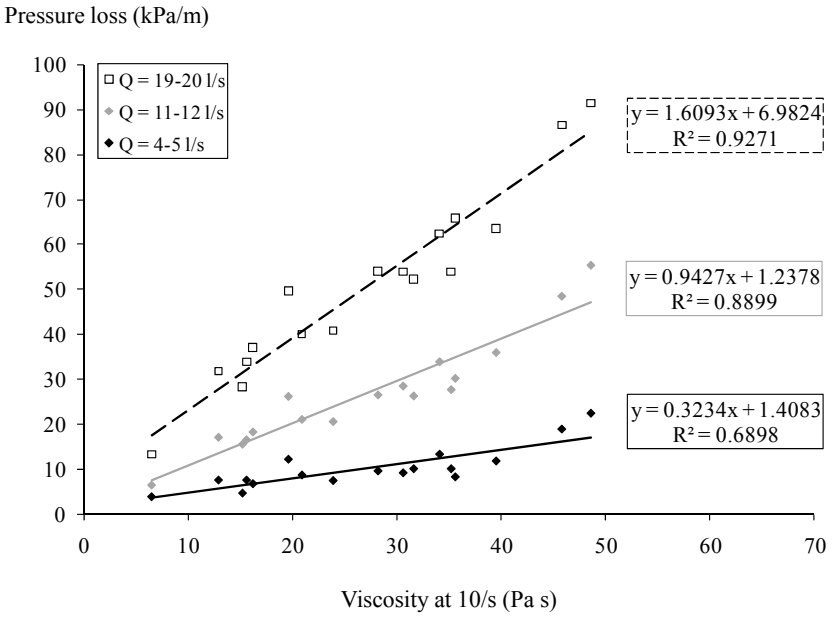

Figure 4. Variations of pressure loss with plastic viscosity of SCC determined at different discharge rates.

Note that these results are empirical and the relationship will change with varying discharge rate and pipe diameter. On the other hand, it is clearly shown that viscosity of SCC, rather than the yield stress, is the main factor influencing pressure loss. Such pressure loss corresponds to the required pumping pressure. Further research should be carried out to identify the relative importance of the lubrication layer for pumping SCC.

Pressure loss in bends

As in case for pure water, existing literature delivers non-conclusive results regarding pressure loss in bends of pipelines for CVC. For example, Kaplan [1] and Chapdelaine [2] did not observe any noticeable additional pressure losses in bends in during their field pumping experiments, while practical guides for pumping introduce the concept of equivalent length to account for the presence of bends in pumplines [3, 4]: e.g. one bend of 90° is equivalent to 3 m of straight pipes [4].

For SCC flowing in bends, an additional pressure loss was observed during the pumping experiments in the long circuits, which appears to be larger compared to CVC. It is important to note that the large scatter of the results prevents accurate conclusion on the level of increase in pressure loss in bends [7]. As the concrete flow needs to change direction across a bend, it is estimated that pressure loss in bends is influenced by a large number of parameters, including viscosity, inertia, coarse aggregate properties, bending radius and helicoidal flow velocity. As a result, further research is needed to capture these phenomena in details in order to develop guidelines and models that can take into account flow of SCC in bends.

Conclusions

By means of the results available in literature for CVC and experimental research project on pumping of SCC, comparison between pumping of CVC and SCC was made. The velocity profile for CVC flowing through pipes is composed of a lubrication layer with a large velocity gradient and a plug in which the velocity is constant. For SCC, the radius of the plug is much smaller than for CVC, and a smaller velocity gradient is present between the lubrication layer and the plug. As a result, a part of the concrete volume is also sheared in the pipes. The pumping parameters for CVC depend mainly on the properties of the lubrication layer, while for SCC, a good relationship between concrete viscosity and pressure loss was established. The flow in bends is complicated leading to non-conclusive results for both CVC and SCC. Further research is required to clarify the influencing factors.

Acknowledgements

The authors would like to acknowledge the Research Foundation in Flanders (FWO) for the financial support of the project and the technical staff of the Magnel and Hydraulics Laboratory at Ghent University for the preparation and execution of the full scale pumping tests.

References

[1] Kaplan, D. (2001), Pumping of concretes, Ph.D. Dissertation (in French), Laboratoire Central des Ponts et Chausées, Paris.
[2] Chapdelaine, F. (2007), Fundamental and practical study on the pumping of concrete, Ph-D-thesis (in French), Université Laval, Laval.
[3] Guptill, N.R. et al. (ACI-Comm 304) (1998), Placing concrete by pumping methods, American Concrete Institute, Farmington Hills.
[4] Crepas, R.A. (1997), Pumping Concrete, Techniques and Applications, 3rd edition, Crepas and Associates, Inc., Elmhurst.
[5] Beitzel, H. and Beitzel. M. (2008), Pump application for self-compacting concrete under extreme conditions, Proc. of the 3rd North-American Conf. on the Design and Use of Self-Consolidating Concrete, Chicago.
[6] Ouchi, M. and Sakue, J. (2008), Self-compactability of fresh concrete in terms of dispersion and coagulation of particles of cement subject to pumping, Proc. of the 3rd North-American Conf. on the Design and Use of Self-Consolidating Concrete, Chicago.
[7] Feys, D. (2009), Interactions between rheological properties and pumping of self-compacting concrete, Ph.D. Thesis, Ghent University, Ghent.
[8] De Schutter, G., Bartos, P., Domone, P. and Gibbs, J. (2008), Self-Compacting Concrete, Whittles Publishing, Caithness.
[9] Tattersall, G.H. and Banfill, P.F.G. (1983), The Rheology of Fresh Concrete, Pitman, London.
[10] Wallevik, O.H. (2003), Rheology – A scientific approach to develop self-compacting concrete, Proc. of the 3rd Int. Symp. on Self-Compacting Concrete, Reykjavik, pp. 23-31.
[11] Wallevik, J.E. (2009), Rheological properties of cement paste: Thixotropic behavior and structural breakdown, *Cem. Conc. Res.,* vol. 39, pp. 14-29.
[12] Ede, A.N. (1957), The resistance of concrete pumped through pipelines, *Mag. Conc. Res.,* vol. 9, pp. 129-140.
[13] Browne, R.D. and Bamforth, P.B. (1977), Tests to establish concrete pumpability, *ACI Journal,* vol. 74, pp. 193-203.

Flow of SCC along Surfaces

Stefan Jacobsen[1], Hedda Vikan[2] and Lars Haugan[2]

[1] Dept. of Structural Eng., Norwegian University of Science and Techn., Norway
[2] SINTEF Byggforsk AS, Norway

Abstract. The flow conditions near solid surfaces (no-slip, slip, lubrication) were investigated using the results of gravimetric flow tests, full scale instrumented pump tests and rheological measurements on matrix, mortar and self-compacting concrete. Modeling with the measured data could fit plug-flow with a 0.6-1 mm thick lubrication layer of matrix having similar lubrication layer viscosity as the lower values of Kaplan: 175-320 Pa·s/m. Visualization of boundary flow conditions and flow profiles and measurements of concrete sticking to different pipe materials related to increased flow rate along smooth acryl and reduced along rougher rubber surfaces. The existence of plug flow during SCC pumping may be questioned and possible causes for formation of a lubricating layer and a plug are discussed as well as a brief review of void formation at the surface.

Introduction

In production of concrete structures surfaces free of voids and other imperfections can be difficult to obtain. Contractors regard this as a major problem [1]. It is also presently a research field within the COncrete INnovation centre [2]. Research was therefore made on flow along surfaces during pumping [3-7], relation to rheology and surface condition.

Flow of Concrete towards Surface

At a concrete surface there is increased paste content due to the wall effect. The coarse aggregate content is almost halved at a distance approximately equal to half the maximum aggregate diameter resulting in low local aggregate packing [8]. Furthermore, during flow the rate of shear is usually highest near the surface and aggregate particles tend to move towards lower rate of shear away from the surface.

K.H. Khayat and D. Feys (eds.), *Design, Production and Placement of Self-Consolidating Concrete*, RILEM Bookseries 1,
DOI 10.1007/978-90-481-9664-7_14, © RILEM 2010

The rate and length of flow along the surface during form filling probably play important roles for the existence or absence of surface voids [9]. The formation and characteristics of different flow conditions at a solid surface have, to our knowledge, not been investigated in detail yet. Except for studies on concrete pumping, few physical characteristics beyond those reviewed in [5] exist. Some early studies like [10-13] mainly pointed to the existence of slip layers to be able to model flow. In newer studies like [6, 7, 14-16] further work was made. In [14] an atmospheric pressure tribometer was developed for determination of slip layer viscosity. In [15] three different ways of formulating SCC-flow towards the solid were proposed: No-slip, Navier-slip and lubrication.

No-slip means a homogeneous fluid with zero flow at the wall and is the standard boundary flow condition, for example for Poiseuille flow of a Newtonian fluid. The Navier-slip [15] models a certain minimum flow rate in homogeneous fluid at the wall and constant shear stress in the flowing concrete. The increase of flow rate parallel to the solid surface is proportional to shear stress parallel to the wall, the proportionality being a slip coefficient. The third surface flow model is a lubrication-layer between the solid surface and the bulk concrete. The layer has lower rheological properties than the bulk concrete and zero flow at the wall. Towards the bulk concrete the lubrication layer and the bulk have equal flow rate. However, no physical data (surface flow rate, slip coefficient) were given in [15]. The physics must of course be realistic and so we must assume that Navier-slip is based on surface friction like in [10], whereas no-slip and lubrication are based on fluid flow like in [11, 14].

Experiments and Results

In our investigations on flow, pumpability and rheology of concrete and mortar, different matrices were made with w/b = 0.50 and 0.56, CEM II 42.5 with 20% fly ash (ground with clinker), silica fume, co-polymeric SP and VMA, see Table I.

Table I. Matrix composition (all material < 0.125 mm) - % of cement mass.

Mixture	w/b	SP	SF	filler	VMA
51	0.50	1	0	20	
52 *	0.50	2	2.5	20	1
53	0.50	1.2	5	28	
54	0.50	0.8	5	20	
55	0.56	2	2.5	20	1

*: Concrete with this matrix neither SCC nor pumpable

The rheological properties of the matrix were investigated in a Physica parallel plate rheometer [6] to a maximum rate of shear 100 s^{-1}. The results are given in

Table II. Measurements of gel strength (yield stress from rest) were made with the procedure described in [17]. Plastic viscosity and yield stress of matrix Mixes 51-55 were derived from the Bingham model in Table II with correlation coefficients R^2 = 0.81-1.00. Due to shear thinning the Herschel-Bulkley model fitted slightly better. The BML-viscometer measures rheological parameters according to the Bingham model and this model is also used in the Buckingham-Reiner equation [11-14]. It was therefore used both for matrix and concrete.

Table II. Matrix rheology: Bingham plastic viscosity (μ), yield (τ_0), gel strength.

Mixture	μ (Pa·s)	τ_0 (Pa)	Gel strength 1 (init.) (Pa)	Gel strength 2 (+10 min) (Pa)	≈structural build-up (Pa/s)
		dynamic	Static	Static	Static
51	0.32	1	0	6	0.010
52	0.10	26	41	50	0.015
53	0.24	7	7	11	0.007
54	0.26	14	14	14	0
55	0.11	17	21	27	0.01

Pipe flow conditions (slip, velocity profile) were studied on mini-concrete with 25% coarse aggregate (4-8 mm), 35% sand (0.125-8 mm) and 40 volume % matrix [5]. Pumpability (flow, pressure) was studied on mortar with 60% sand (0.125-8 mm). The granitic aggregate was a mixture of natural and crushed with particle density 2760 kg/m^3 and 0.5% absorption in coarse and 0.8% in fine aggregate. The content of particles < 0.125 mm was 6.5% in the sand, resulting in the 20% filler in matrix shown in Table I. Mixture 53 was added 8% extra filler of the same composition. Proportioning of concrete and mortar was done according to the particle- matrix approach [18, 19]. The matrix shown in Table I provides information regarding solid particles < 0.125 mm and liquid in the concrete, and probably represents the lubricating layer [6]. Above a matrix volume of around 360 liters per m^3 of concrete the matrix behaviour can be assumed to dominate concrete rheology [19].

Gravitational pipe flow condition experiments

Coloured and gray concrete were poured in a gravity based pipe flow experiment [5] made as an up-scaled flow-cyl test [18, 19]. Observations of flow rates and flow profiles were made. The details on how flow profiles were obtained, including limitations and uncertainties due to the colouring agent, low pressure etc, are discussed in [5]. Some interesting observations with relevance to the preceding pumping experiments were made. Figures 1 and 2 present examples of the results showing that in the gravimetric flow experiments [5] all three types of boundary

flow models reviewed in [15]; no-slip, Navier-slip and lubrication are possible depending on type of concrete and surface.

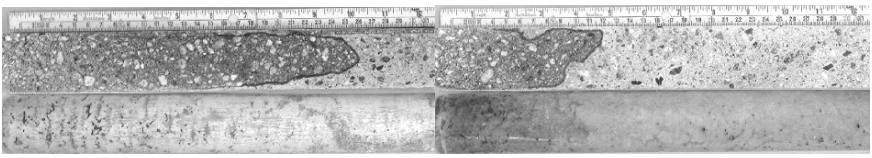

Figure 1. Flow profile (up) and slip layer (down) for rubber at 0.2 m/s (left) and acryl pipe (right) at 0.4 m/s, mixture 51 [5].

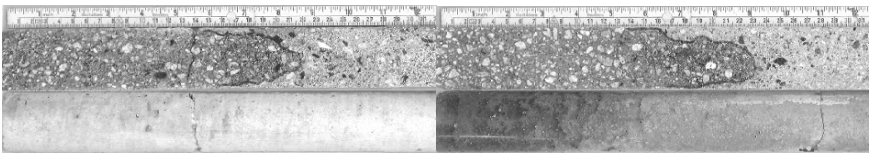

Figure 2. Flow profile (up) and slip layer (down) for rubber at 0.3 m/s (left) and acryl pipe (right) at 0.3 m/s, mixture 52 [5].

Figure 1 shows flow along the rough rubber pipe surface (30-50 μm bumps with 50-100 μm distances seen on the rubber surface in SEM [5]). Flow rate was ≈ zero at the wall, implicating a no-slip or lubrication condition at rubber. A Navier-type slip yields for the smooth acryl pipe (smooth surface seen on acryl in SEM [5]) with less variation in flow rate over the cross section. Furthermore, a long coloured slip layer was seen on the hardened concrete towards the acryl. This difference between rubber and acryl surfaces was seen for all four mixes 51-54 [5]. In addition, less surface voids were seen on the concrete surfaces hardened towards the acryl than on concrete hardened towards the rubber. (Note the difference between lubrication layer and slip layer!)

The adherence of fresh concrete mixture 51 to three different pipe materials (acryl, steel and rubber) was measured. A 1 m long pipe was filled vertically and emptied like in a slump test and mass increase of the pipe noted. Three parallel tests were made on each pipe of acryl, steel and rubber, respectively. The amounts sticking to the pipe surfaces were 0.36, 0.64 and 0.84 kg/m^2 (coefficient of variation 23-40%). This corresponded to an average matrix thickness of 0.1-0.3 mm, increasing with increasing pipe roughness and decreasing rate of flow in the flow experiments [5]. Both surface material roughness and concrete properties may thus affect boundary flow in line with the observations in Figures 1 and 2. Also friction may play a role for pump flow as suggested already in [10].

Pumping experiments

Figure 3 shows the instrumented full-scale pump set-up. It consisted of a screw pump and 70 m of Ø 50 mm rubber hose. Flow and pressure gradient were recorded during pumping at 25 and 50 Hz pump frequency. Rheological measurements (BML-viscometer, slump flow) were also made on the pumped mortars and are shown in Table III.

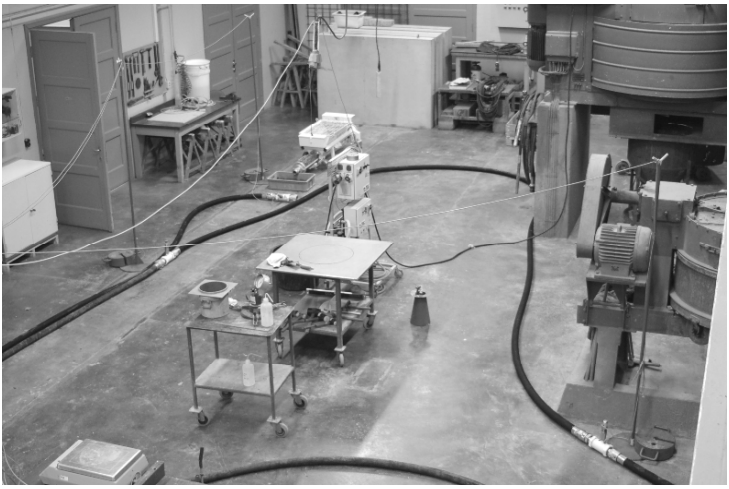

Figure 3. Pump and hose circuit with pressure sensors. The BML viscometer was located in the neighbouring room.

The screw pump works quite differently from a piston pump with a steel screw rotating inside a rubber stator. This gives a constant pressure over time and not the alternating pressure/suction behaviour in piston pumping [4]. However, the maximum aggregate size affects how tightly the steel rotor can move in the rubber stator without so-called back flow, affecting pumpability. A very limited amount of aggregate larger than 8 mm could be used before the pumping pressure dropped due to back flow. The "4 – 8 mm" used in the pipe flow experiments had too much oversize so only 0 – 8 mm sand was used for the mortar in the pumping test.

As in the pipe flow experiments, only the matrix quality varied between the pumped mortars. Composition and content of aggregate above 0.125 mm was kept constant. The rheological properties of the mortar for the pumping experiments therefore varied less than for matrix, see Tables II and III. The measured yield stresses and plastic viscosities were, respectively, 2-3 and 30-100 times higher in mortar than in matrix. This is in line with most results reviewed in [20]. Also in [21] conventional viscometers gave less relative increase in yield stress than in

plastic viscosity when going from matrix to concrete. The large effect on yield stress of aggregate deduced in [22] we attribute to that yield stress was only measured on concrete with different paste volumes and not on the paste itself. Also note that the high rate of shear in the matrix between large particles in concrete causes a problem in the comparison of pure matrix and concrete rheology [23].

Table III. Rheological properties of pumped mortars.

Mixture	Measurement before/after pump	τ_0 (yield stress) (Pa)	μ (plastic viscosity) (Pa·s)	Slump flow (mm)	Slump (mm)
51	Before	7	9.8	690	280
	After	24	7.7	670	280
52	Before	86	32.0	470	250
	After	Not pumpable			
53	Before	39	10.7	580	270
	After	54	8.0	500	260
54	Before	46	8.2	580	270
	After	88	8.4	520	265
55	Before	25	8.0	670	280
	After	8	3.7	760	280

Compared to the yield stress from rest, where quite high values are often observed [20, 24], slip conditions during viscometer measurements could be deceiving due to similar slip- or boundary flow variations as in pipe flow. Still, dynamic properties should be considered more relevant for mixing, pumping and form filling including flow along formwork surfaces. Measurements from rest are mainly relevant for formwork pressure and for the first period at rest where the escape of voids from the surface could be affected by the structural build-up indicated in Table II.

The measured flow in the pumping experiments was much higher than flow calculated with the Buckingham-Reiner equation using homogeneous Bingham fluid properties measured in the BML and measured pressure. Depending on pump frequency and mortar the measured pressure gradient (dp/dx) was only $1/7^{th}$ to $1/5^{th}$ of the pressure necessary to calculate the observed flow [7]. This is in accordance with earlier studies [3, 4, 6, 11, 14, 16, 25, 26]. The most common explanation is that the concrete is not flowing under shear but like a plug. Furthermore, flowable concrete with high dosages of water reducers (HPC, SCC) give higher pumping pressure than plastic concrete [14, 25]. We found [3, 4, 6, 7, 26] that pressure at ≈ constant flow in a given pump set-up increases with increasing plastic viscosity.

Lubrication modeling based on observations in pumping experiments

Due to the large deviation between observed and calculated flow we modified the prediction by using a lubrication model [6, 7, 15]. Bingham rheological parameters of matrix were used to represent the lubrication layer, whereas the mortar properties were used in the plug. The calculation [7] was extended from the Buckingham-Reiner equation. The lubrication layer between the pipe wall and the plug was flowing under shear between zero velocity at the rubber wall (no slip) and the velocity of the plug. The plastic viscosity of the matrix, μ in Table II, is the main parameter of the lubrication layer. τ_0 had little effect on layer thickness when fitting calculated flow to measured pump flow. τ_0 of the mortar is of course important since its existence is the basis for the formation of a plug during flow.

One would expect that mortars with self-compacting properties, like the ones studied here, would flow under shear in pipes as seen in Figures 1 and 2 [5]. However, a fully sheared flow cannot explain why the flow based on homogeneous fluid properties differs so much from that predicted by the Buckingham Reiner equation. We therefore have started our modeling with the relatively simple lubrication model described above. Furthermore, we assume that the concrete closest to the rubber pipe wall has zero flow velocity, Figures 1 and 2.

Figure 4 shows an example of a calculated plug flow profile fitted to measured flow for the 45 mm diameter at the tapered joints between the individual hoses of the 70 m long pumping circuit.

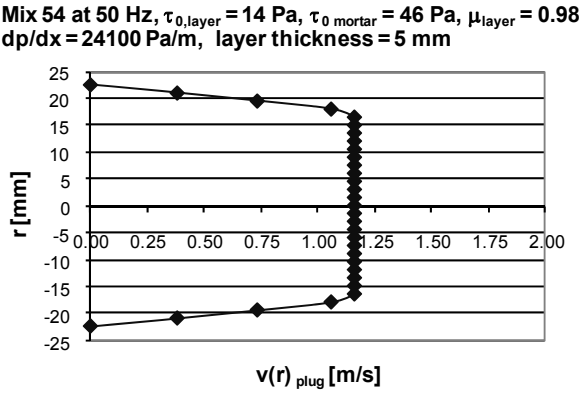

Figure 4. Example of plug-flow profile fitted to measured flow with lubrication layer and measured flow and pressure gradient.

When fitting measured and calculated flow this way surprisingly thin lubrication layers resulted with the measured rheological properties of the matrix in Table II.

The results are all in the lower range of the values reported in [14]; 175-320 Pa·s/m lubrication layer viscosity and 0.6-1 mm thickness. Furthermore, the results were fairly independent of flow rate and compositions for the different w/b = 0.50- 0.56 mortars investigated [6, 7]. It is surprising that the theoretical lubrication layers are similar to those of Kaplan [14] in spite of many differences both in materials, pumping equipment and method of determining layer thickness and quality. Figures 5 and 6 show photos of the liquid-like appearance observed on flowing mortar both in the BML-viscometer and at the hose end. A few grams of a fine white filler powder helped to visualize the shear during viscometer measurements. No visualisation aid was used for the pumped mortar flowing from the hose.

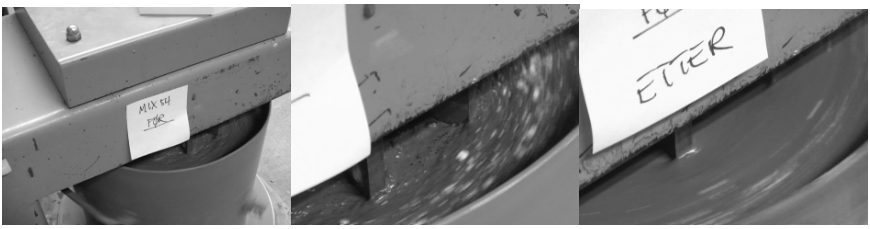

Figure 5. Liquid-like flow in BML of mortar in pump study with a few grams of white filler sprinkled on top - no sign of plug.

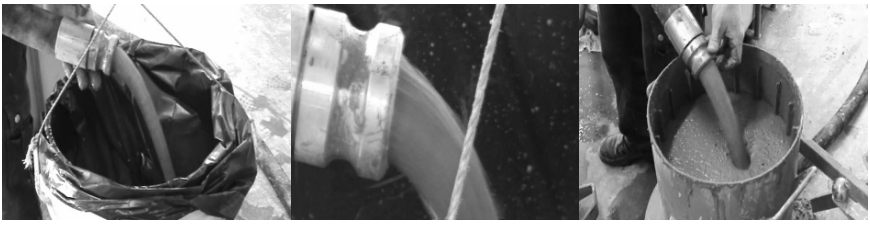

Figure 6. Liquid-like flow and no sign of plug flow during pump flow recording (Mixture 55 and Mixture 54 at 25 Hz) and filling of BML (Mixture 55).

The appearance of the flowing material in Figures 5 and 6 indicates that the mortar flows under shear. Thus the lubrication layer and plug flow calculation fitting measured and calculated flow seems unrealistic. If there is a plug it probably forms during flow and then disappears before the concrete leaves the hose.

The lubrication layer could be due to the wall effect mentioned in the introduction, and possibly from water squeezed out due to the pressure during pumping. However, a plug formation is much more difficult to explain in the present mixes than in more plastic concrete. Kaplan [14] discussed segregation under shear which would increase the coarse aggregate concentration in the center of the hose and

thus radial gradients of rheological properties in the pipe. (This local increase of aggregate packing during flow in passages narrow compared to maximum aggregate size also happens between rebars, and between rebar and formwork.) Together with a lubrication layer this could explain the high pump flow compared to the Buckingham-Reiner equation. Structural build-up [24] could perhaps contribute to plug formation if there is already low shear due to high local packing. Flow rates of around 0.5 and 1 m/s at the two pump frequencies (25 and 50 Hz) of the screw pump gives around 1-2 minutes spent at steady state in the 70 m hose. A low increase of the matrix yield stress of 1-2 Pa is expected from the estimated structural build-up of 0-0.015 Pa/s in Table II. Similar stiffening may be deduced for three of the four pumped mortars from Table III. However, due to the visual appearance it seems that we cannot explain the mode of flow of SCC in a pipe yet.

Air Voids and Their Escape near a Surface

A main obstacle to create beautiful surfaces is often too many and too large irregular surface voids. The formation of air voids, effect of flow and their escape depend on a number of factors. For example, if the concrete flows like a fluid under shear with no-slip at the formwork surface, then Bernoulli yields a reduced pressure at the highest flow rate (away from the surface) and consequently possibility for drawing voids away from the surface. On the other hand a slip at the surface could yield a plug flow with less pressure variation across the flowing concrete, more stiffening and less possibility for air void movement. Consequently it is difficult to say what flow conditions that favour void formation at the surface. At the same time we know that air voids have a positive effect on consistency, both in stabilizing and increasing paste volume [27, 28].

The formation and stability of entrained and natural air voids at a cement paste surface was reviewed and investigated in a recent study [29]. Air voids, once formed, can change within the fresh and young concrete during several hours after placement. The experiments [29] studied voids escaped from fresh paste of w/c = 0.42. Observations were made on their behaviour (change of size, coalescence, disappearance) over the first hours at rest. Experiments performed at atmospheric pressure and 0.7 bars showed that natural air voids coalesced easier to form larger voids than those entrained with AEA. The voids were observed as they entered water on the surface of fresh paste. Still, the results should relate to the conditions in fresh concrete considering the acceptable correlation often found between air void structure in fresh and hardened concrete [30]. Future research should thus study formation, size, coalescence and escape of natural air voids as flow, surface roughness and rheology including structural build-up varies.

Conclusions

Lubrication layers were calculated with data from instrumented full scale pumping tests and rheological measurements on self-compacting mortars and matrix. They show only about 1 mm thickness with 175-320 Pa·s/m layer viscosity. The implicit theoretical plug flow is hard to prove from visual flow observations. Some factors that may cause plug formation during flow are discussed. Clearly there is a need for more research to understand SCC flow along surfaces. Also the formation of air voids at SCC-surfaces is discussed briefly, also deserving more research.

Acknowledgements

The work is part of the COncrete INnovation centre (COIN) at SINTEF and NTNU supported by The Norwegian research council, Aker Solutions, Norcem Heidelberg, St. Gobain, Skanska, Rescon Mapei, UNICON, Veidekke, Consolis and the Road Auth. Thanks to O. Loraas, S.F. Lee and G. Loraas at NTNU, Dept. of Structural Engineering, L-S. Bolduc, Université Laval, M.Ekelin and B. Jensen of St. Gobain Weber Maxit for the work they performed with the experiments, to J.H. Mork and also to the critics and comments from the reviewer.

References

[1] Smeplass, S. (2009), Personal communication.
[2] www.coinweb.no
[3] Jacobsen, S. and Mork, J.H. (2007), Norw. concrete day, SINTEF/NTNU, 18 pp.
[4] Jacobsen, S., Mork, J., Lee, S. and Haugan L. (2008), SINTEF COIN Rep. 5, 42 pp.
[5] Jacobsen, S., Haugan, L. and Hammer, T. (2009), *Cem. Conc. Res.*, vol. 39, pp. 997-1006.
[6] Vikan, H., Jacobsen, S. and Haugan, L. (2009), RILEM PRO 68, pp. 88-96.
[7] Jacobsen, S., Haugan, L. and Vikan H. (2010), SINTEF draft COIN rep 67p.
[8] Sedran, T. and de Larrard, F. (1996), RILEM PRO 32, pp. 439-450.
[9] Thrane, L. (2009), Personal communication DTI/3. Dec.
[10] Ede, A.N. (1957), *Mag of Conc Res*, pp. 129-140.
[11] Rössig, M. (1974), Dr.ing, RWTH Aachen, Westdeutscher Verlag, 132 + 92 pp.
[12] Browne, R.D. and Bamforth, P.B. (1977), *ACI Journal,* pp. 193-203.
[13] Tattersall, G.H. and Banfill, P.F.G. (1983), Pitman Books Ltd., 356 pp.
[14] Kaplan, D. (2001), PhD ENPC/ LCPC, 228 pp (in French).
[15] Thrane, L.H. (2007), PhD DTI/DTU Denmark, 269 pp.
[16] Feys, D. (2009), PhD University of Ghent, 270 pp.

[17] Vikan, H. (2005), PhD Norw Univ of Sc and Tech 2005:189, 332p.
[18] Smeplass, S. and Mørtsell, E. (2001), Proc 2nd Int. Symp SCC, Tokyo, pp. 267-276.
[19] Smeplass, S. and Mørtsell, E. (2003), *NCR Publ*, n. 29, 13p.
[20] Mahaut, F. et al. (2008), *Cem. Conc. Res.,* vol. 38, pp. 1276-1285.
[21] Pedersen, B. (2004), PhD Norw Univ of Sc and Tech 2004:92, 198p.+app.
[22] Geiker, M.R. et al (2002), *Cement Concrete and Aggregates*, vol. 24, n. 91, pp. 3-6.
[23] Wallevik, J.E. (2003), PhD Norw Univ of Sc and Tech 2003:18, 397p.
[24] Billberg, P. (2006), PhD, KTH Stockholm, 91p. + 5 papers.
[25] Hu, C., de Larrard, F. and Sedran, T. (1996), 4th Int Symp HPC, LCPC, pp. 179-186.
[26] Jacobsen, S. and Mork. J.H, (2008), Proc XX Nord Conc Res meeting, pp. 8-9.
[27] Powers, T.C. (1968), Properties of fresh concrete. John Wiley & Sons, 664p.
[28] Hammer, T.A. and Johansen, K. (2005), Proc XIX NCR-meet, pp. 153–155.
[29] Ley M. et al (2009), *Cem. Conc. Res.*, vol. 39, pp. 1276-1285.
[30] Taylor, P., et al (2006), Fed. Highw Adm. Publ. No. FHWA-HRT-06-079, 151p.

Optimisation of the Mixing Process for Producing Self-Compacting High-Performance Concrete

Harald Beitzel

Institute of Building Process and Environmental Technology, Trier, Germany

Abstract. Today's concrete structures call for high-tech construction materials, for example self-compacting high-performance concrete (SCHPC) as self-compacting high-strength concrete (SCHSC) and self-compacting ultra-high-strength concrete (SCUHSC). These concretes are defined as concretes with special properties. This development aims to increase the packing density through the selection of coarse and fine aggregates combined with a reduction in the water-to-binder ratio (*w/b*). To achieve this goal, state-of-the-art concrete plants need to meet certain minimum requirements. In an effort to realize shorter construction times and develop new concrete process technologies, and in view of ever-increasing degrees of component loading, international research has been going on for approximately 30 years for materials that have led, among other things, to the development of high-performance concrete. A trend towards the development of customized concretes, for example of SCHPC, can also be observed in the German construction industry.

Introduction

The concrete-technological aspects for the use of SCHPC are the optimization and increase of compressive strength, porosity, density, the resistance to the aggressive action of freeze with de-icing salt, creep and shrinkage. From these concrete-technological requirements result a number of economic advantages. SCHPC can be installed even in densely reinforced areas without the aid of compaction, retaining at the same time the properties of normal concrete (NC).

SCHPC is the consistent further development of flowable concrete in the direction of a robust, workable and environmentally sound concrete. The SCHPC's increasing application can be expected in particular in the construction of bridges, high-rise buildings, special civil engineering works, tunnel and precast construction. SCHPC is particularly intended for application in architectural and

K.H. Khayat and D. Feys (eds.), *Design, Production and Placement of Self-Consolidating Concrete*, RILEM Bookseries 1,
DOI 10.1007/978-90-481-9664-7_15, © RILEM 2010

fair-faced concrete, for densely reinforced structural members and for slender members, members of complex geometry and for building in a noise-sensitive environment or on existing buildings.

Concrete Mixing Process

SCHPC is distinguished through its advantageous rheological and "self-deairating" properties. At the same time, SCHPC has good resistance to segregation. Other characteristics of correctly processed SCHPC are high surface density, improved durability, increased wear resistance and higher freeze-thaw resistance. The processing properties of SCHPC, with a compressive strength > 65 N/mm², differ from the processing properties of NC as defined in DIN EN 206-1 [1]. The main reason for this is the changed constitutive composition with a high powder content and the use of innovative superplasticizers which create the extraordinarily good flow properties. Constant processing properties are requisite for a uniform concrete production process. Here, the superplasticizers are of great significance. Only through the addition of these admixtures does SCHPC achieve its temporary flow properties. The time factor thus plays an important role with regard to the workability and quality assurance of SCHPC [2].

In the production of these concretes, the mixture constituents should be distributed as homogeneously as possible in the mixture. Being the central process step in the concrete plant, the mixing operation offers the optimization reserves required to enhance the favourable material properties and improve the economic efficiency of the process. Mixing processes in concrete technology are stochastic processes, meaning that there is only a certain probability of any elementary particle in the mixture being able to occupy a certain position in the mixing chamber. A state characterized as uniform random mixture can only be achieved if there is an identical probability of movement. Physical and chemical processes can prevent the probabilistically ideal random mixture from being produced. These processes, as well as any particle agglomerations present in the mixture, are called segregation. Segregation may also be caused by unfavourable filling levels in the mixing chamber, different velocity gradients of the mixture constituents, and different angles of rest at the interior walls and tools of the concrete mixer. There are process-related potentials for optimizing the mixing process. These exist in particular with regard to mixing time, mixing process, nominal capacity, mixing speed, addition of water and dosing sequence. Optimization tests should aim to determine the dimensionless mixture quality indicators on the basis of these influencing factors. Taking into account the dimensional analysis, the dimensionless variables listed in Table I can be computed in accordance with the Buckingham π theorem from the following dimensional parameters: tool width B, mixing chamber diameter D_M, mixing chamber height H_M, tool height H, filling height T, effective grain diameter d_W, mixing speed v_W, mixing chamber radius r, gravitational acceleration g and mixing time t [3]. From a certain minimum

nominal content, the results achieved can be roughly transferred to different mixer sizes based on similarity theory. This is not possible with the standard laboratory-scale mixers. The homogeneity of the mixture is classified and assessed in accordance with RILEM TC 150-ECM Final Report [4]. For the assessment of homogeneity, both the number of samples to be assessed and the sample size in accordance with the requirements specified in [4] are of vital importance.

Table I. Buckingham parameters.

Parameter	Dimensionless variable	Denotation
$\pi 1$	v	Coefficient of variation
$\pi 2$	D_M/B	Relative mixer diameter
$\pi 3$	H_M/B	Relative mixer height
$\pi 4$	H/B	Relative tool width
$\pi 5$	α	Cutting angle
$\pi 6$	T/B	Relative immersion
$\pi 7$	B/d_W	Mix/tool parameter
$\pi 8$	ρ'	Angle of the internal friction
$\pi 9$	$v_W^2/r{\cdot}g$	Froude number
$\pi 10$	$v_W{\cdot}t/B$	Mixing parameter

The following criteria are used for assessing the mixing times [5]:

- mixture quality test results
- homogenization test results
- processing test results
- strength test results

The minimum mixing times of conventional concrete mixers must be assumed to be longer for the production of SCHPC than for the production of NC. The composition of SCHPC, in comparison to NC, contains significantly higher powder content. For the homogenization in the mixing process this means that the movements of the mixing tools - due to a higher energy input - must produce many shear planes in the mixture. Here, thorough distribution and mixing of the superplasticizers, in low quantitative proportion compared to the remaining mixture constituents, is also of special significance.

At present, the fact that the material cost for the manufacturing of SCHPC is still greater than the cost of a comparable NC, is a disadvantage. These extra costs can be compensated for by improving the production and placement process. By utilizing all processing and operational resources, the final product SCHPC can thus be manufactured in a quality-assured and cost-efficient manner.

Effects of Process Engineering

The influencing variables necessary for describing the mixing process are shown in Figure 1. The characteristic parameters, which are independent of each other and which influence the overall mixing process, can therefore generally be classified into the following groups:

- system-technical influences
- operations-technical influence

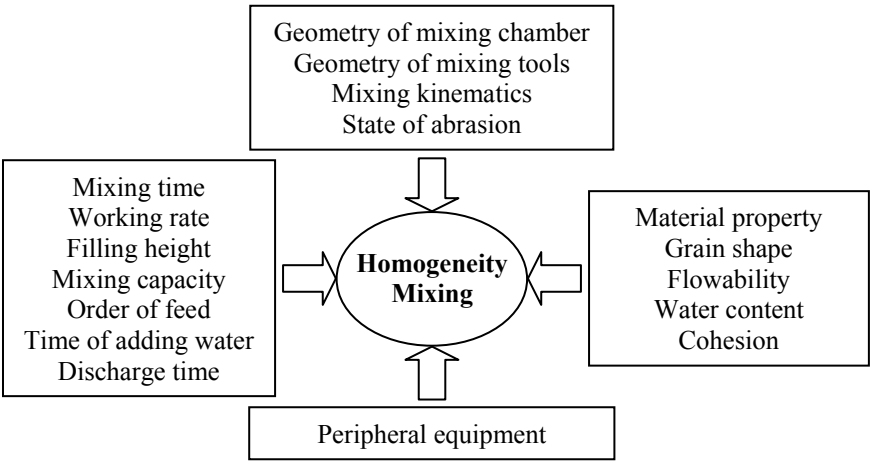

Figure 1. Effects of process engineering on the mixture quality.

The movement of the mixing tools introduces horizontal radial and tangential as well as vertical movements in the mixture. These quasi-laminar and quasi-turbulent basic movement processes determine the kinematics within the mixture. The maximum processing rate in the outermost zone of the mixing space is assumed to be the critical magnitude on the mixing process.

The operational parameters are determined by the flow of operations in the concrete plant. The filling height implicates the filling level for a constant mixer diameter. The mixing time begins when the last mixture component is added and ends at the onset of the discharge process. The feed arrangement is another output variable for improving the quality of the mixture. In contrast to the system-related and operational influencing variables, the selection of the concrete-technological influencing variables poses considerable difficulties.

In order to ensure the optimal processing properties of SCHPC, optimization of the constitutive materials is required, as well as the adjustment of the mechanical equipment for its manufacture imperative. At present, e.g. uneconomically long

mixing periods that diminish the effectiveness of concrete mixing plant must be scheduled for the production of SCHPC. To what extent the mechanical engineering typically used in the manufacturing of conventional flow concrete can also be used for the production of SCHPC and what modifications should be made, cannot currently be answered conclusively. Technical literature has so far not reported on the influence of the mechanical engineering parameters for quality-ensured production of SCHPC. As a result, numerous questions in day-to-day practice arise among operators of concrete production plants. Owing to the special requirements made on SCHPC in respect of batching and mixing, there is a lack of, e.g., proof of the fitness for use of the conventional concrete mixers and commonly used truck mixers for its processing. The present knowledge is still insufficient with regard to the mixing process, the required mixing times, the possible processing time and the necessary machine adjustments.

The mixing processes in concrete technology are stochastic processes. This means that a random elementary particle of the mixture can occupy a specific position in the mixing space only with a certain probability. A stationary distribution state is reached after an interminably long mixing time, as the result of the mixture particle's individual probability of movement. A state described as uniform random mixture is attained only in case of the same probability of movement. The assessment of the quality of the mixture is regulated in DIN 459-2 [6] and in RILEM TC 150-ECM Final Report [4]. In these, the scope of testing for determining the concrete mixture quality is described for defined experimental concretes. On the assumption that the random sample results are normally distributed, the number of samples can be calculated from the confidence interval of the mean value:

$$\mu = \bar{x} \pm \frac{t \cdot s}{\sqrt{n}} \tag{1}$$

This indicates, with statistical certainty, the interval within which the mathematical expectation μ of the parent population is contained. It is calculated with the aid of the mean value $\bar{x}$ of the random sample, the standard deviation s and the number of individual samples n, while t is a correction factor that takes account of a small random sample size with a statistical certainty of 95 percent. The accuracy p (confidence interval) of the mean values is determined as follows:

$$p = \frac{t \cdot s}{\bar{x} \cdot \sqrt{n}} \cdot 100\,[\%] \tag{2}$$

When replacing the expression ($s/\bar{x} \cdot 100$) in Eqn. (2) by the coefficient of variation v, we obtain:

$$p = \frac{v \cdot t}{\sqrt{n}} [\%] \quad (3)$$

To better assess the velocity effect on the homogeneity of the mixture, the coefficient of variation v is compared as a function of the Froude number Fr. The mass of the individual specimens should be high that the components of the mixture that are available in only small proportions can be captured through the individual specimens. The maximum particle size should, if possible, also be included in the probability approach.

Based on a survey conducted by the author and the investigations carried out, approx. 30% of the manufacturers of concrete mixers have obtained a certificate in compliance with [4] and [6] on the production of SCHPC and other concretes. The remaining manufacturers do not have equivalent, objective proof of the performance capability of their concrete mixers.

Quality Assessment

The experimental investigations relating to the production of SCHPC were aimed at optimizing the process-related parameters for quality assurance. In this process, mixer-specific details could be defined relating to the following parameters:

- dosing sequence
- dosing accuracy
- mixing effectiveness
- mixing time
- mixing speed
- special energy inputs
- nominal capacity

As a general rule, longer mixing times are required for the production of SCHPC than for the mixing of standard concretes when using mixers of conventional design. Efficient mixing times can be achieved with almost all types of conventional concrete mixers by varying both the mixing tools and the mixing speed. In terms of the mixture quality of SCHPC, the designs were grouped into the mixer classifications stated in contingent on the mixing time.

Four concrete mixers, as described in [4], were tested. The test results are shown in Figure 2 by way of example, comparing the standard mixers No. 1′ and No. 2′ with mixers No. 1 and No. 2 previously modified by varying the mixing speeds. They show that, for the production of SCHPC of reliable quality, shorter mixing times are possible by varying the mixing speeds of the concrete mixers.

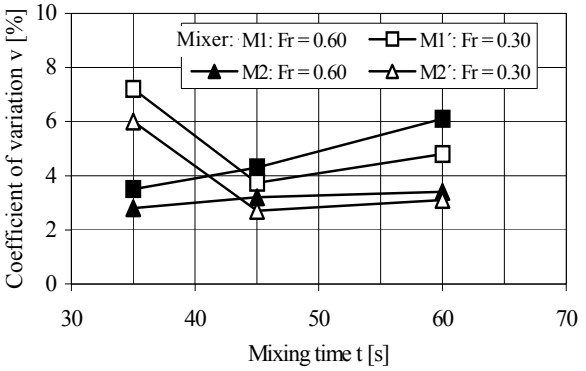

Figure 2. Coefficient of variation as a function of the mixing time with different Froude numbers.

The influence of the mixer types and mixing times on the homogeneity described by the coefficient of variation, as well as on the constituents limiting mixture quality in the individual classifications, is illustrated in Figure 3 for two mixer types. It shows the results for the 4/8 mm and 0/0.25 mm aggregate sizes, as well as for the water w and the water/fines-ratio (w/f). As can be seen from Figure 3, both mixers met the requirements to be classified as high-performance mixers (HPM).

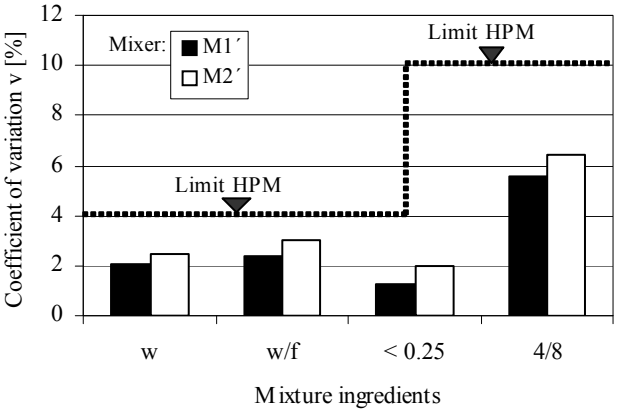

Figure 3. Classification according to [2].

In these experimental mixer investigations cube compressive strengths of up to 70 N/mm² were measured (see Figure 4). The mean compressive strength after 28 d with the modified concrete mixer type 3 after a mixing time of 60 s can be

classified as a SCHPC. The concretes made with the other mixers and mixing times were normal SCC. With regard to the processing of SCC, a slump flow of over 650 mm was moreover attained for all concretes in the investigations. The variations of the compressive strengths were due to the different workability, air content and bulk density in dependence of the mixing kinematics.

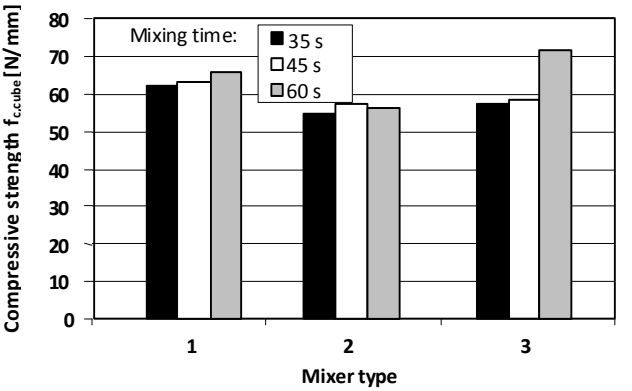

Figure 4. Cube compression strength.

Summary and Outlook

The processing properties of SCHPC differ from the processing properties of NC as defined in [1]. The main reason for this is the changed constitutive composition with high powder content and the use of innovative superplasticizers which create the extraordinarily good flow properties. For a reliable concrete production process, constant processing properties must be ensured. Here, the superplasticizers are of great significance. Only through the addition of these admixtures does SCHPC achieve its temporary flow properties. The time factor thus plays an important role with regard to the workability and quality assurance of SCHPC.

The assessment of the quality of the mixture is regulated in [4] and [6]. In these, the scope of testing for determining the concrete mixture quality is described for defined experimental concretes. Only approximately 30% of the manufacturers of concrete mixers have obtained a certificate in compliance with [4] and [6] on the production of SCHPC and other concretes.

The fine-grained composition of the SCHPC means for the homogenization in the mixing process that the movements of the mixing tools – due to a higher energy input – must produce many shear planes in the mixture. Here, thorough distribution

and mixing of the superplasticizers, in low quantitative proportion compared to the remaining mixture constituents, is also of special significance.

A stationary distribution state is reached after an interminable long mixing time, as the result of the mixture particle's individual probability of movement. A state described as uniform random mixture is attained only in case of the same probability of movement.

The classification and assessment of the homogeneity of the mixture follows from [4], with the boundary proportions of the mixture quality specified in Table I. Accordingly, the classification categories standard mixers, performance mixers and high-performance mixers are possible. Quality-assured SCHPC can be manufactured in high-performance mixers economically short mixing times.

Most conventional concrete mixers are suitable for the production of SCHPC, with differences in quality depending on the mixing time and energy consumption. The concrete mixture quality can be assessed by means of [4]. The mixing time can be reduced by varying the mixing parameters. It can be assumed that it will be possible in the future to reduce these mixing times by using innovative superplasticizers and continuously adjustable mixer speeds.

References

[1] DIN Deutsches Institut für Normung (2001), DIN EN 206-1 – Concrete – Part 1: Specification, performance, production and conformity, Beuth, Berlin (in German).

[2] Beitzel, H. (2009), Future Trends in the processing of ready-mixed high-strength self-compacting concrete, Proceedings of the 2nd International Conference on Advances in Concrete Technology in the Middle East – Self Compacting Concrete, Abu Dhabi.

[3] Beitzel, H. (2007), Quality-assured manufacture of self-compacting concrete (SCC) by changing the relevant machine parameters in the concrete mixer, *Concrete Plant + Precast Technology*, vol. 01/2007 (in German).

[4] Beitzel, H., Charonnat, Y. and Beitzel, M. (2003), RILEM TC-150 ECM – Efficiency of Concrete Mixers, Final Report, *Materials and Structures*, vol. 26, pp. 256.

[5] Beitzel, H. (2007), Process optimisation for the mixing of self-compacting concrete, Proceedings of the 5th International RILEM Symposium on Self-Compacting Concrete, vol. 1, Ghent.

[6] DIN Deutsches Institut für Normung (1995), DIN 459-2 – Building material machines – Mixers for concrete and mortar – Part 2: Procedure for the examination of the mixing efficiency of concrete mixers, Beuth, Berlin (in German).

Theme 5: Flow Modeling of SCC

Computational Modeling of SCC Flow through Reinforced Sections

Ksenija Vasilic[1], Nicolas Roussel[2], Birgit Meng[1] and Hans-Carsten Kühne[1]

[1] BAM, Federal Institute for Material Research and Testing, Berlin, Germany
[2] Université Paris Est, Laboratoire Central des Ponts et Chaussées, Paris, France

Abstract. Computational modeling of fresh SCC flow is a comprehensive and time consuming task. The computational time is additionally increased when simulating casting of reinforced sections, where each single reinforcement bar has to be modeled. In order to deal with this issue and to decrease the computational time, an innovative approach of treating a reinforcement network as a porous medium is applied. This contribution presents the model for concrete flow through reinforced sections, based on Computational Fluid Dynamics (CFD), coupling a single-phase flow model for SCC and a continuum macroscopic model for porous medium. In the last part of this paper, numerical simulations are compared with experimental results obtained on model fluids.

Introduction

In recent years the numerical modeling of fresh concrete gained importance, showing potentials to become a tool for prediction and optimisation of concrete casting [1, 2]. The modeling of the concrete flow is a comprehensive task and even when using simplified approximate models, it leads to complex and time consuming simulations. When simulating casting of real elements, which are always reinforced, the influence of the reinforcement on the flow has to be taken into account as well. Modeling of the rebars one by one makes the simulation more complex, significantly increasing not only computational time, but also the pre-processing time (the time needed for geometry generation and meshing). In order to simplify pre-processing and to reduce total simulation time the approach of treating reinforcement as a porous medium is proposed [3, 4]. Instead of modeling rebars one by one, the reinforcement network is presented as a homogenous porous zone (schematically shown in Figure 1).

K.H. Khayat and D. Feys (eds.), *Design, Production and Placement of Self-Consolidating Concrete*, RILEM Bookseries 1,
DOI 10.1007/978-90-481-9664-7_16, © RILEM 2010

Consequently, the flow of SCC through a reinforcement zone is regarded as a flow of a non-Newtonian fluid through the porous medium (PM). By defining characteristic parameters of the PM (permeability, porosity, etc.), its influence on the flow (i.e. the relationship between the viscometric behaviour and the observed behaviour in the porous matrix) can be defined. Defining characteristics of the PM for different reinforcement geometries and classes should significantly simplify mathematical and numerical modeling of reinforced sections.

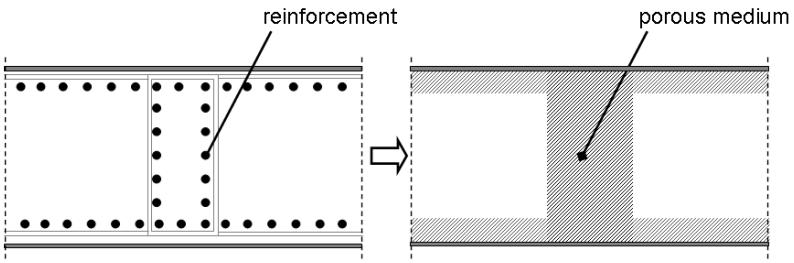

Figure 1. Schematic representation of the basic idea, reinforcement modeled as a porous medium: a) real position, b) model.

This contribution will present a CFD model for concrete flow through reinforcement and discuss its applicability on numerical modeling of SCC casting. The fresh concrete is here treated as a non-Newtonian fluid and the reinforcement is modeled as a porous matrix, accounting for its influence on the flow by defining the corresponding PM parameters.

Model of Concrete Flow and Influence of Reinforcement

Model of the flow

Involving complex material behaviour, moving free surfaces and fluid-structure interfaces, computational modeling of fresh concrete flow is a comprehensive and time consuming task. Due to its complexity an exact model of the flow does not exist and simplified models are in use (reviewed in [2]). From the modeling point of view, the fresh concrete can be considered as a fluid when a particular degree of flowability is achieved (slump at least 100 mm [5]) and when the concrete is homogeneous. Due to its extreme flowability, SCC in general satisfies the above-mentioned constraint and is here therefore modeled as a Bingham fluid:

$$\eta(\dot{\gamma}) = \frac{\tau_0}{\dot{\gamma}} + \eta_{pl}\,;\ \eta(D_{II}) = \left(\frac{\tau_0}{\sqrt{2D_{II}}} + \eta_{pl} \right) \tag{1}$$

where η is the apparent viscosity, τ_0 is yield stress and η_{pl} is plastic viscosity. D_{II} is the second invariant of the deformation rate tensor and corresponds to the shear rate in 2D problems. Furthermore, the fluid flow is described by continuity equations (i.e. mass and momentum conservation equations for the incompressible fluid):

$$\underline{\nabla} \cdot \underline{v} = 0; \qquad \rho \frac{D\underline{v}}{Dt} = -\underline{\nabla} p + \underline{\nabla} \cdot \underline{\underline{S}} + \rho \underline{g} \tag{2}$$

where $\underline{v}$ is velocity vector, ρ is density, p is pressure and $\underline{g}$ denotes gravity. The non-Newtonian effects are reflected in definition of the extra stress tensor $\underline{S}$, which depends on above defined bulk viscosity as $\underline{\underline{S}} = 2\eta(\dot{\gamma}) \cdot \underline{\underline{D}}$.

Model of the flow through reinforcement / porous medium

Aside from [3], there are no attempts to model the flow of cementitious materials through reinforced sections as a flow of a non-Newtonian fluid through PM. On the contrary, in other engineering fields the flow of complex suspensions through PM has been studied a lot and some very sophisticated models are developed. Overview of the work can be found in [6] and more recently in [7]. However, to include the influence of PM on the flow common practice is to use continuum macroscopic approach e.g. to modify model equations to account for presence of the porous matrix as a continuous medium [8]. The model used in this work is hence a macroscopic approach, accounting for influence of the PM on the flow in description on apparent shear rate and apparent viscosity. The resulting macroscopic flow laws look like a modified version of the Darcy's law with some equivalent or apparent viscosities in PM:

$$\eta_{app} = \frac{k}{v_D} \frac{\Delta p}{\Delta L} \tag{3}$$

where η_{app} is apparent viscosity of the fluid in the PM, k is its permeability of the medium, v_D is Darcy's velocity of the fluid and $\Delta p/\Delta L$ is pressure gradient within the medium. Furthermore, since the strain field within the PM is unknown, one defines so-called "apparent" or "in-situ" shear rate within the medium $\dot{\gamma}_{app}$:

$$\dot{\gamma}_{app} = \frac{\alpha \cdot v_D}{\sqrt{k \cdot \phi}} = \frac{v_D}{c_1} \tag{4}$$

where ϕ is porosity of the porous medium and α is a shift factor, which can be experimentally and analytically determined [8]. c_1 is then a factor having dimensions of length [m], depending on the shift factor, porosity and permeability

of the PM. By introducing the shear rate into Eqn. (1), the constitutive equation for the viscosity in PM becomes:

$$\eta_{app}(\dot{\gamma}_{pm}) = \frac{\tau_0}{\dot{\gamma}_{pm}} + \eta_{pl} = \frac{c_1 \cdot \tau_0}{v_D} + \eta_{pl} \tag{5}$$

Implementation of porous model into CFD software

For the purpose of numerical studies, the porous model explained above is implemented into the CFD solver FLUENT©. The porous medium is modeled by the addition of a momentum source term to the standard momentum flow equations (the right side of Eqn. (2)). Since a laminar flow is assumed, the inertial loss can be neglected and the source term is composed of a viscous loss term only. The model reduces to Darcy's law and for the 2D case the added momentum source term in the flow direction is given as:

$$S_x = -\frac{\eta}{k} v_{D,x} \tag{6}$$

where S_x is momentum source and v_{Dx} is Darcy's velocity in the flow direction x. For the Bingham material, by introducing the definition of viscosity from equation 6, the previous equation becomes:

$$S_x = -\frac{1}{k}(c_1 \cdot \tau_0 + \eta_{pl} \cdot v_{D,x}) \tag{7}$$

and accounts for the influence of the porous zone on the material flow.

Numerical Studies and Experimental Validation

Case studies

Using the described numerical model, series of the preliminary numerical case studies on different simple geometries are conducted. The goals of these tests were to validate the basic idea of the study (to show that the reinforcement can be assumed and modeled as a porous medium), to prove applicability of the model on realistic materials and geometries and to test comparability with experimental results.

One of the 2D test-geometries is schematically shown in Figure 2, while a 3D case is shown in Figure 3. The setup consists of a rectangular tube with vertical rebars (Figures 2a, 3a); a test-fluid is poured with a constant velocity through the inlet

(left) and flows in the direction of the outlet (right). The corresponding porous medium geometry is shown in Figures 2b and 3b.

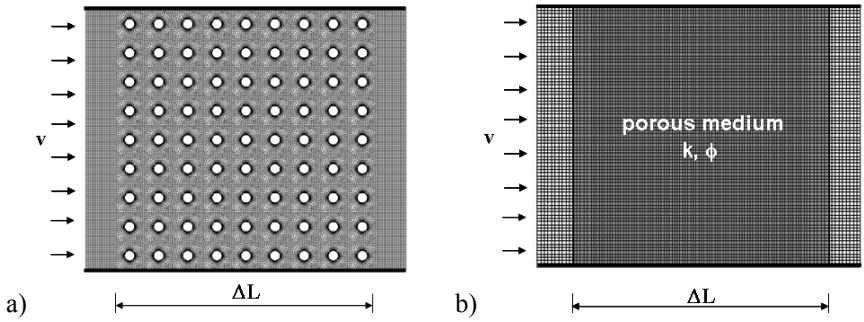

Figure 2. 2D test-geometry: a) reinforcement b) porous medium model.

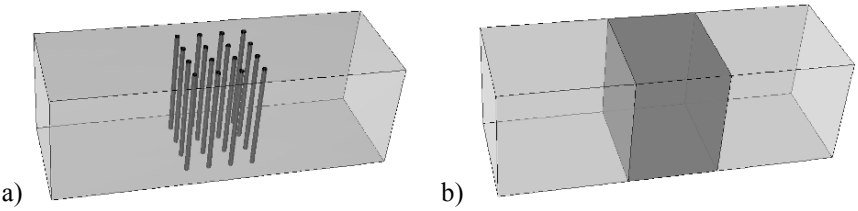

Figure 3. 3D test-geometry: a) reinforcement b) porous medium model.

The simulations with the PM geometry are conducted by implementing the porous media model explained in previous chapter into FLUENT©. The unknown permeability is calculated from the simulations with the Newtonian material for the reinforcement case (Figure 2a), by implementing numerically obtained pressure drop into Eqn. (3) (in this case η_{app} is the actual Newtonian viscosity $\eta = 1$ Pas). The calculated value of permeability is then used as a characteristic permeability of the porous zone for the further simulations with PM geometry. The unknown coefficient c_1, which relates shear rate in PM to Darcy's velocity, is obtained by performing numerical tests where the distance between the rebars is varied. From these tests, the following approximate relation between the Darcy's velocity and the apparent shear rate is found as:

$$c_1 = \frac{v_D}{\dot{\gamma}_{app}} \approx \sqrt{k \cdot \phi} \tag{8}$$

In the first case study to be presented here, simulations with the depicted 2D geometry (Figure 2) and a Bingham test-material are conducted. Here the bar

diameter was d = 3 mm and the distance between the bars is varied from δ = 6 mm to δ = 8 mm. All the test-material properties are set to the unity-values. The second and more "realistic" 3D study is performed using a cementitious-like material with material properties typical for self-compacting mortar (Bingham material: τ_0 = 5 Pa, η_{pl} = 5 Pas) and realistic geometry measures (box dimensions: 25 x 25 x 75 cm, bar diameter: d = 2 cm, distance between the bars: δ = 5 cm).

The simulations for the reinforcement and PM cases are compared in terms of flow front and pressure drop within the reinforcement/porous zone.

Experimental validation

In order to study the permeability of the reinforcement network, preliminary experimental studies were conducted at LCPC [3]. The used experimental setup is shown in Figure 4. The setup consists of a 20 x 20 x 60 cm container made of Plexiglas, enabling observation of the flow front of the poured fluid. The adaptable modulus in the middle of the box, holds the vertical rebars (d = 3 mm) and allows modification of the number and the distance between the bars. The used test material was a Carbopol gel, a yield stress fluid having the following properties: yield stress τ_0 = 40 Pa, plastic viscosity η_{pl} = 1 Pas and density ρ = 990 kg/m^3. The fluid is poured from above into the corner of the form and the flow is observed. When the flow stops, the length and the height difference of the final material shape are measured. From these values, the pressure drop within the rebar zone is obtained and using Eqn. (3) and (5) the factor k/c_1 is calculated. Varying the number of the bars and the distance between them, the experimental procedure is repeated and k/c_1 is calculated for different network geometries. The experiment is then simulated using the software FLUENT (Figure 5) and experimentally and numerically obtained results for the coefficient k/c_1 are compared.

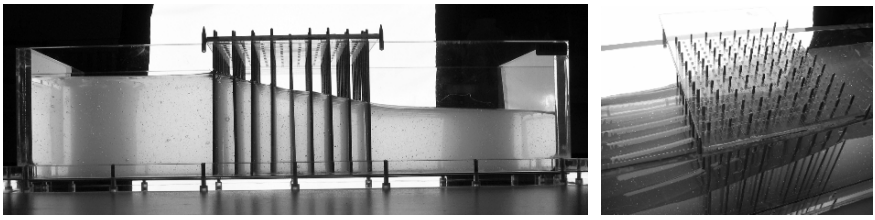

Figure 4. Experimental setup, performed experiments with Carbopol gel.

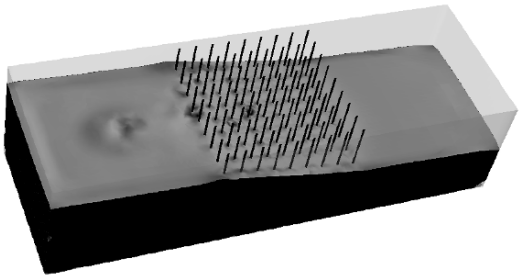

Figure 5. Numerical simulation of the test experiment.

Results and Discussion

Results of the numerical simulations with the 2D geometry and unity Bingham fluid are shown in Figure 6. The configuration of the rebars is varied so that the relative distance between the bars (the distance between the bars divided by the bar diameter) is X = 2 and X = 2.7. The simulations are performed for different inlet velocities and the pressure drop is calculated. The diagrams show an excellent agreement when comparing the reinforcement and PM geometry, where the maximal discrepancy for the calculated pressure drop between reinforcement and PM case is found to be 0.4%.

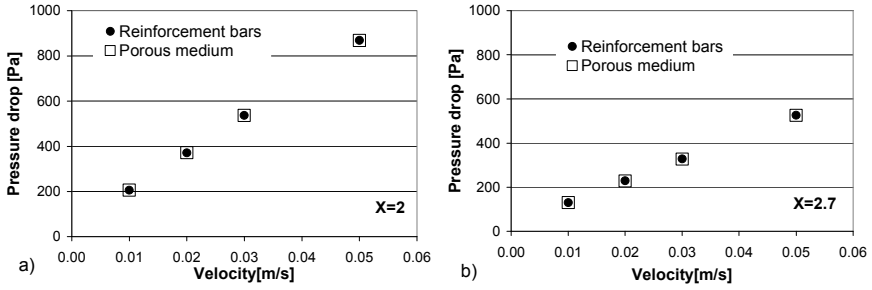

Figure 6. Comparison of the model with bars and PM model, pressure drop as a function of inlet velocity for a) X = 2 b) X = 2.7. X is the relative distance between the rebars.

The results of the 3D simulations with the cementitious-like material are shown in Figure 7. The picture shows the comparison of the flow front after 0.5 seconds, for the reinforcement and porous medium case in 3D and 2D representation.

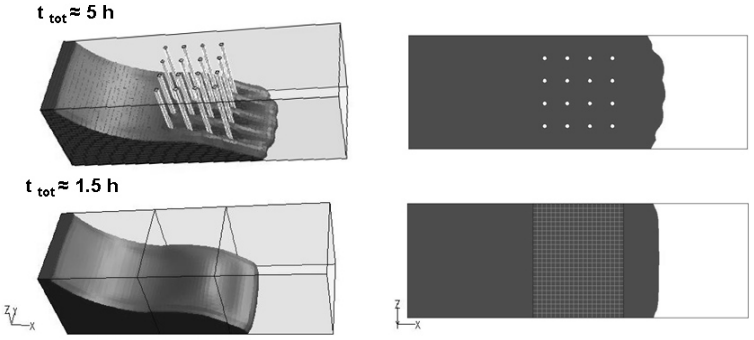

Figure 7. Comparison of the model with bars and porous medium model, flow front development after 0.5 sec. t_{tot} is the total time needed for simulation.

In terms of flow distance, a good match can be seen between these two simulations. t_{tot} shown in this figure denotes the total simulation time: time needed for geometry and meshing together with the computation time. It can be seen, that even for the simple geometry studied here, the computations with rebars are much more time-consuming than the ones with PM model.

The comparison of the experimental and numerical permeability studies is shown in Figure 8. The diagrams shows the factor k/c_1 plotted vs. relative distance between the bars X (X is the distance between the bars δ divided by the bar diameter d). A good match between the numerical and experimental results can be seen, validating the basic mathematical postulates of the used approach particularly the assumptions concerning permeability of reinforcement network.

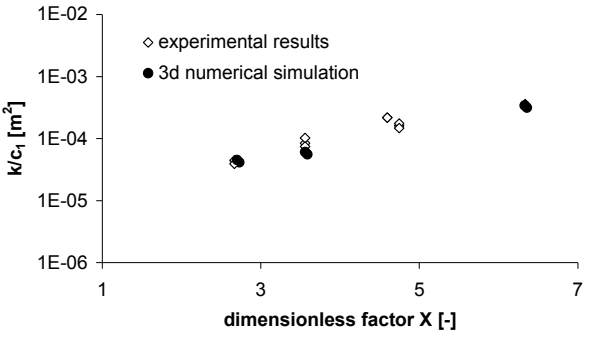

Figure 8. Comparison of the experimental and numerical results, factor k/c_1 plotted versus dimensionless distance between the bars X.

Conclusions and Outlook

The preliminary numerical studies showed that the time needed for the computations with PM model was significantly shorter than for the simulations with reinforcement, which proves accomplishment of the basic aim of the study: reduction of the computational time by using PM model. The studies with the test and the realistic materials showed that the proposed model for PM gives good results for pressure drop and flow front development. This validates the basic postulate of the study i.e. capability of the presented mathematical approach to model cementitious material flow through reinforcement zones. Furthermore, the performed experimental studies and the good congruence between the experimental and numerical results, verified the correctness of the numerical tests and of the assumptions regarding permeability of the reinforced zones.

Further work will focus on experimental and numerical studies with different reinforcement geometries, with the goal of defining the porous medium parameters for various classes of reinforcement.

References

[1] Roussel, N. (2007), Rheology of fresh concrete: From measurements to predictions of casting processes, *RILEM Materials and Structures,* vol. 40, n. 10, pp. 1001-1012.

[2] Roussel, N., Geiker, M.R., Dufour, F., Thrane, L.N. and Szabo, P. (2007), Computational modelling of concrete flow: General overview, *Cement and Concrete Research,* vol. 37, n. 9, p. 1298-1307.

[3] Nguyen, T.L.H. (2007), Modeling tools for casting concrete, PhD Thesis, Ecole Nationale des Ponts et Chaussées (in French).

[4] Vasilic, K., Roussel, N., Meng, B. and Kühne, H.-C. (2009), Computational modelling of SCC flow: reinforcement network modelled as porous medium, In: *Rheology of Cement Suspensions such as Fresh Concrete*, Proceedings of the 3rd International RILEM Symposium, Rilem Publications S.A.R.L , Bagneux, France, pp. 148-154.

[5] Ferraris, C., de Larrard, F. and Martys, N. (2001), Fresh concrete rheology: Recent developments, *Materials Science of Concrete VI*, pp. 215-241.

[6] Sorbie, K.S., Clifford, P.J. and Jones, E.R.W. (1989), The rheology of pseudoplastic fluids in porous media using network modeling, *J. Colloid Interface Sci.*, vol. 130, p. 508.

[7] Lopez, X., Valvatne, P.H. and Blunt, M. (2003), Predictive network modeling of single-phase non-Newtonian flow in porous media, *J. Colloid Interface Sci.*, vol. 264 (1), pp. 256-265.

[8] Pearson, J.R.A. and Tardy, P.M.J. (2002), Models for flow of non-Newtonian and complex fluids through porous media, *J. Non-Newtonian Fluid Mechanics*, vol. 102, n. 2, pp. 447-473.

Simulation and Testing of the Grout Backfill Process in a Case-Study Related to a Nuclear Waste Disposal Gallery

P. Bakker[1], V. Ramohalli Gopala[2], J.A. Lycklama à Nijeholt[2], E. Koenders[3], S. Grünewald[4] and J. Walraven[4]

[1] Van Hattum en Blankevoort, Woerden, The Netherlands, before: Delft University of Technology, Delft, The Netherlands
[2] Nuclear Research & Consultancy Group (NRG), Petten, The Netherlands
[3] Microlab, Delft University of Technology, Delft, The Netherlands
[4] Section of Concrete Structures, Delft University of Technology, Delft, The Netherlands

Abstract. The simulation of the flow of fresh grout allows predicting the filling behavior at defined conditions. Hereby, the production process can be optimized.
In Mol (Belgium), a field testing site for storage of nuclear waste material has been developed in the past decades. At this location, the Economic Interest Grouping EURIDICE investigates the possibility to store containers with nuclear waste material in horizontal underground tunnels. The space between the tunnel lining and the waste containers could be filled with a cement-based grout. The aim is to create a solid body without voids that can withstand ground settlements. Since the filling process cannot be visually observed a study was carried out in order to predict the filling by simulating the fresh grout flow with computer software. The objective of the study was to determine a proper filling strategy for this project. The experiments were carried out at the Delft University of Technology in The Netherlands. The Nuclear Research & Consultancy Group in Petten, The Netherlands, simulated the filling process with OpenFOAM, a software package that is based on Computational Fluid Dynamics (CFD). The study consisted of three parts: firstly, the rheological characteristics (thixotropy, yield value and plastic viscosity) of the fresh grout were determined, secondly, a parameter-study was carried out on the filling behavior of the grout with a scaled Plexiglas version (maximum length: 5.76 m) of the underground tunnel and finally, simulations were performed and compared to experimental results.
This paper describes the case-study and experimental results, and compares the filling behavior determined from experiments and computer simulations using CFD.

K.H. Khayat and D. Feys (eds.), *Design, Production and Placement of Self-Consolidating Concrete*, RILEM Bookseries 1,
DOI 10.1007/978-90-481-9664-7_17, © RILEM 2010

Introduction

The study on the disposal of nuclear waste material combines material testing, downsized tests and the simulation of the grout flow. With the material characteristics as input parameters, experimental results were compared with simulations. First, the background theory of flow simulations is discussed. Thereafter, the rheological testing is described that was used as an input for the simulations. Next, the downsized setup and tests are described. Finally, simulations and experiments are compared and conclusions are drawn.

Simulation of flow

Different numerical methods have been developed for the simulation of transient arbitrary free surface flow. The two most applied methods are the discrete particle approach and the homogeneous fluid method.

Discrete particle approach. The aim of the discrete particle approach is to carry out detailed studies on the movement, the direction, the rotation and the interaction of particles. This method is therefore applicable to heterogeneous materials since it describes both simulations on the macroscopic level as well as the local behavior of granular materials and suspensions. A limited number of studies have been performed on the form filling ability and flow patterns, and the relation between simulations and experiments is not clear. One of the uncertainties of this method concerns the input parameters describing the contact laws between particles. These are not measureable quantities: they need to be fitted in order to get the best comparison between numerical predictions and experimental results.

Homogeneous fluid method. The homogeneous fluid method refers to the simulation of ideal fluids without particle inclusions and is part of the overall framework of Computational Fluid Dynamics (CFD). The flow characteristics are obtained by solving the governing equations of mass, momentum and energy using a numerical solution method. The material properties comprise for example density, viscosity, specific heat, and thermal conductivity. Few studies have been carried out on the process of casting cementitious materials using a homogeneous fluid approach. For self-compacting concrete (SCC) Thrane [1] registered consistency between the experimental and simulated flow behaviour for the slump flow test, the L-box test, and form filling tests and found reasonable agreement between rheological parameters determined in the viscometer and those applied to simulate the flow.

OpenFOAM and VOF. The software package used in this research study is OpenFOAM. With a mesh consisting of finite volumes of the geometrical model, the boundary conditions such as velocity at the inlet, outlet dimensions, wall resistance and the physical (rheological) parameters of grout and air, OpenFOAM

calculates the flow characteristics in each of these cells at every time step [2]. The Volume Of Fluid method (VOF) is used to track the interface of the two phase flow situation (grout and air). The volume fraction V is defined in each cell such that $V = 1$ for grout filled cells, $V = 0$ for air filled cells and $0 < V < 1$ for cells containing both grout and air. Cells with $0 < V < 1$ together form the grout front for a certain time step [3].

Rheological parameters. The flow of cementitious mixtures can be described with the Bingham model [4, 5]. The rheological behaviour is characterized by two parameters: yield stress and plastic viscosity. It also behaves as a thixotropic material with an internal structure that builds up during rest and is broken down while in motion [6]. The thixotropic behaviour has not been included in the CFD model.

Rheological Testing

Experimental methods

During the grouting experiment the material is either in constant motion, or is subjected to motion after rest, and finally reaches its destination in the setup. The rheological parameters used in the simulations were determined with the BML-viscometer [7]. The apparatus consists of a standardized bucket and a measuring device that is inserted in the bucket. The bucket is filled with grout and rotates on a horizontal platform, while the measuring device measures the torque that is exerted to it. From this, the yield stress and the plastic viscosity could be derived. For the grout being in constant motion as well as for grout that is subjected to motion after a period of rest, test methods were developed.

Grout in constant motion. It is unfavourable to exert motion to the mixture for several hours using the BML-viscometer. When the mixture is at rest and afterwards subjected to motion in the mixer for 60 seconds, the thixotropic structure that was build up during rest will be broken down. It is assumed that similar rheological parameters are obtained as for the material being in constant motion.

Grout in motion after a period of rest. It is also unfavourable to keep the inner cylinder of the BML-viscometer inside the grout during a long period of rest. For this test, it is therefore assumed that similar results are obtained when the inner cylinder is lowered into the mixture very slowly after the resting period.

In both cases, the rheological behaviour was determined after a rest period of 3, 4, 5 and 6 hours. The mix design can be found in Table I. Water is added until a water cement ratio of 1.325 (m/m) is reached.

Table I. Mixture composition.

10% (m/m)	Cement	CEM I 52.5N HSR LA
30% (m/m)	Limestone powder	$CaCO_3$
0.03% (m/m)	Superplasticiser	PCE-type
59.97% (m/m)	Sand	Calibrated river sand Dmin = 0 mm Dmax = 4 mm

Results of the rheological testing

Plastic viscosity. For the mixture being remixed in the mixer after a period of rest, and for the mixture not being remixed, similar values for the plastic viscosity were found up to a period of 6 hours after mixing. The plastic viscosity in both cases was found in the range of 9 to 13 Pa·s, which is low compared to the plastic viscosity of self-compacting concrete for example. The results are plotted in Figure 1, with the resting period on the horizontal axis and the plastic viscosity (μ) on the vertical axis.

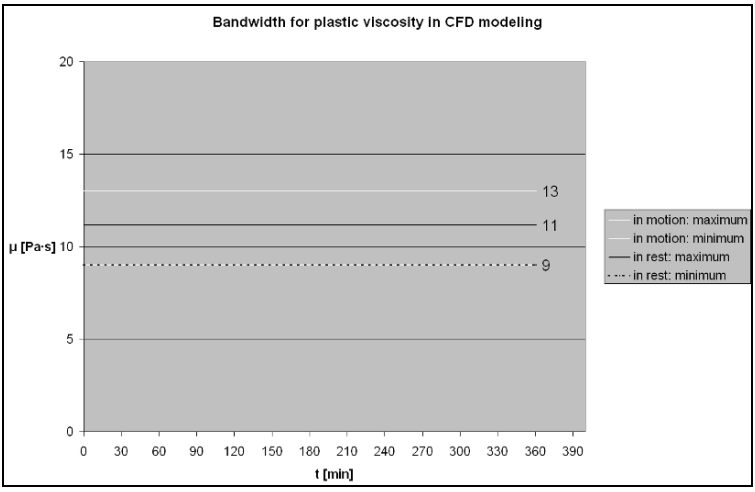

Figure 1. Plastic viscosity development in time.

Yield stress. The yield stress increased during the rest period (3, 4, 5 and 6 hours). When the material was remixed after the resting period, the yield stress was in the range of 0 and 4 Pa, while values between 25 and 47 Pa were found for the material being tested without remixing after the resting period. The idealized yield stress is plotted in Figure 2, with the resting period after mixing on the horizontal axis and the yield stress (τ_0) on the vertical axis.

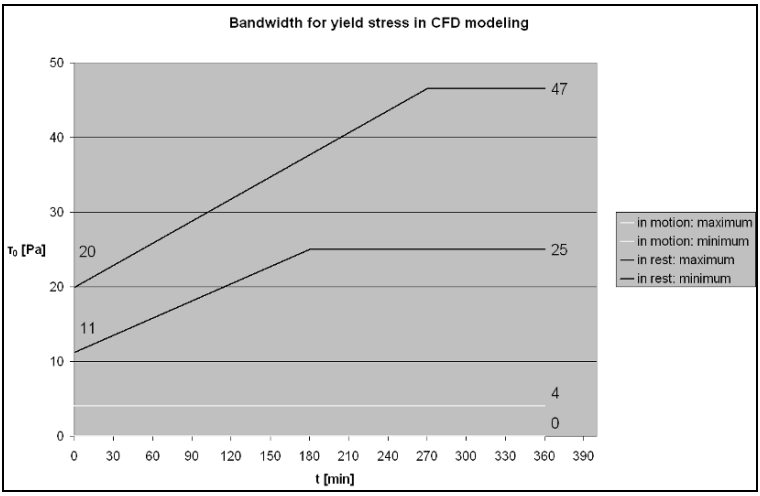

Figure 2. Yield stress development in time.

In the model a constant yield stress and plastic viscosity have been assumed as rheological properties of the grout. Also segregation of the grout is excluded because the CFD model is based on the homogeneous fluid approach, which does not allow taking into account segregation.

Grouting Experiment

Test set-up

The flow experiments were carried out to validate the model and to simulate the flow of grout when injecting it into the underground galleries. The model will also be used to simulate future casting situations, because visual inspection of the filling process is not possible. The Plexiglas model represents the underground tunnel and is downsized with a factor 12.5. A picture is shown in Figure 3. The space to be filled with grout is shown in Figure 4.

Three sections of Plexiglas with an inner diameter of 24 cm and a length of 1.92 m were constructed, which were coupled to a total length of 5.76 m. Tests were also performed with only one section and with two sections coupled. Additional tubes with an outer diameter of 16 cm represent a row of waste containers in the tunnel and are placed inside the Plexiglas setup. This smaller tube rests on line supports along the setup. The filling strategy proposed by EURIDICE is called backfill technology. With this technique, the grout fills the space from the back on, with the air venting at the front. In this study, the grout is injected via a hose and a pump that was filled directly from the mixer. With the chosen experimental setup it was

possible to fill the setup via the front or via the back endplate with the air vent opened at the other site of the setup (Figures 5 and 6). The backfill method is the closest to the real casting situation.

Figure 3. Picture of one of the three sections of the Plexiglas setup.

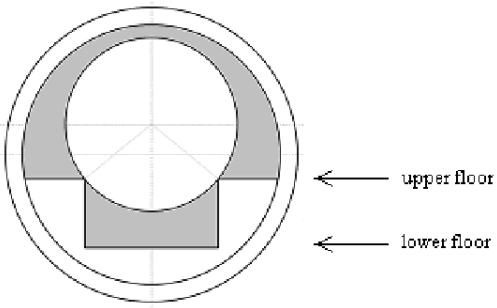

Figure 4. Space of the cross-section of the tunnel to be filled with grout (in grey).

Figure 5. Schematisation of the frontfill method.

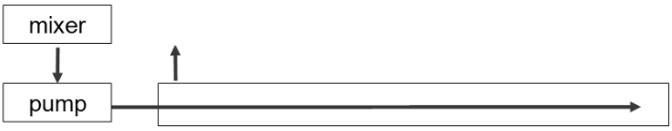

Figure 6. Schematisation of the backfill method.

Outside the Plexiglas tube, a grid was placed to record the progress of the grout front in time. The progress of the grout front was compared to positions in the simulation. Segregation tests were carried out at every 1.92 m along the setup. Three frontfill tests were carried out, whereby the length was increased from 1.92 to 3.84 and ultimately to 5.76 m. Thereafter, two backfill tests were carried out using a setup of 5.76 m in length with the injection pipe on the lower and on the upper floor, respectively. Discharge rates of 0.60 up to 1.80 liters per minute were used. After each test the setup was completely cleaned and prepared for the following test. In the picture below, a section is shown during one of the experiments.

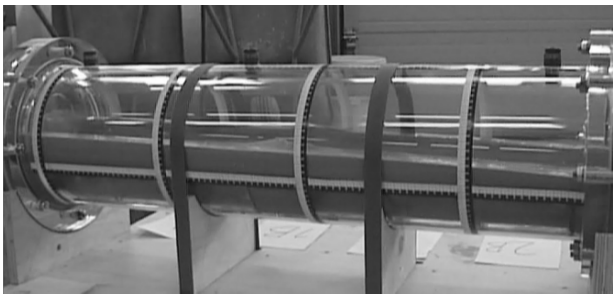

Figure 7. Setup with grout and grid for time-position measurements of grout front.

Results of the grouting experiment

General conclusions and mixture analysis.

- Independent of the length of the setup or the filling method, the inner tube was always immersed in the grout; no air entrapments were observed. At the top of the tube – especially close to the air outlet – a foam-like material appeared.
- The inner tube was not completely covered (due to the foam). However, since the experiment is a downsized version of the underground tunnel this does not necessarily mean that this also yields for the real situation.
- The frontfill experiment was carried out with one, two and three sections coupled. In general, it can be concluded that the worst results are always obtained in the section most far from the injection point. Independent of the length of the setup, the following results were obtained:
    - Segregation of the grout (less coarse material at the most far end of the injection point) was observed. The mixture composition was not homogenous throughout the Plexiglas tube.
    - Because of the high flowability of the grout and the closed end plate the grout front was almost horizontal. For the grout it is therefore not possible to push the air towards the end of the setup.

  - The foam that rises to the grout surface will not force air to flow to the end of the setup. After some grout passed the air outlet, the filling ratio did not increase and hardly any air could escape thereafter.
- The backfill method was also applied using an injection tube on either the lower or the upper floor. With three sections coupled and the injection tube positioned at the lower floor, similar results (regarding aggregate segregation, the formation of a horizontal front and the occurrence of foam) were obtained.

Time measurements

- The grout front reaches the end of the 1.92 m long Plexiglas setup after 6 minutes (at a discharge rate of about 0.60 liters per minute).
- The grout front reaches the top of the Plexiglas setup after 12 minutes at the front plate and after 15 minutes at the end plate at the same discharge rate.

Table II. Position of the grout front in time.

	Front plate (0 cm)	End plate (1.92 m)
Grout observed on floor	0 minutes	6 minutes
Grout reaches top	12 minutes	15 minutes

Comparison between Experiments and CFD Simulations

The CFD model has first been applied to predict the flow of grout in a funnel test. The results from the CFD model have been compared with a funnel test performed in the laboratory as a first validation step of the CFD model. Very good agreement between the experimental and the simulated funnel time was found (Figure 8). In the experiment, a funnel time of 9.0 seconds was recorded. In the CFD simulation, a funnel time of 10.0 seconds was found. Because of the results mentioned above, a CFD model was constructed to predict the flow of grout through the Plexiglas setup. The frontfill test using one section of 1.92 m was compared to a CFD simulation.

The presented data yield only 5% of the time-position points that were collected during all five frontfill and backfill tests. Therefore the conclusions drawn here are related to this set of data. The other four tests (with 95% of the time-position points) will be compared with equivalent CFD models in a follow-up study in the near future. The simulation (Figure 9) predicts that the grout climbs through all openings between the supports at almost the same point in time, which was not observed in the experiments.

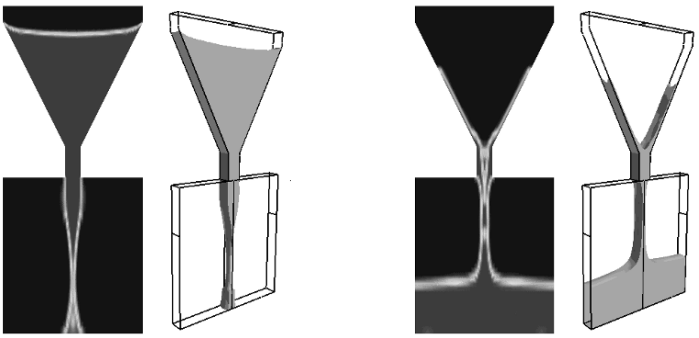

Figure 8. Emptying of a funnel after 1 and 10 seconds predicted by CFD.

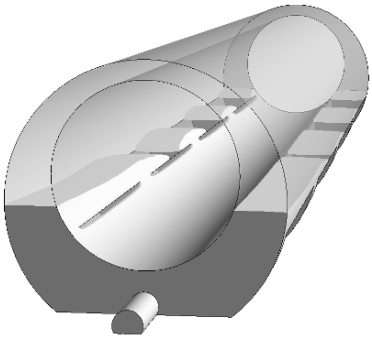

Figure 9. Predicted grout interface during the backfill test by the CFD model. (The grout ascends from the gaps in between the line supports.)

Time measurements

In the horizontal direction, CFD requires 52% more time to reach the end of the tube (distance: 1.92 m) compared to the grout front in the Plexiglas setup. In Figure 10, the time-position graph of the grout front at the lower floor is plotted.

The setup has a length of 1.92 m. At each 0.48 m, the vertical rising of the grout front is recorded. In Figure 11, the data at a distance of 1.44 m is shown. From Figure 10, it can be seen that the grout front reaches 1.44 m at t = 4 minutes 23 s. At this position, the grout starts rising after 4 minutes 23 s, and therefore the first measuring point in Figure 11 is also at 4 minutes 23 s. The height here is already 4 cm, since the floor lies at 4 cm from the bottom of the tube, see also Figure 4.

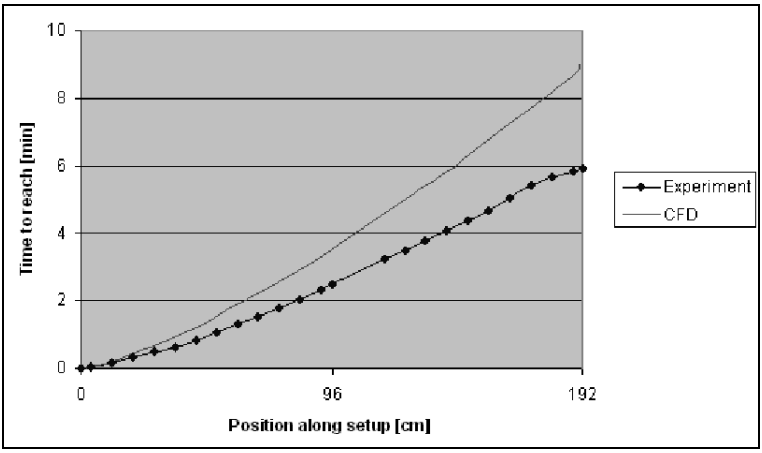

Figure 10. Comparison of the grout front in the horizontal direction.

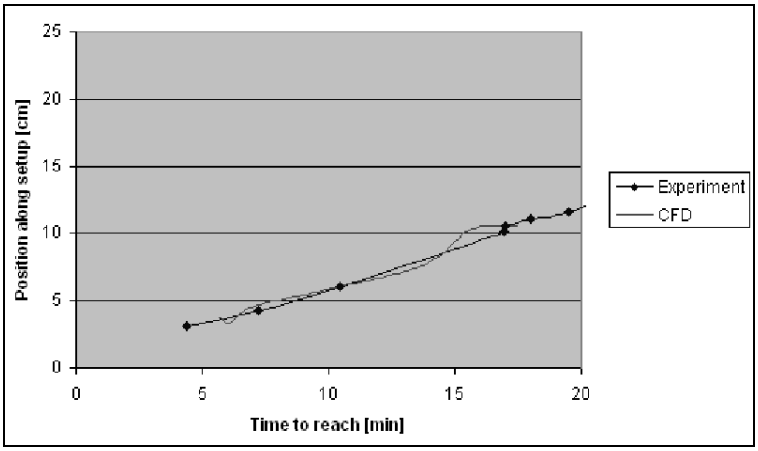

Figure 11. Comparison of the grout front in the vertical direction.

In the vertical direction, the grout front of the CFD model is up to 18% slower in the first half of the tube (distance < 0.96 m) compared to the material in the Plexiglas setup. The vertical rising of the grout front in the second half of the tube shows good agreement with the simulation. An example is given in Figure 11 (three quarters of the setup, at a distance of 1.44 m from the front plate). However, in the simulations an acceleration in the rising speed is found, which was not observed in the experiments; the position in CFD after 16 minutes is 2 cm higher than the position found in the experiment, which is the maximum difference in Figure 11.

Figure 11 indicates small differences between the rising speed in experiments and simulations in vertical direction. In horizontal direction, see Figure 10, the speed of the casting front was underestimated. The difference can be explained by the fact that a thin layer of segregating paste precedes the bulk of the grout. The CFD model assumes a homogeneous fluid, whereas the grout itself is heterogeneous. The most likely cause for the differences here are the rheological parameters and/or segregation of the material. A relatively small segregated volume of the grout has different rheological properties compared to the bulk. Due to a lower plastic viscosity of the grout front and the thixotropic behaviour of the material differences between simulations and experimental results can be explained.

Conclusions

Based on the experimental results and simulations on the filling behavior of fresh grout the following conclusions can be drawn:

Rheological parameters

- The plastic viscosity was between 9 and 13 Pa·s independent of the period of rest.
- The yield stress was in the range of 0 and 4 Pa after remixing and between 25 and 47 Pa after 3 or more hours of rest.

Grouting experiment

- The inner tube was always immersed in the grout. However, a foam-like material appeared at the top site.
- Segregation of the material (less coarse material) was observed in the sections most far from the injection point.
- After the grout passed the air outlet, no more air was driven out via the air vent.
- Similar filling processes were found for the frontfill as well as for the backfill method; when taking into account the position of the grout inlet, the time-position points of the grout front using the frontfill method are well comparable with the points resulting from the backfill method.

Comparison between experiments and CFD simulations

- In the horizontal direction, the grout front in the CFD model is slower than the material in the Plexiglas setup.
- In the vertical direction, the grout front in the first half of the CFD model is slower than the material in the setup. The vertical grout front in the second half showed good agreement with the flow in the Plexiglas setup.
- A very good agreement between the experimental funnel test and the CFD prediction of the funnel test was found.

- The differences between the CFD prediction and the Plexiglas test are most probably caused by the effects of segregation and the thixotropic behaviour of the grout. These effects have not yet been implemented in the rheological CFD model of the grout.

Acknowledgement

The present work has technically and financially been supported by NRG by means of funding from the Dutch ministry of Economic affairs (EZ).

References

[1] Thrane, L.N. (2008), Form filling with self-compacting concrete, PhD Thesis, Eurographic A/S, Technical University of Denmark, Denmark.

[2] Gopala, V.R., Van Wachem, B.G.M. and Andersson, B. (2007), Analysis and validation of the breakup of fluid particles using volume of fluid method, Chalmers University of Technology, Gothenburg, Sweden.

[3] Gopala, V.R. and Van Wachem, B.G.M. (2008), Volume of fluid methods for immiscible-fluid and free-surface flows, *Chemical Engineering Journal,* vol. 141, pp. 204-221.

[4] Wallevik, O.H. (2003), Rheology – A scientific approach to develop self-compacting concrete, Proceedings of the 3rd International RILEM Symposium on SCC, Reykjavik, Iceland.

[5] Grünewald, S. (2004), Performance-based design of self-compacting fibre reinforced concrete, Delft University Press, Delft, the Netherlands, pp. 6-8.

[6] Roussel, N. (2006), A thixotropy model for fresh fluid concretes: Theory, validation and applications, *Cement and Concrete Research,* vol. 36, pp. 1797-1806.

[7] Wallevik, O.H. (2000), Rheological measurements on fresh cement paste, mortar and concrete by use of a coaxial cylinder viscometer. The Icelandic Building Research Institute, Keldnaholt, Iceland.

Prediction of the Impact of Flow-Induced Inhomogeneities in Self-Compacting Concrete (SCC)

J. Spangenberg[1], N. Roussel[2], J. H. Hattel[1], J. Thorborg[1,3], M. R. Geiker[4], H. Stang[4] and J. Skocek[4]

[1] Department of Mechanical Engineering, Technical University of Denmark (DTU), Denmark
[2] Université Paris Est, Laboratoire Central des Ponts et Chaussées (LCPC), France
[3] MAGMA GmbH, Germany
[4] Department of Civil Engineering, Technical University of Denmark (DTU), Denmark

Abstract. SCC is nowadays a worldwide used construction material. However, heterogeneities induced by casting may lead to variations of local properties and hence to a potential decrease of the structure's load carrying capacity. The heterogeneities in SCC are primarily caused by static and dynamic segregation. The present paper reports property maps for a beam based on particle distributions at the end of casting derived from numerical flow simulations. A finite volume based numerical model is used to predict particle distributions at the end of casting, which are then converted into property maps using semi-empirical relations from the literature.

Introduction

The ideal mix design of a SCC is located somewhere between two opposite objectives. On one hand, the SCC has to be as fluid as possible to ensure that it will fill the formwork under its own weight. On the other hand, it has to be a stable mixture as flow in such a confined zone as a reinforced formwork may cause the components of the material to separate during casting. Therefore, a compromise between fluidity and stability has to be reached. The available method in the traditional toolbox of the civil engineer is to try various mix designs and, for each of them, cast the real size element and choose the most suitable mixture (if there is one). This is expensive, time consuming and does not guarantee that an answer will be obtained. However, in the last twenty years, the numerical tools of non-Newtonian fluid dynamics have allowed for the numerical simulations of casting processes and, for a very low cost in time and money, the identification of the

K.H. Khayat and D. Feys (eds.), *Design, Production and Placement of Self-Consolidating Concrete*, RILEM Bookseries 1,
DOI 10.1007/978-90-481-9664-7_18, © RILEM 2010

minimum needed fluidity [1]. Mori and Tanigawa [2] first demonstrated the applicability of Viscoplastic Divided Element Method (VDEM) to simulate the flow of concrete in a reinforced beam section and the filling of a reinforced wall whereas Kitaoji et al. [3] confirmed the applicability of 2D VDEM to simulate the flow of fresh concrete cast into a formwork. The results of a form filling experiment in a vertical wall have also been compared with the corresponding 3D simulation [4]. The results show good correlation with respect to detection of the free surface location, dead zones and particle paths. Numerical simulations were recently also applied to an industrial casting of a very high strength concrete pre-cambered composite beam by Roussel et al. [5]. The results of the simulations carried out for various values of the rheological parameters helped to determine the value of the minimum fluidity needed to cast the element. In most applications, a satisfactory agreement was found between the predicted and the actual global flow of the material within the formwork. It can therefore be expected that, in the future, computational modeling of flow will become a practical tool allowing for the simulation of either total form filling as described above or detailed flow behavior such as particle migration or fiber orientation. These methods could then be gathered in order to create a casting process engineering toolbox and bring rheology from the laboratory to the field.

The present paper shows a glimpse at this future by illustrating how it is possible to extract a map of properties in the hardened state of a structural element from numerical simulations of casting processes coupled with numerical simulations of the segregation of the coarsest particles. In the first part of this paper, we describe the numerical techniques and assumptions needed to simulate the segregation phenomenon during casting of SCC. In the second part, we present maps of coarse aggregates distribution through and at the end of the casting process. Finally, using simple semi-empirical correlations from literature, we deduct from these results maps of local properties or local phenomena such as elastic modulus, compressive strength and drying shrinkage.

Numerical Simulations Description

Most numerical simulations of concrete flows in literature consist in either considering a homogeneous fluid implicitly containing particles or taking explicitly into account the presence of the particles using for example Discrete Element Methods (DEM). The homogeneous approach is easier to implement but is valid only when the smallest characteristic dimension of the flow (size of the mould or spacing between bars) is high compared to the size of the largest particles (five times larger for example in [6]). In this paper, we will assume that these conditions are fulfilled and use a homogeneous approach to calculate the velocity field. As accepted in literature, a Bingham model is, in this case, an acceptable rheological model to describe the concrete rheological behavior. From this velocity field, we then calculate the trajectories of the particles. Meaning, a one-way momentum

coupling is applied such that the fluid affects the particles but not vice versa.

The computational fluid dynamics (CFD) code Flow3D® [7] is used here to solve the Navier Stokes equations. FLOW3D® is a general-purpose computer program with many capabilities. Using input data, the user can select different physical options to represent a wide variety of fluid flow phenomena. The program can be operated in several modes corresponding to different limiting cases of the general Navier Stokes equations. More details about the numerical methods used to model flow of concrete with FLOW3D® can be found in [8]. We consider in this paper an SCC with a yield stress of 50 Pa and a plastic viscosity of 50 Pa s. These are common orders of magnitude for standard SCC in housing construction that may be prone to segregation during casting. We moreover consider in this paper that concrete can be considered by a two phases approach as rigid particles suspended in a continuous phase. The suspended particles considered here correspond to the 25% coarsest particles in the material. The volume fraction of these particles is assumed to be in the order of 15-20% in practice and can be associated to a characteristics average diameter of 15 mm. By doing so, we assume that the 75% finest aggregate particles are sufficiently small to be stable and do not segregate during flow. We moreover assume that the viscosity of the continuous phase is 10 times lower than the viscosity of the SCC. This is in agreement with the orders of magnitudes of viscosities of standard materials from the construction field (cement paste 0.5-1 Pa., mortar 5-10 Pa.s and concrete 50-100 Pa.s). In the following, we either assume that a) the particles have the same density as the suspending fluid (2200 kg/m^3) when we show results for which no segregation occurs or b) have a density of 2700 kg/m^3 when we focus on segregation during casting. It has to be noted that, in the following simulations, all interactions between particles are neglected and that the rheological parameters of the concrete do not vary due to local volume fraction changes. The only thing that is simulated is gravity and the hydrodynamic effects of the fluid on the moving particle. We simulate the casting of a 3 m long and 30 cm thick beam. The casting point is located at the center of the beam and the material is assumed to be homogenous at the entry point. We neglect the presence of any steel bars and perform the calculation in 2D, and therefore also neglecting the influence of the lateral walls. We impose the casting rate so that the front velocity is of the order of 30 cm/s.

Particle Distributions

The casting process simulations are illustrated in Figure 1 at successive time steps. Through the casting, the density difference between the coarse particle and the continuous phase is at the origin governed by a slow migration of the particles towards the bottom of the formwork. This migration is slowed down by the viscosity of the continuous phase but is not fully prevented. In the case of the SCC studied here the results are within the frame of our assumptions.

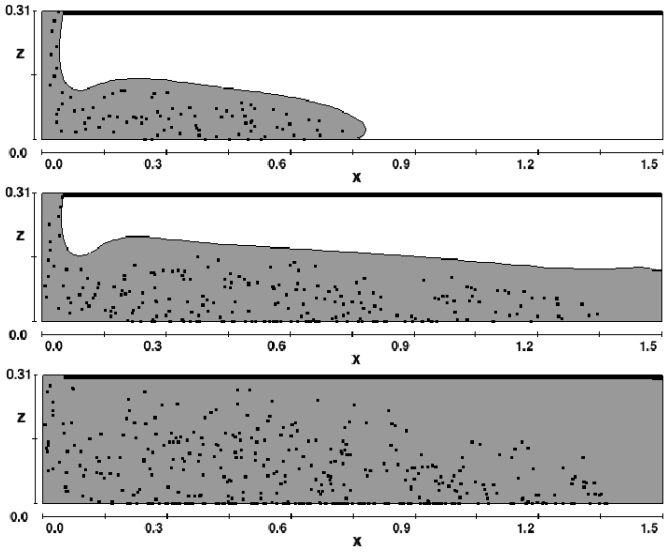

Figure 1. Particle distribution through the casting process. Only the right half of the beam is shown. Vertical and horizontal distances are in (m).

It can be noted that there exist zones at the bottom of the formwork where the volume fraction of the coarse aggregates is predicted to be higher than the maximum volume fraction at the end of casting. This source of error is due to the fact that we do not take into account any interactions between particles and between particles and walls. The particles therefore accumulate without any hindrances at the bottom wall.

In Figure 2 we plot the total aggregates (sand and gravel) volume fraction at the end of casting. In order to obtain this value, we add the local volume fraction of the coarsest particles to the volume fraction of the stable finer aggregates. The top figure in Figure 2 represents the case of particles having the same density as the continuous phase. While a homogeneous distribution of the particles is expected in this case at the end of casting, we see in this figure some heterogeneities. These are due to the sampling and particles counting method and to the random generation of particles at the flow inlet. These "natural" heterogeneities are of the order of ±0.03 (5%) compared to the homogeneous concrete with an aggregate volume fraction of 0.64. The bottom figure in Figure 2 shows the heterogeneities in the beam at the end of casting in the case of particles with a density of 2700 kg/m^3 in a continuous phase with a density of 2200 kg/m^3. In this case, these heterogeneities are of the order of ±0.20 (25%). These are five times higher than the heterogeneities associated with the counting and sampling technique. Because of the stacking of the coarsest particles at the bottom of the formwork described above, there exist zones at the bottom of the formwork where the total aggregates volume fraction is

predicted to be higher than the maximum volume packing fraction at the end of casting. In the zones where this happens, we consider in Figure 2 and in the following sections that the volume fraction of the particles in these zones is equal to the maximum packing fraction of the order of 0.8.

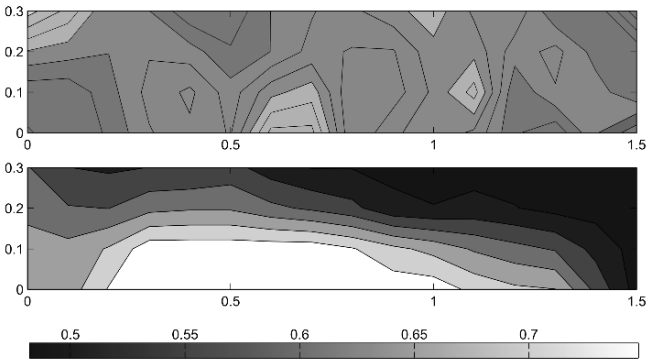

Figure 2. Aggregate volume fraction map. (top) "homogeneous" distribution of particles (homogeneous aggregate volume fraction is 0.64) (bottom) segregated particles. Vertical and horizontal distances are in (m).

Property Maps

In Figures 3 and 4 we plot the maps of the relative elastic modulus (*i.e.* the ratio between the local elastic modulus and the elastic modulus of the homogenous reference concrete) and the relative compression strength (*i.e.* the ratio between the local compressive strength and the compressive strength of the homogenous reference concrete) extracted from the bottom figure in Figure 2 using the simple models proposed in [9] and [10]. The variations induced by segregation are of the order of 10% for these two properties.

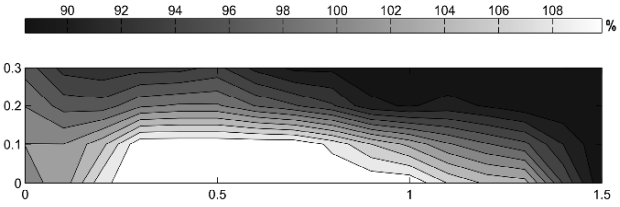

Figure 3. Relative elastic modulus map. Vertical and horizontal distances are in (m).

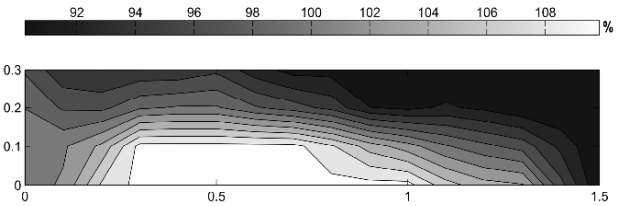

Figure 4. Relative compressive strength map. Vertical and horizontal distances are in (m).

In Figure 5 we plot the map of the relative drying shrinkage strain (*i.e.* the ratio between the local drying shrinkage strain and the drying shrinkage strain of the homogenous reference concrete) using the relation given in [11]. The variations are of the order of 25% and could induce a strong concentration of shrinkage in specific zones of the beam, which could in turn induce some cracking.

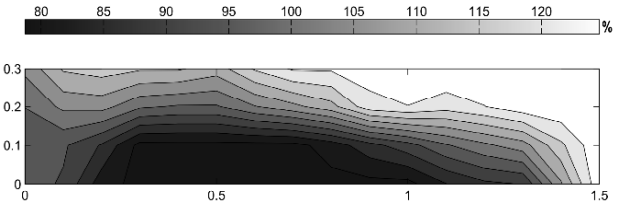

Figure 5. Relative drying shrinkage strain map. Vertical and horizontal distances are in (m).

Conclusions

We have shown in this paper how it is possible to use a CFD calculation of the casting process coupled with numerical modeling of the segregation of the coarsest particles to produce a map of properties in the hardened state of a structural element. We have plotted maps of local properties and phenomena such as elastic modulus, compressive strength and drying shrinkage strain for a beam filled with SCC, using simple semi-empirical correlations from literature.

References

[1] Roussel, N., Geiker, M.R., Dufour, F., Thrane, L.N. and Szabo, P. (2007), Computational modeling of concrete flow: General overview, *Cement and Concrete Research*, vol. 37, n. 9, pp. 1298-1307.

[2] Mori, H. and Tanigawa, Y. (1992), Simulation methods for fluidity of fresh concrete, *Memoirs of the School of Engineering, Nagoya University*, vol. 44, pp. 71-133.

[3] Kitaoji, H., Tanigawa, Y., Mori, H., Kurokawa, Y. and Urano, S. (1996), Flow simulation of fresh concrete cast into wall structure by viscoplastic divided space element method, *Trans. of the Japan concrete institute*, vol. 16, pp. 45-52.

[4] Thrane, L.N., Szabo, P., Geiker, M.R., Glavind, M. and Stang, H. (2005), Simulation and verification of flow in SCC test methods, Proc. of 4th int. RILEM Symp. on SCC, Chicago.

[5] Roussel, N., Staquet, L., D'Aloia Schwarzentruber, L., Le Roy, R. and Toutlemonde, F. (2007), SCC casting prediction for the realization of prototype VHPC-precambered composite beams, *Materials and Structures*, vol. 40, n. 9, pp. 877-887.

[6] Coussot, P. and Ancey (1999), Rheophysics of pastes and suspensions, EDP Sciences (in French).

[7] Flow3D version 8.1 (2004), User's manual 1.

[8] Roussel, N. and Coussot, P. (2005), "Fifty-cent rheometer" for yield stress measurements: from slump to spreading flow, *Journal of Rheology*, vol. 49, n. 3, pp. 705-718.

[9] de Larrard, F. and Le Roy, R. (1992), Correlations between mix design and some mechanical properties of high performance concretes, *Materials and Structures*, vol. 25, pp. 464-475 (in French).

[10] de Larrard, F. (1999), Concrete mixture proportioning – A scientific approach, Modern Concrete Technology, series 9.

[11] Eguchi, K. and Teranishi, K. (2005), Prediction equation of drying shrinkage of concrete based on composite model, *Cement and Concrete Research*, vol. 35, pp. 483-493.

Theme 6: Formwork Pressure of SCC

Influence of Rheological Properties of Pourable Concrete on Formwork Pressure

Carsten Bohnemann and Wolfgang Brameshuber

Institute of Building Materials Research, RWTH Aachen University, Germany

Abstract. In the course of the wider use of concretes with pourable consistency more and more practice-relevant and economic questions arise. The pressure of concrete on formwork is one of those questions. In the literature very contradictory statements are depicted partially to the pressure of concrete on formwork when using concretes with pourable consistency. Therefore the aim of the research project was to examine the influence of the rheological properties of self-consolidating concretes (SCC) and vibrated concretes (VC) with consistencies F5/F6 according to DIN EN 206-1:2001-07 on the formwork pressure. The research project was divided into two steps: "Development and investigation of model mixtures for self-compacting concrete (SCC) and vibrated concrete (VC) respectively" and "Measurements of formwork pressure in constructional elements like walls". In the first step basis mixtures had to be developed. Concretes with F5/F6 consistencies, two powder-type SCC (PT), and two viscosity-agent-type SCC (VAT) were used. The latter mixtures differed considerably in viscosity. Thus all relevant cases regarding the rheological properties were covered by these pourable concrete mixtures. In the second step systematic investigations were conducted to determine the effect of the rheological properties on the fresh concrete pressure on the formwork of constructional elements (walls). By concreting in a precast element plant a reference to practice was given.

Fresh Concrete Pressure on Vertical Formwork

At the present time, the investigation of the new material SCC has already provided a secure knowledge to numerous technical issues. Nevertheless, there are still contradictory results for the formwork pressure of SCC and concretes with consistency classes F5/F6 [1-7]. Systematic studies on the influence of individual parameters showed that the height and distribution of fresh concrete depends on several parameters. The following are the key factors that are described in [8]:

- Rheological properties,

K.H. Khayat and D. Feys (eds.), *Design, Production and Placement of Self-Consolidating Concrete*, RILEM Bookseries 1,
DOI 10.1007/978-90-481-9664-7_19, © RILEM 2010

- Casting rate,
- Method of casting,
- Formwork geometry and
- Reinforcement

In the research project only the influence of the first three parameters was determined on the fresh concrete pressure.

Investigations

Concrete mixtures

First, different model mixtures for concretes of the consistency classes F5, F6 and SCC were developed (Table I).

Table I. Concrete mixtures.

material	unit	Content/value					
		SCC PT-hv	SCC PT-lv	SCC VAT-hv	SCC VAT-lv	VC F5	VC F6
1	2	3	4	5	6	7	8
CEM II/A-LL 32.5 R	kg/m³	300		340		395	
fly ash		250		100		75	
water content		160	190	180	200	170	180
aggregate		1664	1584	1742	1689	1750	1723
superplasticizer	% per mass (cement)	3.9	2.1	2.7	1.7	1.2	1.5
stabilizer		1.0				-	1.0
air content	% per volume	1.5					
w/c_{eq}	-	0.47	0.56	0.47	0.52	0.4	0.42

PT: powder-type
VAT: viscosity-agent-type
hv: high viscosity
lv: low viscosity
superplaticizer based on polycarboxylate ether (PCE)
stabilizer based on synthetic polymers
F5/F6: adjustment of the consistency of vibrated concretes by superplasticizer

The four self-compacting concretes chosen for the investigations can be classified as a low-viscosity and a high-viscosity powder-type and as a viscosity-agent-type SCC with a low viscosity and a high viscosity, respectively. The investigations concerning the measurements of the fresh concrete pressure were conducted in a precast element plant. Therefore the raw materials and the mix designs had to be adjusted to the production in the precast element plant [9]. The applied high-viscosity powder-type SCC is a concrete with a general technical approval, which is used in the precast plant to produce precast elements made of reinforced concrete. The other SCC were developed from this standardised concrete. Also the vibrated concretes (VC) are based on a standardized mixture of the precast element plant.

To characterize the concretes, the fresh concrete temperature, the fresh concrete density and the setting time were determined both in the laboratory and in the precast plant. To verify the rheological properties of the concretes investigations of appropriate mortars (SCM) have been conducted with the Viskomat NT in the laboratory. It is necessary to determine the rheological properties of SCM, because the flow properties of concrete are affected mainly by the properties of cement paste or mortar. The evolution of rheological parameters (viscosity, yield stress) was not determined.

Experimental setup of the model walls

The investigations of the influence of the rheological properties on the fresh concrete pressure were conducted on model walls with the dimensions 3.30 x 2.56 x 0.24 m. The fresh concrete pressure was determined at different casting rates and with different methods of casting. The pressure was determined using load cells. The load cells were attached to the medium formwork element 0.15, 0.75, 1.35, and 2.55 m above the formwork bottom edge (Figure 1). The load cells consisted of a pressure sensor (steel disc), locking concisely with the formwork shell, which was connected with a load cell by a threaded rod (Figure 2). For sealing a thin PE-foil was adhered over the pressure sensors at the inside of the formwork. The concrete was casted either with a concrete bucket from above or with a pump by using a special connection in the lower formwork area.

The marking of the load cells for the evaluation of the results was chosen as follows:

bottom:	0.15 m above the formwork bottom edge
2nd from bottom:	0.75 m above the formwork bottom edge
2nd from top:	1.35 m above the formwork bottom edge
top:	2.55 m above the formwork bottom edge

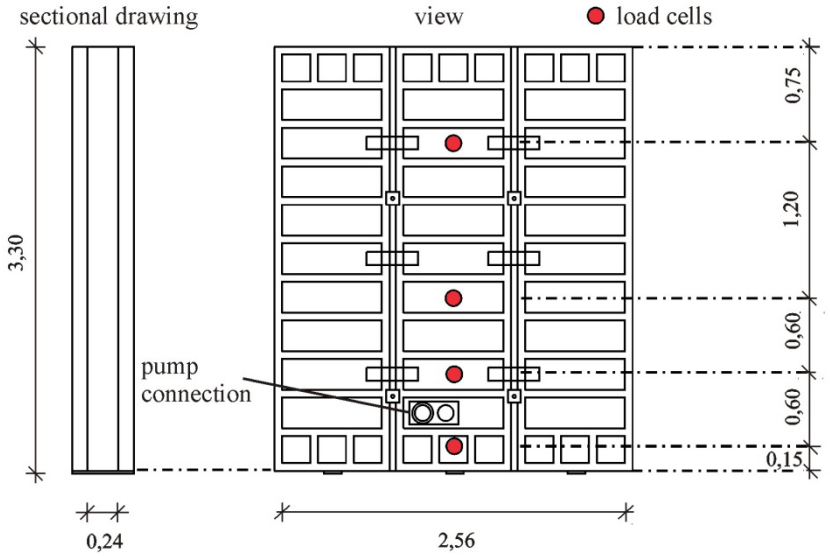

Figure 1. Test setup and installation height of load cells.

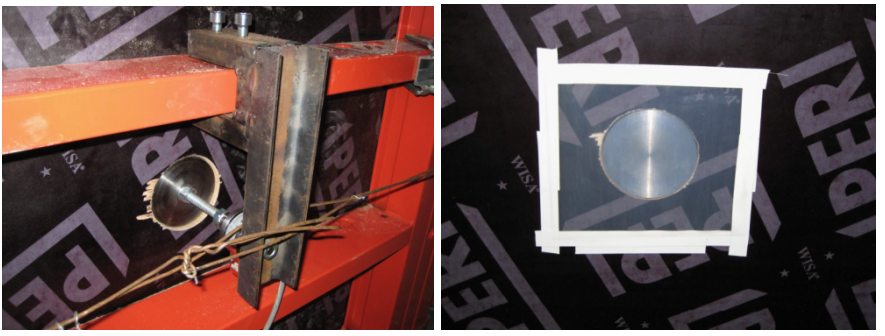

Figure 2. Anchorage and sealing of pressure cells.

Experimental procedure

For the investigations in the precast plant eleven model walls were produced. For each wall three batches of concrete were required. The casting rate was set through the speed of emptying the bucket or at the pump device and was controlled via one lateral formwork element made of acrylic glass. During the production interruptions between different batches occurred as it is usual in practice. The vibrated concretes were compacted with an internal vibrator. During the casting of concrete from above the height of fall between the concrete bucket and the bottom of formwork was max. 3.30 m. An ambient temperature between 17.4 and 29.9°C

was measured. The walls were distinguished by the concrete type, the casting rate and the method of casting (Table II). The medium rates of the casting rate were amounted to 2 m/h and 10 m/h. A small casting rate of 2 m/h was selected, in order to reproduce a casting of construction member with large dimensions (height, length, width). Due to the small casting rate (v_c = 2 m/h) no pump pressures could determined at the concrete pump.

Table II. Overview of the research program of concreting in a precast element plant.

wall	concrete	method of casting	casting rate
1	SCC-PT-hv	concrete bucket	2.0 m/h
2	SCC-PT-lv		
3	SCC-VAT-hv		
4	SCC-VAT-lv		
5	VC-F5		
6	VC-F6		
7	SCC-PT-hv		10.0 m/h
8	SCC-PT-lv		
9	SCC-PT-hv	pump	2.0 m/h
10	SCC-PT-lv		
11	SCC-VAT-lv		

Results

Laboratory tests

The slump flow of the SCC after mixing lay between 715 and 740 mm. The V-funnel time t_{Tr} was amounted between 1.2 and 3.4 s. The fresh concrete density was averaged between 2365 and 2297 kg/m³. Therefore the parameters of consistency and the fresh concrete density were within the normal range of the used SCC. The setting time of the SCC amounted to about 7 h at a fresh concrete temperature between 18 and 21°C. The investigated vibrated concretes showed a slump flow of 635 and 670 mm immediately after mixing. They had a fresh concrete density of 2365 kg/m³. The setting times of the VC were 5.5 h. For the tests in the Viskomat NT, the self-compacting mortars (SCM) were recruited to a

slump flow of 290 mm. The V-funnel flow times t_{Tr} were between 2.3 and 6.5 s. The mortar of the vibrated concretes (VM) had been set to a spread of 230 and 265 mm. Figure 3 shows the results of the investigations with the Viskomat NT illustrated by flow curves.

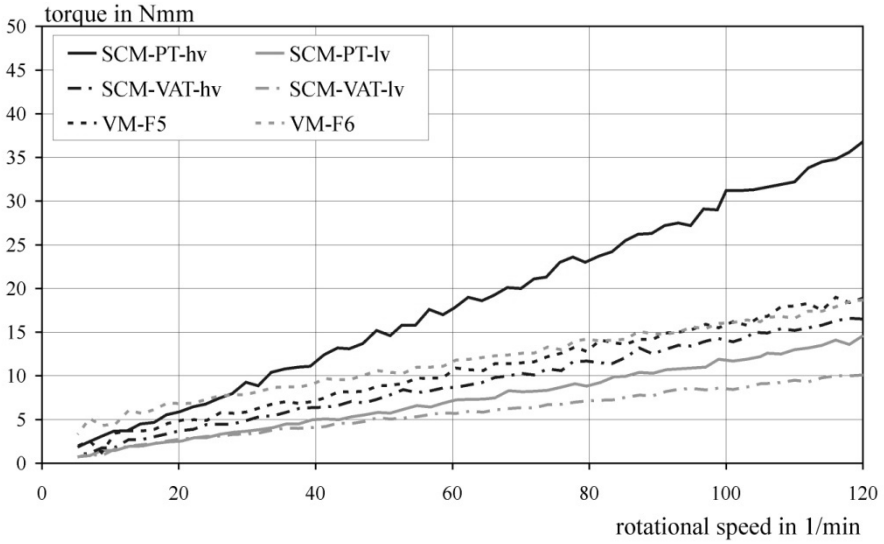

Figure 3. Flow curves of SCM and VC.

The slope of the yield curve corresponds to the viscosity of the mortar. For the SCM the V-funnel flow time was comparable to the order of the relative viscosities. Both powder-type SCM had higher viscosities than the viscosity-agent-type SCM. This is caused by the larger amount of finest fractions (fly ash) of the powder-type SCM. For a start this confirms the qualitative relationship between the V-funnel flow time and the viscosity. It was evident that the higher viscosity of the SVM-PT-hv showed a slightly dilatant behavior, while the flow curves of the other mortars were similar to Bingham fluids. The mortar of the vibrated concrete showed a Bingham behavior with viscosities in the range of the viscosity of the SCM-VAT-hv.

Pressure measurements on the model walls

In the precast plant the fresh concrete characteristics were determined at each first filling of the walls. Additionally the setting behaviour was investigated by Knead-Bag tests [10]. For the casting of batch two and three only the slump flow or the spread was determined. Furthermore, the temporal evolution of the consistency of each first batch was measured. At the beginning of the concreting the slump flow

amounted to 705 to 740 mm. 30 minutes later the slump flow was between 645 and 695 mm. The spread of the VC laid between 620 and 680 mm and after 30 minutes it was between 500 and 645 mm. The V-funnel times t_{TR} for the SCC with higher viscosity (hv) ranged between 11 and 15 s and for the SCC with a lower viscosity (lv) between 5 and 7 s. The fresh concrete densities were determined between 2181 and 2328 kg/m³. The setting times of the SCC were between 8.0 and 10.0 h and for the VC between 5.5 h and 6.5 h. The fresh concrete temperatures were measured between 22.1 to 28.6°C.

In Figure 4 the temporal developments of the fresh concrete pressure during the casting of the wall 1 (SCC-PT-hv) at a velocity of placing of 2 m/h is illustrated. In addition the filling level and the hydrostatic fresh concrete pressure are shown in the figure. The fresh concrete pressures of the SCC in the lower area increased continuously up to the first casting break at a casting height of 1.20 m. After the casting break the fresh concrete pressures at the two lower pressure measuring points increased until the second casting break. The increase of pressure was slower after the casting break. This is to be ascribed to the thixotropy of the concrete which had already been filled in. The pressure at the second measuring point form top increased up to the second casting break continuously. After the second casting break until the casting end no increasing of the fresh concrete pressure were determined. Only the fresh concrete pressure at the top measuring point increased.

It is shown that at a filling level of about 2.2 m the fresh concrete pressure escalated at three pressure measuring points. At this filling level the weight of the concrete in the upper area was larger than the supporting effect and the structure formation of the concrete in lower area. The maximum fresh concrete pressures amounted to about 55% of the hydrostatic fresh concrete pressure.

After the casting the fresh concrete pressure decreased at the lower pressure measuring point to about 66% of its maximum pressure. These relationships were also observed in the concreting of the walls 2 to 4. The fresh concrete pressure in the course of time is presented in [9]. Due to the test conditions the measurement of the pressure of fresh concrete was stopped after 12 h, so that a cancelation time could not be determined. A decay of pressure could be ascertained from 2 up to 3 hours after the beginning of concreting for nearly all castings. At longer casting breaks, the fresh concrete pressure already decreased at the two lower measuring points already decreased during the casting process. When casting the vibrated concretes [9], the maximum fresh concrete pressures lay within the range of the hydrostatic fresh concrete pressure. The irregular course of the fresh concrete pressures could be ascribed to the periodic compaction with the internal vibrator. A decrease in the fresh concrete pressure during the casting could also be observed.

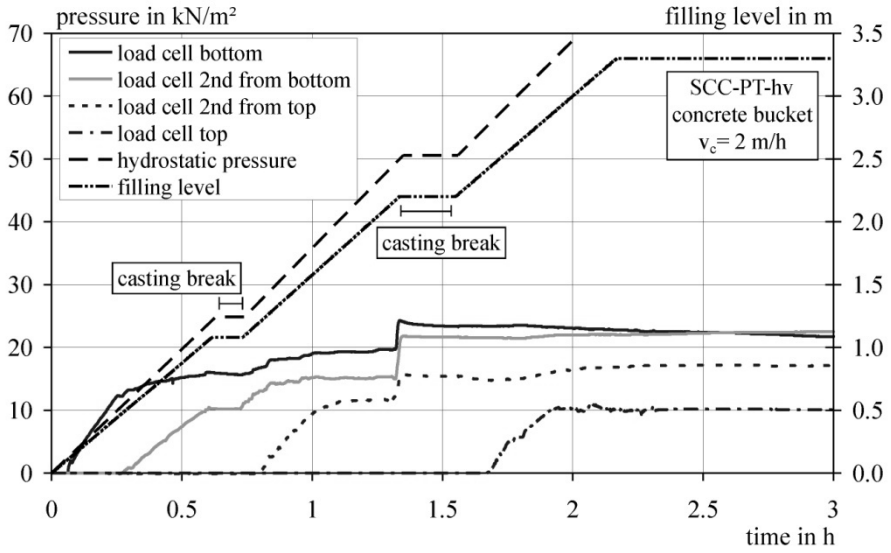

Figure 4. Development of the fresh concrete pressures with time of the wall 1 depending on the filling height for a casting rate of 2 m/h.

Figure 5 illustrates the fresh concrete pressures at the lowest pressure measuring point at a casting rate of v_c = 2 m/h for the walls 1 to 6. The vibrated concretes featured the highest fresh concrete pressures because of the compaction. At the self-compacting concretes (SCC), the fresh concrete pressures of the low-viscosity SCC types are higher than those of the high-viscosity SCC types. An influence of the SCC type on the fresh concrete pressure could not be discerned as the pressures of the respective high and low-viscosity mixtures were almost identical. When casting the powder-type SCC with a bucket from above at a casting rate of v_c = 10 m/h, the maximum fresh concrete pressures ranged near the hydrostatic fresh concrete pressure and they were approximately equal for both different viscosities at this rate of placement [9]. When casting the high-viscosity powder-type SCC at a casting rate of 10 m/h, the fresh concrete pressure was considerably higher than at a rate of 2 m/h. This is presumably due to the fact that the concrete started stiffening at the lower casting rate. At the low-viscosity powder-type, it could be observed that the fresh concrete pressures were almost identical [9].

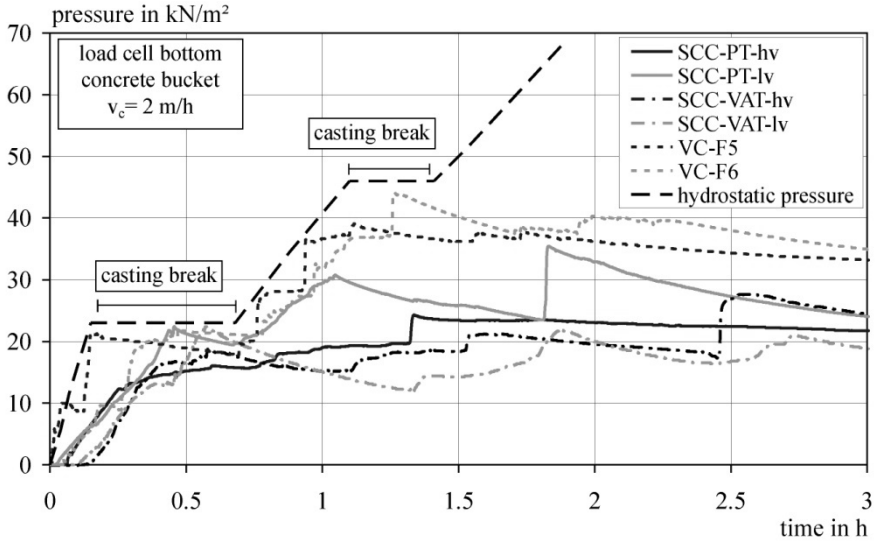

Figure 5. Development of the fresh concrete pressures with time at the lowest measuring point of the walls 1 to 6 for a casting rate of 2 m/h.

Figure 6 shows the results of the castings of walls 9 to 11 from the bottom with a concrete pump at a placement rate of v_c = 2 m/h. In this case, the maximum fresh concrete pressures lay within the range of the hydrostatic fresh concrete pressure. An effect of SCC type and viscosity could not be discerned at the pumping from the bottom and a placement rate of 2 m/h. The maximum fresh concrete pressures were almost identical. When comparing the pressures induced by the high-viscosity powder-type SCC measured at the lowest measuring point, it was observed that the fresh concrete pressures were significantly higher during the pumping than during the pressureless casting from the top. The pressure at the lowest measuring point was 2.5 times higher at the casting from the bottom than at the pressureless casting from the top. The reason was that the developing pressure of the fresh concrete was increased by the pressure caused by the concrete pump. This was necessary to cast the concrete against the concrete which had already been in the formwork (fresh concrete pressure, wall friction).

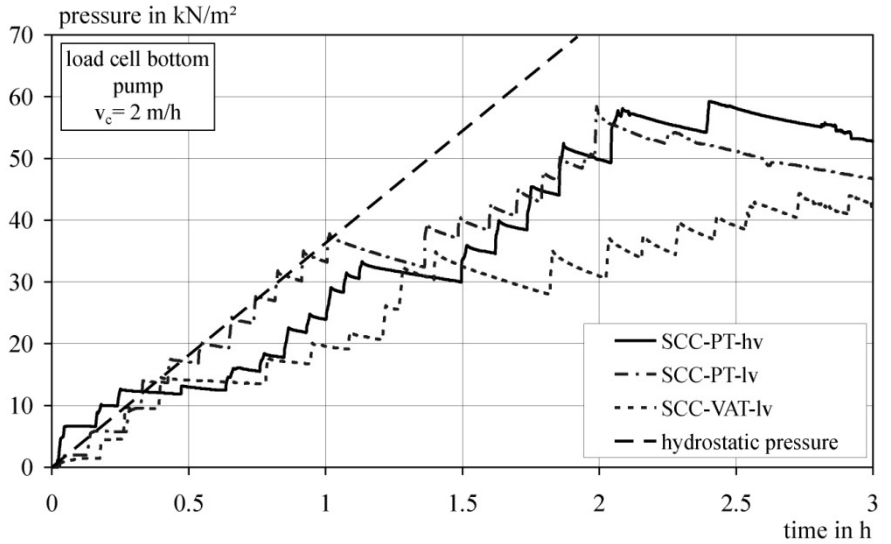

Figure 6. Development of the fresh concrete pressures with time at the lowest measuring point of the walls 9, 10 and 11 for a casting rate of 2 m/h.

Summary

The specification of the formwork pressure caused by high-performance concretes with a pourable consistency was the topic of the investigations. To clear quickly the restraints opposite to the use of this innovative material, the work was focused on the essential fields of application of pourable concretes and vertical formworks. The influence of the concrete type (different SCC, F5 and F6 concretes), the rheological property (viscosity), the method of casting and the casting rates on the fresh concrete pressure were investigated in casting of model walls. The walls were filled with casting rates of 10 and 2 m/h conventional used in practice. The casting was executed alternatively with a concrete bucket from the top or with a concrete pump near the formwork bottom.

It was determined that the influence of SCC-type on the fresh concrete pressure was low. At low casing rates and casting from top a reduction of the viscosity increased the fresh concrete pressure. But in this case the pressure lay below hydrostatic conditions. At higher casting rates the fresh concrete pressure was about 2.5 times higher and reached hydrostatic pressure conditions. In this case the change of viscosity had no effect on the fresh concrete pressure. The pressure of vibrated concretes reached up to the half filling level hydrostatic pressure conditions, afterwards the increase of the pressure up to the final filling level

became smaller and the fresh concrete pressure reached 60% of the hydrostatic pressure. The method of casting had a high influence on the fresh concrete pressure. When filling with a concrete pump from the bottom the maximum fresh concrete pressure was approximately 2 times higher as filling from top with the concrete bucket. The pressure across the entire wall height was almost in the range of the hydrostatic concrete pressure. Only for the high-viscosity powder-type SCC the pressure of fresh concrete was above the hydrostatic pressure up to a third of the filling level.

If the SCC should be used more economical, higher casting rates than 2 m/h are required. In this case the design and the construction of formwork for concretes with consistency class F5 and F6 as well as SCC should be done on the basis of hydrostatic pressure conditions. At low casting rates a minor fresh concrete pressure can be applied depending on the casting rate and the consistency class. For this purpose a calculation of the fresh concrete pressure according to the design models described in [11] is necessary. Thereby the maximum pressure of fresh concrete depends on three parameters: the setting time t_E, the casting rate v_C and a factor $K_{tot,k}$ which describes the consistency of the concrete type [11].

References

[1] Assaad, J., Khayat, K.H. and Mesbah, H. (2003), Variation of Formwork Pressure with Thixotropy of Self-Consolidating Concrete. *ACI Materials Journal,* vol. 100, n. 1, pp. 29-37.

[2] Bernabeu, A. (2000), Form-System and Surface Quality. Brite Euram Proposal No. BE96-3801. Brussels.

[3] Billberg, P. and Österberg, T., Self-Compacting Concrete – Technique of application. CBI Rapport. (www.cbi.se/ra022a.htm).

[4] Vanhove, Y., Djelal, C., Magnin, A. and Martin, D. (2001), Study of Self-Compacting Concrete Pressure on Formwork, Proceedings of the Second International Symposium on Self-Compacting Concrete, Tokyo, Ozawa, K. and Ouchi, M. (Eds.), pp. 585-594.

[5] Khayat, K.H., Assaad, J. and Mesbah, H. (2002), Variations of Formwork Pressure of Self-Consolidating Concrete – Effect of Section Width and Casting Rate, First North American Conference on the Design and Use of Self-Consolidating Concrete, Evanston, IL, USA, pp. 295-302.

[6] Skarendahl, A. (2001), Use of Self-Compacting Concrete in One-Site Constructions, ERMCO-Congress, Berlin.

[7] Walraven, J.C. (2001), Applications of Self-Compacting Concretes in the Netherlands. In: Self-Compacting Concrete, First Symposium of Leipzig, Innovations in Civil Engineering, Leipzig, pp. 205-219 (in German).

[8] Graubner, C.-A., Beitzel, H., Beitzel, M., Brameshuber, W., Brunner, M., Dehn, F., Glowienka, S., Hertle, R., Huth, J., Leitzbach, O., Meyer, L., Motzko, Ch., Müller, H.S., Proske, T., Rathfelder, M., Schuon, M. and

Uebachs S. (2006), Progress Report Fresh Concrete Pressure of Concretes with Pourable Consistency, Series of the German Commission for Reinforced Concrete, vol. 567, Beuth-Verlag, Berlin, p. 75 (in German).

[9] Graubner, C.-A., Beitzel, H., Beitzel, M., Bohnemann, C., Boska, E., Brameshuber, W., Dehn, F., König, A., Lingemann, J., Motzko, C., Müller, H.S., Pistol, K., Proske, T., Stettner, C. and Zilch, K. (2008), Formwork Pressure Asserted by Highly Workable Concretes – A Joint Research Project of German Research Institutes, Final Report F09-7-2008, TU Darmstadt, Institut für Massivbau (in German).

[10] Reinhardt, H.W. et al. (2001), Progress Report Self-Compacting Concrete (SCC), Series of the German Commission for Reinforced Concrete, vol. 516, Beuth, Berlin (in German).

[11] DIN 18218:2010-01: Fresh Concrete Pressure on Vertical Formworks (in German).

Prediction of SCC Formwork Pressure in Full-Scale Elements

Kamal H. Khayat[1], Ahmed F. Omran[1] and Matthew D'Ambrosia[2]

[1] Université de Sherbrooke, Québec, Canada
[2] CTLGroup, Skokie, IL, USA

Abstract. Various prediction models, based on experimental results to evaluate formwork pressure exerted by self-consolidating concrete were established based on extensive laboratory evaluation. The models are based on the measurements of the structural build-up of the concrete with rest time and placement characteristics of the concrete. The latter includes the rate of rise of the concrete in the formwork, concrete temperature, and minimum dimension of the formwork. This paper presents the results of two campaigns of field validation carried out at Sherbrooke, Quebec, and Skokie, Illinois, to validate the prediction models. The results confirm that the established models offer adequate prediction of form pressure exerted by self-consolidating concrete.

Introduction

The use of self-consolidating concrete (SCC) in cast-in-place applications, such as infrastructure and building construction, has been hindered in part due to the lack of understanding of lateral pressure characteristics exerted by such highly flowable concrete. It is generally understood that lateral pressure is greater than that of conventional vibrated concrete (CVC). Without adequate prediction methods, the only option left to the engineer is to design for full hydrostatic pressure or monitor pressure during placement and adjust the rate of placement. Since formwork pressure is a life-safety related issue, with significant construction collapse as a consequence, the only viable option remaining is to monitor the form pressure during placement until prediction models can be developed and validated. Well documented case studies involving casting of SCC in vertical elements in construction and repair applications are reported in [1].

An extensive investigation was carried out to evaluate the effect of mixture parameters and placement conditions on form pressure exerted by SCC [2, 3].

K.H. Khayat and D. Feys (eds.), *Design, Production and Placement of Self-Consolidating Concrete*, RILEM Bookseries 1,
DOI 10.1007/978-90-481-9664-7_20, © RILEM 2010

Concrete mixture parameters and rheological properties are captured in a single property which is related to the thixotropy of the SCC. The thixotropy can be defined as the behavior of certain gels, fluids, or suspensions that flow or become thin (less viscous) over time when shaken, agitated, or otherwise stressed, but become thicker (more viscous) when at left rest. Field-oriented measurement techniques were developed to correlate the structural build-up of flowable concrete with time of rest; this included the inclined plane and portable vane methods [4]. The prediction models also take into consideration the casting rate, formwork width, concrete temperature, and waiting period between successive lifts.

Different Specifications, Standards, and even the researchers were fretful by developing prediction models for the evaluation of SCC formwork pressure. Vanhove et al. [5], Roussel and Ovarlez [6], and Graubner and Proske [7] have developed prediction models based on theoretical approaches. Khayat and Assaad [8] proposed prediction models based on experimental investigations. The developed guidelines took into account concrete properties, formwork dimensions, and casting rate. The capability of these models to reflect the actual formwork pressure through comparing the predicted results to the real field observations was not extremely investigated.

The objective of the study presented here is to validate the form pressure prediction models using two sets of field casting of SCC. In total, eight wall elements and eight column elements were cast using concrete mixtures of different thixotropic levels and placement rates for the field validation.

Experimental Approach

Testing program and mixtures for wall elements

A summary of the testing program undertaken for field validation of wall elements is given in Table I. These walls were cast at the Université de Sherbrooke during the construction of a new research facility dedicated to material and structural engineering. In total, eight wall elements of two different heights were cast. Walls # 1 through # 4 were cast in level # 1 of the laboratory and measured 3.7 m in height. Walls # 5 through # 8 were cast in level # 2 and measured 4.4 m in height, as shown in Figure 1. The structural walls are of 0.20 m in width and 5.6 m in length and are reinforced in both directions. The concrete was cast by pumping from top at a rate of rise (R) that was varied between 5 and 15 m/h.

Variations of lateral pressure were monitored using six pressure sensors that were mounted at 0.5 m intervals along each wall element. The sensors were set flush with the inner surface of the cast concrete using steel plates fixed to the formwork. Two thermocouples were attached at the center of each wall at 1 m from the top to

monitor temperature variations. Data from the pressure sensors and thermocouples were collected using acquisition system at 90-s intervals for 24 h following casting.

Table I. Experimental program for eight wall elements.

	Effect of casting rate (H = 3.7 m)				Effect of thixotropy (H = 4.4 m)			
Wall	#1	#2	#3	#4	#5	#6	#7	#8
Concrete	CVC	SCC1	SCC1	SCC1	CVC	SCC1	SCC2	SCC3
Slump flow/ slump*, mm	120* ± 30	650 ± 25			120* ± 30	650 ± 25		
HRWRA type	--	PCE1			--	PCE1		PNS
Paste vol., l/m^3	--	330			--	330	370	330
Casting rate, m/h	7.5	5	10	15	7.5	10		
w/cm	0.40	0.35			0.40	0.37	0.35	0.42+VMA1
Air content ≤ 3.5%, T = 22 - 30°C, Casting were pumped from top								

Three SCC mixtures (SCC1, SCC2, and SCC3) covering a wide range of mix designs and one CVC were used in casting the wall elements. The target slump flow (ϕ) and slump values for the SCC and CVC mixtures were 650 ± 25 mm and 120 ± 30 mm, respectively. Ternary cement (CSA Type GU-bF/S) were used for the SCC mixtures, and a binary cement (CSA Type GU-bS) was used for the CVC. SCC1 and SCC3 were proportioned with a paste volume (V_p) of 330 and SCC2 had V_p of 370 l/m^3. The *w/cm* was 0.35, 0.37, and 0.42 for SCC1, SCC2, and SCC3, respectively. Crushed limestone aggregate with maximum size of aggregate (MSA) of 10, 14, and 20 mm and siliceous river-bed sand were used. Polycarboxylate ether (PCE1)-based high range water reducing agent (HRWRA) and polynaphthalene sulphonate (PNS)-based HRWRA were employed. A liquid-based viscosity-modifying admixture (VMA1) was used in SCC3 to enhance stability. Set retarder and water-reducing agents were also incorporated.

A portable pressure column device, UofS2 pressure column [2], was employed to evaluate maximum lateral pressure for simulating casting depths similar to those employed in the field. Variations of lateral pressure until pressure cancellation were determined using the sacrificial 1.2-m high PVC column [9]. Material properties were measured before each wall casting at the Material Laboratory of Université de Sherbrooke, including slump flow (ASTM C 1611), temperature (ASTM C 1064), unit weight (ASTM C 138), and air content (ASTM C 231). The portable vane (PV) test [2, 3] was employed to determine the structural build-up at rest of concrete, which was required for the prediction model of form pressure.

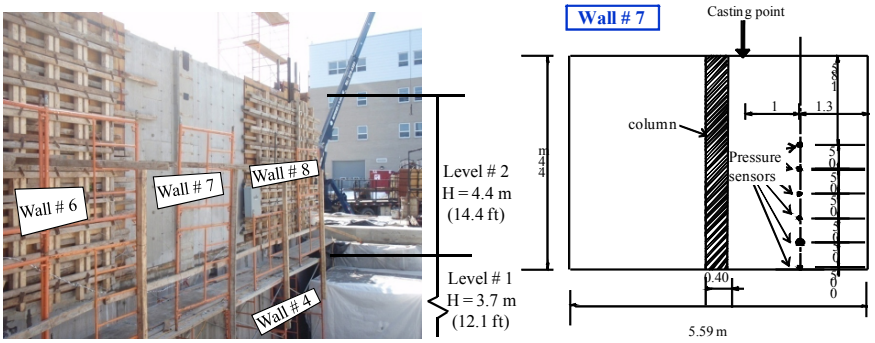

Figure 1. Photo of wall elements and positioning of pressure sensors.

Testing program and mixtures for column elements

Summary of the testing program carried out on column elements cast at the CTLGroup facility in Skokie, Illinois, is given in Table II. In total, eight circular steel columns measuring 3.66 m in height and 0.61 m in diameter were used. Each column was instrumented with two pressure sensors fixed at depths of 2.74 and 3.35 m, as illustrated in Figure 2. The concrete was placed at casting rates varied between 2 and 22 m/h. A waiting period (WP) of 20 min was introduced at mid casting of column # 8 with SCC5. The UofS2 pressure device was employed to estimate maximum pressure. Fresh properties and structural build-up at rest, similar to those of the wall elements, were measured before casting each column.

Table II. Test matrix for column elements.

Mixture		SCC4	SCC5	SCC6
Slump flow, mm		660 ± 20	610 ± 20	610 ± 20
Relative thixotropy		Low	Medium	High
Casting rate, m/h	2	--	--	Col.#5
	5	--	Col.#7	Col.#3
	5 + WP of 20 min	--	Col.#8	--
	10	--	--	Col.#4
	13	Col.#1	--	--
	15	--	--	Col.#6
	22	Col.#2	--	--

Three SCC mixtures (SCC4 through SCC6) of various degrees of thixotropy were used for casting the columns. ASTM Type I cement and class C fly ash were used for SCC4 and SCC5, and ASTM Type II cement was employed for SCC6. The concrete was prepared with crushed aggregate of 14 mm MSA. Polycarboxylate

ether (PCE2)-based HRWRA, VMA2, and air-entraining agent (AEA) were used. SCC4 and SCC5 are similar in composition, except for a lower dose of PCE2 and a slightly higher dosage of VMA2 in the latter mixture. SCC5 was proportioned with 0.34 *w/cm*, a V_p of 320 l/m^3, and AEA. SCC6 had a lower *w/cm* of 0.31, a V_p of 290 l/m^3, and higher dosage of HRWRA without any AEA.

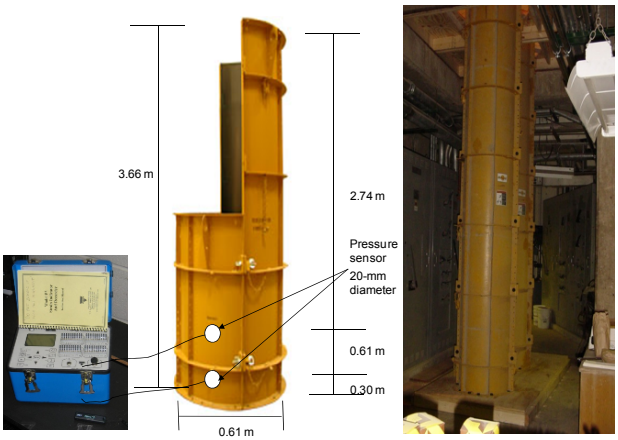

Figure 2. Configuration of column elements.

Table III. Fresh properties of mixtures used in casting wall and column elements.

Wall #	1	2	3	4	5	6	7	8
Mixture	CVC	SCC1	SCC1	SCC1	CVC	SCC1	SCC2	SCC3
Slump flow/slump*, mm	130*	620	670	630	90*	630	655	665
Air content, %	1.8	2	1.5	1.4	1.5	2.7	1.7	1.6
Unit weight, kg/m^3	2389	2388	2401	2381	2386	2406	2385	2391
Concrete temperature, ^{o}C	13.3	22	25.3	21.8	13.6	23.5	15	25.7
$PV\tau_{0rest@15min}$, Pa	1815	425	220	325	1905	410	245	505
$PV\tau_{0rest}(t)$, Pa/min	21.5	8.3	6.8	5.9	11.4	6.2	4.2	15
Column #	1	2	3	4	5	6	7	8
Mixture	SCC4		SCC6		SCC6		SCC5	
Slump flow, mm	640		600		600		620	
Air volume, %	5.5		3		3.6		4.7	
Unit weight, kg/m^3	2330		2386		2358		2323	
Concrete temperature, ºC	22.2		12.8		8.1		16.7	
$PV\tau_{0rest@15min}$, Pa	345		1080		1220		710	
$PV\tau_{0rest}(t)$, Pa/min	3.5		23.1		65.2		18.6	

Fresh concrete properties, including structural build-up characteristics of the concrete used for the wall and column elements are summarized in Table III. The structural build-up characteristics were determined using the PV test and included the static yield stress at 15 min time of rest, $PV\tau_{0rest@15min}$, and the rate of gain in static yield stress between 15 and 60 min, $PV\tau_{0rest}(t)$.

Test Results and Discussion

Lateral pressure variations with time at different concrete depths (H) for wall # 6 are shown in Figure 3. The variations of concrete temperature with time are also indicated. Wall # 6 was cast using SCC1 at R of 10 m/h. These pressure variations were compared to the pressure decay obtained from the 1.2-m high PVC column cast in laboratory at the same rate. The maximum lateral pressure (P_{max}) is shown to increase with the increase in depth. Values for P_{max} of 36, 51, and 58 kPa were obtained at depths of 1.8, 3.3, and 3.9 m, respectively, for wall # 6. Pressure cancellation took place at the same time as concrete temperature started to increase considerably, corresponding to setting. The profile of the lateral pressure decay determined using the 1.2-m high PVC column was similar to those of field measurements.

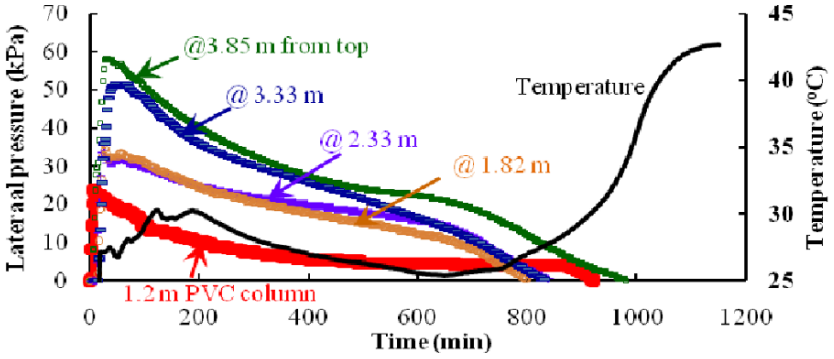

Figure 3. Variations in lateral pressure and concrete temperature with time, wall # 6.

Lateral pressure variations with time of SCC6 designed with high thixotropy employed for Col. # 5 and 6 are plotted in Figure 4. The variations in lateral pressure measured from the column elements are compared to those determined using a 0.9-m high PVC column measuring 0.25 m in diameter. Pressure variations for casting Col. # 5 at a low rate of rise of 1.9 m/h are significantly lower than those determined at R of 13.7 m/h in the case of Col. # 6. P_{max} values of 46 and 75 kPa were determined from the pressure sensors located at a depth of 3.35 m for the

concrete cast at R of 1.9 and 13.7 m/h, respectively. For SCC6 cast, P_{max} values of 39 and 46 kPa were obtained at depths of 2.74 and 3.35 m, respectively.

It is interesting to note that no cancellation time was obtained for the columns. This can be due to thermal expansion of concrete. Lateral pressure cancellation can be obtained when the deformation due to thermal expansion is taken into consideration [10]. The 0.9-m high PVC column resulted in pressure decay similar to that obtained from the full-scale column elements at early stages; however, the lateral pressure of the PVC column had pressure cancellation after 13 h.

Variations of P_{max} with height of SCC1 cast at 5, 10, and 15 m/h (walls # 2, 3, and 4, respectively) are shown in Figure 5 (left). These variations are similar to those obtained using the UofS2 pressure column, presented in Figure 5 (right). The lateral pressure envelops in the two cases were close to hydrostatic values given the shallow casting depth of 3.7 m and low thixotropy of SCC1. As expected, the increase in casting rate led to an increase in P_{max}. However, this increase was not significant since the thixotropy of SCC1 was variable for different concrete deliveries. Indeed, the $PV\tau_{0rest@15min}$ values for SCC1 cast at 5, 10, and 15 m/h received on different days were 425, 220, and 325 Pa, respectively, although the slump flow was within the range of specified values.

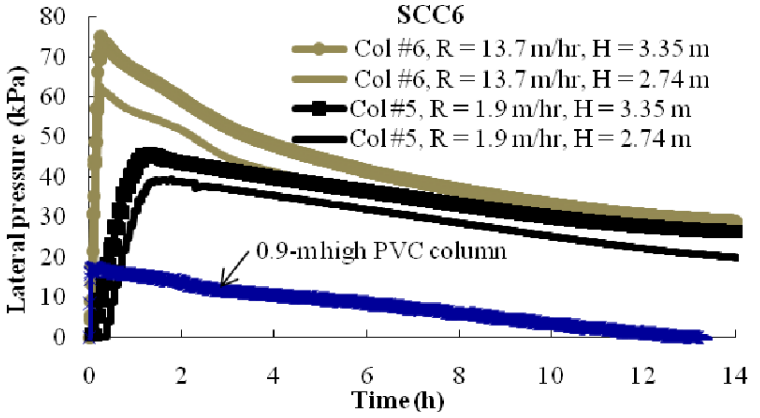

Figure 4. Variations of lateral pressure with time for col. # 5 and 6.

The lateral pressure envelop of Col. # 7 cast continuously at 5 m/h is compared in Figure 6 to Col. # 8 cast at the same rate, except with a waiting period (WP) of 20 min at the mid height. Both columns were cast using SCC5, which has relatively medium thixotropy. As illustrated in Figure 6, the interruption of casting by 20 min resulted in a reduction in P_{max}.

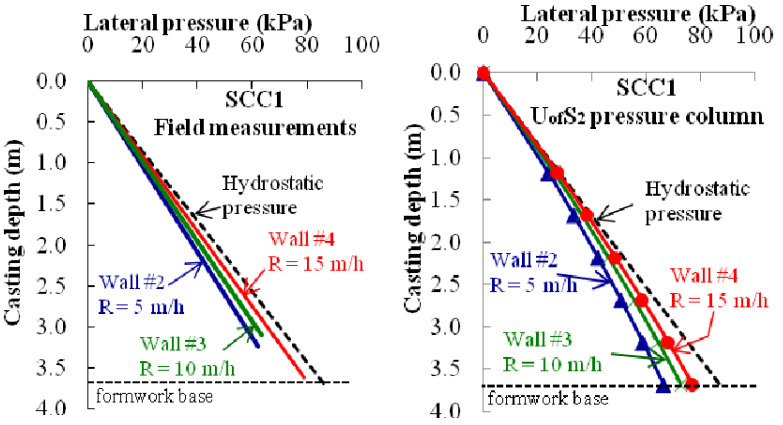

Figure 5. Effect of casting rate on lateral pressure envelops from field observations (left) and using the UofS2 pressure column (right) (SCC1, walls # 2, 3, and 4).

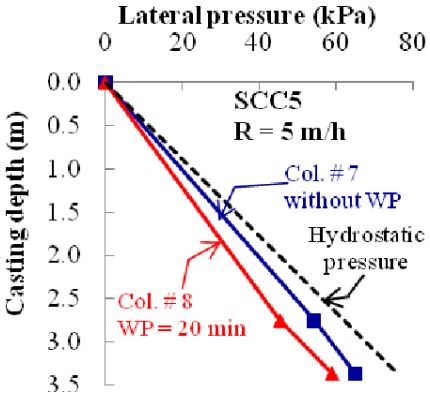

Figure 6. Effect of waiting period on lateral pressure envelop.

Validation of prediction models

P_{max} values monitored using pressure sensors mounted at different depths of six wall elements (walls # 2 to 4 and 6 to 8) and eight column elements (Col. # 1 to 8) cast with SCC are compared in Figure 7 to values obtained from an established prediction model , UofS model, using the PV test [3, 4] (Eqn. (1)). The upper and lower limits corresponding to 90% confidence level are indicated in Figure 7. These limits were calculated as reported in [11]. Excellent correlation between the measured and predicted P_{max} values was obtained indicating the validity of the UofS prediction model of Eqn. (1).

$$P_{max} = \rho.g.H\,[98 - 3.82\,H + 0.63\,R + 0.011\,D_{min} - 0.021\,PV\tau_{0rest@15min@Ti}]\,f_{MSA}\,.\,f_{WP} \quad (1)$$

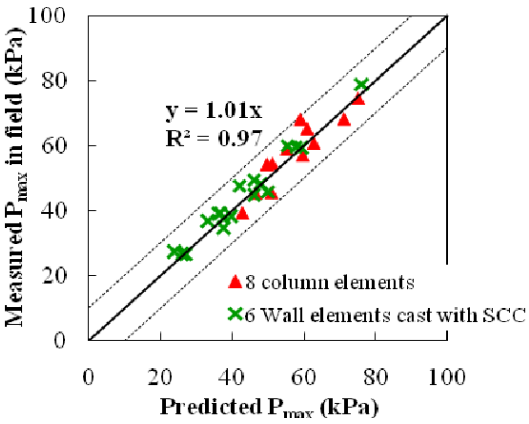

Figure 7. Measured-to-predicted lateral pressure using wall and column elements.

UofS Model vs. Roussel and Ovarlez Model

Roussel and Ovarlez [6] proposed the two models shown in Eqns. (2) and (3) for the prediction of lateral pressure of SCC on formwork of rectangular and circular cross section, respectively.

Rectangular formwork $$\sigma_{xx} = \sigma_{yy} = KH\left(\rho g - \frac{HA_{thix}}{eR}\right) \quad (2)$$

Circular column $$\sigma_{xx} = \sigma_{yy} = KH\left(\rho g - \frac{HA_{thix}}{rR}\right). \quad (3)$$

where: R = casting rate (m/h)
A_{thix} = flocculation coef. (Pa/s)
H = concrete height (m)
K = coefficient related to Poisson's ratio (v_p) = $v_p/(1-v_p)$
ρ = unit weight of SCC (kg/m^3)
e = formwork width (for circular column, e = r: radius) (m)

Corresponding to the field measurements, the P_{max} values obtained from the UofS model (Eqn. (1)) are compared to those obtained using the models of Roussel and Ovarlez (Eqns. (2) and (3)) in Figure 8. Six wall elements cast with SCC (wall # 2-4 and # 6-8) and seven column elements (Col. #1-7). Col. # 8 with a waiting period was eliminated from the comparison. The results indicate that the Roussel and

Ovarlez models give slightly higher estimation of the field measurements (7%) compared to the UofS model.

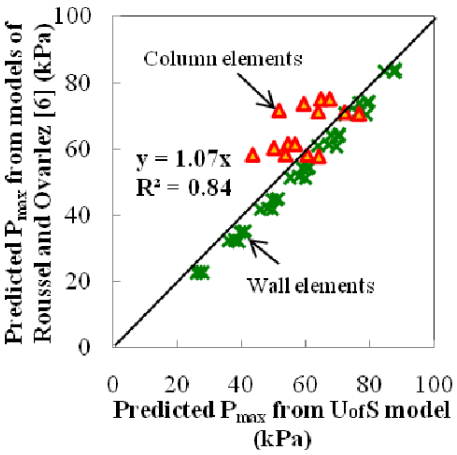

Figure 8. Comparison between predicted formwork pressure obtained using the UofS model vs. the models of Roussel and Ovarlez [6].

Conclusions

Based on the results of the field validations presented here, the following results can be drawn:

- The prediction models for lateral pressure are successfully validated using full-scale wall and column elements. The relationship between the measured and predicted maximum lateral pressure values resulted in high R^2 of 0.97.
- The portable vane test is successfully used to determine the structural build-up at rest of SCC used for lateral pressure prediction. Information from this test can then be useful to differentiate between mixtures of various compositions and help in material selection and mix design of thixotropic concrete.
- The UofS2 pressure device resulted in similar lateral pressure envelopes as those of wall and column elements. The pressure device reflected well the effect of casting rate of the SCC.
- Pressure decay obtained from the small scale PVC column was similar to that obtained from wall and column castings. The sacrificial PVC column can then be used to assess the effect of mixture composition and concrete temperature on the variations in lateral pressure with time.
- The prediction models of Roussel and Ovarlez [6] give slightly higher estimation of the field measurements (7%) compared to the UofS model.

Acknowledgements

The authors would like to acknowledge the National Ready-Mix Concrete Research & Education Foundation, the Strategic Development Council (SDC) of the American Concrete Institute, and SDC members for sponsoring this project. Special thanks go to David Lange from University of Illinois at Urbana-Champaign for his donation of the column formwork to CTLGroup to be used in this study. The authors would also like to thank Meyer Material Company for their significant efforts supplying the ready-mix concrete to CTLGroup for this project.

References

[1] Khayat, K.H. and Omran, A.F. (2007), State-of-the-art review of form pressure Exerted by self-consolidating concrete, National Ready-Mix Concrete Research & Education Foundation and the Strategic Development Council of the American Concrete Institute (ACI), 200 pp. http://www.rmc-foundation.org.

[2] Khayat, K.H., Omran, A.F., Neji, S., Billberg, P. and Yahia, A. (2008), Test methods to evaluate form pressure of SCC, Proceedings of the International Conference of ACBM on SCC (SCC 2008), Chicago, USA, 7 pp.

[3] Khayat, K.H. and Omran A.F. (2009), Evaluation of SCC formwork pressure, Second International Symposium on Design, Performance and use of Self-Consolidating Concrete, Beijing, China, pp. 43-55.

[4] Khayat, K.H. and Omran A.F. (2009), Evaluation of SCC formwork pressure, *Concrete Infocus Magazine*, Publication National Ready-Mixed Concrete Association – Self-Consolidating Concrete: Developing Guidelines to Lower Lateral Pressure, pp. 16-19.

[5] Vanhove, Y., Djelal, C. and Magnin, A. (2004), *Magazine of Concrete Research*, vol. 56, n. 1, pp. 55-62.

[6] Roussel, N. and Ovarlez, G. (2005), A physical model for the prediction of pressure profiles in a formwork, Proceedings of the 2nd North American conference on the Design and Use of Self-Consolidating Concrete (SCC 2005) and the 4th International RILEM Symposium on Self-Compacting Concrete, Eds. Shah, S. P., Chicago, pp. 647-654.

[7] Graubner, C.-A. and Proske, T. (2005), Formwork pressure: A new concept for the calculation, Proceedings of the 2nd North American conference on the Design and Use of Self-Consolidating Concrete (SCC 2005) and the 4th International RILEM Symposium on Self-Compacting Concrete, Eds. Shah, S. P., Chicago, pp. 605-613.

[8] Khayat, K. H. and Assaad, J. (2005), Use of rheological properties of SCC to predict formwork pressure, Proceedings of the 2nd North American Conference on the Design and Use of Self-Consolidating Concrete (SCC 2005), and the 4th International RILEM Symposium on Self-Compacting Concrete, Chicago, Eds. Shah, S. P., pp. 671-677.

[9] Assaad, J. and Khayat, K.H. (2006), *ACI Materials Journal*, vol. 103, n. 4, pp. 280-287.

[10] NRMCA-SDC Final Report, (2009), SCC formwork pressure, submitted to the National Ready-Mix Concrete Research & Education Foundation and the Strategic Development Council of the American Concrete Institute, 549 pp.

[11] Assaad, J. (2004), Formwork pressure of self-consolidating concrete – Influence of thixotropy, Ph.D. Thesis, Department of Civil Engineering, Université de Sherbrooke, 453 pp.

Modeling Fresh Concrete Pressure of Normal and Self-Compacting Concrete

Marc Beitzel

IBU, Institute of Building Process and Environmental Technology, Trier, Germany

Abstract. A material model for fresh concrete pressure, if designed on a physically sound basis, enables the calculation of the formwork pressure of different kinds of concrete, depending on their rheological properties. In this paper, the concept and results of experimental and rheological investigations on fresh concrete pressure are presented. Within this experimental program a special formwork model for the fresh concrete pressure was designed. A material model was developed, describing the behaviour of formwork pressure, depending on various aspects and materials. In order to verify and adjust this material model, a series of experiments on real formwork systems were performed.

Introduction

A reliable prediction of the horizontal formwork loading is essential for the safety and the economical efficiency of concrete sites. Having neglected the recent developments in concrete technology, the existent design standards are only valid for normal weight (NC) and lightweight concrete. Hence, they are not applicable, e.g. for self-compacting concrete (SCC) or fiber-reinforced concrete respectively. The actual standards are simply based on empirical models, without any satisfying theoretical background. This lack results in inaccurate formwork design for NC and a design on the safe side applying a hydrostatic approach for SCC. Due to the high impact of formwork costs on the total construction costs, an inadequate design of the formwork may lead to higher building costs.

Besides numerous influencing factors, the resulting concrete pressure is mainly affected by the unit weight and cohesiveness of the concrete, rate of casting and formwork stiffness. As a consequence of these effects the formwork pressure is dependent on the rheological concrete properties, the stationary and unstationary pressure characteristics, and the active and passive formwork reactions. Today, the effects of these dominating factors are not sufficiently considered in view of the

K.H. Khayat and D. Feys (eds.), *Design, Production and Placement of Self-Consolidating Concrete*, RILEM Bookseries 1,
DOI 10.1007/978-90-481-9664-7_21, © RILEM 2010

modeling of formwork pressure of different types of concretes, due to the lack of a physically sound model.

Applying the new designed formwork model in combination with the use of a rotational rheometer, a physically sound model was developed, describing the behaviour of fresh concrete pressure on vertical formwork [1]. Field tests on a real formwork system have been carried out, in order to verify and calibrate the material model, see [2].

Experimental Investigations and Results

Investigations

For the formwork model, ordinary wooden formwork panels similar to actual dimensions measuring 150 x 200 x 25 cm (height x width x thickness) were used. The main purpose of these experiments was to investigate whether the formwork pressure of NC and SCC respectively is dependent on the rheological properties, the stationary and unstationary pressure characteristics, and the active and passive formwork reactions. The casting rate was thus chosen as the main varying parameter.

Although the height of the formwork model was only 1.50 m, the simulated filling height was up to 6.50 m. The formwork model included the following components: hydraulic pump and cylinder unit, steel frame and formwork. To simulate the different filling heights, the steel frame was developed on which the single-acting cylinder-pump set was attached on top, see Figure 1, left. The principle of the load application was as follows: depending on the mixture's density, the corresponding loads were calculated and applied by using the single-acting cylinder-pump set.

In order to register the horizontal formwork pressure values of the casting, pressure capsules, three on equal heights, were installed along the height of the formwork system, see Figure 1, right. Strain gauges were installed in order to register any formwork deflections due to the resulting formwork pressure. These were located on the second formwork panel, situated exactly opposite the pressure capsules.

After emptying the mixer, the concrete was directly filled into the formwork. To cover a broad range of casting rates different values were chosen. The concrete was simultaneously filled into the measuring container of the rheometer. The rheological measuring process began at the same time as the start of the filling process.

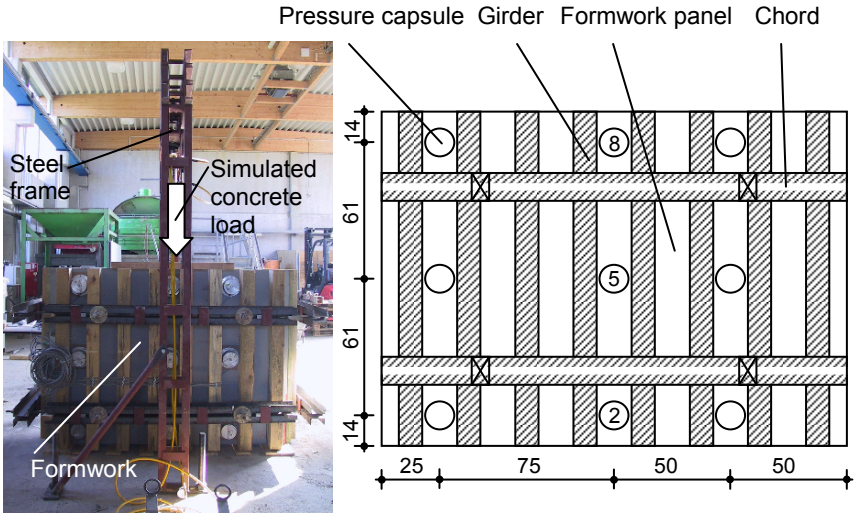

Figure 1. Set up of the tests on formwork model castings (left) and design of the formwork model (right); all dimensions in [cm].

A rotational rheometer was used in order to investigate the rheological properties of a casting. The time dependent yield stress characteristics were linear, which confirmed the results presented in [3] and [4] respectively, as well as with a measuring time < 3 h in [5]. With the thixotropy coefficient C_{thix} generally ranging between 0.1 Pa/s and 0.5 Pa/s the concretes could be classified as thixotropic according to [6]. Correspondingly, C_{thix} approximated the values measured in [4] and [7] (0.1-0.2 Pa/s), as well as in [8] (0.6 Pa/s). With regards to NC the compaction process was thereby taken into account, leading to higher values. For all castings of every concrete type the mixture was identical producing a compressive strength of concrete corresponding to grade C 30/37 according DIN EN 206 [9].

The field tests for the fresh concrete pressure for self-compacting concrete were carried out on a panel wall formwork system with its geometry resulting in the casting dimensions measuring 300 x 125 x 30 cm (height x width x thickness), see Figure 2.

A detailed description of the experimental investigations, i.e. the experimental program, formwork model, concrete composition as well as the fresh and hardened concrete properties, is given in [2].

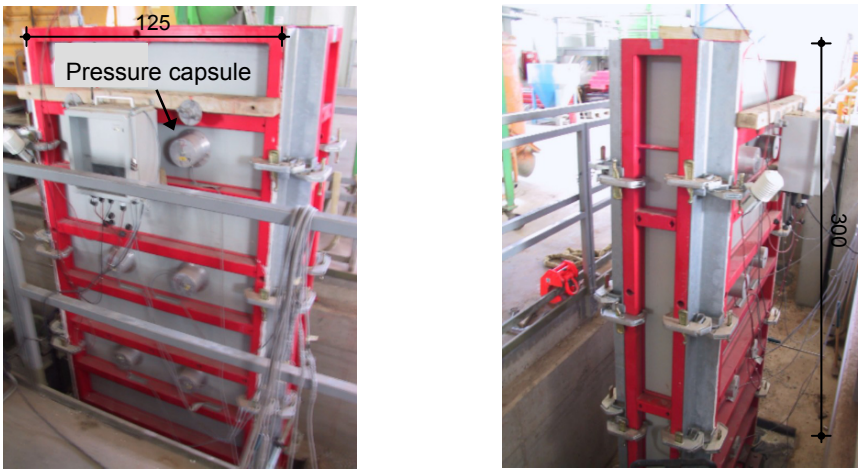

Figure 2. Panel wall formwork system for the field tests – front view (left) and side view (right); all dimensions in [cm].

Results and discussion

The experiments measuring the influence of casting rates were carried out in a constant environment using NC and SCC. The applied casting rates were 3.5 m/h and 14 m/h for NC, as well as 3.5 m/h, 7 m/h, 14 m/h, 28 m/h and 56 m/h for SCC.

Figures 3 and 4 exemplary depict the standard relationship between the casting rate and formwork pressure of NC and SCC at different casting heights measured by pressure capsule PC 5. Whereas the results of the concrete at a casting height of h = 1 m were actually tested using conventional casting processes, those pressure results measured at higher casting heights (see Figures 3 and 4, h = 3 m and 6 m) were simulated using the model described in [2]. Therefore, an analysis of the curve representing the results of the tested concretes shows that influence of the casting rate increases with the casting height.

Thus, Figures 3 and 4 demonstrate that there is a dependency between the formwork pressure and casting rate between v = 3.5 m/h and 14 m/h for NC and accordingly 3.5 m/h and 7 m/h for SCC: the corresponding increase in formwork pressure is almost not visible in Figures 3 and 4 at a height h = 1 m but is evident, for example, at h = 6 m, when the differences of 41.58 kPa for NC (Figure 3) and 28.72 kPa for SCC (Figure 4) are measured. Comparatively, the pressure increases are greater at the higher casting heights than at the lower casting heights. Furthermore, the results of the experiments carried out with SCC show that casting rates greater than 7 m/h do not have that significant effect on the formwork

pressure. Between casting rates from 7 m/h to 14 m/h the casting rate shows a modest influence on the formwork pressure, see Figure 4.

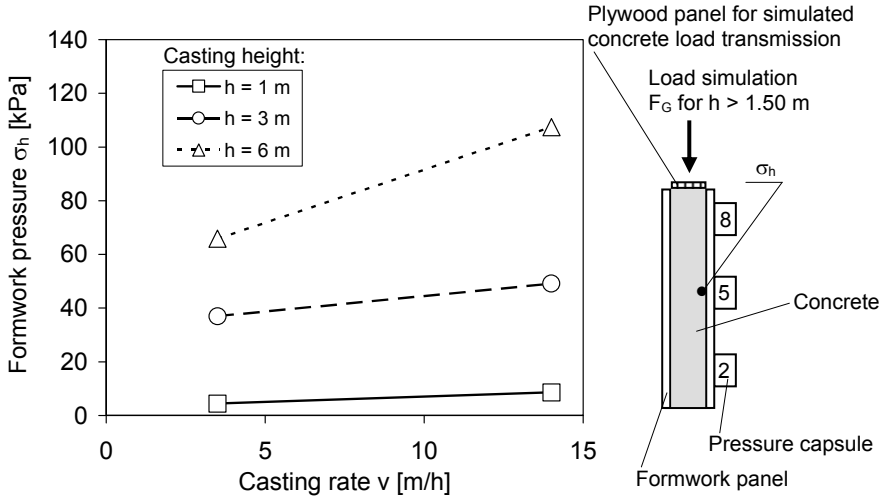

Figure 3. Influence of the casting rate on the formwork pressure of NC at different casting heights.

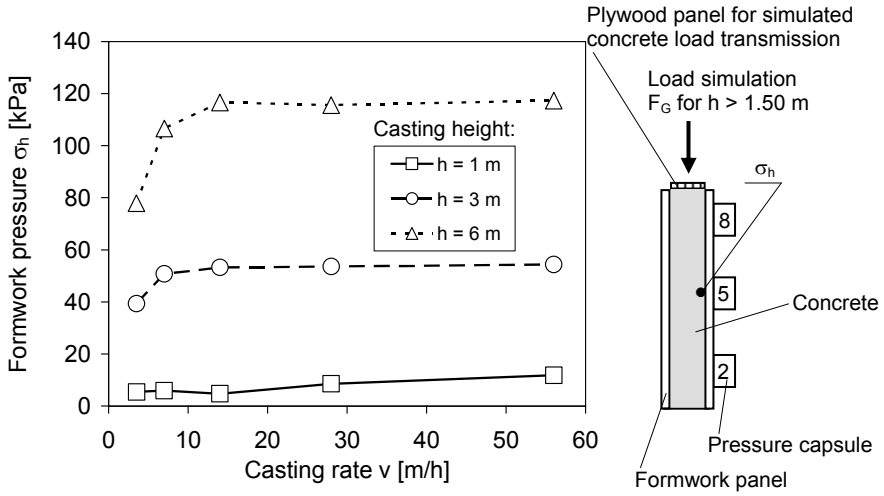

Figure 4. Influence of the casting rate on the formwork pressure of SCC at different casting heights.

Due to the formwork dimensions, the concrete could not be poured in continuously at the casting rate of 3.5 m/h. However, at a casting rate of v = 7 m/h the casting

process did not have to be interrupted, which was one of the reasons the results in Figures 3 and 4 show the depicted relationship between formwork pressure and casting rate. A detailed presentation and discussion of the experimental results can be found in [2].

Figure 5 shows the mean peak formwork pressure values of SCC over the casting height for the field tests. Amongst others, the casting rates were 15 m/h and 30 m/h respectively.

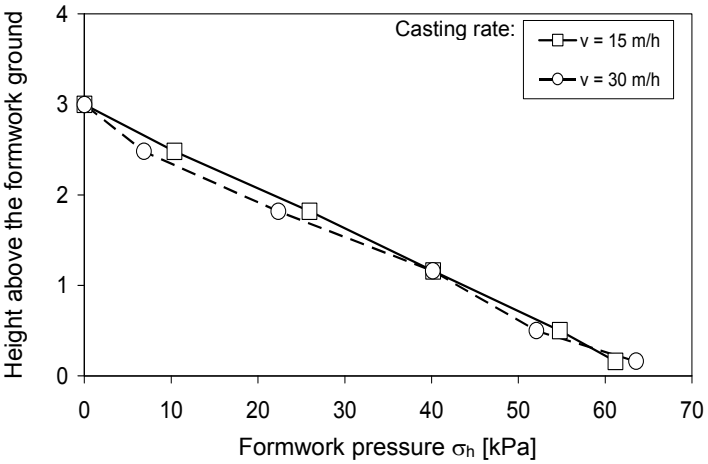

Figure 5. Mean formwork pressure values of SCC over the formwork height at different casting rates.

The peak values σ_h for the SCC's formwork pressure at a formwork height of 16 cm were 61.19 kPa (v = 15 m/h) and 63.55 kPa (v = 30 m/h) respectively. These results confirm the results of the formwork model experiments and show that for casting rates > 14 m/h the casting rate has minor influence on the formwork pressure.

Physical Model

The physical development of the model had to take into account both the rheological and mechanical effects of the concrete's formwork pressure. Therefore, specific parameters for the physical model were selected. In addition to considering the time dependency of the yield stress, see [3] and [4] respectively, the casting impulse and formwork deflection parameters were of significant

importance, see [1]. Due to the relatively small shear zone of SCC at the higher casting area, when compared to the formwork height, see [4], it does not need to be considered in the material model.

The elaboration of the physical material model for the calculation of the horizontal formwork pressure of NC and SCC respectively is presented in [2].

Mechanical casting influences

According to the impulse equation found in NEWTON's second law, see [10], the impulse load of the concrete increases the vertical load as it is filled into the formwork during the casting process. This impulse load is in addition to the unit weight of the material, which is still to be poured in. In this context the upper concrete layer, for instance, behaves like a deflection plate, see [2], on which the poured concrete impinges on.

Thus, using the casting impulse load σ_{imp} measured from the casting process, the concrete's density ρ and the casting rate v the following equation can be derived:

$$\sigma_{imp} = \rho \cdot v^2 \tag{1}$$

The casting impulse load presented here (see Eqn. (1)) must be considered explicitly in terms of the pouring of the concrete and is constant throughout the casting process (if the casting rate does not change).

Mechanical equilibrium

In order to calculate the derivation of the physical material model the balance of forces is attached to the JANSSEN equation [2]. However, as already seen in [4], the formwork friction variable τ_w has been replaced by the yield stress variable τ_0 in the material model. Further, the analysis will be of a casting condition where the majority of the concrete, with the exception of the upper shear zone, is in a static state (see [4]).

In order to determine the formwork's vertical load conditions from the balance of forces depicted in Figure 6, one needs, as already established in [3] and [4], the time dependent development of the yield stress (not taking into account the initial yield stress $\tau_{0,i}$), $\tau_0(t) = C_{thix} \cdot t$ (with the thixotropy coefficient C_{thix} and the casting time t), and the formulation of the casting height increase corresponding to $dh = v \cdot dt$. The initial yield stress $\tau_{0,I}$ can be neglected compared to the yield stress increase over the time [4] and due to the compaction process for NC. Accordingly, the formwork's vertical load conditions during the casting process are determined by the above and in Figure 6 defined variables. By using Eqn. (2)

$$\sigma_v = \gamma \cdot h + \sigma_{imp} \cdot \frac{d_A}{d} - \frac{C_{thix} \cdot h^2}{v \cdot d} \quad (2)$$

these vertical formwork loads σ_v can be calculated.

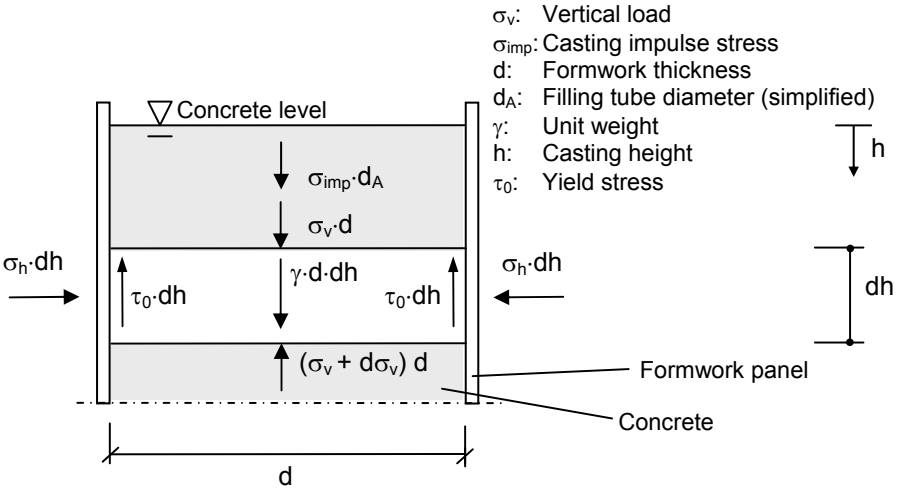

Figure 6. The equilibrium of forces in the formwork during the filling process of the concrete.

Stress ratio and horizontal formwork pressure

As a result of the continuum mechanics the stress ratio, $\lambda = \sigma_h/\sigma_v$, can be derived from the MOHR model (see [11]) [2], see Figure 7. Figure 7 shows MOHR's circle for stress for the principal stresses $\sigma_1 = \sigma_v$ and $\sigma_2 = \sigma_h$ as well as the maximum shear stress $\tau_{max} = \tau_0$ in an absolute state of compressive stress.

Therefore, the horizontal formwork pressure σ_h can be calculated by the following equation:

$$\sigma_h = \sigma_v - 2 \cdot C_{thix} \cdot \frac{h}{v} \quad (3)$$

As already stated above, the initial yield stress $\tau_{0,i}$ was not taken into account. Hence, the stress ratio is derived from the principal stresses of the material as well as the yield stress, defined as the maximum shear stress.

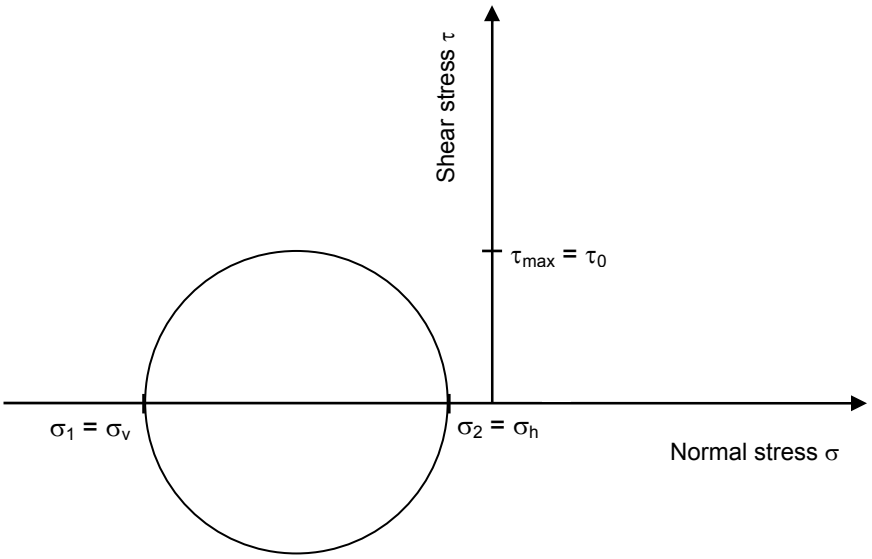

Figure 7. Mohr's circle for stress for determination of the maximum shear stress τ_{max} from the principal stresses σ_1 and σ_2; on the basis of [11].

Furthermore, as the material model concentrates on the physical properties, the reinforcement's influence on the formwork pressure (see [12]) had been neglected. Taking into account the casting impulse load and under consideration of the filling pipe diameter d_A, the horizontal formwork pressure $\overline{\sigma}_h$ can be calculated as follows:

$$\overline{\sigma}_h = \gamma \cdot h_E - \frac{K_{thix} \cdot h_E^2}{v \cdot d} - 2 \cdot K_{thix} \cdot \frac{h_E}{v} + \rho \cdot v^2 \cdot \frac{d_A}{d} \quad (4)$$

As the casting impulse load in Eqn. (4) was only calculated mathematically, further investigations are necessary on its effective influence on the formwork pressure.

A comparison with the experimental results showed a considerably good correlation with the formwork pressures calculated with Eqn. (3), see [2]. For a casting height h = 6 m and varying casting rates, Figure 8 exemplary depicts the comparison between the SCC's experimentally measured formwork pressures and the ones calculated with Eqn. (3).

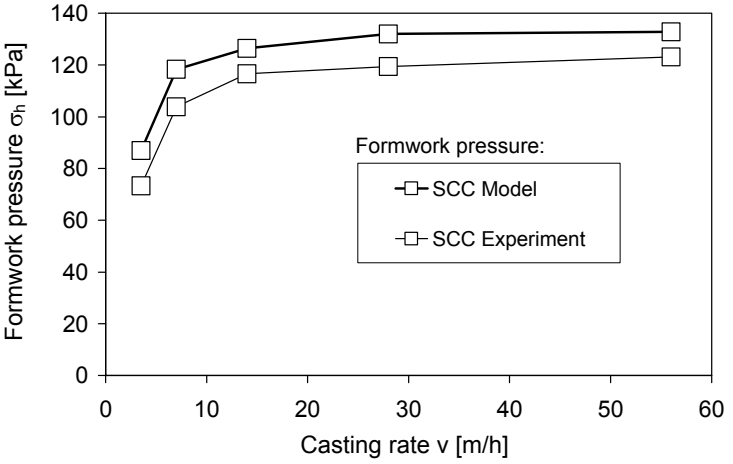

Figure 8. Comparison between calculated and experimentally measured formwork pressures with varying casting rates for SCC (h = 6 m).

Structural formwork characteristics

In order to determine the relationship between the formwork deflection and the formwork pressure, the formwork bedding modulus will now be established. The equilibrium conditions needed for this can be found in the following equation:

$$k = \frac{\sigma_h}{f} \tag{5}$$

$$k = \frac{\bar{\sigma}_h}{f} \tag{6}$$

where k = formwork bedding modulus
f = formwork deflection

Both, Eqn. (5) and (6) build on a parameter called the bedding modulus, which originates from soil mechanics (see [13]). Accordingly, the formwork can be compared to a spring system.

Conclusions

Investigations of both NC and SCC on a newly designed formwork model show that present knowledge is not sufficient for the modeling of its formwork pressure. By determining the rheological properties of the concretes with a rotational rheometer, it can be shown that there is not only a clear relation between the fresh concrete pressure and the casting rate but also with the unit weight, filling height, formwork deflection and rheological properties. These influencing factors will mainly affect a material model to describe the formwork pressure.

Finally, the corresponding physical model for the calculation of the formwork pressure of both NC and SCC has been proposed, which not only takes into account the concrete's rheological properties but also the casting process and the formwork deflection. More detailed information can be found in [2].

References

[1] Beitzel, M. (2006), New knowledge of fresh concrete's formwork pressure behaviour, Abridged Report, Institute for Concrete Structures and Building Materials, Karlsruhe Institute of Technology (in German).

[2] Beitzel, M. (2009), Formwork pressure behaviour of fresh concrete under consideration of the rheological properties, PhD Thesis, Institute for Concrete Structures and Building Materials, Karlsruhe Institute of Technology (in German).

[3] Billberg, P. (2006), Form pressure generated by self-compacting concrete – Influence of thixotropy and structural behaviour at rest, Doctoral Thesis in Concrete Structures, School of Architecture and the Built Environment, Division of Concrete Structures, Royal Institute of Technology, Stockholm.

[4] Ovarlez, G. and Roussel, N. (2006), A physical model for the prediction of lateral stress exerted by self-compacting concrete on formwork, *Materials and Structures*, vol. 39, n. 2.

[5] Amziane, S. and Ferraris, C.F. (2007), Cementitious paste setting using rheological and pressure measurements, *ACI Materials Journal*, vol. 104, n. 2.

[6] Roussel, N. (2006), A thixotropy model for fresh fluid concretes: Theory, validation and applications, *Cement and Concrete Research*, vol. 36, n. 10.

[7] Khayat, K.H. et al. (2005), Effect of section width and casting rate on variations of formwork pressure of self-compacting concrete, *Materials and Structures*, vol. 38, n. 1.

[8] Billberg, P. (2003), Form pressure generated by self-compacting concrete. Proceedings of the 3rd International RILEM Symposium on Self-Compacting Concrete, RILEM pro 33, RILEM Publications, Bagneux.

[9] Deutsches Institut für Normung (2001). DIN-Technical Report 100 – Concrete, Beuth, Berlin (in German).

[10] Jirka, G.H. (2008), Introduction to Hydromechanics, Karlsruhe Institute of Technology, KIT Scientific Publishing, Karlsruhe (in German).
[11] Gross, D., Hauger, W. and Schnell, W. (1992), Technical Mechanics 2 – Elastostatics, Springer, Berlin (in German).
[12] Tchamba, J.C. et al. (2008), Lateral stress exerted by fresh fluid concrete on formwork: laboratory experiments, *Cement and Concrete Research*, vol. 28, n. 11.
[13] Springmann, S. (2006), Geotechnics III – Part 2, V Surface Foundations, Institute for Geotechnics, Swiss Federal Institute of Technology, Zürich.

Formwork Pressure of Highly Workable Concrete – Experiments Focused on Setting, Vibration and Design Approach

Tilo Proske and Carl-Alexander Graubner

Technische Universität Darmstadt, Institut für Massivbau, Germany

Abstract. The presented investigations were conducted at the Institut für Massivbau and contributed to a joint research project including several German research institutes [1]. A number of experimental tests on highly workable concretes were carried out. Small scale material analyses as well as measurements of the formwork pressure on large specimens were carried out. Based on the test results an analytical model for the calculation of the concrete pressure on vertical formwork was developed. The analytical model takes into account the time dependent material parameters of the fresh concrete, the specific properties of highly workable vibrated concretes and self-compacting concretes (SCC) as well as operation aspects. A proposal for the design of formwork, based on the experimental tests and the semi-probabilistic safety concept was developed. It was found that even for highly workable concretes, the design load is often lower than the hydrostatic concrete pressure.

Material Analyses

Introduction

In small-scale material tests, the friction behaviour of fresh concrete in early age was analysed and the influence on the concrete pressure verified. The difference between inner friction resistance and contact friction was distinguished. The inner friction is the shear resistance of the (concrete) material, applying a shear strain, and is generated by the friction between the solid particles. At rest, the inner friction resistance is further highly influenced by various chemical and physical bonds. All these effects contribute to the yield stress [2]. If the shear rate is larger than zero, fluids generate an inner friction resistance which in this case is called viscosity. The contact friction is the shear resistance in the contact zone between the fresh concrete and the limiting (formwork) surface.

K.H. Khayat and D. Feys (eds.), *Design, Production and Placement of Self-Consolidating Concrete*, RILEM Bookseries 1,
DOI 10.1007/978-90-481-9664-7_22, © RILEM 2010

Test device

The test device for the inner friction tests on highly workable concretes is described in detail by Proske [2]. On concrete samples with dimensions 250 x 250 x 250 mm, a casting process with increasing concrete level can be simulated by a stepwise increase of vertical pressure. The lateral concrete pressure was measured in the horizontal direction with two pressure sensors, opposite to each other. The vertical formwork panels can be displaced in horizontal direction. Applying stepwise a controlled slip, the influence of the formwork stiffness on the formwork pressure was analysed. Unintended vibrations during the casting (e. g. by the casting process itself, hammer or bucket impact) were simulated by impact with a pendulum (mass 1 kg, length 200 mm). The generated energy per impact was $E \approx 2.0$ J. The influence of concrete vibrators or vibration by construction operation was investigated using a vibrator that was fixed to the formwork, with a power of 700 W and a rotation speed of 2700 revolutions per minute.

The friction resistance between the concrete and the formwork surface was investigated using the same apparatus. In this case, a steel element with cross-sectional dimensions of 100 x 6 mm was additionally installed and inserted in the concrete. The friction resistance (i.e. the friction coefficient μ) was calculated based on the pull-out force, which was measured during and after an imposed translation of the element. In addition, the displacement resistance between fresh concrete and the reinforcement was measured, fixing two plain steel bars (diameter = 8 mm, length = 100 mm) at a distance of 25 mm from the friction element, perpendicular to the direction of displacement. The roughness parameters of the steel element surface were measured according to DIN EN ISO 4287:1998-10, with R_a = 1.3-3.8 µm, R_t = 8.3-18.6 µm and R_z = 11.3-29.8 µm.

Characteristics of the fresh concrete

The mix design of the used concretes with consistency class F5, F6 and self-compacting concretes (SCC) is shown in Table I. The concretes vary in flowability and viscosity. The influence of different parameters like the paste volume, cement type, water-powder ratio, volume of fly ash, the type of superplasticizer as well as the setting time (from 5 h to 13 h) could be investigated.

The initial slump flow (*sf*) of the SCC was set at 740 ± 20 mm. The initial V-funnel time t_v of the used concretes according should be 5 ± 1 s for the low-viscosity concretes (SCC-1, -3, -5) and 13 ± 2 s for the high-viscosity concretes (SCC-2 and -4). The initial spread (*a*) of the concrete with consistency class F5 according to DIN EN 12350-5 should amount to 600 ± 20 mm this corresponds to $sf \approx 600$ mm. The initial spread *a* of the concrete with consistency class F6 according to DIN EN 12350-5 should amount to 680 ± 20 mm this correspondents to $sf \approx 680$ mm (more details in [1]).

Table I. Mixture proportion of the used concretes.

		F5-1*	F6-1**	F6-2	F6-3	SCC-1	SCC-2*	SCC-3	SCC-4	SCC-5
CEM I 42,5 R	[kg/m³]	274	336		274		273	272	274	273
CEM II A/S-52.5 R	[kg/m³]			274		385				
Fly ash (DIN EN 450-1)	[kg/m³]	137	112	137	137	193	300	300	178	178
Water	[kg/m³]	165	178.0	163.0	163.0	187	165	198	164	199
Superplasticizer 1	[kg/m³]	1.5	1.5	2.7		3.4	3.5			
Superplasticizer 2	[kg/m³]				3.0			2.8	4.5	2.8
Stabiliser	[kg/m³]								0.2	0.2
River sand 0/2 mm	[kg/m³]	646	638	646	646	534	566	613	582	639
River gravel 2/8 mm	[kg/m³]	434	413	434	434	393	393	342	439	383
River gravel 8/16 mm	[kg/m³]	664	633	664	664	602	602	524	672	586
w/cement	[-]	0.61	0.53	0.60	0.60	0.49	0.61	0.73	0.61	0.74
w/powder	[-]	1.13	1.14	1.13	1.12	0.92	0.77	0.93	1.02	1.22
Paste	[l]	314	337	312	314	396	384	416	333	366
* also investigated with Superplasticizer 2; ** also investigated with Superplasticizer 2, 3, 4, 5										

Small-scale simulation tests

Using the described test apparatus, the development of the fresh concrete pressure was investigated in a number of test series. The casting process with constant casting rate was simulated by applying a vertical load with a hydraulic press on a sealed formwork element. The initial vertical pressure was applied 15 minutes after the end of mixing and was increased until the final setting of the concrete (t_E) according to DIN EN 480-2:2006-11 (Vicat-test) which is approximately the initial setting time according to ASTM C403/C403M-05. The mortar for the setting tests with a maximum aggregate diameter of 4 mm was sieved from the concrete charge. The influences on the formwork pressure of the mixture components and the rheological properties as well as the factors which are independent of the mixture design like formwork stiffness, casting rate v (1, 2, 4, 8 m/h) and intensity of vibration were analysed.

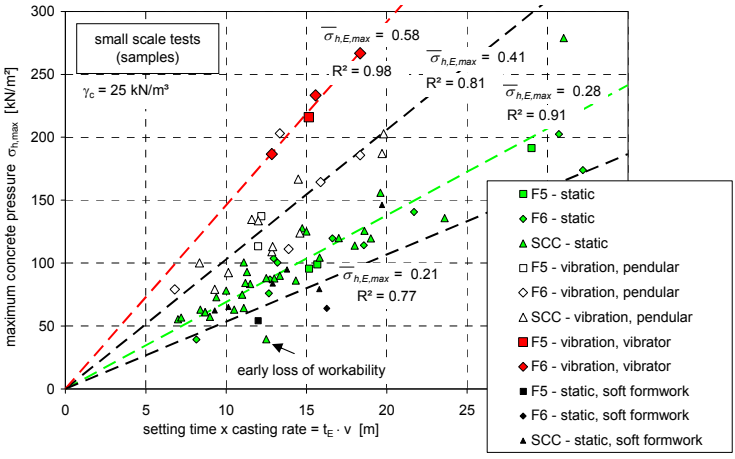

Figure 1. Results of the small-scale simulation test.

The maximum concrete pressure ($\sigma_{h,max}$) as well as the time-dependent inner friction angle (φ) can be determined based on the measured pressure and formwork deformation. The measured maximum concrete pressure ($\sigma_{h,max}$) of all test series in this research project [1] and in additional tests with SCC [2] plotted against the simulated casting rate v and the final setting time t_E is presented in Figure 1. The results are further plotted against the intensity of vibration and the formwork stiffness. For the same boundary condition the fresh concrete pressure varies linearly with the product of casting rate and final setting time $v \cdot t_E$.

The lines in Figure 1 characterise the mean of the pressure development. The slope of the lines represents the normalized concrete pressure ($\overline{\sigma}_{h,E,max}$) and is given in Eqn. (1). The specific concrete weight is $\gamma_c = \rho_c \cdot g$, with density ρ_c and gravity constant g. The value $\overline{\sigma}_{h,E,max} = 1.0$ represents the hydrostatic concrete pressure with the height $h_E = v \cdot t_E$, considering the hydrostatic concrete pressure approaching the position of the already hardened concrete.

$$\overline{\sigma}_{h,E,\max} = \frac{\sigma_{h,\max}}{v \cdot t_E \cdot \rho_c \cdot g} = \frac{\sigma_{h,\max}}{v \cdot t_E \cdot \gamma_c} \tag{1}$$

For highly workable concretes including SCC, the following approximation of the maximum concrete pressure $\sigma_{h,max}$ based on the final setting time t_E, the casting rate v and specific weight γ_c was found:

$$\sigma_{h,\max} = 0.28 \cdot v \cdot \gamma_c \cdot t_E \qquad R^2 = 0.91 \tag{2}$$

The difference of the concrete pressure between consistency F5, F6 and SCC is not significant. However, the self-compacting concretes with a high paste volume (> 390 liter) showed a slightly higher lateral pressure than the vibrated concretes. The concretes with high workability loss included significantly lower formwork pressure compared to the normal workability. However, having a relatively low workability loss, the influence of concrete mix design and respective the rheological properties was accounted sufficiently by the integral parameter final setting time t_E. Furthermore, a significant influence of dynamic exposure on the concrete pressure was observed. Ten impacts with the pendulum every 15 minutes increased the lateral pressure by approx. 50% compared to static conditions. For this situation, the mean of the maximum pressure is given in Eqn. (3).

$$\sigma_{h,\max} = 0.41 \cdot v \cdot t_E \cdot \gamma_c \qquad R^2 = 0.81 \tag{3}$$

In the case of dynamic exposure of the concrete by the vibrator fixed to the test apparatus (10 s every hour until the final setting state), the maximum pressure increased by approx. 100% compared to the reference test under static conditions (see Eqn. (4)).

$$\sigma_{h,\max} = 0.58 \cdot v \cdot t_E \cdot \gamma_c \qquad R^2 = 0.98 \tag{4}$$

The tests with formwork slip and without vibration showed a decrease in the lateral pressure compared to the reference tests with stiff formwork (see Eqn. (5)), especially for the concretes with consistency F5 and F6.

$$\sigma_{h,\max} = 0.21 \cdot v \cdot t_E \cdot \gamma_c \qquad R^2 = 0.77 \tag{5}$$

In addition to the setting time t_E according to the Vicat-penetration test, the setting time of all concrete mixtures was measured with the Setting-bag test according to DIN 18218:2010-01 [3]. The final-setting state $t_{E,KB}$ occurs when the concrete is penetrable by thumb less than 1.0 mm (with a force of 50 N). For concretes with relatively high paste content, Eqn. (6) was found to describe the relation between the specific setting values. With decreasing paste volume the factor F_E will normally increase.

$$t_E = F_E \cdot t_{E,KB} \approx 1.25 \cdot t_{E,KB} \tag{6}$$

$R^2 = 0.92$ for SCC with paste > 390 l/m³, $R^2 = 0.76$ for all concretes

A sufficient prediction of the setting time based on the early age structural behaviour was not identified. The structure formation and the setting process are influenced by the various admixtures and additions often in a different way and independent of each other.

Friction between concrete, formwork and reinforcement

The friction between the fresh concrete and the formwork surface was determined in tribometric tests. In particular the influence of the reinforcement, the paste volume V_{paste}, the vibration and the setting behaviour on the friction resistance was analysed. The results of the tests on SCC are shown in Figure 2. The friction coefficient μ is plotted against the ratio of concrete age t and final setting time $t_{E,KB}$. The friction coefficient μ was calculated according to Eqn. (7), considering the tensile force F_{R1} at the friction element, the effective friction area of the friction element A_n and the normal stress σ_n. The results in Figure 2 based on an applied vertical load of $\sigma_v = 85$ kN/m².

$$\mu = \frac{F_{R1}}{A_n \cdot \sigma_n} = \frac{\tau}{\sigma_n} \tag{7}$$

It can be seen that there are significant differences between the friction resistance for the plain surface and the resistance including reinforcement. At early age, the measured friction was very low ($\mu \leq 0.01$) for the most part. With time, the friction

increased only slightly in the plain surface test, notwithstanding the increased stiffening and setting of the concrete. This is a result of the lubricating paste layer in the contact zone between the fresh concrete and the element surface [2]. In contrast to the surface friction, in the tests with reinforcement a significant increase in displacement resistance was measured after $t/t_{E,KB} = 0.25$ at the latest. Furthermore, Figure 2 reveals that the SCC with low paste content shows a much faster increase in friction resistance than the SCC with high paste content. Additional tests showed that the friction resistance of concretes with consistency F5 and F6 is similar to SCC. Furthermore, a significant reduction of the friction coefficient μ by applied vibration up to $t/t_{E,KB} = 0.60$ was determined (not shown).

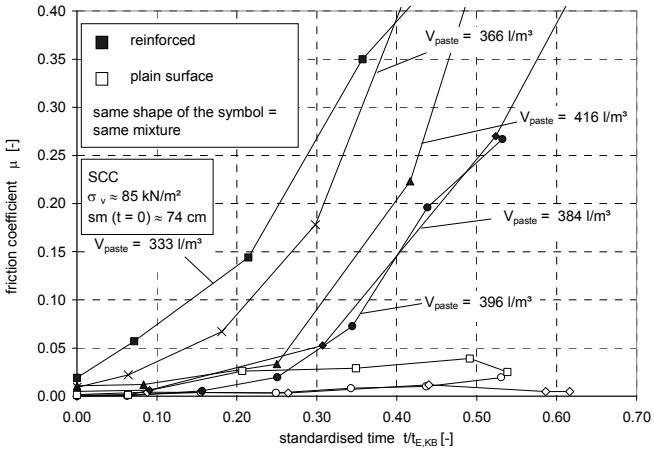

Figure 2. Development of the friction coefficient of SCC.

Modeling of the Fresh Concrete Pressure

The topic of fresh concrete pressure has been discussed recently with high intensity [4-8]. Different models were developed which often consider the material properties of the concrete merely under static conditions and neglecting the load dependent part of the yield stress (inner friction) as well as the construction operations aspects. The determination of the model parameters in the practice like the thixotropy or the friction parameters is often problematic. Based on experimental tests, a new model will be presented here. It tries to include both the reality and practicability to a large extent. The typical development of the fresh concrete pressure on vertical formwork during the casting of a member is presented in Figure 3. The casting rate is assumed constant and the concrete production continuous. For the design of vertical formwork using two opposite formwork panels, the maximum formwork pressure is of particular interest.

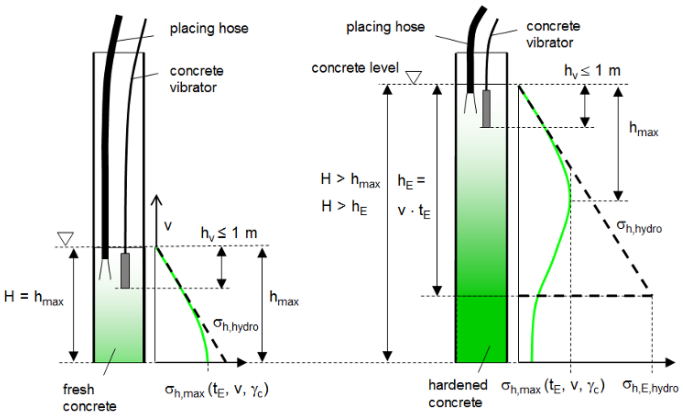

Figure 3. Typical distribution of fresh concrete pressure during casting.

Hydrostatic pressure $\sigma_{h,hydro}$ in the section H must be assumed initially, due to the very low inner friction of the fresh concrete as well as the dynamic impact during the casting. The increase in pressure will be reduced with the duration of casting and the concrete height h respectively, as a result of the increasing yield stress. The maximum pressure $\sigma_{h,max}$ is located at the height h_{max}. The subsequent decrease in the formwork pressure is caused by the build-up of the concrete structure. A reduction of the inner strain condition (the strain is a result of the elastic deformation of the formwork caused by the maximum pressure) must be realised by shrinkage of the concrete, a horizontal deformation or release of the formwork [2]. If the concrete is in the state of final setting (with setting time t_E) no support by the formwork is necessary anymore. This behaviour was confirmed in the present research project [1], using stiff and soft formwork (deformation < 0.02 mm/kPa and > 0.05 mm/kPa) in the full-scale tests.

The development of the concrete level during the concreting implies different load cases. However, the maximum pressure $\sigma_{h,max}$ is of primary importance. In the following, a new analytical model for the calculation of the maximum formwork pressure $\sigma_{h,max}$ asserted by highly workable concretes will be presented using the normalized maximum formwork pressure $\overline{\sigma}_{h,E,\max}$ (see Eqn. (1)). If the value $\overline{\sigma}_{h,E,\max}$ is given, the maximum formwork pressure can be calculated according to (8), with the casting rate v and the setting time t_E.

$$\sigma_{h,\max} = \overline{\sigma}_{h,E,\max} \cdot v \cdot t_E \cdot \gamma_c \tag{8}$$

A proposal for $\overline{\sigma}_{h,E,\max}$ was developed based on the tests on small concrete samples (simulation tests) and full-scale tests, assuming a constant casting rate v. For each consistency class, the simulation tests showed that the value $\overline{\sigma}_{h,E,\max}$ is to a large extent independent of the concrete design if the boundary conditions

such as formwork stiffness and vibration are constant. Frequent vibrations have a significant influence on $\overline{\sigma}_{h,E,\max}$. Therefore, for each consistency, the value $\overline{\sigma}_{h,E,\max}$ is not assumed constant in the model (if concreting from the top), but depends on the height $h_E = v \cdot t_E$ and consequently considers the influence of the filling and compacting technology as well as external vibrations on formwork pressure (see Figure 4 and Eqn. (9) and (10)).

$$\text{Consistency class F5 and F6: } \overline{\sigma}_{h,\max} = 0.18 + \frac{1}{h_E} \le 1 \tag{9}$$

$$\text{SCC: } \overline{\sigma}_{h,\max} = 0.16 + \frac{0.8}{h_E} \le 1 \tag{10}$$

The lower the value h_E the lower the distance between the position of the dynamic impact caused by the concreting technology and the position of the maximum formwork pressure (h_{max}). Because of the reduction of the inner friction resistance close to the maximum pressure, the normalized concrete pressure $\overline{\sigma}_{h,E,\max}$ increases with decreasing h_E-value. In contrast, a larger h_E-value will decrease the influence of vibration and hence reduce the value $\overline{\sigma}_{h,E,\max}$.

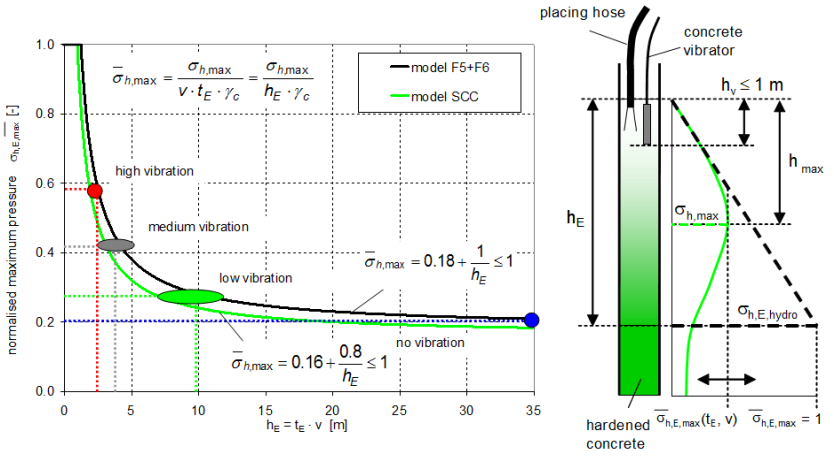

Figure 4. Development of the normalized maximum pressure $\overline{\sigma}_{h,E,\max}$.

For consistency class F5 and F6, no significant differences between $\overline{\sigma}_{h,E,\max}$-values were measured in the material test. Hence the model was chosen similarly. If the height h_E is approx. 2.5 m, a very high influence of vibration must be assumed. In this case the value $\sigma_{h,E,\max} = 0.58$, measured in the material test with direct vibration, is implemented in the model. If $h_E \approx 4$ m, a high influence is still expected and $\sigma_{h,E,\max} = 0.41$ is assumed in the model. The influence of

compaction can be neglected if $h_E \geq 10$ m. If the age of the concrete is larger than t_E the formwork pressure cannot be increased even by strong_and constant vibration. Therefore the upper limit of the normalized pressure is $\sigma_{h,E,\max} = 1.0$. For SCC, the influence of vibration - as a result of the casting process – on the formwork pressure is much lower compared to the vibrated concretes. Furthermore, the silo-effect will reduce the formwork pressure [3]. Hence the $\sigma_{h,E,\max}$ -values of SCC were determined to be lower (see Eqn. (10)). An analytical model, with explicit incorporation of the friction between concrete, formwork and reinforcement is presented by Graubner and Proske [4].

The friction resistance between the concrete and both the formwork surface and the reinforcement can be reduced significantly by vibration [1]. As concretes with consistencies F5 and F6 are compacted with intense vibration and certain vibrations cannot be excluded using SCC, the pressure reducing influence of the silo-effect is not considered explicitly in the analytical model. However, positive effects can be introduced in the calculation of the model (un)certainties, which are used for the calibration of design values. Figure 5 presents the maximum horizontal pressure $\sigma_{h,max}$, insert Eqn. (9) and (10) in Eqn. (8). The fresh concrete pressure varies linearly with the casting rate v and the setting time t_E. The value $\gamma_c = 25$ kN/m³ leads to Eqn. (11) and (12).

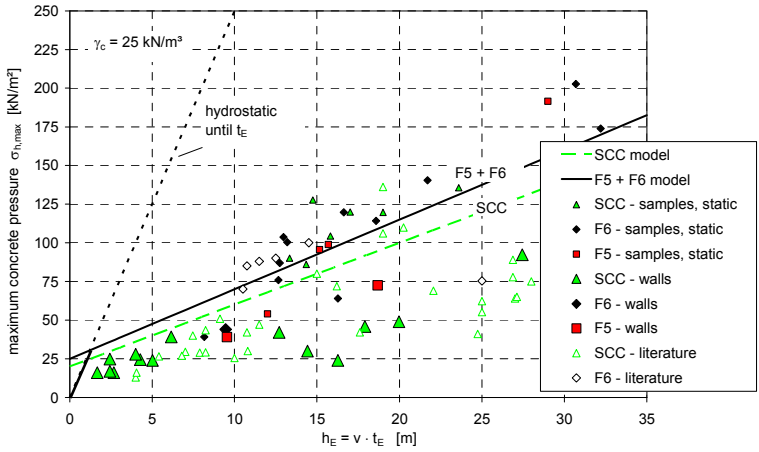

Figure 5. Fresh concrete pressure $\sigma_{h,max}$ according to the analytical models and measured fresh concrete pressure.

$$\text{Consistency F5 and F6: } \sigma_{h,\max} = 25\ kN/m^2 + 4.5 \cdot v \cdot t_E \leq \sigma_{h,E,hydro} \quad (11)$$

$$\text{SCC: } \sigma_{h,\max} = 20\ kN/m^2 + 4.0 \cdot v \cdot t_E \leq \sigma_{h,E,hydro} \quad (12)$$

The hydrostatic concrete pressure $\sigma_{h,E,hydro} = v \cdot t_E \cdot \gamma_c$ is an upper limit value. However, for practical applications it should be considered a minimum value of 25 kN/m² for the concrete consistency F5 and F6 and 20 kN/m² for SCC, giving variation in the operation process. Figure 5 shows a good correlation between the analytical model and test results. The pressure on the walls was determined using pressure sensors and measuring the tension forces of the formwork ties.

Proposed Formwork Design Approach

The bilinear pressure distribution was chosen for the design of the formwork and presented in Figure 6. Accordingly, the concrete pressure must be assumed hydrostatic until the maximum horizontal pressure $\sigma_{h,max}$ and the respective height h_s is reached. Further, the horizontal pressure is constant in the remaining section of $h_E = v \cdot t_E$. If the concrete has an age of t_E no concrete pressure must be considered anymore. This simplified distribution has the advantage of applying the maximum pressure over a large distance. In reality, the position of the maximum formwork pressure h_{max} is influenced by a number of parameters, like formwork stiffness or early shrinkage and cannot be predicted exactly. Below the section of h_{max} a significantly lower pressure than $\sigma_{h,max}$ will occur. However, for the design of formwork the "safe" bilinear distribution is of advantage, considering the variation of the setting time t_E, the casting rate v and the height h_E respectively (see Figure 6). Assuming the hydrostatic pressure up to h_s, uncertainties due to discontinues casting rate and vibrations can be considered. A good correlation between test results and the calculation of σ_h is observed with $R^2 = 0.74$.

The design of formwork and falsework must fulfill the requirements for safety and reliability of the construction. According to the semi-probabilistic safety concept the design value of the formwork pressure σ_{hd} can be calculated with Eqn. (13). The characteristic value σ_{hk} must be multiplied by the partial safety coefficient γ_F.

$$\sigma_{hd} = \sigma_{hk} \cdot \gamma_F \tag{13}$$

Like the analytical model (approx. mean value), the distribution of the characteristic pressure σ_{hk} and the design value σ_{hd} is chosen bilinear (see Figure 6). The characteristic value of the maximum concrete pressure $\sigma_{hk,max}$ was calculated using the full probabilistic method and the Monte-Carlo method. The calculation of $\sigma_{hk,max}$ was based on the analytical models as well as the full-scale tests. The partial safety factor on the load in the ultimate limit state was predefined as $\gamma_F = 1.5$. The limit state function for the calibration of the characteristic formwork pressure was developed from the relation between impact E and resistance R.

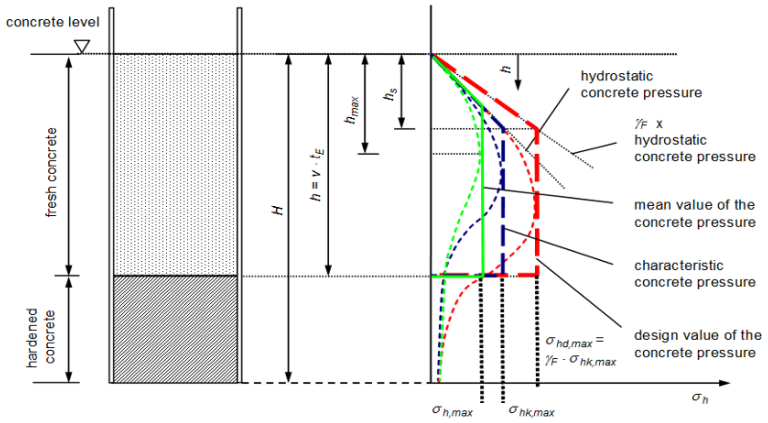

Figure 6. Distribution of the horizontal fresh concrete pressure on formwork.

A formwork collapse has relatively low negative effects on life and material. Hence the failure probability in the ultimate limit state was defined as $P_f = 10^{-4}$. The statistical parameters were derived from the experimental tests and values found in the literature. The casting rate v has the highest influence on the spread with a variation coefficient $V = 0.25$. The reason is mainly insufficient control of the casting process. A high spread is further seen in the setting time t_E. The model uncertainties θ_E were calculated based on the measured and calculated pressures. For the calculation of the maximum characteristic pressure the Eqn. (14) to (16) were determined ([m] – unit meter).

$$\text{SCC: } \sigma_{hk,\max} = h_s \cdot \gamma_c = \left(1\,[m] + 0.26 \cdot v \cdot t_E\right) \cdot \gamma_c \tag{14}$$

$$\text{Consistency F6: } \sigma_{hk,\max} = h_s \cdot \gamma_c = \left(1\,[m] + 0.30 \cdot v \cdot t_E\right) \cdot \gamma_c \tag{15}$$

$$\text{Consistency F5: } \sigma_{hk,\max} = h_s \cdot \gamma_c = \left(1\,[m] + 0.24 \cdot v \cdot t_E\right) \cdot \gamma_c \tag{16}$$

According to the analytical model the characteristic values for SCC are lower than for consistency F6. The values for consistency F5 are lower than both SCC and F6 because of the lower model uncertainties of concrete F5 and lower spread of t_E. Using SCC and neglecting the influence of unintended vibrations, the pressure of SCC is lower than the pressure of the vibrated concretes. In this case, the higher workability of SCC has less influence on the formwork pressure than the mechanical compaction.

The experience on construction sites shows that a vibration depth of 2 m cannot be excluded. However, the material tests showed that a change in the concrete consistency due to vibration can be achieved up to a concrete age of approximately $0.65 \cdot t_E$ and a depth of $0.65 \cdot h_E$ respective. Figure 7 shows that the pressures accounting for this additional requirement are mostly included in the characteristic equation. Further on, special loads like the impact of the concrete bucket, impacts

of the trailer pump hoses or continuous external vibration with intense vibration are considered adequately in the design model. The proposed model - based on the setting time - gives an upper characteristic formwork pressure and hence leads to safe formwork. If the workability loss or the thixotropy of the concrete is comparatively high and only low vibrations are asserted the real formwork pressure should be significant lower than the model values. Also a lower spread of the model parameters would reduce the design load.

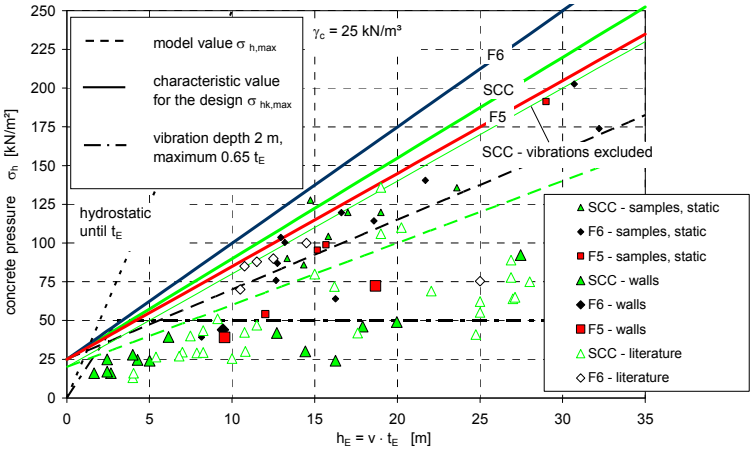

Figure 7. Concrete pressure for the design $\sigma_{hk,max}$ and measured values.

Conclusions and Further Research

A proposal for the design of formwork, based on the experimental tests and the semi-probabilistic safety concept was developed. It was found that even for highly workable concretes, the design load is often lower than the hydrostatic concrete pressure. The here presented proposal for the calculation of formwork pressure was implemented in the German standard DIN 18218 “Pressure of fresh concrete on vertical formwork” DIN 18218:2010-01 [3] mostly unchanged.

Future research work should involve the numerical simulation and the pressure asserted on formwork for structures having geometrically complicated shapes. First finite element analyses [2] show the significant influence of the formwork inclination on the concrete pressure asserted by SCC. Also the introduction of the early structural behaviour in the design model would be advantageous and will further help to reduce the design pressure and therefore the formwork cost.

Acknowledgement

The research presented in this paper received financial support from the German Federal ministry of transport, building and urban affairs (BMVBS), Güteschutzverband Betonschalungen e.V., Bilfinger Berger AG, Wayss & Freytag Ingenieurbau AG, Max Bögl Bauunternehmen GmbH and RSB Schalungstechnik GmbH.

References

[1] Graubner, C.-A., Beitzel, H., Beitzel, M., Bohnemann, C., Boska, E., Brameshuber, W., Dehn, F., König, A., Lingemann, J., Motzko, C., Müller, H.S., Pistol, K., Proske, T., Stettner, C. and Zilch, K. (2008), Formwork pressure asserted by highly workable concretes, F09-7-2008, TU Darmstadt, Institut für Massivbau (in German).

[2] Proske, T. (2007), Formwork pressure asserted by self-compacting concrete Ph.D. Thesis, Technische Universität Darmstadt (in German).

[3] DIN 18218:2010-01 (2010), Pressure of fresh concrete on vertical formwork, Beuth Verlag (in German).

[4] Graubner, C.-A. and Proske, T. (2007), Formwork Pressure of Concretes with High Workability, Advances in Construction Materials, Stuttgart, Springer-Verlag.

[5] Vanhove, Y. et al. (2001), Study of self-compacting concrete pressure on formwork, Proceedings of the Second International Symposium on Self-Compacting-Concrete, COMS Eng. Corporation, Fukui/ Japan.

[6] Ovarlez, G. and Roussel, N. (2006), A physical model for the prediction of lateral stress exerted by self-compacting concrete on formwork, *Materials and Structures*, vol. 39.

[7] Khayat, K. H. and Assaad, J. (2008), Use of thixotropy-enhancing agent to reduce formwork pressure exerted by self-consolidating concrete, *ACI Materials Journal*, vol. 105, n. 1.

[8] Gregori, A., Ferron, R., Sun, Z. and Shah, S.P. (2008), Experimental simulation of self-consolidating concrete formwork pressure, *ACI Materials Journal*, vol. 105, n. 1.

Theme 7: Properties of Hardened SCC

Drying Shrinkage of SCC – Influence of the Composition of Ternary Composite Cements

Hedda Vikan[1], Tor Arne Hammer[1] and Knut O. Kjellsen[2]

[1] COIN - Concrete Innovation Centre, SINTEF Building and Infrastructure, Oslo, Norway
[2] Norcem AS, Heidelberg Cement Group, Brevik, Norway

Abstract. There is an increasing interest of developing and using composite cements, e.g. to reduce CO_2-emmissions in cement production. This paper discusses results from an investigation of the influence of composition of ternary composite cements on the drying shrinkage of a typical low cost SCC for buildings (*w/cm* = 0.55) as used in Norway. Various Portland cements (CEM I), Portland fly ash cements (CEM II/A-V), Portland limestone cements (CEM II/A-L) and a Portland-composite cement (CEM II/B-M) were tested. The fineness of clinker phase, fly ash and limestone were varied systematically in the cements. Shrinkage was determined from length measurements of 500 mm long prisms, 100 x 100 mm in cross section, stored in water from demoulding until 7 days of age and then at 50% RH until 12 months of age.
As expected, increased fineness and early reactivity of the cements increased shrinkage. The results showed, however, that the drying shrinkage was not significantly affected by the cement type. I.e. replacing up to 35% of the clinker by fly ash and limestone did not influence the drying shrinkage.

Introduction

During cement production large amounts of CO_2 are emitted. Strategies to reduce these emissions include alternative fuels, optimized energy consumption (e.g. regeneration of heat, optimization of clinker composition with mineral additives, etc.) and replacing part of the clinker with other materials such as slag, limestone powder, fly ash, silica fume, natural pozzolans etc. The type of replacement materials used depends normally on their availability (amount available, price, transportation) [1]. Limestone powder and fly ash are available at the Norwegian cement factories. Optimizing the replacement of clinker by these two components

K.H. Khayat and D. Feys (eds.), *Design, Production and Placement of Self-Consolidating Concrete*, RILEM Bookseries 1,
DOI 10.1007/978-90-481-9664-7_23, © RILEM 2010

would enable Norwegian factories to produce more sustainable cement. Currently, Norcem manufactures CEM I and CEM II/A-V cements.

Clinker replacing materials may influence fresh and hardened concrete properties. The literature suggests that several mechanisms dominate in different ranges of internal pore humidity [2-4]. When considering concrete shrinkage in the 45-90% relative humidity range, capillary stress appears to be the predominant mechanism. When pore water evaporates from capillary pores in hardened concrete, tension in the liquid is transferred to the walls, resulting in shrinkage. Quite frequently these tensile stresses lead to cracks that are aesthetically undesirable and may reduce the concrete performance. For a given pore structure, the internal stress generated upon evaporation is proportional with the surface tension of the pore water and inverse proportional with the pore radius as described by the Kelvin-LaPlace equation for a circular meniscus:

$$p^a - p^l = \Delta P = -\frac{RT}{v^l} \ln \frac{p}{p_o^g}^g = \frac{2\gamma^{lg}}{r \cdot \cos\Theta} \quad (1)$$

where ΔP is the capillary tension, T is the temperature, R is the universal gas constant, v^l is the molar volume of the pore solution, γ^{lg} is the surface tension of the pore solution, r is the pore radius and Θ is the wetting angle.

Conflicting results are reported about the effect of supplementary cementitious materials on drying shrinkage. It is, however, likely that shrinkage is governed by the dosage, way of addition, particle size distribution and reactivity of the material [5-7]. Self-compacting concrete has normally very different powder contents and composition compared to a traditionally vibrated concrete. It is correspondingly difficult to predict the drying shrinkage potential for these types of concrete [8].

Experimental

Materials

Limestone powder and low-calcium fly ash were used to replace part of the Portland cement clinker. The raw materials used for the cements are given in Table I while their chemical compositions are given in Table II. Compositions and densities of the cements are given in Table III and IV respectively. All cements were blended on volume basis.

A polycarboxylate based superplasticizer with solid content of 18% was used for all mixes. The gneiss/granite aggregates consisted of the fractions 0-2 mm, 0-8 mm, and 8-16 mm.

Table I. Materials for the trial cements. Note that cement C contained 20 volume percent fly ash intermixed by the producer.

Material	Denomination	Intermixed limestone (%)	Blaine (m^2/kg)	Density (g/cm^3)
CEM I 42.5 RR	A	2.7	598	3.14
CEM I 42.5 R	B	4.5	390	3.12
CEM II A-V 42.5R	C	-	461	2.95
Fly Ash	FA	-	359	2.37
Fly Ash finely milled	FA^{FM}	-	537	2.57
Limestone powder	LS	-	362	2.73
Limestone powder finely milled	LS^{FM}	-	490	2.77

Table II. Characteristics of the different raw materials used to compose the trial cements.

	Fly ash	Limestone	CEM A	CEM B	CEM C
CaO (%)	4.1	79.8	61.8	61.6	-
SiO_2 (%)	54.4	12.9	19.8	20.0	-
Al_2O_3 (%)	22.0	2.7	4.3	4.5	-
Fe_2O_3 (%)	5.8	2.0	3.8	3.6	-
SO_3 (%)	0.5	-	3.6	3.3	2.68
MgO (%)	2.2	1.8	2.2	2.2	-
Free CaO (%)	-	-	1.5	1.76	0.78
K_2O (%)	2.20	0.62	1.07	1.00	-
Na_2O (%)	1.15	0.49	0.38	0.43	-
Eqv. Na_2O (%)	2.60	0.90	1.08	1.10	-
Carbon (%)	3.64	-	-	-	-
LOI (%)	4.08	37.66	1.72	2.38	1.82
C_3S (%)	-	-	56.0	34.8	-
C_2S (%)	-	-	14.0	31.0	-
C_3A (%)	-	-	5.0	7.4	-
C_4AF (%)	-	-	11.4	10.3	-

Table III. Composition of the trial cements (volume percent).

Denomination	**No**	**C (%)**	**A (%)**	**B (%)**	**FA (%)**	**FA^{FM} (%)**	**LS (%)**	**LS^{FM} (%)**
100C (CEM II/A-V)	Ref	100						
100A (CEM I)	1		100					
100B (CEM I)	2			100				
80A-20FA (CEM II/A-V)	3		80		20			
80A-20FA^{FM} (CEM II/A-V)	4		80			20		
80A-20LS (CEM II/A-L)	5		80				20	
80A-20LS^{FM} (CEM II/A-L)	6		80					20
65A-20FA15LS (CEM II/B-M)	7		65		20		15	
80B-20FA (CEM II/A-V)	8			80	20			
80B-20LS (CEM II/A-L)	9			80			20	

Table IV. Densities of the trial cements.

Denomination	**No.**	**Density (g/cm^3)**
100C	Ref	2.95
100A	1	3.14
100B	2	3.12
80A-20FA	3	2.99
80A-20FA^{FM}	4	3.03
80A-20LS	5	3.06
80A-20LS^{FM}	6	3.07
65A-20FA15LS	7	2.93
80B-20FA	8	2.97
80B-20LS	9	3.04

Concrete recipes

The concrete mixture design was based on a typical low cost SCC for buildings (*w/cm* = 0.55) as used in Norway. All concretes had a water-cement ratio of 0.55. The reference had a cement paste and matrix volume (here defined as cement paste + filler from the aggregates with particle size smaller than 0.125 mm) of 290 and 320 l/m^3 respectively. The aggregates consisted of 1018 kg/m^3 0-8 mm sand and 822 kg/m^3 8-16 mm gravel. The superplasticizer dosage was 2.3%.

Mixture 1-9 had a cement paste volume of 310 l/m^3, and matrix volume of 345 l/m^3. The aggregates consisted of 144 kg/m^3 0-2 mm sand, 987 kg/m^3 0-8 mm sand and 643 kg/m^3 8-16 mm gravel. The superplasticizer dosage was 3.2%.

Note that the densities of the cements were somewhat reduced as limestone and/or fly ash were added as replacements. The amount of powder and water was correspondingly reduced in order to keep both matrix volume and *w/cm* constant. Mixture 7, having the lowest density of all in this study, had thus 3% less added water than mixture 2.

Mixing and preparation of test samples

A forced pan mixer with a volume of 50 liters was used to prepare the concretes. All dry materials were first blended during 1 minute. Water and half of the superplasticizer were thereafter added and the mixture was blended for 2 minutes. The remaining superplasticizer was added after 2 minutes rest. The concrete was finally mixed for 1 minute. Following procedure was performed after mixing:

- Measurement of slump flow
- Measurement of density and air in fresh concrete (NS-EN 12350)
- Casting of 3 prisms per mixture (500 x 100 x 100 mm) with cast-in measurement points for use of extensometer. Drying shrinkage was determined as length change of the prisms. The samples were demoulded after 24 hours and then put into a 20^{o}C water bath for 6 days. Differences in swelling during the 6 days the samples were stored in water bath are not considered to be significant for the accuracy of the measurements. The samples were thereafter stored at 50% relative humidity and 20°C. Measurements of length and weight change were performed at the following ages: 1 day (by demoulding), 7, 14 and 28 days as well as 2, 3, 6 and 12 months. The procedure is based on Swedish Standard SS 13 72 15.
- Casting of six 100 mm cubes per mixture for determination of compressive strength after 1 and 28 days (NS-EN 12390-3)

Results and Discussion

Air content, slump flow and compressive strength

All concretes were stable and none of them showed signs of separation.

Table V. Fresh concrete properties.

Mixture Composition	No.	Slump flow (mm)	Air (%)
100C	Ref	545	2.1
100A	1	502	3.6
100B	2	574	2.9
80A-20FA	3	535	2.9
80A-20FA^{FM}	4	536	2.7
80A-20LS	5	553	3.4
80A-20LS^{FM}	6	535	3.4
65A-20FA15LS	7	555	3.2
80B-20FA	8	595	2.9
80B-20LS	9	585	3.2

Table VI. Hardened concrete properties.

Mixture Composition	No.	Density (kg/m^3)*	Compressive strength	
			1 day (MPa)	28 days (MPa)
100C	Ref	2400	18.6	46.8
100A	1	2342	27.9	54.4
100B	2	2365	19.0	50.4
80A-20FA	3	2354	20.7	46.6
80A-20FA^{FM}	4	2353	21.9	49.2
80A-20LS	5	2344	21.4	47.7
80A-20LS^{FM}	6	2343	22.0	46.8
65A-20FA15LS	7	2354	17.1	42.0
80B-20FA	8	2358	15.4	46.7
80B-20LS	9	2366	15.4	41.1

* calculated from the weight of the cubes after demoulding, assuming volume of 0.001 m^3

The slump flow data given in Table V generally show that the slump flow increases as 20-35% cement is replaced with limestone powder and/or fly ash (confer mixture 1 vs. 3, 4, 5 and 6, mixture 2 vs. 8 and 9). Note that mixture 2, 8

and 9 have relatively high slump flow. This is probably due to lower surface area (and thus water demand) of cement B compared to cement A.

The compressive strength (Table VI) was as expected reduced as clinker was replaced with the supplementary materials. Extra milling of the fly ash resulted in slightly increased compressive strength at both ages, while increased fineness of the limestone powder only slightly increased the 1 day compressive strength.

Drying shrinkage

Influence of cement type. Figure 1 shows that samples based on cement B tended to produce less drying shrinkage than samples based on cement A. Possible explanations for this finding are the higher surface fineness and early reactivity of Cement A as indicated by the 1 day compressive strength in Table VI. Figure 2 shows that samples consisting of Cement A or B released less water during curing than the composite cements. This finding is expected, since less water is bound by hydration products as Portland cement is partly replaced by limestone powder and/or fly ash. Composite cements based on CEM A tended to produce higher shrinkage than cements based on B. The differences are, however, minor. No conclusions can thus be drawn upon the effect of chemical composition of cement on drying shrinkage. The trends are, however, in accordance with other studies reporting that increased fineness of the cement results in increased shrinkage [5]. Reasons for this effect might be refined pore structure and thus increased capillary pressure in the partly filled pores and/or increased degree of hydration leading to increased autogenous shrinkage. Shrinkage has also been reported to increase with increasing alumina content [9]. In this case, the relatively high surface fineness of CEM A seems to overpower any effect of higher alumina content of cement B. Note that Bogue estimations probably not are accurate enough for determination of cement composition and its influence on early reactivity. Previous studies have shown that mineralogical determination obtained by quantitative X-ray diffraction (QXRD) and Rietveld analyses is far more useful than Bogue estimations for study of early cement reactivity [10].

Influence of type and fineness of cement replacement. Note that the reference mixture (100C) had somewhat lower cement paste and matrix content compared to the other concretes (20 – 25 liter/m^3). Still, the shrinkage (Figure 1) and weight loss (Figure 2) of this concrete is approximately the same as for cement B. This indicates that cement C has somewhat higher shrinkage potential than cement B. This is probably due to the higher Blaine surface of cement C compared to the trial cements 80B-20FA and 80B-20LS.

Figure 1 shows that the drying shrinkage in the first approximately 2 months tends to increase when cement A is replaced by 20% limestone powder or fly ash. This is accompanied by increased water loss as seen Figure 2. Increased water loss is probably caused by less amount of water being bound by hydration products.

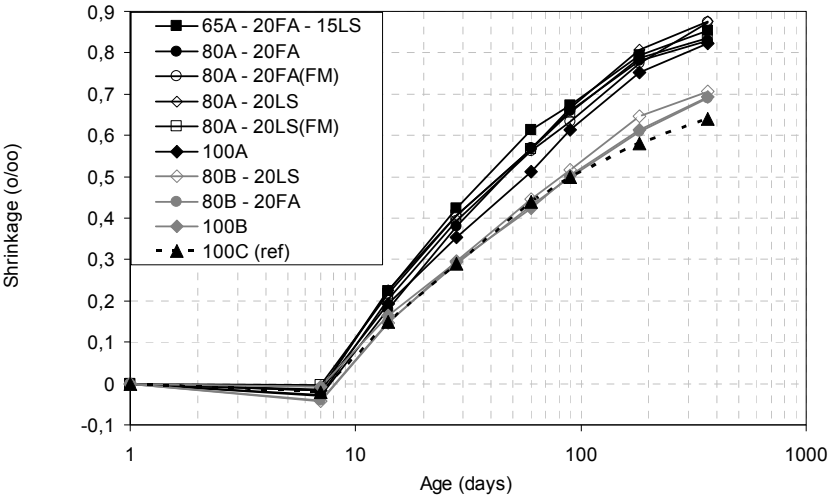

Figure 1. Shrinkage for concretes based on clinker A, B and C (reference). Note that the reference mixture had a cement paste volume of 290 l/m^{3}while the other concretes had a cement paste volume of 310 l/m^3.

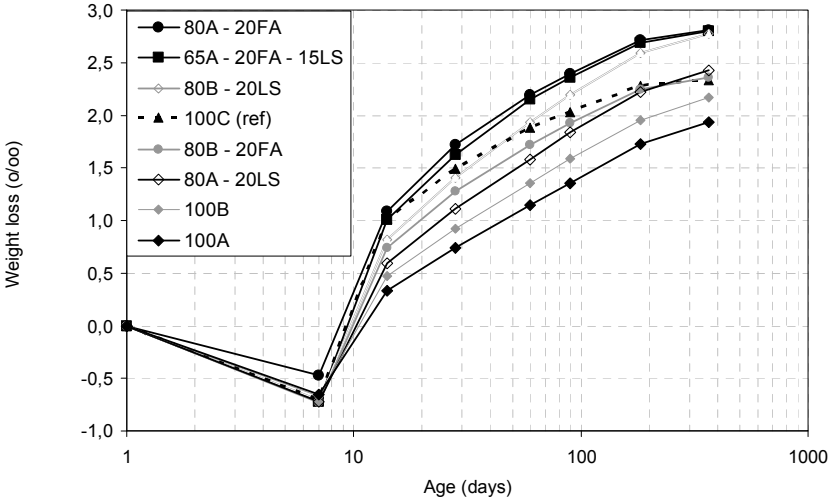

Figure 2. Weight loss for concretes based on clinker A, B, and C (reference). Note that the reference mixture had a cement paste volume of 290 l/m^{3}while the other concretes had a cement paste volume of 310 l/m^3.

Moreover, the Blaine finenesses of both fly ash and limestone powder were lower than Cement A. Increased water loss by cement replacement could thus also be an indication of more and/or coarser capillary pores. But still, the relative difference in shrinkage is not considerable, probably caused by coarser capillary pores and thus reduced capillary tension (Eqn. (1)).

Interestingly, type of cement replacement (fly ash or limestone) did not have any effect on the drying shrinkage a seen by Figure 1. Figure 2 shows no clear effects for water loss since mixes based on cement A indicate that fly ash replacement results in higher water loss than limestone powder, while mixes based on cement B indicate the opposite. Note that the Blaine fineness of fly ash (FA) and limestone powder (LS) were almost identical, namely 359 and 362 m^2/kg respectively. The pozzolanic effect seems thus not to influence the drying shrinkage in these experiments.

Fineness of the cement replacing powders did not influence the drying shrinkage as seen by comparing samples with un-milled and finely milled fly ash and limestone powder. Less weight loss was, however, measured for finely milled than un-milled fly ash, indicating finer pore structure.

Replacing cement with both fly ash and limestone powder did not influence the shrinkage even though the replacement ratio increased from 20 to 35%. Figure 2 and 3 show that concretes with blended cements exhibited the highest weight loss during drying. These concretes seem thus to have a more open/coarser pore structure and/or more evaporable water. It is not clear by comparing the two figures if fly ash or limestone powder results in largest amount of evaporable water.

No marked effect of cement replacement can be found for cement B. This cement had a Blaine surface fineness in the same range as the replacement materials. The slump flow increased correspondingly only 10-20 mm as cement B was replaced by fly ash or limestone. Note that only the coarser limestone powder and fly ash was used to replace cement B.

The results found in this study are in line with other reports. Fly ash has been reported to increase drying shrinkage or have no influence at all [5, 11]. No references have been found to other studies with similar replacement ratios of limestone powder.

Ratios between shrinkage and weight loss are given in Figure 4. Concretes based on CEM A exhibited the highest values of shrinkage relative to the content of evaporated water. Possible explanations for this finding are the relatively high surface fineness and early reactivity of this cement (see Table VI). This confirms the theory of shrinkage being driven by capillary forces that are inversely

proportional with the pore size; the finest pores producing the largest capillary forces and thus the largest shrinkage.

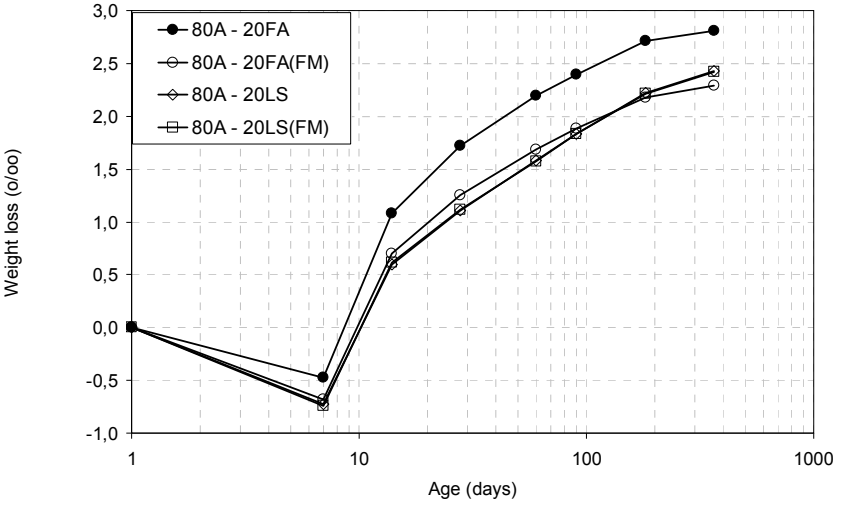

Figure 3. Influence of finely milling fly ash and limestone powder on the weight loss.

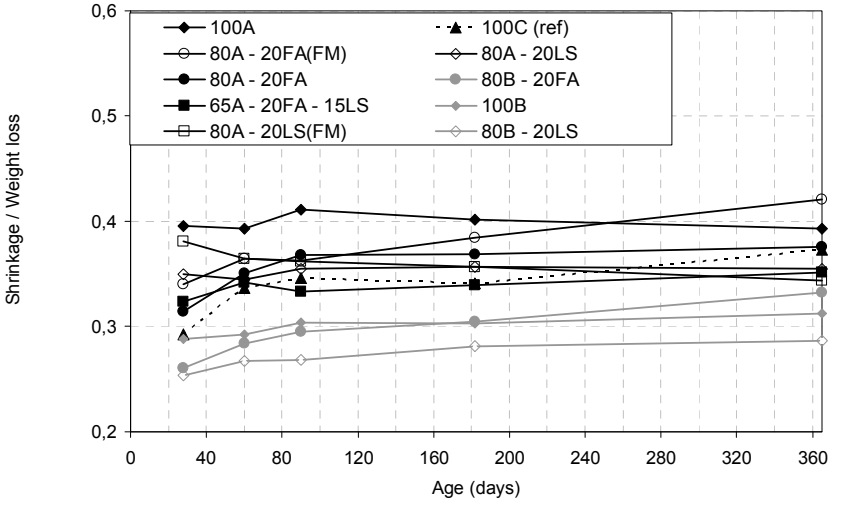

Figure 4. Ratio between weight loss and shrinkage from 14 days for all concretes.

Replacing parts of the cement with fly ash/and or limestone resulted in reduced density of the composite cement. Amount of powder and water were correspondingly somewhat reduced in order to keep both matrix volume and *w/cm* constant. Mixture 7, having the lowest density of all in this study, had thus 3% less added water than mixture 2. No trends could, however, be found between amount of added water (given in kg/m^3) and shrinkage/water loss. It is thus believed that the difference of amount of added water is too low to significantly influence the measurements.

Conclusions

The results revealed that the tested trial cements of the type Portland-fly ash cements (CEM II/A-V), Portland –limestone cement (CEM II/A-L) and Portland – composite cement (CEM II/B-M) increased the slump flow of concrete compared to comparable CEM I cements. Thus, the reduced water (or superplasticizer) demand makes these tested blended cements well suited for SCC.

The results do not show any clear influence of fly ash and limestone filler replacing Portland cement (here up to 35% replacement). There was not found any notable difference between fly ash and limestone filler as replacement, or any influence of the fineness of the two supplementary materials. CEM II/A-V and CEM II/B-M provide similar drying shrinkage as CEM I in SCC. However, the drying shrinkage of the tested concretes increased with increasing fineness of the cements.

References

[1] Justnes, H. (2007), Principles of making cement with reduced CO_2 emission – State of the art, SINTEF Report, ISBN 978-82-536-0982-9, downloadable from www.coinweb.no.

[2] Ronbing, B. and Jian, S. (2005), Synthesis and evaluation of shrinkage-reducing admixture for cementitious materials, *Cem. Concr. Res.*, vol. 35 pp. 445-448.

[3] Taylor, H.F.W. (1990), Cement Chemistry, Academic Press Limited, London, pp.270-272.

[4] Bentz, D. (2005), Curing with shrinkage-reducing admixtures, *Concrete International*, October, pp. 55-60.

[5] Neville, A.M. (1995), Properties of Concrete, 4th Ed. Pearson Education Limited, Essex, England.

[6] Brooks, J.J. and Jiang, X. (1997), The influence of chemical admixtures on restrained drying shrinkage of concrete, Fifth CANMET/ACI Conference on Superplasticizers and Other Chemical Admixtures in Concrete, Rome, pp. 249-266.

[7] Jianyong L. and Yan, Y. (2001), A study on creep and drying shrinkage of high performance concrete, *Cem. Concr. Res.,* vol. 31, pp. 1203-1206.
[8] De Schutter, G., Bartos, P.J.M., Domone, P. and Gibbs, J. (2008), Self-Compacting Concrete, Whittles Publishing, Scotland, p. 200.
[9] ACI 209.1R-05, Report on Factors Affecting Shrinkage and Creep of Hardened Concrete.
[10] Vikan, H., Justnes, H., Winnefeld, F. and Figi, R. (2007), Correlating cement characteristics with rheology of paste, *Cem. Concr. Res.,* vol. 37, pp. 1502-1511.
[11] Brooks, J.J. (1999), How admixtures affect shrinkage and creep, *Concr. Int.,* vol. 21, pp. 35-38.

Properties of Low-Shrinkage, High-Strength SCC Using Shrinkage-Reducing Admixture, Blast Furnace Slag and Limestone Aggregates

K. Saito[1], M. Kinoshita[1], H. Umehara[2] and R. Yoshida[2]

[1] Takemoto oil & Fat Co., Ltd., Aichi, Japan
[2] Nagoya Institute of Technology, Aichi, Japan

Abstract. It is indicated that the risk of early age shrinkage cracking on high-strength self-compacting concrete (SCC) increases due to autogenous shrinkage caused by low water-to-cement ratio (*w/c*) and high cement content. For the purpose of reducing the shrinkage strain of high-strength SCC, three kinds of shrinkage-reducing concrete materials, shrinkage-reducing admixture (SRA), blast furnace slag aggregate (BFS) and limestone aggregates were examined. It was found that these materials each showed excellent shrinkage-reducing effect better than each ordinary material when they were used separately. In addition, the authors have found that the shrinkage-reducing mechanisms were individually different and the shrinkage-reducing effect was approximately 45% to 61% when used all together.

Introduction

In recent years, high-strength SCC has been increasingly used for high-rise RC building in urban areas. As *w/c* becomes lower, drying shrinkage strain of high-strength concrete generally decreases, but autogenous shrinkage increases due to the high cement content, and the risk of early age shrinkage cracking increases [1, 2]. In order to prevent shrinkage cracking, the shrinkage strain of high-strength SCC should be decreased and it is known that SRA can reduce autogenous shrinkage as well as drying shrinkage [3, 4]. With this background, the authors have applied three kinds of shrinkage-reducing concrete materials, SRA, BFS [5] and limestone aggregate [6] to high-strength SCC with a target strength of 60 to 150 MPa and *w/c* of 0.30, 0.25 and 0.15, and experimentally examined their effectiveness.

K.H. Khayat and D. Feys (eds.), *Design, Production and Placement of Self-Consolidating Concrete*, RILEM Bookseries 1,
DOI 10.1007/978-90-481-9664-7_24, © RILEM 2010

Experimental Procedure

Materials

Admixture. A polycarboxylic high-range water-reducing admixture (HP) was used for the concretes with *w/c* of 0.30 and 0.25, and a polycarboxylic high-range water-reducing admixture (SSP) which is configured by polymeric molecular design having improved water-reducing performance on the ultra high-strength concrete [7] was used for the concrete with *w/c* of 0.15. A polyether type shrinkage-reducing admixture (SRA) was used. Their chemical compositions are given in Table I.

Table I. Chemical composition of admixtures.

Symbol	Type	Admixture Composition	Conc. (%)
HP	high-range water-reducing admixture	Maleic type polycarboxylate-based copolymer	25
SSP	high-range water-reducing admixture for ultra high-strength	Mixture with SP1 and SRA	30
SRA	Shrinkage-reducing admixture	Polyether derivative	100

Cement. Normal Portland cement (N), moderate heat Portland cement (M), and silica fume cement (SFC) were used. SFC is a premixed cement containing silica fume (SF) in place of 10 wt% of low heat Portland cement (L). Their chemical and physical properties are given in Table II.

Table II. Characteristics of cement.

Type of cement	Phase composition (%)				Surface area (m^2/kg)	Density (g/cm^3)
	C_3S	C_2S	C_3A	C_4AF		
Normal Portland (N)	52	23	9	9	325	3.16
Moderate heat Portland (M)	35	43	5	9	340	3.22
Low heat Portland (L)	27	58	2	8	335	3.22
Silica fume cement (SFC)	L (90%) + SF (10%)				560	3.08

Aggregate. Blast furnace slag aggregate (SG) which met the requirement of JIS A 5011 (Slag aggregate for concrete) was used as fine aggregate. And a crushed sand (S) which is generally used on high-strength concrete was used for comparison. A crushed limestone (LG) was used as coarse aggregate. And a crushed stone of sandstone (G) which is generally used on high-strength concrete was used for comparison. Their physical properties are given in Table III.

Table III. Characteristics of aggregate.

Kind of aggregate	Symbol	Type	SSD Density (g/cm^3)	Water absorption rate (%)	Fineness modulus	Solid volume percentage (%)	Max size (mm)
Fine aggregate	SG	Blast furnace slag aggregate	2.77	0.45	2.56	56.7	5
	S	Crushed sand	2.64	1.24	2.67	65.8	5
Coarse aggregate	LG	Limestone	2.70	0.29	6.74	61.2	20
	G	Crushed stone	2.66	0.67	6.75	60.6	20

Procedures

Mixture proportioning. Table IV gives the mixture proportions of concrete. N cement, M cement and SFC were used for the concrete with a target strength of 60, 80, and 150 MPa, respectively. The target slump flow of concrete with *w/c* of 0.30, 0.25 and 0.15 were set to 60 ± 5 cm, 65 ± 5 cm and 70 ± 5 cm, respectively. Considering freezing and thawing resistance, the concrete with *w/c* of 0.30 and 0.25 were entrained with target air content as 3.0 ± 1.0%, respectively, whereas a concrete with *w/c* of 0.15 was not air-entrained (under 2%) because a previous study showed that high-strength concrete with a *w/c* lower than 0.20 has sufficient freezing and thawing resistance without entraining air [8].

Table IV. Mixture proportions of concrete.

Symbol	Target strength (MPa)	Cem-ent	*w/c*	SRA (kg/m^3)	SG	LG	Slump flow (cm)	Air (%)	Unit weight (kg/m^3)					
									W	C	SG	S	LG	G
30N	60	N	0.30	-	-	-	60	3	160	533	-	853	-	854
30N-SG				-	○	-					895	-	-	854
30N-LG				-	-	○					-	853	875	-
30N-SR				6	-	-					-	853	-	854
30N-All				6	○	○					895	-	875	-
25M	80	M	0.25	-	-	-	65	3	160	640		774	-	854
25M-SG				-	○	-					812	-	-	854
25M-LG				-	-	○					-	774	875	-
25M-SR				6	-	-					-	774	-	854
25M-All				6	○	○					812	-	875	-
15S	150	SFC	0.15	-	-	-	70	2	160	1067	412	-	-	854
15S-SG				-	○	-					-	432	-	854
15S-SR				6	-	-					412	-	-	854
15S-SR-SG				6	○	○					-	432	-	854

Mixing concrete. Concretes were mixed using a forced-mixing-type mixer with a capacity of 100 liters as follows: Dry mix fine aggregate and cement for 15 sec. Add water and admixture and mix for 60, 90, and 300 sec for *w/c* of 0.30, 0.25, and

0.15, respectively. Add coarse aggregate and mix for 120 sec. The test temperature was set to 20°C.

Test methods. Slump flow was measured in accordance with JIS A 1150. L-flow velocity (Lv) was measured by using L-flow test meter [8] shown in Figure 1. The flow speed of concrete between 5 and 10 cm from the flow start line of the L-flow test meter was defined as L-flow velocity.

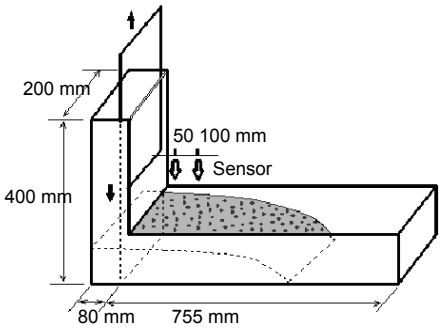

Figure 1. L-flow test meter.

Setting time was measured in accordance with JIS A 1147 by means of penetration resistance measurements on mortar sieved from the concrete. Drying shrinkage tests were conducted in accordance with JIS A 1129. The specimens for length change were molded in 100 x 100 x 400 mm prisms and were demolded after 24 hours, cured in water until the age of 7 days and kept in a room with a temperature of 20°C and 60% RH for 182 days. The base length of the specimen was measured at the age of 7 days.

Autogenous shrinkage tests were conducted following the method established by JCI Research Committee for Autogenous Shrinkage [9]. The strain was measured by the data logger using embedded strain gauges in the middle section of the form shown in Figure 2, and the changes in the strain after initial setting were regarded as autogenous shrinkage strain. The specimens molded in 100 x 100 x 400 mm prisms were sealed and kept in a room with a temperature of 20°C until the age of 182 days.

Compressive strengths were determined with 200 x 100 mm cylinder specimens in accordance with JIS A 1108. The specimens were water-cured immediately after being demolded until compression testing at 7, 28, and 91 days. For the simplified adiabatic curing, the specimens were sealed-cured and placed in a thermal insulated box for 7 days, and then they were sealed and cured at 20°C until compression testing at 28 and 91 days. Freezing and thawing resistance tests were conducted in accordance with ASTM C 666 (procedure A). The specimens molded

in 100 x 100 x 400 mm prisms were subjected to the test after 28 days curing in water at 20°C. They were frozen in water at a temperature of -18 ± 2°C and thawed at 5 ± 2°C for 300 cycles.

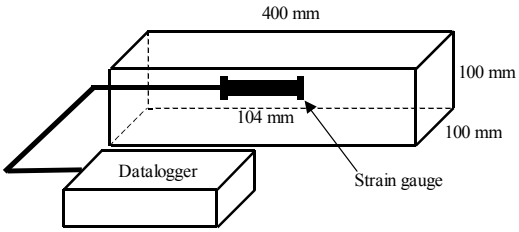

Figure 2. Autogenous shrinkage strain tester.

Results and Discussion

Properties of fresh concrete

The fresh concrete test results are given in Table V. High-range water-reducing admixture dosage slightly increased when SG was used, and slightly decreased when SRA was used. With the surface-active function of SRA, the Lv of concrete using SRA was slightly larger than other concretes. The Lv of concrete using SG was low. The difference of setting time due to the aggregate difference and SRA presence was limited.

Table V. Properties of fresh concrete.

Symbol	Admixture	Dosage (C×%)	Slump flow (cm)	Lv (cm/s)	Air content (%)	Concrete temp. (°C)	Setting time (hours)	
							initial	final
30N	HP	1.20	60.0	9.4	3.2	21	5.4	7.6
30N-SG	HP	1.35	63.0	7.2	4.3	21	6.2	8.6
30N-LG	HP	1.20	65.0	9.1	3.6	21	5.8	8.3
30N-SR	HP	1.15	64.5	10.7	3.4	21	5.5	7.9
30N-All	HP	1.20	61.0	8.2	3.1	22	6.3	8.8
25M	HP	1.25	63.0	9.1	3.0	21	6	8.4
25M-SG	HP	1.25	63.5	7.4	3.9	22	6.3	8.9
25M-LG	HP	1.25	63.5	7.7	3.8	22	5.7	8.1
25M-SR	HP	1.15	69.5	9.7	2.5	22	6.4	8.9
25M-All	HP	1.15	67.0	9.0	3.4	22	6.6	9.4
15S	SSP	1.20	70.0	6.2	2.3	23	6.5	9.0
15S-SG	SSP	1.20	67.0	6.0	2.7	23	6.2	8.5
15S-SR	SSP	1.15	68.0	7.5	1.9	23	7.3	10.1
15S-SR-SG	SSP	1.10	71.5	7.7	1.6	23	7.2	9.8

Properties of hardened concrete

Drying shrinkage. Table VI shows the summary of shrinkage test results and Figure 3 shows the changes in the drying shrinkage strain versus time. Concretes using SG (30N-SG, 25M-SG and 15S-SG) reduced the drying shrinkage strain by approximately 7% to 31% at the age of 189 days. The drying shrinkage-reducing mechanism of SG is considered as follows. (1) Microstructure on the slag aggregate surface was densified with hydration reaction of latent hydraulicity. (2) Because the water absorption rate of SG is small, the water amount in the concrete using SG was low and the drying mass loss was therefore limited. Concretes using LG (30N-LG, 25M-LG) reduced the drying shrinkage strain by approximately 14% to 16% at the age of 189 days. The drying shrinkage-reducing mechanism of LG is considered as follows. (1) Calcium carbo-aluminate produced by the reaction of cement and limestone took in the water as crystal water. (2) Microstructure on the limestone surface was densified with hydration and micropore amount decreased. Concretes using SRA (30N-SR, 25M-SR and 15S-SR) reduced the drying shrinkage strain by approximately 23% to 32% at the age of 189 days. The drying shrinkage-reducing mechanism of SRA is considered that SRA reduces surface tension of water in the capillary void and the capillary tension is reduced. Concretes using SG, LG and SRA (30N-All, 25M-All) and using SG and SRA (15S-SR-SG) reduced the drying shrinkage strain by approximately 32% to 60% at 189 days. These results indicate that the use of these materials in combination can reduce drying shrinkage more effectively because their shrinkage-reducing mechanisms were individually different.

Table VI. Summary of shrinkage test results.

Symbol	Drying shrinkage		Autogenous shrinkage			Total shrinkage (1)+(2)	
	(1) (189 days)		(2) (7 days)	(182 days)		(182 days)	
	Strain ($\times 10^{-6}$)	Percentage of shrinkage reduction (%)	Strain ($\times 10^{-6}$)	Strain ($\times 10^{-6}$)	Percentage of shrinkage reduction (%)	Strain ($\times 10^{-6}$)	Percentage of shrinkage reduction (%)
30N	525	-	202	362	-	727	-
30N-SG	363	30.9	102	250	30.9	465	36
30N-LG	442	15.8	157	285	21.3	599	17.6
30N-SR	359	31.6	110	226	37.6	469	35.5
30N-All	208	60.4	95	172	52.5	303	58.3
25M	432	-	178	244	-	610	-
25M-SG	330	23.6	158	216	11.5	488	20
25M-LG	373	13.7	146	190	22.1	519	14.9
25M-SR	282	34.7	71	104	57.4	353	42.1
25M-All	195	54.9	43	88	63.9	238	61
15S	520	-	403	692	-	923	-
15S-SG	486	6.5	314	575	16.9	800	13.3
15S-SR	400	23.1	205	402	41.9	605	34.5
15S-SR-SG	355	31.7	152	331	52.2	507	45.1

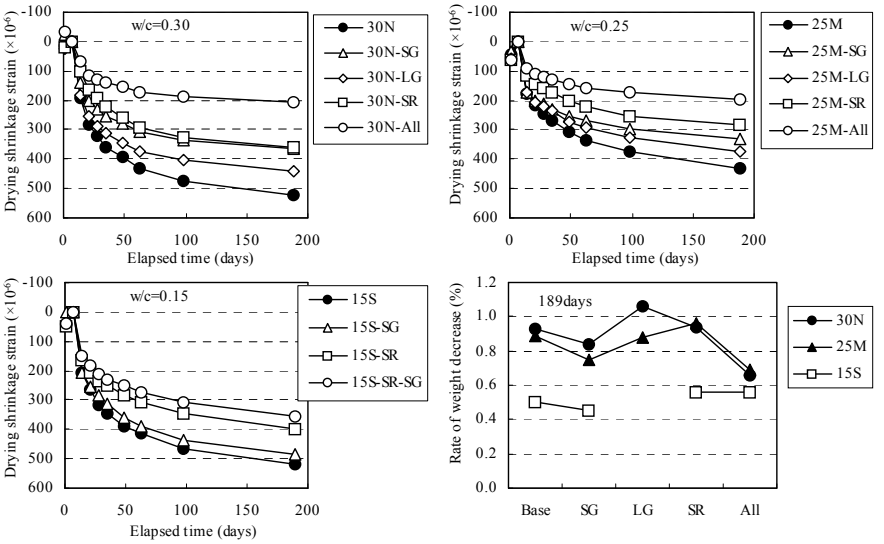

Figure 3. Drying shrinkage strain versus time.

Autogenous shrinkage. Table VI shows the summary of shrinkage test results and Figure 4 shows the changes in the autogenous shrinkage strain versus time. Concretes using SG (30N-SG, 25M-SG and 15S-SG) reduced the autogenous strain by approximately 17% to 31% at the age of 182 days. Concretes using LG (30N-LG, 25M-LG and 15S-LG) reduced the autogenous shrinkage strain by approximately 21% to 22% at the age of 182 days. Concretes using SRA (30N-SR, 25M-SR and 15S-SR) reduced the autogenous shrinkage strain by approximately 38% to 57% at the age of 182 days. Concretes using SG, LG and SRA (30N-All, 25M-All) and using SG and SRA (15S-SR-SG) reduced the autogenous shrinkage strain by approximately 52% to 64% at the age of 182 days. These results indicate that the use of these materials in combination can reduce autogenous shrinkage more effectively. It is considered that the autogenous shrinkage-reducing mechanism of SG and LG is the same as the drying shrinkage-reducing mechanism of SG and LG. Further investigation is required to elucidate the mechanism.

Total shrinkage. Figure 5 shows the total shrinkage strain and percentage of shrinkage reduction. In this paper, the total shrinkage strain is defined as the sum of the autogenous shrinkage strain at the age of 7 days and the drying shrinkage strain at the age of 189 days. The total shrinkage strain became larger according to *w/c* of 0.15, 0.30, 0.25 and the shrinkage-reducing effect increased according to SRA, SG, and LG within the limits of this study. Concretes using SG, LG and SRA (30N-All, 25M-All) and using SG and SRA (15S-SR-SG) reduced the total shrinkage strain by approximately 400×10^{-6} and showed the shrinkage-reducing effect of approximately 45% to 61%.

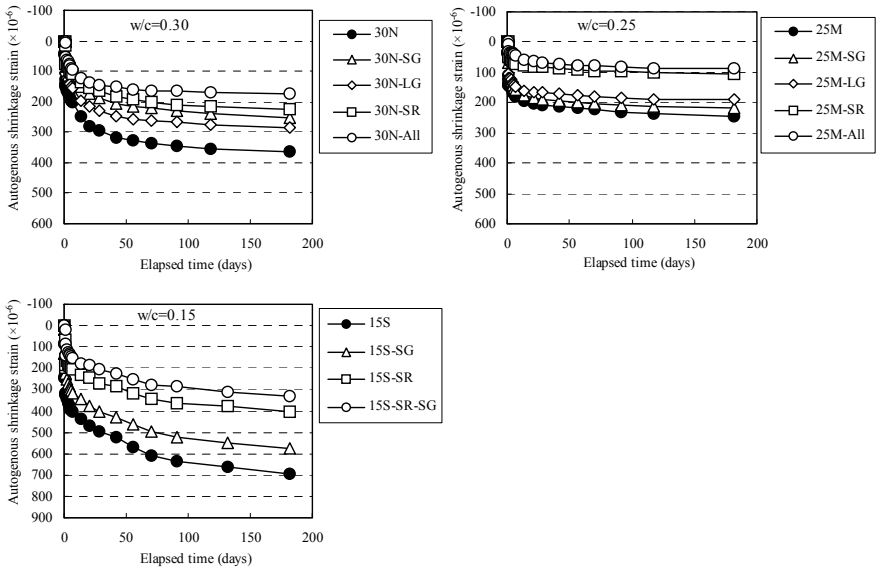

Figure 4. Autogenous shrinkage strain versus time.

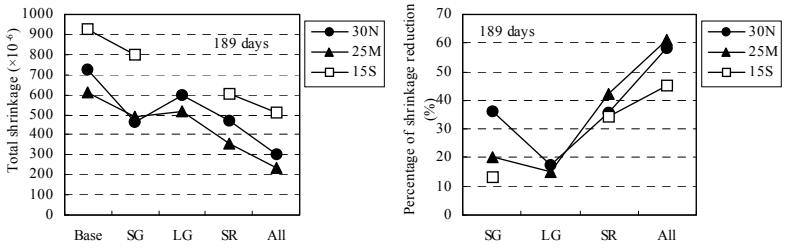

Figure 5. Total shrinkage strain and percentage of shrinkage reduction at 189 days
Note: Base: 30N, 25M and 15S, SG: 30N-SG, 25M-SG and 15S-SG,
LG: 30N-LG and 25M-LG, All: 30N-All, 25M-All and 15S-SR-SG.

Compressive strength. Figure 6 shows the compression test results. Although compressive strengths of concrete using BFS and/or SRA at the age of 7 days were slightly lower than that of standard concretes (30N, 25M, 15S), the difference became smaller at the long term strength. The concretes using limestone aggregate showed about the same compressive strength development as standard concrete (30N, 25M). All concretes achieved strengths equivalent to the target strength by the age of 7, 28, or 91 days.

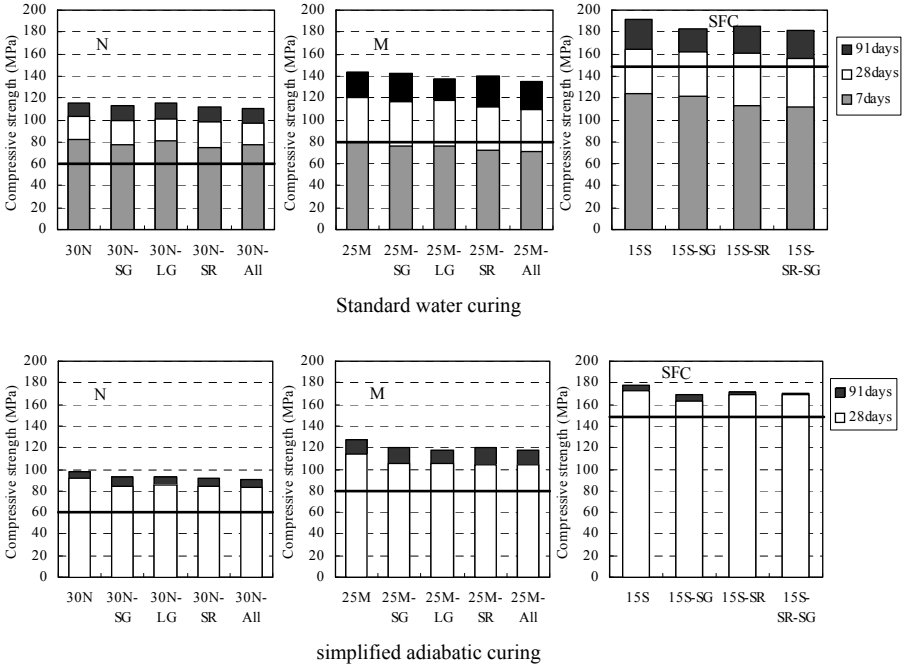

Figure 6. Compressive strength development.

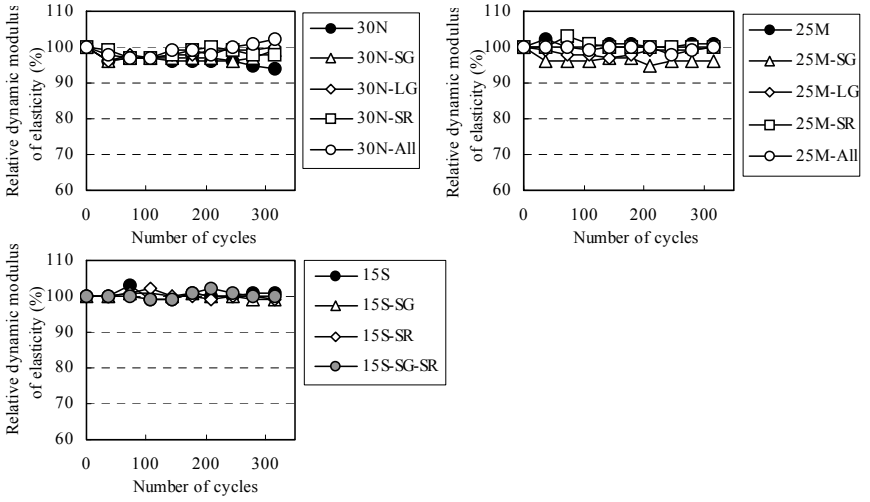

Figure 7. Results of freezing and thawing test.

Freezing and thawing resistance. Figure 7 gives the results of the freezing and thawing tests. All concrete mixtures showed sufficient resistance with relative dynamic modulus of elasticity above 90% after 300 cycles of freezing and thawing.

Conclusions

Three kinds of shrinkage-reducing concrete materials, SRA, BFS and limestone aggregate to high-strength SCC with a target strength of 60 to 150 MPa and experimentally examined their effectiveness. The following are the obtained conclusions:

- Properties of fresh concrete using SG, LG and SRA were almost same as those of standard concrete using S, G.
- SG, LG and SRA showed drying shrinkage-reducing effect of approximately 7% to 32% when they were used separately, and showed a reduction in the shrinkage of approximately 32% to 60% when they were used all together.
- SG, LG and SRA showed autogenous shrinkage-reducing effect of approximately 17% to 57% when they were used separately, and showed a reduction in the shrinkage of approximately 52% to 64% when they were used all together.
- Concretes using SG, LG and SRA in combination reduced the total shrinkage strain by approximately 400×10^{-6} and showed the shrinkage-reducing effect of approximately 45% to 61%. These results indicate that the use of these materials in combination can reduce total shrinkage more effectively.
- Although compressive strengths of concrete using BFS and/or SRA at the age of 7 days were slightly lower than that of standard concretes, the difference became smaller at the long term strength. The concretes using limestone aggregate showed about the same compressive strength development as standard concrete.
- All concrete mixtures showed sufficient resistance with relative dynamic modulus of elasticity above 90% after 300 cycles of freezing and thawing.
- Consequently, it is expected that the application of shrinkage-reducing admixture, blast furnace slag aggregate and limestone aggregate could help produce low shrinkage high-strength self-compacting concrete.

References

[1] Persson, B. (2001), A comparison between mechanical properties of self-compacting concrete and the corresponding properties of normal concrete, *Cement and Concrete Research*, vol. 31, n. 3, pp. 413-420.

[2] Persson, B. (2002), Eight-year exploration of shrinkage in high-performance concrete, *Cement and Concrete Research*, vol. 32, n. 8, pp. 1229-1237.

[3] Folliard, K.J. and Berke. N.S. (1997), Properties of high-performance concrete containing shrinkage-reducing admixture, *Cement and Concrete Research*, vol. 27, n. 9, pp. 1357-1364.

[4] Berke, N.S. and Li, L. (2003), Effectiveness of shrinkage reducing admixtures inreducing total shrinkage, *Advances in Cement and Concrete*, Proceedings of a conference held at Copper Mountain, Colorado, USA, pp. 101-109.

[5] Saito, K., Kinoshita, M., Ihara, T. and Yoshizawa, C. (2009), Performance of high durability concrete using blast furnace slag aggregate, *Proceedings of JCI*, vol. 31, n. 1, pp. 139-144 (in Japanese).

[6] Bui, V.K., and Montgomery, D. (1999), Drying shrinkage of self-compacting concrete containing milled limestone, SCC RILEM publications S.A.R.L. Stokholm, Sweden, pp. 227-239.

[7] Kinoshita, M., Suzuki, T., Soeda, K. and Nawa, T. (1997), Properties of methacrylic water-soluble polymer as a superplasticizer for ultra high-strength concrete, *Superplasticizers and Other Chemical Admixtures in Concrete,* Proceedings of the Fifth CANMET/ACI International conference, Rome, Italy, (SP-173), pp. 143-162.

[8] Mitsui, K., Yonezawa, T., Kinoshita, M. and Shimono, T. (1994), Application of a new superplasticizer for ultra high-strength concrete. Superplasticizers and other chemical admixtures in concrete. Proceedings of the Fourth CANMET/ACI International Conference, Montreal, Canada, 1994 (SP-148), pp. 27-46.

[9] JCI Committee (2002), Report by Autogenous Shrinkage of Concrete Committee, Japan Concrete Institute, pp. 51-54.

Plastic Shrinkage Evaluation of Self-Consolidating Concrete as Repair Materials Based on Restrained and Free Strain Measurements

Parviz Ghoddousi[1] and Ali Akbar Shirzadi Javid[2]

[1] Civil Engineering, Iran University of Science and Technology (IUST), Iran
[2] Construction Engineering and Management, IUST, Iran

Abstract. One of the most challenging problems that can confront a repair engineer is that the completed structure is a monolithic mass that is free from cracks, especially with regard to the plastic shrinkage cracking in concrete flatwork. The more roughness in the surface of substrate, there will be more bond strength between substrate and repair overlay. But, meanwhile, the more roughness, more restraints induced in overlay, which during shrinkage, tensile stresses will be generated in repair materials. The results of investigation reported herein concern the effect of the type of repair materials on free and restrained plastic shrinkage properties. Four types of repair materials were used in this work are plane self-consolidating concrete (SCC), SCC containing silica fume (SF), SCC containing SF and latex (Styrene Butadiene Rubber), and SCC containing SF, latex, and fiber. To roughen the surface of substrate base, dents were used to provide restraints. The panels were subjected to severe combination of wind, temperature, and relative humidity. The test program includes: settlement strain, free and restrained shrinkage strain, evaporation and bleeding rates, and crack characteristic measurements. The results show that, while the rates of evaporation and bleeding affect shrinkage, it is over shadowed by other factors, such as fiber type, binder type and use of latex. The results show that, a significant improvement was observed for SCC with latex and fiber exhibiting the lowest plastic settlement and shrinkage strains, as well as crack area and longest time to first cracking. The plane SCC exhibited almost twice the settlement and shrinkage strains than SCC with latex and fiber.

Introduction

Recently, SCC has also been used for repair of concrete infrastructure where it is used to ensure proper filling of restricted areas including the bottom sides of structural beams and girders and column and wall elements that can necessitate the filling narrow sections with restricted access to placement and consolidation [1].

K.H. Khayat and D. Feys (eds.), *Design, Production and Placement of Self-Consolidating Concrete*, RILEM Bookseries 1,
DOI 10.1007/978-90-481-9664-7_25, © RILEM 2010

But one of the most important problems of concern in hot climate is plastic behaviour of concrete especially used in repair. The climate conditions in the hot and arid areas of the world are considered to be very aggressive for concrete. The sudden and continuous variations in temperature and humidity accelerate the cracking of concrete due to expansion/contraction [2]. Therefore, plastic shrinkage is a primary problem after placement of concrete in hot weather condition. When water evaporates from the surface of plastic concrete in a higher rate than bleeding water, the concrete is prone to cracking by plastic shrinkage. The free plastic shrinkage does not induce cracking, but restrained shrinkage provided by the surface of substrate develops tensile stresses in repair concrete and hence resulting in cracks on the surface of concrete. Therefore, the combination of environmental conditions, restraint conditions, and concrete itself affects plastic shrinkage performance of concrete.

When only the concrete mixture is concerned there are many factors increasing or decreasing plastic shrinkage. The factors, such as mixture design, binder type, aggregate content, fiber, and chemical admixtures [1-6]. The studies showed that, addition of fibers to the concrete are beneficial for limiting plastic shrinkage cracking. Branch et al. [6] found that the crack area reduced between 40% and 85% for the inclusion of two different types of polypropylene fibers at 0.1% by volume in a high strength concrete. Ma et al. [7] found that with fiber addition the number of larger cracks decreases, but the finer cracks increase. The initial cracking time can be delayed for more than 30 min. Based on probability theory, they concluded that the order of effectiveness for each variable on plastic shrinkage cracking, is fiber content > temperature > relative humidity. Wongtanakitcharoen and Naaman [8] conducted experimental investigations on the effect of different fibers such as carbon fibers on plastic shrinkage. They observed that fiber-reinforced concretes behave similarly to plain concrete in the first few hours after casting. However, the addition of fibers to fresh concrete, to 0.4% by volume, led overall to an average 34% decrease in free shrinkage strain at 24 hr age. At 0.1% volume fraction the average decrease was about 30%. They noted that, an increase in fiber volume faction from 0.1% to 0.4% does not lead to a significant improvement. They have also found that the addition of fibers does not have any influence on the cumulative loss of water from fresh concrete by evaporation. It was concluded that, fibers do not play some role as bleeding channels.

As already mentioned, when a concrete is on a debonded surface and it has free movement, concrete does not crack. But if shrinkage of concrete is restrained, concrete becomes susceptible to cracking. Meanwhile, the strains usually measured are different from restrained strain. In fact, the actual strain, which is measured experimentally, does not give true picture of shrinkage behaviour. But, the calculated restrained strain is related to the crack parameters, as mentioned by the authors in another study [9]. By subtracting free strain, ε_{fc}, by measured strain, ε_{mc}, the restrained strain, ε_{rc}, is calculated as follows:

$$\varepsilon_{rc} = \varepsilon_{fc} - \varepsilon_{mc} \quad (1)$$

where ε_{rc} is restrained strain, ε_{fc} is free strain (debonded), and ε_{mc} is measured strain. The restrained strain can be expressed in terms of restraint factor as:

$$\varepsilon_{rc} = R\,\varepsilon_{fc} \quad (2)$$

or

$$\varepsilon_{mc} = (1-R)\,\varepsilon_{fc} \quad (3)$$

If there is free movement of the member R=0, and $\varepsilon_{mc} = \varepsilon_{fc}$. For a fully restrained member, R=1 and hence $\varepsilon_{rc} = \varepsilon_{fc}$. There are, however, few studies on plastic shrinkage of self-consolidating concrete [5], and behavior of SCC as repair material [1, 3].

The purpose of the present study is to investigate experimentally the effects of fiber, acrylic latex, and silica fume on restrained strain and plastic settlement and restrained plastic shrinkage cracking.

Experimental Program

Mixture proportioning

In the present study for repair concretes, Portland cement Type II was used. River sand with a specific gravity of 2.60 was used as fine aggregate. Crushed limestone with maximum size of 9.5 mm and specific gravity of 2.68 was used as coarse aggregate. The grading curve according to national standard is used, which is mixture gradation (sand and coarse aggregate). This includes four gradings with the $C_{9.5}$ grading having highest proportion of fine aggregate used. Before choosing the grading curve and the amount of powder, many trial mixtures with different grading curves and amount of powders were made. The results showed that the grading curve $C_{9.5}$ combined with 212 kg/m^3 powder resulted in enhanced SCC properties. In other words, it was found that addition of more amount of powder to concrete can improve their fluidity and stability. Figure 1 shows the grading curve for repair concretes. Silica fume (SF) and limestone powder (LP) with Blaine fineness of 410 m^2/kg were used. In all mixtures, a polycarboxylate high-range water reducing admixture (HRWR) was used; also the Styrene Butadiene Rubber (SBR) was used as latex-modifier. Commercial straight polypropylene fibers of 19 mm in length were employed. The specific gravity of the fibers was 0.90. Four types of the repair concretes were used in this work are plane self-consolidating concrete (SCC), SCC containing silica fume (SF), SCC containing SF and latex and SCC containing SF, Latex and fiber.

Table I. The mixture proportions and 28-day compressive strength.

Mixture	Quantities (kg/m^3)				HRWR (% cement)	Fiber (% Volume)	28-day Compressive Strength (MPa)
	PC	SF	*w/cm*	LP			
S	400	-	0.45	212	0.6	-	43
SS	368	32	0.45	212	0.6	-	48
SSL	368	32	0.45	212	0.6	-	30
SSLF	368	32	0.45	212	0.8	0.2	31

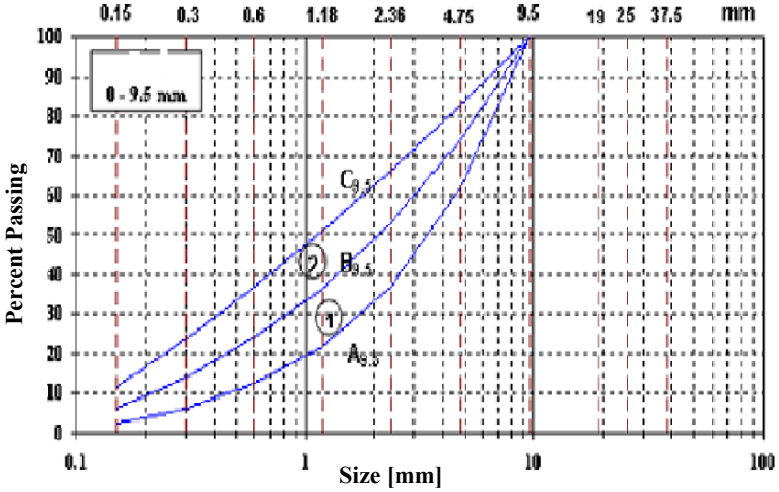

Figure 1. The grading curve for repair concretes.

The mixture proportions of four self-consolidating repair concrete (SCRC) are given in Table I. Water-to-cementitious materials ratio was 0.45 for all the mixtures. The substrate was ordinary concrete made with 350 kg/m^3 ordinary Portland cement, 710 kg/m^3 fine aggregate, and 1102 kg/m^3 coarse aggregate. Its compressive strength at 28 day was 22 MPa and water-to-cement ratio was 0.55. The substrate base was 600×400 mm with 100 mm thickness. To roughen the surface of the other substrate bases, dents provided while the concrete were in fresh state. The cross section of dents was semi-circular. These dents were made to provide restraint. Figure 2 shows substrate with dents.

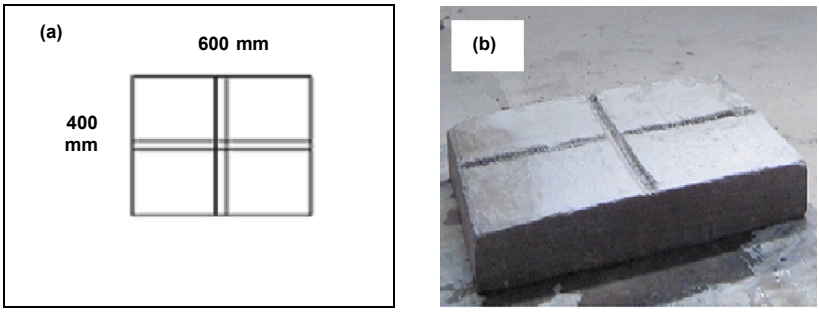

Figure 2. a) Plan view of substrate slab with dents b) with substrate slab.

Test procedure

Environmental conditions. The exposure condition of the slabs was controlled to simulate hot weather. Hence, a chamber was made, which equipped with heater and fan. The fan generated wind velocity of 3 km/h, and the temperature was maintained at 40˚C. The relative humidity (RH) of the chamber was same as laboratory RH, which was between 30% and 35%. Since, differential shrinkage between substrate concrete and repair concrete may have effect on the testing results; the substrate bases were cured using wet burlap and plastic sheet for three months prior to overlay application. On the day of the test, repair concrete poured over the substrate base and finished with a steel trowel. Then, the whole base and overlay transferred to the exposure chamber.

Fresh properties. The Slump flow, T_{50} time, V-funnel, L-box, and J-ring tests and visual stability indices were performed in accordance with PCI [10].

Bleeding. To monitor the rate of evaporation for each type of concrete mixture, one panel was placed adjacent to the testing slab and weighted at each 20 minutes. A pan of water was also placed and weighted to monitor rate of evaporation from a water surface. The rate of bleeding was measured according to ASTM C 232 [11]. In order to reduce the evaporation as much as possible, the testing panels containing different repair concretes were kept in the control room with RH of 100% and 40˚C temperature.

Plastic shrinkage. The shrinkage was measured horizontal displacement of two plastic studs which were specially designed and made for this purpose. The bases of studs were embedded into concrete surface which were 300 mm apart. The reflection of laser beam on the tips of studs could be observed as two black Points on a wall, in front of the slab. The displacement of the studs due to deformation of concrete cannot be measured by ordinary tools. Therefore, to magnifying the

movement of the studs, laser beam was used. At desire time intervals, the distance of two points on the wall was measured. The test set up is shown in Figure 3.

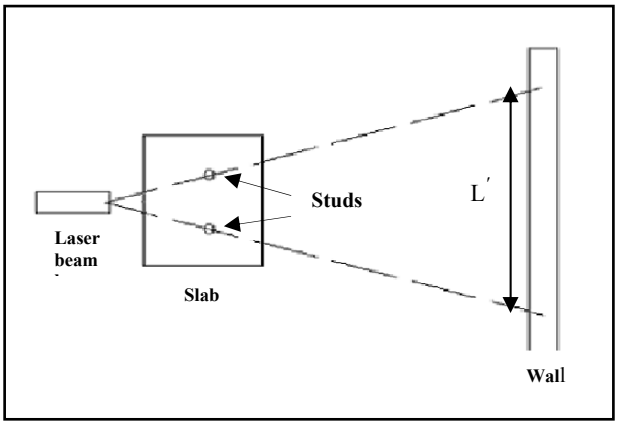

Figure 3. Test setup to measure shrinkage.

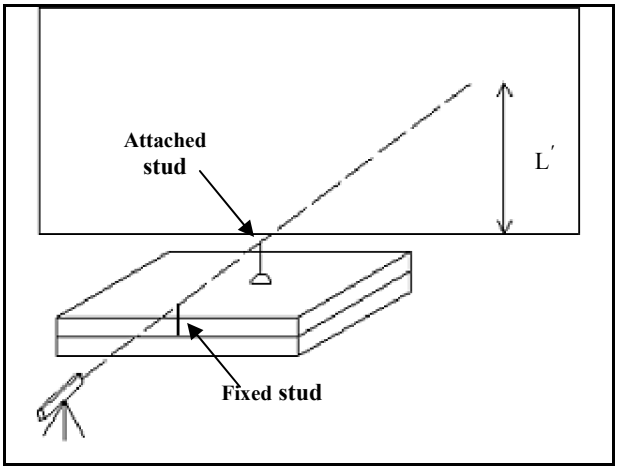

Figure 4. Test setup to measure settlement.

By considering, the distance of the wall from studs, the horizontal deformation as plastic shrinkage (measured strain) is calculated by following equation:

$$\varepsilon = (L'_0 - L'_t)/L'_0 \tag{4}$$

where ε is plastic shrinkage strain, L'_0 is initial magnified distance on the wall and L'_t is magnified distance on the wall at desire time intervals.

Plastic settlement. The test arrangement for measurement of settlement was similar to shrinkage set up. Except that, one stud embedded into concrete, and the other stud attached on the top of the mould. During concrete settlement, the embedded stud moves downward, and the stud attached on the top of the mould is considered as fixed point. Then, the distance between the two studs can be measured by laser beam as mentioned for shrinkage measurement. The test set up is shown in Figure 4.

Crack parameters

During the course of plastic shrinkage tests, crack width and crack length were recorded at every 20 min. interval. Crack width was measured using hand-held microscope to an accuracy of 0.02 mm. The initial cracking time was also recorded. Then, the crack parameters such as total length, total crack area, maximum and average crack width were determined. To calculate the mean crack width a total of 10 arbitrary points was chosen along the crack profile.

Results and Discussion

Properties of fresh concrete

The results of fresh SCC properties for all types of the mixtures are given in Table II. It can be seen that, the addition of fibers (SSLF) increased the J-ring value, and decreased the h_2/h_1, in L-box test. The slump flow also reduced due to fiber inclusion. However, the slump flow value of 610 mm for SSLF can be considered in the range of SCC.

Table II. Fresh concrete properties.

Mixture	Slump flow		V-funnel (s)	L – box (h_2 / h_1)	J – ring (mm)	VSI
	Spread (mm)	T_{50} (s)				
S	730	3.0	3.5	1.00	6	1
SS	620	1.6	3.7	0.96	7	1
SSL	760	1.2	2.7	0.90	9	2
SSLF	610	2.5	6	0.81	15	2

Figure 5 shows the measurement results of evaporation rate and bleeding rates for four SCC mixtures. The environmental conditions were chosen so that the evaporation rate from the water pan exceeds 1.0 kg/m^2/hr. The mixture containing SF exhibited the minimum rate of bleeding, which can be considered as nearly zero bleeding. Comparing bleeding rate of ‘SSL’ and ‘SSLF’ mixture indicated that addition of fiber to the mixture significantly reduced the rate of bleeding. This is

not in agreement of the results found by Wongtanakitcharoen and Naaman [8]. However, more research is needed on this subject.

Plastic shrinkage

A comparison is made in Figure 6 of the free shrinkage strains of concrete mixtures. The term free shrinkage used in this study is defined as the shrinkage of the debonded overlay induced by plastic sheets. It is clear that Latex reduced the free shrinkage. The difference between mixture with silica fume (SS) and mixture with silica fume and Latex (SSL) is about 2000 μs at maximum strain. But the mixture with fibers showed the lowest shrinkage strains. The strains of SS mixture and SSLF mixture show more than 5000 μs difference. In another words, the results imply that, the addition of fibers can reduce significantly the free shrinkage. These results are in consistency with literature advocating the shrinkage reduction of fibers [8]. Figure 7 shows the measurement results of the shrinkage of different concrete at the same restraint. Inspection of Figure 7 reveals that there is significant concrete type effect on the measured shrinkage. The highest increase in measured strain belonged to the silica fume SCC (SS).

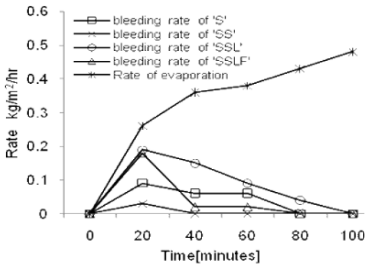

Figure 5. Rate of bleeding for different concrete mixtures and rate of evaporation.

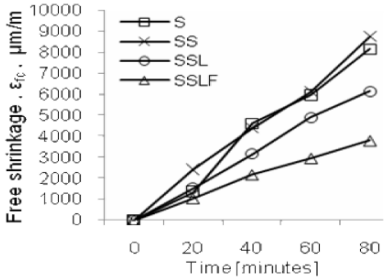

Figure 6. Free shrinkage strain vs. time of testing for different concretes.

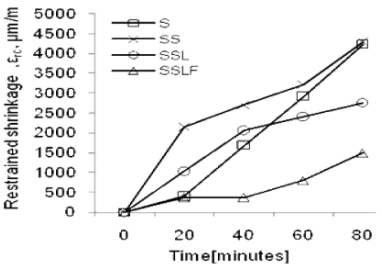

Figure 7. Measured shrinkage strain vs. time of testing for different concretes.

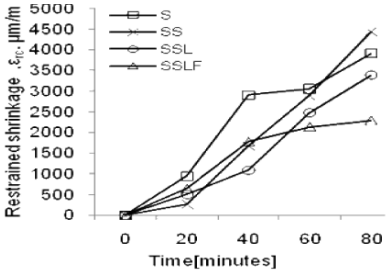

Figure 8. Restrained shrinkage strain vs. time of testing for different concretes.

This may be attributed to the lack of bleeding in the mixture. The lowest strain belongs to SSLF mixture. A similar trend was exhibited in free shrinkage strains (Figure 6). According to the Eqn. (1), the restrained shrinkage is given by:

$$\varepsilon_{rc} = \varepsilon_{fc} - \varepsilon_{mc} \tag{5}$$

The calculated values of the restrained strains are plotted in Figure 8 for the different concrete studied. Inspection of Figures 6-8 reveals that, the free shrinkage (ε_{fc}), measured shrinkage (ε_{mc}), and restrained shrinkage (ε_{rc}) are minimal for SSLF mixture and maximum for SS mixture.

Plastic settlement

In Figure 9 plastic settlement for different concretes are plotted against time. All curves have the same trend with rapid increase in strains and then settlement rates are almost constant after the maximum strains are reached. This founding is in agreement with results of Hammer [4], and Turcry and Loukili [5]. No significant difference is observed between the plastic settlement of concrete SS containing silica fume and concrete S without silica fume. Similar behaviour was observed by Hammer [4]. The final settlement values for concretes S and SS were about 6000 μs while the settlements for concrete SSL and SSLF were about 3000 μs. These results indicate that the bleeding rate is not the only controlling factor for settlement, but other factors like composition of the mixture play important role. This result is not in agreement with Turcry and Loukili [5], who stated that difference in settlement between two types of concrete is mainly due to the difference in bleeding. According to Turcry and Loukili [5], at phase 1, a high settlement rate is recorded and at phase 2, volumetric contraction is transmitted horizontally little by little.

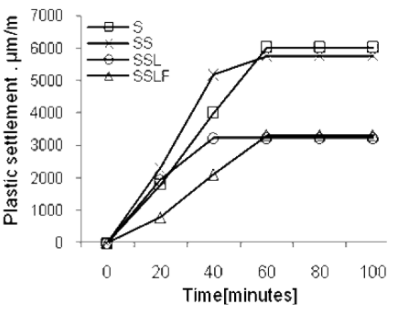

Figure 9. Plastic settlement vs. time for different concretes.

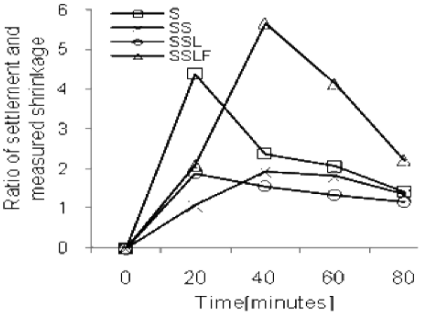

Figure 10. Ratio of plastic settlement and measured shrinkage (ε_{mc}).

To find out this trend for the results of this study, the ratio between settlement strains and measured shrinkage strains (ε_{mc}) for different concrete at time intervals are calculated. Results from this study as shown in Figure 10 confirm that, during one hour after placement of concrete, the volumetric contraction is mainly due to high settlement rate. But, after about one hour, volumetric contraction is transmitted horizontally. Therefore, the ratio of settlement and shrinkage is decreased after one hour.

Crack parameters

Table III compares the crack parameters of different concretes at their final state. None of the concretes were cracked when plastic sheet provided between the repair layer and substrate surface (fully free shrinkage). These results are not presented in the table. The repair layer made of 'SSLF' mixture also did not show any sign of crack during the time of testing. The minimum crack initiation time and highest number of crack and average crack width belong to concrete with silica fume (SS). Addition of latex to concrete mixture (SSL) improved crack characteristic substantially. The crack initiation time increased and number of cracks and also crack length decreased significantly for 'SSL' concrete comparing to 'S' and 'SS' concretes. This cannot be attributed to forming of polymeric network, because the mixture still is in plastic state, and such network can be formed when the concrete is in dry state. Therefore, there is a need for more investigation on this subject. As mentioned earlier, it was found that, addition of silica fume makes the concrete more susceptible to plastic shrinkage cracking. Similar results were found by Ghoddousi et al. [12] and Samman et al. [13]. The authors attributed the cracking tendency of silica fume concretes to rate of evaporation. But cracking tendency cannot be attributed solely on rate of evaporation. Based on the results in this study, the rate of evaporation of 'SSLF' concrete was less than 'S' and 'SSL' concrete (Figure 5), but no crack was observed in 'SSLF' concrete. On contrary, Al-Amoudi et al. [2] did not observe in the silica fume concrete slab. The authors pointed out that, even though the plastic shrinkage strain in the silica fume concrete slabs was more than that in the plain concrete slabs, they were not high enough to cause cracking. The authors attributed the result to threshold value of plastic shrinkage strain that could result in cracking which is 1100 μs, and plastic shrinkage strain in the silica fume concrete was less than 800 μs**.** But, inspection of Table III reveals that all concretes were cracked exhibited strain more than 3000 μs, with highest strain (more than 4000 μs) which belongs to silica fume concrete. The lowest strain (lower than 2500 μs) belongs to 'SSLF' concrete which did not divulge crack. This conclusion can be seen clearly in Figure 11.

Table III. Crack parameters for different repair concretes.

Concrete type	Crack initiation time (min)	No. of cracks	Crack length (mm)	Average crack width (mm)	Total cracking area (mm^2)
S	95	6	760	0.3	2533
SS	85	9	890	0.54	1648
SSL	120	2	340	0.31	1096
SSLF	-	-	-	-	-

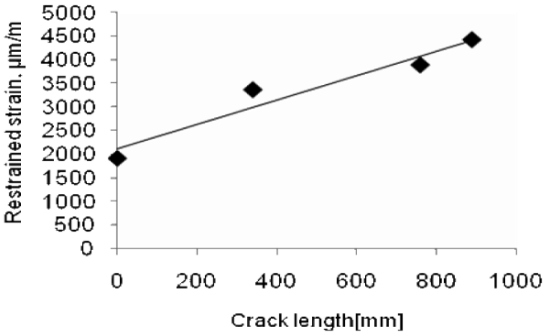

Figure 11. Correlation between restrained strain and crack length for different concretes.

Conclusions

Based on the results obtained in this study, the following conclusions can be stated:

- One should be distinguished between measured deformation of restrained shrinkage, ε_{mc}, and restrained strain, ε_{rc}. In fact, ε_{mc} is measured experimentally does not give true picture of shrinkage. But, there is a close correlation between ε_{rc} and shrinkage behaviour of concrete including crack parameters. ε_{rc} is the difference between the free shrinkage, ε_{fc} , and the measured shrinkage, ε_{mc}.
- Restrained plastic shrinkage strain not only affected by rate of bleeding, but restraint conditions, silica fume, styrene butadiene rubber (SBR) latex, and fiber play significant roles. Concrete made with silica fume, styrene butadiene rubber (SBR) Latex, and fiber play significant roles. Concrete

made with silica fume exhibited highest restrained strain (4430 μs) and concrete made with silica fume, fiber and latex showed lowest restrained strain (1920 μs). The same trends observed in plastic settlement measurements.

- There was no direct correlation between rate of evaporation and cracking characteristic. No crack was observed for concrete made with fiber (SSLF) even with less rate of evaporation comparing to concrete without fiber (SSL). Crack initiation time was shortest for concrete made with silica fume, SS (85 minutes), and longest for concrete made with latex and silica fume, SSL (120 minutes). Similar results were found from number of cracks, and crack length point of view.
- There was significant correlation between restrained strain values and crack length measurements.

References

[1] Khayat, K.H. and Hwang, S.D. (2005), Durability of self-consolidating concrete used in repair applications, Proceedings of the international symposium on durability of concrete, Alejandro, D. (Ed.), FIC-UANL academic group on concrete technology, Mexico, pp. 121-141.

[2] Al-Amoudi, O.S.B., Moslehuddin, M., Shameem M. and Ibrahim, M. (2007), *Cem. Concr. Compos.*, vol. 29, p. 690.

[3] Hwang, S.D. and Khayat, K.H. (2008), *ACI Mater.* J., vol. 105, n. 5, p. 499.

[4] Hammer, T.A. (2001), *Mater. struct.,* vol. 34, p. 273.

[5] Turcry, P. and Loukili, A. (2006), *ACI Mater. J.*, vol.103, n. 4, p. 272.

[6] Branch, J., Rawling, A., Hannat, D.J. and Mulheron, M. (2002), *Mater. struct.,* vol. 35, p. 189.

[7] Ma, Y., Tan, Z.M. and Wu, K. (2004), *Mater. Struct.*, vol. 37, p. 92.

[8] Wongtanakitcharoen, T. and Naaman, A. (2007), *Mater. Struct.,* vol. 40, p. 289.

[9] Abbasnia, R., Ghoddousi, P. and Ahmadi, J. (2005), *Cem. Concr. Res.* vol. 35, p. 1909.

[10] PCI (2003), Intern guidelines for the use of self-consolidating concrete in precast/prestressed concrete institute member plants, USA.

[11] PCI (2003), Standard test method for bleeding, vol. 4.02, Annual book of ASTM standards, Pennsylvania, USA.

[12] Ghoddousi, P., Raiss Ghasemi, A.M. and Parhizkar, T. (2007), *International Journal of Civil Eng.*, vol. 5, n. 4, p. 266.

[13] Samman, T., Mirza, W.H. and Wafa, F.F. (1996), *ACI Mater. J.,* vol. 93, n. 1, p. 36.

Acceleration of Hardening Kinetics of SCC

François Jacquemot, Patrick Rougeau and Nicolas Flahault

CERIB (Centre d'Etudes et de Recherches de l'Industrie du Béton), Epernon, France

Abstract. Shortening the hardening time of SCC allows the precast concrete industry to respond to its challenge of productivity and extend the scope of application of these materials. Indeed, reducing the elapsed time between mixing fresh concrete and demoulding the concrete products represents a key factor for a faster rotation of the equipment and reduces the global cost of production. The results of the study show that it is possible to accelerate significantly the hardening kinetics of SCC.
Applying an optimized thermal treatment on SCC mixture based on conventional constituents and suitable admixtures enables one to produce concrete that stays workable for 30 minutes and reaches compressive strength up to 25 MPa after 4 hours of curing and more than 80 MPa at 28 days. The influence of the thermal treatment, the use of hardening accelerator and ultrafine particles were evaluated.

Introduction

Self-compacting concretes (SCC) are being more and more widely employed in the precast concrete industry. However, the hardening kinetics of SCC is not always equivalent to the traditional concrete as the admixtures that are necessary to obtain SCC generally present a secondary retarding effect. Shortening the hardening time of SCC would thus allow the precast concrete industry to respond to its challenge of productivity and extend the scope of application of these materials. Indeed, reducing the elapsed time between mixing fresh concrete and demoulding the concrete products represents a key factor for a faster rotation of the equipment and reduces the global cost of production.

One of the aims of the study was to identify among the mix design and the manufacturing process of concrete products the main factors that accelerate the hardening kinetics of SCC. The proposed solutions had to meet the following specifications:

K.H. Khayat and D. Feys (eds.), *Design, Production and Placement of Self-Consolidating Concrete*, RILEM Bookseries 1,
DOI 10.1007/978-90-481-9664-7_26, © RILEM 2010

- in the fresh state, SCC presents a spread at the slump flow test of 70 (± 5) cm, remains homogeneous and workable for at least 30 minutes,
- in the hardened state, the compressive strength of SCC reaches 25 MPa at 4 hours.
- the extra cost of the solution does not exceed 20% compared with traditional SCC.

The method that was developed in this study consists of applying a suitable thermal treatment to SCC designed with available constituents used in the precast concrete industry. The influence of the thermal treatment, the use of hardening accelerator and ultrafine mineral additions were evaluated.

Experimental Procedures and Constituents

The 40 liter concrete batches were produced in a planetary mixer. The aggregates, the fillers and the cement were first dry-mixed. The water (with the accelerating admixture diluted) was then added at the time T0. The superplasticizer was introduced later on until SCC reaches the intended flowability.

When a thermal treatment was applied, the moulds were immediately placed after being filled (T0+15 min), in a thermal chamber until T0+4 hours. The specimens were protected from desiccation using a special wrapping membrane. At the age of 24 hours, the samples were demoulded and stored in a moist curing room (20°C, 100% HR) until the age of 28 days.

The slump-flow test was carried out conforming to prEN 12350-8 [1] at T0+10 min and T0+30 min. Compressive strength tests were carried out on 10 x 10 x 10 cm cubic specimens conforming to EN 12390-3 [2] at T0+4 hours (± 10 min) and at T0+28 days.

The siliceous limestone river aggregate employed were 0/4 mm and 4/12 mm size. Ordinary Portland Cement of type CEM I 52.5 R conforming to Standard EN 197-1 [3] and limestone filler conforming to Standard EN 12620 [4] were used to produce SCC mixtures. Their characteristics are given in Table I.

Table I. Characteristics of the constituents used is the experiments.

	Composition (%)					Specific gravity (g/cm^3)	Blaine specific area (cm^2/g)
	C_3S	C_2S	C_3A	C_4AF	$CaCO_3$		
OPC	68.9	8.9	9.0	7.5		3.1	5180
Limestone filler					98.5	2.7	5300

Two chemical admixtures were employed in SCC mixtures:

- a commercially available polycarboxylate based superplasticizer which presents little retardant effect
- a chloride-free hardening accelerator.

The admixture content in SCC mixtures is expressed as a ratio of the mass of liquid admixture to the mass of cement (%C).

The cost calculation of SCC mixtures was estimated on the basis of the current price in France of their constituents.

Influence of Thermal Treatment

Thermal treatment is widely employed in precast concrete industry. This part of the study aimed to choose the most efficient treatment for a given SCC mixture. Several thermal treatments were tested on the same concrete mixture (SCC1). The mixture proportion of SCC1 is given in Table II.

Because of the objective of compressive strength at very early age, the thermal treatments studied are compared to a traditional thermal treatment. The characteristics of the studied thermal treatments take into account the specifications of standard EN 13369 [5]. They all begin at T0+15 min and include a 15 min pre-treatment phase at 35°C, a temperature increase phase leveling off at 65°C and a natural cooling phase for 30 min. Three thermal treatments are presented in Table III. They differ by the temperature increase (from 12°C/h for TT1 to 20°C/h for TT3) and by the duration of the plateau at 65°C (from 30 min for TT1 to 90 min for TT3).

The concrete specimens were demoulded during the cooling phase. Particular care has to be taken during the cooling phase to avoid cracking by limiting the gradient of temperature between the core and the surface of the concrete products. Table IV shows the compressive strength results for SCC1 at 4 hours.

No cracks were detected on thermally treated concrete specimens and their long term properties did not seem to be affected; their compressive strengths measured at 28 days were equivalent to specimens that did not undergo thermal treatment.

Table II. Mixture proportion of SCC1.

	Cement	Limestone filler	0/4 mm aggregates	4/12 mm aggregates	Superplasti-cizer (%C)	Accelerator (%C)	Water
SCC1	400	180	880	720	0.72	2.00	160

Table III. Characteristics of the thermal treatments studied.

	Duration of pre-treatment at 35°C	Rate of temperature increase	Duration of the plateau at 65°C	Duration of cooling phase	Total duration of the cycle
TT1	15 min	12°C/h	30 min	30 min	225 min
TT2	15 min	15°C/h	60 min	30 min	225 min
TT3	15 min	20°C/h	90 min	30 min	225 min

Table IV. Compressive strength results at 4 hours.

	TT1	TT2	TT3
Compressive strength fc, cube,4 h (MPa)	6.0	21.0	27.0

Table V. Characteristics of hardening accelerators.

	Dry extract	Density	pH	Na_2Oeq	Cl^- ion content
Acc1	61.5%	1.45	6.0	≤ 2.7%	≤ 0.10%
Acc2	39.5%	1.30	9.5	≤ 14.7%	≤ 0.10%
Acc3	51.5%	1.39	4.8	≤ 2.5%	≤ 0.10%

The range of the results shows the considerable influence of thermal treatment on compressive strength and maturity of concrete. The most efficient treatment is TT3, characterized by the highest rate of temperature increase and the longest duration of the plateau at 65°C. Consequently, TT3 was chosen to be applied to the following experiments. The extra cost induced by TT3 is evaluated at +10% when compared to the cost of SCC mixture raw materials.

Influence of Hardening Accelerator

In addition to thermal treatment, the use of hardening accelerators is one of the traditional ways to shorten the hardening time of concrete. The hardening accelerators that were studied are commercially available; they are chloride-free and recommended for producing reinforced concrete. Three accelerators were tested. Their characteristics are presented in Table V. The influence of these three hardening accelerators on workability and compressive strength was evaluated on SCC mixtures exposed to TT3 thermal treatment. The mixture proportion of the tested SCC and the results are given in Tables VI and VII respectively. Raw material extra cost of SCC mixtures is compared to SCC0 mixture.

Table VI. Mixture proportion of SCC designed with different hardening accelerators.

	Cement	Limestone Filler	0/4 mm aggregates	4/12 mm aggregates	Superplasticizer (%C)	Accelerator (%C)			Water
						Acc1	Acc2	Acc3	
SCC0	400	180	880	720	0.76				160
SCC1	400	180	880	720	0.72	2.00			160
SCC2	400	180	880	720	0.73		2.00		160
SCC3	400	180	880	720	0.71			2.00	160

Table VII. Characteristics of SCC designed with different hardening accelerators.

	Spread at slump flow test at T0+10 min (cm)	Spread at slump flow test at T0+30 min (cm)	Compressive strength at T0+4 h (MPa)	Compressive strength at T0+28 days (MPa)	Raw material extra cost (%)
SCC0	67	48	1.5	65.0	0
SCC1	65	43	27.0	83.5	10
SCC2	75	53	12.5	65.5	7
SCC3	75	63	10.0	66.5	11

The range of the results of compressive strength at T0+4 h shows the considerable influence of the choice of the hardening accelerator. With regard to mechanical strength, accelerator Acc1 is the most efficient. Its influence on the loss of workability is notable but it enables SCC to be easily casted during 15 minutes at least, which is generally enough for precast products. Consequently, Acc1 was chosen as accelerator within the following SCC mixtures.

Influence of Different Ultrafine Mineral Additions

Ultrafine mineral additions are particles finer than cement (median diameter D_{50} < 5 µm). When incorporated in concrete, they increase its compactness. Experience [6] shows that ultrafine mineral additions endow concrete with better long term properties in terms of mechanical strength and durability. Generally acting as nucleation site, their influence on hardening time of SCC at very early age was studied.

The ultrafine mineral additions that were employed are:

- LS: limestone microfiller slurry (65% dry material)
- MK: ultrafine metakaolin
- SF: silica fume

The characteristics of these additions are presented in Table VIII.

Table VIII. Characteristics of ultrafine mineral additions.

	Specific gravity (g/cm^3)	BET specific area (m^2/g)	D_{50} (µm)
LS: Limestone filler (slurry)	1.7	5.5	2.0
MK: Ultrafine metakaolin	2.2	19	1.5
SF: Silica fume	2.2	23	-

Table IX. Mixture proportion of SCC designed with ultrafine mineral additions.

	Cement	Limestone Filler	Addition			0/4 mm aggregates	4/12 mm aggregates	Superplast. (%C)	Acc1 (%C)	Water
			LS	MK	SF					
SCC1	400	180				880	720	0.72	2.00	160
SCC4	400	180	50			880	720	0.60	2.00	160
SCC5	400	180		30		880	720	1.03	2.00	160
SCC6	400	180			30	880	720	0.97	2.00	160

Table X. Characteristics of SCC designed with different ultrafine mineral additions.

	Spread at slump flow test at T0+10 min (cm)	Spread at slump flow test at T0+30 min (cm)	Compressive strength at T0+4 h (MPa)	Compressive strength at T0+28 days (MPa)	Raw material extra cost (%)
SCC1	65	43	27.0	83.5	10
SCC4	75	60	25.5	70.5	18
SCC5	73	66	13.0	87.5	24
SCC6	65	51	22.0	81.0	27

The ultrafine addition content in SCC mixtures was defined such that the extra cost of raw material does not exceed about 20% when compared to SCC0 mixture. Table IX shows the mixture proportion of SCC tested to evaluate the influence of ultrafine mineral additions. Results are presented in Table X.

The use of different ultrafine mineral additions was shown to be of minor interest through the tests achieved as they do not seem reactive enough at very early age, even with thermal treatment.

Kinetics of Hardening

The thermal treatment TT3 applied to SCC1 mixture is considered to be the most satisfactory solution in terms of workability, compressive strength and extra cost. Including thermal treatment and raw materials, this solution is about 20% more expensive than a traditional SCC formula. The kinetics of hardening of such a

solution were studied more deeply on three very similar SCC mixtures whose mixture proportion and characteristics are given in Table XI and Table XII respectively. Small variations of mixture proportions lead to significant variations of compressive strength at T0+4h.

The evolution of the compressive strength of these SCC versus time at very early age appears in Figure 1. The evolution of compressive strength at the end of the 4-hour thermal treatment gives an almost linear time-line. A variation of 10 min around T0+4h represents a variation of about 4 MPa of compressive strength. Temperature measurements inside SCC samples show that the amount of heat brought to concrete is an essential parameter influencing hardening kinetics of SCC.

The control of the industrial implementation of such a solution that leads to demould concrete products at very early age requires the monitoring of the mechanical strength by the maturimetry method. The maturimetry method [7-9] enables one to link compressive strength of a concrete to its history of temperature. Temperature can easily be recorded anywhere inside a concrete product by thermocouples. Thus, the suitable duration of thermal treatment necessary to achieve a given compressive strength of a concrete product can be precisely and almost immediately evaluated without mechanical test on concrete samples.

Table XI. Mixture proportion of SCC designed to study kinetics of hardening.

	Cement	Limestone filler	0/4 mm aggregates	4/12 mm aggregates	Superplasticizer (%C)	Acc1 (%C)	Water
SCC7	400	180	880	720	0.72	2.00	160
SCC8	400	180	880	720	0.68	2.00	160
SCC9	400	180	880	720	0.68	2.00	155

Table XII. Characteristics of SCC designed to study kinetics of hardening.

	Spread at slump flow test at T0+10 min (cm)	Spread at slump flow test at T0+30 min (cm)	Compressive strength at T0+4 h (MPa)	Compressive strength at T0+28 days (MPa)	Raw material extra cost (%)
SCC7	71	68	20.0	64.0	10
SCC8	72	58	17.5	81.0	10
SCC9	70	57	26.0	87.5	10

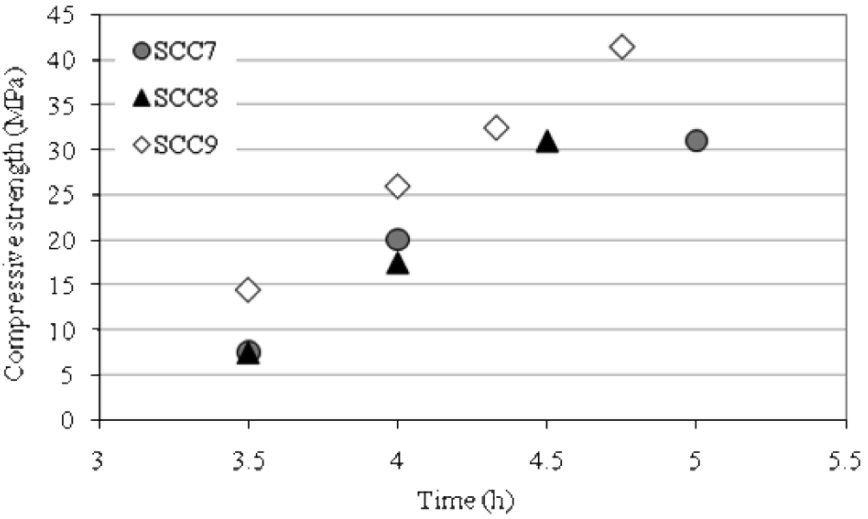

Figure 1. Evolution of compressive strength versus time.

The maturimetry method defines the equivalent time as the time that would need a concrete, that is maintained at a constant reference temperature (20°C), to reach the same maturity as in real conditions. A suitable indicator of the maturity of a concrete is its compressive strength. Thus, the equivalent time (t_{eq}) is a function of real time and temperature, as shown in Eqn. (1).

$$t_{eq} = \int_0^t \exp\left(-\frac{E_a}{R}\left(\frac{1}{T(t)} - \frac{1}{293}\right)\right)dt \quad (1)$$

where: t = the time (s)
E_a = the activation energy of the cement ($J.mol^{-1}$)
R = the perfect gas constant, 8.314 ($J.mol^{-1}.K^{-1}$)
T(t) = the absolute temperature (K)

Temperature was measured in SCC7 and SCC8. Figure 2 shows the evolution of their compressive strength versus equivalent time with E_a/R = 4000 K (value suggested by annex B of Eurocode 2 [10]).

When compared on the real time scale, kinetics of hardening of SCC7 and SCC8 are well distinct (Figure 1), but when compared on the equivalent time scale, their kinetics of hardening are very similar (Figure 2). As the equivalent time integrates the history of temperature of the concrete, one can deduce that the amount of heat

brought to concrete is the essential parameter influencing hardening kinetics of these SCC.

The maturimetry method is shown to provide a simple and efficient way to control thermal treatment length and compressive strength of these SCC for an industrial implementation.

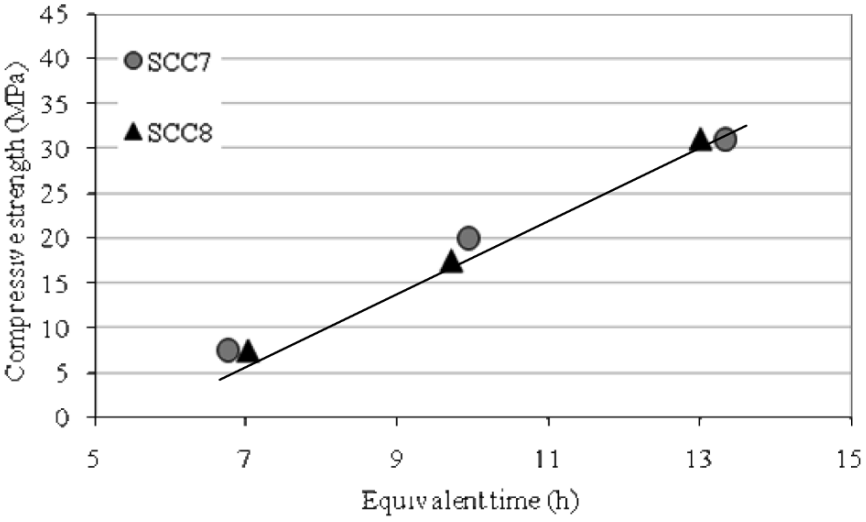

Figure 2. Evolution of compressive strength versus equivalent time.

Conclusions

Applying an optimized thermal treatment on SCC mixture based on conventional constituents and suitable admixtures enables one to produce concrete that stays workable for about 30 minutes and reaches compressive strength up to 25 MPa after 4 hours of curing and more than 80 MPa at 28 days.

Including thermal treatment and raw materials, the proposed solution is only 20% more expensive than traditional SCC that would reach the same properties after one day of natural curing. Thus, by increasing concreting productivity, this solution seems technically and economically attractive.

The control of the industrial implementation of such a solution that leads to demould concrete products at early age needs the mechanical strength to be monitored by the maturimetry method.

References

[1] prEN 12350-8 Testing fresh concrete – Part 8: Slump flow test.
[2] EN 12390-3 Testing hardened concrete – Part 3: Compressive strength of test specimens.
[3] EN 197-1 Cement – Part 1: Composition, specifications and conformity criteria for common cements.
[4] EN 12620 Aggregates for concrete.
[5] EN 13369 Common rules for precast concrete products.
[6] Rougeau, P. and Borys, B. (2004), Making HPC or UHPC products with ultrafines other than silica fume, CERIB Report n°DDP 114 (in French).
[7] Saul, A.G.A. (1951), *Magazine of Concrete Research*, vol. 2, n. 6, pp. 127-140.
[8] Plowman, J.M. (1956), *Magazine of Concrete Research*, vol. 8, n. 22, pp. 13-22.
[9] Carino, N.J. (1984), *Journal of Cement, Concrete, and Aggregates*, vol. 6, n. 2, pp. 61-73.
[10] EN 1992-1-1 Eurocode 2 – Design of concrete structures – Part 1-1: General rules and rules for buildings.

Time Evolution of Properties of SCC Mixtures Produced Using Crushed Limestone Aggregate and High Content of Limestone Filler

Violeta Bokan Bosiljkov[1], David Duh[2], Vlatko Bosiljkov[1] and Roko Zarnic[1]

[1] University of Ljubljana, Faculty of Civil and Geodetic Engineering, Ljubljana, Slovenia
[2] TRC-JUB, Dol pri Ljubljani, Slovenia

Abstract. The paper deals with time-dependent increase of compressive strength, splitting tensile strength and modulus of elasticity as well as with compressive stress-strain curves of self-compacting concrete (SCC) made with crushed limestone aggregate and high content of limestone filler. The characteristics under consideration were tested at the ages of 1, 3, 7, 28, 180, 360 and 720 days. Time evolution of the strength characteristics and modulus of elasticity was estimated with analytical models given in European code Eurocode 2. The study revealed that the models can adequately predict time evolution of the SCC characteristics, when coefficient *s* in the models is equal to 0.17, 0.08 and 0.25 for compressive strength, tensile strength and modulus of elasticity, respectively. These values of coefficient *s* are quite different from the value 0.2 proposed by Eurocode 2 for used cement strength class.

Introduction

Self-compacting concrete (SCC) mixes produced in Slovenia are mostly made using crushed limestone aggregate with maximum aggregate size (D_{max}) of 16 mm and with relatively high content of limestone filler [1]. In the period between 2000 and 2008 comprehensive study of short term mechanical, physical and durability properties of the SCC mixes were carried out at the University of Ljubljana [2]. However, data about time evolution of the most important mechanical characteristics of concrete, such as compressive and tensile strength, modulus of elasticity and compressive stress-strain relationship, were not available for the SCC mixes. Therefore, in 2007 a systematical 2 year study of typical Slovenian SCC mixture with adequate durability for civil engineering application started, to obtain the missing data. Experimentally obtained results were compared with analytical

K.H. Khayat and D. Feys (eds.), *Design, Production and Placement of Self-Consolidating Concrete*, RILEM Bookseries 1,
DOI 10.1007/978-90-481-9664-7_27,

models given in the European Code for Design of Concrete Structures, Eurocode 2 (EC 2, [3]), in order to find out whether commonly accepted models can be used also for the estimation of the time evolution of the SCC characteristics.

Experimental Work

Materials, proportions and fresh concrete properties

The SCC mixture was prepared using:

- Portland cement CEM II/A-S 42.5R (EN 197-1 [4]) with up to 15% of ground granulated blast furnace slag and with Blaine fineness of 3730 cm^2/g,
- coarse (combination of 4-8 and 8-16 mm fractions) and fine (combination of 0-2 and 0-4 mm fractions) crushed limestone aggregate, with compressive strength of the parent rock around 200 MPa,
- limestone filler (LF) produced in quarrying operation, with Blaine fineness of 2670 cm^2/g (limestone dust that contained 100% of calcite and originates from the same parent rock as the aggregate),
- tap water, and
- polycarboxylate-based superplasticizer (SP).

In Figure 1 particle size distributions of the cement and LF are presented and in Table I relative density of basic materials and proportions of the SCC are given.

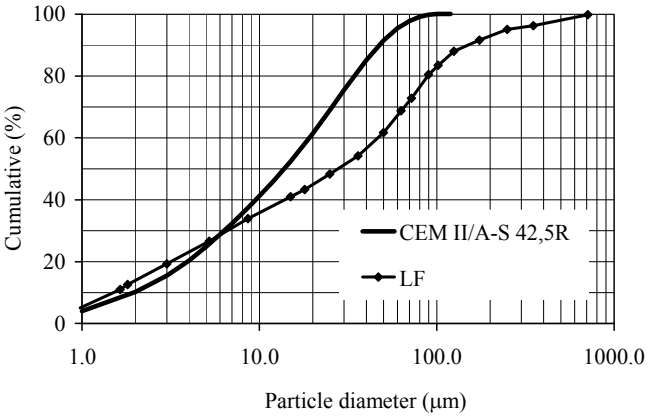

Figure 1. Particle size distribution of the cement and LF.

Batches of fresh SCC had the following properties: Slump-Flow 740±20 mm, T500 4.8±0.2 s, V-funnel Time 14.0±1.0 s, L-box ratio ≥ 0.82 (L-box with 2 rebars) and air content of 2%.

Table I. Relative density of basic materials and proportions of the SCC.

	CEM II/ A-S 42.5R	LF	coarse aggregate	fine aggregate	water	SP
density (kg/m^3)	3.08	2.75	2.71	2.71	1.0	1.10
content (kg/m^3)	400	250	710	870	170	4.81

Preparation of test specimens, curing and testing

To determine compressive strength (EN 12390-3 [5]) and tensile splitting strength (EN 12390-6 [6]), standard concrete cubes with nominal size of 150 mm were cast. To determine the modulus of elasticity (DIN 1048 Teil 5, [7]) and compressive stress-strain curves standard concrete prisms 100x100x400 mm were used. Making and curing specimens for the tests followed the procedures according to EN 12390-2 [8], without mechanical compaction. The age of test specimens at testing was 1, 3, 7, 28, 180, 360, and 720 days. For each test method and age of concrete 5 specimens were tested.

Test Results and Discussion

Compressive test

The results of compressive test are given in Table II as average compressive strength $f_{cm}(t)$, ratio between average compressive strength at selected age and the age of 28 days, and coefficient of variation of compressive strength results.

Table II. Results of compressive test of SCC.

t [days]	1	3	7	28	180	360	720
$f_{cm}(t)$ [MPa]	42	54	60	69	78	80	86
$f_{cm}(t)/ f_{cm}(28)$	0.61	0.78	0.87	1.00	1.13	1.16	1.25
COV [%]	1	1	1	2	4	1	1

From the results in Table II it can be concluded that the used SCC mixture can be classified in compressive strength class C50/60, according to European standard

EN 206-1 [9]. C50/60 is the upper limit of the compressive strength classes for normal strength concrete. Compared to vibrated concrete mixture with the same cement type and content, the same aggregate and the same water to cement ratio, but without the LF [2], 28 day compressive strength of the SCC is higher by 10 MPa.

Figure 2 presents the time evolution of the SCC's compressive strength and the estimation of its compressive strength at various ages according to the analytical model given in EC 2 [3]:

$$f_{cm}(t) = \beta_{cc}(t) f_{cm}; \quad \beta_{cc}(t) = e^{s\left(1-\sqrt{28/t}\right)} \tag{1}$$

where: $f_{cm}(t)$ = the mean concrete compressive strength at an age of t days
f_{cm} = the mean compressive strength at 28 days
$\beta_{cc}(t)$ = a coefficient which depends on the age of concrete t
t = the age of concrete in days
s = a coefficient which depends on the type of cement: 0.2 for cement of strength classes CEM 42.5 R, CEM 52.5 N and CEM 52.5 R [4], 0.25 for cement of strength classes CEM 42.5 N and CEM 32.5 [4].

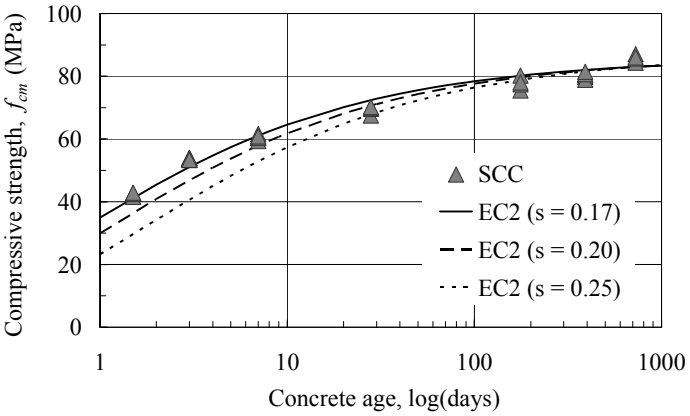

Figure 2. Time evolution of compressive strength of the SCC and its estimation using analytical model (Eqn. (1)).

For the model approximately the same long-term compressive strength at 360 and 720 days was assumed as obtained with the compressive test. Based on this assumption, f_{cm} in Eqn. (1) was evaluated for different values of coefficient s. The

same approach was adopted also for tensile strength and for the modulus of elasticity.

Since binder in the SCC mixture was a combination of cement with strength class of CEM 42.5R (400 kg/m^3) and LF (250 kg/m^3), we expected coefficient 0.25 to be adequate choice for the evaluation of time-compressive strength relationship of the SCC with Eqn. (1). However, even with coefficient of 0.2, the compressive strength of the SCC at early ages was underestimated, as it can be seen in Figure 2.

The chi-squared test revealed that the statistic H^{χ^2} from testing agreement of Eqn. (1) with the results of compressive tests is minimal for coefficient *s* equal to 0.17:

$$f_{cm}^{SCC_{am}}(t) = e^{0,17\left(1-\sqrt{28/t}\right)} f_{cm} \tag{2}$$

The addition of LF to Portland cement has several effects on the properties of hardened concrete. The LF grains act as nucleation sites for CH and C-S-H reaction products at early hydration ages, and they accelerate the hydration of clinker minerals, especially C_3S, resulting in an improvement in early strength [10, 11]. Improvement of fine-particle packing can considerably increase the density of paste matrix and interfacial transition zone (ITZ) [12-14]. Thus, compared to plain concrete with the same water to cement ratio and PC type, concrete with a high LF content with suitable particle size distribution generally possesses improved strength characteristics, especially at early ages [15, 16]. Despite faster strength increase at early ages for the SCC with high content of LF, Eqn. (1) can still be used to estimate the time evolution of the SCC's compressive strength, if allowing coefficient *s* to be lower than 0.2.

Tensile test

Results of tensile splitting test are given in Table III as average tensile splitting strength $f_{ctm,sp}$ (t), average axial tensile strength f_{ctm} (t), which is 90% of $f_{ctm,sp}$ (t) according to EC 2 [3], ratio between average tensile strength at selected age and the age of 28 days, and coefficient of variation of tensile strength results.

Table III. Results of tensile test of SCC.

t [days]	1	3	7	28	180	360	720
$f_{ctm,sp}$ (t) [MPa]	3.4	3.6	3.8	3.8	4.1	4.3	4.2
f_{ctm} (t) [MPa]	3.0	3.2	3.4	3.4	3.7	3.9	3.8
f_{ctm} (t)/ f_{ctm} (28)	0.89	0.95	1.00	1.00	1.08	1.13	1.11
COV [%]	7	4	6	8	9	12	3

By using analytical relation between tensile strength f_{ctm} and characteristic cylinder compressive strength f_{ck} given in EC 2 [3], the average 28 day tensile strength of 4.1 MPa would be expected for average compressive cube strength of 69 MPa. Analytically obtained value is about 20% higher than the SCC average tensile strength at the same age. Similar results were obtained in the study carried out by Parra et.al [17], where splitting tensile strength of SCC mixes were on average 18% lower than for vibrated concrete mixes with the same compressive strength.

Figure 3 presents time evolution of the SCC's tensile strength and the estimation of its tensile strength at various ages according to the analytical model given in EC2 [3]:

$$f_{ctm}(t) = \left(\beta_{cc}(t)\right)^{\lambda} \cdot f_{ctm} \tag{3}$$

where: f_{ctm} = the mean tensile strength at 28 days
$\beta_{cc}(t)$ = a coefficient given by Eqn. (1)
$\lambda = 1$ for $t < 28$ and $\lambda = 2/3$ for $t \geq 28$

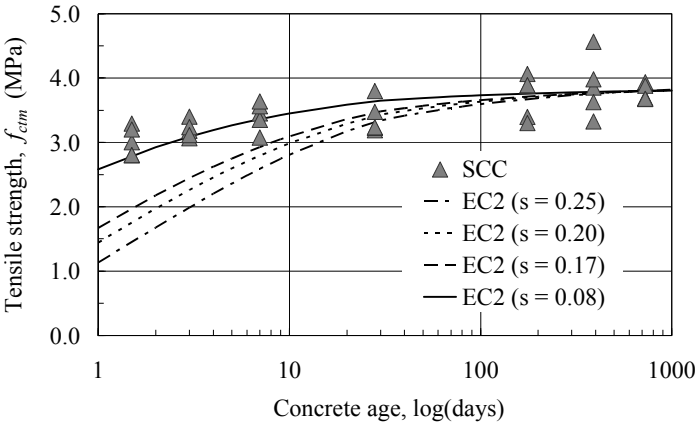

Figure 3. Time evolution of the SCC's tensile strength and its estimation using analytical model (Eqn. (3)).

Figure 3 shows that the estimation of tensile strength–concrete age relationship of the SCC with Eqn. (3) considerably underestimates tensile strength of the concrete for early ages up to 7 days, when coefficient *s* is equal to 0.25 or 0.2. This is true also for *s* equal to 0.17, the value belonging to the best fit for the compressive strength–concrete age relationship of the SCC. In case of tensile strength the best fit of Eqn. (3) with experimentally obtained results was obtained for *s* equal to

0.08. Thus, we can conclude that the analytical model (Eqn. (3)) given in EC 2 [3] can also be used for the estimation of the tensile strength increase with time of the SCC, but with the value of coefficient *s* much lower than given by the code.

By comparing the test results in Table II and Table III it is clear that the rate of tensile strength increase of the SCC with time is up to 28 days much higher than that of the compressive strength. However, after 28 days only the increase of tensile strength up to 10% can be expected. The ratio between mean tensile and compressive strength of the standard cube is between 7% and 6% for early ages, and 5% at 28 days and later on.

Modulus of elasticity

According to EC 2 [3], modulus of elasticity E_{cm} is secant value between compressive stress equal to zero and stress equal to $0.4 \cdot f_{cm}$ of the compressive stress-strain curve. Results for modulus of elasticity are given in Table IV as average modulus of elasticity $E_{cm}(t)$, ratio between average modulus of elasticity at selected age and the age of 28 days, and coefficient of variation of modulus of elasticity test results.

Table IV. Results of modulus of elasticity of SCC.

t [days]	1	3	7	28	180	360	720
$E_{cm}(t)$ [GPa]	32	39	40	43	45	46	46
$E_{cm}(t)/ E_{cm}(28)$	0.74	0.91	0.93	1.00	1.05	1.07	1.07
COV [%]	1	2	1	1	2	1	1

Comparison of the mean modulus of elasticity at 28 days with the value given in EC 2 [3] for the same compressive strength class reveals that the modulus of elasticity of the SCC is about 6 GPa higher, most likely due to the selected crushed limestone aggregate incorporated in the SCC mix. More relevant comparison of E-moduli is between the SCC and the vibrated concrete with the same mean compressive strength and basic materials (the same cement type and content, the same aggregate, and water to cement ratio equaling 0.40), and without LF [18]. At mean 28 day compressive strength equal to 68 MPa, E_{cm} of vibrated concrete was 44 GPa. This value is close to the mean 28 day modulus of elasticity of the SCC. Despite lower content of the aggregate in the SCC mix, modulus of elasticity remained unchanged, compared to the vibrated concrete, probably due to high modulus of elasticity of the LF (compressive strength of parent rock around 200 MPa), and increased density and homogeneity of paste matrix and ITZ in hardened concrete.

Figure 4 presents the time evolution of the SCC's modulus of elasticity and its estimation at various ages according to the analytical model given in EC2 [3]:

$$E_{cm}(t) = \left(e^{0,25\left(1-\sqrt{28/t}\right)} \right)^{0,3} E_{cm} \tag{4}$$

For the modulus of elasticity best fit of the analytical model was obtained for coefficient s equal to 0.25 (Figure 4, Eqn. (4)). The increase of the modulus of elasticity of the SCC with time is important up to the age of 28 days. Later on only increase of a few percents can be expected.

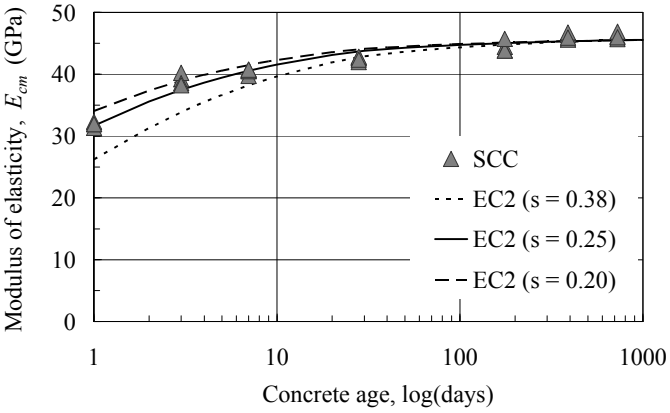

Figure 4. Time evolution of the SCC's modulus of elasticity and its estimation using analytical model in EC 2 [3].

Compressive stress-strain curves

Figure 5 presents compressive stress-strain curves of the SCC at the ages equal to 1, 3, 7, 28, 180, 360, and 720 days, up to the strain at peak stress. From the figure we can see that the linear part of the curves is increasing with concrete age. At age of 1 day it attained 25% of the compressive peak stress and at ages of 3 and 7 days 35% and 45%, respectively. At ages of 28 and 180 days the stress-strain curve of the SCC is linear at least to 50% of the compressive peak stress, and at ages of 1 and 2 years this value is close to 60%. These results indicate that density and strength of the ITZ in the SCC are increasing with time, resulting in more homogenous concrete material without pronounced ITZ, compared to vibrated ordinary concrete.

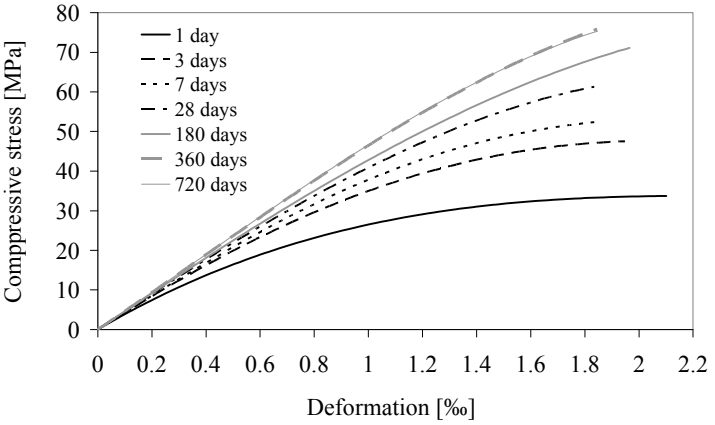

Figure 5. Compressive stress-strain curves of the SCC.

Conclusions

Results of the study presented in the paper show that for the SCC mixture with 400 kg/m^3 of PC, water to cement ratio of 0.43 and high content of LF (250 kg/m^3) about 10 MPa higher 28 days compressive strength can be expected, compared to the control vibrated concrete with the same type and content of PC and the same water to cement ratio, but without the LF. The tensile strength of the SCC is about 20% lower and its modulus of elasticity is approximately the same as at the control vibrated concrete with the same compressive strength.

Analytical models for time dependant increase of compressive and tensile strength and modulus of elasticity given in EC 2 [3] can also be used for estimating the same characteristics of the SCC. However, adequate value of coefficient *s* is quite different than that recommended by the code for particular cement strength class. At the same time *s* has different value for each of characteristics under consideration: 0.17, 0.08, and 0.25 for compressive strength, tensile strength and modulus of elasticity, respectively.

References

[1] Cotič, Z., Koglot, K., Žarnić, R. and Bokan Bosiljkov, V. (2008), Experience with SCC mixes used for precast elements and field applications in Slovenia, Conference Proceedings – SCC 2008: Challenges and Barriers to Application, 6 pp., ACBM.

[2] Duh, D. (2008), Self-compacting and vibrated concretes with limestone powder, Doctoral thesis, University of Ljubljana, Slovenia, 200 pp. (in Slovenian).
[3] EN 1992-1-1:2005. Eurocode 2: Design of concrete structures – Part 1-1: General rules and rules for buildings.
[4] EN 197-1, Cement – Part 1: Composition, specifications and conformity criteria for common cements. CEN.
[5] EN 12390-3, Testing hardened concrete – Part 3: Compressive strength of test specimens.
[6] EN 12390-6, Testing hardened concrete – Part 6: Tensile splitting strength of test specimens.
[7] DIN 1048 Teil 5. 1991. Testing methods for concrete: Hardened concrete, specially prepared specimens (in German).
[8] EN 12390-2, Testing hardened concrete – Part 2: Making and curing specimens for strength tests.
[9] EN 206-1, Concrete – Part 1: Specification, performance, production and conformity.
[10] Pera, J., Husson, S. and Guilhot, B. (1999), Influence of finely ground limestone on cement hydration, *Cem. Concr. Comp*., vol. 21, n. 6, pp. 99-105.
[11] Bonavetti, V., Donza, H., Rahhal, V. and Irassar E. (2000), Influence of initial curing on the properties of concrete containing limestone blended cement, *Cem. Concr. Res.,* vol. 30, n. 5, pp. 703-708.
[12] Trägårdh, J. (1999), Microstructural features and related properties of self-compacting concrete, Proceedings of the First International RILEM Symposium on Self-Compacting Concrete, Skarendahl, A., Petersson, O. (Eds.), RILEM Publications S.A.R.L, Cachan, Cedex, pp. 175-186.
[13] Billberg, P. (1999), Energy modified cement in SCC, Proceedings of the First International RILEM Symposium on Self-Compacting Concrete, Skarendahl, A., Petersson, O. (Eds.), RILEM Publications S.A.R.L, Cachan, pp. 591-602.
[14] Heikal, M., El-Didamony, H. and Morsy, M.S. (2000), Limestone-filled pozzolanic cement, *Cem. Concr. Res.*, vol. 30, n. 11, pp. 1827-1834.
[15] Sonebi, M., Bartos, P.J.M., Zhu, W., Gibbs, J. and Tamimi, A. (2000), Task 4 – Properties of hardened concrete, Final report, Brite EuRam Project No. BE96-3801/Contact BRPR-CT96-0366, 73p.
[16] Petersson, O. (2001), Limestone powder as filler in self-compacting concrete – Frost resistance and compressive strength, Proceedings of the Second International Symposium on Self-Compacting Concrete, Ozawa, K., Ouchi, M. (Eds.), COMS Engineering Corporation, Kochi, pp. 277-284.
[17] Parra, C., Valcuende, M. and Benlloch, J. (2007), Mechanical properties of self-compacting concretes. Proceedings SCC 2007: 5th International

RILEM Symposium on Self-Compacting Concrete, De Schutter, G., Boel, V. (Eds.), RILEM Publications, S.A.R.L, Bagneux, pp. 645-650.

[18] Bokan-Bosiljkov, V. and Žarnić, R. (2008), Optimum rehabilitation of concrete bridge decks on Slovene motorways using latex modified concrete overlays, Final report, 88 pp., University of Ljubljana.

Effect of Freezing-Thawing Cycles on the Resistance of Self-Consolidating Concrete to Sulfate Attack

M.T. Bassuoni and M. Sonebi

Centre for Built Environment Research, Queen's University Belfast, UK

Abstract. SCC has been used in various applications, such as pavements, marine structures, shallow foundations, etc. that can be concomitantly exposed to sulfate-rich environments and frost action. To evaluate the resistance of SCC mixtures to sulfate attack considering the effect of frost action, the present study introduces accelerated testing procedure combining the exposure to aggressive magnesium and mixed magnesium-sodium sulfate solutions with freezing-thawing cycles. After five months of exposure, the results showed that SCC mixtures incorporating high dosage of fillers (limestone and ultrafine kaolin) had inferior physico-mechanical properties relative to the other SCC mixtures. Thermal and microscopy analyses indicated that mutual effects of sulfate attack and freezing-thawing cycles caused severe distress in such cementitious systems.

Introduction

Since the last decade SCC has been progressively used in various infrastructural applications in urban, coastal, agricultural and industrial zones. Various aspects on the durability of SCC were compiled by the RILEM Technical Committee on the durability of SCC (TC205-DSC) in a state-of-the-art report [1]. Limited data, however, are currently available on the long-term performance of elements/structures made of SCC under field conditions. Therefore, research on the performance of various SCC mixture designs under different field-like exposures is needed [2].

From a durability perspective, SCC may be sensitive to chemical attack as it has a high-volume of paste incorporating large dosages of supplementary cementitious materials (e.g. fly ash, silica fume, etc.) and/or fillers (e.g. limestone powder). In particular, SCC has been used in various applications such as pavements, partially embedded structures, marine/coastal structures, etc. that can be exposed to sulfate-rich environments. In a previous study [3], it was reported that the use of high

K.H. Khayat and D. Feys (eds.), *Design, Production and Placement of Self-Consolidating Concrete*, RILEM Bookseries 1,
DOI 10.1007/978-90-481-9664-7_28, © RILEM 2010

amounts of limestone filler (94-375 kg/m^3) in SCC did not cause adverse effects, for example due to thaumasite sulfate attack, on SCC specimens continuously immersed in 1.8% Na_2SO_4 maintained at a low temperature (5°C) up to 900 days. On the other hand, the currently used full immersion test methods for evaluating the sulfate resistance of cement-based materials have been criticized for overlooking important parameters (e.g. environmental conditions) affecting the field performance of concrete structures exposed to sulfate attack [4-6].

Since deterioration of concrete in service often occurs due to a multitude of damage mechanisms (e.g. chemical and physical), it is believed that accelerated field-like exposure tests can reliably capture performance risks associated with conventional and emerging types of concrete. Thus, for evaluating the resistance of SCC to sulfate attack, environmental actions (e.g. freezing-thawing cycles) should be introduced in the test methods. The current study investigates the performance of SCC mixtures under sulfate solutions when freezing-thawing cycles are incorporated in the test procedure. The results are compared to that of a full immersion test, which is commonly used as the sole performance measure to qualify concrete for service in sulfate-rich environments [5]. The SCC mixtures incorporated various combinations of ordinary Portland cement, silica fume and fillers (limestone and ultrafine kaolin). High dosages of limestone filler were incorporated in the SCC mixtures to test their vulnerability to sulfate attack under both testing procedures.

Experimental Program

Materials

Seven SCC mixtures with a water-powder ratio (*w/p*) of 0.33 were prepared using single and binary binders with fillers. The binders used included ordinary Portland cement (OPC) and silica fume (SF), while the fillers were limestone (LF) and ultrafine kaolin (K). The chemical and physical properties of the binders and fillers are listed in Table I. The control SCC mixture was prepared with 100% OPC. SCC mixtures made from single binders and fillers included 85% OPC with 15% LF, 65% OPC with 35%LF, 57.5% OPC with 35% LF and 7.5% K and 50% OPC with 35% LF and 15% K. SCC mixtures prepared with binary binders and fillers included 60% OPC with 35% LF and 5% SF and 55% OPC with 35% LF and 10% SF.

The total powder content was kept constant at 550 kg/m^3 to provide a high volume of fine materials (paste volume of 360-375 l/m^3) conforming to the ranges stated in common SCC mixture design guidelines [7]. The fine aggregate was natural siliceous sand with a fineness modulus of 2.9, a saturated surface dry specific gravity of 2.60 and water absorption of 1.5%. Crushed basalt with a maximum

nominal size of 20 mm, a saturated surface dry specific gravity of 2.65 and water absorption of 0.8% was also used. A polycarboxylic-based superplasticizer was used to enhance the flowability of the SCC mixtures. The dosage of superplasticizer was adjusted to maintain a slump flow of 650±30 mm and L-box ratio (H_2/H_1) not less than 0.75 for all mixtures. A detergent-based air-entraining agent was used to obtain a fresh air content of 5±1%.

Table I. Chemical and physical properties of the binders and fillers used.

	OPC	Silica Fume	Limestone	Kaolin
SiO_2 (%)	19.8	94.0	0.3	47.0
CaO (%)	63.2	0.4	--	0.1
Al_2O_3 (%)	5.0	0.1	--	38.0
Fe_2O_3 (%)	2.4	0.1	--	0.8
MgO (%)	3.3	0.4	--	0.2
K_2O (%)	1.2	0.9	--	2.1
SO_3 (%)	3.0	1.3	--	--
Na_2O (%)	0.1	0.1	--	0.1
TiO_2 (%)	0.3	0.3	--	--
$CaCO_3$ (%)	--	--	99.0	--
Specific surface area, [m^2/kg]	410	19000	600	14000
Specific gravity	3.17	2.12	2.70	2.60

Procedures

Constituent materials were mixed in a mechanical mixer in accordance to the ASTM C 192. Table II shows the proportions of the tested SCC mixtures. Visual inspection and the T-50 (time to reach a flow diameter of 500 mm) were used as secondary quality control measures for the SCC mixtures. Visual inspection was done to ensure that there was no segregation of coarse aggregates implied by paste/mortar haloes. Also, the T-50 was set to be at least 4 s. Any single mixture not satisfying the fundamental requirements of slump flow and L-box along with the ancillary requirements of visual inspection and T-50 was rejected and adjustments were accordingly made to the dosage of HRWRA.

The mortar fraction (passing #4 sieve/4.75 mm) was extracted to cast replicates of 50 x 50 x 50 mm cubes and 50 x 50 x 250 mm prisms without compaction. All specimens were demolded after 24 hours and immersed in a curing tank (20°C) for

28 days. A reference exposure was similar to that for ASTM C 1012 [8] in which specimens were fully immersed in a magnesium sulfate solution or a mixed magnesium-sodium sulfate solution with a concentration of 39,900 ppm SO_4^{-2}. In the mixed sulfate solution, half (19,950 ppm SO_4^{-2}) of the sulfate concentration was from magnesium sulfate and the other half from sodium sulfate. The temperature of the solutions was maintained around 20±2°C. The solutions were renewed each 8 weeks, and the pH was controlled at a range of 6.0-8.0 by titration with diluted sulfuric acid solutions at regular time intervals (5 days). Regular stirring was conducted to allow for a homogenous distribution of the solution.

Table II. Proportions of tested mixtures per cubic meter of concrete.

Mixture ID	OPC [kg]	Silica Fume [kg]	Lime-stone [kg]	Kaolin [kg]	*w/cm*	Fine Aggregate [kg]	Coarse Aggregate [kg]	f'_c 28 days [MPa]
OPC	550	--	--	--	0.33	850	835	81
OPC-15LF	467.5	--	82.5	--	0.39	840	800	70
OPC-35LF	357.5	--	192.5	--	0.50	830	780	42
OPC-35LF-5SF	330	27.5	192.5	--	0.50	810	795	66
OPC-35LF-10SF	302.5	55	192.5	--	0.50	810	785	60
OPC-35LF-7.5K	316	--	192.5	41.5	0.58	820	785	39
OPC-35LF-15K	275	--	192.5	82.5	0.66	810	785	24

Notes: *w/p* and air contents of all mixtures are 0.33 and 5±1%, respectively

A second exposure involved concomitant chemical and physical attacks: magnesium or mixed magnesium-sodium sulfate and frost action. Specimens were subjected to successive freezing-thawing cycles interrupted by wetting and drying periods. A full exposure cycle consisted of 7 days of immersion in a magnesium sulfate or mixed magnesium-sodium sulfate solution at 20°C, 5 days (25 freezing-

thawing cycles) in an automated freezing-thawing cabinet adjusted to the ASTM C 666 procedure A expect that a magnesium sulfate or mixed magnesium-sodium sulfate solution was used instead of water, and 2 days of drying at 20°C and 50% RH. The concentration of sulfate solutions was similar to that of the reference exposure, i.e. 39,900 ppm SO_4^{-2}. Replacement of solutions and pH control were done similar to the reference full immersion exposure.

Before recording the initial physico-mechanical properties, specimens were preconditioned to a saturated surface dry state. For the cubes, the initial mass, compressive strength (ASTM C 109) and pulse velocity (ASTM C 597) at 28 days were recorded to calculate the change in mass and pulse velocity versus time of exposure and the residual compressive strength of deteriorating specimens, respectively. For the prisms, the initial length (ASTM C 1012), was recorded to calculate the change in length versus time of exposure. To analyse the reaction products associated with damage, differential thermogravimetric analysis (DTG) was conducted on powder samples passing #200 sieve (75 μm) collected from the surface (within a range of 0-15 mm from the exposed surface) of selected specimens. Secondary scanning electron microscopy (SEM) with energy dispersive X-ray analysis (EDX) was also conducted on selected fracture surfaces.

Results and Discussion

Reference exposure

After five months, visual inspection for all specimens fully immersed in either the magnesium sulfate or mixed magnesium-sodium sulfate solutions showed no visible features of damage. The results of this exposure are summarized in Table III. The mass of specimens gradually increased throughout the time of exposure, but it was generally less than 1% for most SCC specimens. The mass gain was the highest (up to 1.69%) for SCC specimens incorporating high dosage of fillers (OPC-35LF-15K). In the full immersion experiments, mass gain of specimens is customarily observed in early stages due to absorption of solutions and formation of reaction products in voids. For such sizes of specimens, failure of mortar exposed to sulfate attack is generally indicated by an expansion beyond 0.1%, a relative pulse velocity (pulse velocity at a certain time relative to its initial value) of less than 60% and a mass loss of more than 5%. These values usually correspond to a drop in strength of more than 25% [6, 9].

Up to five months, all expansion values in both solutions were low and did not exceed 0.02%. The ultrasonic pulse velocity results complied with that of visual inspection, mass change and length change. Reduction of pulse velocity relative to its initial values indicates internal cracking of specimens. In this exposure, the

relative pulse velocity increased (maximum of 115%) for all the SCC cubes immersed in both solutions due to infilling of voids with sulfate reaction products.

Table III. Results for specimens fully immersed in the magnesium sulfate and mixed magnesium-sodium sulfate solutions for up to five months.

	$MgSO_4$			$MgSO_4 + Na_2SO_4$		
Mixture ID	Mass Gain [%]	Expansion [%]	Relative Pulse Velocity [%]	Mass Gain [%]	Expansion [%]	Relative Pulse Velocity [%]
OPC	0.68	0.011	109	0.45	0.015	111
OPC-15LF	0.68	0.009	108	0.45	0.013	113
OPC-35LF	0.77	0.013	109	0.67	0.016	111
OPC-35LF-5SF	1.15	0.015	112	0.84	0.020	109
OPC-35LF-10SF	0.48	0.010	111	0.58	0.014	109
OPC-35LF-7.5K	0.94	0.012	112	0.76	0.016	112
OPC-35LF-15K	1.15	0.016	114	1.69	0.022	115

Irrespective of the type of binder and filler, the results suggest that the rate of attack is still low. After five months, all the SCC mixtures had high resistance to full immersion in high concentration (39,900 ppm SO_4^{-2}) magnesium sulfate or mixed magnesium-sodium sulfate solutions. This may be ascribed to the physical resistance (low penetrability) of this type of concrete with high powder content and low water-powder ratio that is cast without vibration (homogenous microstructure). However, whether the SCC mixtures will maintain this performance when freezing-thawing cycles are combined with sulfate solutions still needs to be investigated.

Combined exposure: Sulfate attack and freezing-thawing cycles

In the combined exposure, most SCC specimens remained intact and showed no severe features of deterioration up to five months (270 freezing-thawing cycles), except for the specimens incorporating the highest dosage of fillers (OPC-35LF-15K). Similar behaviour was observed under both combined procedures (magnesium sulfate with freezing-thawing cycles and mixed magnesium-sodium sulfate with freezing-thawing cycles). The results of this exposure are summarized in Table IV. Figure 1 shows exemplar results for the change of expansion and relative pulse velocity versus the time of exposure.

Table IV. Results for specimens exposed to the magnesium and mixed magnesium-sodium sulfate solutions with freezing-thawing cycles for up to five months.

	$MgSO_4$			$MgSO_4 + Na_2SO_4$		
Mixture ID	Mass Loss (%)	Expansion (%)	Relative Pulse Velocity (%)	Mass Loss (%)	Expansion (%)	Relative Pulse Velocity (%)
OPC	0	0.031	112	0	0.046	109
OPC-15LF	0	0.034	113	0	0.039	108
OPC-35LF	0.92	0.041	112	0.96	0.047	113
OPC-35LF-5SF	0.37	0.038	101	0.55	0.045	104
OPC-35LF-10SF	1.33	0.021	104	0.93	0.028	105
OPC-35LF-7.5K	1.44	0.031	106	1.59	0.037	102
OPC-35LF-15K	7.2	0.120	64	10.76	0.163	55

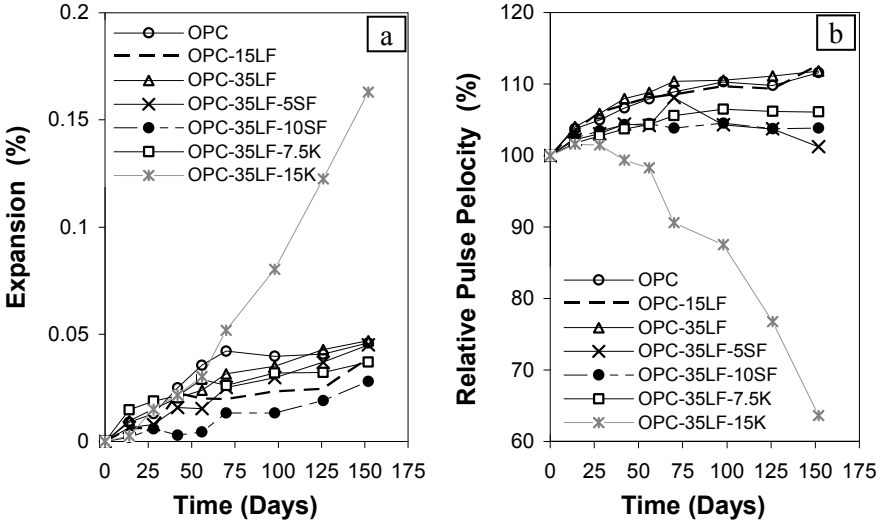

Figure 1. Exemplar results of the combined exposure: (a) $MgSO_4 + Na_2SO_4$, and (b) $MgSO_4$, with freezing-thawing cycles.

Specimens from mixture OPC-35LF-15K started to deteriorate at an early stage (e.g. Figure 1) of the combined exposure. After five months, cubes and prisms made from the powder systems incorporating 50% OPC, 35% limestone filler and 15% ultrafine kaolin suffered softening, spalling and cracking along the edges and

corners (e.g. Figure 2). Cubes had higher level of degradation than that of prisms because of their larger surface-to-volume ratio.

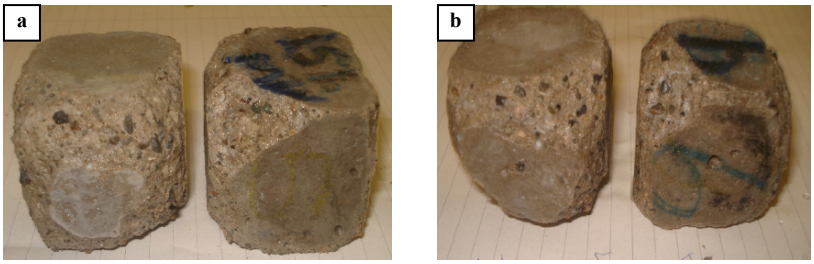

Figure 2. OPC-35LF-15K specimens after five months in the combined exposure: (a) $MgSO_4$, and (b) $MgSO_4 + Na_2SO_4$, with freezing-thawing cycles.

Unlike the reference exposure, mass loss was observed for most SCC specimens in the combined exposure (Table IV). Also, higher expansion values were recorded for prismatic specimens in the combined exposure relative to that in the reference exposure implying a higher rate of damage. High mass loss values of 7 and 11% were recorded for OPC-35LF-15K cube specimens under the exposure involving magnesium sulfate with freezing-thawing cycles and mixed magnesium-sodium sulfate with freezing-thawing cycles, respectively. Those specimens had high loss in compressive strength of 58 and 65%, respectively after five months of exposure. This complies with the low relative pulse velocity (maximum of 64%) recorded for those specimens, and the high expansion (minimum of 0.12%) measured for their prismatic counterparts (Table IV).

Surface scaling of most SCC specimens, as indicated by visual assessment and mass loss results, can be attributed to the mutual effects of sulfate solutions and frost action [2]. The uptake of sulfate solutions in the surface skin of specimens can gradually increase with successive freezing-thawing cycles resulting in supersaturation. Subsequently, differential concentration of sulfate salts likely caused osmotic pressures, which led to the progressive removal of the surface skin in a manner similar to that of de-icing salts.

For the SCC specimens made from the single binder with the highest dosage of fillers (35% LF and 15% K), the damage was mainly driven by its higher penetrability relative to the other SCC mixtures. In this powder system, the OPC content was diluted with a large dosage (225 kg/m^3) of relatively inert fillers. Although such fine and ultrafine particles has a physical filling effect, it did not offset the adverse effect of low OPC content generating a less volume of calcium-silicate-hydrate (C-S-H) and more porous matrix. This was reflected by the significantly lower compressive strength (24 MPa) of mixture OPC-35LF-15K relative to that of the other SCC mixtures (Table II). While this trend was not

captured in the full immersion exposure up to five months, such matrices were more vulnerable to freezing-thawing cycles at an early stage of the combined exposure (Figure 1) because of the higher degree of saturation. This caused a network of micro-cracks in the subsurface zone (e.g. Figure 3), thus further enhancing the penetrability of the sulfate solutions.

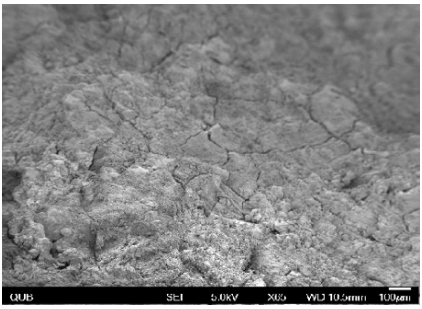

Figure 3. SEM micrograph for OPC-35LF-15K specimen showing a network of micro-cracks near the exposed surface after three cycles in the combined exposure.

DTG on powder samples extracted from the surface zone (0-15 mm) of OPC-35LF-15K specimens under the combined exposure (both magnesium sulfate and mixed magnesium-sodium sulfate with freezing-thawing cycles) showed significant progress of sulfate attack reactions. For example, Figure 4 illustrates the depletion of portlandite (absence of a dehydroxylation peak at a temperature around 450°C) and formation of thaumasite (5.3% of the sample mass), gypsum (13.6% of the sample mass) and brucite (4.4% of the sample mass) as shown by the endothermic peaks at temperatures of 110, 150 and 390°C, respectively.

As explained earlier, the ingress of sulfate solutions in the cementitious systems with the highest dosage of fillers was facilitated by repetitive freezing-thawing cycles. Sodium sulfate and magnesium sulfate react with portlandite to form gypsum. Brucite is also produced in the case of magnesium sulfate. Gypsum can further react with hydrated calcium aluminate, monosulfate or unhydrated tricalcium aluminate to produce secondary ettringite, which is expansive in nature thus leading to the destruction of cementitious matrices. In addition, magnesium sulfate has deleterious effects on the cementitious matrix as it directly attacks (decalcifies) C-S-H forming gypsum and non-cementitious magnesium silicate hydrate [6]. If carbonate/bicarbonate are available in the cementitious matrix with abundance of moisture and a prevailing low temperature (below 15°C), thaumasite can readily form and eventually lead to thaumasite sulfate attack (TSA) turning concrete into a non-cohesive mass [6, 10]. In the current study, DTG showed that thaumasite formation was significant in OPC-35LF-15K specimens due to the inclusion of a large dosage of limestone and the conditions of the combined

exposure that involved sulfate-rich media and temperatures cycling between freezing-thawing.

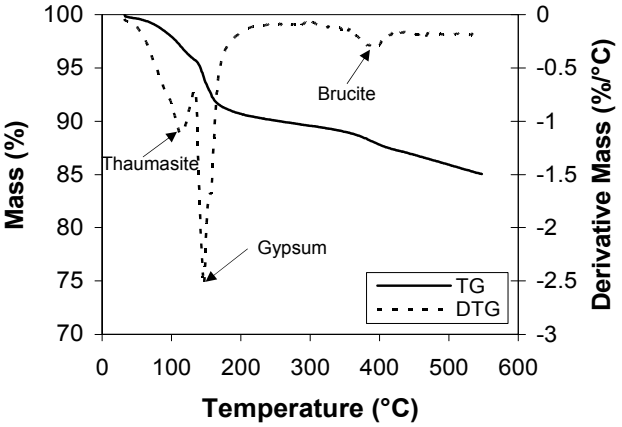

Figure 4. DTG for OPC-35LF-15K specimens after five months in the combined exposure (mixed magnesium-sodium sulfate and freezing-thawing cycles).

SEM analysis complied with the DTG results confirming the abundant formation of tabular gypsum and acicular (ettringite-thaumasite) crystals in those specimens (e.g. Figure 5a-b). The dissolution of portlandite and C-S-H and the significant formation of gypsum and thaumasite caused softening of the matrix as manifested by the marked loss in compressive strength that reached up to 65%.

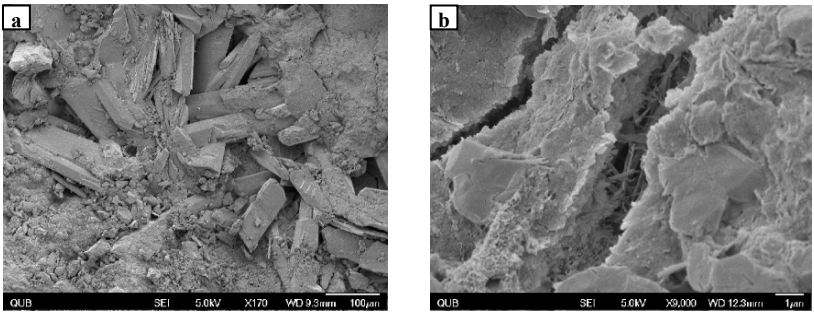

Figure 5. (a) Gypsum, and (b) ettringite-thaumasite formation in OPC-35LF-15K specimens (magnesium sulfate with freezing-thawing cycles).

It was observed that thaumasite and ettringite crystals were present in intimate assemblages, and the structure of thaumasite often had an inclusion of aluminium (e.g. Figure 6). This may imply that thaumasite formed through the Woodfordite

route as a result of reaction between ettringite and C-S-H [10]. The high Al_2O_3 content in kaolin perhaps acted as a precursor for ettringite and subsequently thaumasite formation through the Woodfordite route.

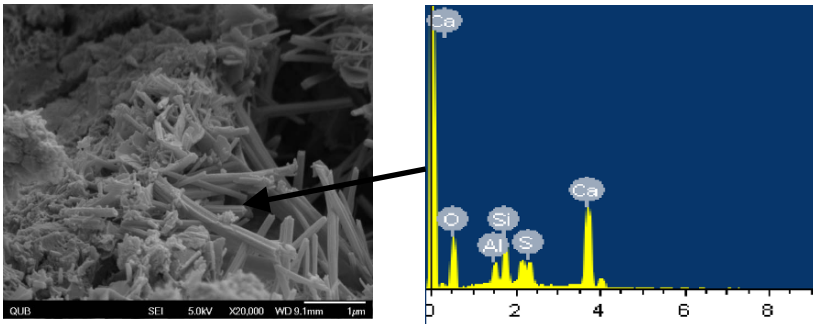

Figure 6. Thaumasite crystals in OPC-35LF-15K specimens (magnesium sulfate with freezing-thawing cycles).

Conclusions

- Up to five months, the full immersion tests suggested that all SCC mixtures tested in this study were resistant to aggressive magnesium sulfate or mixed magnesium-sodium sulfate solutions. However, this test could not capture potential risks that may arise if frost action is combined with sulfate solutions.
- The combination of sulfate solutions and freezing-thawing cycles in a performance testing procedure showed inferior physico-mechanical properties associated with SCC made from powder systems incorporating 50% OPC and 50% fillers (35% limestone and 15% Kaolin).
- In the combined exposure, the damage of cementitious systems comprising OPC with high dosage of limestone and kaolin fillers was mainly driven by their higher penetrability and surface micro-cracking induced by repetitive freezing-thawing cycles, which enhanced the ingress of sulfate solutions into those matrices.
- Mutual effects of sulfate attack and freezing-thawing cycles led to complex forms of damage in the cementitious systems incorporating high dosage of limestone and kaolin fillers. Osmotic pressures, dissolution of portlandite and C-S-H and accumulation of sulfate reaction products, together with progression of thaumasite sulfate attack were responsible for the distress of specimens made from such powder systems.
- While the results after five-months under the combined exposure may suggest that certain combinations of binders and fillers at low *w/p* may offer

a solution for mitigating thaumasite sulfate attack on SCC containing high dosages of limestone filler, further research is needed to substantiate this observation.

References

[1] De Schutter, G. and Audenaert, K. (Eds.) (2007) Durability of self-compacting concrete, State-of-the-art Report of RILEM TC 205-DSC, RILEM Report 38.

[2] Nehdi, M. L. and Bassuoni, M. T. (2008), Durability of self-consolidating concrete to combined effects of sulfate attack and frost action, *Mater. Struct.*, vol. 41, n. 10, pp. 1657-1679.

[3] Persson, B. (2003), Sulphate resistance of self-compacting concrete, *Cem. Concr. Res.*, vol. 33, n. 12, pp. 1933-1938.

[4] Clifton, J., Frohnsdorff, G. and Ferraris, C. (1999), Standards for evaluating the susceptibility of cement-based materials to external sulfate attack, In: *Materials Science of Concrete Special Volume: Sulfate Attack Mechanisms*, Marchand, J. and Skalny, J. (Eds.), The American Ceramic Society, Westerville, OH, pp. 337-355.

[5] Day, R. L. (2000), Development of performance tests for sulfate attack on cementitious systems, *Cem. Concr. Aggr.*, vol. 22, n. 2, pp. 169-176.

[6] Skalny, J., Marchand, J. and Odler, I. (2002), Sulfate attack on concrete, Spon Press, UK.

[7] The European guidelines for self-compacting concrete (2005), BIBM, CEMBUREAU, ERMCO, EFCA, EFNARC, www. efnarc.org.

[8] ASTM C 1012 (2009), Standard test method for length change of hydraulic-cement mortar exposed to a sulfate solution, *Annual Book of American Society for Testing Materials*, vol. 4.01, West Conshohocken, PA.

[9] Cohen, M. and Mather, B. (1991), Sulfate attack on concrete-research needs, *ACI Mater. J.*, vol. 88, n. 1, pp. 62-69.

[10] Bensted, J. (2003), Thaumasite-direct, Woodfordite and other possible formation routes, *Cem. Concr. Compos.*, vol. 25, n. 8, pp. 873-877.

Theme 8: Bond Strength of SCC

Bond Behaviour and Shear Capacity of Self-Compacting Concrete

Veerle Boel[1,2], Peter Helincks[1,2], Pieter Desnerck[2] and Geert De Schutter[2]

[1] Department of Construction, Faculty of Applied Engineering Sciences, University College Ghent, Belgium
[2] Faculty of Engineering Sciences, Ghent University, Belgium

Abstract. In this paper the bond mechanism of steel reinforcement to concrete and the shear capacity are examined. Tests have been conducted on conventional vibrated concrete (CVC) and self-compacting concrete (SCC). The results from pull-out tests on 200 mm cube specimens show that for the same compressive strength the maximum bond stress for SCC is as high or higher than for CVC and this for all tested diameters (8, 12 or 16 mm). The bond stress increases with increasing bar diameter. The specimens were loaded at constant rate and during testing the slip of the bars and the applied load were recorded. The four-point loading tests point out a slightly decreased shear capacity of SCC in respect to CVC with the same compressive strength. The shear capacity decreases with increasing shear span-to-depth ratio a/d (2 to 3) for all the tested concrete types. During the testing the maximum applied load was recorded and the crack and failure mechanism were observed.

Introduction

A substantial amount of research has already been performed on fresh, mechanical and transport properties and durability of self-compacting concrete (SCC) [1-3]. Still, more fundamental knowledge regarding the bond behaviour and the shear resistance of SCC can assist the designers and engineers when SCC is used in civil structures.

The bond between steel and concrete is important when considering anchorage lengths required for reinforcement. According to [4] the bond behaviour of the reinforcement is to a large extent depending on the surface texture and the geometry of the bars. In addition to those two aspects, also the quality of the concrete will influence the bond behaviour of the reinforcement. Changes in the

K.H. Khayat and D. Feys (eds.), *Design, Production and Placement of Self-Consolidating Concrete*, RILEM Bookseries 1,
DOI 10.1007/978-90-481-9664-7_29, © RILEM 2010

mix design or the placing of the material, which is the case with SCC, can modify the steel-to-concrete bond.

Shear failure of reinforced concrete signifies rapid strength degradation. In order to avoid this sudden failure mode, the shear resistance of the concrete element should be higher than the resistance to other failure modes which do not suddenly appear, as for instance flexural failure. Since the composition of SCC is different from CVC, a lower amount of coarse aggregates, and a larger amount of fine materials (e.g. filler), there could be a significant influence on the shear capacity [5].

In the first part of this paper the bond strength of rebars in three different concrete types is discussed (one CVC and two SCC mixtures). The test parameters include concrete type (CVC/SCC) and diameter of rebars (8/12/16 mm). Maximum and characteristic bond stress and slip are recorded and compared for different test members. In the second part of this paper the shear capacity is discussed. Test parameters include concrete type (CVC/SCC) and shear span-to-depth ratio, a/d (2/2.5/3) ('a' the distance between a point load and a support and 'd' the effective depth of the cross section of the concrete beam). The maximum shear capacity is recorded and the experimental results are also compared with theoretical values deduced from code based design equations.

Experimental Program

Mixture design

The experiments are performed on SCC and CVC. Five different concrete mixtures were used, three mixtures made in the laboratory (CVC1, SCC1 and SCC2) and two mixtures provided by a local ready-mix concrete supplier (CVC2, SCC3). For each test the results on three mixtures are discussed in this paper. The pull-out tests are performed on SCC1, SCC3 and CVC2. The tests on the shear resistance are performed on SCC1, SCC2 and CVC1.

Laboratory mixtures. One mixture of CVC (CVC1) and two mixtures of SCC (SCC1 and SCC2) have been designed (Table I). SCC1 and CVC1 have the same cement content, 360 kg/m³, and the same W/C of 0.46. SCC2, with a W/C of 0.55, and CVC1 have approximately the same strength. The used materials are sand 0/4, river gravel 2/8, river gravel 8/16, limestone filler, CEM I 52.5 N and a polycarboxylic ether as superplasticizer (PCE). The amount of superplasticizer was determined in order to obtain a suitable flowability without segregation. A slump flow of ± 700 mm was aimed for. The mixture characteristics are shown in Table II (slump, slump flow, V-funnel, compressive strength $f_{c,cub150}$ and f_c at 28 days). The compressive strength f_c was calculated based on the $f_c/f_{c,cub}$ in [6] where the same mixtures and materials were used. The maximum standard deviation of $f_{c,cub150}$ was ± 6 N/mm² (performed on three cubes). Despite the low slump of CVC1 a well

compacted concrete was achieved after vibrating the concrete. The lower compressive strength of CVC in comparison to SCC of the same W/C, can be attributed to the higher capillary porosity, as was demonstrated in [7, 8].

Ready-mix concrete mixtures. Both C40/50 mixtures were provided by a local ready-mix concrete company. The mixtures are designed for an EE2 environment [9]. Cement type CEM III/A 42.5 was used in both cases. The maximum nominal diameter D_{max} was 8 mm in the case of SCC3 and 16 mm in the case of CVC2. The compressive strengths f_c at the age of testing, 56 days, of SCC3 and CVC2 are 53.5 N/mm² and 55.2 N/mm² respectively.

Table I. Mixture proportions.

	CVC1	SCC1	SCC2
CEM I 52.5 N [kg/m³]	360	360	300
Sand 0/4 [kg/m³]	640	853	853
River gravel 2/8 [kg/m³]	462	263	263
River Gravel 8/16 [kg/m³]	762	434	434
Limestone filler [kg/m³]	-	240	300
Water [kg/m³]	165	165	165
PCE superplasticizer [l/m³]	-	2.83	2.40
W/C	0.46	0.46	0.55

Table II. Mixture characteristics.

	CVC1	SCC1	SCC2
Slump [mm]	32	-	-
Slump flow [mm]	-	775	663
V-funnel [s]	-	13.7	16.0
$f_{c,cub150}$ [N/mm²]	56.3	68.2 (1) 60.6 (2)	60.0
f_c [N/mm²]	50.1	60.7 (1) 58.0 (2)	55.8

(1) first batch, used for the shear resistance; (2) second batch, used for the pull-out specimens

Specimens

Pull-out tests. According to the recommendations RC6 part 2 of RILEM (1973), the specimens of the pull-out tests were 200 mm cubes [10]. One steel bar BE 500 S (according to EN 10080) with diameter ϕ 8, 12 or 16 mm was imbedded in each cube with an anchorage length of 3.5 ϕ (Figure 1). For every diameter size, three specimens were made which were stored at 20 ± 2°C until the age of testing. The specimens were sealed until the age of testing.

Shear capacity. The shear capacity was derived by means of four point bending tests on reinforced concrete beams. The longitudinal reinforcement was designed

in order to assure failure due to shear ($\rho_l = \pm 1\%$). The dimensions of the beams are shown in Figure 2. For every mixture and every a/d, four beams were produced. They were stored at 20 ± 2°C until the age of testing. The specimens were sealed until the age of testing.

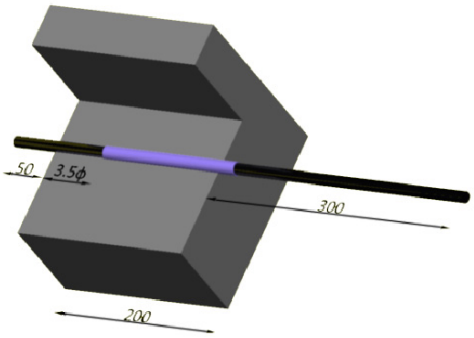

Figure 1. Dimensions and characteristics of the pull-out specimen.

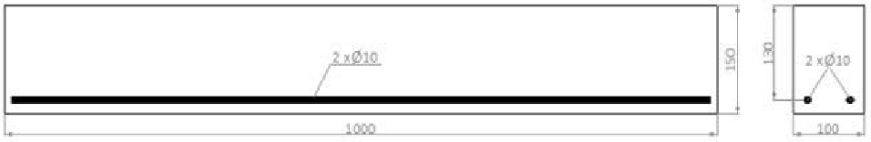

Figure 2. Dimensions and characteristics of the beams.

Test methods

Pull-out tests. The pull-out tests were carried out according to RILEM recommendations [10], except that in this case the force is applied on the rebar instead of on the cube. The pull-out load was applied progressively up to bond failure (0.02 mm/s) and the relative slip of the bar was measured using two symmetric placed laser devices connected to the unloaded end of the bar. The test set-up is shown in Figure 3.

Shear capacity. For the four point bending test, the applied load was divided into two point loads by using a steel spreader profile (type HEB120) (Figure 4). The position of the point loads was varied in order to achieve three different a/d. The force was progressively increased in steps of ± 0.2 kN/s, until shear failure.

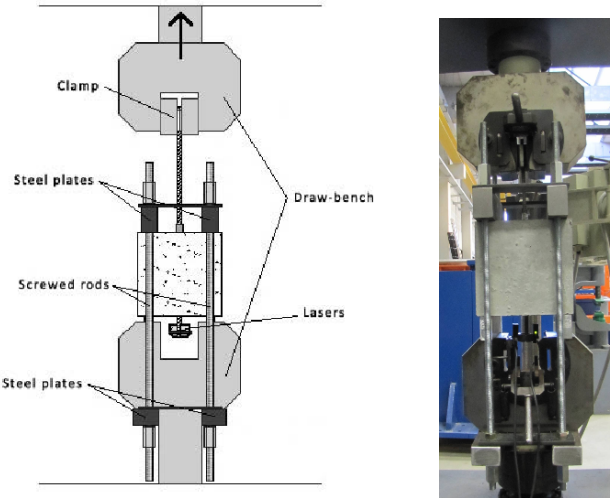

Figure 3. Test set-up of the pull-out test.

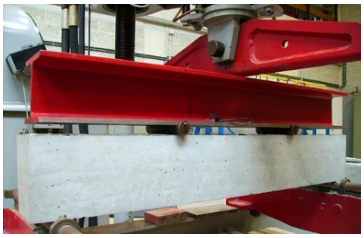

Figure 4. Test set-up four point bending test.

Results and Discussion

Pull-out tests

The pull-out tests are carried out at 56 days. For all specimens, failure was caused by pull-out. The bond stress τ is calculated using Eqn. (1):

$$\tau = \frac{F}{\pi \, \phi \, L} \tag{1}$$

with F, ϕ and L respectively being the applied load, the bar diameter and the anchorage length. All the bond stress–slip curves have the same shape. From these curves the maximum bond stress τ_m and slip s_m are derived. The characteristic bond

stress τ_k is calculated as the arithmetic mean of the stresses recorded at slips of 0.01, 0.10, and 1.00 mm. The values of τ_k, τ_m, the maximum applied load P_m and s_m are listed in Table III.

Table III. Pull-out characteristics.

	τ_k [N/mm²]		τ_m [N/mm²]		P_m [kN]		s_m [mm]	
	mean	stdev	mean	stdev	mean	stdev	mean	stdev
SCC1-8	14.42	1.77	25.88	1.08	18.21	0.78	0.588	0.071
SCC1-12	20.71	3.14	29.86	4.59	47.27	7.26	0.698	0.514
SCC1-16	20.98	2.23	32.32	1.45	90.97	4.07	1.286	0.536
CVC2-8	8.27	0.96	20.07	1.80	14.13	1.26	0.581	0.043
CVC2-12	13.53	3.37	25.23	4.56	39.85	7.37	0.845	0.081
CVC2-16	13.67	1.04	26.03	0.46	73.27	1.28	0.891	0.180
SCC3-8	9.60	1.00	19.92	1.60	14.02	1.13	0.640	0.090
SCC3-12	13.94	1.29	24.39	1.00	38.63	1.53	0.850	0.200
SCC3-16	17.14	1.83	30.64	0.31	86.26	0.87	0.790	0.140

It can be observed that there is little difference between the slip s_m of SCC and CVC. In order to compare the bond strength behaviour of the three concrete mixtures the normalized bond strength can be calculated by expression ($\tau / \sqrt{f_c}$).

Influence of concrete type and mixture. Figure 5 shows the normalized characteristic and maximum bond stress as a function of mixture type. The normalized bond stress of SCC is as high or higher compared to CVC. When the ready-mix concretes CVC2 and SCC3 are compared the difference is small and increases with higher rebar diameter. The increased bond strength of the SCC mixtures might be attributed to a greater uniformity in the interfacial transition zone (ITZ) around the reinforcement bars [8]. The higher normalized bond strength of SCC1 compared to SCC3 might be due to a finer microstructure and therefore a better ITZ. More tests will be carried out to verify this. One should be careful because data scatter exists between different SCC or CVC mixtures of the same strength class. The stability of SCC is an important factor in maintaining bond strength.

Influence of bar diameter. From Figure 5 it can also be seen that the normalized characteristic and maximum bond stress increase with increasing rebar diameter. In [11] results relating bond strength and concrete compressive strength, from several researchers, are studied. It was found that bond strength varies with bar size, bar type (plain or deformed) and concrete strength, and also that there is significant scatter within each program. Nevertheless from those results it is apparent that there is little difference between the bond to SCC and that to CVC when all other variables are constant. The results also indicate an increase in maximum bond stress with increasing diameter.

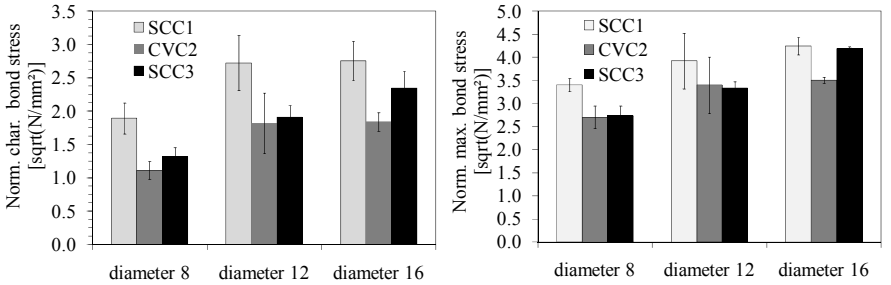

Figure 5. Normalized characteristic/maximum bond stress.

Anchorage length – ultimate bond stress. Based on the limited results above a qualitative validation of the anchorage length and the ultimate bond stress can be made. The theoretical design value of the bond stress f_{bd} according to Belgian standard NBN B15-002 [12] is calculated by Eqn. (2):

$$f_{bd} = \frac{2.25}{\gamma_c} \cdot 0.21 \cdot f_c^{2/3} \tag{2}$$

where the partial factor γ_c was taken as 1. When the bond strength of SCC is higher compared to CVC, Eqn. (2), which is valid for CVC, can still be used.

Shear capacity

The beams have been tested at the age of 28 days. They all failed in shear. The maximum shear capacity V_{max} is listed in Table IV for different a/d. In order to be able to compare several concrete mixtures the shear capacity is normalized ($V / \sqrt{f_c}$). In Figure 6 the normalized shear capacity is plotted as a function of the mixture type and a/d.

Table IV. Maximum shear capacity.

a/d	2		2.5		3	
	V_{max} [kN]	stdev [kN]	V_{max} [kN]	stdev [kN]	V_{max} [kN]	stdev [kN]
CVC1	26.38	2.96	21.73	0.51	20.91	1.10
SCC1	28.37	2.17	23.96	2.33	22.35	0.83
SCC2	25.34	3.47	21.20	0.74	20.31	0.84

Influence of mixture type (Figure 6). The beams made of SCC have a slightly lower shear capacity than those made of CVC1: 98.3% (SCC1) and 91.8% (SCC2) of the shear capacity of CVC1. The mean ratio of SCC compared to CVC is 97.0%. This is

in agreement with [13]: the shear capacity of SCC was found to be 97.3% of the capacity of CVC (ρ_l = 1%, a/d = 2.5). The lower shear capacity might be due to the lower aggregate interlock. There are fewer coarse aggregates to transfer the forces over the shear surfaces. More tests will be carried out in order to verify these results.

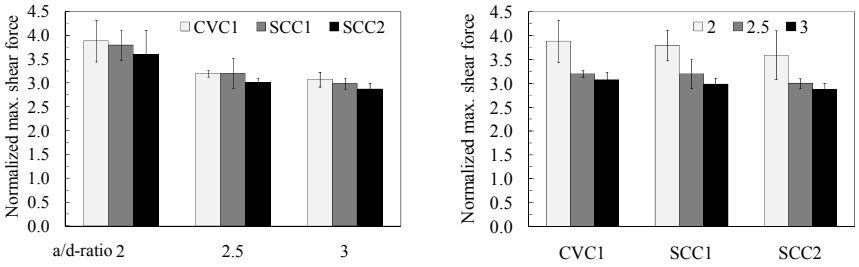

Figure 6. Normalized shear capacity.

Influence of a/d (Figure 6). The shear capacity is lower for a higher a/d. This was also found for CVC in [14-15]. The decrease in shear capacity is of the same order of magnitude for SCC as for CVC. At a/d of 2 there is a bigger transfer of the loading to the supports by compressive struts.

Design shear resistance. Based on the experimentally derived maximum shear capacity V_{max}, it is investigated which formula for the design shear resistance of the member without shear reinforcement $V_{Rd,c}$ gives a good prediction of the experimental values. This could lead to a proposal for the most suitable formula of $V_{Rd,c}$ for SCC mixtures. Formulas from Eurocode 2 [12], Model Code 90 [16], ACI 31 [17], CSA A23.3 [18, 19], BS 8110 [20] and JSCE [21] are taken into consideration. In Table V the $V_{Rd,c}/V_{max}$ is listed for several a/d.

From Table V it can be concluded that most of the formulas tend to underestimate the actual measured shear capacity. Only the formulas out of MC-90 [16] and JSCE-86 [21] give a good approximation of the shear capacity of both SCC and CVC. When the correlation (r^2) of $V_{Rd,c}$ / V_{max} is taken into account, JSCE-86 [21] seems to be the most suitable Eqn. (3):

$$V_{Rd1} = 0{,}20 \cdot \left(0{,}75 + \frac{1{,}4 \cdot d}{a}\right) \cdot f_c'^{1/3} \cdot \left(\frac{1000}{d}\right)^{1/4} \cdot \rho_w^{1/3} \cdot b_w \cdot d \qquad (3)$$

with d the effective depth of the cross section [mm], a the shear span [mm], f_c the characteristic cylindrical compressive strength [N/mm²], ρ_w the geometric reinforcement ratio [%] and b_w the smallest width of the beam [mm]. This is probably due to the fact that in this equation a/d is taken into account which is not the case for the other formulas. Based on the results previously discussed it is expected that, from a certain value of a/d, the influence of a/d becomes negligible.

Ignoring a/d might be seen as an extra safety factor when calculating the value of $V_{Rd,c}$.

Table V. Validity of design shear resistance formulas.

	a/d	$V_{Rd,c}$ / V_{max}						
		EC2-03	MC-90	ACI-05	CSA-94	CSA-04	BS-85	JSCE-86
CVC1	2	0.66	0.84	0.60	0.70	0.49	0.69	0.89
	2.5	0.81	1.02	0.71	0.85	0.61	0.84	0.98
	3	0.84	1.06	0.73	0.88	0.60	0.87	0.94
SCC1	2	0.66	0.88	0.61	0.71	0.48	0.69	0.88
	2.5	0.78	1.05	0.71	0.85	0.57	0.81	0.94
	3	0.84	1.12	0.75	0.91	0.59	0.87	0.94
SCC2	2	0.72	0.94	0.65	0.77	0.56	0.75	0.96
	2.5	0.86	1.12	0.77	0.92	0.67	0.89	1.04
	3	0.89	1.17	0.79	0.96	0.66	0.93	1.01
mean [%]		78.3	102.1	70.2	83.7	58.3	81.7	95.4
st. dev. [%]		8.5	11.4	7.0	9.1	6.6	8.9	5.0
r^2 [%]		7.5	7.7	24.5	7.6	3.6	7.5	85.5

Conclusions

Tests have been carried out on SCC and CVC mixtures in order to examine the bond mechanism of reinforcement steel to concrete and the shear capacity. The results presented in this paper are part of an extended experimental program still in progress. Evidently the scope of this study is too small to provide a definite conclusion of this matter. From the first results the following conclusions can be made.

Bond mechanism:

- The normalized bond stress of SCC is as high or higher compared to CVC when all the other parameters are kept constant;
- The characteristic and maximum bond stress increase with increasing rebar diameter;
- When the bond strength of SCC is as high or higher compared to CVC the formulas valid for CVC can be used in the case of SCC.

Shear capacity:

- The beams made of SCC have a slightly lower shear capacity than those made of CVC;
- The shear capacity is lower for a higher a/d when all the other parameters are kept constant.

References

[1] De Schutter, G. and Audenaert, K. (2007), In: *Durability of Self-Compacting Concrete*, State-of-the-Art Report of RILEM Technical Committee 205-DSC, RILEM Report 38, 185 pp.

[2] De Schutter, G. and Boel, V. (2007), In: *Self-Compacting Concrete SCC2007*, Proceedings of the Fifth International RILEM Symposium on SCC, RILEM Publications S.A.R.L., Proceedings PRO 54, 3 volumes, 1149 pp.

[3] De Schutter, G., Bartos, P., Domone, P. and Gibbs, J. (2008), Self-Compacting Concrete, Whittles Publishing, Caithness, 288 pp.

[4] Valcuende, M. and Parra, C. (2009), Bond behaviour of reinforcement in self-compacting concretes. *Construction and Building Materials*, vol. 23. pp. 162-170.

[5] Desnerck, P., De Schutter, G. and Taerwe, L. (2009), Shear friction of reinforced concrete members in self-compacting concrete, 2nd International Symposium on Design, Performance and Use of Self-Consolidating Concrete, Beijing.

[6] Desnerck, P., De Schutter, G. and Taerwe, L. (2008), Bond behaviour of reinforcing bars in self-compacting concrete: experimental determination by using beam tests, 3rd North American Conference on the Design and Use of Self-Consolidating Concrete, Chicago.

[7] Audenaert, K. (2006), Influence of the capillary porosity on transport mechanisms in relation with carbonation and chloride penetration in self-compacting concrete, PhD Thesis, Ghent University (in Dutch).

[8] Boel, V. (2006), Microstructure of self-compacting concrete in relation with gas permeability and durability aspects, PhD Thesis, Ghent University (in Dutch).

[9] CEN (2000), EN 206-1: Concrete-Part 1: Specification, performance, production and conformity.

[10] RILEM (1970), Technical recommendations for the testing and use of construction materials: RC6, Bond test for reinforcing steel: 2. Pull-out test (7-II-128), *Materials and Structures*, pp. 175-178.

[11] Domone, P.L. (2007), A review of the hardened mechanical properties of self-compacting concrete, *Cement & Concrete Composites,* vol. 29, pp. 1-12.

[12] CEN (2004), Eurocode EN 1992-1-1: Design of concrete structures: General Rules and Rules for Buildings – Belgian standard NBN B15-002.

[13] Hassan, A., Hossain, K. and Lachemi, M. (2008), Behavior of full-scale self-consolidating concrete beams in shear, *Cement & Composites,* vol. 30, pp. 588-596.

[14] Berg, F.J. (1960), Shear strength of reinforced concrete beams without web reinforcement, *Magazine of Concrete Research*, vol. 12, n. 36, pp. 1587-1599.

[15] Imran, A. and Saeed, A. (2008), Evaluation of shear strength of high-strength concrete beams without stirrups, *The Arabian Journal for Science and Engineering*, vol. 33 (2B).
[16] Comité Euro-international du Béton (CEB) and Fédération Internationale de la Préconstrainte (FIP) (1991), European CEB-FIP Model Code 1990, Bulletin d'Information, No. 213/214.
[17] ACI Committee 318 (2005), Building Code Requirements for Structural Concrete (Aci 318-05) and Commentary (318R-05), American Concrete Institute (ACI), Farmington Hills, Mich., 151 pp.
[18] CSA CAN3-A23.3 (1994), Design of concrete structures, Canadian Standards Association, Rexdale, Ontario.
[19] CSA CAN3-A23.3 (2004), Design of concrete structures, Canadian Standards Association, Rexdale, Ontario.
[20] BS 8110 (1985), Structural use of concrete – Part 1: Code of practice for design and construction, British Standard Institution.
[21] JSCE (1986), Specification for design and construction of concrete structures: Design, JSCE Standard, Part 1, Japan Society of Civil Engineers, Tokyo.

Top-Bar Effect in Self-Compacting Concrete Elements

Konstantinos G. Trezos, Ioannis P. Sfikas, Myron S. Palmos and
Ellas K. Sotiropoulou

School of Civil Engineering, National Technical University of Athens, Greece

Abstract. Self-compacting concrete (SCC) can be considered as one of the most revolutionary innovations in the worldwide concrete construction industry and is rapidly gaining acceptance as a potential replacement for normal concrete (NC). Due to its rheological characteristics, fresh SCC has the ability to flow under its own weight and adequately fill highly congested concrete members without the need of external compaction.
The modified composition of SCC, compared to NC, may have consequences on the hardened concrete properties. One of the most important issues is the steel-to-concrete bond, which for NC has been observed to be significantly affected by the concrete depth under the horizontal bars of deep elements, a phenomenon called "top-bar effect". Design codes usually confront this bond reduction by applying a correction factor.
The present paper examines the occurrence of top-bar effect in SCC columns with transverse reinforcement bars in various heights by performing pull-out tests to estimate the anchorage capacity of reinforcement bars, in terms of the bond stress curve as a function of slip.

Introduction

Building codes around the world [1, 2] have currently adopted increased requirements concerning the reinforcement of concrete members, leading to highly congested concrete members. The difficulty of achieving adequate consolidation by means of vibration methods led to a growing interest in using concrete mixtures with higher workability, that require less or no compaction. Self-compacting concrete (SCC) has the ability to flow under its own weight and adequately fill highly congested concrete members without the need of external compaction. The question arising from the use of such mixtures concerns the impact on various hardened concrete properties that are dependable on the adequacy of compaction, like the resulting bond behaviour with steel rebars.

K.H. Khayat and D. Feys (eds.), *Design, Production and Placement of Self-Consolidating Concrete*, RILEM Bookseries 1,
DOI 10.1007/978-90-481-9664-7_30, © RILEM 2010

A very important aspect of steel-to-concrete bond is the reduction of bond strength as a function of concrete depth under the horizontal reinforcement bars in deep concrete elements, a phenomenon known as the "top-bar effect". For normal concrete (NC), building codes have taken this bond reduction into consideration by applying a correction factor that decreases the value of bond strength in the higher parts of the concrete elements. Although SCC is gaining confidence in terms of its steel-to-concrete bond strength [3-6], very few studies [7-9] have been conducted concerning its bond variation in relation to the position of the rebars in deep concrete elements and the significance of top-bar effect, which could lead to a different correction factor and the corresponding required anchorage length for SCC.

Recent studies have led to contradictory results. In particular, Valcuente and Parra [9] studied bond strength of 8 SCC and 4 NC columns with special focus on different water to cement ratio (*w/c*) and different types of cement. The findings indicated that the mean bond strength was higher for SCC specimens, while the difference between the ultimate bond strength of the two concrete types was reduced especially for higher compressive strengths (>50 N/mm^2). Top-bar effect has been found to be more pronounced in NC specimens. Esfahani et al. [7] performed pull-out tests in 12 SCC and NC specimens, each with three embedded bars at different heights, focusing on different concrete cover thicknesses. For equal bond strength at the bottom of NC and SCC columns the values were lower for the latter in the top part of the specimen, resulting in increased top-bar effect due to the degraded settlement of fresh concrete. Hassan et al. [8] examined the effect of different age on bond strength, concluding to higher bond strength of the bottom bars for later ages for same quality NC and SCC. In addition, higher bond stresses have been observed in SCC specimens, resulting in lower top-bar effect compared to NC.

The present paper reports the results of a laboratory investigation concerning the occurrence and the significance of top-bar effect in SCC elements. 8 SCC and 2 reference NC columns with transverse reinforcement bars in various heights have been tested and the bond reduction by height has been evaluated and compared.

Steel-to-Concrete Bond & Top-Bar Effect

Bond strength is critical for reinforced concrete to perform as a uniform structural material. Applied forces are being transferred among concrete and reinforcement bars by adhesion (physicochemical action), friction and bearing (mechanical actions). Quality of concrete and geometry of the reinforcement play an important role in bond strength development. Thus, the resulting bond is significantly affected by any changes in the mixture design, placing method and settlement of concrete, as well as by the position and orientation of reinforcement bars.

One critical aspect related to bond strength is the top-bar effect, which is a phenomenon that mostly acts upon steel bars oriented perpendicularly to the casting direction located near the top casting surface, creating voids under the horizontal bars (Figure 1). The rising bleed water and plastic settlement of concrete during casting may result in the accumulation of water underneath the reinforcement bars. As fresh concrete matures, this trapped water evaporates forming air voids, and thus deteriorating the local quality of the bond between the two materials. This effect is taken into consideration in design codes worldwide by applying a suitable correction factor that increases the required anchorage length. For concrete depths of more than 250 mm beneath horizontal bars, EC2 [2] requires the reduction of the ultimate bond stress to 70% of the characteristic value (valid for shallow sections) and a subsequent increase of anchorage length by 43%. Accordingly, for sections deeper than 300 mm ACI 318R-08 [1] requires an increase in the anchorage length by 30%.

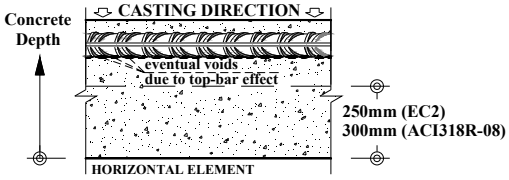

Figure 1. Top-bar effect on reinforcement bars embedded in concrete elements.

Experimental Program

Tested specimens

The bond properties were studied by conducting pull-out tests of reinforcement bars embedded in column elements. Tall specimens were required to observe the phenomenon on a larger scale and reach safer conclusions. The experimental columns were cast in a 1800 mm high plywood mould with a quadratic cross section (200 x 200 mm). Nine horizontal transverse reinforcement bars (numbered from B1 to B9) (B500C, Ø16 mm, L=800 mm) were embedded every 200 mm (Figure 2), starting at 100 mm from the top of the column. The bars were placed perpendicularly to the casting direction and a bond length of 80 mm (5Ø), according to the test method proposed by EN-10080:2005 [10], was achieved by attaching 120 mm plastic sleeves around the rest of the bar length inside the cross section. The sleeves were adjusted into place and secured with sealant (plasticine) in order to avoid inflow of cement paste into the encased reinforcement. The columns were removed from the formwork 3-5 days after casting and cured until the time of testing (28-days). In total, 8 SCC (SCC1 to SCC8) and 2 reference NC columns (NC1 to NC2) have been cast and tested.

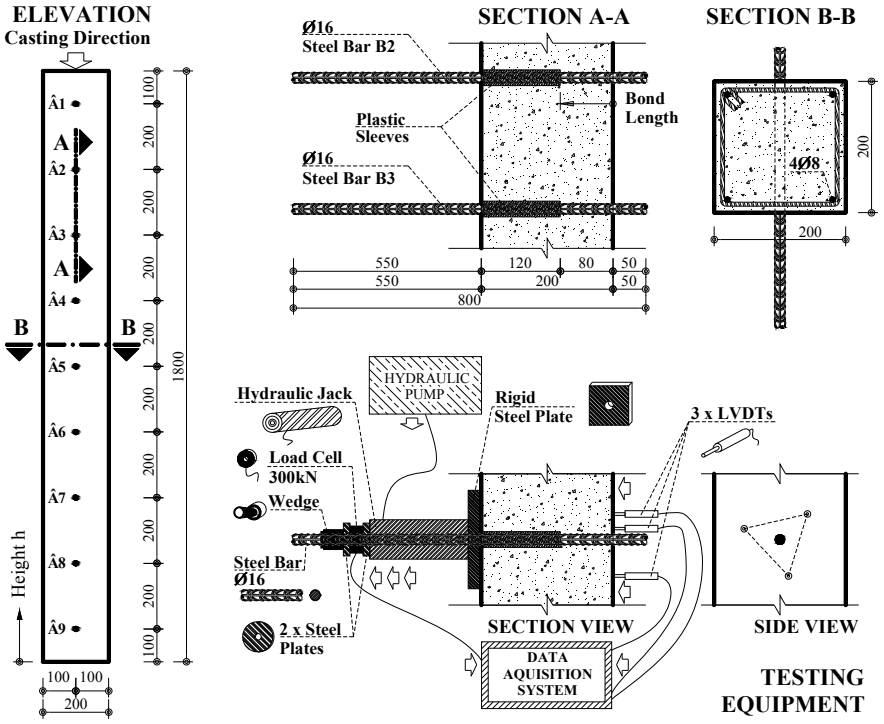

Figure 2. Layout of the tested specimens and testing equipment.

Materials and concrete mixtures

Ordinary Portland cement was used for all concrete mixtures. For all mixtures, the maximum sizes of the crushed limestone aggregates being used were: 4 mm for sand and 16 mm for coarse gravel (with the exception of mixture NC2, where a maximum size of 32 mm has been used). Limestone powder (lp) of different fineness (lp20: purity 97.6% $CaCO_3$, fineness 97% < 18 μm, 15% < 2 μm, lp80: purity 96.5% $CaCO_3$, fineness 97% < 80 μm, 5% < 2 μm) was used as filler in four columns (SCC1, SCC6, SCC7, SCC8) and silica fume (sf) was used in one column (SCC5). Required fluidity and plastic viscosity characteristics of SCC were achieved by using suitable dosage of two different types of polycarboxylic ether superplasticizers (SP). The stability of SCC was enhanced by incorporating Viscosity-Modifying Admixture (VMA). The 28-days compressive strengths, f_{cc}, for SCC varied from 38 to 55 N/mm^2 (for NC: 41 to 44 N/mm^2), while the corresponding tensile strengths, f_{ct}, reached about 10% of f_{cc}. Mixture proportions (kg/m^3), corresponding composition ratios and strengths (N/mm^2) of all concrete mixtures are shown in Table I.

Table I. Mixture proportions (kg/m^3), corresponding composition ratios (-) and strengths (N/mm^2) of the concrete mixtures.

Mixture	SCC1	SCC2	SCC3	SCC4	SCC5	SCC6	SCC7	SCC8	NC1	NC2
c_1 42.5	333	345	390	451	398	289	184	336	124	464
c_2 32.5	-	-	-	-	-	-	-	-	151	-
c_3 22.5	-	-	-	-	-	-	184	-	-	-
sf	-	-	-	-	50	-	-	-	-	-
lp20	-	-	-	-	-	-	-	192	-	-
lp80	48	-	-	-	-	158	105	-	-	-
s 0/4	1043	1202	1141	952	946	955	951	923	1074	849
g_1 4/8	284	319	316	551	548	569	568	501	193	454
g_2 8/16	380	295	292	200	199	208	207	186	386	314
g_3 16/32	-	-	-	-	-	-	-	-	301	-
w	193	194	211	217	242	208	214	240	179	273
SP Type	C347	C347	C347	S628	S628	S628	S628	S628	C347	C347
SP	5.14	6.37	6.21	7.52	7.48	7.01	7.27	5.73	0.10	0.52
VMA	2.01	1.71	2.70	2.30	2.90	1.75	1.82	2.75	-	-
w/c	0.58	0.56	0.54	0.48	0.61	0.72	0.58	0.71	0.65	0.59
w/f	0.38	0.39	0.40	0.41	0.46	0.40	0.39	0.41	0.46	0.52
g/w_{tot}	0.29	0.26	0.25	0.31	0.31	0.32	0.31	0.28	0.37	0.32
p/w_{tot}	0.31	0.30	0.32	0.32	0.32	0.31	0.32	0.35	0.24	0.34
m/w_{tot}	0.77	0.80	0.80	0.71	0.72	0.71	0.71	0.74	0.68	0.70
f_{cc}	45.6	41.0	41.4	56.7	55.4	38.7	46.2	45.6	41.5	43.6
f_{ct}	4.8	4.4	4.3	-	4.8	4.0	4.4	4.7	4.3	4.7

c: cement CEM II A/L 42.5N or 32.5N or 22.5, sf: silica fume, lp: limestone powder, s: sand 0/4, g_1: gravel 4/8, g_2: gravel 8/16, g_3: gravel 16/32, w: water, SP: polycarboxylic ether superplasticizer, VMA: high-performance viscosity-modifying agent, f: fine materials (c+sf+lp+sand fines+gravel fines), w_{tot}: total mixture weight (per m^3), g: total gravel (per m^3), p: paste (f+admixtures+w) (per m^3), m: mortar (p+s) (per m^3), f_{cc}: compressive strength, f_{ct}: tensile strength

Various tests (Slump-flow, J-ring, V-funnel, L-box and U-box) were carried out to evaluate the rheological behaviour of the mixtures and to rank them according to the criteria of the European Guidelines of SCC [5]. According to the Visual Stability Indices (VSI) proposed by Daczko and Kurtz [12] and Struble [13] for fresh and hardened concrete respectively, all mixtures were stable and there were no signs of obvious segregation. The results of the above mentioned tests are shown in Table II.

SCC specimens were not mechanically consolidated during casting and were filled with a continuous uncompacted pour of SCC. NC specimens were filled in three (or four) layers, while thoroughly compacting concrete with a mechanical vibrator, according to the requirements specified in European Standard EN-12390-2:2009 [13]. From each concrete mixture, standard cubes (150 mm) and cylinders (Ø = 150 mm, H = 300 mm) were cast using steel moulds to determine conventional compressive and splitting tensile strengths according to EN-12390-3:2009 [13] and EN-12390-6:2009 [13], respectively. The specimens were demoulded 24 hours after casting and were tested at the time of the pull-out tests (28 days). Deformed steel bars B500C, conforming to EN-10080:2005 [10], were used for both transverse (Ø16 mm) and longitudinal (Ø8 mm) reinforcement.

Table II. SCC rheology tests results & stability evaluation.

	Mixture		SCC1	SCC2	SCC3	SCC4	SCC5	SCC6	SCC7	SCC8
Slump-Flow	S	mm	275	265	270	265	270	275	270	265
	SF	mm	700	665	645	680	575	680	715	645
	SF	-	SF2	SF2	SF1	SF2	SF1	SF2	SF2	SF1
	T_{50}	s	2.7	1.7	3.0	4.2	1.5	3.4	3.1	1.6
	TF	s	19.2	17.7	26.0	33.5	9.8	24.4	30.3	16.9
	VS	-	VS2	VS1	VS2	VS2	VS1	VS2	VS2	VS1
	VSI_f	-	0	0	0	0	0	0	0	0
J-Ring	SF_J	mm	670	600	690	675	585	660	690	605
	B_J	mm	11.3	25.0	10.0	7.5	6.3	11.3	6.3	7.5
V-Fummel	$T_{V,A}$	s	8.2	6.9	4.8	7.9	1.5	7.5	20.5	4.4
	$T_{V,B}$	s	14.6	9.1	5.2	13.3	1.6	9.7	42.1	5.7
	VF	-	VF2	VF1	VF1	VF1	VF1	VF1	VF2	VF1
L-Box	$T_{L,20}$	s	0.5	0.8	1.0	1.6	0.4	0.7	0.8	0.6
	$T_{L,40}$	s	1.1	1.3	1.7	2.8	0.9	1.2	1.9	1.0
	$\lambda_{H,L}$	%	94.7	94.7	94.4	88.5	94.4	94.7	97.8	94.4
	PA	-	PA2	PA2	PA2	PA2	PA2	PA2	PA2	PA2
U-Box	T_U	s	8.6	11.0	3.5	6.3	2.0	8.1	10.9	2.0
	ΔH_U	mm	18	20	5	5	10	10	5	20
28d	VSI_h	-	0	0	0	0	0	1	0	1

SF: flowability class expressed by slump-flow, VS: viscosity class expressed by T_{50}, VSI_f: visual stability index (mortar halo at the slump-flow patty perimeter), VF: viscosity class expressed by V-funnel time, PA: passing ability class expressed by L-box passing ability, VSI_h: visual stability index (hardened concrete)

Testing procedure

For each reinforcement bar the local bond versus the corresponding slip was determined by conducting a pull-out test at the age of T=28 days. The effect of the location of the horizontal reinforcement bars (from B1 in the top to B9 in the bottom) over the height, h, was studied.

Pull-out force was progressively applied using a hydraulic jack, that was connected to a hydraulic pump, up to bond failure and the corresponding slip of the bar was recorded using three linear variable differential transformers (LVDTs) connected by a clamp to the protruding end of the bar at the side closer to the anchored part (Figure 2). A rigid steel plate was placed between the specimen and the hydraulic jack to act as a bearing plate. The applied axial force was acquired by a 300 kN load cell. All hardware parts were connected to a data acquisition system, which was recording the pull-out force versus the slips of the three LVDTs in real-time. The bond stress τ (N/mm^2) at every different moment can be calculated using Eqn. (1), where F (N) the applied force, Ø (mm) the steel bar diameter and L (mm)

the bond length of the corresponding bar, and be plotted as a function of the corresponding mean slip s (mm) of the three LVDTs.

$$\tau = F / \pi \, \text{Ø} L \tag{1}$$

A typical plot for all bars B1 to B9 is shown in Figure 3a. From each curve, five representative bond stresses were retained (Figure 3b): $\tau_{0.01}$, $\tau_{0.10}$, $\tau_{0.25}$ and $\tau_{1.00}$, which correspond to slip values s=0.01 mm, s=0.10 mm, s=0.25 mm and s=1.00 mm, respectively, as well as the maximum reached bond stress, τ_{max}. Additionally, the mean bond stress, τ_m, has also been calculated for each reinforcement bar, using Eqn. (2).

$$\tau_m = \int_0^{s_{\tau max}} \tau ds \Big/ s_{\tau max} \tag{2}$$

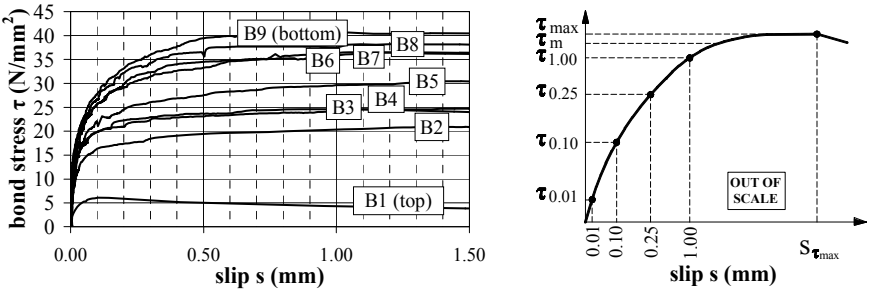

Figure 3. (a) Typical plot of bond stress for bars B1 to B9 as a function of slip and (b) definition of the representative bond stresses and of mean bond stress, τ_m.

After conducting the pull-out test, the reinforcement bars were removed and the columns have been sawn in two parts along the path determined by the positions of the holes. The effective bond length has been measured on each side and the mean value of the two measurements has been used for the calculation of bond stress, τ, instead of the nominal value (5Ø=80 mm) mentioned earlier.

Results and Discussion

Bond reduction coefficient

The measured bond stresses, $\tau_{0.01}$, $\tau_{0.10}$, $\tau_{0.25}$ and $\tau_{1.00}$, as well as the maximum bond stress, τ_{max}, and the mean bond stress, τ_m, are plotted as a function of the distance, h, of each rebar from the bottom of the column in Figures 4. A linear variation with height is evident. The linear regression analysis leads to Eqn. (3), where τ_0 is the

maximum theoretical local bond stress at the bottom of the column and α is a coefficient that defines the linear bond reduction as a function of the height, h, from the bottom of the column. The values of the bond reduction coefficient (slope of the fitted line), are shown in Table III.

$$\tau_h / \tau_0 = 1 - \alpha\, h \tag{3}$$

As it can be seen in Table III, the bond reduction coefficient depends on both mixture and the examined bond stress. SCC develops lower reduction coefficients (ranging from 0.23 to 0.46) than NC (ranging from 0.42 to 0.52) for bond stresses for small slips s=0.01 mm, s=0.10 mm and s=0.25 mm. For slip s=1.00 mm, for the maximum bond stress, τ_{max}, and for the mean bond stress, τ_m, SCC develops higher reduction coefficients (ranging from 0.27 to 0.50) than NC (ranging from 0.22 to 0.40). The highest reduction coefficients are developed for mixture SCC7 (lower quality cement, higher viscosity class VF2), while the lowest bond reduction coefficients are developed for high strength mixture SCC4.

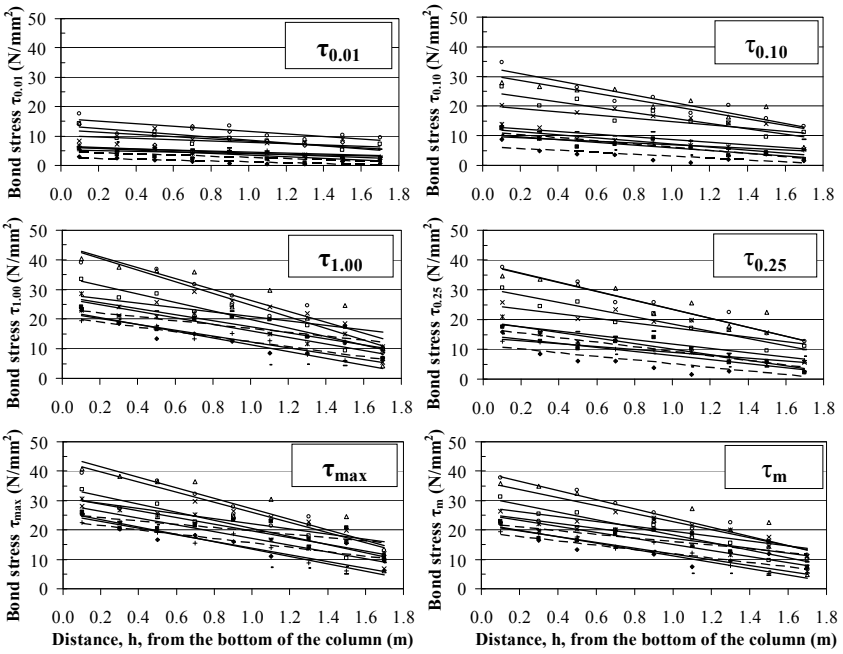

Figure 4. Variation of the representative bond stresses and mean bond stress as a function of the distance from the bottom of the column for the different mixtures (each line corresponds to one mixture).

Table III. Bond reduction coefficients, α, for bond stresses $\tau_{0.01}$, $\tau_{0.10}$, $\tau_{0.25}$ and $\tau_{1.00}$, for the maximum bond stress, τ_{max}, and for the mean bond stress, τ_m.

	SCC1	SCC2	SCC3	SCC4	SCC5	SCC6	SCC7	SCC8	NC1
$\tau_{0.01}$	0.31	0.37	0.27	0.23	0.35	0.25	0.45	0.27	0.42
$\tau_{0.10}$	0.36	0.35	0.36	0.27	0.42	0.30	0.43	0.34	0.46
$\tau_{0.25}$	0.38	0.38	0.38	0.30	0.46	0.34	0.44	0.37	0.43
$\tau_{1.00}$	0.42	0.41	0.44	0.27	0.37	0.45	0.50	0.41	0.28
τ_{max}	0.40	0.40	0.40	0.28	0.37	0.45	0.48	0.40	0.22
τ_m	0.40	0.38	0.36	0.29	0.32	0.43	0.47	0.39	0.27

Mean bond stress reduction

In Figure 5a, the variation of the bond reduction coefficient, α, is plotted for the five representative bond stresses. Figure 5b presents the bond reduction coefficient values, α, that correspond to the mean bond stress, τ_m. As it can be inferred from Figures 5a and 5b, the bond reduction coefficient values, α, corresponding to the mean bond stress, τ_m, are higher for SCC compared to NC mixtures in most cases. The highest values are encountered for mixtures SCC6 (low strength, high filler content, high *w/c*, slight segregation) and SCC7 (lower quality cement, higher viscosity class VF2). The lowest values of bond reduction coefficient are developed for SCC4 (high strength, low *w/c*) and SCC5 (silica fume, high strength).

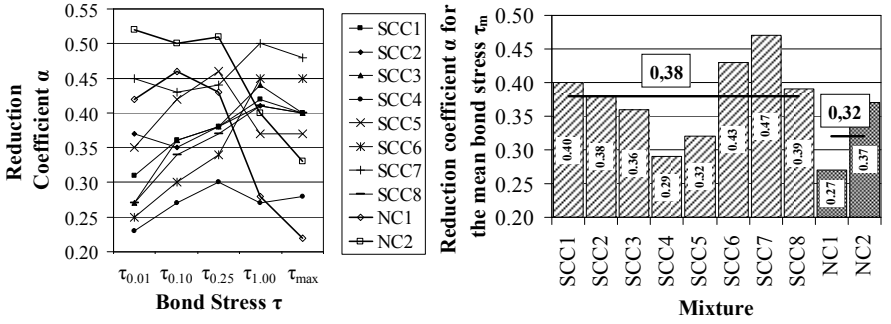

Figure 5. (a) Variation of reduction coefficient, α, for the representative bond stresses and (b) reduction coefficient, α, corresponding to the mean bond stress, τ_m.

Bond strength

The bond strength to be used in the design of anchorage length depends on the selected bond stress. Different criteria can be adopted for selecting the bond strength: (a) According to ACI 318R-08 [1] and recent literature [7, 15], the bond strength can be selected as the stress corresponding to the maximum pull-out force, τ_{max}. (b) FIB [16] proposed the selection of the bond stress, $\tau_{0.25}$, that corresponds

to slip s=0.25 mm, which is lower than the slips (close to or greater than 1.00 mm) at which the maximum stress occurs. (c) In the present study, the selection of mean bond stress, τ_m (Eqn. (2)), as the bond strength is also being examined. The bond strength according to each of the above three criteria is presented and compared in Table IV. The values are normalized by the square root of the compressive strength, $\tau/f_{cc}^{0.5}$ (τ and f_{cc} in N/mm^2).

Table IV. Normalized bond strength, $\tau/f_{cc}^{0.5}$, for all mixtures using different criteria (τ_{max}, $\tau_{0.25}$ and τ_m).

	Mixture	SCC1	SCC2	SCC3	SCC4	SCC5	SCC6	SCC7	SCC8	NC1	NC2
τ_{max}	$\tau_0/f_{cc}^{0.5}$	5.1	7.0	6.7	4.1	4.2	4.0	3.8	4.3	3.9	3.5
	τ_{top}/τ_{bot}	0.33	0.34	0.34	0.53	0.39	0.24	0.19	0.33	0.64	0.46
	α	0.40	0.40	0.40	0.28	0.37	0.45	0.48	0.40	0.22	0.33
$\tau_{0.25}$	$\tau_0/f_{cc}^{0.5}$	4.7	6.2	6.3	3.4	2.7	2.3	2.3	2.9	2.8	1.8
	τ_{top}/τ_{bot}	0.37	0.37	0.37	0.50	0.23	0.43	0.26	0.39	0.28	0.14
	α	0.38	0.38	0.38	0.30	0.46	0.34	0.44	0.37	0.43	0.51
τ_m	$\tau_0/f_{cc}^{0.5}$	4.8	6.4	5.9	3.8	3.6	3.6	3.4	3.9	3.5	3.0
	τ_{top}/τ_{bot}	0.34	0.37	0.40	0.52	0.47	0.28	0.22	0.35	0.56	0.39
	α	0.40	0.38	0.36	0.29	0.32	0.43	0.47	0.39	0.27	0.37

τ_0: bond stress at the bottom of the column (Eq.2), τ_{bot}: bond stress at the bottom bar (B9), τ_{top}: bond stress at the top bar (B1), α: bond reduction coefficient

As it can be seen in Table IV, the maximum normalized theoretical local bond stress at the bottom of the column, $\tau_0/f_{cc}^{0.5}$, is either equal or higher for SCC mixtures compared to NC mixtures, regardless of the criterion selected to estimate bond strength. Mixtures SCC1, SCC2 and SCC3 (high levels of sand, low levels of gravel) develop the highest bond stresses at the bottom of the column. Other researchers [8] have reached similar conclusions for same quality SCC and NC mixtures.

The ratio of the top to bottom bar bond strength (B1 to B9), τ_{top}/τ_{bot}, is a common way of evaluating the bond reduction over height. The ratios should be compared carefully, because they depend on the distance between the two bars in the tested specimens. In the present study (column height: 1800 mm, B1 to B9 distance: 1600 mm), for the maximum stress, τ_{max}, the ratios vary between 19-53% for SCC, while for NC the corresponding range is 46-64%. Other studies [9] resulted in ranges 32-55% for SCC and 60-74% for NC for 1500 mm high columns and edge bars distance 1350 mm. For the bond stress corresponding to slip s=0.25, $\tau_{0.25}$, SCC seems to develop higher ratios than NC, ranging from 23-50% and 14-28%, respectively. Finally, for the mean bond stress, τ_m, top to bottom bar bond strength ratios vary between 22-52% for SCC, while for NC the corresponding range is 39-56%.

The above results can also be expressed in terms of the bond reduction coefficient, α, which expresses the loss of bond strength by height and is not depending on the

distance between the top and the bottom bars. For most SCC mixtures, the values of the bond reduction coefficient seem to be similar, regardless of the selected criterion, ranging from 0.28 to 0.48. In most cases, SCC mixtures develop 19-45% higher bond reduction coefficient values for τ_{max} and τ_m than NC mixtures, the latter ranging from 0.22 to 0.37. In contrast, the bond reduction coefficient for bond stress $\tau_{0.25}$ seems to be higher for NC mixtures, ranging from 0.43 to 0.51.

Conclusions

In the present study, the top-bar effect has been examined for SCC. A linear variation of bond stress as function of concrete depth has been observed. This linear bond stress reduction as a function of the height can be described by the bond reduction coefficient, α, which seems to be more efficient for the evaluation of the top-bar effect than the top to bottom bar bond strength ratio used in literature. The bond reduction coefficient seems to be affected by the cement strength and the resulting concrete strength, the filler type and content, the *w/c*, as well as by the viscosity and the segregation resistance of the mixture. Top-bar effect seems to be less intense in SCC elements for smaller slips, compared to NC. On the contrary, for larger slips, as well as for the maximum bond stress and for the mean bond stress, SCC leads to higher bond reduction coefficients.

Different criteria in selecting the bond strength to be used in the design of anchorage length have been examined. The bond strength developed by SCC mixtures seems to be equal or higher for SCC mixtures compared to same quality NC mixtures, regardless of the selected criterion. The bond reduction coefficient is higher for SCC mixtures, when the maximum bond stress, τ_{max}, or the mean bond stress, τ_m, are selected as the bond strength. The top-bar effect seems to be less intense in SCC, when the stress corresponding to slip s=0.25 mm, $\tau_{0.25}$, is selected as the bond strength.

Acknowledgements

Authors would like to thank (in alphabetical order) BASF Hellas, Dionyssomarble Group, Halyvourgiki Inc., Interbeton Building Materials S.A. and Lafarge for providing the required raw materials for the preparation of concrete mixtures.

References

[1] ACI (2008), Building Code Requirements for Structural Concrete (318-08), and Commentary (318R-08), American Concrete Institute.

[2] Eurocode 2 (2004), EN 1992-1-1: Design of concrete structures, Part 1-1: General rules and rules for buildings, European Committee for Standardization.
[3] Almeida Filho, F.M., El Debs, M.K. and El Debs, A.L.H.C. (2008), Bond-slip behavior of self-compacting concrete and vibrated concrete using pull-out and beam tests, *Materials and Structures*, vol. 41, pp. 1073-1089.
[4] Daoud, A., Lorrain, M. and Elgonnouni, M. (2002), Pull-out behaviour of reinforcement embedded in self-compacting concrete, *Materials and Structures*, vol. 35, pp. 395-401 (in French).
[5] Zhu, W., Gibbs, J.C. and Bartos, P.J.M. (2001), Uniformity of in situ properties of self-compacting concrete in full-scale structural elements, *Cement and Concrete Composites*, vol. 23, pp. 57-64.
[6] Zhu, W., Sonebi, M. and Bartos, P.J.M. (2004), Bond and interfacial properties of reinforcement in self-compacting concrete, *Materials and Structures*, vol. 37, pp. 442-448.
[7] Esfahani, M.R., Lachemi, M. and Kianoush, M.R. (2008), Top-bar effect of steel bars in self-consolidating concrete, *Cement and Concrete Composites*, vol. 30, pp. 52-60.
[8] Hassan, A.A.A., Hossain, K.M.A. and Lachemi, M. (2009), Bond strength of deformed bars in large reinforced concrete members cast with industrial self-consolidating concrete mixture, *Construction and Building Materials*, vol. 24, pp. 520-530.
[9] Valcuende, M. and Parra, C. (2009), Bond behaviour of reinforcement in self-compacting concretes, *Construction and Building Materials*, vol. 23, pp. 162-170.
[10] EN-10080 (2005), Steel for the reinforcement of concrete, CEN.
[11] BIBM, CEMBUREAU, EFCA, EFNARC, ERMCO (2005), European Guidelines for Self-Compacting Concrete: Specification, Production and Use.
[12] Daczko, J.A. and Kurtz, M.A. (2001), Development of high-volume coarse aggregate self-compacting concrete, Proceedings of the Second International Symposium on Self-Compacting Concrete, Tokyo, Japan.
[13] Struble, L (2007), Self Consolidating Concrete*,* CEAT Brown Bag Seminar, Civil and Environmental Engineering University of Illinois.
[14] EN-12390 (2009), Testing hardened concrete, (EN-12390-2:2009) Part 2: Making and curing specimens for strength tests, (EN-12390-3:2009) Part 3: Compressive strength of test specimens, (EN-12390-6:2009) Part 6: Tensile splitting strength of test specimens, CEN.
[15] Foroughi, A., Dilmaghani, S. and Famili H (2008), Bond strength of reinforcement steel in self-compacting concrete, *International Journal of Civil Engineering*. vol. 6, n. 1, pp. 25-33.
[16] FIB (2000), Bulletin 10: Bond of reinforcement in concrete, State-of-Art Report, Lausanne, Switzerland.

Effect of Rheology of SCC on Bond Strength of Ribbed Reinforcement Bars

L.N. Thrane[1], C. Pade[1], C. Idzerda[2] and M. Kaasgaard[1]

[1] Danish Technological Institute, Denmark
[2] Ottawa University, Ontario, Canada

Abstract. SCC can have very different rheological properties depending on the application and local mix design traditions. By definition, SCC should encapsulate the reinforcement bars to ensure proper bond strength, however, variations in bond strength may at least theoretically occur dependent on the rheological properties and the flow characteristics history near the individual bar. Especially, the bond strength may be questioned for SCC with a slump flow in the range 500-580 mm which is often used to obtain good control of flowing concrete as well as high segregation resistance. This paper presents the results of an experimental program investigating the relationship between the rheological parameters yield stress and plastic viscosity and bond strength of reinforcement bars. A reference conventional slump concrete requiring vibration to consolidate and several SCCs of equivalent strength class but with varying rheological parameters as measured by the 4C-Rheometer were prepared. Batches of 250 liters were cast into a formwork containing 12 mm diameter ribbed reinforcement bars fixed horizontally. The distance of SCC flow in the formwork was 2.5 m. Bond and compressive strengths were tested after 7 days of curing. The results indicate that the bond strength is not significantly influenced by the rheological properties of SCC and that the bond strength corresponds to that of conventional concrete.

Introduction

The initial motivation for developing SCC was to reduce the number of casting failures and avoid poorly compacted zones sometimes seen when using conventional vibrated concrete. Thus, the use of SCC would result in a more homogenous concrete quality with better overall structural performance and consequently also less need for repair and maintenance. One of the key properties of reinforced concrete structures is the bond strength. The general conclusion seems to be that a properly designed SCC has similar or better bond strength

K.H. Khayat and D. Feys (eds.), *Design, Production and Placement of Self-Consolidating Concrete*, RILEM Bookseries 1,
DOI 10.1007/978-90-481-9664-7_31, © RILEM 2010

compared to slump concrete [1-8] though also lower bond strength of SCC has been reported [9]. Higher bond strength of SCC may be explained by an often denser microstructure of SCC and the lack of mechanical vibration that can lead to weak zones along reinforcement and aggregate [1-3]. During vibration water may accumulate under the reinforcement bar reducing the bond strength [1-3]. On the other hand, SCC, especially very fluid SCC, may suffer from segregation, which may have a negative impact on the bond strength. However, if stable, it has been found that so-called "top-bar effect" in tall elements (formation of voids under horizontal reinforcement due to settlement) may be of the same order as conventional concrete for SCC [4, 10].

Most studies on bond strength have used relatively fluid SCCs with slump flows above 600 mm with correspondingly low yield stresses. However, much SCC is produced with lower slump flow values for simpler applications such as floors etc., where stability and control of the flowing concrete is essential to a successful hardened concrete quality. One important question using this type of low slump flow SCC is whether it will consolidate sufficiently to encapsulate the reinforcement bars and provide proper bond strength, and whether the plastic viscosity of such SCC plays a role in this respect. Only little previous information can be found regarding the effect of plastic viscosity. However, results from [4] indicate that very high viscosities on the order of 400 Pa·s may lead to inadequate self-consolidation and reduction in bond strength. In terms of the T_{500} value, it is suggested that care should be taken when the T_{500} value is in the range of 6-7 sec for SCC with slump flow of 650-700 mm. On the other hand, mixtures with slump flow of 650-700 mm that are less viscous resulted in proper self-consolidation with uniform bond strength.

The above was the motivation for conducting an experimental study of the bond strength of SCC in the slump flow range 500-600 mm but with quite different plastic viscosities, and comparing the results to the bond strength of slump concrete with the same basic mixture composition.

Experimental

Mix design

The concrete used was a C35 with a target air content of 5%. For five of the seven concretes tested the composition was the same except for the amount of superplasticizer added. The consistence varied between 150 mm slump and 580 mm slump flow. The conventional concrete and the SCC with similar composition are labeled NC, S1, S2, S4, and S6 in Table I.

Two compositions, S3 and S5, had a different mixture composition in order to increase the plastic viscosity. The paste content and equivalent water to cement

ratio was kept almost constant (an acticity factor of 0.5 was used for the fly ash) but the ratio of powder/(powder+water) (by volume) was increased by adding more fly ash.

Table I. Mixture composition and fresh properties of the seven concretes tested.

	NC	**S1**	**S2**	**S3**	**S4**	**S5**	**S6**
CEM I (Rapid Cement) (kg/m^3)	276	276	276	219	276	165	276
Water (kg/m^3)	142	142	142	129	142	119	142
Fly ash (kg/m^3)	92	92	92	158	92	222	92
Total binder (kg/m^3)	368	368	368	377	368	387	368
Aggregate 0/4 (kg/m^3)	803	803	803	803	803	803	803
Aggregate 4/8 (kg/m^3)	989	989	989	989	989	989	989
Paste content (l/m^3)	269	269	269	267	269	267	269
Equivalent w/c	0.44	0.44	0.44	0.43	0.44	0.43	0.44
Powder/(Powder+Water) (vol.)	0.48	0.48	0.48	0.52	0.48	0.56	0.48
Air volume (%)	5.0	5.0	5.0	5.0	5.0	5.0	5.0
Air measured (%)	5.6		4.8	6.6	9.0	6.0	4.5
Slump flow (mm) (*slump)	*150	580	560	580	520	580	530
Yield stress (Pa)		45	53	45	75	45	65
Plastic viscosity (Pa·s)		46	37	81	45	218	60

The mixing of the concrete was performed at Danish Technological Institutes full-scale mixing station comprising a 250 liter pan type counter-current mixer. The 250 liters of concrete required for each was mixed with the mixing sequence being 0/4, 4/8, cement + fly ash, water, superplasticizer in order of addition.

Formwork and casting procedure

A formwork was constructed out of epoxy coated expanded polystyrene to hold 12 mm nominal diameter ribbed reinforcement bars fixed horizontally, see Figure 1. The formwork dimension was 2.40 m x 0.25 m x 0.40 m (length x width x height). Two rows of six bars spaced 0.40 m apart with edge distances of 0.20 m were fixed in the formwork. The two rows of bars were placed 0.10 m and 0.25 m respectively from the bottom of the formwork. Holes were drilled into the side of the formwork and the bars were fixed in place using a wooden brace, ensuring that all bars had an embedment depth of 80 mm.

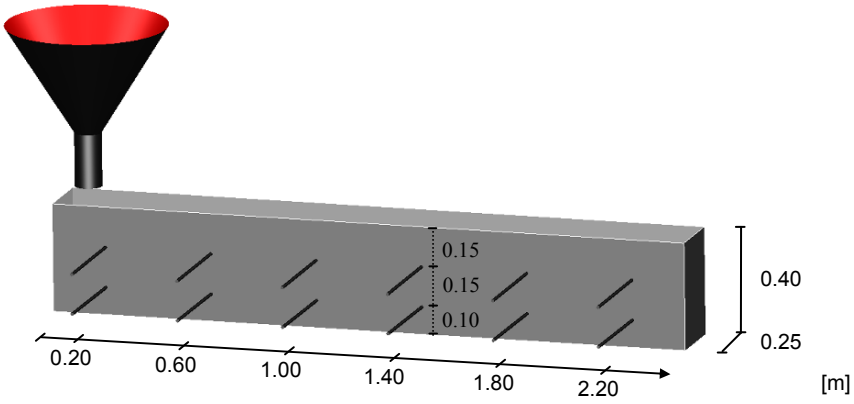

Figure 1. Formwork geometry and placement of reinforcement bars.

All SCC mixes were cast from one consistent location and allowed to flow under its own weight to fill the formwork, see Figure 2. The inlet was at the one end and approximately 250 liters of concrete was poured into the formwork. No mechanical consolidation was applied.

The conventional concrete on the other hand was cast at various locations and consolidation was performed using a poker vibrator.

Figure 2. Pictures of the formwork (left), during casting of SCC (middle), and a close up of the SCC flow near the reinforcement (right).

Testing

Prior to each casting, the flow properties and air content of the concrete was measured, and three 100 x 200 mm cylinders were cast for testing of the

compressive strength simultaneous with testing of bond strength. The flow properties were measured using the 4C-Rheometer (Figure 3), which provides estimates of the yield stress, plastic viscosity, slump flow and T_{500} values [11]. The workability of conventional concrete was characterized by its slump value. The fresh state properties are listed in Table I.

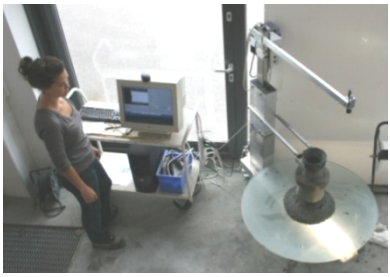

Figure 3. The 4C-Rheometer was used to measure the flow properties of SCC.

The cast cylinders were stored submerged in water at 20°C. The compressive strength and bond strength were tested when the concrete reached seven days of age. The rebars were pulled out using a hydraulic jack setup as shown in Figure 4.

Figure 4. The hydraulic jack setup used for testing the bond strength.

Results and Discussion

Figure 5 shows the measured SCC flow properties in a so-called rheology diagram displaying yield stress and plastic viscosity. The slump flow values varying between 520 mm and 580 mm are shown to the right. The diagram is divided into three sections of yield stress and plastic viscosity – low, medium and high. The sections have been proposed based on practical experiences with casting of SCC and examples of practical impact were given in [11]. As seen, the plastic viscosity

varies from 35 to 220 Pa·s approximately. For the SCC with the highest plastic viscosity the corresponding T_{500} value was roughly 11 seconds. The normal vibrated concrete had a slump value of 150 mm.

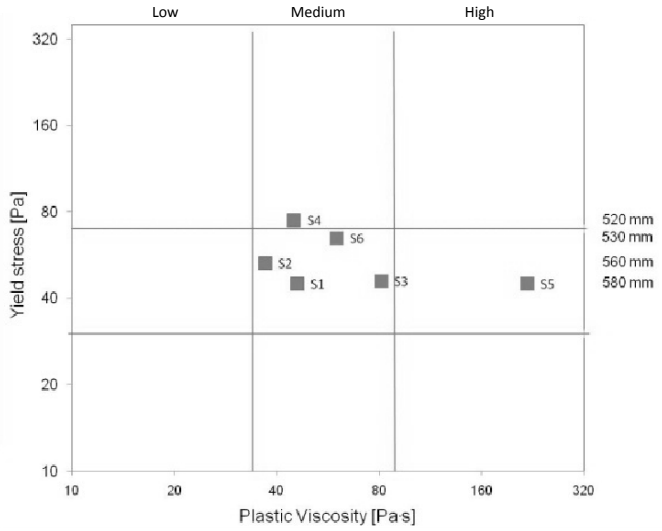

Figure 5. The flow properties of SCC.

When casting SCC the surface will be left with a downward slope depending on the yield stress of the concrete. The slopes of the SCCs S1-S6 are shown in Figure 6.

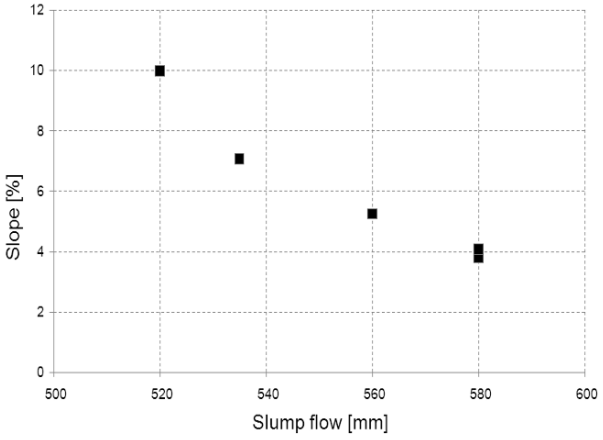

Figure 6. Final slope of the SCCs S1- S6.

The inclination of the SCCs left the top bars with a progressively lower cover distance and for the lowest slump flows the last two rebars in the far end (positioned at 1.80 and 2.20 m) was not covered by concrete at all. The pull-out strength drops with decreasing cover thickness. For comparison with the bottom row, only the top row bars with a concrete cover of minimum 100 mm have been included in calculation of the average bond strength.

Figure 7 shows the average bond strength of the top and bottom row for each concrete. To compare the results these are shown as normalized bond strength given as bond strength, f_b, over concrete tensile stress, f_{ct}. According to the EuroCode2 the design value of the ultimate bond stress, f_{bd}, for ribbed bars may be taken as:

$$f_{bd} = 2.25 \cdot f_{ctd} \tag{1}$$

where, f_{ctd} is the design value of the concrete tensile strength calculated as $f_{ctd} = (f_{cd})^{1/2}$, where f_{cd} is the design compressive strength.

Figure 8 shows the average bond strength of the bottom row for the SCCs as a function of yield stress and plastic viscosity, respectively.

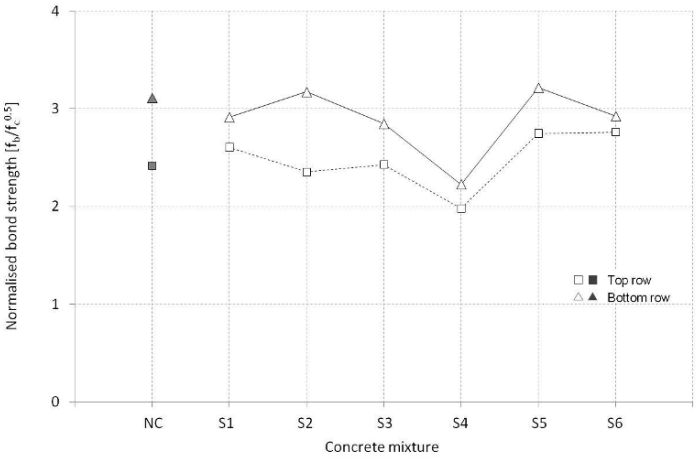

Figure 7. The average normalized bond strength of the top and bottom row of rebars.

For the bottom row the results show that SCCs S1, S2, S3, S5, and S6 are very similar to that of the conventional concrete, and higher than the normalized EC2 design value of 2.25. However, for S4 a significant lower value was obtained. This was the concrete with a slump flow of 520 mm, but it was also the concrete with the highest air content of 9.0%, which may contribute to a weaker interfacial zone

between the paste and rebar. For instance, S6 had a similar slump flow of 530 mm, but a lower air content of 4.5% and did not show a reduction in bond strength.

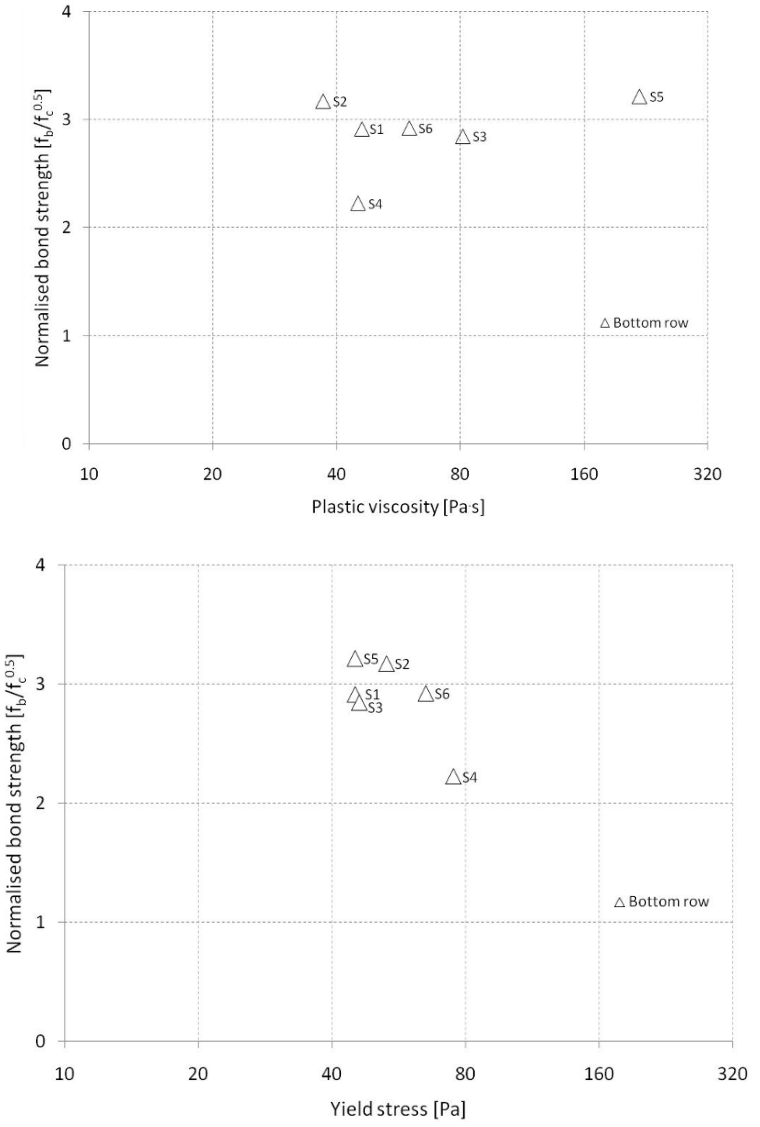

Figure 8. The average normalized bond strength of the SCCs (S1-S6) as a function of the measured yield stress and plastic viscosity. Results are shown for the bottom row.

For the top row, the results again show similar bond strengths to that of the conventional concrete, except for S4 with the high air content. Comparing the difference in bond strength between top and bottom row of rebars the results indicate that the variation for SCC is similar or less than that of conventional concrete. However, this should only be regarded as a weak trend due to the limited number of experiments e.g. only one data set for conventional concrete represented in the present study.

For the effect of rheology, the results indicate that it is possible to obtain bond strengths similar to that of conventional concrete for SCC with relatively high yield stresses (corresponding to slump flow from 520 – 580 mm) within a broad range of plastic viscosities (35 – 220 Pa·s).

Besides the flow properties also the flow pattern may have influence on the bond strength. Figure 9 shows the bond strength for each bar at the bottom row.

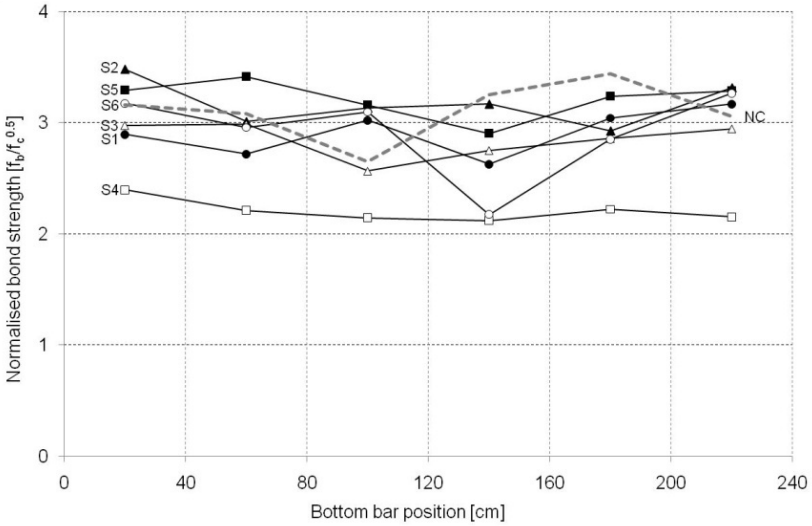

Figure 9. Normalized bond strength of each individual rebar from the bottom row. The dashed line represents the normal concrete (NC). The SCC flew from left towards right, i.e. 240 cm is the far end of the formwork.

During casting of a formwork some rebars may be located in zones of intense flow and others may be placed in more or less dead zones. Simulations, though not performed here, could be used to study the flow patterns and detect variations in flow. The variation seems to be of the same order as for the normal concrete and there seems to be no systematic variation depending on position within the

formwork. However, S6 did show one significantly lower bond strength value at 140 cm, but no real explanation for this could be found.

Conclusions

The bond strength of relatively low slump flow SCC has been compared to that of conventional concrete with similar mixture composition. The results indicate that there is no difference in average bond strength between SCC and slump concrete nor between the individual SCCs of varying plastic viscosities in the low slump flow range from 520-580 mm. The value of the plastic viscosity does not appear to influence the bond strength either, at least not within the investigated relatively broad range of 35-220 Pa·s. One test did show a significant lower bond strength, which seems to be caused by a high air content of 9.0%. Also, the variation in bond strength across the length of the specimen was found to be of the same order in SCC as for the conventional concrete tested indicating that the flow pattern, though unknown, did not influence the results.

References

[1] Sonebi, M., Zhu, W. and Gibbs, J. (2001), Bond of reinforcement in self-compacting concrete, *Concrete*, vol. 35, n. 7, pp. 26-28.

[2] Chan, Y., W., Chen, Y.S. and Liu, Y.S. (2003), Development of bond strength of reinforcement steel in self-compacting concrete, *ACI Structural Journal*, vol. 100, n. 4, pp. 490-498.

[3] Khayat, K.H. (1998), Use of viscosity modifying admixture to reduce top-bar effect of anchored bars cast with fluid concrete, *ACI Materials Journal*, vol. 95, n. 2, pp. 158-167.

[4] Khayat, K.H. and Mitchell, D. (2009), Self-consolidating concrete for precast, prestressed concrete bridge elements, National Corporative Highway Research Program, Report 628.

[5] Desnerck, P., De Schutter, G. and Taerwe, L. (2008), Bond strength of reinforcing bars in self-compacting concrete: Experimental determination, The 3rd North American Conference on the Design and Use of Self-Consolidating Concrete, Chicago.

[6] Cattaneo, S., Muciaccia, G. and Rosati, G. (2008), Bond strength in limestone Self-Compacting Concrete, The 3rd North American Conference on the Design and Use of Self-Consolidating Concrete, Chicago.

[7] Filho, F., Debs, M. and Debs, A. (2008), Bond-slip behavior of self-compacting concrete and vibrated concrete using pull-out and beam tests, *Materials and Structures*, vol. 41, n. 6, pp. 1073-1089.

[8] Valcuende, M. and Parra, C. (2009), Bond behaviour of reinforcement in self-compacting concrete, *Journal of Construction and Building materials*, vol. 23, n. 1, pp. 162-170.

[9] Sherif, Y., Abudayyeh, O., Maurovich, M. and Zalt, A. (2008), Bond strength of Self consolidating concrete, The 3rd North American Conference on the Design and Use of Self-Consolidating Concrete, Chicago.

[10] Söylev, T.A. and Francois, R. (2006), Effects of bar-placement conditions on steel-concrete bond, *Materials and Structures*, vol. 39, n. 2, pp. 211-220.

[11] Thrane, L.N., Pade, C. and Nielsen, C.V. (2010), Determination of rheology of self-consolidating concrete using the 4C-Rheometer and how to make use of the results, *Journal of ASTM International*, vol. 7, n. 1.

Development Length of Carbon-Fiber-Reinforced Polymer Bars in Self-Consolidating Concrete

Slamah Krem and Khaled Soudki

Department of Civil Engineering, University of Waterloo, Canada

Abstract. Self-consolidating concrete (SCC) is widely used in the construction industry. SCC is a high performance concrete with high workability and consistency allowing it to flow under its own weight without vibration and makes the construction of heavily congested structural elements and narrow sections easier. Recently, fiber-reinforced polymer (FRP) reinforcements, with their excellent mechanical and non-corrosive characteristics are being increasingly used as a replacement for conventional steel reinforcement. In spite of the wide spread of SCC applications, the bond behaviour of FRP bars in SCC has not been fully studied.
This paper presents the results of the first phase of an experimental study on the bond characteristics of sand coated CFRP bars in SCC beams. The experimental program of this phase consists of four SCC beams. All beams had the same geometric dimensions and were reinforced with single CFRP bar (12.7 mm in diameter). All beams were tested up to failure by four point bending regime with the shear span vary from 550 to 950 mm. The test results were used to evaluate the bond strength at different embedded lengths. These preliminary test results showed that the ACI 440.1R-06 [1] over estimated the development length of the CFRP bars in SCC, while CAN/CSA-S6-06 [2] equation is unconservative.

Introduction

Self-consolidating concrete (SCC) was developed and introduced to the concrete industry in the late 1980s. SCC can be defined as a highly workable high performance concrete that can flow and fill the target spaces under its own weight without vibration or any other means of consolidation, [3]. SCC provides advantages in both quality and cost reduction over conventional vibrated concrete (CVC) [3, 4]. SCC mixture reduces the potential of bleed water accumulation under horizontally embedded bars. This phenomenon is known as local w/c increase, which locally reduces the compressive strength and the bond strength of concrete [3]. Many researchers reported that the bond strength of steel reinforcing

K.H. Khayat and D. Feys (eds.), *Design, Production and Placement of Self-Consolidating Concrete*, RILEM Bookseries 1,
DOI 10.1007/978-90-481-9664-7_32, © RILEM 2010

bars in SCC is higher than that in CVC of comparable compressive strength [5-8]. Consequently, SCC has become a popular alternative for concrete structures.

Fiber-Reinforced Polymers (FRP) reinforcement was introduced in the last two decades as a promising material that can replace the conventional reinforcing steel; thus resolving the corrosion problem facing infrastructures worldwide. Currently, FRP is used as a primary reinforcement in several concrete structures and bridge decks. The advantages of FRP material are attributed to high-strength to mass ratio, corrosion resistance, and high fatigue resistance [1].

One of the research areas that still unresolved is the use of FRP reinforcement in SCC construction. The bond behavior of Carbon FRP (CFRP) as reinforcing bars in SCC beams is of particular interest. The development length equations in current design codes are based on the bond strength of GFRP bars in CVC, with no material correction factor to account for CFRP bars [1]. Thus a design equation for the development length of CFRP reinforcement bars in SCC is needed [9]. This study will experimentally examine the bond and flexural behavior, and determine the development length of CFRP bars in SCC beams.

Background

The design of reinforced concrete flexural members assumes perfect bond between the reinforcement bars and the concrete. In other words, the reinforcement and the concrete at the level of reinforcement experience the same strain change. This assumption allows engineers to use the strain compatibility analysis approach. To ensure this assumption is valid, reinforcing bars should have an embedded length equal or greater than the development length. A limited research is available on the bond behavior of reinforcing steel bars in SCC. There is no available published work on bond behavior of FRP bars in SCC.

Literature review

Chan et al. [6] conducted research on the bond strength of steel bars in SCC as compared to CVC using pullout specimens. The steel bars were placed at three levels to simulate bottom, middle and top bars. The embedded length was kept constant at 300 mm for all specimens. At 28 days age of concrete, the ultimate bond strength of the reinforcing steel bars in SCC specimens was found to be 9.5 MPa for the bottom bars, 6.98 MPa for the middle bars, and 6.38 MPa for the top bars. For CVC specimens, the ultimate bond strength was 6.38 MPa for the bottom bars, 4.36 MPa for the middle bars, and 3.66 MPa for the top bars. The authors concluded that steel bars in SCC exhibits better bond strength with less significant effects for top bars. Valcuende and Parra [7] found that the bond strength of steel bars in SCC was greater than in CVC. The difference in the bond strength tends to even out as concrete compressive strength increased.

Aly et al. [10] published a study on the tensile lap splice behaviour of Carbon and Glass FRP reinforcing bars in CVC. The test variables included the bar diameter and the splice length. The average concrete compressive strength for CFRP and GFRP specimens were 42 and 44 MPa, respectively. This work concluded that the maximum stress at the ends of spliced FRP bars was proportional to the splice length. The critical bond stresses associated with the critical splice lengths were larger in CFRP bars as compared to GFRP bars. For both bars, the critical bond stress decreased as the bar diameter and splice length increased. The recorded average bond strength for 9.5 and 12.7 mm diameter CFRP bars were 6.4 and 4.4 MPa, respectively, and for 15.9 and 19.1 mm diameter GFRP bars were 4.1 and 3.0 MPa, respectively. The higher bond strength recorded in CFRP specimen results confirms the need for material correction factors in the development length equation provided by ACI 440.1R-06 to account for higher stiffness of CFRP bars.

Rafi et al. [11] carried out an experimental study on the flexural and bond behavior of CFRP-reinforced beams in comparison to steel-reinforced beams. The beams were reinforced with two 9.5 mm diameter CFRP bars or two 10M steel bars and made of CVC. The concrete compressive strength for CFRP specimens was 42.5 MPa. The beams were subjected to four-point bending with a shear span of 675 mm and an additional 115 mm overhang embedded length. Both beam types failed by concrete crushing. In the CFRP-reinforced beams, the CFRP bars reached 80% to 90% of their rupture capacity at the beam failure load. No signs of slip were observed for CFRP-reinforced beams. The recorded average bond strength over the entire embedded length of the CFRP bars was 4.27 MPa, and the average bond strength within the first 400 mm of the embedded length was 5.62 MPa.

Mosley et al. [12] conducted a research study on the bond behavior of FRP reinforcing bars using a beam splice test. Twelve beams were tested in three sets including beams reinforced with steel, GRFP or AFRP bars. All beams had a splice length within the constant moment region. The splice length was varied from 305 to 457 mm. All beams failed by splitting of concrete cover within the splice length. The results indicated that at the same embedded length, the bond strength of the FRP beams was approximately about 50% that of steel bars. The authors conclude that the bond strength is related to the modulus of elasticity of the reinforcement.

Code equations

Based on the literature review there is no equation for development length of FRP bars in SCC. The development length equations in the available codes were formulated based on CVC properties. The Canadian Highway Bridge Design Code (CAN/CSA-S6-06 2006) [2] provides an empirical equation for the development length of FRP bars in CVC. This equation is based on the splitting failure mode.

$$l_d = 0.45 \frac{k_1 k_4}{d_{cs} + k_{tr} \frac{E_{frp}}{E_s}} \left(\frac{f_{frp}}{f_{cr}} \right) A_{frp} \quad (1)$$

where: l_d is the development length in mm, k_1 is the bar location factor, k_4 is the bar surface factor, f_{frp} is the stress in the FRP reinforcement, f_{cr} is the flexural cracking strength of concrete, A_{frp} is the area of FRP bar, E_{frp} is the modulus of elasticity of FRP reinforcement, E_s is the modulus of elasticity of steel, d_{cs} is the smaller of the distance from concrete surface to the bar center and two-thirds of the center to center spacing of bars and k_{tr} is the transverse reinforcement index. The term $(d_{cs} + k_{tr} \frac{E_{frp}}{E_s})$ should not be taken greater than $2.5d_b$.

The American Concrete Institute (ACI) Committee 440 published a series of design guidelines for using FRP reinforcement. ACI 440.1R-03 [13] provides two equations for the development length of FRP bars. The first equation is based on pullout failure, Eqn. (2) and the second one is based on splitting failure, Eqn. (3).

$$l_d = \frac{d_b f_{fu}}{18.5} \propto k \quad (2)$$

where l_d is the development length, d_b is the FRP bar diameter, f_{fu} is the design tensile strength of the FRP bar, α is bar location modification factor and k is the cover modification factor; it varies linearly from 1.5 to 1.0 as the cover varies between d_b and 2 d_b and equal to 1.0 for the cover greater than $2d_b$.

$$l_{frpd} = 0.028 \frac{A_{frp} f_{frpu}}{\sqrt{f'_c}} \quad (3)$$

where l_{frpd} is the development length, A_{frp} is the FRP bar cross section area, f_{frpu} is the tensile strength of FRP bar and f'_c is the concrete compressive strength.

In 2006, ACI 440 Committee published ACI 440.1R-06 [1]. A completely new approach was introduced for development length calculations based on the database collected by Wambeke and Shield [14]. This approach is based on the equilibrium principles for bars anchored in concrete. The normalized average bond stress versus the normalized cover and the embedment length equation were developed, Eqn. (4). This equation is based on results of beams failed by splitting and pullout [1]. The development length equation is given in Eqn. (5).

$$\frac{u}{0.083 \sqrt{f'_c}} = 4.0 + 0.3 \frac{C}{d_b} + 100 \frac{d_b}{l_e} \quad (4)$$

$$l_{d\,split} = \frac{d_b\left(\frac{f_{fu}}{0.083\sqrt{f_c'}} - 340\right)\propto}{13.6 + \frac{c}{d_b}} \quad (5)$$

where u is the bond stress, l_e is the embedment length, l_d is the development length, d_b is the bar diameter, f_{fu} is the design strength of the FRP bar, f_c' is concrete compressive strength, α is the bar location factor, C is taken as the lesser of the cover to the center of the bar or half the center-to-center spacing of the bars being developed, $f_{fu,}$ is the stress in FRP bar.

The database used in Wambeke and Shield [14] analysis is primarily based on beams reinforced with GFRP bars. Although there was no data on CFRP bars included in the calibration of Eqn. (4), ACI Committee 440 mentioned that "it is anticipated that the much larger stiffness of the CFRP bars will likely decrease the required development length." But ACI committee 440 recommended a material modification factor of 1.0 when CFRP bars are used. Additionally, ACI committee 440 set a limit of 3.5 on C/d_b so that Eqn. (4) can be used for either mode of failure: splitting or pullout; however, the specimen that failed in pullout was limited to embedment length to bar diameter ratio (l_d/d_b) between 15 and 30 [14] while specimens with splitting mode of failure had (l_d/d_b) between 19 and 100.

Experimental Program

Material properties

Carbon-fiber-reinforced polymer (CFRP) bars were used in this study. The bars were developed and manufactured in Quebec, Canada. The bars were made of continuous longitudinal fibers impregnated in a thermosetting vinylester resin with a typical fiber content of 73%, and their surfaces were sand-coated. The guaranteed tensile strength is 1765 MPa, the modulus of elasticity is 144 MPa, and the rupture strain is 1.32%. Deformed steel bars No. 10M (d_b = 11.3 mm) with yield stress of 400 MPa were used as the top steel bars and shear reinforcement stirrups. A commercially available SCC was used to cast all test specimens. All specimens were subjected to 7 days of moist curing at room temperature.

Tested beams

Full-scale beams were constructed and tested up to failure. Beam specimens were selected because they provide the actual bond behavior of flexural members. The beam geometry and loading configuration are shown in Figure 1. The length of the beam was selected to provide the required embedded length for testing. The cross section of all beams was maintained constant at 150 x 250 mm. All beams were

reinforced with a single CFRP bar in the tension zone. The concrete cover was selected to prevent splitting failure and it was maintained constant of 38.1 mm, $3d_b$ [1]. To avoid shear failure, all beams were reinforced with 10M closed stirrups spaced at 100 mm. The use of uniform shear reinforcement provides a constant confinement factor for bond strength evaluation.

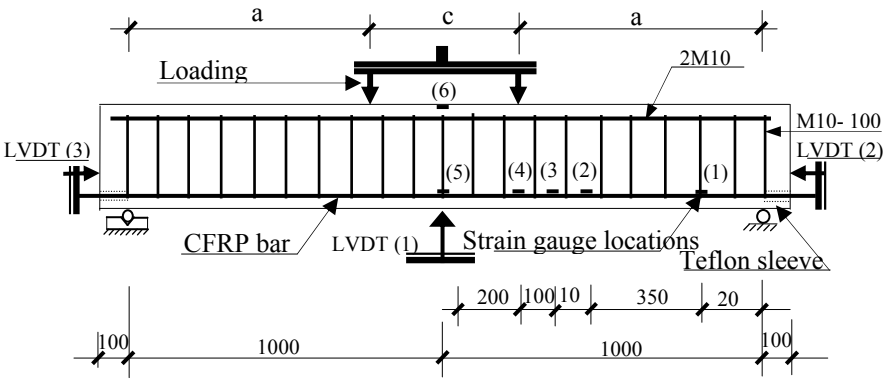

Figure 1. Typical beam geometry, instrumentation, and testing arrangements.

Instrumentations and measurements

Each beam was instrumented with several strain gauges (5 mm length) mounted on the CFRP bars within the shear span and one strain gauge (60 mm in length) on the concrete compression face. Two linear variable differential transducers (LVDTs), ±2.5 mm range, were used to measure the bar slip at each beam end. One LVDT, ±50 mm range, was used to measure the midspan deflection, Figure 1. The beams were tested in a four point bending regime using a universal testing frame of 330 kN capacity under stroke control of 1.5 mm/minute. The shear span was varied from 550 to 950 mm. Measurements of load, midspan deflection (LVDT 1), bar slip at beam ends (LVDT 2 and LVDT 3), strain in CFRP bar, and strain in concrete were collected using a data acquisition system.

Results and Discussion

Sectional analysis model was developed based on force equilibrium and strain compatibility approach to predict the flexural capacity of a beam reinforced with a CFRP bar. The model was capable of determining the section capacity, strain in the CFRP bar and in concrete compression face. Results of sectional analysis are presented and discussed with experimental results below.

Concrete fresh and hardened properties

SCC is flowable high workable concrete. All beams were cast without any vibration. The slump flow was 720 mm and the J-ring slump flow was 690 mm. Figure 2 shows the concrete compressive strength development over 56 days. The average concrete compressive strength at testing was 62.2 MPa.

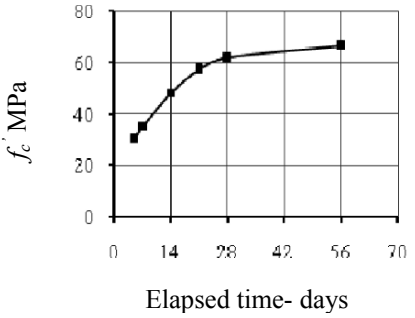

Figure 2. Concrete compressive strength results.

Structural behaviour

Figure 3 shows the moment deflection response for all beams. It is evident that all beams showed bilinear moment-deflection behaviour. The initial linear part of the curve had very steep slope, which correspond to the uncracked stiffness. The behaviour of all beams was similar before cracking with the exception of beam B1 which was tested as a cracked beam.

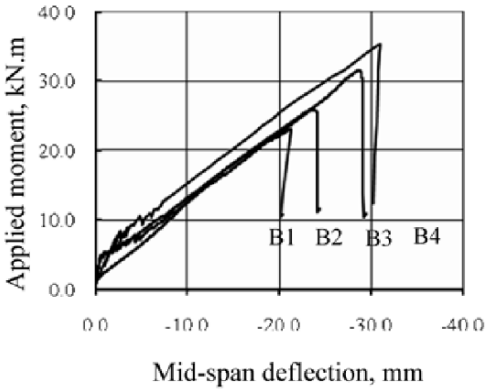

Figure 3. Moment vs. deflection response of all beams (B1, B2, B3 and B4).

In the second part of the curve, flexural cracks started to form. Typically the first crack occurred in the constant moment region. The first part of this segment

showed the influence of the cracks on the moment deflection response. The slope of this part is less than the slope of the first part. The rate of deflection per moment is higher after the beam has cracked which is an indication of the stiffness reduction. As the load increased, the cracks became wider at the bottom and propagated deeper into the beam depth up to 200 mm from the bottom face. Crack mapping indicate that the crack spacing increases as the embedded length increase. At an embedded length of 550 mm, the crack spacing was 110 mm and at embedded length of 950 mm, the crack spacing was 180 mm.

At about 80% of maximum load, an inclined crack began to form in the shear span (close to the constant moment region). This crack increased dramatically as the beam approaches failure. Finally, the beams were failed due to pull-out of the CFRP bar from one end of the beam. At failure, a loud noisy ping/pop sound was heard. The sudden bar slip was recorded by the horizontal LVDT located at the failure crack side (Figure 4-a). No slip was recorded on the other beam end. The summary of flexure test results is shown in Table I.

Table I. Summary of the flexural test results.

Beam	Shear span, mm	M_{exp}, kN.m	$\frac{M_{exp.}}{M_{theo.}}$	f_{frp}, MPa	$\frac{f_{frp}}{f_{frpu}}$	u, MPa
B1	550	23.0	0.56	795	0.45	4.57
B2	650	26.7	0.65	1152	0.65	5.62
B3	750	31.0	0.76	1317	0.75	5.57
B4	950	35.0	0.86	1555	0.88	5.19

where: $M_{exp.}$ is the experimental failure moment; $M_{theo.}$ is the theoretical section moment capacity based on sectional analysis; f_{frp} is the maximum stress in CFRP bar at failure; f_{frp} is the guaranteed tensile strength of the CFRP bar and u is the average bond stress at failure calculated as follows:

$$u_{average} = \frac{E_{cfrp}\varepsilon_{cfrp}A_{cfrp}}{\pi d_b l_{emb}} \quad (6)$$

where E_{cfrp} is the modulus of elasticity of the CFRP bar, ε_{cfrp} is the maximum strain recorded by the strain gauges, A_{cfrp} is the cross section area of the CFRP bar, d_b is the CFRP bar diameter and l_{emb} is the actual embedded length.

Bond analysis

The stresses in the CFRP bar were calculated from the strain gauge readings. The values before section cracking were very small; however, after section cracking the strains in the CFRP bar was increased dramatically. Some gauges experienced a

sudden increase in strain at a given moment. In beam B3 Figure 4-b, for example, the strain gauge at 750 mm from the support experienced a sudden increase in strain at a moment of 5.0 kN.m, which represents the cracking moment of the section. When a crack forms, the full tension force was transferred to the tension bar thus causing an increase in the strain values. Between cracks, tensile stresses were introduced into the concrete and the strain in the tension bar was smaller than at crack location [15]. Similar to the experimental results, the analytical analysis showed a sudden increase in strain of the CFRP bar once the section is cracked.

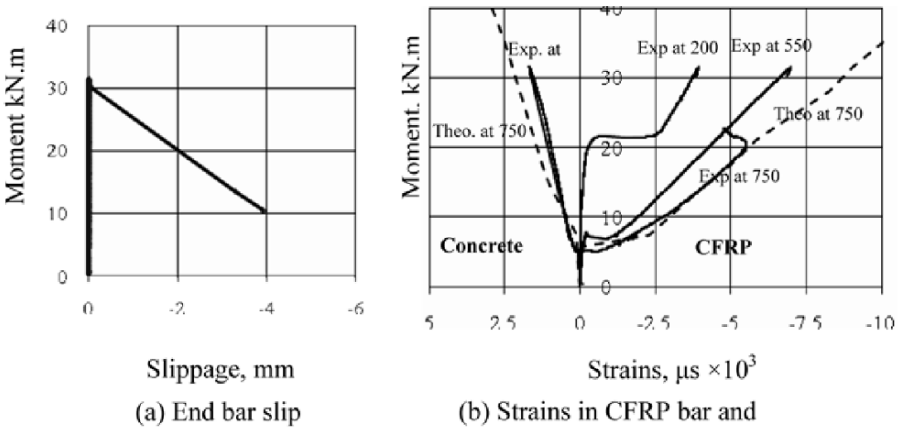

Figure 4. Beam B3 flexural test results.

The normalized bond strength results of the current study were plotted versus the normalized embedded length and compared to the data-base collected by Wambeke [14], Figure 5. Wambeke divided the beams based on mode of failure: pullout mode of failure in group (1), and splitting mode of failure in group (2). Specimens in group (1) had embedment length to bar diameter ratio (l_e/d_b) between 15 and 30 and specimens with splitting mode of failure had (l_e/d_b) up to 95. At comparable (l_e/d_b), the CFRP bars used in SCC beams showed higher bond strength than those of GFRP used in CVC beams. These values were, however, lower than those of GFRP bars used in CVC beams that failed by pullout (l_e/d_b of 15 to 30).

Development length

The failure moment increased from 23 to 35 kN.m as the embedded length increases from 550 to 950 mm, Table I. At an embedded length of 950 mm, the failure moment represented 86% of the theoretical moment capacity. The failure moment versus embedded length relationship is shown in Figure 6. The predicted moment capacity is 40.8 kN.m; therefore the development length of the CFRP bar is expected to be higher than 950 mm. using the average normalized bond strength

of 0.66 (Figure 5), and force equilibrium approach, the development length equation can be formulated as follows:

$$l_{d-pullout} = \frac{d_b f_{fu}}{2.64\sqrt{f'_c}} \quad (7)$$

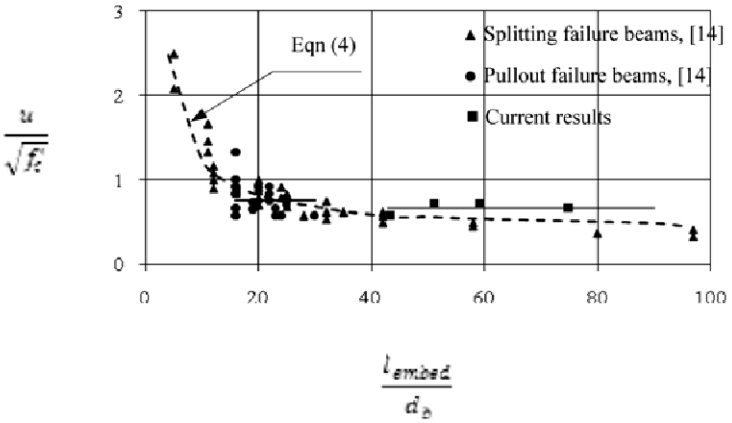

Figure 5. Average normalized bond stress versus normalized embedment length.

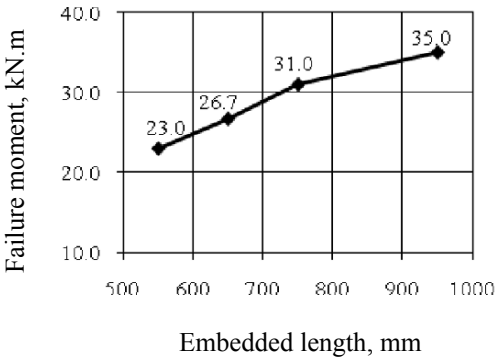

Figure 6. Failure moment versus embedded length relationship.

The development length for a CFRP bar in SCC in the current study was calculated based on Eqn. (7) to be 1080 mm. In comparison, the development lengths were calculated based on available code equations. The CAN/CSA-S6-06 Eqn. (1) gave a value of 834 mm (considering k_4 factor =1.0), unconservative by 28%; ACI 440.1R-03 Eqn. (2) gave a value of 1211 mm (conservative by 12%), while ACI 440.1R-06 Eqn. (5) yields a value of 1750 mm (conservative by 62%). The ACI

440.1R-06 Eqn. (5) resulting in development length to bar diameter ratio (l_d/d_b) greater than 100, which beyond the validity of the ACI 440.1R-06 Eqn. (4).

The ACI 440.1R-03 Eqn. (2), which based on pullout mode of failure, provided closer prediction of the development length for this experimental work than those of Eqn. (1) and Eqn. (5). The CAN/CSA-S6-06 Eqn. (1) was originally developed for the steel bars in CVC [2, 16]. The modulus of elasticity factor $(\frac{E_{frp}}{E_s})$ was introduced in this equation to account for the FRP bars. However, the difference in the bond characteristics was not addressed properly with this factor. Similar results were obtained by Aly et al. [10] for the larger FRP bars in CVC. The bond stress prediction of ACI 440.1R-06 Eqn. (4), which is based on beams reinforced with GFRP bars in CVC with most of them failed in splitting than pullout mode of failure, gives 3.68 MPa. When a bar has sufficient cover to prevent splitting, larger bond stress could be developed as compared to bars with small cover which tend to fail in splitting mode of failure before the full bond strength can be developed. The available literature showed the average bond strength of the CFRP bar in CVC beams is between 4.2 to 4.4 MPa [9-11].

The results of the present study showed that there is an improvement in the bond strength of CFRP in SCC as compared with CFRP in CVC. This is because the homogeneity of concrete around the bar becomes higher in SCC due to more fines. Studying the bond and interfacial properties of steel reinforcement, Zhu et al. [8] found that SCC provides 10–40% higher bond strength than CVC.

Based on the current results, it can be concluded that the CFRP bars in SCC can develop higher bond stress as compared to the GFRP in CVC. The ratio of bond stress of CFRP to GFRP bars is around 1.42. This factor includes combined effect of the bar materials and the concrete type. More research is needed to investigate the effect of concrete type, bar material and bar diameter.

Conclusions

This paper presents an on-going experimental investigation on bond characteristics and the development length of CFRP embedded in SCC. Based on the results of this experimental work, the following conclusions can be drawn:

- Beams made from SCC and reinforced with CFRP bars showed bilinear moment-deflection behavior.
- All beams failed by sudden pullout of the CFRP bar from the concrete. CFRP bar rupture was not observed in all beams. Using a concrete cover of 3 times the bar diameter was sufficient to prevent splitting failure for the tested beams.
- The failure moment increased from 56% to 86% of the beam capacity when the embedded length was increased from 550 to 950 mm.

- Bond strength of the CFRP bars in SCC tested in this study was higher than those of the CFRP and the GFRP in CVC reported in literature.
- An equation for the development length of CFRP bars in SCC was proposed. This equation needs to be verified with other bond parameters such as the bar diameter and concrete compressive strength.
- Predictions of the development length of CFRP bar in SCC using CAN/CSA-S6-06 were unconservative while those using ACI 440.1R-06 were very conservative.
- Further experimental work is recommended to include the effect of concrete type, concrete compressive strength, and CFRP bar diameter.

Acknowledgements

The authors gratefully acknowledge Alfateh University Tripoli – Libya for the scholarship provided to the first author. The financial support provided by NSERC and support by the technical staff at the University of Waterloo is highly appreciated.

References

[1] ACI Committee 440 (2006), ACI 440.1R-06, American Concrete Institute, Farmington Hills, MI.
[2] Canadian Standards Association (2006), CAN/CSA-S6-06, A National Standard of Canada, Mississauga, Ontario, Canada.
[3] ACI Committee 237 (2007), ACI 237R-07, American Concrete Institute, Farmington Hills, MI, USA.
[4] Okamura, H. and Ouchi, M. (2003), *Journal of Advanced Concrete Technology,* vol. 1, n. 1, pp. 5-15.
[5] Domone, P.L. (2007), *Cement & Concrete Composites,* vol. 29, n. 1, pp. 1-12.
[6] Chen, Y.W., Chen, Y.S. and Liu, Y.S. (2003), *ACI Structural Journal,* vol. 100, n. 4, pp. 490-498.
[7] Valcuende, M. and Parra, C. (2009), *Construction and Building Materials,* vol. 23, n. 1, pp. 162-170.
[8] Zhu, W., Sonebi, M. and Bartos, P. (2004), *Material and Structures,* vol. 37, n. 7, pp. 442-448.
[9] Khayat, K. and Mitchell, D. (2009), NCHRP report 628, Transportation Research Board, Washington, D.C. USA.
[10] Aly, R., Benmokrane, B. and Ebead, U. (2006), *ACI Structural Journal,* vol. 103, n. 6, pp. 857-864.
[11] Rafi, M., Nadjai, A. and Ali, F. (2007), *Journal of Composite Materials,* vol. 41, n. 22, pp. 2657-2673.

[12] Mosley, C.P., Tureyen, A.K. and Forsch, R.J. (2008), *ACI Structural Journal,* vol. 105, n. 5, pp. 634-642.
[13] ACI Committee 440 (2003), ACI 440.1R-03, American Concrete Institute, Farmington Hills, MI.
[14] Wambeke, B. and Shield, C. (2006), *ACI Structural Journal,* vol. 103, n. 1, pp. 11-17.
[15] Collins, P.M. and Denis, M. (1997), "Prestressed Concrete Structures," Response Publication, Toronto.
[16] Canadian Standard Association (2006), CSA Standard A23.3-04 – Concrete Design Handbook, third edition, Cement Association of Canada, Ottawa Canada.

Theme 9: Design and Performance of Fiber-Reinforced SCC

Design with Highly Flowable Fiber-Reinforced Concrete: Overview of the Activity of fib TG 8.8

Liberato Ferrara[1], Steffen Grünewald[2] and Frank Dehn[3]

[1] Department of Structural Engineering, Politecnico di Milano, Italy
[2] Delft University of Technology/Hurks Beton, The Netherlands
[3] University of Leipzig/MFPA, Germany

Abstract. Self-compacting fiber-reinforced concrete (SC-FRC) combines the benefits of highly flowable concrete in the fresh state with the enhanced performance in the hardened state in terms of crack control and fracture toughness provided by the wirelike fiber-reinforcement. Thanks to the suitably adapted rheology of the concrete matrix, it is possible to achieve a uniform dispersion of fibers, which is of the foremost importance for a reliable performance of structural elements. Balanced viscosity of concrete may also be helpful to drive the fibers along the concrete flow direction. An ad-hoc designed casting process may hence lead to an orientation of the fibers "tailored" to the intended application, which is along the anticipated directions of the principal tensile stressed within the structural element when in service. This converges towards a "holistic" approach to the design of structure made with highly flowable/self-consolidating FRC, which encompasses the influence of fresh state performance and casting process on fiber dispersion and orientation and the related outcomes in terms of hardened state properties. The fib task Group 8.8 "Structural design with highly flowable concrete", sub-group fiber concrete, appointed in April 2009, aims at drafting recommendations to facilitate and spread the use of these innovative materials, merging together research findings and practical experience.

Introduction

The synergy between Self-compacting concrete (SCC) and fiber-reinforced concrete (FRC) combines the benefits of the former's superior fresh state behaviour with the enhanced performance of the latter in the hardened state. Due to the elimination of compaction and vibration and to the suitably adapted rheology of the concrete matrix, a homogeneous dispersion of fibers within SCFRC elements can be achieved, which is of crucial for a reliable structural performance [1].

K.H. Khayat and D. Feys (eds.), *Design, Production and Placement of Self-Consolidating Concrete*, RILEM Bookseries 1,
DOI 10.1007/978-90-481-9664-7_33, © RILEM 2010

It has been also shown that, thanks to a balanced viscosity of the concrete mixture, fibers can be aligned along the direction of the fresh concrete flow during casting [2]. A suitably designed casting process may thus lead to an orientation of the fibers "tailored" to the intended application, which is along the anticipated direction of principal tensile stresses within the structural element when in service. A superior mechanical performance in the hardened state can hence be achieved along the direction at issue, which may lead to optimized structural dimensions and self weights. This finally results into a more rational design of the supporting structure, and consequently into a more time- and cost-effective construction process, including costs for transportation, capacity of lifting equipments etc.

This converges towards the definition of a "holistic" approach to the design of structures made with highly flowable FRC, which has to encompass the multifold correlation among the fresh state performance, casting procedure, fiber dispersion and orientation and the mechanical properties in the hardened state, including material anisotropy due to the flow-induced orientation of fibers.

To this aim several aspects have to be considered:

- the mix-design, to achieve optimum resistance to static and dynamic segregation of fibers;
- the concepts of suitable test methods and equipment to characterize the fresh state performance, with major focus on fiber dispersing ability;
- the "on-site" (non-destructive) monitoring of fiber dispersion and orientation, and their prediction as a function of the fresh state performance and casting process, also in the sight of designing the latter to achieve an orientation tailored to the intended application;
- the identification of the relevant material properties and of the "constitutive" stress-strain/crack opening relationships as a function of the flow-driven fiber orientation, including the effects of induced anisotropy.

These aspects will be the focus of the activity of the fib TG 8.8 "Structural Design with flowable concrete" – subgroup fiber-reinforced concrete and will be addressed in this paper. The final goal of the TG is to spread and facilitate the use of advanced fiber-reinforced cementitious composites with adapted rheology for high end structural applications by drafting recommendations in which state of the art knowledge and practical experience will be merged.

Mix-Design and Fresh State Performance

Successful casting of highly flowable FRC relies on a solid mix-design methodology to achieve the fresh state performance required for the intended application. The addition of fibers to a concrete matrix affects its fresh state performance, due to both the larger surface area of fibers, which requires more fluid

phase to be properly enveloped and lubricated, and the significant inter-particle friction and interlocking between fibers and between fibers and aggregates [3].

Several mix-design approaches have been proposed, *e.g.* including fibers through a fictitious equivalent diameter into the optimization of the solid particle grading [4-6] and/or accounting for their influence on the packing density of a given polydisperse particle arrangement [7], either empirically [8, 9] or through the so-called perturbed volume concept [10]. Based on referred investigations, it can be reliably stated that the same enhanced fresh state performance of a plain concrete matrix can be guaranteed with the incorporation of fibers, by replacing an amount of (coarse) aggregates equivalent to the addition in terms, e.g., of the specific surface area. This allows one to maintain the same balance between the surface area of solid particles which has to be lubricated by the suspending fluid phase (paste or mortar) and the rheological properties of the latter [6-8, 11-13]. Mix-compositions of different SCSFRCs illustrating the aforementioned concepts are given in Table I and Table II, together with the measured values of slump flow diameter and T_{50}.

Table I. Examples of mix design of plain and fiber-reinforced SCCs – adjustment of aggregate proportions for increased specific surface area of fibers [6].

	SCC1	**SCSFRC1**	**SCC2**	**SCSFRC2**	**SCC3**	**SCSFRC3**
Constituent	**Dosage (kg/m^3)**					
Cement type I	380	380	400	400	450	450
Fly ash Class C	142	142	150	150	167	167
Water (*w/b*)	188 (0.36)	188 (0.36)	177 (0.32)	177 (0.32)	197 (0.32)	197 (0.32)
SP (% binder)	2.4 (0.45)	2.4 (0.45)	3.0 (0.55)	3.0 (0.55)	2.8 (0.45)	2.8 (0.45)
V_{paste}	0.36	0.36	0.36	0.36	0.40	0.40
Sand 0-4.6 mm	936	929	936	929	887	872
Gravel 4.6-9.5 mm	763	754	763	754	715	708
Steel fibers 65/35	=	50	=	50	=	50
Slump flow diam.(mm)	710	690	725	710	750	750
T_{50} (sec)	3	3	5	5	3	3

Table II. Examples of mix design SCSFRCs – influence of different fiber types and dosages [6].

	SCSFRC-A	SCSFRC-B	SCSFRC-C	SCSFRC-D
Constituent	**Dosage (kg/m^3)**			
Cement type I	400	397	390	392
Fly ash Class C	148	148	145	146
Water (*w/b*)	186 (0.34)	185 (0.34)	182 (0.34)	183 (0.34)
SP (% binder)	2.7 (0.5)	2.7 (0.5)	2.6 (0.5)	2.7 (0.5)
V_{paste}	0.37	0.365	0.36	0.36
Sand 0-4.6 mm	918	913	940	931
Gravel 4.6-9.5 mm	749	745	748	749
Steel fibers (type)	50 (65/35)	80 (65/35)	50 (65/60)	25 + 25 (65/35)+(65/60)
Slump flow diam.(mm)	650	600	635	650
T_{50} (sec)	4	4	4.5	4.5

The fresh state performance of highly flowable FRCs deserves further investigation, which the activity of the fib TG 8.8 will encourage and address, with a major focus on test methods and equipments, which may differ from those currently employed for plain SCC. Minimum clear spacing between the obstacles has for example been specified, as a function of the fiber length, aspect ratio and dosage, to avoid blockage in L-box and J-ring tests [14]. The ability of the mixture to guarantee a uniform dispersion of fibers during casting has also been recognized as a peculiarity of these materials. Some early attempts to address the issues related to its measurements have also been reported, either with reference to lab-scale tests [15, 16] and full-scale casting mock-ups [17, 18].

The reliability and the robustness of test methods and measurements have to be assessed together with their correlation with other indicators of the fresh state performance, in the sight of developing standards which support quality control.

Fiber Dispersion and Flow-Induced Orientation

A uniform dispersion of fibers within elements can be achieved with highly flowable/self-compacting SFRC, thanks to the elimination of consolidation and vibration, which would otherwise hinder the aforementioned uniformity, causing

downward settlement, clustering and agglomeration and also resulting in fiber-free or poorly reinforced zones [1, 19]. These, acting as flaws, may seriously affect the structural performance, with reference to either the achievement of the predicted load-bearing capacity and the activation of the anticipated failure mechanisms. Thanks to a suitably balanced viscosity of the fresh concrete, fibers can be also effectively aligned along the direction of the casting flow. Sound evidence to the above said statement was provided by dedicated experimental investigation, performed either at the lab-scale [1, 2, 6, 8, 19-24] and on full scale precast elements [6, 19, 25]. Information on the influence of the casting flow geometry, level of fresh state performance and fiber dosage and aspect ratio was also obtained.

In most of the reported investigations, fiber dispersion and orientation were evaluated by counting fibers on cross sections of specimens, either manually or employing time-consuming image analysis procedures. X-ray pictures of cores or of thin specimen slices were also taken [19, 23, 26]. Though they immediately display fiber orientation, quantitative information could hardly be obtained, either due to the loss of the third dimension and, most of all, in case of higher percentages on short fibers. This points out the need to develop reliable, time- and cost-effective, non-destructive, methods for the on-site monitoring of fiber dispersion related issues, which could be easily implemented into quality control procedures.

Electrical methods based on the effect of fibers on the conductivity of the composite have received much attention in the very last years. Among them the Alternate Current Impedance Spectroscopy (AC-IS) was intensively investigated and proved to be a reliable tool for the purpose at issue [27, 28]. The method is based on the frequency dependant behaviour of cementitious composites reinforced with conductive, such as steel and carbon, fibers. These were in fact shown to be insulating under Direct Current (DC) and low frequencies of Alternate Current (AC) while they are conductive under high frequencies of AC. A wide assessment of the method was performed at the lab-specimen scale [1, 27], also through comparison with image analysis, showing its sensitivity to orientation and to sources of non-uniform fiber dispersion, such as clumping, segregation etc. and addressing its application also to full-scale case studies [28]. So far, the method has been applied by using special and dedicated equipment, which, also due to its higher cost, may not be widely available, e.g. for on site assessment of existing structures or quality control, e.g. in precast factories. The feasibility of simpler equipments as well as of alternative approaches to the measurement of electrical and magnetic properties of the composite is currently under investigation [20, 29-31]. Among the cons of electrical methods, it has to be remarked that their application may result questionable in some cases, such as structural topping of floor and roof decks in precast structures or in structural repair and rehabilitation, where the measurements can be affected by the presence of the original underlying structure. Furthermore they are highly sensitive to moisture gradients, which can hardly be controlled in existing structures [27, 28].

Methods based on the study of heat transients and on the effects of fibers on thermal diffusivity of the composite has also been tentatively applied [32]. Despite temperature fields can easily be surveyed through IR thermography, a major difficulty remains the slow propagation of temperature variations in thick members, which makes it difficult to provide a controlled input excitation over large areas.

Computer Axial Tomography has also been applied to investigate fiber dispersion [21, 33], which is able to provide a nice visualization of the 3D fiber arrangement. The need of dedicated equipment and analysis software still is the major drawback to a wider use of the method at industrial scale.

The prediction of fiber orientation as a function of the fresh concrete properties and of the casting flow geometry stands as a likewise challenging and cutting-edge research need. It would in fact allow to "tailor" the casting process to the intended application, to achieve the aforementioned closer correspondence between the alignment of fibers, along the direction of the fresh concrete flow, and the anticipated direction of the principal tensile stresses.

Numerical modeling of fresh concrete flow has been recently recognized as an effective tool the aforementioned purpose [34]. Computational Fluid Dynamic approaches have been successfully applied to model the flow of fresh concrete in simple tests and a few examples of full scale castings assuming a single fluid behaviour can be found [35-38]. As an alternative to CFD, Discrete Element method, normally employed for modeling the flow of granular media, has been applied to the simulation of the fresh concrete behaviour [39]. Fibers can be modeled as clusters of solid spheres. Calibration of the interaction laws between the particles is a crucial and not simple task which needs to be solved to make comparison quantitatively meaningful.

The improvement and the calibration of numerical predictive tools have also to be performed with reference to significant experimental benchmarks. They are also instrumental to clarify the role of casting geometry, fiber geometry, type and volume fraction as well as of the fundamental rheological properties of the fluid matrix, and to identify suitable parameters able to effectively describe the aforementioned phenomena in the framework of a design-oriented prediction.

Engineering Properties in the Hardened State

Engineering properties of fiber-reinforced cementitious composites, ranging from resistance to shrinkage cracking to fracture toughness, are actually the outcome of the toughening effects due to the dispersed wirelike reinforcement [40]. This actually depends on the fiber geometry, quantity, filament strength, dispersion and orientation with respect to the applied stress and on the fiber-matrix bond [41].

Several experiences on pull-out behavior of single fibers from SCC concrete matrices have been reported [8, 42]. The role of fiber type, embedded length, and inclination angle was investigated, providing sound confirmation to the knowledge on the topic. The comparative investigation between self-compacting and traditional vibrated concrete matrices, featured by the same compressive strength, showed comparable values of maximum bond strength (Figure 1).

The higher paste volume and the lower maximum aggregate size of concrete exhibiting highly flowable/SCC consistency with respect to vibrated ones, result in lower stiffness as well as in a more brittle behaviour in compression. A few related investigations [18, 43-44] confirmed that fibers may temper the inherent higher brittleness of the matrix and also positively affect the stiffness. Further investigation is necessary on this topic, whose major outcomes should also confidently support dedicated design prescriptions.

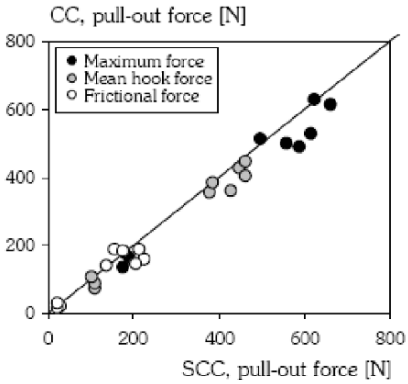

Figure 1. Pull-out fiber force in vibrated concrete (CC) and SCC matrices [8].

The possibility of achieving a randomly uniform dispersion of fibers has been recognized as instrumental to reduce experimental scattering [1] or top-column effect [22, 44], with related outcomes concerning, e.g., the characteristic values of material properties and safety factors [45]. Furthermore, the possibility of achieving a flow-driven orientation of the fibers which can be tailored to match as close as possible with the direction of the principal tensile stresses, has led to establish quantitative correlation between flexural strength and toughness parameters and the fiber orientation factor on the fracture surface [1, 2, 8, 21, 22, 46 – Figure 2]. In all cases specimen manufacturing was carefully designed and performed to trigger fiber orientation along the flow direction of the fresh concrete. This emphasizes the following issues which deserve and need to be addressed:

- the experimental identification of material properties for design calculations as well as the procedure for material qualification and acceptance: not only the specimen geometry and the testing methodology employed to the purpose

have to reproduce either the major characteristics of the geometry and of the stress and strain state of the intended application. The casting procedure employed to manufacturing the specimens, has also to "mimic" as close as possible the one which will be actually employed in the practice, so to achieve a close correspondence between the flow induced orientation of the fibers and the applied state of stress (mainly with reference to the principal tensile stresses);

- the anisotropy due to the flow induced orientation of the fibers, may even cause the material to exhibit significantly different properties in two orthogonal directions (Figure 2). This has to be carefully evaluated and taken into account in the design, mainly whenever significant biaxial stress-states are expected. Experimental investigation on the behaviour under biaxial stress-states, as affected by the orientation of the fibers with respect to the direction of principal stresses, is, in the authors' opinion, a challenge that needs to be addressed by research.

Paving the Way towards High End Structural Applications

In the very last decade SCFRC has been used in a certain number of partially and full load-bearing structural applications, including slabs on grade [48] and overlays [49], precast prestressed beams [18] and roof elements [19], sheet piles and tunnel segments [8], post-tensioned girders for slope stabilization [17], thin-wall houses [50, 51], refractory concrete linings [52] and façade panels [43, 53]. The use of fibers was always cued by the opportunity of partially replacing or even completely substituting traditional reinforcement, e.g. stirrups or welded wire meshes. Superior performance with respect to similar vibrated SFRC applications was recognized and attributed to the improved fiber dispersion [54]. Benefits in terms of the overall efficiency of the construction process were also reported, such as increased speed of construction, reduced crew-size, cost- and energy saving, automation of quality control. The benefits of a tailored orientation of fibers have also been highlighted.

Pilot applications of highly flowable/self-compacting FRC have highlighted the need to converge towards the definition of an integrated design approach which tailors both the material composition and the casting process to the anticipated structural performance. This aims to achieve a tailored orientation of fibers, matching as close as possible with the direction of the principal tensile stress within the structural element when in service, and which may yield to a more efficient structural use of the material. In the design process a desirable closer correspondence between the shape of an element and the function it performs in a structure assembly could hence be pursued. A suitably balanced fresh-state performance of the fiber-reinforced composite would allow to mould the shape of an element and, thanks to a tailored casting process, to orientate the fibers along the direction of the principal tensile stresses resulting from its structural function.

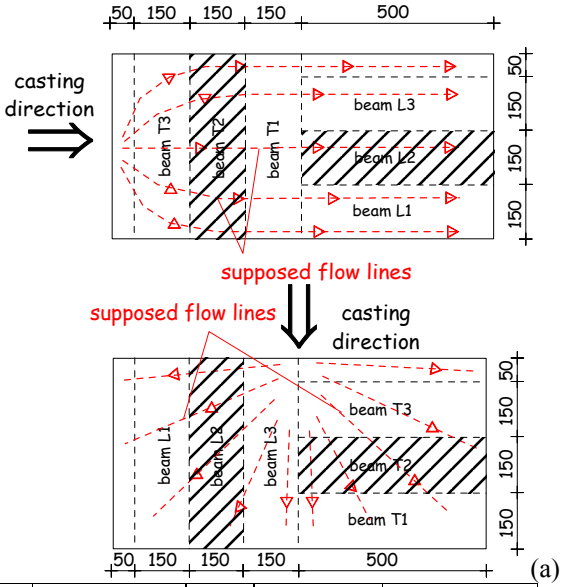

Spec.	cross section area cm² (in²)	n_{fibers}	fibres/cm² (fibers/in²)	$\alpha = n_{fibers} \frac{A_f}{V_f}$
A-L2	45.7 (7.3)	2463	53.9 (337.4)	0.850
A-T2	44.1 (7.0)	1236	28.0 (176.6)	0.442
B-L2	45 (7.2)	2159	48.0 (300)	0.757
B-T2	46.7 (7.5)	1593	34.1 (212.4)	0.538

(b)

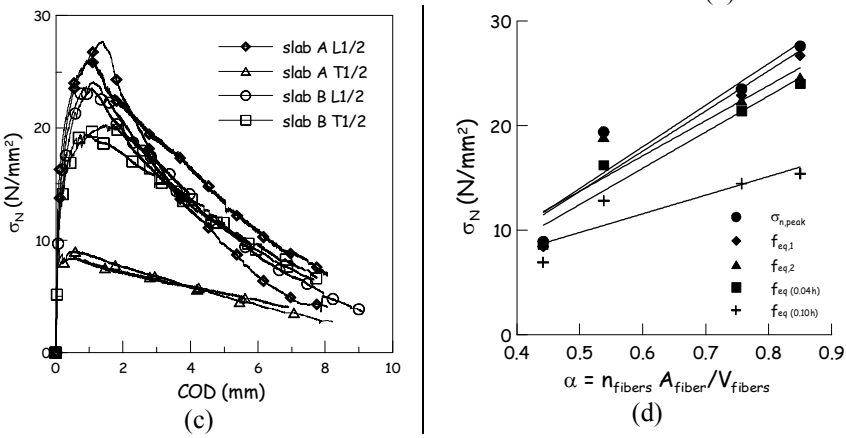

Figure 2. Specimen casting (a), fiber orientation factors on fracture surfaces (b), results of 4pb tests on beams cut with axis at different orientation to the casting flow direction (c), and toughness parameters vs. fiber orientation factors (d) [2].

Concluding Remarks: Envisioning the Activity of fib TG 8.8

fib TG 8.8 will focus on drafting guidelines on the structural design with highly flowable fiber-reinforced concrete providing a synopsis of the several different issues addressed in this paper. This would also hopefully trigger further research to resolve many open problems which still deserve in depth investigation:

- the definition of test methods to characterize the fresh state performance of SCFRC focusing on the resistance to static and dynamic segregation of fibers;
- the development and assessment of techniques for non-destructive, on-the-site, monitoring of fiber dispersion and orientation;
- the prediction of fiber dispersion and orientation as a function of the rheological properties of the mixtures and of the casting geometry, also in the sight of tailoring either the mixture-composition/fresh state performance and the casting process to the intended application;
- the definition of suitable procedures for the identification of material properties in the hardened state, which should be representative of the intended application and encompass the influence of the aforementioned variables;
- the suitable characterization of material anisotropy due to the flow induced orientation of the fibers and the related outcomes on the structural performance.

This would pave the way to spread the use of this kind of advanced fiber-reinforced cement based materials to a broader range of applications, not merely through the study of optimized geometries but also through the development of innovative high-end structure concepts.

References

[1] Ferrara, L., Park, Y.D. and Shah, S.P. (2008), *ASCE J. Mat. Civ. Eng.*, vol. 20, n. 7, pp. 493-501.
[2] Ferrara, L., Ozyurt, N. and di Prisco, M. (2010), *Mat. & Struct*., accepted.
[3] Bayasi, M.Z. and Soroshian, S.P. (1992), *ACI Mat. J.*, vol. 89, n. 4, pp. 369-374.
[4] Yu, B., Zou, R.P. and Standish, N. (1992), *J. Am. Cer.Soc.,* vol. 75 n. 10, pp. 265-272.
[5] Yu, B., Standish, N. and McLean, A. (1993), *J. Am. Cer. Soc.*, vol. 76, n. 11, pp. 2813-2816.
[6] Ferrara, L., Park, Y.D. and Shah, S.P. (2007), *Cem. Concr. Res.*, vol. 37, n. 6, pp. 957-971.
[7] Martinie, L., Rossi, P. and Roussel, N. (2010), *Cem. Concr. Res.*, vol. 40, n. 2, pp. 226-234.
[8] Grunewald, S. (2004), PhD Thesis, Delft University of Technology.

[9] Pereira, E.N.B., Barros, J.A.O., Ribeiro, A.F. and Camoes A. (2004), In: Proceedings BEFIB04, di Prisco, M. et al. (Eds.), RILEM Pubs., Paris, pp. 1371-1380.
[10] De Larrard, F. (1999), E&FN Spoon.
[11] Saak, A.W., Jennings, H.M. and Shah S.P. (2001), *ACI Mat. J.*, vol. 98, n. 6, pp. 429-439.
[12] Bui, V.K., Akkaya, J. and Shah, S.P. (2002), *ACI Mat. J.*, vol. 99, n. 6, pp. 549-559.
[13] Bui, V.K., Geiker, M.R. and Shah, S.P. (2003), In: Proceedings HPFRCC4, Naaman, A. and Rheinhardt, H.W. (Eds.), RILEM Pubs., Paris, pp. 221-231.
[14] Grunewald, S. and Walraven J. (2010), In: ACI SP SC-FRC, Aldea, C.M. and Ferrara, L. (eds.), ACI Farmington Hills, to appear.
[15] Ferrara, L. and Ozyurt, N. (2008), In: Proceedings SCC2008 (paper 1124).
[16] Ozyurt, N. et al. (2009), In: Proceedings Rheo-Iceland 2009. Wallevik, O.H. et al. (Eds.) RILEM Pubs., Paris, pp. 313.321.
[17] di Prisco, C. et al. (2006), In: Proceedings 1st Fib World Conf., (paper 823).
[18] Dhonde, H.B., Mo, Y.L., Hsu, T.T.C. and Vogel, J. (2007), *ACI Mat. J.*, vol. 104, n. 4, pp. 491-500.
[19] Ferrara, L. and Meda, A. (2006), *Mat. & Struct.*, vol. 39, n. 4, pp. 411-420.
[20] Lataste, J.F., Behloul, M. and Breysse, D. (2008), *NDT&E International*, vol. 41, n. 8, pp. 638-647.
[21] Stahli, P., Custer, R. and van Mier, J.G.M. (2008), *Mat. & Struct.*, vol. 41, n. 1, pp. 189-196.
[22] Torrijos, M.C., Tobes, J.M., Barragàn, B.E. and Zerbino, R.L. (2008), In: Proceedings BEFIB 2008, Gettu, R. (Ed.), RILEM Pubs., Paris, pp. 729-738
[23] Vandewalle, L., Heirman, G. and van Rickstal, F. (2008), In: Proceedings BEFIB 2008, Gettu, R. (Ed.), RILEM Pubs., Paris, pp. 719-728.
[24] Yardimci, M.Y., Baradan, B. and Tasdemir, M. (2008), In: Proceedings BEFIB 2008, Gettu, R. (Ed.), RILEM Pubs., Paris, pp. 711-718.
[25] Kooiman, A.G. (2000), PhD Thesis, Delft University of Technology.
[26] Stroeven, P. and Shah, S.P. (1978), In: Testing and Test Methods of Fibre Reinforced CompositesConstr. Press, Lancaster, pp. 345-353.
[27] Özyurt, N., Woo, L.Y., Mason, T.O. and Shah, S.P. (2006), *ACI Mat. J.*, vol. 103, n. 5, pp. 340-347.
[28] Ozyurt, N., Mason, T.O. and Shah, S.P. (2006), *Cem. Concr. Res.*, vol. 36, pp. 1653-1660.
[29] Franchois, A., Taerwe, L. and Van Damme, S. (2004), In: Proceedings BEFIB 2004, di Prisco, M. et al. (Eds.), RILEM Pubs., Paris, pp. 249-256.
[30] Faifer, M. et al. (2009), In: Proceedings IMTC09, pp. 313 - 318.
[31] Faifer, M. et al. (2010), Accepted for presentation at IMTC10.
[32] Felicetti, R. and Ferrara, L. (2008), In: Proceedings BEFIB 2008, Gettu, R. (Ed.), RILEM Pubs., Paris, pp. 525-536.
[33] Molins Borrel, C., Martinez Martinez, J.A. and Arnaiz Alvaro, N. (2008), In: Proceedings 4th ACHE Conference, Valencia.
[34] Roussel, N. et al. (2007), *Cem. Concr. Res.,* vol. 37, pp. 1298-1307.

[35] Roussel, N. (2007), *Mat. & Struct.*, vol. 40, n. 10, pp. 1001-1012.
[36] Roussel, N. et al. (2007), *Mat. & Struct.*, vol. 40, n. 9, pp. 877-887.
[37] Cremonesi, M., Ferrara, L. and Frangi, A. (2010), Accepted BAC 2010.
[38] Shah, S.P. et al. (2009), In: Proceedings SCC2009, Shi, C. et al. (Eds.), RILEM Pubs., Paris, pp. 3-15.
[39] Mechtcherine, V. and Shyshko, S. (2009), In: Proceedings RheoIceland 2009, Wallevik, O.H. et al. (Eds.), RILEM Pubs., Paris, pp. 171-179.
[40] Balaguru, P. N. and Shah. S.P. (1992), McGraw Hill.
[41] Laranjeira, F. (2010), PhD Thesis, Universitat Politecnica de Catalunia, Barcelona.
[42] Cunha, V.M.C.F., Barros, J.O.A. and Sena-Cruz, J.M. (2010), *ASCE J. Mat. Civ. Engrg.,* vol. 22, n. 1, pp. 1-9.
[43] Pereira, E.N.B., Barros, J.O.A. and Camoes, A. (2008), *ASCE J. Struct. Engrg.*, vol. 134, n. 8, pp. 1310-1321.
[44] Aoude, H., Cook, W. and Mitchell, D. (2009), *ACI Struct. J.*, vol. 106, n. 3, pp. 349-357.
[45] di Prisco, M., Plizzari, G. and Vandewalle, L. (2009), *Mat. and Struct.*, vol. 42, n. 9, Special Issue: FRC: Structural applications and standards, pp. 1261-1281.
[46] Ozyurt, N., Mason, T.O. and Shah, S.P. (2007), *Cem. Concr. Comp.*, vol. 29, n. 2, pp. 70-79.
[47] Ferrara, L., Dozio, D. and di Prisco, M. (2007), In: Proceedings HPFRCC5, Naaman, A. and Reinhardt, H.W. (Eds.), RILEM Pubs., Paris, pp. 249-258.
[48] Groth, P. and Nemegeer, D. (1999), In: Proceeding 1st Int. RILEM Symposium on Self-Compacting Concrete, RILEM Pubs., Paris, pp. 497-507.
[49] Carlsward, C. and Emborg, M. (2007), In: Proceedings SCC 2007, De Schutter, G. and Boel, V. (Eds.), RILEM Pubs., Paris, pp. 793-798.
[50] Barragàn, B. et al. (2004), In: Proceedings BEFIB 2004, di Prisco, M. et al. (Eds.), RILEM Pubs., pp. 455-464.
[51] Borralleras, P., Barragàn, B. and Gettu, R. (2007), In Proceedings SCC2007, De Schutter, G. and Boel, V. (Eds.), RILEM Pubs., Paris, pp. 1092-1098.
[52] Romano, G.Q. et al. (2007), In: Proceedings SCC2007, De Schutter, G. and Boel, V. (Eds.), RILEM Pubs., Paris, pp. 881-886.
[53] Bigas, J.P. et al. (2007), In: Proceedings SCC2007, De Schutter, G. and Boel, V. (Eds.), RILEM Pubs., Paris, pp. 1013-1018.
[54] Greenough, T. and Nehdi, M. (2008), *ACI Struct. J.*, vol. 105, n. 5, pp. 468-477.

Fiber-Reinforced Cementitious Materials: From Intrinsic Isotropic Behavior to Fiber Alignment

L. Martinie and N. Roussel

Université Paris Est, Laboratoire Central des Ponts et Chaussées, Paris, France

Abstract. Fiber addition may lead to a strong modification of a cementitious material rheological behavior. First, the existence of a transition in the evolution of the material rheological behavior is shown relatively to the fiber volume fraction, in isotropic state. This transition occurs at a critical fiber volume fraction between a regime in which hydrodynamic effects govern the rheological behavior and a regime in which direct mechanical contacts between fibers are predominant. Then the orientation process induced by a casting flow is highlighted. The effect of yield stress on the orientation process is specially studied. Orientation of large amount of fibers is derived from the equation describing a single fiber orientation.

Introduction

Fibers in cementitious materials can have a very positive influence on the mechanical properties of the composite in its hardened state. It was however shown that addition of fibers decreases the workability of the material. This effect increases with the volume fraction ϕ_f and aspect ratio r of the fibers [1-3]. Many researchers observed a decrease of the yield stress when the product $r\phi_f$, defined as the *fiber factor*, increases [1, 4-10], as presented in a literature review in [11]. In the case of rigid fibers, contrary to spherical rigid inclusions, flow can moreover induce a preferred orientation of the fibers which modifies the material properties in fresh state and, after setting, strongly influences the mechanical properties of the resulting fiber-reinforced composite [12-14]. Often, an orientation factor is defined to deal with the difficulty of manipulating a spatial notion such as orientation through a section [15-18].

In this paper, a prediction of the critical fiber amount leading to a very strong increase of the yield stress of cementitious materials is first derived from the physical phenomena involved in the case of spherical inclusions. Then, fiber

K.H. Khayat and D. Feys (eds.), *Design, Production and Placement of Self-Consolidating Concrete*, RILEM Bookseries 1,
DOI 10.1007/978-90-481-9664-7_34, © RILEM 2010

orientation during casting process is studied. The effect of yield stress on fiber alignment is specifically highlighted in the case of a simple flow between two parallel planes.

Isotropic Behavior

Influence of the addition of rigid inclusions on the yield stress of concrete

The rheological behaviour of a material such as concrete can be described by its yield stress and viscosity. The Krieger-Dougherty relation [19] relates the rheological properties of the suspending fluid and the volume fraction ϕ of the particles to the rheological properties of the mixture through the parameter ϕ/ϕ_m, with ϕ_m the dense packing volume fraction. A similar relation for yield stress relating τ_0^{conc} the yield stress of the concrete and τ_0^{cp} the yield stress of the cement paste, through a function of the parameter ϕ/ϕ_m governing the nature of interactions between inclusions can also be written [20]. It was moreover shown that the material behavior varies between a regime governed by hydrodynamic effects and a regime in which direct mechanical contacts between fibers are predominant [21]. Below the random loose packing fraction, mechanical contacts can be neglected. Inversely, above this value, the behavior of concrete does not depend much on the behavior of the cement paste but mainly on volume fraction and dense packing fraction of the granular skeleton, which dictate the number of contacts in the system [11, 22].

Random loose and dense packing of rigid fibers

The main difficulty when trying to apply the transition concept described above to rigid fibers lies in the determination of the packing fractions of these specific inclusions. Measurements of random loose and dense packing fractions of fibers were carried out in [11] for aspect ratios r between 17 and 100 (r is the ratio between a fiber length and diameter). Philipse [23] has shown that, in the case of high aspect ratio bodies, packing fractions can be written as $\phi_m = \alpha_m / r$ for the dense packing fraction and $\phi_c = \alpha_c / r$ in the case of random loose packing. The fitted values of α_m and α_c in the range of high aspect ratios 50-100 are respectively 4 and 3.2 [11]. It can be noted that α_m is of the same order of magnitude as the value of 5.4 theoretically expected by Philipse [23] and that it is close to the value of order 4.5 which can be extrapolated from the experimental work of Nardin and Papirer [24]. As yield stress and viscosity scale on the ratio ϕ_f / ϕ_m and as ϕ_m scales with $1/r$, the behavior of the mixture should scale on the fiber factor $\phi_f r$.

Cement paste and fibers: Yield stress measurements

In most applications, fibers are combined with sand and gravels. This combination strongly affects the packing density of both aggregates and fibers [25]. In this work, the contribution of each type of inclusion is simply added to the contact network (the assumption of a linear behavior regarding the contribution of each type of inclusion is made). The total relative volume fraction is therefore defined as the sum of the relative volume fraction of the fibers and the relative volume fraction of the granular skeleton $\phi_f r/4 + \phi_s/\phi_{ms}$ where ϕ_s and ϕ_{ms} are respectively the volume fraction and the dense packing fraction of the sand (of the order of 0.5-0.7 depending on the nature of the sand). We consider yield stress measurements obtained in isotropic conditions (*i.e.* non oriented fibers), as described in [11]. Figure 1 plots the relative yield stress *vs.* the total relative volume fraction.

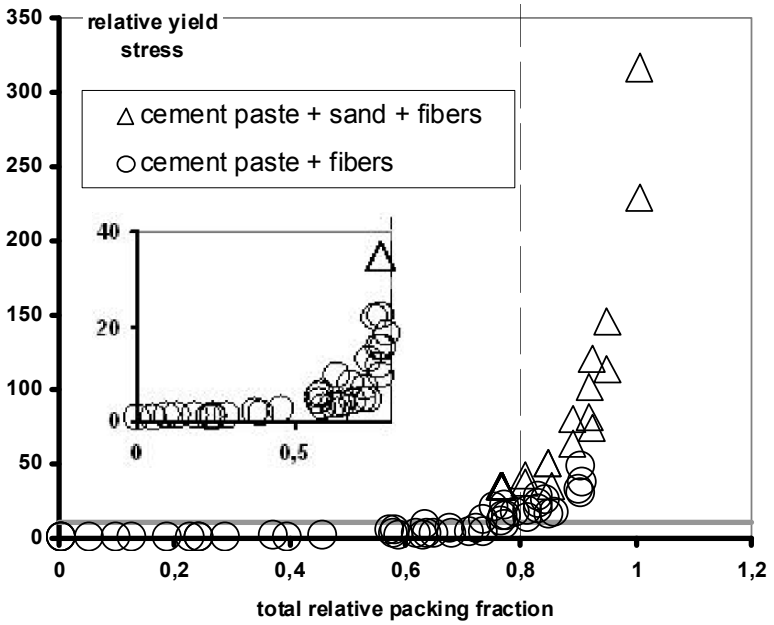

Figure 1. Relative yield stress as a function of the total relative packing fraction. Experimental results from literature or obtained at LCPC.

It can be admitted from this figure that it is possible to combine the effects of both fibers and sand in order to predict the bifurcation in the yield stress of these mixtures around the critical volume fraction at which all these inclusions combine

in order to generate a strong direct contact network in the material. Below this critical value, fibers and inclusions only play a small role and the mixture behavior is very close to the cement paste behavior whereas, above this critical value, the material yield stress increases of several orders of magnitude. It is possible to extract from the Figure 1 a simple helpful mix design criterion for self-compacting materials containing fibers. For the yield stress to keep the same order of magnitude after inclusion addition, and thus for the concrete to roughly display the same of rheological behavior, the non dimensioned yield stress should not increase over a factor 10 (in gray on Figure 1). This criterion is verified for a total relative packing fraction lower than 0.8.

$$\phi_f r/4 + \phi_s/\phi_{ms} \leq 0.8 \tag{1}$$

Fiber Alignment

Background

The second phenomenon which strongly influences reinforced material rheological behavior is the orientation of fibers. The orientational process, first described by Jeffery [26] in 1922, is still of interest for many researchers, mainly in the case of Newtonian fluids [27-40]. Jeffery [26] solved the moment equation of a rotating ellipsoid immersed in an incompressible fluid. He showed that a single rigid, force and torque free ellipsoid slips with a velocity equal to the one of the equivalent undisturbed fluid at the ellipsoid center, while rotating indefinitely along one of an infinite number of Jeffery orbits [26, 36]. However, it has been shown that in the absence of interactions, the ellipsoid spends a large portion of its time nearly aligned with the flow direction. For an ellipsoid represented by its unit vector **p** and its aspect ratio *r*, the orientation evolution is described by the following differential equation [26]:

$$\dot{\mathbf{p}} = W\mathbf{p} + \lambda\left(D\mathbf{p} - D:\mathbf{ppp}\right) \tag{2}$$

with *W* and *D* the vorticity tensor and the rate of strain tensor respectively for the flow unperturbed by the fiber. λ is a parameter representative of the fiber slenderness, $\lambda = (r^2 - 1)/(r^2 + 1)$. To apply this prediction to a yield stress fluid, it is assumed here that in a volume proportional to the gyratory volume around the inclusion and centered on its inertia center, the apparent viscosity $(\eta + \tau_0/\dot{\gamma})$ is constant, so that the Jeffery's equation can locally be applied. It can be noticed that, for this assumption to be valid, the inclusion highest length has to be a lot less than the flow characteristic size.

Aligned fiber assumption

The asymptotic case of an ellipsoid infinitely elongated is commonly used in literature as the *aligned fiber approximation* to represent a cylindrical fiber [38]. In this case, the fiber rotational behavior can be assimilated to the one of a fluid line [41], meaning that the fiber no longer rotates periodically in shear flow but approaches an equilibrium position oriented in the direction of the flow. The consequence of using such an assumption is that no mechanical contacts between fibers are considered, as two fluid lines cannot cross since the fluid velocity field is a single value. This assumption has thus to be considered only in case of negligible interactions between inclusions, which occurs in dilute regimes. However, if fibers tend to align along a preferred direction, the amount of interactions between them decreases and the aligned fiber assumption can be adopted, even for semi-dilute or semi-concentrated regimes [28, 35, 42]. In practical terms, this assumption implies an infinite aspect ratio and thus a parameter λ approaching 1 in Eqn. (2).

Wall effect

From a simple geometrical point of view, it is not possible to find a fiber perpendicular to a wall at a distance lower than half the length of the fiber. Furthermore, hydrodynamic and direct mechanical interactions between fibers are considered to strongly influence the macroscopic orientation over a distance of the order of a fiber length from a wall [15]. This is a critical point for sizing experimental moulds or choosing fibers to reinforce structural elements. Indeed, to avoid too important wall effects and a resulting orientation due to geometrical considerations, flow must spread in an area larger than 5 times fiber length, which implies quite large moulds for longer fibers of several tens of millimeter length.

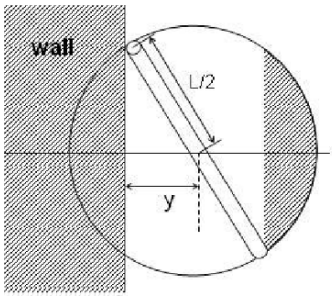

Figure 2. Fiber degree of freedom close to a wall ($y < L/2$).

Yield stress effect

Literature provides only few experimental results in the case of yield stress fluids [12, 28-38, 43-46]. The existence of a critical stress to be overcome to induce flow

causes in the material flowing areas which are not submitted to any deformations, called plug-flow areas. Two orientation regimes can thus be observed. A) Outside the plug flow areas, deformations induced by the flow contribute to the fiber alignment as described by Jeffery, depending on the reinforced material rheological parameters and the fiber initial orientation. High deformation rates are generally localized at the interface with the mold due to non-slip boundary conditions. Thus, in addition to geometrical considerations, the closer to the wall the fiber starts, the quicker it aligns with the flow. Then deformation rates decrease towards free surfaces or symmetrical plans, where stress due to the flow is null. B) Inside the plug-flow areas, the material behaves like a solid. Therefore, a fiber initially inside a plug-flow area keeps its initial orientation.

Application: Shear flow between two parallel planes

A fiber flowing through two infinite planes is submitted to a symmetrical shear stress relatively to the median plan. The shear stress decreases from the wall interface until reaching the material yield stress value at a critical height z_c. The central area is shifted with the fluid at the velocity of the interface with the sheared part.

The evolution of a group of slender fibers with various initial orientations is considered to represent the macroscopic orientation process. Each time step evolution of the orientation of each fiber is directly deduced from the Jeffery equation (2). The number of fibers necessary to provide quantitative results can be discussed, but only a few of them is required to get a qualitative idea of the preferred orientation induced by the flow. Two fibers initially orthogonal and distributed in a range of $[0, \pi]$ angles are considered here as an example (Figure 3). Two types of concrete are studied: an ordinary rheology concrete with a yield stress of 800 Pa and a self-compacting concrete with a yield stress of 50 Pa.

An orientation factor relating the behaviour of N fibers in a two dimensional flow is defined relatively to a direction $\vec{d}$ as the ratio between the total projection of each unit vector $\mathbf{p}$ on this direction and all the projections.

$$\alpha_{\vec{d}} = \frac{\sum_{k=1}^{N} p_{\vec{d}}^{k}}{\sum_{k=1}^{N} (p_1^k + p_2^k)} \tag{3}$$

with $\vec{d}$ the chosen direction between 1 and 2, and $p_{\vec{d}}$ the fiber projection on direction $\vec{d}$. Values of this non-dimensioned factor vary in a range of $[0, 1]$. It can be noticed that this factor is equal to 1 for fibers perfectly aligned with $\vec{d}$, null for fibers orthogonal to this direction, and equal to 0.5 for all fibers isotropic.

Cementitious materials display two main behaviors. Ordinary rheology concrete (ORC) with a yield stress of order of a couple thousands of Pascals flows like a granular paste sliding on a thin layer of fluid material at the wall interface where fibers align quickly with flow direction, while orientation of fiber occurs in a more homogeneous way for self-compacting concrete (SCC) with yield stresses of the order of several tens of Pascals yield stresses (Figure 3).

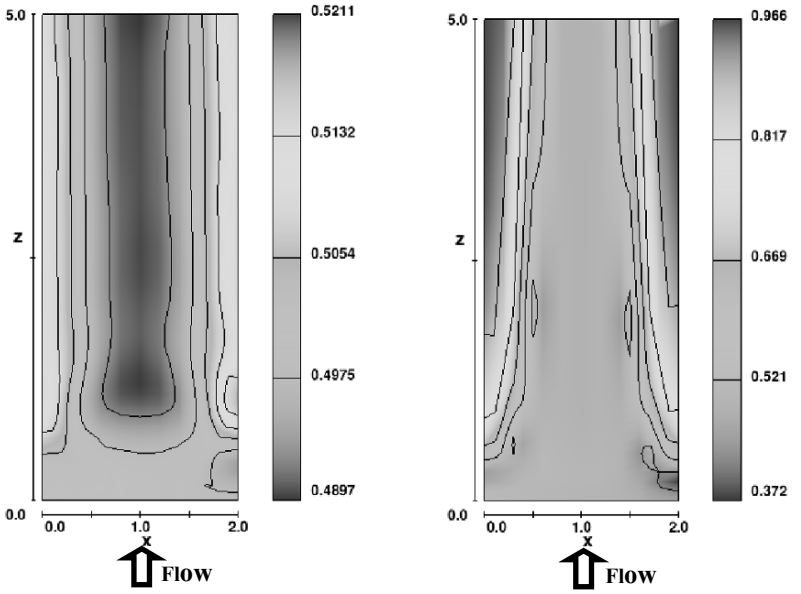

Figure 3. Orientation factor relatively to the flow direction (z) calculated from 2 fibers immersed in an ORC (τ_0 =800 Pa, left) and an SCC (τ_0 =50 Pa, right) of 80 Pa.s plastic viscosity.

The average orientation relatively to the flow direction can then be computed on the channel exit line. Numerical results indicate $\overline{\alpha}_z = 0.50$ in the case of the high yield stress fluid, and $\overline{\alpha}_z = 0.71$ for the low yield stress fluid. Fibers are in average less oriented in the case of ordinary rheology concrete than in the case of self-compacting concrete.

Conclusions

The effect of rigid straight fibers on the yield stress of cementitious materials has been studied thanks to a simple model describing the contacts network between rigid fibers inside the material. Then the process of fiber orientation induced by

casting has been shown to strongly depend on the yield stress of the material. The contrast between a solid material behavior for an ORC sliding along walls and a viscous fluid behavior in the case of SCC has been highlighted. It can be kept in mind that, on average, orientation is stronger in the case of SCC.

References

[1] Grünewald, S. (2004), PhD Thesis, DTU, the Netherlands.
[2] Rossi, P. (1992), *Cem. Concr. Compos.*, vol. 14, n. 16, p. 3.
[3] Mohammadi, Y., Singh, S.P. and Kaushik, S.K. (2008), *Constr. & Build. Mater.*, vol. 22, n. 5, p. 956.
[4] Bayasi, M.Z. and Soroushian, P. (1992), *ACI Mater. J.*, vol. 89, n. 4, p. 369.
[5] Johnston, C.D. (1996), In: *Production Methods and Workability of Concrete*, Proceedings of the RILEM Symposium, P.J.M. Bartos, D.L. Marrs, D.J. Cleland (Eds.), E&FN Spon London, pp. 155–179.
[6] Groth, P. (2004), PhD Thesis, Lulea University of Technology.
[7] Bui, V.K., Geiker, M.R. and Shah, S.P. (2003), Proceedings of the RILEM Symposium, A.E. Naaman, H.W. Reinhardt (Eds.), RILEM Publications Michigan, pp. 221–231.
[8] Ding, Y., Liu, S., Zhang, Y. and Thomas, A. (2008), *Const. & Build. Mater.*, vol. 22, n. 7, p. 1462.
[9] Ferrara, L., Park, Y.D. and Shah, S.P. (2007), *Cem. Concr. Res.*, vol. 37, n. 6, p. 957.
[10] Banfill, P.F.G., Starrs, G., Derruau, G., McCarter, W.J. and Chrisp, T.M. (2006), *Cem. Concr. Compos.*, vol. 28, n. 9, p. 773.
[11] Martinie, L., Rossi, P., and Roussel, N. (2010), *Cem. Concr. Res.*, vol. 40, p. 226.
[12] Kooiman, A.G. (2000), PhD Thesis, DTU, the Netherlands.
[13] Markovic, I. (2006), PhD Thesis, DTU, the Netherlands.
[14] Stähli, P. and van Mier, J.G.M. (2007), *Eng. Fract. Mech.*, vol.74, n. 1-2, p. 223.
[15] Dupont, D. and Vandewalle, L. (2005), *Cem. Conc. Comp.*, vol. 27, p. 391.
[16] Laranjeira, F., Aguado, A. and Molins, C. (2009), *Mater. Struct.*, published online.
[17] Ferrara, L. and Meda, A. (2006), *Mater. Struct.*, vol. 39, p. 411.
[18] Robins, P.J., Austin, S.A. and Jones, P.A. (2003), *Mag. Conc. Res.*, vol. 55, n. 3, p. 225.
[19] Krieger, I.M., Dougherty, T.J. (1959), *Trans. Soc. Rheol.*, vol. 3, p. 137.
[20] Mahaut, F., Mokkedem, S., Chateau, X., Roussel, N. and Ovarlez, G. (2008), *Cem. Concr. Res.*, vol. 38, n. 11, p. 1276.
[21] Yammine, J., Chaouche, M., Guerinet, M., Moranville, M. and Roussel, N. (2008), *Cem. Concr. Res.*, vol. 38, n. 7, p. 890.
[22] Roussel, N., Lemaitre, A., Flatt, R.J. and Coussot, P. (2010), *Cem. Concr. Res.*, vol. 40, p. 77.

[23] Philipse, A.P. (1996), *Langmuir*, vol. 12, p. 1127.
[24] Nardin, M. and Papirer, E. (1985), *Powder Technology*, vol. 44, p. 131.
[25] Barthos, P.J.M. and Hoy, C.W. (1996), In: *Production Methods and Workability of Concrete*, Proceedings of the RILEM Symposium, P.J.M. Bartos, D.L. Marrs, D.J. Cleland (Eds.), E&FN Spon, London, pp. 451-461.
[26] Jeffery, G.B. (1922), *Proc. Royal Soc. A*, vol. 102, pp. 161-179.
[27] Folgar, F. and Tucker, C.F. (1984), *J. Reinf. Plast. Comp.*, vol. 3, p. 98.
[28] Rahnama, M., Koch, D.L. and Shaqfeh, E.S.G. (1995), *Phys. Fluids*, vol. 7, n. 3, p. 487.
[29] Anczurowski, E. and Mason, S.G. (1967), *J. Colloïd Interface Sci.*, vol. 23, p. 522.
[30] Trevelyan B.J. and Mason, S.G. (1951), *J. Colloïd Sci.*, vol. 6, p. 354.
[31] Mason, S.G. and Manley, R. St. (1957), *Proc. Royal Soc.*, vol. 238 series A, p. 117.
[32] Harris, J.B. and Pittman, J.F.T. (1975), *J. Colloïd Interface Sci.*, vol. 50, n. 2, p. 280.
[33] Bibbo, M.A., Dinh, S.M. and Armstrong, R.C. (1985), *J. Rheol.*, vol. 29, n. , p. 905.
[34] Kameswara Rao, C.V.S. (1979), *Cem. Concr. Res.,* vol. 9, p. 685.
[35] Dinh, S.M. and Armstrong, S.M. (1984), *J. Rheol.*, vol. 28, n. 3, p. 207.
[36] Bretherton, F.P. (1962), *J. Fluid Mech.*, vol. 14, p. 284.
[37] Goldsmith, H.L. and Mason, S.G. (1967), In: *Rheology: Theory and Applications*, vol. 4, chapter 2, pp. 85-250, New York.
[38] Lipscomb, G.G. and Denn, M.M. (1988), *J. Non-Newt. Fluid Mech.*, vol. 26, p. 297.
[39] Vincent, M. (1984), PhD Thesis, ENS des Mines de Paris.
[40] Taskernam-Kroser, R. and Ziabicki, A. (1963), *J. Polymer Sciences*, vol. 1, n. 6, p. 491.
[41] Sunadararjakumar, R.R. and Koch, D.L. (1997), *J. Non-Newt. Fluid Mech.*, vol. 73, p. 205.
[42] Koch, D.L. and Shaqfeh, E.S.G. (1990), *Phys. Fluids A*, vol. 2, p. 2093.
[43] Ozyurt, N., Mason, T.O. and Shah, S.P. (2006), *Cem. Concr. Res.*, vol. 36, p. 1653.
[44] Lataste, J.F., Behloul, M. and Breysse, D. (2007), Proceedings of the AUGC Symposium, Bordeaux (France).
[45] Boulekbache, B., Hamrat, M., Chemrouk, M. and Amziane, S. (1985), *EJECE*.
[46] Ozyurt, N., Woo, N.Y., Mason, T.O. and Shah, S.P. (2006), *ACI Materials Journal*, vol. 103, n. 5, p. 340.

Flow-Induced Fiber Orientation in SCSFRC: Monitoring and Prediction

Liberato Ferrara[1], Nathan Tregger[2] and Surendra P. Shah[2]

[1] Department of Structural Engineering, Politecnico di Milano, Italy
[2] ACBM, Northwestern University, Evanston, IL, USA

Abstract. The dispersion and the orientation of fibers in concrete can be governed through a suitably balanced set of fresh state properties and a carefully designed casting procedure, if proved effective. This would allow one to achieve a mechanical performance of the fiber-reinforced cementitious composite which is optimal to the foreseen structural application, even keeping the fiber content at relatively low values (e.g. maximum 1% by volume) and aligning them with the direction of the principal tensile stress within the structural element when in service.
Modeling the casting of fresh concrete, through suitable numerical tools, in order to anticipate the direction of flow lines, along which fibers may orient, and optimize the whole process to the foreseen structural application is of the foremost importance.
Monitoring fiber dispersion related issues through suitable non destructive methods would also be crucial for reliable, time and cost-effective quality control.
In this paper a pioneer study has been performed in the above said framework. The results are really encouraging and pave the way towards a holistic approach to the design of self-consolidating fiber-reinforced concrete structures.

Introduction

The dispersion and orientation features of the distributed reinforcement consisting of short steel fibers in Steel Fiber-Reinforced Cementitious Composites (SFRCC) represent a major factor influencing the performance of the composite. The efficiency for stress transfer by fibers across a crack, which has been recognized to be governed by the so-called fiber factor (i.e. the product of fiber volume fraction V_f, fiber aspect ratio l_f/d_f and interfacial friction stress τ_f) is in fact likely to be affected by the non-alignment of fibers and principal tensile stresses [1]. Furthermore, poorly reinforced or even fiber-free spots, e.g. caused by improper

K.H. Khayat and D. Feys (eds.), *Design, Production and Placement of Self-Consolidating Concrete*, RILEM Bookseries 1,
DOI 10.1007/978-90-481-9664-7_35, © RILEM 2010

placement and compaction, also affected by the well known worsening effects of fibers on the mixture workability, may act as flaws in a structural element which jeopardize its performance, as anticipated in design calculations, with reduction of load bearing capacity and activation of unforeseen failure mechanisms [2].

Sound theoretical approaches have been provided over the past years to explain, through stereological micromechanics concepts, the effects of fiber orientation on the mechanical performance of SFRCC, which proved to satisfactorily explain experimental evidence [1, 3, 4].

In the very last years, thanks to the widespread diffusion of concrete and cementitious composites with adapted rheology, intense research efforts have been dedicated to investigate the connections between the fresh state performance and the dispersion and orientation of fibers, as also influence by the casting flow properties and geometry [5-7]. The possibility of governing the dispersion and the orientation of fibers in concrete through a suitably balanced set of fresh state properties and a carefully designed casting procedure hence represents a cutting edge topic for research and technology transfer. This, if proved effective, would be a feasible way to achieve a performance of the SFRCC which is optimal to the foreseen structural application, even keeping the fiber content at relatively low values (e.g. around 1% by volume). The key idea of the whole process is that the fluid mixture has to be first of all self-consolidating, in order to fill the formwork without any vibration or manual compaction, which may hinder homogeneous fiber dispersion. The fresh state performance of the mixture must be characterized by an adequate viscosity, to drive the fibers along the direction of the flow and orient them according to the fluid velocity field lines. Furthermore, to achieve the anticipated benefits in terms of structural performance, the casting process must be designed in order to make the flow direction of fresh concrete and the orientation of fibers to match as close as possible with the direction of the principal tensile stress within the structural element when in service.

Such a “holistic” design approach tailors both the material composition and the casting process to the anticipated structural performance, by making the orientation of fibers to match as close as possible with the direction of the principal tensile stress within the structural element when in service. In this way a more efficient structural use of the material can be reliably achieved. This would allow to pursue, in the design process, a desirable closer correspondence between the shape of an element and the function it performs in a structure assembly. A suitably balanced fresh-state performance of the fiber-reinforced cementitious composite would allow to mould the shape of an element and, thanks to a tailored casting process, to orient the fibers along the direction of the principal tensile stresses resulting from its structural function.

In the above said framework three main issues can be highlighted which need to be further investigated in order to transfer the proposed approach into the engineering

practice:

- monitoring fiber dispersion and orientation in a time- and cost-effective way, e.g. through suitably developed non-destructive methodologies, these should also be effectively implemented into quality control and acceptance procedure for an immediate check and validation of the previous step output;
- predicting the orientation of fibers as a function of the casting flow properties and geometry (this should be an integrated part with both architectural and structural design as well as with the mix-design selection);
- identifying material properties relevant to the structural design by means of test specimens and methodologies suitably designed, manufactured and set-up to "reproduce" as close as possible the dispersion and orientation features of fibers which are likely to occur in the designed structural application, also with reference to the alignment with principal tensile stresses.

This paper summarizes related research findings by the authors, focusing on the first two issues listed above.

Research Significance and Background

Fiber dispersion and orientation are crucial for the structural performance of applications with SFRC and have to be effectively checked at the production stage for a sound quality.

The majorities of studies published so far, referred to "manual" counting of the number of fibers over selected surfaces and employed either formulae derived from stereological models or image analysis techniques to calculate orientation-related parameters [1, 3, 4, 8]. Methods based on electrical conductivity measurements received in the very last years much of the researcher's attention [8-10]. Among them, Alternate Current Impedance Spectroscopy AC-IS [8] has been proved able to provide reliable information in a fast and effective way and lots of work has been done, also by the authors, either to calibrate the method and address the possibility of employing it on an industrial scale [6, 8, 11].

The prediction of fiber orientation as a function of the casting flow properties represents the next frontier for research and technology transfer. The final aim would be to design the casting process in such a way to achieve the orientation of the fibers which is most suitable for the selected application, mainly with reference to the alignment with the direction of the principal tensile stresses.

Computational Fluid Dynamics (CFD) modeling of fresh concrete flow has been recently recognized as an effective tool to simulate casting processes and optimize them with reference to specific applications, also including the selection of the most appropriate set of fresh state properties of concrete [8]. Embedding discrete elongate particles such as fibers into a complex fluid flow is a not trivial task [9]

and distance still has to be travelled before such an approach could be applied to real casting flow modeling. Homogeneous single fluid approach, despite rougher, may provide enough information, mainly the magnitude and direction of the shear rate vectors, which drive the fibers along the flow [12, 13].

The study presented in this paper encompasses the aforementioned concepts, in an attempt to address the research needs. First of all, SFRCs with suitable compositions were designed to achieve different levels of fresh state performance. Slab specimens were cast to provide experimental evidence of the influence of the fresh concrete viscosity to orient the fibers along its flow. Non destructive monitoring of fiber dispersion was then performed by means of AC-IS, thus providing a thorough assessment of the possibility to employ the method for quality control at an industrial scale. Finally an example of CFD modeling of one of the experimentally investigated cases addresses the issue of prediction of fiber orientation.

Monitoring Fiber Dispersion and Orientation via AC-IS

In the very last years Impedance Spectroscopy has been applied as an analyzing tool to investigate properties of fiber-reinforced cementitious composites [14], which are featured by a frequency dependent behavior. Conductive fibers, such as steel, due to an oxide film forming at the fiber/electrolyte interface, were in fact shown to be insulating under Direct Current (DC) and low frequencies of Alternate Current (AC), while they are conductive under high frequencies of AC [8, 15].

The method consists of applying to the specimen a voltage excitation (1V) over a range of frequencies (10 MHz-1Hz was the range employed in this study, uniformly stepped down along a log-scale by 20 steps per decade) and measuring the amplitude and phase of the output current. When the calculated real and imaginary parts of the impedance Z are plotted on the so-called Nyquist diagram, SFRCCs exhibit a “dual-arc” behavior (Figure 1). The rightmost cusp, occurring under low frequencies (fibers act insulating), gives the resistance of the matrix, R_m, also detected on the single arc behavior in the case of unreinforced composites, and the leftmost cusp, occurring under high frequencies (fibers are conductive) corresponds to the resistance of the fiber-reinforced composite R.

To define fiber dispersion the so-called matrix normalized conductivity is used:

$$\frac{R_m}{R} = \frac{\sigma}{\sigma_m} = 1 + [\sigma_{fibers}] V_f \quad (1)$$

where σ and σ_m are the conductivity of the fiber-reinforced composite and of the matrix respectively and $[\sigma_{fibers}]$ is the intrinsic conductivity of the fibers which

depends on the ratio of the fiber conductivity to the matrix conductivity [16].

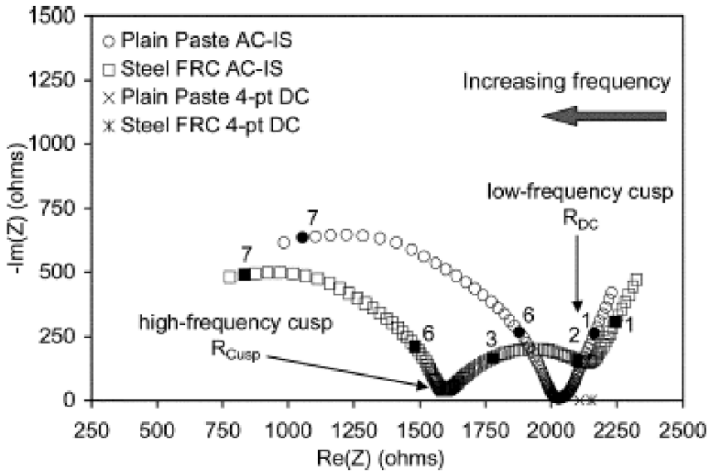

Figure 1. Sample Nyquist plot for plain and FRC paste [8].

The Role of Fresh State Performance on Fiber Dispersion and Orientation

In order to assess the reliability of AC-IS for non-destructive monitoring of fiber dispersion and orientation and at the same time investigate as these are influenced by the casting flow properties, three SFRC mixtures were designed and characterized by three different levels of fresh state performance, namely Vibrated SFRC, Self-Consolidating SFRC (SC-SFRC) and a very loose mixture prone to segregation. Design of mixture compositions was performed in the framework of the approach proposed by Ferrara et al. [17], in whose paper all the details can be found. It is worth here remarking that for all three mixtures the same content was employed (50 kg/m^3) of hooked end steel fibers, 35 mm long and with an aspect ratio equal to 65.

Square slabs 600 mm wide and 60 mm thick were hence cast. The geometry and casting modalities were accurately defined with reference to potential applications, with the aim of reproducing as close as possible the dispersion and orientation of fibers with respect to the applied stress direction, as it is likely to occur in the structural elements when in service. For both self- and segregation-consolidating SFRC, one plate was cast allowing a radial spread of the fluid concrete from the center towards the edges of the mould, and two were cast from one side, the formwork being filled by a flow of the fresh concrete parallel to formwork edges. For vibrated SFRC only two plates were cast, both according to the first modality.

AC-IS monitoring of fiber dispersion was then performed. The experimental set-up sketched in Figure 2 was used. A 120 mm spaced grid was drawn on the mould-finished surface of the specimen to locate measuring points. Stainless steel 80 mm square plates were employed as electrodes, constantly spaced at 240 mm; the electrical contact with the specimen surface was guaranteed by means of same size (when wet) sponges, soaked in a 1M NaOH-KOH solution. The AC-IS measures were taken in both x- and y- direction, coherently with the foreseen structural applications the specimens were meant to represent, i.e. thin walled elements, for which through thickness information was regarded as not significant. Due to the reduced thickness (actually less than twice the fiber length), fibers tend to lie flat and are hence likely to affect to a low, if not negligible, extent the electrical behavior of the composite in the out-of-plane direction. Thirty AC-IS measures for each plate were taken, fifteen in each direction: both in x and y directions for the nine central cells (7-9, 12-14, 17-19 - Figure 2), while for twelve edge cells information only on either the x (2-4,22-24) or y (6, 11, 16, 10, 15, 20) direction was garnered. No measure was taken for the four corner cells (1, 5, 21, 25).

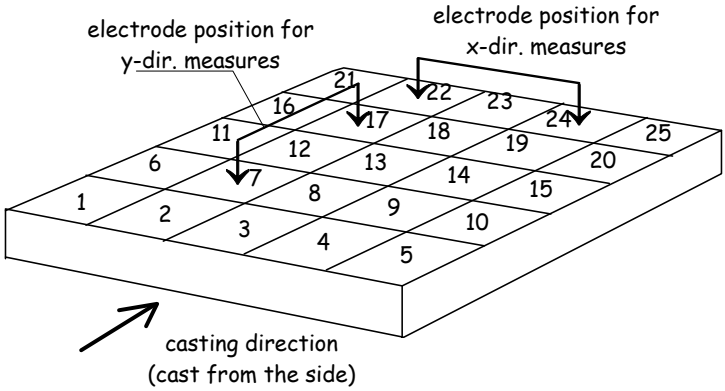

Figure 2. Scheme for AC-IS measurements.

The average values and standard deviations of the matrix normalized conductivity are listed in Table I. The measured values of the R_m/R have also been plotted, highlighting the influence of the fresh state properties of concrete on fiber dispersion. Self-consolidating concrete is effective in guaranteeing a more uniform dispersion of fibers within the specimen, as well as in effectively orienting them along the casting direction (Figures 3a-b), the exceptions along the edges of the center cast plate being consistent with the wall effect of the formwork. Vibrated SFRC plate shows, with respect to self-consolidating ones, a dispersion of fibers almost twice as much scattered (Figure 4). The same holds also for segregation-consolidating SFRC plates, where, when cast from the side, a strong decrease in the matrix normalized conductivity along the direction of casting is also observed

(Figure 5). This corresponds to dynamical segregation of fibers, due to poor concrete viscosity.

Table I. matrix normalized and fractional conductivities.

Specimen	$(R_m/R)_X$ average (std. dev.)	$(R_m/R)_Y$ average (std. dev.)	f_x	f_Y	f_x/f_Y
Vibrated SFRC	1.40 (0.22)	1.41 (0.27)	0.50	0.50	1.00
Self-consolidating SFRC					
A – center cast	1.43 (0.14)	1.38 (0.13)	0.56	0.44	1.27
B – side cast	1.53 (0.19)	1.59 (0.19)	0.37	0.63	0.59
C – side cast	1.50 (0.13)	1.74 (0.16)	0.40	0.60	0.67
Segregating SFRC					
A – center cast	2.35 (0.55)	2.45 (0.69)	0.52	0.48	1.08
B – side cast	1.36 (0.22)	1.33 (0.19)	0.39	0.61	0.64
C – side cast	1.52 (0.23)	1.48 (0.20)	0.44	0.55	0.80

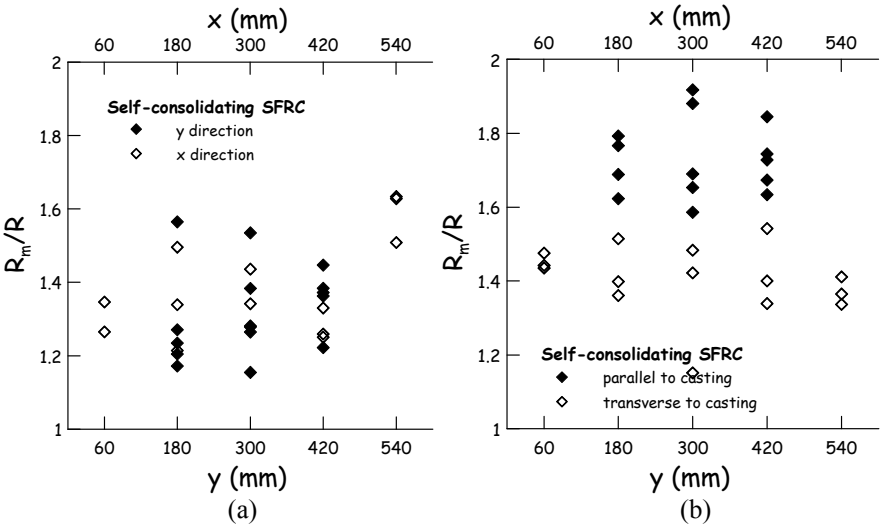

Figure 3. R_m/R for SC SFRC plate cast from the center (a) and from the side (b).

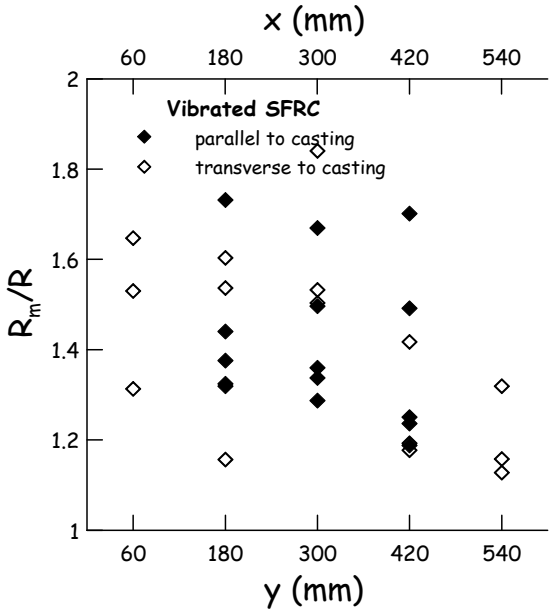

Figure 4. R_m/R for vibrated SFRC plate (cast from the center).

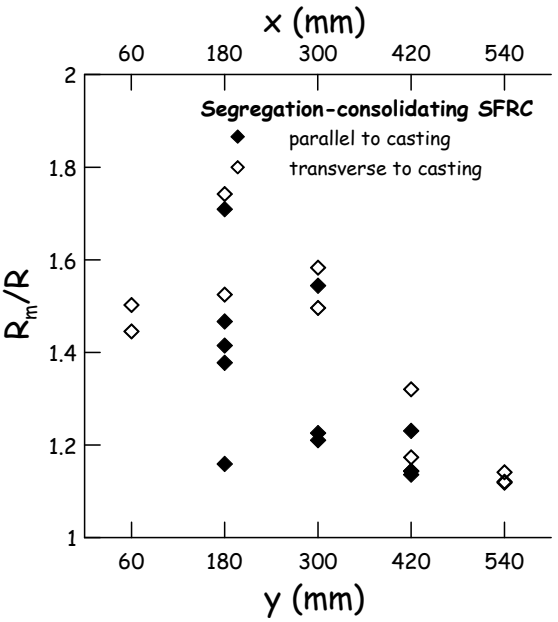

Figure 5. R_m/R for segregating SFRC plate cast from the side.

Further information can be obtained on the orientation of fibers, by calculating the conductivity of fibers in both x and y direction, neglecting the influence of the electrical behavior in the out-of-plane direction and defining a fractional conductivity:

$$[\sigma]_{\text{fibers x,y}} = \frac{\left(\frac{R_m}{R}\right)_{x,y} - 1}{V_f} \tag{2}$$

$$f_{\text{fibers x,y}} = \frac{[\sigma]_{\text{fibers x,y}}}{[\sigma]_{\text{fibers x}} + [\sigma]_{\text{fibers y}}} \tag{3}$$

Results in Table I, referring only to the nine central cells for which data in both x and y directions were gathered, confirm what above said with reference to the possibility of orienting the fibers along the casting direction thanks to the suitably "selected" fresh state performance of the concrete. Since a linear correlation holds between the matrix normalized conductivity and the orientation number of fibers [8], the ratio $[f_{\text{fibers x}}/f_{\text{fibers y}}]$ can be regarded as representative of the ratio between orientation factors orthogonal and parallel to casting.

Predicting Fiber Orientation: Computational Fluid Dynamics Modeling of Fresh Concrete Flow

The issue of casting flow modeling as a tool for predicting fiber orientation as a function of the flow properties and geometry, and hence optimize them with reference to the specific application, is addressed hereafter. As an example, a Computation Fluid Dynamics simulation has been performed of one among the experimental cases described in the previous section, namely the self-consolidating SFRC plate cast from the center. This has been chosen because of its twofold symmetry, which allowed only one quarter of the plate to be modeled, greatly reducing computational effort and time. A single fluid approach has been employed, using Polyflow, a CFD code developed by ANSYS and already quite successfully employed by the authors [18] to assess calculations between fundamental rheological properties of cement paste and measurements from field tests. A Bingham model has been employed to describe the behavior of fresh concrete with a yield stress τ_0 = 100 Pa and a plastic viscosity μ = 100 Pas. These values were estimated, also by means of well assessed relationships [19] for the SCSFRC dealt with in the present study [17]. Figure 6 shows the formwork filling sequence as modeled. In order to consistently compare the results of the CFD modeling with information obtained through non destructive monitoring of fiber dispersion and orientation based on AC-IS, the same scheme employed for the latter (Figure 2) has been also employed to process output data from the former.

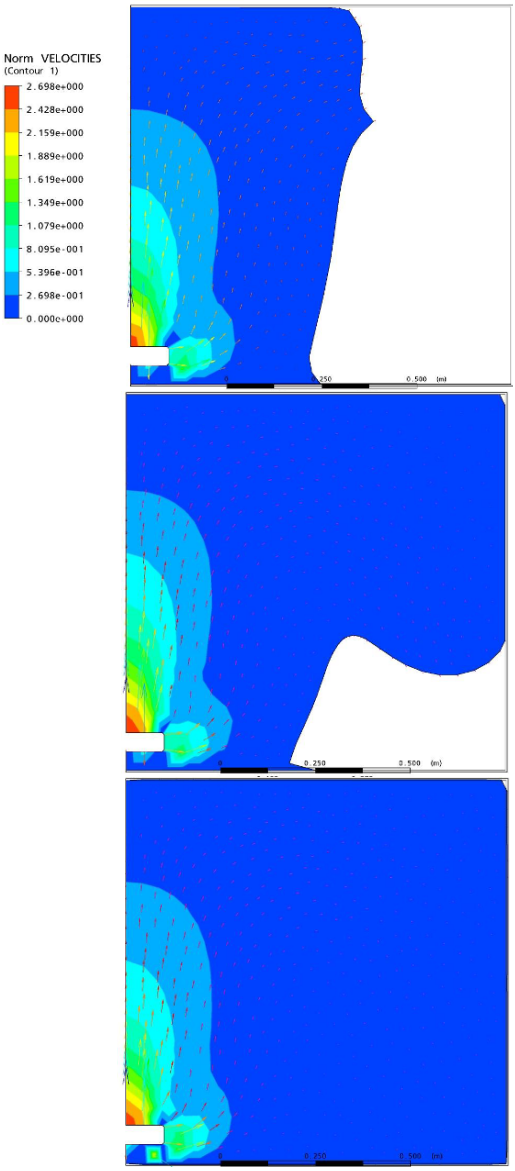

Figure 6. Schematic sequence of formwork filling as from CFD modeling: SCSFRC plate cast from the center (modeling refers to one quarter of the plate).

Reference has been made to the sinus of inclination angles of the shear rate vectors with respect to horizontal and vertical directions, $\sin\alpha_x$ and $\sin\alpha_y$ respectively. A fractional orientation factor has been computed as:

$$(\text{Fractional Orientation})_{x,y} = \frac{sin\alpha_{x,y}}{sin\alpha_x + sin\alpha_y} \tag{4}$$

to make consistent the comparison with fractional conductivities calculated from Eqn. (3). The comparison between non-destructive monitoring measures and numerical modeling predictions (Figure 7) is really encouraging, also accounting for the simplificity of the modeling approach herein pursued, and paves the way towards dedicated improvements.

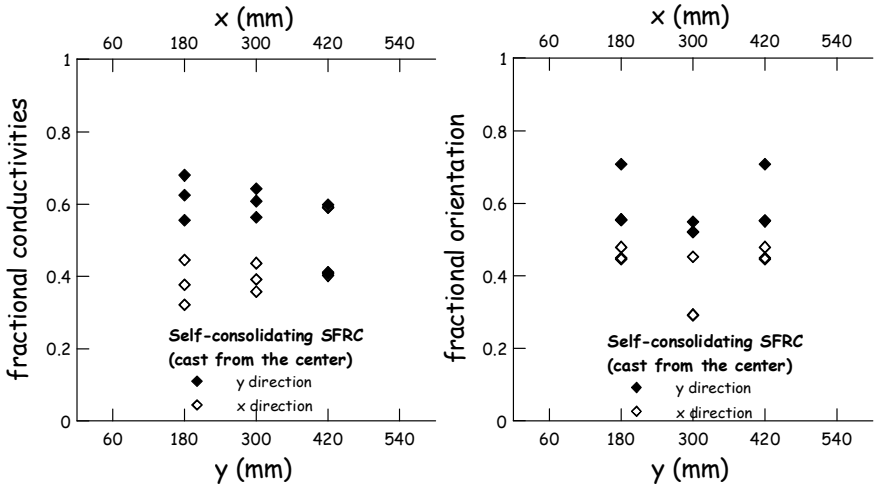

Figure 7. Comparison of fractional conductivities from AC-IS measurements and fractional orientation from CFD modeling.

Concluding Remarks

In this study the issues related to monitoring and predicting flow-driven fiber orientation in SCSFRC have been assessed. The results herein shown pave the way to "embed" non destructive monitoring and predictive modeling of fiber orientation into a holistic design and testing approach for SCSFRC structures. This allows, through selected material composition, suitably adapted rheology and tailored casting process, to orientate the fibers as close as possible along the direction of the principal tensile stresses within a structural element when in service.

Acknowledgements

The first part of this work was performed during a period spent by the first author at ACBM Northwestern University with a Fulbright scholarship. The CFD modeling was part of the work performed by the second author during a period spent at Politecnico di Milano, Polo Regionale di Lecco, under a grant by the Regional Council of Lombardia. Both financial supports are gratefully acknowledged.

References

[1] Stroeven, P. (2009), *ACI Mat. J.*, vol. 106, n. 3, pp. 213-222.
[2] Ferrara, L. and Meda, A. (2006), *Mat. & Struct.*, vol. 39, n. 4, pp. 411-420.
[3] Soroushian, P. and Lee, C.D. (1990), *ACI Mat. J.*, vol. 87, n. 5, pp. 433-439.
[4] Soroushian, P. and Lee, C.D. (1990), *ACI Mat. J.*, Vol. 87, n. 6, pp. 541-546.
[5] Stähli, P., Custer, R. and van Mier, J.G.M., (2008), *Mat. & Struct.*, vol. 41, n. 1, pp. 1891-196.
[6] Ferrara, L., Park, Y.D and, Shah, S.P. (2008), *ASCE J. Mat. Civ. Engrg*, vol. 20, n. 7, pp. 493-501.
[7] Ferrara, L., Ozyurt, N. and di Prisco, M. (2010), *Mat. & Struct.*, accepted.
[8] Ozyurt, N., Woo, L.Y., Mason, T.O. and Shah, S.P. (2006), *ACI Mat. J*, vol. 103 n. 5, pp. 340-347.
[9] Lataste, J.F., Mouloud, B. and Breysse, D. (2008), *NDT&E In.t*, vol. 41, n. 8, pp. 638-647.
[10] Faifer, M. et al. (2009), In: Proceedings IMTC09, pp. 313-318.
[11] Ozyurt, N., Mason, T.O. and Shah, S.P. (2006), *Cem. Concr. Res.*, vol. 36, pp. 1653-1660.
[12] Roussel, N. et al. (2007), *Cem. Concr. Res.*, vol. 37, n. 9, pp. 1298-1307.
[13] Petrie, C.S.J. (1999), *J. Non-Newt. Fluid Mechs*, vol. 87, pp. 369-402.
[14] Mason, T.O., Campo, M.A., Hixson, A.D. and Woo, L.Y. (2002), *Cem. Concr. Comp.*, vol. 24, pp. 457-465.
[15] Woo, L.Y. et al. (2005), *Cem. Concr. Comp.*, vol. 27, pp. 627-636.
[16] Douglas, J.F. and Garboczi, E.J. (1995), *Adv. Chem. Phys.*, XCI, Wiley, pp. 2265-2270.
[17] Ferrara, L., Park, Y.D. and Shah, S.P. (2007), *Cem. Concr. Res.*, vol. 37, n. 6, pp. 957-971.
[18] Tregger, N., Ferrara, L. and Shah, S.P. (2008), *ACI Mat. J.*, vol. 105, n. 6, pp. 558-566.
[19] Roussel, N. and Coussot, P. (2005), *J. Rheol.*, vol. 49, pp. 705-718.

Shear Behavior of Self-Compacting Concrete and Fiber-Reinforced Concrete Push-Off Specimens

Estefanía Cuenca and Pedro Serna

Universidad Politécnica de Valencia, ICITECH, Spain

Abstract. The shear behavior of reinforced "Z"-shaped push-off specimens made with self-compacting concrete (SCC) and self-compacting fiber-reinforced concrete (SCFRC) was analyzed by means of experimental tests. Testing consisted of two phases. Firstly, specimens were precracked subjected to linear load along the shear plane. During this first phase three precracked levels were distinguished (without precrack, thin and thick precrack). Then, precracked specimens were tested under direct shear load. The shear behavior along the shear plane was analyzed by means of the crack opening and shear displacement versus shear load process. Variables were: the type of concrete (SCC, or SCFRC with different fibers contents: 40 kg/m^3 or 60 kg/m^3), the transversal reinforcement (TR) and the precrack width. The analysis was specially focused on the study of aggregate interlocking. The failure occurrence is better controlled thanks to the presence of fibers, the shear behavior is more ductile.

Introduction

Shear failures of concrete elements can be brittle and fibers are able to increase the ductility of concrete [1]. To evaluate the fiber contribution, it is interesting to analyze the shear behavior of fiber-reinforced concrete (FRC). Dupont & Vandewalle [2] showed that addition of steel fibers to concrete improves its postcrack behavior in tension. Shear tests on steel fiber-reinforced concrete beams without stirrups have shown that if the fiber dosage is high enough no other transverse reinforcement is necessary to achieve the desired shear capacity [2]. Casanova et al. [3] proposed that fibers act as transverse reinforcement.

Different kinds of specimens and testing methods have been proposed to determine shear strength and to analyze the behavior in a local failure plane. Test of Z-specimens has been quite common in the determination of the shear behavior of

K.H. Khayat and D. Feys (eds.), *Design, Production and Placement of Self-Consolidating Concrete*, RILEM Bookseries 1,
DOI 10.1007/978-90-481-9664-7_36, © RILEM 2010

concrete [4-13]. But, there are not previous experiences with self-compacting fiber-reinforced concretes (SCFRC) push-off tests.

Research Significance

This research is focused on the analysis of the influence of the fiber addition in SCFRC on the shear behavior. The main objectives are:

- To analyze the fibers' influence on the aggregate interlock contribution to shear and to compare it with the influence of traditional rebars.
- To analyze the shear capacity of push-off test on Z-shaped specimens, to study and to differentiate failure modes and to evaluate the influencing parameters.

Experimental Program

Materials

Three different SCC made with steel fiber contents of 0, 40 or 60 kg/m^3 were analyzed. All concretes contain the same cement, water and aggregate type and mixture proportioning (Table I). Filler, sand and coarse aggregates were crushed limestone. A superplasticizer was used and dosed to reach a slump flow (UNE 83361:2007) close to 600 mm for each fiber content.

Table I. Concrete dosages (kg/m^3).

Concrete mix (kg/m^3)	SCC	FRC-40	FRC-60
Cement CEM I-52.5R	423		
Crushed Sand	950		
Gravel 4/7	200		
Gravel 7/12	523		
Filler	83		
Water	196		
Fibers 65/35	0	40	60
Superplasticizer	7.19 (1.7%)	9.73 (2.3%)	10.58 (2.6%)

A Bolomey reference sieve curve [14] with "a=18" parameter was selected to have the minimum fines content need to guaranty the required flowability and avoid any segregation risk. A good agreement between theoretical versus actual aggregate curves was obtained (Figure 1).

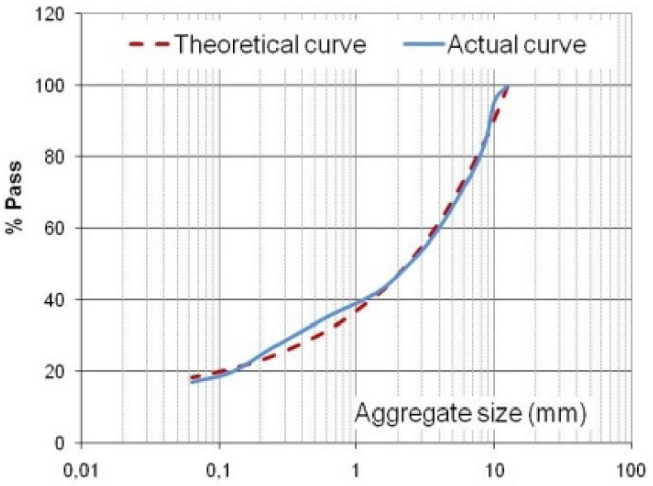

Figure 1. Concretes particle size distribution.

Methodology

The dimensions and test set-up of the Z-shaped push-off specimens are shown in Figure 2 [15-17]. In order to localize the ruptured section and to avoid parasite cracks (cracks which appear out of the shear zone) a notch (5 mm depth and 5 mm width) was sawn on the two sides of the theoretical shear zone and rebars crossing this zone were placed in the specimens. Along the shear plane, the crack opening and shear displacement were measured by means of several displacement meters (Figures 2 and 3).

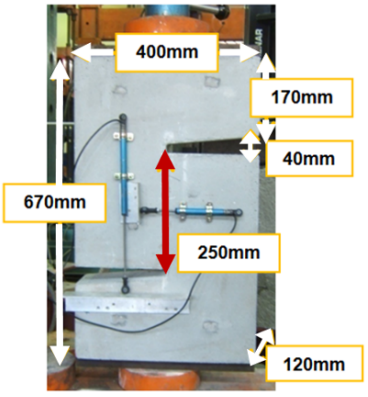

Figure 2. Specimen dimensions. Displacements measure (face A).

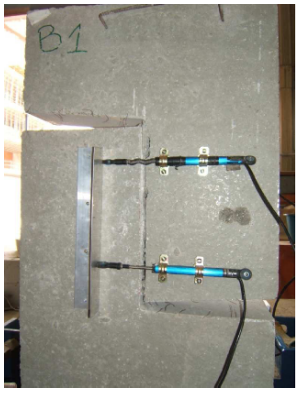

Figure 3. Displacements measure (face B).

In order to control crack opening and avoid brittle failure of the push-off specimens made without fibers, rebars were provided across the anticipated shear failure region (Figure 4).

Before executing the push-off test, a precrack was forced in the failure section; a localized splitting load was applied as shown in Figure 5 by means of metallic load plates. The crack width was determined during the process by calculating the difference between displacements at both sides of the specimens. So, the average was taken by putting one displacement measurement unit in the middle of each side of the specimen.

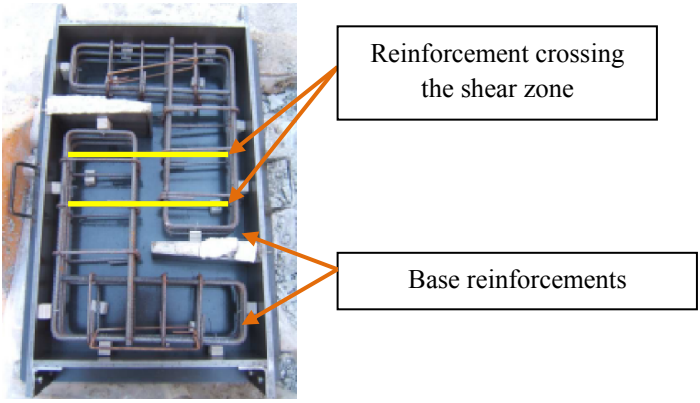

Figure 4. Base reinforcements with the stirrups as reinforcement crossing the shear zone.

Tests variables

Variables were:

- steel fibers dosage (0, 40, 60 kg/m^3)
- the amount of traditional reinforcement crossing the crack section; 2 or 3 ϕ 6
- the maximum precrack opening: No cracked, fine crack (0.28-0.76 mm) and thick crack (0.96-1.76 mm).

Two Z-specimens were produced for each combination of variables. So, there were 26 specimens in total. The complete test program is shown in Table II.

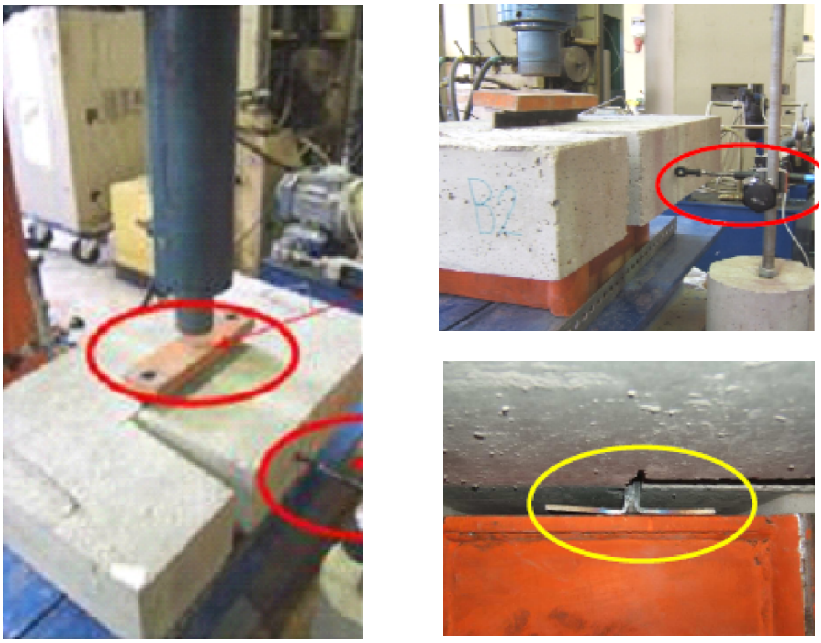

Figure 5. Precrack process before the push-off tests.

Complementary tests

Three cylinders (150 x 300 mm) for each mixture and two additional prismatic specimens (150 x 150 x 600 mm) for each SCFRC mixture were cast with the same batch for push-off specimens. Then, compressive strength EN 12390-3 [18] and residual flexural strength EN 14651 [19], were determined 28 days after their production.

Results and Discussion

Failure modes

The different failure modes are shown in Figure 6. When the specimen does not have transversal reinforcement (TR), the failure pattern is clearly brittle. When, fibers or rebars were placed, the test is better controlled and a ductile failure can be observed.


SCC and no TR


FRC with precrack


FRC without precrack


Precracked SCC with TR

Precracked SCC without TR

Figure 6. Different failure modes obtained during the push-off tests.

Test results

The shear behavior was analyzed by means of the crack opening or shear displacement versus shear load curves during the push-off tests. At Figures 7 and 8 a general example is presented. Those kinds of curves (Figure 7) present a load peak, a post-peak softening and finally a practically constant residual strength until 133 kN for specimens with rebars and until 25 kN for specimens with fibers.

Table II shows the concrete compressive strength and residual flexural strength $f_{R,1}$ and $f_{R,3}$ according to (EN 14651) and the main push-off test results. Results are the average value of all specimens test.

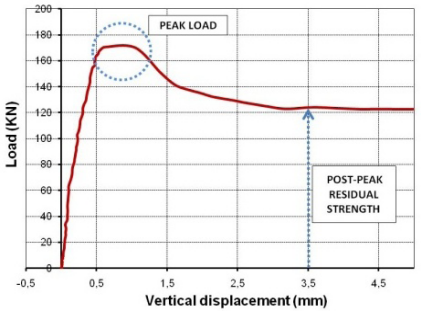

Figure 7. Load-Vertical displacement (Push-off test).

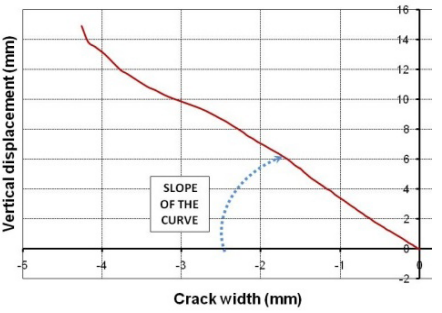

Figure 8. Vertical displacement-Crack width (Push-off test).

Table II. Tests results.

EXPERIMENTAL PROGRAM			CONCRETE PROPERTIES				TEST RESULTS	
Transversal Reinforcement	Concrete	Precrack	Slump Flow (mm)	f_c (Mpa)	$f_{R,1,k}$ (Mpa)	$f_{R,3,k}$ (Mpa)	Max. Load (kN)	Residual load (kN)
No	SCC	No	500	47	-------		150	-
2ϕ6		No	550	50			211	105
		Fine					110	
		Thick					Without peak	
3ϕ6		No					244	133
		Fine					133	
		Thick					Without peak	
No	FRC-40	No	620	55	6.9	4.5	151	16.5
		Fine					72	
		Thick					30	
	FRC-60	No	525	65	8.7	6.3	218	25
		Fine					93	
		Thick					37	

Figures 9 and 10 show some crack opening and shear displacement curves. The maximum load increases with the fiber content and the rebars presence, and is much reduced when the specimens were precracked. Not precracked specimens with 3ϕ6 TR reached the highest maximum load; 40 kg/m^3 fibers and SCC specimens without any reinforcement a 38.5% lower than 3ϕ6 TR and, 2ϕ6 TR or 60 kg/m^3 of fibers specimens (both reached similar load peak) a 12.3% lower than 3ϕ6 TR. The maximum load is also influenced by the precrack level. A load peak for the curve load-vertical displacement on precracked specimens with TR 3ϕ6 is not detected. But, with 2ϕ6 TR or with fibers a load peak was observed (Figures 9 and 10). This maximum load is about 60% higher with fine precracks (72 kN for 40 kg/m^3 and 93 kN for 60 kg/m^3) compared to thick precrack (30 kN for 40 kg/m^3 and 37 kN for 60 kg/m^3). Residual load also increases with the fiber content but is not influenced by the precrack level. In this case, rebars are more efficient than

fibers. Specimens with 2ϕ6 (105 kN) show a residual load 4 times compared to 60 kg/m^3 fibers. Fibers cause a ductile behavior.

With high levels of precracking, a high vertical displacement is obtained (Figures 11 and 12). With fibers (Figure 11) the differences between thick precrack and fine precrack are more pronounced compared to TR 2ϕ6 (Figure 12). At a larger original crack width, TR achieves a better sewing effect than fibers. But, for fine precracks both (fibers and TR) have similar behavior. At small crack widths, the vertical displacement is smaller in the case of fibers compared to TR; fibers are more efficient then TR and control better the relative displacement between the two crack faces.

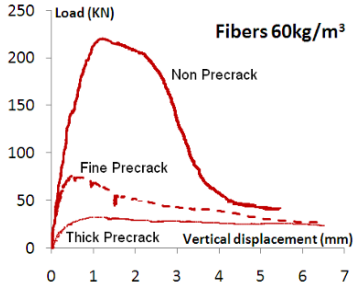

Figure 9. Load - vertical displacement (SCFRC 60 kg/m^3).

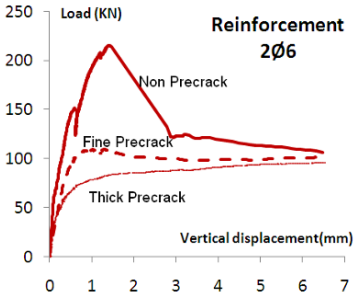

Figure 10. Load - vertical displacement (SCC 2ϕ6).

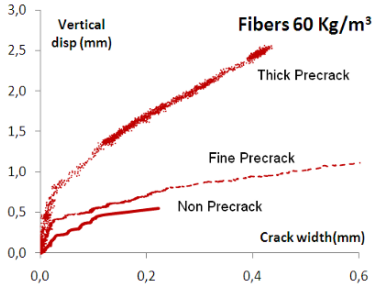

Figure 11. Vertical displacement versus crack width (SCFRC 60 kg/m^3).

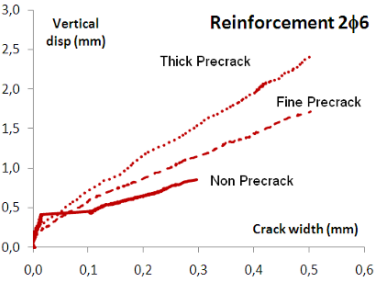

Figure 12. Vertical displacement versus crack width (SCC 2ϕ6).

Conclusions

The main objectives of this research were to analyze the influence of fibers on the aggregate interlock contribution to shear and, to analyze the shear behavior for push-off test on Z-shaped specimens, studying failure modes and influencing parameters.

In total 26 "Z"-specimens made of SCC with different fibers dosages (0, 40, 60 kg/m^3), amount of transversal reinforcement (2 or 3ϕ6) and levels of precrack (no, fine or thick) were tested to analyze the influence on the shear behavior.

From the present study, the following conclusions may be drawn:

- The maximum load increases with the fiber content and due to the rebars presence.
- The maximum load is influenced by the precrack level; precracking decreases the maximum load. The maximum load is 60% higher for fine precracking compared to thick precrack. With high levels of precrack, a high vertical displacement is obtained.
- The residual load also increases with the fiber content but is not influenced by the precrack level. With this respect, rebars are more efficient than fibers. With fibers a ductile behavior is obtained.
- With fibers, the differences on behavior between thick precrack and fine precrack are bigger than for traditional reinforcement.

Acknowledgements

Funding from the Spanish Ministry of Education and Science, through grants BIA2006-15471-C02-01 and PSE 11-2005, PSE-380000-2006-4, PSE-380000-2007-1: "HABITAT 2030", is greatly appreciated.

This research project was financed by PREVALESA (Collaborator Precast industry) and IMPIVA (Instituto de la Pequeña y Mediana Industria Valenciana)-2008.

References

[1] ACI (1996), Report on Fiber Reinforced Concrete, ACI Committee 544 (Ed.), ACI 544.2R-96, ACI Manual of Concrete Practice, Part 6.

[2] Dupont, D. and Vandewalle, L., (2000), In: Proceedings ACI Fall Convention 2000, ACI-SP-216-6, American Concrete Institute (Ed.), Detroit, USA, pp. 79-94.

[3] Casanova, P., Rossi, P. and Schaller, I. (1997), *ACI Materials Journal*, vol. 94-M41, pp. 341-354.
[4] Barr, B. (1987), The Fracture Characteristics of FRC Materials in Shear, Fiber Reinforced Concrete: Properties and Applications, SP-105, ACI (Ed.), pp. 27-53.
[5] Barragán, B., Gettu, R., Agulló, L. and Zerbino, R. (2006), *ACI Materials Journal*, vol. 103, pp. 251-257.
[6] Carmona, S. and Cabrera, M. (2009), *Construction Engineering Magazine*, vol. 24, n. 1, pp. 79-94 (in Spanish).
[7] Frénay, J.W., Reinhardt, H.W. and Walraven, J.C. (1991), *Journal of Structural Engineering, ASCE*, vol. 117, n. 10, pp. 2900-2918.
[8] Hwang, S-J., Yu, H-W and Lee, H-J, (2000), *Journal of Structural Engineering, ASCE*, vol. 126, n. 6, pp. 700-707.
[9] Mansur, M.A., Vinayagam, T. and Tan, K-H. (2008), *Journal of Materials in Civil Engineering, ASCE*, vol. 20, n. 4, pp. 294-302.
[10] Reinhardt, H.W. and Walraven, J.C. (1982) *Journal of the Structural Division, Proceedings of the American Society of Civil Engineers, ASCE*, vol. 108-ST1, pp. 207-224.
[11] Serna, P. (1984), Study of the contribution of steel fibers in concrete on shear behavior, École Nationale des Ponts et Chaussées, France (in French).
[12] Van De Loock, L. (1988), *Journal of Materials Science Letters*, vol. 7, pp. 225-226.
[13] Walraven, J.C. (1981), *Journal of the Structural Division, Proceedings of the American Society of Civil Engineers, ASCE*, vol. 107-ST11.
[14] Arredondo, F. (1969), Concrete Mix Design, Instituto Eduardo Torroja (Ed.), Madrid (in Spanish).
[15] Cuenca E. (2008), Shear behavior on self-compacting and fiber reinforced concrete elements, Master thesis, UPV, Spain (in Spanish).
[16] Cuenca E. (2008), Study of shear behavior on self-compacting elements. Application to industrial precast beams, PFC, UPV, Spain (in Spanish).
[17] Figuet, E. and Serna, P. (2009), Shear behavior on self-compacting fiber-reinforced concrete "Z" specimens, PFC, UPV, Spain (in French).
[18] Committee AEN/CTN 83 Concrete, (2009), UNE-EN 12390-3: Hard state concrete tests. Part 3: Concrete strength determination on specimens (in Spanish).
[19] Committee AEN/CTN 83 Concrete, (2007), UNE-EN 14651: Steel fiber reinforced concrete test method. Tensile strength determination by flexure (proportionality limit (LOP), residual strength) (in Spanish).

Long-Term Behaviour of Fiber-Reinforced Self-Compacting Concrete Beams

Nicola Buratti, Claudio Mazzotti and Marco Savoia

DISTART-Structural Engineering, University of Bologna, Italy

Abstract. This paper describes the results of an experimental campaign aimed at investigating the long-term behaviour of beams cast using fiber-reinforced self-compacting concretes containing either steel or synthetic fibers in comparison with that of plain self-compacting concrete beams with standard reinforcement. The flexural behaviour of six different beams was investigated in a long-term four point bending test under constant loading. All the beams were pre-cracked before the long-term test.
The tests showed that fibers have an important role in controlling the increase of crack opening over time. The greatest reduction in the delayed crack opening was obtained using a mixture of steel and macro synthetic fibers.

Introduction

In the last few years the construction industry has recognized that concrete pavements have to be designed as actual structural elements, which must comply with some prescribed limit states [1]. The design of the concrete pavements is mainly addressed by requirements in terms of serviceability limit states (short and long-term deformations, cracking) and only marginally by requirements in terms of ultimate limit states. As far as the serviceability limit states are concerned, it is important that the performance levels to be satisfied are defined by taking into account the reference time interval of application of the corresponding actions (characteristic, frequent and persistent values). In order to fulfill these types of requirements, in the last years there have been a great deal of technical developments concerning construction materials, among which high performance concretes (e.g. self-compacting concrete, SCC) and fiber-reinforced concretes have generated noteworthy advances in concrete industrial-pavement technology [2-9]. As an example, the traditional reinforcement mesh may, in some cases, be reduced or completely removed by using fiber-reinforced concretes; in this respect, the self-compacting concrete is an ideal medium to spread homogeneously the fibers into

K.H. Khayat and D. Feys (eds.), *Design, Production and Placement of Self-Consolidating Concrete*, RILEM Bookseries 1,
DOI 10.1007/978-90-481-9664-7_37,

the fresh concrete, avoiding segregation. On the other hand, the verification of the required performance levels may be complicated in terms of both the evaluation of the effects of the applied actions and the proper definition of the target level of performance. Equally complex is the assessment of the floor performance with respect to the long-term actions. In this case, the dependence of strains and crack openings on time must be considered because of their effect on durability [10-12].

The present paper is a first attempt in understanding the long-term behaviour of fiber-reinforced self-compacting concretes (FRSCC) for serviceability loads. In particular, it discusses the results of tests comparing the long-term behaviour, in terms of mid-span deflection and crack opening increases with time, of a plain SCC beam with conventional reinforcing bars with the behaviour of fiber-reinforced SCC beams, containing steel or synthetic fibers, without conventional reinforcement.

The Experimental Campaign

Experimental program

Six 300 x 120 x 2000 mm (width x height x length) beams were considered in the present study, as summarized in Table I. The geometry of the beams was defined in order to be representative of a strip of concrete floor. The first beam, named REBAR in the following, was cast using plain SCC concrete and contained conventional steel reinforcing bars (ϕ8/10 cm, i.e. three steel bars in total). All the other beams were cast using fiber-reinforced SCC and did not contain any reinforcing bar. Three different FRSCCs were used; two containing different dosages, 25 kg/m^3 and 35 kg/m^3 respectively, of steel fibers and one containing a combination of steel and synthetic fibers (see Table I and Table II). Two beams were cast for each of the first two FRSCCs (named SF25a, SF25b, SF35a and SF35b in the following). Only one beam was cast with the concrete containing the combination of fibers (named MIX in the following). The synthetic fibers used in this last beam are usually employed to reduce shrinkage induced cracking in industrial pavements.

For each concrete mixture, two prisms with dimensions 150 x 150 x 550 mm were also cast and used to characterize the short-term properties of the concrete.

Material properties

Self-compacting-concrete properties. The SCC used in the tests has normal compressive strength, it is suitable for cast-in-place applications and has been cast in a ready-mix plant. In order to achieve the self-compactability without increasing the number of silos required at the concrete production site, the cement has been used also as filler. The details of the mixture as well as some important mixture design parameters (w/c, being w = water, c = cement content by mass) are reported in Table III for the mixtures used to cast the beams. In particular, the mixture used

for the REBAR beam is plain SCC, while in the remaining mixtures fibers were added. The superplasticizer used is based on acrylic polymers (with no formaldehyde) and the viscosity agent is an active polymer-based admixture. No segregation was observed during the casting phases.

Table I. Summary of the beams considered. The fiber dosage is given both as mass per volume unit and as volume percentage.

Beam	Fiber type	Fiber dosage	Rebar
MIX	Steel A & B + Synthetic	17 kg/m^3 – 0.21% (St. A) + 3 kg/m^3 – 0.04% (St. B) + 0.3 kg/m^3 – 0.003% (Synth.)	-
SF25a	Steel A	25 kg/m^3 – 0.32%	-
SF25b	Steel A	25 kg/m^3 – 0.32%	-
SF35a	Steel A	35 kg/m^3 – 0.45%	-
SF35b	Steel A	35 kg/m^3 – 0.45%	-
REBAR	-	-	ϕ8/10”

Table II. Geometry of the fibers used.

Fiber type	D [mm]	L [mm]
Steel A	0.75	50
Steel B	0.6	33
Synthetic	18×10^{-3}	6

Table III. Concrete mixture design parameters for the different casts performed.

Component	Type	Unit	REBAR	SF25a	SF25b	SF35a	SF35b	MIX
Cement	II/A-L 32.5R	kg/m^3	390	390	390	390	390	390
Fine sand	0-4 mm	kg/m^3	125	125	125	125	125	125
Gravel	8-15 mm	kg/m^3	425	425	425	425	425	425
Water		lt/ m^3	225	225	225	225	225	225
w/c = w/b			0.57	0.57	0.57	0.57	0.57	0.57
Superplasticizer		lt/ m^3	2.75	3.98	2.30	3.98	4.30	2.30
Viscosity agent		lt/ m^3	-	0.4	-	-	-	-

Before casting the slump flow, J-ring and V-Funnel tests were performed in order to characterize the fresh properties of the concretes. These test were performed

according to Italian standards for SCC (UNI 10041 [13]), obtaining the values reported in Table IV. In some cases, the conventional fresh-state tests were not completed because fiber length of 50 mm (steel fibers) is too high for J-ring with bar spacing of about 45 mm. The compressive strength of the hardened concrete was also measured at 7 and 28 days, obtaining the results given in Table V. The mean yielding stress of the steel reinforcement bars used in the REBAR beam is f_{ym}=540 MPa.

Table IV. Fresh properties of the concretes used to cast the different beams.

Cast	Slump flow [mm]	V-funnel [sec]	J-ring [mm]
MIX	580	8	-*
SF25a	670	3.5	630
SF25b	580	-*	-*
SF35a	610	4.5	500
SF35b	620	-*	-*
REBAR	660	4.5	660

* These values could not be measured due to problems during the test caused by the presence of fibers

Table V. Cube compressive strength of the concrete for the different casts.

Cast	R_{cm} (7 days) MPa	R_{cm} (28 days) [MPa]
MIX	27.3	33.4
SF25a	31.5	40.1
SF25b	34.2	42.2
SF35a	31.0	39.9
SF35b	32.6	40.1
REBAR	31.4	42.0

Short-term mechanical properties of FRSCC. The short-term mechanical properties of the FRCs considered in the present study were characterized by performing four-point bending tests on 150 x 150 x 550 mm (height x width x length) notched prisms (see Figure 1). The test procedure adopted is consistent with the guidelines given by UNI EN 11039-2 [14]. The specimens were notched at mid-span (the height of the notch is 45 mm), in order to control the triggering of the crack.

The specimens were cured in moulds, under polyethylene sheeting, for 24 h after casting and then demoulded and subjected to water curing at 20°C for further 26 days. At the end of the curing period, the specimens were prepared for the test and tested 28 days after casting. The tests characterized the tensile behaviour of the FRCs by means of force-Crack Mouth Opening Displacement (CMOD) and force-Crack Tip Opening Displacement (CTOD) curves that allowed to calculate the residual strength at different values of crack-opening. The testing machine used

operates under displacement control with a constant rate of displacement (CMOD or deflection), and has sufficient stiffness to avoid unstable loading phenomena.

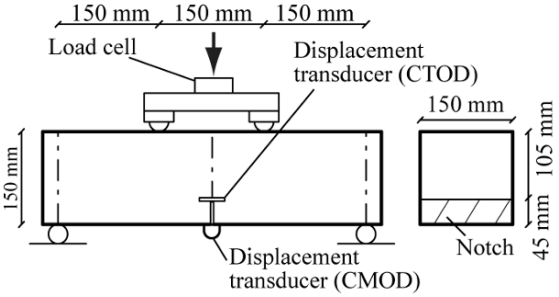

Figure 1. Short-term tests on the 150 x 150 x 550 mm: tests set-up.

During the tests, according to UNI EN 11039-2 [14], the rate of increase of the CMOD was controlled: 0.05 mm/min for CMOD ≤ 0.65 mm and 0.5 mm/min for CMOD > 0.65 mm. All the tests were terminated at CMOD = 4 mm.

The force-CMOD and force-CTOD curves obtained from the tests are given in Figure 2 which shows that, on average, even though the number of specimens is small, the post-peak performance of the FRCs increases as the fiber dosage increases, and that the specimens with steel fibers have a greater toughness than those with the combination of steel and synthetic fibers. Figure 2 also draws the attention to the high scatter of the curves in the post peak region, especially as far as steel fibers are concerned. This is a consequence of the statistical variability of the number of fibers crossing the crack surface and it is particularly high for steel fibers. This variability depends on the geometry of the fibers with respect to that of the specimen and on their dosage and type [15-17].

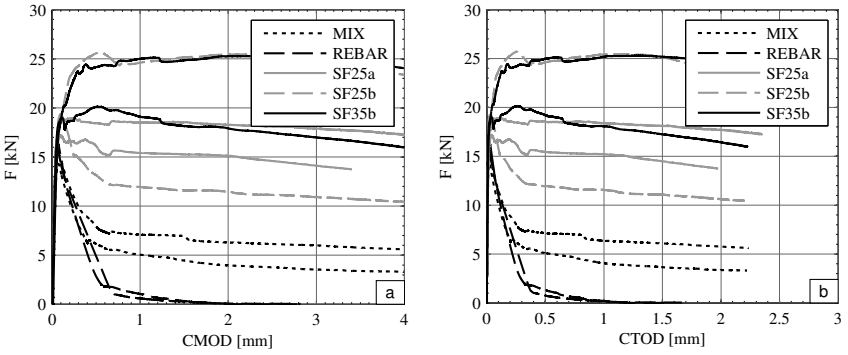

Figure 2. Short-term tests on the 150 x 150 x 550 mm prisms: (a) force-CMOD curves, and (b) force-CTOD curves.

Pre-cracking and definition of loading

Prior to the long-term tests, the beams have been pre-cracked up to a CMOD of 0.2 mm. This value has been assumed as representative of the crack width of concrete floors at the serviceability limit state. In order to better control the position of the crack, all beams have been notched at mid-span (notch 10 mm deep). In this phase, a three-point bending scheme was adopted, and the tests were run under mid-span deflection control. The same machine used for the 150x150x550 mm specimens (which was adapted to the beam size) was employed in this phase and a distance between the supports of 80 cm was set (see Figure 3a). Figure 4a and 4b show the behaviour of some of the beams in this phase by means of force-CMOD curves (Figure 4a) and nominal strength-CMOD curves (Figure 4b). The nominal strength is calculate as $\sigma = M/W$, where M is the bending moment at mid-span and W is the section modulus of the net cross-section at mid-span. The SF25b, SF35a, MIX beams showed similar behaviour, characterized by a slightly softening branch after the peak of the force-CMOD curve.

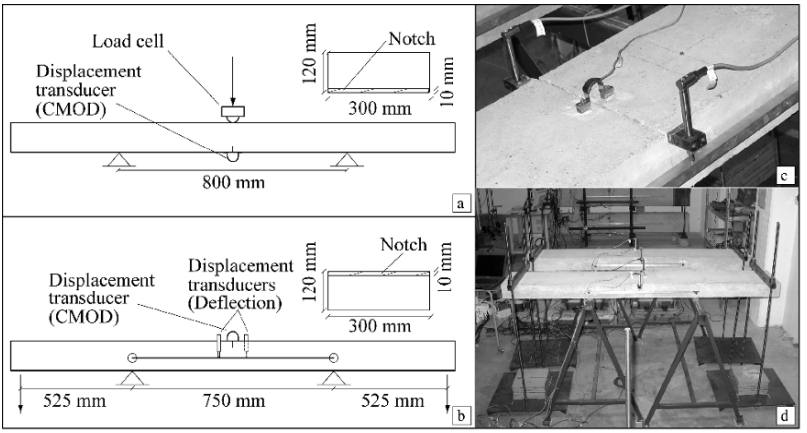

Figure 3. Test set-up for pre-cracking the beams (a); test set-up for the long-term tests (b); detail of the transducers used in the long-term tests (c); two beams during the long-term test (d).

The forces measured at CMOD = 0.2 mm and the residual crack mouth openings after the complete unloading were similar as well; they ranged from 11.0 kN to 14.5 kN and from 0.08 to 0.11 mm, respectively. The SF35b beam had a different behaviour; in fact, the force-CMOD curve related to this beam had an appreciable strain-hardening without showing a clear peak stress point. Looking for this peak, the test was carried out up to a greater CMOD value, i.e. CMOD = 0.35 mm.

Since the long-term tests described in the present paper are not standard, there are no acknowledged criteria on how to define the loading value to be applied permanently. In the present work, it was chosen to apply a loading value able to produce a bending moment in the cracked section equal to the 50% of that observed at CMOD = 0.2 mm in the pre-cracking test.

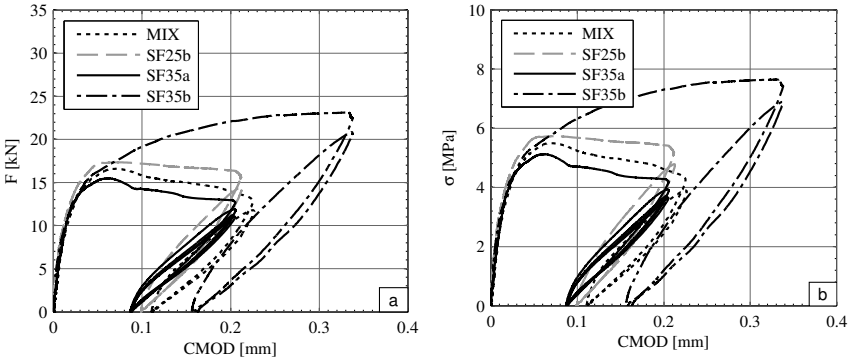

Figure 4. Force-CMOD curves (a) and nominal stress-CMOD curves (b) obtained pre-cracking the beams.

Experimental set-up for the long-term tests

After the cracking phase, the long-term tests were performed using a four-point bending scheme. Figure 3b-d show the experimental setup. Each beam is sustained by two steel systems at the intermediate supports, thus creating a central span of 750 mm, where the bending moment is constant and the shear is null. The dead loads were applied at the beams extremities at a distance of 525 mm from the inner supports, by using concrete blocks; they were supported by a steel system composed of a base plate connected by two threaded rods to transverse hollow rods placed on the top of the beam (Figure 3d). The load values, calculated following the criterion described at the end of the previous section, are reported in Table VI.

Table VI. Loads applied on each end of the beams during the long-term test.

Beam	Load (kN)
MIX	2.50
SF25a	2.53
SF25b	2.51
SF35a	2.14
SF35b	3.36
REBAR	2.56

On each beam, the crack-opening at mid-span (notched section) as well as the mid-span deflection respect to the intermediate supports have been measured. The crack opening was measured by using a bridge-based displacement transducer while the deflection was measured, on both sides of the beams, by using LVDT transducers. In order to evaluate the relative deflection between mid-span and the intermediate supports, two aluminium bars, supported by pins glued over the supports, on both sides of the beams were used. During the long-term tests, the beams were kept in a climate room, at 20°C and 60% RH.

Results of the Long-Term Tests

Loading phase

As described in the previous section, the loads used in the long-term tests were applied using concrete weight (see Figure 3d). The force-CMOD and the force-mid-span deflection curves recorded during the loading phase are given in Figure 5. Those curves are clearly not-continuous because the loading was applied in discrete steps. Force-CMOD and force-mid-span deflection relations show a moderately non-linear behaviour for low force values, when the crack re-opening process occurs, and then are almost linear. All the beams showed a similar flexural stiffness. The REBAR beam was the most flexible while the MIX beam was the stiffest. In terms of force-CMOD relations, a higher scattering of the results was observed, being the curves dependent only from the flexural behaviour of the cracked section. Nevertheless, the REBAR and MIX beams show again smaller and higher stiffness, respectively, compared to the other beams.

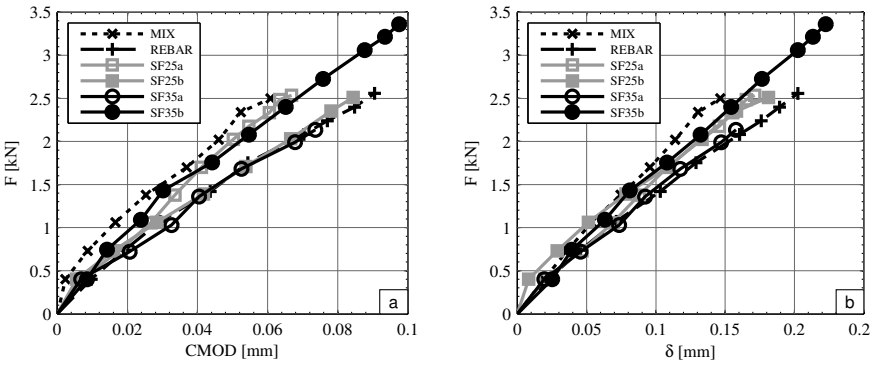

Figure 5. Force-CMOD (a) and force-mid-span deflection curves (b) recorded while applying the loads used in the long-term tests.

Long-term tests

Figure 6 shows the long-term behaviour of the beams considered in terms of CMOD and mid-span deflection increases with time. To make the figure more easily readable only the average behaviour of the two couples of beams with the same dosage of fibers, i.e. SF25a/SF25b and SF35a/SF35b, have been plotted. Figure 6a shows the CMOD increase over time: the different rates of increase of the delayed deformations for the different concretes considered can be observed. In particular, confirming the instantaneous behaviour, the rate of delayed deformations for the REBAR beam is the highest while the lowest is provided by the MIX beam. The curves for the concretes SF25 and SF35 are included between these two limits and in general their slope decreases as the fiber dosage increases.

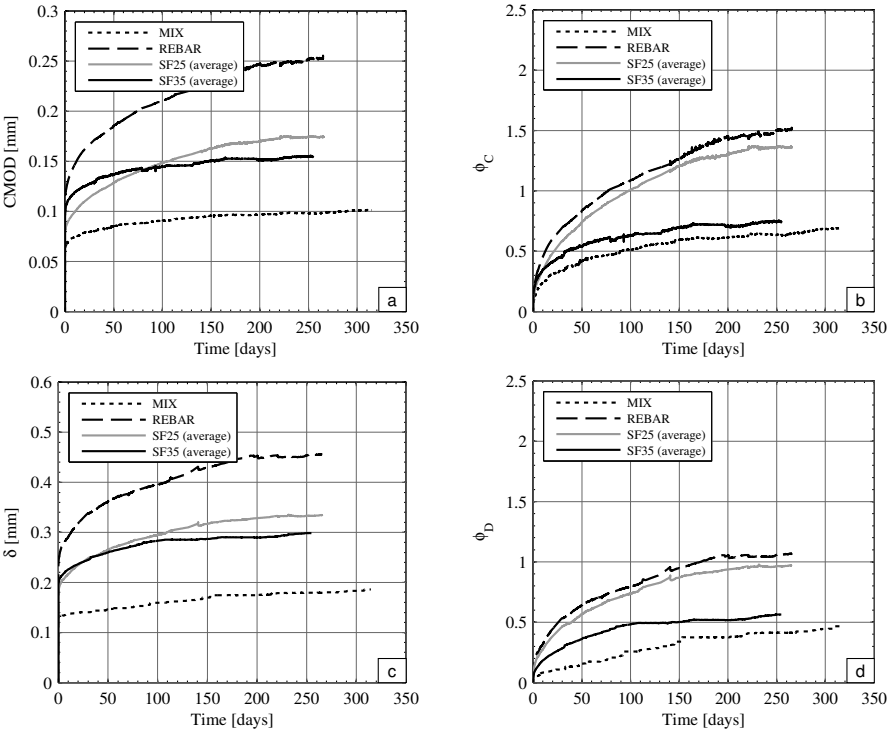

Figure 6. CMOD increase over time (a); creep coefficient in terms of CMOD (b); mid-span deflection increase over time (c); creep coefficient in terms of mid-span deflection (d).

In order to better compare the long-term results in terms of CMOD, the delayed CMOD increase can be reported in terms of coefficient of viscosity, ϕ_C, according to the expression $\phi_C = CMOD(t) - CMOD(t_0)/CMOD(t_0)$, where t is the generic

time instant and t_0 is the time at the end of the loading phase (see Figure 5). Figure 6b shows the so obtained curves. This plot allows to appreciate the importance of delayed deformations, in fact, for example, after 250 days since the end of the loading phase the CMOD increase was 63% for the MIX beam, 74% on average for the SF35a and SF35b beams, 136% on average for the SF25a and SF25b beams and 150% for the REBAR beam. Similar comments can be made on the results in terms of mid-span deflection, which are reported in Figure 6c. This plot shows the mid-span deflection increase over time. In general, the behaviour is similar to that observed in terms of CMOD.

Figure 6d shows the evolution with time of the coefficient of delayed deflection ϕ_D, calculated as $\phi_D = \delta(t) - \delta(t_0)/\delta(t_0)$, where $\delta(t)$ is the mid-span deflection at time t and $\delta(t_0)$ is the mid-span deflection at the end of the loading phase (see Figure 5). Comparing this figure with Figure 6b it is possible to observe that the delayed deformations in terms of mid-span deflection are smaller than those in terms of CMOD. In fact, for example, the delayed deformations in terms of mid-span deflection after 250 days since the end of the loading phase are 41% of the instantaneous deflection for the MIX beam, 56% on average for the SF35a and SF35b beams, 97% on average for the SF25a and SF25b beams and 106% for the REBAR beam. This confirms the effectiveness of the fibers compared to the use of a conventional steel mesh.

Failure tests

The REBAR and SF25a beams were unloaded after 265 days since the beginning of the test and loaded up to failure in a three point bending scheme. The same experimental set-up used to pre-crack the beams was adopted. Figure 7 shows the force-CMOD curves measured during the failure tests.

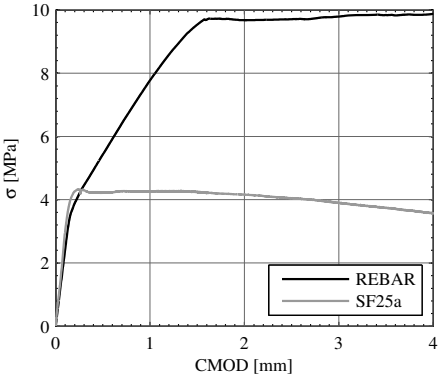

Figure 7. Force-CMOD curves recorded during the failure test performer on REBAR and SF25a beams at the end of the long-term loading.

As expected, the two curves are quite different: in fact, the beam containing the reinforcing steel bars (REBAR) shows a force-CMOD curve constituted of three quasi-linear branches and clearly shows plastic behaviour after yielding. On the contrary, the force-CMOD curve concerning the SF25a beam shows a clear peak with a corresponding force value of 13 kN, after which a slightly softening behaviour can be observed. The remaining beams have not yet been unloaded.

Conclusions

The experimental campaign described in the present paper investigated the long-term behaviour of cracked beams cast with FRSCC. In particular, the CMOD and the mid-span deflection developments over time of six different beams were measured and compared. The tests performed showed that the magnitude of the delayed deformation can be high, up to 150% of the instantaneous counterpart. The rate of delayed deformation increased at lower rates for the fiber-reinforced SCC beams than for the plain SCC beam containing standard reinforcing bars. In particular, the lowest long-term damage was obtained for the specimen containing a combination of steel fibers of different sizes and of synthetic fibers usually employed to reduce shrinkage.

Acknowledgements

The authors would like to thank MAPEI, Maccaferri and Lombarda Calcestruzzi for providing the materials and casting the specimens. The financial support of (Italian) MIUR (PRIN 2006 Grant: “Structural application of self-compacting concrete”) is also gratefully acknowledged.

References

[1] Sorelli, L.G., Meda, A. and Plizzari, G.A. (2006), Steel fiber concrete slabs on ground: a structural matter, *ACI Structural Journal*, vol. 103, pp. 551-558.

[2] Torrijos, M.C., Barragán, B.E. and Zerbino, R.L. (2010), Placing conditions, mesostructural characteristics and post-cracking response of fibre reinforced self-compacting concretes, *Construction and Building Materials*, vol. 24, pp. 1078-1085.

[3] Pons, G., Mouret, M., Alcantara, M. and Granju, J. (2007), Mechanical behaviour of self-compacting concrete with hybrid fibre reinforcement, *Materials and Structures*, vol. 40, pp. 201-210.

[4] Okamura, H. (1997), Self-compacting high-performance concrete, *Concrete International.*, vol. 19, pp. 50-54.

[5] Ferrara, L. and Meda, A. (2006), Relationships between fibre distribution, workability and the mechanical properties of SFRC applied to precast roof elements, *Materials and Structures*, vol. 39, pp. 411-420.

[6] Ferrara, L., Park, Y.-D. and Shah, S.P. (2007), A method for mix-design of fiber-reinforced self-compacting concrete, *Cement and Concrete Research*, vol. 37, pp. 957-971.

[7] Brouwers, H.J.H. and Radix, H.J., (2005) Self-compacting concrete: Theoretical and experimental study, *Cement and Concrete Research*, vol. 35, pp. 2116-2136.

[8] Corinaldesi, V. and Moriconi, G. (2004), Durable fiber reinforced self-compacting concrete, *Cement and Concrete Research*, vol. 34, pp. 249-254.

[9] Ding, Y., Zhang, Y. and Thomas, A. (2009), The investigation on strength and flexural toughness of fibre cocktail reinforced self-compacting high performance concrete, *Construction and Building Materials*, vol. 23, pp. 448-452.

[10] Grzybowski, M. and Shah, S.P. (1990), Shrinkage cracking of fiber reinforced conrete, *ACI Materials Journal*, vol. 87, pp. 138-148.

[11] Miltenberger, M., Attiogbe, E. and Bissonnette, B. (2007), Behavior of conventional reinforcement and a steel-polypropylene fiber blend in slabs-on-grade, *Materials and Structures*, vol. 40, pp. 279-288.

[12] Rouse, J.M. and Billington, S.L. (2007), Creep and shrinkage of high-performance fiber-reinforced cementitious composites, *ACI Materials Journal*, vol. 104, pp. 129-136.

[13] UNI, 10041 (2003), Testing procedure on fresh self compacting concrete, Evaluation of the slump flow and of the flow time (in Italian).

[14] UNI, 11039-2 (2003), Steel fibre reinforced concrete. Test method for determination of first crach strength and ductility.

[15] Buratti, N., Mazzotti, C. and Savoia, M., (2008), Experimental study on the mehanical behaviour of steel and macro-synthetic fibre reinforced concretes, Proceedings of the 17th Conference of the Italian Association of Concrete Precasting Industries (CTE), Rome, pp. 511-520 (in Italian).

[16] Gettu, R., Gardner, D.R., Saldivar, H. and Barragan, B.E. (2005), Study of the distribution and orientation of fibers in SFRC specimens, *Materials and Structures*, vol. 38, pp. 31-37.

[17] Dupont, D. and Vandewalle, L. (2004), Comparison between the round plate test and the RILEM 3-point bending test, 6th RILEM Symposium on Fibre-Reinforced Concretes (FRC) - BEFIB, Di Prisco, M., Felicetti, F. and Plizzari, G.A. (Eds.), RILEM Publications S.A.R.L., Varenna, pp. 101-110.

Author Index

REUNION INTERNATIONALE DES LABORATOIRES ET EXPERTS DES MATERIAUX, SYSTEMES DE CONSTRUCTION ET OUVRAGES

INTERNATIONAL UNION OF LABORATORIES AND EXPERTS IN CONSTRUCTION MATERIALS, SYSTEMS AND STRUCTURES

RILEM Publications - 2 April 2010

The following list is presenting the current global offer, sorted by series.

RILEM PROCEEDINGS

PRO 1: Durability of High Performance Concrete (ISBN: 2-912143-03-9); *Ed. H. Sommer*

PRO 2: Chloride Penetration into Concrete (ISBN: 2-912143-00-04), *Eds. L.-O. Nilsson and J.-P. Ollivier*

PRO 3: Evaluation and Strengthening of Existing Masonry Structures (ISBN: 2-912143-02-0); *Eds. L. Binda and C. Modena*

PRO 4: Concrete: From Material to Structure (ISBN: 2-912143-04-7), *Eds. J.-P. Bournazel and Y. Malier*

PRO 5: The Role of Admixtures in High Performance Concrete (ISBN: 2-912143-05-5); *Eds. J. G. Cabrera and R. Rivera-Villarreal*

PRO 6: High Performance Fiber Reinforced Cement Composites (HPFRCC 3) (ISBN: 2-912143-06-3); *Eds. H. W. Reinhardt and A. E. Naaman*

PRO 7: 1st International RILEM Symposium on Self-Compacting Concrete (ISBN: 2-912143-09-8); *Eds. Å. Skarendahl and Ö. Petersson*

PRO 8: International RILEM Symposium on Timber Engineering (ISBN: 2-912143-10-1); *Ed. L. Boström*

PRO 9: 2nd International RILEM Symposium on Adhesion between Polymers and Concrete ISAP '99 (ISBN: 2-912143-11-X); *Eds. Y. Ohama and M. Puterman*

PRO 10: 3rd International RILEM Symposium on Durability of Building and Construction Sealants (ISBN: 2-912143-13-6); *Eds. A. T. Wolf*

PRO 11: 4th International RILEM Conference on Reflective Cracking in Pavements (ISBN: 2-912143-14-4); *Eds. A. O. Abd El Halim, D.A. Taylor and El H. H. Mohamed*

PRO 12: International RILEM Workshop on Historic Mortars: Characteristics and Tests (ISBN: 2-912143-15-2); *Eds. P. Bartos, C. Groot and J. J. Hughes*

PRO 13: 2nd International RILEM Symposium on Hydration and Setting (ISBN: 2-912143-16-0); *Ed. A. Nonat*

PRO 14: Integrated Life-Cycle Design of Materials and Structures (ILCDES 2000) (ISBN: 951-758-408-3), (ISSN: 0356-9403); *Ed. S. Sarja*

PRO 15: Fifth RILEM Symposium on Fibre-Reinforced Concretes (FRC) - BEFIB' 2000 (ISBN: 2-912143-18-7); *Eds. P. Rossi and G. Chanvillard*

PRO 16: Life Prediction and Management of Concrete Structures (ISBN: 2-912143-19-5); *Ed. D. Naus*

PRO 17: Shrinkage of Concrete - Shrinkage 2000 (ISBN: 2-912143-20-9)
Eds. V. Baroghel-Bouny and P.-C. Aïtcin

PRO 18: Measurement and Interpretation of the On-Site Corrosion Rate (ISBN: 2-912143-21-7)
Eds. C. Andrade, C. Alonso, J. Fullea, J. Polimon and J. Rodriguez

PRO 19: Testing and Modelling the Chloride Ingress into Concrete - 516 pp. - ISBN: 2-912143-22-5 - Soft cover, *Eds. C. Andrade and J. Kropp*

PRO 20: 1st International RILEM Workshop on Microbial Impacts on Building Materials (2000); *Ed. M. Ribas Silva (CD 02)*

PRO 21: International RILEM Symposium on Connections between Steel and Concrete (ISBN: 2-912143-25-X); *Ed. R. Eligehausen*

PRO 22: International RILEM Symposium on Joints in Timber Structures (ISBN: 2-912143-28-4); *Eds. S. Aicher and H.-W. Reinhardt*

PRO 23: International RILEM Conference on Early Age Cracking in Cementitious Systems (ISBN: 2-912143-29-2); *Eds. K. Kovler and A. Bentur*

PRO 24: 2nd International RILEM Workshop on Frost Resistance of Concrete (ISBN: 2-912143-30-6) Hard back; *Eds. M. J. Setzer, R. Auberg and H.-J. Keck*

PRO 25: International RILEM Workshop on Frost Damage in Concrete (ISBN: 2-912143-31-4) - Soft cover; *Eds. D. J. Janssen, M. J. Setzer and M. B. Snyder*

PRO 26: International RILEM Workshop on On-Site Control and Evaluation of Masonry Structures (ISBN: 2-912143-34-9) - Soft cover; *Eds. L. Binda and R. C. de Vekey*

PRO 27: International RILEM Symposium on Building Joint Sealants (1988) (CD03); *Ed. A.T. Wolf,* 2003

PRO 28: 6th International RILEM Symposium on Performance Testing and Evaluation of Bituminous Materials, PTEBM'03, Zurich, Switzerland (2003) (ISBN: 2-912143-35-7) - Soft cover; *Ed. M.N. Partl, (CD06)*

PRO 29: 2nd International RILEM Workshop on Life Prediction and Ageing Management of Concrete Structures, Paris, France (2003) (ISBN: 2-912143-36-5) - Soft cover; *Ed. D.J. Naus*

PRO 30: 4th International RILEM Workshop on High Performance Fiber Reinforced Cement Composites – HPFRCC 4, University of Michigan, Ann Arbor, USA (2003) (ISBN: 2-912143-37-3) Hard back; *Eds. A.E. Naaman and H.W. Reinhardt*

PRO 31: International RILEM Workshop on Test and Design Methods for Steel Fibre Reinforced Concrete: Background and Experiences (2003) (ISBN: 2-912143-38-1) - Soft cover; *Eds. B. Schnütgen and L. Vandewalle*

PRO 32: International Conference on Advances in Concrete and Structures (2003), 2 vol. (ISBN (set): 2-912143-41-1) - Soft cover; *Eds. Ying-shu Yuan, Surendra P. Shah and Heng-lin Lü*

PRO 33: 3rd International Symposium on Self-Compacting Concrete (2003) (ISBN: 2-912143-42-X) - Soft cover; *Eds. Ó. Wallevik and I. Níelsson*

PRO 34: International RILEM Conference on Microbial Impact on Building Materials (2003) (ISBN: 2-912143-43-8); *Ed. M. Ribas Silva*

PRO 35: International RILEM TC 186-ISA on Internal Sulfate Attack and Delayed Ettringite Formation (2002) (ISBN: 2-912143-44-6) - Soft cover; *Eds. K. Scrivener and J. Skalny*

PRO 36: International RILEM Symposium on Concrete Science and Engineering – A Tribute to Arnon Bentur (2004) (ISBN: 2-912143-46-2) Hard back
Eds. K. Kovler, J. Marchand, S. Mindess and J. Weiss

PRO 37: 5th International RILEM Conference on Cracking in Pavements – Mitigation, Risk Assessment and Prevention (2004), (ISBN: 2-912143-47-0) Hard back
Eds. C. Petit, I. Al-Qadi and A. Millien

PRO 38: 3rd International RILEM Workshop on Testing and Modelling the Chloride Ingress into Concrete (2002) (ISBN: 2-912143-48-9) - Soft cover; *Eds. C. Andrade and J. Kropp*

PRO 39: 6th International RILEM Symposium on Fibre-Reinforced Concretes (BEFIB 2004), (ISBN: 2-912143-51-9) Hard back; *Eds. M. Di Prisco, R. Felicetti and G. A. Plizzari*

PRO 40: International RILEM Conference on the Use of Recycled Materials in Buildings and Structures (2004) (ISBN: 2-912143-52-7) - Soft cover; *Eds. E. Vázquez, Ch. F. Hendriks and G. M. T. Janssen*

PRO 41: RILEM International Symposium on Environment-Conscious Materials and Systems for Sustainable Development (2004) (ISBN: 2-912143-55-1) - Soft cover; *Eds. N. Kashino and Y. Ohama*

PRO 42: SCC'2005 – China: 1st International Symposium on Design, Performance and Use of Self-Consolidating Concrete (2005) (ISBN: 2-912143-61-6) Hard back; *Eds. Zhiwu Yu, Caijun Shi, Kamal Henri Khayat and Youjun Xie*

PRO 43: International RILEM Workshop on Bonded Concrete Overlays (2004) (e-ISBN: 2-912143-83-7); *Eds. J.L. Granju and J. Silfwerbrand*

PRO 44: 2nd International RILEM Workshop on Microbial Impacts on Building Materials (Brazil 2004) (CD11) e-ISBN: 2-912143-84-5; *Ed. M. Ribas Silva*

PRO 45: 2nd International Symposium on Nanotechnology in Construction, Bilbao, Spain (2005) - ISBN: 2-912143-87-X - Soft cover; *Eds. Peter J.M. Bartos, Yolanda de Miguel and Antonio Porro;* 2006

PRO 46: ConcreteLife'06 - International RILEM-JCI Seminar on Concrete Durability and Service Life Planning: Curing, Crack Control, Performance in Harsh Environments (2006) - ISBN: 2-912143-89-6, Hard back; *Ed. K. Kovler*

PRO 47: International RILEM Workshop on Performance Based Evaluation and Indicators for Concrete Durability (2006) - ISBN: 978-2-912143-95-2- Soft cover; *Eds. V. Baroghel-Bouny, C. Andrade, R. Torrent and K. Scrivener ;* 2007

PRO 48: 1st International RILEM Symposium on Advances in Concrete through Science and Engineering (2004) e-ISBN: 2-912143-92-6; *Eds. J. Weiss, K. Kovler, J. Marchand, and S. Mindess*

PRO 49: International RILEM Workshop on High Performance Fiber Reinforced Cementitious Composites in Structural Applications (2006) ISBN: 2-912143-93-4 - Soft cover; *Eds. G. Fischer and V.C. Li*

PRO 50: 1st International RILEM Symposium on Textile Reinforced Concrete (2006) ISBN: 2-912143-97-7 - Soft cover; *Eds. Josef Hegger, Wolfgang Brameshuber and Norbert Will*

PRO 51: 2nd International Symposium on Advances in Concrete through Science and Engineering (2006) ISBN: 2-35158-003-6; e-ISBN: 2351580028 Hard back; *Eds. J. Marchand, B. Bissonnette, R. Gagné, M. Jolin and F. Paradis*

PRO 52: Volume Changes of Hardening Concrete: Testing and Mitigation (2006) ISBN: 2-35158-004-4; e-ISBN: 2351580052 - Soft cover; *Eds. O. M. Jensen, P. Lura and K. Kovler*

PRO 53: High Performance Fiber Reinforced Cement Composites HPFRCC5 (2007) 542 pp. ISBN: 978-2-35158-046-2 Hard back; *Eds. H.W. Reinhardt and A.E. Naaman*

PRO 54: 5th International RILEM Symposium on Self-Compacting Concrete (2007) 1198 pp. ISBN: 978-2-35158-047-9 - Soft cover; *Eds. G. De Schutter and V. Boel*

PRO 55: International RILEM Symposium Photocatalysis, Environment and Construction Materials (2007) 350 pp. ISBN: 978-2-35158-056-1 - Soft cover; *Eds. P. Baglioni and L. Cassar*

PRO56: International RILEM Workshop on Integral Service Life Modelling of Concrete Structures (2007) 458 pp. ISBN 978-2-35158-058-5 - Hard back, *Eds. R. M. Ferreira, J. Gulikers and C. Andrade*

PRO57: RILEM Workshop on Performance of cement-based materials in aggressive aqueous environments (2008) 132 pp. e-ISBN: 978-2-35158-059-2, *Ed. N. De Belie*

PRO58: International RILEM Symposium on Concrete Modelling CONMOD'08 (2008) 847 pp., ISBN: 978-2-35158-060-8, Soft cover, *Eds. E. Schlangen and G. De Schutter*

PRO 59: International RILEM Conference on On Site Assessment of Concrete, Masonry and Timber Structures SACoMaTiS 2008 (2008)., ISBN: 978-2-35158-061-5 (set) - Hard back, *Eds. L. Binda, M. di Prisco and R. Felicetti*

PRO 60: Seventh RILEM International Symposium (BEFIB 2008) on Fibre Reinforced Concrete: Design and Applications (2008) 1181 pp, ISBN: 978-2-35158-064-6 - Hard back, *Ed. R. Gettu*

PRO 61: 1st International Conference on Microstructure Related Durability of Cementitious Composites *(Nanjing),* 2 volumes, (2008), 1524 pp., ISBN: 978-2-35158-065-3 - Soft cover, *Edited by W. Sun, K. van Breugel, C. Miao, G. Ye and H. Chen*

PRO 62: NSF/ RILEM Workshop: In-situ Evaluation of Historic Wood and Masonry Structures (2008), e-ISBN: 978-2-35158-068-4, *Edited by B. Kasal, R. Anthony and M. Drdacky*

PRO 63: Concrete in Aggressive Aqueous Environments: Performance, Testing and Modelling, 2 volumes, (2009) 594 pp., ISBN: 978-2-35158-071-4 - Soft cover, *Eds. M.G. Alexander and A. Bertron*

PRO 64: Long Term Performance of Cementitious Barriers and Reinforced Concrete in Nuclear Power Plants and Waste Management - NUCPERF 2009 (2009), Soft cover - ISBN: 978-2-35158-072-1, 359 pp., *Edited by V. L'Hostis, R. Gens, C. Gallé*

PRO 65: Design Performance and Use of Self-consolidating Concrete, SCC'2009, (2009), ISBN: 978-2-35158-073-8 - *Eds. C. Shi, Z. Yu, K. H. Khayat and P. Yan*

PRO 66: Concrete Durability and Service Life Planning, 2nd International RILEM Workshop, ConcreteLife'09, (2009) 602 pp., ISBN: 978-2-35158-074-5 - *Eds.K. Kovler, A. Bentur*

PRO 67: Repairs Mortars for Historic Masonry, (2009) – 397 pp. – e-ISBN: 978-2-35158-083-7 – *Ed. by C. Groot*

PRO 68: Proceedings of the 3rd International RILEM Symposium on "Rheology of Cement Suspensions such as Fresh Concrete" - 372 pp. - ISBN 978-2-35158-091-2 - *Edited by O. H. Wallevik, S. Kubens and S. Oesterheld*

PRO 69: 3rd International PhD Student Workshop on "Modelling the Durability of Reinforced Concrete" - ISBN: 978-2-35158-095-0 - *Edited by R. M. Ferreira, J. Gulikers and C. Andrade*

PRO 71: Advances in Civil Engineering Materials, Proceedings of the "The 50-year Teaching Anniversary of Prof. Sun Wei", ISBN: 978-2-35158-098-1, e-ISBN: 978-2-35158-099-8 - *Edited by C. Miao, G. Ye, and H. Chen*

RILEM REPORTS

Report 19: Considerations for Use in Managing the Aging of Nuclear Power Plant Concrete Structures (ISBN: 2-912143-07-1); *Ed. D. J. Naus,* 1999

Report 20: Engineering and Transport Properties of the Interfacial Transition Zone in Cementitious Composites (ISBN: 2-912143-08-X)
Eds. M. G. Alexander, G. Arliguie, G. Ballivy, A. Bentur and J. Marchand, 1999

Report 21: Durability of Building Sealants (ISBN: 2-912143-12-8); *Eds. A. T. Wolf, 1999*

Report 22: Sustainable Raw Materials – Construction and Demolition Waste (ISBN: 2-912143-17-9); *Eds. C. F. Hendriks and H. S. Pietersen,* 2000

Report 23: Self-Compacting Concrete state-of-the-art report (ISBN: 2-912143-23-3) - Soft cover; *Eds. Å. Skarendahl and Ö. Petersson,* 2001

Report 24: Workability and Rheology of Fresh Concrete: Compendium of Tests (ISBN: 2-912143-32-2) - Soft cover; *Eds. P.J.M. Bartos, M. Sonebi and A.K. Tamimi,* 2002

Report 25: Early Age Cracking in Cementitious Systems (ISBN: 2-912143-33-0) - Soft cover *Ed. A. Bentur,* 2003

Report 26: Towards Sustainable Roofing (Joint Committee CIB/RILEM) (CD 07); *Eds. Thomas W. Hutchinson and Keith Roberts,* 2001

Report 27: Condition Assessment of Roofs (Joint Committee CIB/RILEM) (CD 08), 2003

Report 28: Final report of RILEM TC 167-COM 'Characterisation of Old Mortars with Respect to their Repair', 192 pp. (ISBN: 978-2-912143-56-3) - Soft cover; *Eds. C. Groot, G. Ashall and J. Hughes ,* 2007

Report 29: Pavement Performance Prediction and Evaluation (PPPE): Interlaboratory Tests, (e-ISBN: 2-912143-68-3); *Eds. M. Partl and H. Piber,* 2005

Report 30: Final Report of RILEM TC 198-URM 'Use of Recycled Materials', (ISBN: 2-912143-82-9; e-ISBN: 2-912143-69-1) - Soft cover; *Eds. Ch. F. Hendriks, G.M.T. Janssen and E. Vázquez,* 2005

Report 31: Final Report of RILEM TC 185-ATC 'Advanced testing of cement-based materials during setting and hardening', (ISBN: 2-912143-81-0; e-ISBN: 2-912143-70-5) - Soft cover; *Eds. H.W. Reinhardt and C.U. Grosse*, 2005

Report 32: Probabilistic Assessment of Existing Structures. A JCSS publication - 176pp. ISBN 2-912143-24-1 - Hard back; *Ed. D. Diamantidis*, 2001

Report 33: State-of-the-Art Report of RILEM Technical Committee TC 184-IFE 'Industrial Floors', - 158 pp. ISBN 2-35158-006-0 – Soft cover; *Ed. P. Seidler,* 2006

Report 34: Report of RILEM Technical Committee TC 147-FMB 'Fracture mechanics appli-cations to anchorage and bond' Tension of Reinforced Concrete Prisms – Round Robin Analysis and Tests on Bond, - 248 pp. e-ISBN 2-912143-91-8 – Online; *Eds. L. Elfgren and K. Noghabai*, 2001

Report 35: Final Report of RILEM Technical Committee TC 188-CSC 'Casting of Self Compacting Concrete', 40 pp. ISBN 2-35158-001-X; e-ISBN: 2-912143-98-5 - Soft cover; *Eds. Å. Skarendahl and P. Billberg*, 2006

Report 36: State-of-the-Art Report of RILEM Technical Committee TC 201-TRC 'Textile Reinforced Concrete', 292 pp. ISBN 2-912143-99-3 - Soft cover; *Ed. W. Brameshuber*, 2006

Report 37: State-of-the-Art Report of RILEM Technical Committee TC 192-ECM 'Environment-conscious construction materials and systems', 88 pp. ISBN: 978-2-35158-053-0 - Soft cover; *Eds. N. Kashino, D. Van Gemert and K. Imamoto*, 2007

Report 38: State-of-the-Art Report of RILEM Technical Committee TC 205-DSC 'Durability of Self-Compacting Concrete', 204 pp. ISBN: 978-2-35158-048-6 - Soft cover; *Eds. G. De Schutter and K. Audenaert*, 2007

Report 39: Final Report of RILEM Technical Committee TC 187-SOC 'Experimental determination of the stress-crack opening curve for concrete in tension', 54 pp. ISBN 978-2-35158-049-3 - Soft cover; *Ed. J. Planas*, 2007

Report 40: State-of-the-Art Report of RILEM Technical Committee TC 189-NEC 'Non-Destructive Evaluation of the Penetrability and Thickness of the Concrete Cover', 246 pp. ISBN 978-2-35158-054-7 - Soft cover; *Eds. R. Torrent and L. Fernández Luco*, 2007

Report 41: State-of-the-Art Report of RILEM Technical Committee TC 196-ICC 'Internal Curing of Concrete', 164 pp. ISBN 978-2-35158-009-7 - Soft cover; *Eds. K. Kovler and O.M. Jensen*, 2007

RILEM COMPENDIUMS

COMP 01: Trilingual Dictionary for Materials and Structures (English-French-German) (CD01) (1970)

COMP 02: 1947-1997: 50 years of evolution of Building Materials and Structures - e-ISBN: 2-912143-86-1; *Ed. F. Wittmann*

COMP 03: General Conference of RILEM TCs' Chairmen and RILEM Seminar 'Advancing the Knowledge in Materials and Structures' (CD10) (2000) e-ISBN: 2-912143-85-3

COMP 06: Concrete Science and Engineering Journal - Vol. 1, 2, 3, 4 (1999-2002) (CD05)

COMP 13: RILEM Technical Day, Moscow (2005) e-ISBN: 2-35158-045-1